The Elastic Sphere Under Concentrated Loads

By E. STERNBERG[1] and F. ROSENTHAL,[2] CHICAGO, ILL.

This paper contains an exact solution for the stress distribution in an elastic sphere under two equal and opposite concentrated loads, applied at the end points of a diameter. The solution is based on the Boussinesq stress-function approach to axisymmetric problems and is represented as a sum of two solutions: A singular solution in closed form, and a series solution corresponding to surface tractions which are finite and continuous throughout the surface of the sphere. It is shown that the singularity at the points of application of the loads is not identical with that arising at a concentrated load acting normal to a plane boundary. The existence of pseudosolutions to the problem under consideration, as well as to concentrated-force problems in general, is illustrated, and the validity of the present solution is confirmed through a limit process applied to the case of tractions uniformly distributed over a portion of the boundary. The numerical results for the normal stress on the plane of symmetry perpendicular to the load axis, are compared with the corresponding stress values obtained in a recent three-dimensional photoelastic investigation of the same problem by Frocht and Guernsey (1).[3]

Statement of Problem

THE problem of the sphere in the classical theory of elasticity has an extensive literature.[4] Although there is available a variety of general solutions to this problem, in series or integral form, the singularities encountered in the presence of concentrated loads require special attention if the solutions corresponding to such singular loading cases are to be practically useful. In the current paper we consider the axisymmetric problem of a sphere which is under the action of two equal and opposite concentrated loads, applied at the end points of a diameter, the body forces being assumed to vanish identically. This particular problem is perhaps of interest in connection with the stress analysis of ball bearings. Moreover, the treatment of the singularities, developed here, remains applicable to any configuration of radial concentrated loads. Finally, the current work is a prerequisite for, and has been applied in obtaining an exact solution to, the problem of the spherical shell of arbitrary thickness under the same loading conditions; the results of this investigation will be communicated in a later publication.

The solution sought presently must meet the following requirements: (*a*) It must satisfy the basic field equations of elasticity theory; (*b*) it must conform to surface tractions which vanish throughout the surface of the sphere; (*c*) it must possess singularities at each load point such that the tractions on any surface enclosing the point, and lying wholly in the region occupied by the medium, are statically equivalent to the prescribed concentrated load. These conditions, however, though necessary, represent an incomplete formulation of the problem, and do not uniquely characterize the solution.[5] In a recent paper (5), W. Leutert presented a solution in closed form, satisfying the foregoing requirements for the problem of an elastic sphere under the action of its own weight which is balanced by a single concentrated force applied to the surface of the sphere. It is evident that the solution to this problem, by virtue of the principle of superposition, is readily extended to the problem considered here. The solution so obtained, of course, again meets the foregoing three requirements; however, Leutert's singularity at the load point, as the radius of the sphere approaches infinity, does not tend toward the singularity appropriate to a concentrated force acting normal to the plane boundary of a semi-infinite medium. Moreover, the solution reached on the basis of Leutert's results, is a pseudosolution of the present problem in the sense that it does not coincide with the solution corresponding to tractions uniformly distributed over regions of the boundary which surround the points of application of the forces, in the limit as these regions are contracted to the load points and the resultants of the distributed tractions are made to approach the given concentrated loads. It is such a limit condition which must be added to the three conditions already cited, and which provides an ultimate criterion for the validity of solutions to concentrated-force problems.

Boussinesq Approach to Axisymmetric Problems, Spherical and Spherical Dipolar Co-Ordinates

The solution of the problem just stated will be based on the stress-function approach originated by Boussinesq (6). According to Boussinesq (7), the general solution of the displacement equations of equilibrium in case of torsion-free rotational symmetry about the z-axis, and in the absence of body forces, is representable as the sum of the following two displacement fields which are referred to cylindrical co-ordinates (ρ, γ, z)

$$2G\,[u_\rho, u_\gamma, u_z] = \text{grad}\ \phi \quad \ldots\ldots [1]$$

$$2G\,[u_\rho, u_\gamma, u_z] = \text{grad}\ (z\psi) - [0, 0, 4(1-\nu)\psi] \quad \ldots\ldots [2]$$

where

$$\nabla^2\phi(\rho, z) = 0, \quad \nabla^2\psi(\rho, z) = 0 \quad \ldots\ldots [3]$$

Here $[u_\rho, u_\gamma, u_z]$ designate the radial, transverse, and axial components of displacement, G denotes the shear modulus, and ν is Poisson's ratio.

The displacement fields Equations [1] and [2], together with their associated fields of stress, constitute the first and second Boussinesq solutions, whose general axisymmetric curvilinear transforms were given in (7).

In what follows we shall have occasion to refer, in particular, to spherical and spherical dipolar co-ordinates. If (x, y, z) denote Cartesian co-ordinates, the spherical co-ordinates (r, θ, γ) are introduced through the transformation

$$\left.\begin{aligned} x = r\sin\theta\cos\gamma,\ y = r\sin\theta\sin\gamma,\ z = r\cos\theta \\ 0 \le r < \infty,\ 0 \le \theta \le \pi,\ 0 \le \gamma < 2\pi \end{aligned}\right\} \quad \ldots [4]$$

---

[1] Professor of Mechanics, Illinois Institute of Technology. Jun. ASME.

[2] Associate Research Engineer, Armour Research Foundation.

[3] Numbers in parentheses refer to the Bibliography at the end of the paper.

[4] A complete bibliography of this subject is beyond the scope of this paper; see (2, 3, 4) for references.

Presented at the National Conference of the Applied Mechanics Division, State College, Pa., June 19–21, 1952, of The American Society of Mechanical Engineers.

Discussion of this paper should be addressed to the Secretary, ASME, 29 West 39th Street, New York, N. Y., and will be accepted until January 10, 1953, for publication at a later date. Discussion received after the closing date will be returned.

Note: Statements and opinions advanced in papers are to be understood as individual expressions of their authors and not those of the Society. Manuscript received by ASME Applied Mechanics Division, February 25, 1952. Paper No. 52—APM-37.

[5] This fact, in view of the singular loading conditions, is not in contradiction with the uniqueness theorems of elasticity theory.

whereas the spherical dipolar co-ordinates (α, β, γ) are defined by

$$\left.\begin{aligned} x &= \frac{r_0 \sin\beta}{\cosh\alpha - \cos\beta}\cos\gamma \\ y &= \frac{r_0 \sin\beta}{\cosh\alpha - \cos\beta}\sin\gamma \\ z &= -\frac{r_0 \sinh\alpha}{\cosh\alpha - \cos\beta} \\ -\infty < \alpha < \infty,\ 0 \le \beta \le \pi,\ 0 \le \gamma &< 2\pi \end{aligned}\right\} \quad \ldots\ldots [5]$$

where r_0 is a positive constant. The co-ordinate surfaces of the dipolar system were discussed in an earlier paper (8), and the traces of the surfaces α = const, β = const upon a meridional half-plane γ = const, are reproduced in Fig. 1. This figure also

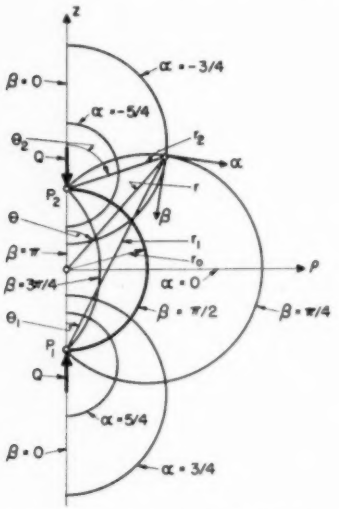

FIG. 1 SPHERICAL AND DIPOLAR CO-ORDINATE SYSTEMS

shows the polar co-ordinates (r, θ), as well as the "displaced" polar co-ordinates (r_1, θ_1) and (r_2, θ_2), the origins of which coincide with the poles of the dipolar system and are located on the z-axis at $z = -r_0$ and $z = r_0$, respectively. We now introduce the auxiliary notations

$$\left.\begin{aligned} c &= \cos\theta,\ c_1 = \cos\theta_1,\ c_2 = \cos\theta_2 \\ s &= \sin\theta,\ s_1 = \sin\theta_1,\ s_2 = \sin\theta_2 \\ p &= \cos\beta,\ q = \cosh\alpha \\ \bar{p} &= \sin\beta,\ \bar{q} = \sinh\alpha \\ \mu &= (q-p)^{1/2} \end{aligned}\right\} \quad \ldots\ldots [6]$$

and note the identities

$$\left.\begin{aligned} \bar{p} &= 2r_0 rs\,[(r_0^2 + r^2)^2 - 4r_0^2 r^2 c^2]^{-1/2},\ \bar{q} = \frac{-cp}{s} \\ r_1 &= \frac{\sqrt{2}r_0 e^{-\alpha/2}}{\mu}, \qquad c_1 = \frac{(q-p-\bar{q})e^{\alpha/2}}{\sqrt{2}\mu} \\ r_2 &= \frac{\sqrt{2}r_0 e^{\alpha/2}}{\mu}, \qquad c_2 = \frac{(p-q-\bar{q})e^{-\alpha/2}}{\sqrt{2}\mu} \end{aligned}\right\} \quad \ldots [7]$$

which relate the four sets of co-ordinates under consideration. With the aid of the law of stress transformation we arrive at the relations

$$\left.\begin{aligned} (q^2-p^2)^{1/2}u_r &= -p\bar{q}u_\alpha - \bar{p}qu_\beta \\ (q^2-p^2)^{1/2}u_\theta &= \bar{p}qu_\alpha - p\bar{q}u_\beta \\ (q^2-p^2)\sigma_r &= p^2\bar{q}^2\sigma_\alpha + \bar{p}^2q^2\sigma_\beta + 2p\bar{p}q\bar{q}\tau_{\alpha\beta} \\ (q^2-p^2)\sigma_\theta &= \bar{p}^2q^2\sigma_\alpha + p^2\bar{q}^2\sigma_\beta - 2p\bar{p}q\bar{q}\,\tau_{\alpha\beta} \\ (q^2-p^2)\,\tau_{r\theta} &= -p\bar{p}q\bar{q}(\sigma_\alpha - \sigma_\beta) + (p^2\bar{q}^2 - \bar{p}^2q^2)\tau_{\alpha\beta} \end{aligned}\right\} \quad \ldots [8]$$

which connect the spherical and dipolar components of displacement and stress. The normal stress σ_γ is common to both reference systems whereas the displacement u_γ, as well as the stresses $\tau_{\gamma r}, \tau_{\gamma\theta}, \tau_{\gamma\alpha}, \tau_{\gamma\beta}$, vanish identically in view of the rotational symmetry.

The first and second Boussinesq solutions were referred to spherical co-ordinates in (4) and to spherical dipolar co-ordinates in (8); for the sake of convenience, we record at this place the corresponding formulas for the displacements and stresses. In spherical co-ordinates

$$2Gu_r = \phi_r,\ 2Gu_\theta = -\frac{s\phi_c}{r} \quad \ldots\ldots [9]^6$$

$$\left.\begin{aligned} \sigma_r &= \phi_{rr}, \qquad \sigma_\theta = \frac{s^2}{r^2}\phi_{cc} - \frac{c}{r^2}\phi_c + \frac{\phi_r}{r} \\ \sigma_\gamma &= \frac{\phi_r}{r} - \frac{c}{r^2}\phi_c, \qquad \tau_{r\theta} = \frac{s}{r}\left(\frac{\phi_c}{r} - \phi_{rc}\right) \end{aligned}\right\} \quad \ldots [10]$$

$$\left.\begin{aligned} 2Gu_r &= c[r\psi_r - (3-4\nu)\psi] \\ 2Gu_\theta &= -s[c\psi_c - (3-4\nu)\psi] \end{aligned}\right\} \quad \ldots\ldots [11]$$

$$\left.\begin{aligned} \sigma_r &= rc\psi_{rr} - 2(1-\nu)c\psi_r - \frac{2\nu s^2}{r}\psi_c \\ \sigma_\theta &= \frac{cs^2}{r}\psi_{rc} + (1-2\nu)c\psi_r - [1+(1-2\nu)s^2]\frac{\psi_c}{r} \\ \sigma_\gamma &= (1-2\nu)c\psi_r - (c^2+2\nu s^2)\frac{\psi_c}{r} \\ \tau_{r\theta} &= -s\left[c\psi_{rr} - (1-2\nu)\psi_r - 2(1-\nu)\frac{\psi_c}{r}\right] \end{aligned}\right\} \quad \ldots [12]$$

In spherical dipolar co-ordinates

$$2Gr_0u_\alpha = \mu^2\phi_\alpha,\ 2Gr_0u_\beta = -\mu^2p\phi_p \quad \ldots\ldots [13]$$

$$\left.\begin{aligned} r_0^2\,\sigma_\alpha &= \mu^2(\mu^2\phi_{\alpha\alpha} + \bar{q}\phi_\alpha + \bar{p}^2\phi_p) \\ r_0^2\,\sigma_\beta &= \mu^2[\mu^2\bar{p}^2\phi_{pp} - (\mu^2p + \bar{p}^2)\phi_p - \bar{q}\phi_\alpha] \\ r_0^2\,\sigma_\gamma &= -\mu^2[\bar{q}\phi_\alpha - (1-qp)\phi_p] \\ r_0^2\,\tau_{\alpha\beta} &= -\mu^2\bar{p}[\mu^2\phi_{\alpha p} - \phi_\alpha + \bar{q}\phi_p] \end{aligned}\right\} \quad \ldots [14]$$

$$\left.\begin{aligned} 2Gu_\alpha &= -\left[\bar{q}\psi_\alpha + (3-4\nu)\frac{qp-1}{\mu^2}\psi\right] \\ 2Gu_\beta &= \bar{p}\bar{q}\left[\psi_p - (3-4\nu)\frac{\psi}{\mu^2}\right] \end{aligned}\right\} \quad \ldots [15]$$

$$\left.\begin{aligned} r_0\sigma_\alpha &= -\mu^2\bar{q}\psi_{\alpha\alpha} - [\bar{q}^2 + 2(1-\nu)(qp-1)]\,\psi_\alpha \\ &\quad - (1-2\nu)\bar{q}\,p^2\,\psi_p \\ r_0\sigma_\beta &= -\mu^2\bar{q}\,p^2\,\psi_{pp} + [\mu^2\bar{q}p + (3-2\nu)\bar{q}\,p^2]\psi_p \\ &\quad + [\bar{q}^2 - 2\nu(qp-1)]\psi_\alpha \\ r_0\,\sigma_\gamma &= [\bar{q}^2 - 2\nu(qp-1)]\psi_\alpha + [qp - 1 + 2\nu p^2]\,\bar{q}\,\psi_p \\ r_0\,\tau_{\alpha\beta} &= \mu^2\bar{q}\,\bar{p}\,\psi_{\alpha p} - 2(1-\nu)\bar{q}\,p\,\psi_\alpha \\ &\quad + [\bar{q}^2 + (1-2\nu)(qp-1)]\,p\psi_p \end{aligned}\right\} \quad \ldots [16]$$

[6] Subscripts attached to functions which originally bear no subscript denote partial differentiation with respect to the argument indicated.

Basic Solutions in Spherical Co-Ordinates

In this section we compile a catalog of certain basic solutions in spherical co-ordinates of the field equations of elasticity theory, which are needed in the subsequent analysis of the problem under consideration. The following are the pertinent Boussinesq stress functions, which all satisfy Laplace's equation, together with the designations of the solutions so generated[7]

$$\left.\begin{aligned}
&\phi = r^{-n-1}P_n(c) \quad (n = 0, \pm1, \pm2, \dots) \dots [A_n]\\
&\psi = r^{-n-1}P_n(c) \quad (n = 0, \pm1, \pm2, \dots) \dots [C_n]\\
&\phi = \omega(r, c) \dots [D_1]\\
&\psi = \omega(r, c) \dots [E_1]\\
&\phi = r(c\omega - 1) \dots [D_2]\\
&\psi = r(c\omega - 1) \dots [E_2]\\
&\phi = r^2[(1 - 3c^2)\omega + c^2 + 3c - 1] \dots [D_3]
\end{aligned}\right\} \dots [17]$$

where P_n is the Legendre polynomial of order n, and

$$\omega(r, c) = \log \frac{r(1 + c)}{2r_0} \equiv \log \frac{r + z}{2r_0} \dots [18][8]$$

The displacements and stresses appropriate to the solutions defined by Equations [17] follow from Equations [9] to [12]. We cite here merely the components of stress.

Solution $[A_n]$

$$\left.\begin{aligned}
\sigma_r &= (n + 1)(n + 2)\frac{P_n}{r^{n+2}}\\
\sigma_\theta &= \frac{1}{r^{n+2}}[P_{n+1}' - (n + 1)(n + 2)P_n]\\
\sigma_\gamma &= -\frac{P_{n+1}'}{r^{n+2}}, \qquad \tau_{r\theta} = \frac{n + 2}{r^{n+2}}sP_n'
\end{aligned}\right\} \dots [19][9]$$

For reasons indicated in (4) it is expedient to replace $[C_n]$ by the linear combination

$$[B_n] = (2n + 1)[C_n] - (n + 4 - 4\nu)[A_{n-1}] \dots [20]$$

We thus reach

Solution $[B_n]$

$$\left.\begin{aligned}
\sigma_r &= (n + 1)[(n + 1)(n + 4) - 2\nu]\frac{P_{n+1}}{r^{n+2}}\\
\sigma_\theta &= -\frac{1}{r^{n+2}}[(n + 1)(n^2 - n + 1 - 2\nu)P_{n+1}\\
&\qquad -(n - 3 + 4\nu)P_n']\\
\sigma_\gamma &= -\frac{1}{r^{n+2}}[(1 - 2\nu)(n + 1)(2n + 1)P_{n+1}\\
&\qquad + (n - 3 + 4\nu)P_n']\\
\tau_{r\theta} &= (n^2 + 2n - 1 + 2\nu)\,s\,\frac{P_{n+1}'}{r^{n+2}}
\end{aligned}\right\} \dots [21]$$

Solution $[D_1]$

$$\left.\begin{aligned}
\sigma_r &= -\frac{1}{r^2}, \qquad \sigma_\theta = \frac{c}{r^2(1 + c)}\\
\sigma_\gamma &= \frac{1}{r^2(1 + c)}, \qquad \tau_{r\theta} = \frac{s}{r^2(1 + c)}
\end{aligned}\right\} \dots [22]$$

Solution $[E_1]$

$$\left.\begin{aligned}
\sigma_r &= \frac{1}{r}[-(3 - 4\nu)c - 2\nu]\\
\sigma_\theta &= \frac{1}{r(1 + c)}[(3 - 4\nu)c^2 - 2\nu c - 2(1 - \nu)]\\
\sigma_\gamma &= \frac{1}{r(1 + c)}[(1 - 2\nu)c - 2\nu]\\
\tau_{r\theta} &= \frac{s}{r(1 + c)}[(3 - 4\nu)c + 1 - 2\nu]
\end{aligned}\right\} \dots [23]$$

Solution $[D_2]$

$$\left.\begin{aligned}
\sigma_r &= \frac{c}{r}, \qquad \sigma_\theta = -\frac{c^2 + c - 1}{r(1 + c)}\\
\sigma_\gamma &= \frac{-1}{r(1 + c)}, \qquad \tau_{r\theta} = -\frac{s}{r}
\end{aligned}\right\} \dots [24]$$

Solution $[E_2]$

$$\left.\begin{aligned}
\sigma_r &= -(1 - 4\nu)c^2 + 2(1 - 2\nu)c\\
&\qquad - \omega[2(1 - 2\nu)c^2 + 2\nu]\\
\sigma_\theta &= \frac{-c}{1 + c}[(1 - 4\nu)s^2 + c]\\
&\qquad + \omega[2(1 - 2\nu)c^2 - 2(1 - \nu)]\\
\sigma_\gamma &= -\frac{c}{1 + c} - 2\nu\omega\\
\tau_{r\theta} &= \frac{s}{1 + c}[(1 - 4\nu)c^2 - c - (1 - 2\nu)]\\
&\qquad + 2(1 - 2\nu)cs\omega
\end{aligned}\right\} \dots [25]$$

Solution $[D_3]$

$$\left.\begin{aligned}
\sigma_r &= 2(1 - 3c^2)\omega - 7c^2 + 6c + 1\\
\sigma_\theta &= 2(3c^2 - 2)\omega + \frac{1 - c}{1 + c} + 7c^2 - 6c - 1\\
\sigma_\gamma &= 2\omega + \frac{c - 1}{c + 1}\\
\tau_{r\theta} &= s\left[6c\omega + \frac{7c^2 + c - 4}{1 + c}\right]
\end{aligned}\right\} \dots [26]$$

Solutions $[A_n]$ and $[B_n]$ were also discussed in (4) where their physical significance was examined. These solutions are regular throughout the finite Cartesian space, for $n < 0$; for $n \geq 0$, they are generated by the sequence of stress functions obtained from the potential $1/r$ through successive z-differentiations, and as n increases possess progressively stronger singularities at the origin. In particular, $[A_0]$ and $[B_0]$ correspond, respectively, to a center of dilatation and a concentrated force at $r = 0$ in an infinite medium.

Solutions $[D_1]$, $[D_2]$, $[D_3]$, and $[E_1]$, $[E_2]$, on the other hand, are generated by the initial members of the sequence of stress functions arising from $1/r$ through successive z-integrations. Indeed

$$\left.\begin{aligned}
&\frac{\partial\omega}{\partial z} = \frac{1}{r}, \qquad \frac{\partial}{\partial z}[r(c\omega - 1)] = \omega\\
&\frac{\partial}{\partial z}\{r^2[(1 - 3c^2)\omega + c^2 + 3c - 1]\} = -4r(c\omega - 1)
\end{aligned}\right\} \dots [27]$$

These solutions possess progressively weaker singularities along the negative z-axis. Solution $[D_1]$, in particular, represents a half-line of dilatation.

Finally, we consider the stress resultants of the tractions acting

---

[7] Throughout this paper, capital letters in brackets denote either the displacement vector-field or the stress tensor-field of the corresponding solution, and equality, addition, as well as multiplication by a scalar, are to be interpreted accordingly.

[8] The constant denominator in the argument of the logarithm is introduced for later convenience.

[9] The argument of P_n, unless otherwise specified, is henceforth assumed to be c, and $P_n' = \frac{dP_n}{dc}$.

on a hemispherical surface of radius r, centered at the origin and lying in the half-space $z \geq 0$, for the basic solutions listed in Equations [17]. Let $Z(r)$ be the resultant force in question. Furthermore, let the outer normal to the surface be directed toward the origin and let Z be positive if acting in the positive z-direction. A trivial computation yields

$$\left.\begin{aligned}
&[A_n] \ldots\ldots Z(r) = -2\pi(n+1)r^{-n-1}P_n(0)\\
&[C_n] \ldots\ldots Z(r) = -4\pi(1-\nu)r^{-n}P_{n-1}(0)\\
&[D_1] \ldots\ldots Z(r) = 2\pi\\
&[E_1] \ldots\ldots Z(r) = 4\pi(1-\nu)r\\
&[D_2] \ldots\ldots Z(r) = -2\pi r\\
&[E_2] \ldots\ldots Z(r) = \pi(1-\nu)r^2(\log r^2/4r_0^2 - 1)\\
&[D_3] \ldots\ldots Z(r) = 2\pi r^2(\log r^2/4r_0^2 - 1) \ldots\ldots
\end{aligned}\right\} \ldots [28]$$

where

$$P_{2n+1}(0) = 0,\ P_{2n}(0) = (-1)^n \frac{|2n}{2^{2n}(|n)^2} \ldots\ldots [29]$$

Determination of Singularities for Sphere Under Concentrated Loads

We return here to the particular problem to be considered. Let the sphere occupy the region $r \leq r_0$, and let the two forces, each of magnitude $|Q|$, be applied at the poles P_1, P_2, Fig. 1. For $Q > 0$, both forces are supposed to be directed toward the center of the sphere.

The well-known solution, due to Boussinesq (6), corresponding to a concentrated load Q applied at $r = 0$ perpendicular to the plane boundary of a medium occupying the half-space $z \geq 0$, in our notation appears as[10]

$$[S_0] = -\frac{Q}{2\pi}\{[B_0] + (1-2\nu)[D_1]\} \ldots\ldots [30]$$

with $[B_0]$, $[D_1]$ defined by Equations [17], [20]. The desired solution $[S]$ to the problem is now assumed as

$$[S] = [\bar{S}_0] + [R_0] \ldots\ldots [31]$$

where $[\bar{S}_0]$ is the "symmetrized" form of $[S_0]$, that is, the sum of the two solutions which represent, respectively, an upward force Q acting on the boundary $z = -r_0$ of the half-space $z \geq -r_0$ and a downward force Q acting on the boundary $z = r_0$ of the half-space $z \leq r_0$, both forces being applied along the z-axis. On the other hand, $[R_0]$ is the solution of a "residual problem," the formulation of which is implicit in Equation [31]. The approach indicated by Equation [31] is strictly analogous to that commonly employed in developing the solution to the corresponding plane problem[11] of the circular disk under diametrically opposed concentrated loads, where the counterpart of $[R_0]$ turns out to be characterized by a uniform, hydrostatic field of stress.

Solution $[\bar{S}_0]$ is obtained from $[S_0]$ by a symmetrization process which we define presently in general terms. Thus let $[T]$ be any axisymmetric solution of the field equations, given by the displacements

$$u_r = F(r, \theta),\ u_\theta = H(r, \theta) \ldots\ldots [32]$$

Then the displacement field of the symmetrized form[12] $[\bar{T}]$ of $[T]$ is defined as the vector sum of the two displacement fields

$$\left.\begin{aligned}
u_{r_1} &= F(r_1, \theta_1), & u_{\theta_1} &= H(r_1, \theta_1)\\
u_{r_2} &= F(r_2, \pi - \theta_2) & u_{\theta_2} &= -H(r_2, \pi - \theta_2)
\end{aligned}\right\} \ldots [33]$$

where (u_{r_1}, u_{θ_1}) and (u_{r_2}, u_{θ_2}) are the components of the displacement vector with reference to the displaced polar co-ordinate systems. According to Equations [33], [9], [11], if $[T]$ is the sum of the first and second Boussinesq solutions generated by

$$\phi = \Phi(r, c),\ \psi = \Psi(r, c) \ldots\ldots [34]$$

then $[T]$ is the sum of the two Boussinesq solutions derived from

$$\left.\begin{aligned}
\phi &= \Phi(r_1, c_1) + \Phi(r_2, -c_2)\\
&\quad + r_0[\Psi(r_1, c_1) + \Psi(r_2, -c_2)]\\
\psi &= \Psi(r_1, c_1) - \Psi(r_2, -c_2)
\end{aligned}\right\} \ldots [35]$$

Equations [35] permit the determination of $[\bar{T}]$ on the basis of the stress functions appropriate to $[T]$. Returning to $[\bar{S}_0]$, we note that according to Equation [30]

$$[\bar{S}_0] = -\frac{Q}{2\pi}\{[B_0] + (1-2\nu)[D_1]\} \ldots\ldots [36]$$

We next examine the tractions to which $[\bar{S}_0]$ gives rise on the sphere $r = r_0$, and which are to be removed by superposition of $[R_0]$, as indicated by Equation [31]. In order to ascertain whether these tractions, and hence the boundary stresses of $[R_0]$, are regular, it suffices to examine the local behavior of the normal and shearing stresses, designated by $\sigma(c)$ and $\tau(c)$, arising from $[\bar{S}_0]$ on the displaced sphere $r = 2r_0c$, in the neighborhood of the origin, where $c = 0$. An elementary computation, based on Equations [30], [21], [22], and on the law of stress transformation, yields

For $[\bar{S}_0]$

$$\left.\begin{aligned}
\sigma(c) &= 0(1)\\
\tau(c) &= \frac{Q}{8\pi r_0^2}\left[\frac{-2(1-2\nu)}{c} + 5 - 4\nu\right] + 0(0)
\end{aligned}\right\} \ldots [37]$$

where $0(1)$ and $0(0)$, respectively, denote terms which approach a finite limit or zero, as $c \to 0$.

Equations [37] reveal the important fact that in contrast to the situation encountered in the analogous plane problem of the circular disk, the shearing stress of $[\bar{S}_0]$ on $r = r_0$, and hence the surface shearing-tractions of $[R_0]$, become infinite at the poles P_1, P_2. This implies, furthermore, that in the three-dimensional problem of the sphere, the singularity at a point of application of a radial concentrated force is not identical with that arising in the presence of a concentrated force acting normal to a plane boundary.

In view of these observations, we seek to modify the singular solution $[\bar{S}_0]$ so as to arrive at a new residual problem, governed by boundary stresses which are finite and continuous throughout the surface of the sphere. In this attempt we are guided by the requirement that the modified singularities at the poles must remain dominated by those of $[\bar{S}_0]$, if the solution $[S]$ to the problem is to approach the proper limit as $r_0 \to \infty$. This leads us to assume[13]

$$[S] = [\bar{S}_2] + [R_2] \ldots\ldots [38]$$

with

$$[S_2] = [S_0] + e_1[E_1] + d_2[D_2] + e_2[E_2] + d_3[D_3] \ldots [39]$$

where the coefficients e_1, d_2, e_2, d_3 are to be determined so as to assure[14] $\sigma(c) = 0(1)$ and $\tau(c) = 0(0)$ for $[S_2]$, the notation being

[10] See also (2), p. 191, and (9), p. 362. If $Q > 0$, the force acts in the positive z-direction.

[11] See, for example (9), p. 107.

[12] A bar placed over a letter designating a solution of the field equations will henceforth denote symmetrization.

[13] See discussion, at end of preceding section, regarding relative strength of singularities present in aggregate of solutions defined by Equations [17].

[14] It should be recalled that $\tau(c) = 0(1)$ would correspond to a discontinuity at the poles in the shearing stress of $[R_2]$, and is therefore inadmissible.

that of Equations [37]. With the aid of Equations [23] to [26], we find that the foregoing two conditions uniquely determine the unknown coefficients of superposition in Equation [39], and thus reach

$$\left.\begin{aligned}[\bar{S}_2] &= [\bar{S}_0] + \frac{(1-2\nu)Q}{2\pi r_0}\,[\bar{L}_1] \\ &\quad + \frac{(1+12\nu-16\nu^2)Q}{16\pi r_0^2}\,[\bar{L}_2] \\ [L_1] &= [E_1] + 2(1-\nu)\,[D_2] \\ [L_2] &= 2[E_2] - (1-\nu)\,[D_2]\end{aligned}\right\} \ldots [40]$$

It remains to be seen whether the singularities of $[\bar{S}_2]$ give rise to the required stress resultant Q at the poles of the sphere $r = r_0$. This is confirmed by means of Equations [40] and [28], which imply that the stress resultant $Z(r)$ vanishes identically and individually for solutions $[L_1]$ and $[L_2]$.[16]

We observe, parenthetically, that letting

$$\left.\begin{aligned}[S] &= [\bar{S}_1] + [R_1] \\ [\bar{S}_1] &= [\bar{S}_0] + \frac{(1-2\nu)Q}{2\pi r_0}\,[\bar{L}_1]\end{aligned}\right\} \ldots\ldots\ldots [41][16]$$

leads to a residual problem, the solution $[R_1]$ of which is governed by finite and continuous normal tractions at the boundary, and by shearing tractions which remain finite but exhibit a discontinuity at the poles of the sphere. The sequence of singular solutions $[\bar{S}_0]$, $[\bar{S}_1]$, $[\bar{S}_2]$ thus gives rise to a sequence of solutions $[R_0]$, $[R_1]$, $[R_2]$ to the associated residual problems, which are characterized by progressively increasing regularity in the corresponding boundary conditions; this is also reflected by successive improvements in the convergence of the series which are found to represent this sequence of solutions. It should be emphasized that whereas the boundary stresses of $[R_2]$ are finite and continuous throughout the surface of the sphere, they are by no means analytic.[17] For this reason, $[\bar{S}_2]$ does not contain the complete singularity inherent in the problem. The process of successive "regularization" of the residual problem, which was terminated with $[R_2]$, could be continued in an obvious manner; however, this would seem to serve no particular purpose.

The Singular Solution in Dipolar Co-Ordinates

The singular solution $[\bar{S}_2]$, defined in Equations [40], assumes a comparatively simple form when referred to spherical dipolar co-ordinates. To this end we first determine the stress functions of the basic component solutions which enter $[\bar{S}_2]$. By aid of Equations [17] and the symmetrization Equations [35], we obtain

$$\left.\begin{aligned}&[A_0] \ldots\ldots \phi = \frac{1}{r_1} + \frac{1}{r_2},\ \psi = 0 \\ &[B_0] \ldots\ldots \phi = r_0\left(\frac{1}{r_1} + \frac{1}{r_2}\right),\ \psi = \frac{1}{r_1} - \frac{1}{r_2} \\ &[D_1] \ldots\ldots \phi = \omega_1 + \omega_2,\ \psi = 0 \\ &[\bar{E}_1] \ldots\ldots \phi = r_0(\omega_1 + \omega_2),\ \psi = \omega_1 - \omega_2 \\ &[\bar{D}_2] \ldots\ldots \phi = r_1(c_1\omega_1 - 1) - r_2(c_2\omega_2 + 1),\ \psi = 0\end{aligned}\right\} \ldots [42]$$

[16] It is interesting to note that $[L_1]$ and $[L_2]$ are the only linear combinations of solutions $[E_1]$, $[D_2]$ and $[E_2]$, $[D_2]$, which are self-equilibrated in this sense.

[17] Note that the coefficient of $[\bar{L}_1]$ is the same in Equations [41] and [40].

[18] The derivatives with respect to θ, of these stresses, do not remain finite at the poles; see footnote 19.

$$\left.\begin{aligned}&[\bar{E}_2] \ldots\ldots \phi = r_0[r_1(c_1\omega_1 - 1) - r_2(c_2\omega_2 + 1)] \\ &\qquad\qquad \psi = r_1(c_1\omega_1 - 1) + r_2(c_2\omega_2 + 1) \\ &[\bar{D}_2] \ldots\ldots \phi = r_1^2[(1-3c_1^2)\omega_1 + c_1^2 + 3c_1 - 1] \\ &\qquad + r_2^2[(1-3c_2^2)\omega_2 + c_2^2 - 3c_2 - 1],\ \psi = 0\end{aligned}\right\} \ldots [42]\ (cont.)$$

where

$$\omega_1 = \log\frac{r_1(1+c_1)}{2r_0}, \qquad \omega_2 = \log\frac{r_2(1-c_2)}{2r_0} \ldots [43]$$

The dipolar components of displacement and stress for the component solutions $[\bar{S}_0]$, $[\bar{L}_1]$, $[\bar{L}_2]$ of $[\bar{S}_2]$ are now established with the aid of Equations [36], [40], [42], the co-ordinate Relations [7], and the general dipolar Transforms [14] to [16]. We record here the results of these cumbersome computations, so far as stresses are concerned.

Solution $[\bar{S}_0]$

$$\left.\begin{aligned}\sigma_\alpha &= \frac{Q}{2\pi r_0^2}\left\{2(1-2\nu)\bar{q}^2 + \frac{\sqrt{q+1}}{4\mu}\,[8(2-\nu)q^2p\right. \\ &\quad - 3p^2(4q-p-1) - 4(1-2\nu)q^2 - 6q(p+1) \\ &\quad \left.- (1-8\nu)p + (7-8\nu)]\right\} \\ \sigma_\beta &= \frac{Q}{2\pi r_0^2}\left\{2(1-2\nu)\frac{(qp-1)^2}{p^2} - \frac{\sqrt{q+1}}{4\mu(1+p)}\right. \\ &\quad \left.[4(1-2\nu)qp(qp-2) + 3p^2(p^2-2) + (7-8\nu)]\right\} \\ \sigma_\gamma &= \frac{Q(1-2\nu)}{2\pi r_0^2}\left\{-2\frac{\mu^4}{p^2} + \frac{\mu\sqrt{q+1}}{2(1+p)}\right. \\ &\quad \left.[-2qp(p+1) + p^2 + 2q + 1]\right\} \\ \tau_{\alpha\beta} &= \frac{Q\bar{q}}{2\pi r_0^2 p}\left\{-2(1-2\nu)(qp-1) + \frac{1-p}{4\mu\sqrt{q+1}}\right. \\ &\quad [4(1-\nu)q^2p + 3p(2qp - p^2 - p - 1) \\ &\quad \left.+ 2(5-4\nu)qp - 4(1-2\nu)q - (7-8\nu)]\right\}\end{aligned}\right\} \ldots [44]$$

Solution $[\bar{L}_1]$

$$\left.\begin{aligned}\sigma_\alpha &= -\frac{2(3-2\nu)}{r_0}\,\bar{q}^2 + \frac{\sqrt{q+1}}{2\mu r_0} \\ &\quad [4(3-2\nu)q^2 - p(4q+p) - 6\mu^2 - (7-8\nu)] \\ \sigma_\beta &= -\frac{2(3-2\nu)}{r_0}\frac{(qp-1)^2}{p^2} + \frac{\sqrt{q+1}}{2\mu r_0 p^2} \\ &\quad [4(3-2\nu)q^2p^2 - p^3(4q+p) \\ &\quad -4(5-4\nu)qp + 6p^2 + (7-8\nu)] \\ \sigma_\gamma &= \frac{2(3-2\nu)}{r_0}\frac{\mu^4}{p^2} + \frac{\mu\sqrt{q+1}}{r_0 p^2} \\ &\quad [(1-2\nu)p^2 - 2(3-2\nu)\mu^2] \\ \tau_{\alpha\beta} &= \frac{2(3-2\nu)}{r_0}\frac{\bar{q}(qp-1)}{\bar{p}} + \frac{\bar{q}}{2p\mu r_0\sqrt{q+1}} \\ &\quad [-4(3-2\nu)q^2p + p^2(4q+p) \\ &\quad -10qp + 3p(p-1) + 2(5-4\nu)q + (7-8\nu)]\end{aligned}\right\} \ldots [45]$$

Solution $[\bar{L}_4]$

$$\left.\begin{aligned}
\sigma_\alpha &= -2(1+\nu)\frac{\bar{q}^3p^2\tilde{\omega}}{\mu^4} + \frac{2}{\mu^4}[-4(2-\nu)q^4 \\
&\quad + 4(4-\nu)qp\bar{q}^2 - (3-\nu)p^2\bar{q}^2 + (3-5\nu)q^2 \\
&\quad + (5+\nu)] + \frac{2\sqrt{q+1}}{\mu^3}[2(2-\nu)q^2(2q-1) \\
&\quad - 2(6-\nu)q^2p + p(2qp+7q-p) \\
&\quad - (1-4\nu)q + (3-2\nu)p - 2(1+\nu)] \\
\sigma_\beta &= -\frac{2(1+\nu)(qp-1)^2\tilde{\omega}}{\mu^4} + \frac{2}{\mu^4p^2}[-4(2-\nu)q^4p^2 \\
&\quad + 4(4-\nu)q^3p^2 - (3-\nu)q^2p^2(p^2+7) + 8(1-\nu)q^2p \\
&\quad - 2(1+\nu)qp^2 + 4\nu q^2 + 2(5-\nu)qp - (5+\nu)p^2] \\
&\quad + \frac{2\sqrt{q+1}}{\mu^3p^2}[2(2-\nu)q^2p^2(2q-1) - 2(6-\nu)q^2p^3 \\
&\quad + p^2(2qp+7q-p-1) - 8(1-\nu)q^2p \\
&\quad + (13-4\nu)qp^2 + (1-4\nu)q(p+1) - 5p^2 \\
&\quad - (3-2\nu)p + 2(1+\nu)] \\
\sigma_\gamma &= -2(1+\nu)\tilde{\omega} - 2(3-\nu) + 8(2-\nu)\frac{q\mu^2}{p^2} \\
&\quad - 4(2-\nu)(2q-p-1)\frac{\mu\sqrt{q+1}}{p^2} \\
\tau_{\alpha\beta} &= \frac{2(1+\nu)\bar{q}p(qp-1)\tilde{\omega}}{\mu^4} + \frac{2\bar{q}}{\mu^4p}[4(2-\nu)q^3p \\
&\quad - 4(4-\nu)q^2p^2 + (3-\nu)qp^3 - 4(1-\nu)q^2 \\
&\quad + (13-3\nu)qp + (1+\nu)p^2 - (5+\nu)] \\
&\quad + \frac{2\bar{q}}{\mu^3p\sqrt{q+1}}[-2(2-\nu)q^2p(2q+1) \\
&\quad + 2(6-\nu)q^2p^2 - p^3(2qp+p+2) + (5-2\nu)qp^2 \\
&\quad + 4(1-\nu)q^2 - 6qp + (3-2\nu)\mu^2 + 2(1+\nu)]
\end{aligned}\right\} \quad \ldots [46]$$

where

$$\tilde{\omega} = \log\frac{(1-p)(\sqrt{q+1}+\mu)^2}{4\mu^4} \quad \ldots\ldots [47]$$

Solution of Residual Problem

In accordance with Equations [38], the solution $[R_3]$ of the residual problem obeys the boundary conditions

$$\left.\begin{aligned}
\sigma_r(r_0,\theta) &= -\sigma_\beta(\alpha,\pi/2) \\
\tau_{r\theta}(r_0,\theta) &= \tau_{\alpha\beta}(\alpha,\pi/2)
\end{aligned}\right\} \quad \ldots\ldots [48][18]$$

where σ_β, $\tau_{\alpha\beta}$ are dipolar components of stress belonging to the singular solution $[\bar{S}_3]$. By means of Equations [40], [44] to [47] and observing from Equations [6] and [7] that $q = 1/s$ for $\beta = \pi/2$, we reach

$$\left.\begin{aligned}
\sigma_r(r_0,\theta) &= \frac{Q}{8\pi r_0^2}\{(1+12\nu-16\nu^2) \\
&\quad [(1+\nu)(s^2\tilde{\omega}_0 - 2s\epsilon) + (5+\nu)s^2] \\
&\quad - 4(1-4\nu)(2+\nu-4\nu^2)\epsilon \\
&\quad + 4(4-13\nu-4\nu^2+16\nu^3)\} \\
\tau_{r\theta}(r_0,\theta) &= \frac{Qs}{8\pi r_0^2}\left\{(1+12\nu-16\nu^2)\right. \\
&\quad [(1+\nu)(c\tilde{\omega}_0 - 2\lambda) + (5+\nu)c] \\
&\quad \left.+ 2(1-\nu)(5+4\nu-16\nu^2)\left[\frac{2c}{s^2} - \frac{\lambda}{s}\left(1+\frac{2}{s}\right)\right]\right\}
\end{aligned}\right\} \quad \ldots [49]$$

where

$$\left.\begin{aligned}
\tilde{\omega}_0 &= \log\left[\frac{s}{4}(2+2\epsilon+s)\right] \\
\epsilon &= \left(\frac{1+c}{2}\right)^{1/2} + \left(\frac{1-c}{2}\right)^{1/2}, \\
\lambda &= \left(\frac{1+c}{2}\right)^{1/2} - \left(\frac{1-c}{2}\right)^{1/2}
\end{aligned}\right\} \quad \ldots [50][19]$$

We now approach the solution of the residual problem which is subject to the boundary Conditions [49], on the basis of the general solution to the axisymmetric problem of the sphere, presented in (4). To this end we expand the boundary Tractions [49] as Fourier-Legendre series of the form

$$\left.\begin{aligned}
\sigma_r(r_0,\theta) &= \sum_{n=0}^{\infty}\xi_{2n}P_{2n} \\
\tau_{r\theta}(r_0,\theta) &= s\sum_{n=1}^{\infty}\eta_{2n}P_{2n}'
\end{aligned}\right\} \quad \ldots\ldots [51]$$

and find

$$\left.\begin{aligned}
\xi_0 &= \frac{Q}{6\pi r_0^2}(5-8\nu^2) \\
\xi_2 &= -\frac{Q}{84\pi r_0^2}(7+327\nu-364\nu^2-48\nu^3) \\
\eta_2 &= \frac{Q}{84\pi r_0^2}(7+143\nu-196\nu^2+16\nu^3) \\
\xi_{2n} &= \frac{Q}{4\pi r_0^2}\frac{24(1+2\nu-4\nu^2)n^2 + 8(-2+7\nu+8\nu^2-16\nu^3)n - (1+\nu)(1+12\nu-16\nu^2)}{n(n-1)(4n-1)(4n+3)} \\
\eta_{2n} &= \frac{Q}{8\pi r_0^2}\frac{-16(1+\nu)(1+12\nu-16\nu^2)n^2 - 36(1+2\nu-4\nu^2)n + (31+7\nu-124\nu^2+80\nu^3)}{n(n-1)(4n-1)(4n+3)(2n+1)} \\
&\quad (n=2,3,4,\ldots)
\end{aligned}\right\} \quad [52]$$

[18] See also Fig. 1.

[19] Equations [49], [50] display the nonanalytic character of the boundary stresses of $[R_3]$ at the poles P_1, P_2.

By virtue of Equations [27] and [39] of reference (4), the desired solution $[R_3]$ is given by

$$[R_3] = \sum_{n=1}^{\infty} a_{-2n-1}[A_{-2n-1}] + \sum_{n=0}^{\infty} b_{-2n-2}[B_{-2n-2}] \quad \ldots [53]$$

where

$$\left.\begin{aligned} a_{-2n-1} &= \frac{(4n^2+4n-1+2\nu)\xi_{2n} + (2n+1)(4n^2-2n-2-2\nu)\eta_{2n}}{2(2n-1)[4n^2+2(1+2\nu)n+1+\nu]r_0^{2n-2}} \\ b_{-2n-2} &= \frac{\xi_{2n}+2n\eta_{2n}}{2[4n^2+2(1+2\nu)n+1+\nu]r_0^{2n}} \end{aligned}\right\} \quad \ldots [54]$$

Equations [52] to [54], together with Equation [17], constitute the complete solution $[R_3]$ of the residual problem. The stresses of the component solutions $[A_{-2n-1}]$ and $[B_{-2n-2}]$ are given explicitly in Equations [19] and [21], respectively. The series for the components of displacement and stress of $[R_3]$ converge uniformly throughout the region $0 \leq r \leq r_0$, including the boundary[20] $r = r_0$. The convergence of the stress series remains fairly rapid even at $r = r_0$, where it is least favorable. In fact, for $r = r_0$, the nth term in each of these series is at most of the order P_{2n}/n^2, as compared to the orders P_{2n}/n and P_{2n}, which are found to characterize the behavior of the corresponding series representing $[R_1]$ and $[R_2]$, respectively.[21] This observation demonstrates the acceleration in convergence derived from the successive regularization of the residual problem.

Confirmation of Solution Through a Limit Process, the Sphere Under Partial Distributed Loading

Solution $[S]$, the formal determination of which is now complete, clearly satisfies the three necessary conditions stated in the opening section of the paper. We proceed to confirm the validity of $[S]$ through a limit process, by considering the problem[22] of a sphere which is subjected to a radial pressure of intensity $w > 0$, uniformly distributed over two spherical caps surrounding the poles P_1, P_2. The appropriate boundary conditions appear as

$$\left.\begin{aligned} \sigma_r(r_0,\theta) &= -w \text{ for } 0 \leq \theta \leq \theta_0 < \pi/2,\ \pi-\theta_0 \leq \theta \leq \pi \\ \sigma_r(r_0,\theta) &= 0 \text{ for } \theta_0 < \theta < \pi-\theta_0 \\ \tau_{r\theta}(r_0,\theta) &= 0 \text{ for } 0 \leq \theta \leq \pi \end{aligned}\right\} \quad \ldots [55]$$

Expanding the tractions given in Equations [55] as Fourier-Legendre series of the form [51], and setting $\cos\theta_0 = c_0$, we find

$$\left.\begin{aligned} \xi_0 &= -w(1-c_0),\ \xi_{2n} = -\frac{w(4n+1)}{2n(2n+1)}(1-c_0^2)P_{2n}'(c_0) \\ \eta_{2n} &= 0 \quad (n = 1, 2, 3, \ldots) \end{aligned}\right\} \quad \ldots [56]$$

and the desired solution $[S_0]$ to the problem stated in Equations [55] is thus equal to the right-hand member of Equations [53], provided the coefficients of superposition are now taken to be defined by Equations [54], [56].

Next, we consider the limit $[S_L]$ of $[S_0]$ as the loaded spherical caps are shrunk to the poles of the sphere, while the total load is made to approach Q. Thus

$$\left.\begin{aligned} [S_L] &= \lim [S_0] \\ &\text{as } c_0 \to 1,\ w\pi r_0^2(1-c_0^2) \to Q \end{aligned}\right\} \quad \ldots [57]$$

In this manner we are led to

$$\left.\begin{aligned} [S_L] &= \sum_{n=1}^{\infty} a_{-2n-1}[A_{-2n-1}] + \sum_{n=0}^{\infty} b_{-2n-2}[B_{-2n-2}] \\ a_{-2n-1} &= -\frac{(4n^2+4n-1+2\nu)(4n+1)Q}{4\pi(2n-1)[4n^2+2(1+2\nu)n+(1+\nu)]r_0^{2n}} \\ b_{-2n-2} &= -\frac{(4n+1)Q}{4\pi[4n^2+2(1+2\nu)n+(1+\nu)]r_0^{2n+2}} \end{aligned}\right\} \quad \ldots [58]$$

Equations [58] constitute a complete solution in series form to the main problem treated previously. However, the convergence of this solution, particularly in the vicinity of the boundary, is exceedingly poor and the stress series are divergent for $r = r_0$, as is to be anticipated. The identity of $[S_L]$ and $[S]$ is established most efficiently by comparing the corresponding two pairs of generating stress functions. This, in turn, necessitates the expansion of ϕ and ψ for the closed portion $[\bar{S}_2]$ of $[S]$, as series of interior spherical harmonics. A tedious computation, based on Equations [42], [40], [27], and on the identities

$$\left.\begin{aligned} \frac{1}{r_1}+\frac{1}{r_2} &= \frac{2}{r_0}\sum_{n=0}^{\infty}\left(\frac{r}{r_0}\right)^{2n}P_{2n} \\ \frac{1}{r_1}-\frac{1}{r_2} &= \frac{-2}{r_0}\sum_{n=0}^{\infty}\left(\frac{r}{r_0}\right)^{2n+1}P_{2n+1} \end{aligned}\right\} \quad \ldots [59]$$

yields for $[\bar{S}_2]$

$$\left.\begin{aligned} \phi &= \frac{Q}{8\pi r_0^2}\left\{(1-12\nu)r^2P_2 + r_0^2\sum_{n=2}^{\infty}\frac{-16n^3+24n^2+(1-12\nu)n+(-10+\nu+28\nu^2-16\nu^3)}{n(n-1)(2n-1)}\left(\frac{r}{r_0}\right)^{2n}P_{2n}\right\} \\ \psi &= \frac{Q}{8\pi r_0^2}\left\{16(1-\nu)rP_1 + r_0\sum_{n=1}^{\infty}\frac{16n^2+16(1-\nu)n-(1+12\nu-16\nu^2)}{n(2n+1)}\left(\frac{r}{r_0}\right)^{2n+1}P_{2n+1}\right\} \end{aligned}\right\} \quad \ldots [60][23]$$

---

[20] For $0 \leq r \leq \delta < r_0$, also all derivatives of finite order with respect to r and θ of the series under consideration converge uniformly and absolutely.

[21] See Equations [31], [41], and the discussion following Equation [41]. The series solutions $[R_1]$ and $[R_0]$ are not included in this paper.

[22] The authors are indebted to Prof. E. H. Lee of Brown University, for directing their attention to reference (10) in which, they understand, this problem is also treated. Unfortunately, this report, which is apparently still classified, has not been available.

[23] In the formula for ϕ an unessential additive constant has been suppressed.

Equations [17], [38], [52], [53], [54], [58], and [60] are found to imply $[S] \equiv [S_L]$; this confirms the validity of solution $[S]$.

Numerical Evaluations, Discussion

The complete solution $[S]$ to the problem under consideration is given by Equation [38] and has been represented as the sum of the closed, singular solution $[\bar{S}_2]$, defined by Equations [30] to [40] and [42], and of the series solution $[R_3]$, defined by Equations [52] to [54] and [17]. The stresses of $[\bar{S}_2]$ are given explicitly, with reference to dipolar co-ordinates, by Equations [40] and (44] to [47]; those of $[R_3]$ follow explicitly, with reference to spherical co-ordinates, from Equations [52] to [54], [19], and [21]. The transition from dipolar to spherical co-ordinates is effected by aid of Equations [7], [8].

Particular simplifications arise on the equator plane $z = 0$, where $\theta = \pi/2$, $c = 0$, $\alpha = 0$, $q = 1$, and at the surface $r = r_0$, where $\beta = \pi/2$, $p = 0$. The contribution from $[\bar{S}_2]$ to the normal stress on the equator plane is found to be

$$\left.\begin{aligned}[\bar{S}_2]: \quad & \sigma_s(z = 0) = \sigma_\alpha(\alpha = 0) \\ &= \frac{-Q\sqrt{2(1-p)}}{8\pi r_0^2}\,[3p^2 - 4(2-\nu)p + 4(1-2\nu)^2] \\ & p = \frac{(r/r_0)^2 - 1}{(r/r_0)^2 + 1}\end{aligned}\right\} \quad \ldots [61]$$

At the center of the sphere the series solution $[R_3]$ terminates, and the complete value of σ_s for solution $[S]$ is represented by the closed formula

$$\sigma_s(r = 0) = -\frac{3Q(14 + 5\nu)}{2\pi r_0^2(7 + 5\nu)} \quad \ldots [62]$$

Fig. 2 shows the variation of σ_s at $z = 0$ for $\nu = 0.25$ and $\nu = 0.48$. In order to establish the stress value at $r = r_0$ within three characteristic places, ten terms had to be considered in the series contribution to σ_s, and toward the interior of the sphere the convergence is found to accelerate rapidly. The curve for $\nu = 0.48$ is to be compared with the dashed curve, which represents the experimental values obtained by Frocht and Guernsey (1)[24] who used a photoelastic material of that Poisson ratio. It is seen that, although there is some discrepancy near the surface of the sphere where the stress is relatively low, the agreement between theoretical and experimental values is remarkably good in the neighborhood of the center of the sphere. For purposes of comparison, the figure also shows the corresponding stress values taken from the analogous plane solution to the problem of a circular disk under diametrically opposed concentrated forces.[25] In this instance the stress distribution, of course, is independent of the elastic constants. In the three-dimensional problem, the influence of Poisson's ratio upon σ_s at $r = 0$, is illustrated by Fig. 3.

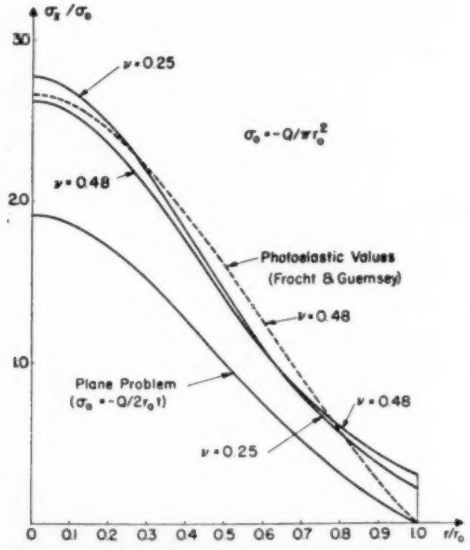

Fig. 2 Normal Stress on Equator Plane

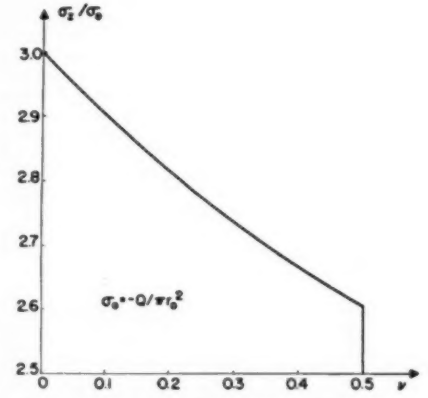

Fig. 3 σ_s at $r = 0$ as a Function of Poisson's Ratio

It is evident from Equations [30], [38], [40], [52] to [54], and [19] to [26], that the state of stress at a fixed point of the space interior to the sphere, approaches that consistent with solution $[S_0]$ alone, in the limit as r_0 tends to infinity while the pole P_1 is maintained in its original position. This limit process thus yields Boussinesq's solution to the problem of the semi-infinite body under a concentrated load acting perpendicular to its plane boundary.

Acknowledgment

The authors are greatly indebted to Prof. R. D. Mindlin of Columbia University, for most valuable discussions and several illuminating comments. The occasional advice and assistance of Mr. R. A. Eubanks, Research Assistant at Illinois Institute of Technology, is gratefully acknowledged. Finally, thanks are due to the Division of Engineering Mechanics Research of the Armour Research Foundation, for generous support of this investigation.

BIBLIOGRAPHY

1 "A Special Investigation to Develop a General Method for

[24] The authors are indebted to the NACA for permission to include this curve.

[25] See (9), p. 108. In connection with this curve it should be noted that here the average stress $\sigma_0 = Q/2\pi rt$, where r_0 and t are the radius and thickness of the disk, respectively.

Three-Dimensional Photoelastic Stress Analysis," by M. M. Frocht and R. Guernsey, Jr., Report to the NACA under Contract No. NAw-5959, September 15, 1951.

2 "A Treatise on the Mathematical Theory of Elasticity," by A. E. H. Love, fourth edition, Dover Publications, New York, N. Y., 1944.

3 "Die erste und zweite Randwertaufgabe der linearen Elastizitätstheorie für die Kugelschale," by Werner Leutert, Dissertation, Eidgenössische Technische Hochschule in Zürich, Art. Institut Orell Füssli A. G., Zürich, Switerland, 1948.

4 "On the Axisymmetric Problem of Elasticity Theory for a Region Bounded by Two Concentric Spheres," by E. Sternberg, R. A. Eubanks, and M. A. Sadowsky, presented at the First U. S. National Congress of Applied Mechanics, Chicago, Ill., June, 1951; to appear in the forthcoming Proceedings of the Congress.

5 "The Heavy Sphere Supported by a Concentrated Force," by Werner Leutert, *Pacific Journal of Mathematics*, vol. 1, no. 1, 1951, pp. 97–101.

6 "Application des Potentiels," by J. Boussinesq, Gauthiers-Villars, Paris, France, 1885.

7 "On the Stress-Function Approaches of Boussinesq and Timpe to the Axisymmetric Problem of Elasticity Theory," by E. Sternberg, R. A. Eubanks, and M. A. Sadowsky, *Journal of Applied Physics*, vol. 22, no. 9, 1951, pp. 1121–1124.

8 "On the Axisymmetric Problem of the Theory of Elasticity for an Infinite Region Containing Two Spherical Cavities," by E. Sternberg and M. A. Sadowsky, JOURNAL OF APPLIED MECHANICS, Trans. ASME, vol. 74, March, 1952, pp. 19–27.

9 "Theory of Elasticity," by S. Timoshenko and J. N. Goodier, second edition, McGraw-Hill Book Company, Inc., New York, N. Y., 1951.

10 "The Distribution of Stress in a Decelerating Sphere," by W. R. Dean, I. N. Sneddon, and H. W. Parsons, Theoretical Research Report No. 33/44, Armaments Research Department, Sevenoaks, Kent, England, 1944.

11 "Fourier Transforms," by I. N. Sneddon, first edition, McGraw-Hill Book Company, Inc., New York, N. Y., 1951.

Appendix

PSEUDOSOLUTIONS TO CONCENTRATED FORCE PROBLEMS

At this place we exemplify the existence of pseudosolutions to concentrated force problems, that is, of solutions which satisfy the three necessary conditions stated in the beginning of the paper, but fail to coincide with the corresponding limit solutions described there.

In connection with the problem of Boussinesq, consider the solution

$$\left.\begin{aligned}[S_0'] &= [S_0] + \sum_{n=0}^{N} k_n \{f(n)\,[A_{2n}] + (2n+1)\,[B_{2n+1}]\} \\ &+ \sum_{n=0}^{N} \rho_n \{f(n+1)\,[A_{2n+1}] + (2n+2)\,[B_{2n+2}]\} \\ f(n) &= 4n^2 + 4n - 1 + 2\nu\end{aligned}\right\} \quad \ldots [63]$$

whose component solutions are defined by Equations [30], [20], and [17]. It follows from Equations [19], [21], [22] that $[S_0']$ clears the plane $z = 0$ from tractions and possesses vanishing stresses at infinity for arbitrary choice of the coefficients k_n, ρ_n. Furthermore, Equations [28] and [20] imply that $Z(r) = Q$ for $[S_0']$. However, $[S_0']$ coincides with the appropriate limit of the solution corresponding to a normal load which is uniformly distributed over a circular region surrounding the origin,[26] only if $k_n = \rho_n = 0$. Thus $[S_0]$, which is the solution given by Boussinesq (6), represents the correct solution to the problem. It is not difficult to show[27] that Boussinesq's solution is identical with the limit of the solution corresponding to an arbitrary continuous distribution of normal tractions applied over any region surrounding the origin, as the region is shrunk to the origin while the total load is held constant.

The existence of pseudosolutions to the problem of Boussinesq stems from the existence of solutions which satisfy the field equations for $z \geq 0$, are singular at the origin, and leave the plane $z = 0$ as well as infinity free from stress. In order to examine the physical significance of these self-equilibrated singular solutions, which when added to $[S_0]$ give rise to pseudosolutions of the problem, we consider the first term in the series appearing in Equations [63]

$$-(1 - 2\nu)\,[A_0] + [B_1] \quad \ldots [64]$$

and recall the well-known solution[28] for a concentrated tangential force at the boundary $z = 0$ of a semi-infinite medium occupying the half-space $z \geq 0$. Next, consider the solution appropriate to four mutually orthogonal tangential forces, each of magnitude P, applied at a distance Δ from the origin in such a way that the four lines of action intersect at the origin. A routine computation yields the Solution [64] in the limit as $\Delta \to 0$, $P \to \infty$, whereas the product of Δ and P is made to tend to a finite limit. Thus, the solution given by [64] corresponds to two mutually perpendicular tangential force doublets at $r = 0$ and represents what might be referred to as a surface center of compression. The remaining terms in the series of Equations [63] admit a similar physical interpretation on the basis of higher self-equilibrated axisymmetric singularities at the origin.

With reference to the problem treated in this paper, the symmetrization of Leutert's results (5) yields the solution

$$\left.\begin{aligned}[S'] &= \frac{-Q}{120\pi r_0(1-\nu)} \\ &\{30(1-\nu)\,[[\bar{D}_2] - r_0[\bar{D}_1]] + 20r_0^2(1-2\nu)\,[\bar{A}_0] \\ &+ 4r_0^2(7+2\nu)\,[\bar{A}_1] + 15r_0[B_0] - 20r_0^2[B_1] \\ &+ 8r_0^3[\bar{B}_2]\}\end{aligned}\right\} \quad \ldots [65]$$

whose component solutions are given by Equations [17]. Solution $[S']$ leaves the surface of the sphere $r = r_0$ free from stress and, as is readily confirmed by aid of Equations [28] and [20], gives rise to the required stress-resultant Q at the poles of the sphere. It is, nevertheless, a pseudosolution to the problem since it is not identical with the limit solution $[S_L]$, given by Equations [58]. The pseudo-character of solution $[S']$ is also evident from the observation that its singularities at the poles P_1 and P_2 are of a higher order than that of $[S_0]$ at the origin. For this reason $[S']$ does not exhibit the proper limit behavior as r_0 approaches infinity. Computing σ_z at the center of the sphere on the basis of $[S_0']$, we find

$$\sigma_z(r = 0) = -\frac{3Q(4-\nu)}{2\pi r_0^2(1-\nu)} \quad \ldots [66]$$

as compared to the correct value given by Equation [62]. In particular, for $\nu = 0.48$, the stress value obtained from Equation [66] is almost 4 times that consistent with Equation [62], the latter being within 2 per cent of the photoelastic result. This comparison shows that any expectation, based on an appeal to Saint Venant's principle, of deriving useful approximations to $[S]$ from the closed solution $[S']$, is unfounded.

[26] See, for example (11), p. 470.

[27] See (2), p. 242.

[28] See, for example (2), p. 203.

The Analysis of Fully Restrained Slabs Under Concentrated Loads

By C. A. M. GRAY,[1] SYDNEY, N. S. W., AUSTRALIA

THE analysis of fully restrained, thin, elastic slabs under concentrated loads is usually made by adding suitable edge moments to the simply supported solution. In this paper use is made of Muschelisvili's solution[2] of the biharmonic equation. From it we determine two analytic functions $\Omega(z)$ and $w(z)$ of the complex variable z, given, for simply connected areas, by two integral equations of which a direct solution is possible, provided that the boundary conditions are in a suitable form, and the transformation of the loaded area to a unit circle is known. For fully restrained slabs under concentrated loads, provided the singularities introduced at the loading points are removed, the boundary conditions are of a suitable form for a direct application of Muschelisvili's equations. In this paper the load-point singularities are removed by taking the solution for a fully restrained circular slab inscribed in the given area and similarly loaded. Two illustrations of the method are given: an infinitely long rectangle loaded at the center, and a square slab loaded at the center. In both cases the solution is obtained for the edge moments without an excessive amount of labor.

Theory

It is well known that the deflection of a thin elastic slab by a concentrated load satisfies the biharmonic equation at all points, except at the load point, and is of the form

$$v = \frac{P}{8\pi D} R^2 \log R + v_0 \qquad [1]$$

where

P = concentrated load
v = deflection at any point x, y
R = distance of any point from load point
v_0 = biharmonic over area of slab

If the slab is fully restrained on all edges and ν is the direction of the normal to the boundary, the boundary conditions for v are

$$v = 0$$
$$\frac{\partial v}{\partial \nu} = 0$$

On the boundary these conditions are equivalent to the two conditions

$$\frac{\partial v}{\partial x} = \frac{\partial v}{\partial y} = 0$$

Following Muschelisvili, we define two functions $\Omega(z)$ and $w'(z)$ of the complex variable z by

$$\left.\begin{aligned} \nabla_1^2 v &= {}^1/_2 \left[\Omega'(z) + \bar{\Omega}'(\bar{z})\right] \\ \frac{\partial^2 v}{\partial y^2} - \frac{\partial^2 v}{\partial x^2} - 2i \frac{\partial^2 v}{\partial x\, \partial y} &= -\frac{1}{2}\left[z\,\bar{\Omega}''(\bar{z}) + \bar{w}''(\bar{z})\right] \end{aligned}\right\} \qquad [2]$$

where the bars denote the conjugate function, and the dashes differentiation with regard to z.

The deflection is now given by

$$v = \frac{1}{4} R[z\,\Omega(z) + w(z)]$$

and on the boundary, $z = z_B$

$$\Omega(z_B) + z_B\,\bar{\Omega}'(\bar{z}_B) + \bar{w}'(\bar{z}_B) = \frac{\partial v}{\partial x} + i\frac{\partial v}{\partial y} \qquad [3]$$

Thus for a fully restrained slab Equation [3] becomes

$$\Omega(z_B) + z_B\,\bar{\Omega}'(\bar{z}_B) + \bar{w}'(\bar{z}_B) = 0 \qquad [4]$$

and from Equation [1], Ω and w' have the form

$$\left.\begin{aligned} \Omega(z) &= \frac{P}{2\pi D}\left[z \log (z - z_1) - z_1 \log (z - z_1)\right] + \Omega_0(z) \\ w(z) &= \frac{-P}{2\pi D}\left[z\bar{z}_1 \log (z - z_1) - z_1\bar{z}_1 \log (z - z_1)\right] + w_0(z) \end{aligned}\right\} \qquad [5]$$

where Ω_0 and w_0 are analytic over the whole of the area in the z-plane.

Suppose we transform the area conformally in the z-plane to a unit circle γ: $|\zeta| \leq 1$ in the ζ-plane, by the transformation

$$z = f(\zeta) = \sum_{r=0} u_r \zeta^r$$

so that the load point z_1 goes to ζ_1.

Then Equation [4] becomes

$$\Omega\left[f(\sigma)\right] + f(\sigma)\,\bar{\Omega}_z'(\bar{\sigma}) + \bar{w}'(\bar{\sigma}) = 0$$

where

$$\Omega_z' = \frac{d}{d\zeta}\left\{\Omega[f(\zeta)]\right\}\frac{d\zeta}{dz}$$

and $\sigma = e^{i\theta}$ is the value of ζ on the unit circle.

$$\text{But } \log (z - z_1) = \log\left\{\frac{z - z_1}{\zeta - \zeta_1}\beta(\zeta - \zeta_2)\right\} + \log\frac{\zeta - \zeta_1}{\beta(\zeta - \zeta_2)}$$

where ζ_2 is the point in the ζ-plane inverse to the point ζ_1 with respect to the unit circle γ, and $\zeta_1 = \beta e^{i\gamma}$. Then the first term

[1] University of Sydney.

[2] "Practical Solution of the Fundamental Boundary Value Problems of Elasticity in a Plane for Various Contours," by N. Muschelisvili, *Zeitschrift für angewandte Mathematik und Mechanik*, vol. 13, August, 1933, pp. 264–282.

Contributed by the Applied Mechanics Division and presented at the Fall Meeting, Chicago, Ill., September 8-11, 1952, of The American Society of Mechanical Engineers.

Discussion of this paper should be addressed to the Secretary, ASME, 29 West 39th Street, New York, N. Y., and will be accepted until January 10, 1953, for publication at a later date. Discussion received after the closing date will be returned.

Note: Statements and opinions advanced in papers are to be understood as individual expressions of their authors and not those of the Society. Manuscript received by ASME Applied Mechanics Division, October 22, 1951. Paper No. 52—F-13.

on the right-hand side is analytic within the circle and we can replace Equation [5] by

$$\left.\begin{aligned}\Omega(z) &= \frac{P}{2\pi D}(z-z_1)\log\frac{\zeta-\zeta_1}{\beta(\zeta-\zeta_2)}+\Omega_0(z)\\ w(z) &= \frac{-P}{2\pi D}\bar{z}_1(z-z_1)\log\frac{\zeta-\zeta_1}{\beta(\zeta-\zeta_2)}+w_0(z)\end{aligned}\right\}\quad\ldots[6]$$

Equation [4] then becomes

$$\begin{aligned}&\Omega_0[f(\sigma)]+f(\sigma)\bar{\Omega}_0'(\bar{\sigma})+\bar{w}_0'(\bar{\sigma})\\ &\quad=\frac{-P}{2\pi D}\frac{(\bar{\zeta}_1-\bar{\zeta}_2)(z_B-z_1)(\bar{z}_B-\bar{z}_1)}{(\bar{\sigma}-\bar{\zeta}_1)(\bar{\sigma}-\bar{\zeta}_2)}\frac{\overline{d\zeta}}{dz}\\ &\quad=F_1+iF_2\qquad\ldots[7]\end{aligned}$$

This equation is identical with that occurring in the first boundary problem of plane elasticity, and the functional solution has been given by Muschelisvili as

$$\Omega_0=\frac{1}{2\pi i}\int_\gamma(F_1+iF_2)\frac{d\sigma}{\sigma-\zeta}-\frac{1}{2\pi i}\int_\gamma f(\sigma)\bar{\Omega}_0'(\bar{\sigma})\frac{d\sigma}{\sigma-\zeta}$$

and

$$w_0'=\frac{1}{2\pi i}\int_\gamma(F_1-iF_2)\frac{d\sigma}{\sigma-\zeta}-\frac{1}{2\pi i}\int_\gamma\bar{f}(\bar{\sigma})\bar{\Omega}_0'(\sigma)\frac{d\sigma}{\sigma-\zeta}$$

Since Ω_0' is given by the power series

$$\Omega_0'=\sum_{r=0}b_r\zeta^n,\ |\zeta|<1$$

the coefficients may be determined from the following set of infinite simultaneous equations

$$\sum_{\nu=0}^{\nu=n}(1+\nu)\,u_{1+\nu}b_{n-\nu}+(1+n)\sum_{\nu=0}^{\alpha}u_{1+n+\nu}\bar{b}_\nu=p_n\quad[8]$$

where

$$\frac{d}{d\zeta}\left[\frac{1}{2\pi i}\int_\gamma(F_1+iF_2)\frac{d\sigma}{\sigma-\zeta}\right]=\sum_{r=0}p_r\zeta^r$$

To determine the function w' given by the series $w'=\sum_{r=0}f_r\zeta^r$ we have

$$f_r=q_r-c_r\qquad\ldots[9]$$

where

$$\frac{1}{2\pi i}\int_\gamma(F_1-iF_2)\frac{d\sigma}{\sigma-\zeta}=\sum_{r=0}q_r\zeta^r$$

and

$$c_r=\sum_{r=0}\bar{u}_n b_{n+r}$$

The derivation of Equations [8] and [9] is given in a previous paper by the author.[3]

Method of Solution

Once we have the solution of Equation [8] the remainder of the solution follows directly. Now no method is available to obtain a complete solution of Equation [8], although we can obtain approximations to the unknowns by either an iterative process or by some method of successive approximation. In either case the b's will only be determined approximately, although if sufficent labor is expended we can determine them to as high an accuracy as is desired. Using an iterative process we obtain each term successively so that after, say, 8 iterations the first few terms are obtained to a high order of accuracy and the subsequent ones are increasingly inaccurate. By virtue of the fact that a fully restrained circular slab inscribed in the given area and similarly loaded must deflect similarly to the given slab, at least at the center, $R\Omega_0'$ must be in the nature of a correction which will be continuous on the actual boundary, and consequently its nth term will at least be of the order $1/n^3$. Thus we may expect that the series for Ω_0' will converge sufficiently rapidly for its first few terms to be a sufficiently good approximation for practical use. To illustrate, two examples, a square slab loaded at the center and an infinitely long rectangular slab also loaded at the center, will be considered.

Example 1. Consider a square slab loaded with a concentrated load P at the center. The transformation for a square of side $2a$ in the z-plane to the unit circle $|\zeta|\leq 1$ is given by

$$z=\frac{-2ia}{K}\left[\zeta-\frac{\zeta^5}{10}+\frac{\zeta^9}{24}-0.02404\,\zeta^{13}\ldots\ldots\right]$$

where $K=1.85407$.

Since the load is at the center, $\zeta_1=0$. Hence

$$F_1+iF_2=\frac{-P}{2\pi D}\frac{z_B\bar{z}_B}{\bar{\delta}}\left(\frac{d\bar{\zeta}}{dz}\right)_{\zeta=\sigma}$$

Whence

$$\frac{d}{d\zeta}\left[\frac{1}{2\pi i}\int_\gamma(F_1+iF_2)\frac{d\sigma}{\sigma-\zeta}\right]=\frac{-2ia}{K}$$
$$[0.95262-0.385295\,\zeta^4+0.263403\,\zeta^8\ldots\ldots]$$

Equations [8] become, since the b's are obviously real

$$\begin{aligned}2b_0-0.1\,b_4+0.041667\,b_8-0.02404\,b_{12}\ldots\ldots &= 0.95262\\ -b_0+1.20834\,b_4-0.12020\,b_8-0.080420\,b_{12}\ldots &= -0.385295\\ 0.75\,b_0-0.71636\,b_4+1.14475\,b_8\ldots\ldots\ldots\ldots &= 0.263403\end{aligned}$$

and so on.

The results of 3 iterations are given in Table 1.

TABLE 1

Iterate	$b_0 \div -P/2\pi D$	$b_4 \div -P/2\pi D$	$b_8 \div -P/2\pi D$
1	0.47631	0.075324	
2	0.48008	0.078439	−0.035346
3	0.48097	0.075666	−0.035938

Thus

$$\Omega_0'=\frac{-P}{2\pi D}[0.48097+0.07566\,\zeta^4-0.035938\,\zeta^8\ldots\ldots]$$

Hence

$$\Omega_z'=\frac{P}{2\pi D}\left[\log\zeta+\frac{iK}{2a}\frac{z}{\zeta}(1+\zeta^4)^{1/2}-0.48097\right.$$
$$\left.-0.07566\,\zeta^4+0.035938\,\zeta^8\ldots\ldots\right]$$

Using the conventions given by Timoshenko[4] we have immediately that the edge moments are given by

$$M=\frac{P}{2\pi}R_e\left[\log\sigma+\frac{\bar{z}_B}{\sigma}\frac{iK}{2a}(1+\sigma^4)^{1/2}-0.48097\right.$$
$$\left.-0.07566\,\sigma^4+0.035938\,\sigma^8\ldots\ldots\right]\qquad\ldots[10]$$

[3] "Polynomial Approximations in Plane Elastic Problems," by C. A. M. Gray, *Quarterly Journal of Mechanics and Applied Mathematics*, vol 4, part 4, 1951, pp. 444–448.

TABLE 4

Iteration	$b_0 \div -P/2\pi D$	$b_2 \div -P/2\pi D$	$b_4 \div -P/2\pi D$	$b_6 \div -P/2\pi D$	$b_8 \div -P/2\pi D$
6	0.406747	−0.159761	−0.074882	−0.043088	−0.028408
7	0.406959	−0.158033	−0.073397	−0.042246	−0.028325

Table 2 gives values from Timoshenko[4] and from Equation [10].

TABLE 2

	$M_{y=0}$	
x/a	Timoshenko	Equation [10]
0	$-0.126P$	$-0.126P$
0.278	$-0.102P$	$-0.099P$
0.450	$-0.069P$	$-0.071P$
0.689	$-0.030P$	$-0.025P$

Example 2. Consider a concentrated load of P at the point $x = 0$, $y = 0$ of an infinitely long, fully restrained rectangular slab of width $2h$.

The transformation from this case is

$$z = \frac{-4ih}{\pi}(\zeta + \zeta^3/3 + \zeta^5/5 + \zeta^7/7 \ldots)$$

Since the load is at the center, $\zeta_1 = 0$. Hence

$$F_1 + iF_2 = \frac{-P}{2\pi D}\frac{z_p \bar{z}_p}{\delta}\left[\frac{d\bar{\zeta}}{dz}\right]_{\zeta=\sigma}$$

[4] "Theory of Plates and Shells," by S. Timoshenko, McGraw-Hill Book Company, Inc., New York, N. Y., and London, England, 1940.

Table 3 gives the computed values of p_n.

TABLE 3

$p_0 = -0.733698i4h/\pi$	$p_5 = -0.277146i4h/\pi$
$p_1 = -0.5i4h/\pi$	$p_6 = -0.244343i4h/\pi$
$p_2 = -0.388885i4h/\pi$	$p_7 = -0.215826i4h/\pi$
$p_3 = -0.322224i4h/\pi$	$p_8 = -0.199350i4h/\pi$
$p_4 = -0.322224i4h/\pi$	

The results for the 6th and 7th iteration of Equation [8] for this case are given in Table 4. Hence

$$\Omega_s' = \frac{P}{2\pi D}\left[\log\zeta + \frac{i\pi}{4h}\frac{z}{\zeta}(1-\zeta^2)\right]\frac{-P}{2\pi D}(0.406959 - 0.158033\,\zeta^2 - 0.073397\,\zeta^4 - 0.042246\,\zeta^6 - 0.028325\,\zeta^8 \ldots\ldots) \quad \ldots\ldots [11]$$

For this case Timoshenko[5] gives only the value of the edge moment at the point $x = h$, $y = 0$, so that a comparison is available only at this point.

From Equation [11] we obtain $M_{\substack{x=h \\ y=0}} = -0.1695P$, taking the terms shown in the series and from Timoshenko[4],

$$M_{\substack{x=h \\ y=0}} = -0.1674P.$$

[5] Ibid., p. 231.

Pressure Drops in the Pneumatic Conveyance of Solids

By OSCAR PINKUS,[1] TROY, N. Y.

With the object of studying the characteristics of the horizontal flow of a mixture of solids and air a theoretical analysis of the flow pattern was attempted. Experiments were performed whose object was to determine the relationship between pressure loss, solids flow rate, and air velocity, and to obtain values for the frictional constants involved in the analysis. A justification for the developed equations was sought. It was found that the presence of the solid phase causes an appreciable pressure loss which is a linear function of both solid and gas flow rate. This justified the theoretical equations which predicted such a relationship. Experiments with two sizes of the same sand showed a higher pressure drop for the larger particles, other conditions being equal. These experiments, however, question the validity of applying the Fanning equation to a solid phase. The equation holds for a given solid but does not take into account variations in its size. The introduction of the dimensionless group d/D is proposed. On the basis of this investigation, it is concluded that the drag coefficient C is a function of the Reynolds number. The ratio of solids velocity to gas velocity is 0.5–0.6 for the small and 0.3 for the large sand. Following results of this work it would seem desirable to operate pneumatic systems at low gas velocities and high solid rates. Recommendations for further investigations are made.

Nomenclature

The following nomenclature is used in the paper:

Subscripts:

- a = acceleration
- D = duct
- ds = dispersion of solids
- f = fluid
- F = force
- fs = friction of solids
- g = gas
- p = particle
- s = solids
- o = air

Symbols:

- a = acceleration, fps per sec
- A = projected area of particle, sq ft
- C = drag coefficient, dimensionless
- d = diameter of particle, ft
- D = diameter of duct, ft
- f = Fanning friction factor, dimensionless
- F = frictional head, ft
- g = constant of gravitational acceleration, fps per sec
- G_s = solids mass flow, lb/sq ft-sec
- L = length, ft
- m = mass of particle, lb-sec^2/ft
- N = number
- P = pressure, lb per sq ft
- Re = Reynolds number, dimensionless
- s = distance, ft
- t = time, sec
- v = velocity, fps
- V = specific volume, ft^3/lb
- ρ = density, lb-sec^2/ft^4
- ρ_{ds} = dispersed solids density, p/cf of pipe
- μ = viscosity, (lb-sec)/sq ft

Introduction

In comparison with the extensive analytical and experimental work done in the field of flow of pure gases or liquids there has been very little attention given the case of solid-gas flow. The problem is of considerable importance in many fields of mechanical and chemical engineering. It arises in burners and boilers using pulverized coal as a fuel, in all pneumatic systems, in dust separators, and conveyers. The future has in store the possibility of replacing liquid fuels by solid fuels in internal-combustion engines, and recently the problem became of paramount importance in the chemical industry where fluidized systems are used as catalysts. A deeper knowledge of the mechanism of pneumatic conveyance and the expected pressure losses becomes essential.

There is very little in the literature about the characteristics of solid-fluid flow. Almost all of the work that has been done was purely experimental with little, if any, thought given the analytical aspect of the situation. Wood and Bailey (1)[2] and Cramp (2) did some experimentation but their results are of limited use for general situations. Vogt and White (3) tried to correlate analytically the solid and fluid properties with the pressure drop but were only partially successful. The most successful analysis is due to Hariu and Molstad (4) who very convincingly presented the case of vertical flow. But, as the authors themselves point out, they included acceleration pressure losses in the frictional pressure drop, obscuring the results.

The purpose of this investigation was to attempt a theoretical analysis of the problem of pneumatic conveyance and, by a series of experiments, to verify the validity of the obtained correlations, and obtain experimental constants involved in the theoretical work. The most important phase was obtaining a correlation between pressure losses, solids flow rate, and fluid flow. The second purpose was to develop some means of estimating the relative velocity between the solids and the gas which is an extremely important parameter in the whole analysis. Only the case of horizontal flow was considered. No attempt was made

[1] At present with General Electric Company, Schenectady, N. Y. Jun. ASME.

Presented at the National Conference of the Applied Mechanics Division, State College, Pa., June 19–21, 1952, of The American Society of Mechanical Engineers.

Discussion of this paper should be addressed to the Secretary, ASME, 29 West 39th Street, New York, N. Y., and will be accepted until January 10, 1953, for publication at a later date. Discussion received after the closing date will be returned.

Note: Statements and opinions advanced in papers are to be understood as individual expressions of their authors and not those of the Society. Manuscript received by ASME Applied Mechanics Division, July 12, 1951. Paper No. 52—APM-30.

[2] Numbers in parentheses refer to the Bibliography at the end of the paper.

to investigate the effect of various solids on the flow pattern; only two sizes of the same kind of sand were used.

Theoretical Analysis

Equations of Motion. Let a particle move in the two-dimensional field x, y, as shown in Fig. 1. We have then

$$m\frac{dv_x}{dt} = -R_F\cos\alpha \quad [1]$$

$$m\frac{dv_y}{dt} = mg\left(\frac{\rho-\rho_0}{\rho}\right) - R_F\sin\alpha \quad [2]$$

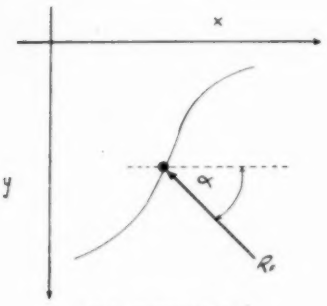

Fig. 1 Particle Flow

Since

$$\cos\alpha = \frac{v_x}{v},\ \sin\alpha = \frac{v_y}{v}$$

and by definition (5)

$$R_F = -\frac{\rho_0 v^2}{2}CA \quad [3]$$

where C, in general, is a function of Reynolds number, then substituting in Equations [1] and [2] the appropriate expressions for R_F we have

$$\frac{dv_x}{dt} = -\frac{\rho_0 CAv(v_x)}{2m} \quad [4]$$

$$\frac{dv_y}{dt} = g\left(\frac{\rho-\rho_0}{\rho}\right) - \frac{\rho_0 CAv(v_y)}{2m} \quad [5]$$

These equations are true for a fluid at rest. If the fluid itself is moving, the velocities have to be taken relative to the fluid. Considering only the case of horizontal flow we write $v = (v_f - v_s)$ and using this in Equation [4] we obtain

$$\frac{dv}{dt} = \frac{\rho_0 CA\,(v_f - v_s)^2}{2m} \quad [6]$$

The value of C as a function of Reynolds number is given in several references (4, 6). Dalla Valle (5) expresses this relation by means of the following equation

$$\sqrt{C} = 0.63 + \frac{4.8}{\sqrt{\mathrm{Re}}} \quad [7]$$

where Re, the Reynolds number, for moving particles is given by

$$\mathrm{Re} = \frac{v\rho_0 d}{\mu}$$

For pure fluids the criterion for streamline flow is given by $\mathrm{Re} < 2500$; for particles by $\mathrm{Re} < 2$. Since turbulent flow denotes the destruction of the parallel shearing forces, this last criterion becomes of doubtful validity when the air itself is already in a state of turbulent motion. The following criterion is given by Dalla Valle:

1 If the fluid flow is in the streamline region then for the particle injected into the stream the value of C is a function of Reynolds number where v is given by the relative velocity.

2 If the fluid is in turbulent motion, the motion of the particle will always be turbulent regardless of the relative velocity.

It will be a part of this investigation to examine the truth of these assertions. Accordingly, equations will be developed assuming the constancy of C and others, assuming C to be a function of Reynolds number. (The motion of the fluid in this experiment was always turbulent.)

Equation [6] as developed previously is true for bodies moving through fluids of infinite extent. If the flow takes place in a duct there will be retarding forces acting on the particles. Collisions between the particles themselves, between the solids and the pipe walls and the occasional sliding on the bottom of the pipe constitute opposing forces to the flow of the solids and these forces will cause a frictional pressure loss due to the solid phase.

Following Vogt and White (7) and Hariu and Molstad (4) an assumption is now made that the Fanning equation

$$F = \frac{\Delta P}{\rho g} = \frac{2fLv_s^2}{gD} \quad [8]$$

holds also for a solid phase. The friction factor f is to account for the frictional losses due to the lost momentum and sliding. Equations [8] and [6] constitute two opposing forces which will be equal only at steady-state conditions. In the transient phase the difference between the two forces will be balanced by an inertia term. This is expressed by the following differential equation

$$\frac{dv_s}{dt} = \frac{\rho_0 CA}{2m}(v_f - v_s)^2 - \frac{2fv_s^2}{D} \quad [9]$$

Now, as pointed out previously, two separate cases will be considered; one on the assumption that C is a variable, the other based on Dalla Valle's assertions of the constancy of C once the air is in the turbulent region. The latter case is taken up first.

Case 1: C = const

Let v denote in this section the particle velocity and let

$$\frac{\rho_0 CA}{2m} = c_1 \qquad \frac{2f}{D} = c_2$$

then

$$\frac{dv}{dt} = c_1(v_f - v)^2 - c_2v^2$$

and

$$t = \int \frac{dv}{c_1v_f^2 - 2c_1v_fv + (c_1 - c_2)v^2}$$

Integrating we obtain

$$t = \frac{1}{2\sqrt{c_1c_2}v_f}\ln\frac{2(c_1-c_2)v - 2c_1v_f - 2\sqrt{c_1c_2}\,v_f}{2(c_1-c_2)v - 2c_1v_f + 2\sqrt{c_1c_2}\,v_f} + C$$

when $t = 0$ so that after some simplification

$v = 0$

$$t = \frac{1}{2\sqrt{c_1c_2}\,v_f} \ln \frac{c_1v_f - (c_1 - \sqrt{c_1c_2})\,v}{c_1v_f - (c_1 + \sqrt{c_1c_2})\,v} \quad \ldots\ldots [10]$$

or

$$v = \frac{c_1v_f\left[1 - e^{-2\sqrt{c_1c_2}\,v_f t}\right]}{(c_1 + \sqrt{c_1c_2}) - (c_1 - \sqrt{c_1c_2})\,e^{-2\sqrt{c_1c_2}\,v_f t}} \quad \ldots [11]$$

The terminal velocity that the particles reach is obtained from

$$\lim_{t \to \infty} v = \frac{c_1v_f}{c_1 + \sqrt{c_1c_2}} = \frac{v_f}{1 + \sqrt{\frac{c_2}{c_1}}}$$

or replacing the symbols

$$v_s = \frac{v_f}{1 + \sqrt{\frac{4fm}{D\rho_0CA}}} \quad \ldots\ldots [12]$$

It can be seen from Equation [12] that the particles never reach the fluid velocity unless the value of the radical in the denominator becomes zero. This is possible only if $f = 0$ or D is very large, theoretically infinite.

The result of Equation [12] could have been obtained directly from Equation [9] by letting $(dv)/(dt) = 0$.

Case 2: $C = f(\mathrm{Re})$

In this section let v denote the relative velocity between the gas and the particles or $v = (v_f - v_s)$. Rewriting Equation [9]

$$\frac{dv}{dt} = -\frac{\rho_0CA}{2m}\,v^2 + \frac{2f}{D}\,(v_f - v)^2 \quad \ldots\ldots [13]$$

Let

$$-\frac{\rho_0\,A}{2m} = k_2, \quad -\frac{2f}{D} = k_3$$

Now

$$\sqrt{C} = 0.63 + \frac{4.8}{\sqrt{\mathrm{Re}}}, \text{ and } \mathrm{Re} = k_1v, \text{ where } k_1 = \frac{\rho_0 d}{\mu}$$

so when the expression for Re is used in C and the result substituted in Equation [13] it yields the expression for $(dv)/(dt)$ as

$$\frac{dv}{dt} = (0.4k_2 - k_3)\,v^2 + \left(23\,\frac{k_2}{k_1} + 2k_3v_f\right)v + 6.05\,\frac{k_2}{k_1}\,v^{3/2} - k_3v_f^2 \quad \ldots [14]$$

In order to integrate Equation [14] an approximation in the term

$$6.05\,\frac{k_2}{k_1}\,v^{3/2}$$

is convenient. This v assumes values ranging from v_f ($v_s = 0$) to v terminal. Since it is expected that the terminal $v \sim (v_f/2)$ (reference 2) we replace $v^{3/2}$ by $\sqrt{3v_f/4}$. (It can be shown that the effect of this transformation on the final result is very small.)

Letting

$$23\,\frac{k_2}{k_1} + 2\,k_3v_f + 6.05\,\frac{k_2}{k_1}\sqrt{\frac{3v_f}{4}} = S$$

$$(0.4k_2 - k_3) = P, \quad -k_3v_f^2 = T$$

Equation [14] becomes

$$\frac{dv}{dt} = P\,v^2 + S\,v + T$$

$$t = \int \frac{dv}{P\,v^2 + S\,v + T} = \frac{1}{\Delta} \ln \frac{2\,P\,v + S - \Delta}{2\,P\,v + S + \Delta} + C$$

where

$$\Delta = \sqrt{S^2 - 4PT}$$

For

$$t = 0, \; v = v_f$$

and

$$t = \frac{1}{\Delta} \ln \left[\left(\frac{2\,P\,v + S - \Delta}{2\,P\,v + S + \Delta}\right)\left(\frac{2\,P\,v_f + S + \Delta}{2\,P\,v_f + S - \Delta}\right)\right] \quad [15]$$

Letting

$$S - \Delta = c_1, \; 2\,P\,v_f + S + \Delta = c_2$$

$$S + \Delta = c_3, \; 2\,P\,v_f + S - \Delta = c_4$$

and solving Equation [15] for v

$$v = \frac{c_2c_4 - c_1c_3\,e^{-\Delta t}}{2P\,(c_3\,e^{-\Delta t} - c_4)} \quad \ldots\ldots [16]$$

From this the terminal velocity becomes

$$\lim_{t \to \infty} v = -\frac{c_4}{2P} = -\frac{S + \Delta}{2P}$$

The absolute terminal velocity of the solids is given by

$$v_s = v_f + \frac{S + \Delta}{2P} \quad \ldots\ldots [17]$$

Frictional Losses. Applying the Fanning equation to the flow of solids in a horizontal pipe we have

$$\Delta P_{fs} = \frac{2\,f\,L\,v_s^2\rho_{ds}}{g\,D} \quad \ldots\ldots [18]$$

Since

$$\rho_{ds} = \frac{G_s}{v_s}$$

$$\frac{\Delta P_{fs}}{LG_s} = \frac{2fv_s}{gD} \quad \ldots\ldots [19]$$

where ΔP_{fs} is the drop in pressure due to the solids friction in the pipe.

If the functional relationship between pressure drop, solids flow rate, and gas velocity is correct, then the pressure drop is a linear function of both solids velocity and flow rate. A plot of ΔP_{fs} against G_s at constant v_s, and against v_s at a constant G_s ought, therefore, to represent straight lines.

From previous considerations

$$m\,\frac{dv}{dt} = F = \frac{\rho_0\,CA\,(v_f - v_s)^2}{2}$$

all per one particle.

The number of particles present in a given length of pipe is

$$V_p\,\rho_pN = \rho_{ds}A_D\,L = \frac{G_s}{v_s}\,A_D\,L$$

$$N = \frac{G_s\,A_D\,L}{V_p\,\rho_pv_s} \quad \ldots\ldots [20]$$

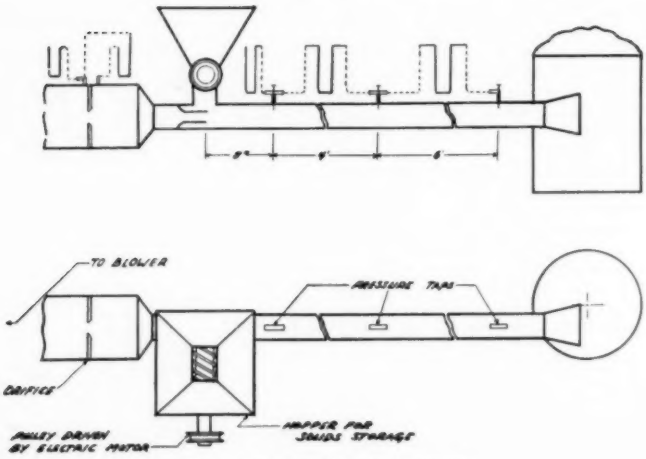

FIG. 2 SCHEMATIC VIEW OF APPARATUS

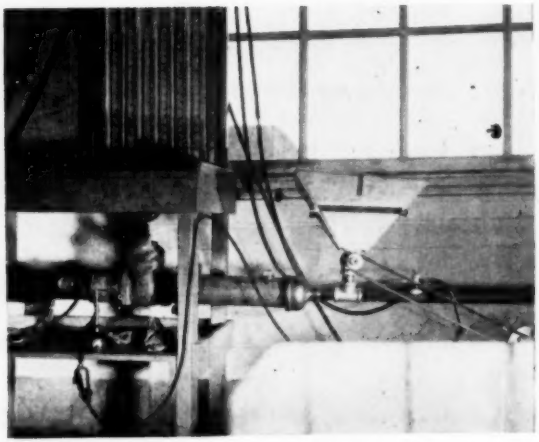

FIG. 3 PARTIAL VIEW OF APPARATUS

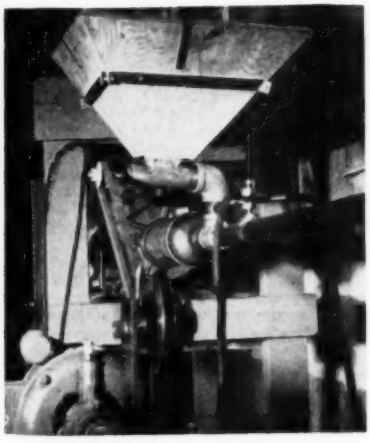

FIG. 4 FEEDING SECTION

The total force exerted on the solids in a given length is

$$F = \frac{\rho_0 C A\,(v_f - v_s)^2}{2} \frac{G_s\, A_D\, L}{V_p\, \rho_p\, v_s}$$

or dividing both sides by A_p and $G_s L$

$$\frac{\Delta P_{f_s}}{G_s\, L} = \frac{C\,\rho_0\,(v_f - v_s)^2}{2\,d\,\rho_p\, v_s} \qquad [21]$$

Equation [18] represents the force required to overcome the solids friction in the pipe. Equation [21] is the force exerted by the air on the gas. At the steady state the two forces will be equal and this equality served to compute the friction factor f.

The total pressure drop across a given length of pipe will be composed of the following three parts

$$\Delta P = \Delta P_a + \Delta P_f + \Delta P_{f_s} \qquad [22]$$

Experimental Investigation

The apparatus used for the experiments is shown in Fig. 2 and parts of it in Figs. 3 and 4. Air was supplied by a 1.5-hp blower and the air velocity measured with a standard ASME orifice. All pressure heads were measured with water manometers calibrated in 0.1 in. The data of ΔP_{fa} was taken with an inclined water manometer calibrated in 0.01 in.

The feeding of the solids into the air presented considerable difficulties and required a careful arrangement. The vital part of the feeding mechanism was the screw which was manufactured by brazing its flights to a steel shaft and placing it in a brass pipe. The brass pipe had an opening at the top exposing a part of the screw on which a hopper was placed and soldered to the pipe. The general arrangement and dimensions of the feeding section are shown in Fig. 5 and in Figs. 3 and 4.

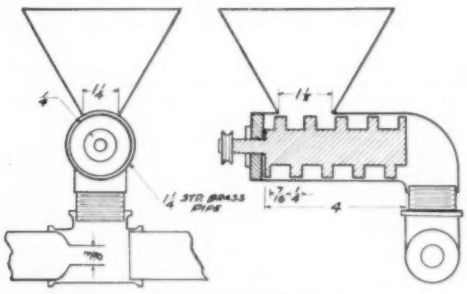

Fig. 5 Feeding Mechanism

In preliminary operation the back pressure, being above atmospheric, prevented the screw from feeding the solids into the pipe. This was quite surprising since the back pressure amounted to no more than 4 or 5 in. of water. The pressure at the feeding point was lowered by introducing a nozzle made from a $^3/_8$-in. pipe projecting up to the feeding point. This produced a high-velocity jet and lowered the pressure.

Another source of trouble was the stopping of the screw by sand particles which entered the clearance space between the screw and brass pipe. The screw had to be turned down from an original clearance of 0.01 to 0.02 in. for the small and 0.03 in. for the large sand. With these changes made the feeding was smooth and continuous. The screw was driven by a gear motor with a system of pulleys giving six different speeds ranging from 20 to 200 rpm.

The test section was a standard 1-in. iron pipe with an over-all length of 11 ft. Measuring from the feeding point, pressure pick-up stations were located at a distance of 0.66, 4.66, and 10.66 ft. The static pressure openings were $^1/_{16}$ in. diam. In each pressure-tap lock a thin rod sealed with graphite rope packing was introduced to clean the pressure openings when they were filled with sand.

The solids discharged into a circular can covered with a muslin cloth which permitted the air to escape but retained the solids.

The material used in this experiment was New Jersey silica sand. The sand was sieved on a Ro-Tap machine with a Tyler standard screen allowing 15 min for batches about 4 lb each. The density of the sand was determined by the water-displacement method. Table 1 gives the general characteristics of the solids.

Preliminary work done before actual data were taken includes the determination of the pressure drop due to the flow of air alone and the calibration of the solids feeding rate as determined by the speed of the motor.

TABLE 1 CHARACTERISTICS OF SOLIDS

Name	Mesh range	Mesh opening, in.	Diam, ft	Spec. weight, p/cf
Large sand....	28–48	0.0232–0.0116	0.00145	162
Small sand....	60–100	0.0098–0.0058	0.00065	162

The screw was calibrated as follows: The hopper was filled with sand to an indicated level. The rest of the sand kept in a bucket was weighed carefully. At a given time the feeding started. The sand was constantly kept at its original level. After 15 min the flow was stopped and the remaining sand weighed. The decrease in weight divided by the time interval gave the solids flow rate.

The runs consisted of taking pressure-drop readings at various air velocities and solid flow rates. The range of air velocities was 20–70 fps; the solids flow rate 17–100 lb per hr.

Results and Discussion

The direct experimental results, a plot of the pressure drop due to the flow of air alone and the additional frictional pressure drop due to the presence of a solid phase, are shown in Figs. 6, 7, and 8. As pointed out in the introduction, the functional relationship between the pressure losses and the flow rates of the solids and air is the main result of the experiments. According to these plots the pressure losses are a linear function of these two parameters. The fact that ΔP_{fa} is plotted against v_f instead of v_s makes no substantial difference since, as shown later, v_s/v_f is practically a constant. Consequently, the experimental results confirm the validity of the theoretical equations.

Referring to Fig. 11, it can be seen that the unit pressure drop is somewhat higher for larger particles. This is caused by several factors. It follows from Equation [21] that an increase in particle diameter decreases the pressure losses directly but indirectly they are increased by changing the value of the slip velocity. This result would indicate that in addition to the desirability of operating pneumatic systems at low gas velocities a choice of finer solids is preferred.

The plot in Fig. 12 should bring out the salient factors in the flow of gas-solid mixtures. On this curve the ratio of mixture-pressure losses over air-pressure loss is plotted against the ratio of the flow rates of the solid and gaseous phases. Since the air pressure drop increases as the square of the velocity while the solids pressure drop is a linear function of the velocity, it is obvious that the curve must have a decreasing slope. At sufficiently high flow rates, the curve will reach a peak and eventually decrease. Consequently, when air-pressure losses are taken into account it is more economical to use high solid-air ratios. Settling of the solids probably will limit solid-air ratios. In these experiments this occurred at a rate of 140 lb per hr.

In setting up the experiment, extreme care was taken not to include the acceleration pressure losses in the data for the frictional losses. For this purpose the test pipe was divided in two sections—one 4 ft long following the feeding section and another 6 ft long. It turned out, however, that the acceleration effects ceased almost completely in the short distance of 8 in. which separated the first pipe section from the feeding point. Thus, while in vertical risers acceleration effects were still present several feet above the feeding point (reference 4), in horizontal-flow systems they cease shortly after the solids are entrained. This, however, does not mean that the pressure drops at the feeding point are negligible or even small. In fact, it can be shown that the losses in the entrainment region are rather high.

Using Dalla Valle's expression for C and Equation [21], the solids velocity was computed for both Cases 1 and 2. There is

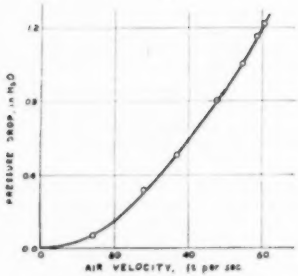

FIG. 6 PRESSURE LOSSES FOR PURE AIR
(Length of pipe = 6 ft.)

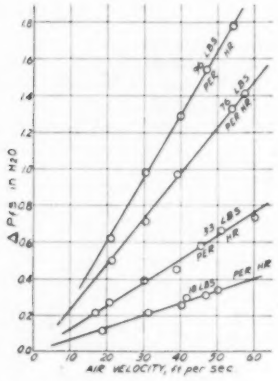

FIG. 7 SOLIDS PRESSURE DROP VERSUS AIR VELOCITY FOR SMALL SAND
(Length of pipe = 6 ft.)

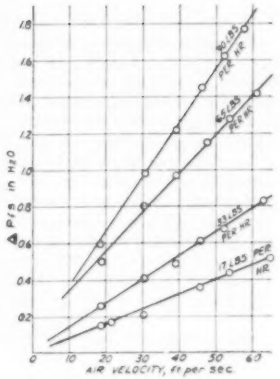

FIG. 8 SOLIDS PRESSURE DROP VERSUS AIR VELOCITY FOR LARGE SAND
(Length of pipe = 6 ft.)

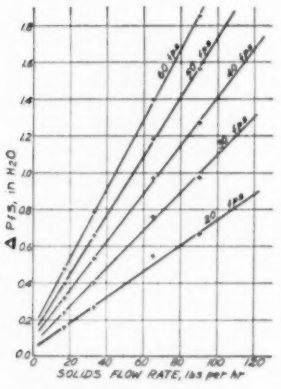

FIG. 9 SOLIDS PRESSURE DROP VERSUS SOLIDS FLOW RATE FOR SMALL SAND
(Length of pipe = 6 ft.)

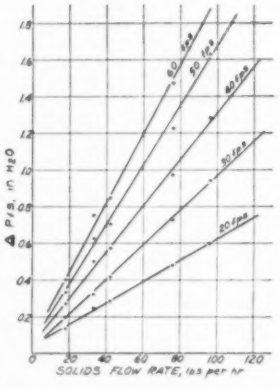

FIG. 10 SOLIDS PRESSURE DROP VERSUS SOLIDS FLOW RATE FOR LARGE SAND
(Length of pipe = 6 ft.)

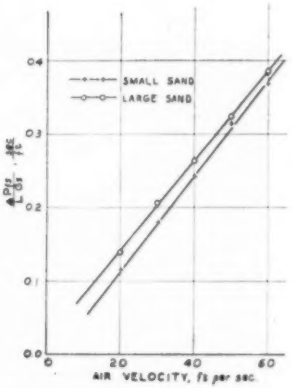

FIG. 11 UNIT SOLIDS PRESSURE DROP

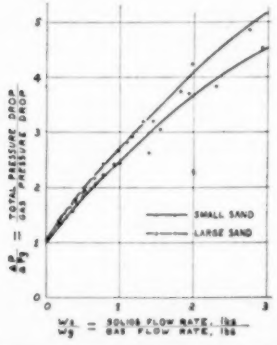

FIG. 12 PRESSURE-DROP RATIO VERSUS FLOW-RATE RATIO

very little data in the literature to compare these values with. The only values given are those by Cramp (2) which were obtained for grain flowing in a horizontal pipe. The values for the particle velocity were obtained in the following manner: He let the grain discharge into the atmosphere, and measuring the distance they traveled and the height from which they fell, he calculated the original velocity of the particles. Although this method of measurement is somewhat problematical and the shapes of the bodies were different, the similarity of the two systems justifies a comparison of the results. The values for the ratio of v_s/v_f, as given by Cramp, range from 0.4 to 0.47. The values obtained in this experiment are given in Table 2. It is clear that the values obtained for v_s by treating C as a variable are more reasonable and in a closer agreement with Cramp's results.

A comparison of the present results with those obtained by

TABLE 2 RESULTS OF EXPERIMENT TO DETERMINE v_s/v_f

	C = const = 0.44	$C = f$ (Re)
Small sand....	0.33	0.5 –0.6
Large sand....	0.20	0.28–0.33

Hariu and Molstad (4) from a more reliable and direct method will further support the thesis that C is a function of the Reynolds number. Although Hariu and Molstad used a glass riser which would give higher v_s/v_f, the presence of a gravity force and the small diameters of the conduits ($^1/_4$ and $^1/_2$ in. diam) would oppose such an increase and compensate for the first effect. Table 3 gives values taken from Hariu and Molstad:

TABLE 3 VALUES OF v_s/v_f FROM REFERENCE (4)

	Diam, ft	v_s/v_f
Small sand.....	0.007	0.66–0.74
Large sand.....	0.00165	0.25–0.28

Thus the values obtained in this experiment agree fairly well with the values obtained from direct measurements. The values of 0.33 and 0.2 obtained by treating C as a constant are decisively out of the range of expected values. On the basis of this experiment, Dalla Valle's assertion could not be justified. The drag coefficient remains a function of Reynolds number.

The values obtained for the velocity of the particles support also the proposition that the C-curve can be applied to the flow of solids in pipes, something which cannot be justified from a pure theoretical standpoint.

It was said previously that the Fanning equation is introduced on the assumption that it will account for the solids-pressure losses as it does for fluids. It could be a useful relation, because with f determined from experiments and v_s found from Equation [12], the expected pressure losses could be computed. A close investigation of the Fanning equation

$$\Delta P_{f_s} = \frac{2 f v_s L G_s}{g D}$$

raises, however, some questions. From the expressions for the solids velocity, it can be seen that it decreases with an increase in particle diameter. Therefore the value of f in the Fanning equation could stay constant only, and only if, the pressure loss ΔP_{f_s} drops correspondingly. This, however, was not the case. By using the same kind of solids but of larger particle diameter, the pressure drop was higher. The solids velocity being appreciably smaller, both factors contributed to almost doubling the value of f, from 0.015 to 0.03.

On the basis of this work, it can be said that the Fanning equation is correct in its application to a solid phase inasmuch as it bears a linear relationship to the pressure drop. With a known value of f it may supply a means of estimating the pressure losses. The equation, however, bears no correlation to the kind of solids used or to different sizes of the same solid. Therefore, this lack of generality makes it of limited use.

However, a modification of the Fanning equation might be possible. It seems that the introduction of the dimensionless group d/D would take into account the variation in particle diameter. From Figs. 13 and 14 it is seen that multiplying the friction factor by 2, which is the ratio of the diameters of the small and large sands, will bring the value of f back to approximately 0.025. To justify such a modification, however, more extensive experiments with various sand sizes, and possibly various kinds of solids, are required.

Recommendations

For a complete understanding of solid-gas flow, further study is necessary. The following seem to the author to be of the greatest importance:

1 A method for direct measurement of the particle velocity.

2 Extensive experimentation with solids of various sizes, shapes, and surface characteristics.

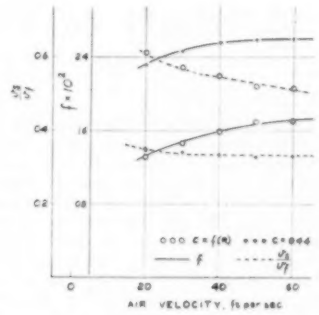

Fig. 13 Velocity Ratio and Friction Factor for Small Sand

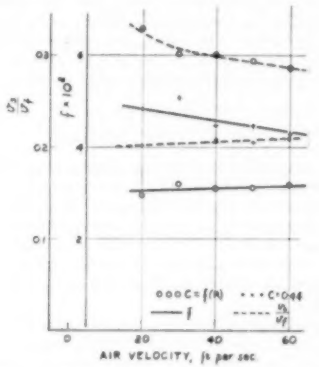

Fig. 14 Velocity Ratio and Friction Factor for Large Sand

3 Measurement of the acceleration pressure losses at the feeding section and at bends.

Acknowledgment

Acknowledgment is due to Professors N. P. Bailey and J. J. Devine of Rensselaer Polytechnic Institute, whose invaluable suggestions and assistance made this work possible.

Bibliography

1 "Horizontal Carriage of Granular Material by an Injector-Driven Air Stream," by S. A. Wood and A. J. Bailey, *Proceedings of the Journal of The Institute of Mechanical Engineers*, vol. 142, 1939, p. 149.

2 "Pneumatic Transport Plants," by W. Cramp, Trans. Society of the Chemical Industry, vol. 44, 1925, p. 207.

3 "Applied Hydro and Aeromechanics," by L. Prandtl, McGraw-Hill Book Company, Inc., New York, N. Y., chapter 5, 1934.

4 "Dynamics of Fluid-Solid Systems," by O. H. Hariu and O. C. Molstad, *Industrial and Engineering Chemistry*, vol. 41, 1949, p. 1148.

5 "Micromeritics," by J. M. Dalla Valle, Pitman Publishing Company, New York, N. Y., 1948.

6 "Chemical Calculation of Particle Trajectories," by C. E. Lapple and C. B. Shepherd, *Industrial and Engineering Chemistry*, vol. 32, 1940, p. 605.

7 "Friction in the Flow of Suspensions," by E. G. Vogt and R. R. White, *Industrial and Engineering Chemistry*, vol. 40, 1948, p. 1731.

8 "Chemical Engineers Handbook," by J. H. Perry, McGraw-Hill Book Co., Inc., New York, N. Y., second edition, 1941, p. 807.

9 "Conveyance of Solid Particles by Fluid Suspension," by R. F. Davis, *Engineering*, vol. 140, 1935, p. 124.

A Study of Vanes Singing in Water

By C. A. GONGWER[1] AZUSA, CALIF.

In the course of propulsion experiments in the ring-channel and rotating-boom facility at the Aerojet Engineering Corporation, it was discovered that certain struts which are used to support underwater bodies would "sing" at surprisingly low speeds, e.g., 5 to 7 knots. Tail surfaces also sang. The note emitted was a clear musical tone in most instances, and, as the speed was increased, the note would fade, disappear, and then reappear as a note of higher frequency. This singing caused considerable apprehension as it was feared that the strut would fail at high speeds due to build-up of the vibrations. Analysis for flutter stability and torsional divergence had been conducted, and it was known that the operation was well away from the ranges where flutter or torsional divergence might occur. However, the severity of the singing did not tend to become greater at high speeds, and there were usually quiet speed zones at high speeds as well as at low speeds.

Review of the Literature

THE unclassified literature on singing propellers has been thoroughly reviewed by C. E. Work in a paper[2] which also contains an extensive bibliography. A study of this reference reveals that the cause of singing is generally ascribed to "hydrodynamic excitation." Further study of the literature reveals that many different remedies are used to cure singing troubles and that their efficacy is very uncertain and varies widely and irreproducibly.

One investigator[3] relates that frequency was observed to increase in direct proportion to speed. This suggests that singing is caused by the shedding of a von Kármán vortex street; such streets have a characteristic correlation between frequency, speed, and length. Other investigators have attempted to relate the frequency of the supposed vortex street to a characteristic dimension of the blade, such as the maximum thickness or the chord. However, the frequency-speed relationships were found to be of the wrong order for the characteristic length used and not to be related to changes in thickness and chord.

The investigations presented here show that the observation made by Gutsche[3] is of primary importance as a clue to the cause of singing.

Experimental Procedure

Test Facility. The facility used in the tests was the 80-ft rotating-boom and ring-channel test facility at the Aerojet plant.

Vanes. Solid steel struts of diamond or double-wedge section profile of 12 in. chord and $^3/_8$ and $^3/_4$ in. maximum thickness were used. The trailing edges were initially $^1/_8$ in. thick, ($^1/_{16}$ in. radius), and these were sharpened down in successive steps. The leading edges also were of $^1/_8$ in. thickness, but for high-speed operation it was found necessary to sharpen the leading edge in order to suppress strip cavitation. It was necessary to use an antiaeration vane placed horizontally just under the water surface at the trailing edge to prevent air from running down the back of the strut. The span or length submerged was usually about 1 ft. The ridge at the half-chord point on each side, characteristic of diamond sections, was rounded to about a 3 in. radius. Each vane was polished with fine emery paper to a finish of about 10 microinches rms.

Speeds. The speed was carried as high as the torsional-divergence limit would allow. This limited the speed on the $^3/_8$-in-thick vane to about 45 knots. The $^3/_4$-in-thick vane was run at speeds as high as 60 knots.

Attitudes. The vanes were tested with both vertical (meaning trailing edge and leading edges perpendicular to the flow) and swept forward 30 deg attitudes. Most of the tests were at zero angle of attack, but some tests were made with angles of attack of 1, 2, and 3 deg.

Photography. Edgerton microflash pictures were taken from the underwater observation windows as the strut passed. The pictures were timed by a cam on the boom. Underwater mirrors were used to concentrate the light of the flash lamps.

Frequency Measurement. The frequency of the singing was measured using a cathode-ray oscilloscope which compared the frequency of the strut as picked up by a stationary microphone at the edge of the pool in the air with a signal of known frequency generated by an oscillator. As the strut passed the microphone, the Doppler effect caused a frequency shift, making exact measurement difficult. Therefore on later tests the microphone was mounted on the rotating boom and connected through slip rings. Later, frequency measurements were made with a General Radio sound analyzer.

Speed Measurement. The speed of travel of the vane was measured by a tachometer which was calibrated regularly by timing the revolutions of the boom. The relative water speed is nearly the absolute speed because the drag-around of the water in the channel is negligible for a body of such low drag as the streamlined struts.

Curvature of Path. All tests were run with the strut at the 40.6-ft radius of the boom.

Flow Visibility. The flow is made visible, or at least partly so, by cavitation and, in some tests, by aeration. Under some conditions the vortex street associated with the singing was visible because the cores of the vortexes cavitated. This core cavitation is the principal means of identifying the streets photographically. When the aeration plate is absent, the trailing edge aerates when vertical and the vortex cores are visible from this aeration at speeds below that necessary for cavitation to occur. However, aeration has little significance in propeller uses. When the strut is swept forward 30 deg, no aeration plate is necessary.

Test Results

Strut Vertical. In the first set of experiments the strut was vertical, i.e., flow direction was normal to the leading and trailing edges of the strut. Figs. 1(*a*) and 1(*b*) show frequency plotted

[1] Manager, Underwater Engine Division, Aerojet Engineering Corporation. Mem. ASME.

[2] "Review of Marine Propeller Noise and Vibration Studies," by C. E. Work, U. S. Naval Ordnance Test Station Propulsion Memorandum 74, September 7, 1950.

[3] "The Singing of Ships' Propellers," by F. Gutsche, *Zeitschrift des Vereines deutscher Ingenieure*, vol. 81, July 3, 1937, pp. 882–883.

Presented at the National Conference of the Applied Mechanics Division, State College, Pa., June 19–21, 1952, of The American Society of Mechanical Engineers.

Discussion of this paper should be addressed to the Secretary, ASME, 29 West 39th Street, New York, N. Y., and will be accepted until January 10, 1953, for publication at a later date. Discussion received after the closing date will be returned.

Note: Statements and opinions advanced in papers are to be understood as individual expressions of their authors and not those of the Society. Manuscript received by ASME Applied Mechanics Division, December 6, 1951. Paper No. 52—APM-33.

against speed for a number of different trailing-edge thicknesses. It can be seen that each note holds at nearly constant frequency over a short range of speed. The notes jump up or down in frequency as speed is increased or decreased. At some points a zone of silence occurs between various speeds. The lines enclosing the note segments on the plot were formed by extending straight lines from the origin. For purposes of analysis, the characteristic of frequency versus speed is taken as the slope of a straight line bisecting the tone area. As the trailing edge is reduced in thickness by successive steps, new zones of notes are entered. It is seen that Gutsche's observation[3] of proportionality between frequency and speed for propeller singing is borne out.

Microflash photographs of a vane with trailing-edge thickness (rounded) of 0.125 in. are shown in Figs. 2, 3, 4, and 5, for speeds of 28, 38, 44, and 46 knots, respectively. The angle of attack is zero degrees. The cavitating cores of the trailing vortex street can be seen faintly in Fig. 2 and more strongly in the other figures. The division of the trailing edge into vibrating segments is shown clearly by the separation of the streets into separate streams. As the speed increases and the frequencies rise, as shown in Figs. 1(*a*) and 1(*b*), the trailing-edge vibration jumps in stages into higher modes of oscillation until, at 44 knots, four distinct and separate streets can be seen emerging in phase from four separate segments of the trailing edge. It follows that, under these conditions, the adjacent streets must be of opposite sign; this will be shown later.

Strut Swept Forward 30 Deg. The plot of frequency versus speed for a strut swept forward 30 deg is shown in Fig. 6. The relationship of separate notes to changes in speed is much the same for this strut as it is for the vertical strut, except the frequencies are not as high as those of the vertical strut at the same trailing-edge thickness.

Photographs of this strut at 37 and 44 knots are shown in Figs. 7 and 8. The vortex streets are not as visible as those in the photographs of the vertical strut, as the cavitation appears fainter. The singing was as loud in these tests as it was in the tests of the vertical strut, however. In Fig. 7 progressive aeration of the vortex cores from the surface with increasing distance behind the strut can be seen. Because this strut was swept forward, its speed of torsional divergence was reduced greatly, and it was necessary to decrease the submergence to about 8 in.

Strut at Different Angles of Attack. The tests with the vane at varying angles of attack showed that the vane sings at the same notes (at the same approximate speeds) as when zero angle of attack was used. This can be seen in Fig. 9. However, the zones of speed where silence prevails are wider, in some instances, the greater the angle of attack. Fig. 10 shows that the strength of the vortexes is reduced at increased angles of attack. The pictures show the suction side of the blade. At an attack angle of 3 deg, no cavitating cores could be discerned, whereas for the same speed and an attack angle of about 2 deg, the cores are visible. The transverse, or lift, force was so great at 3 deg, that the speed could not be increased beyond 50 knots because of the possibility of strut failure, even though the strut thickness was increased to 1/4 in. for these tests. The tests with a 2-deg angle of attack were carried to 58 knots.

Progressive Thinning of Trailing Edge. Reducing the thickness of the trailing edge was found to raise the frequency of vibration for a given speed. This can be seen in Figs. 1(*a*) and 1(*b*). With a thickness of 0.015 in., some high-frequency notes were obtained;

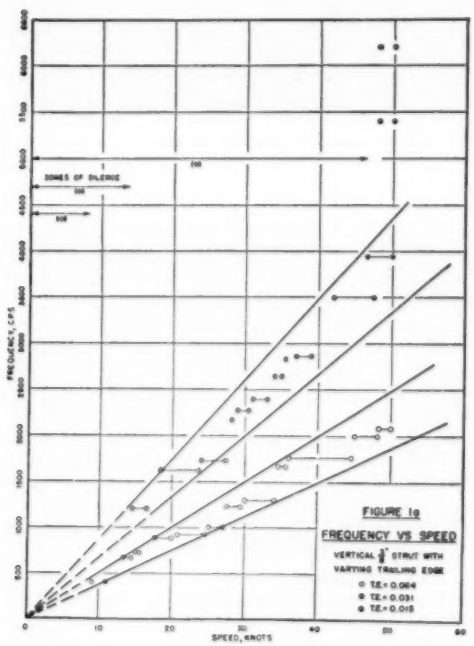

FIG. 1(*a*)

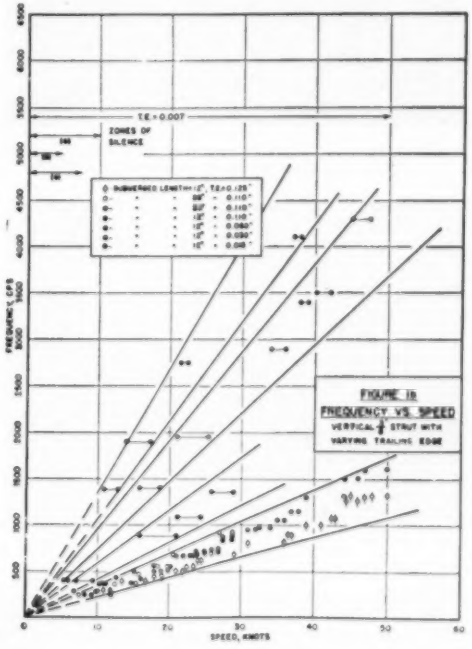

FIG. 1(*b*)

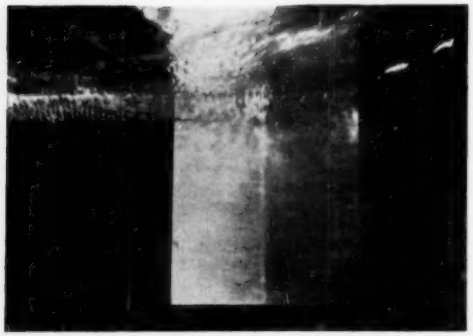

FIG. 2 CAVITATING VORTEX STREET SHED FROM VERTICAL STRUT WHILE SINGING, ZERO ANGLE OF ATTACK, SPEED 28 KNOTS

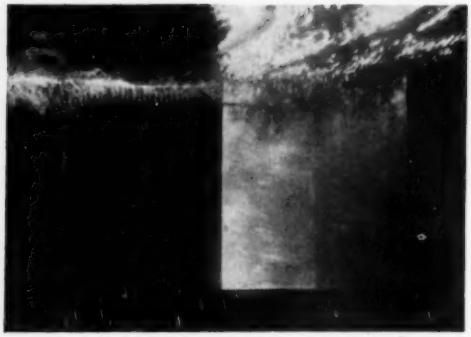

FIG. 3 CAVITATING VORTEX STREET SHED FROM VERTICAL STRUT WHILE SINGING, ZERO ANGLE OF ATTACK, SPEED 38 KNOTS

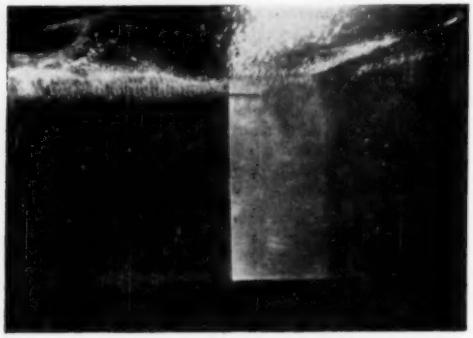

FIG. 4 CAVITATING VORTEX STREET SHED FROM VERTICAL STRUT WHILE SINGING, ZERO ANGLE OF ATTACK, SPEED 44 KNOTS

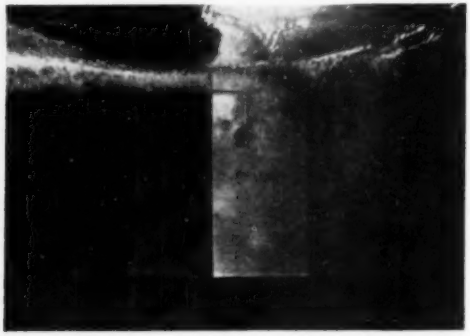

FIG. 5 CAVITATING VORTEX STREET SHED FROM VERTICAL STRUT WHILE SINGING, ZERO ANGLE OF ATTACK, SPEED 46 KNOTS

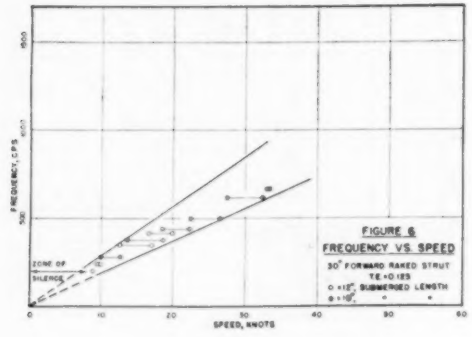

FIG. 6

with a thickness of 0.007 in. no singing occurred at any speed. It can be observed that, for a fixed speed, as the trailing edge is thinned, the frequency increases in inverse proportion, but with very thin edges, the increase in frequency is at a slower rate. This is treated in the section which follows.

DISCUSSION OF TEST RESULTS

Vertical Strut. It is apparent from inspection of Figs. 1(*a*) and 1(*b*) and the succeeding photographs that the hydrodynamic clapper effect mentioned in the literature is the von Kármán vortex street. This street can be correlated with the trailing-edge thickness b through the Strouhal number, Nb/U, and b/a where N is the frequency of shedding of the alternate vortexes, here taken to be the frequency of the note of the singing strut; U is the forward speed; and a is the spacing between alternate vortexes. Consistent units must be used throughout. (That the frequency of shedding is the note frequency can be checked by dividing vane velocity diminished by the street velocity of about 0.1 U)[4] by the vortex spacing. This has been found to check.) Goldstein gives value of Nb/U of 0.18, Re = 10^4, for a cylinder and 0.148 to 0.18 for a flat plate normal to the flow. For the points in Figs. 1(*a*) and 1(*b*) at a speed of 15 knots the values given in Table 1 obtain for different trailing-edge thicknesses. It can be seen that Nb/U decreases as the trailing edge thins. It has been found that the arbitrary addition of 0.016 in. to the thickness b causes Nb/U to remain substantially constant, as shown in the last row of Table 1. This corrected value is called Nb'/U and is about 0.18, or substantially the same as that for the cylinder.

[4] "Modern Developments in Fluid Dynamics," by S. Goldstein, Oxford University Press, London, England, vol. 2, 1938.

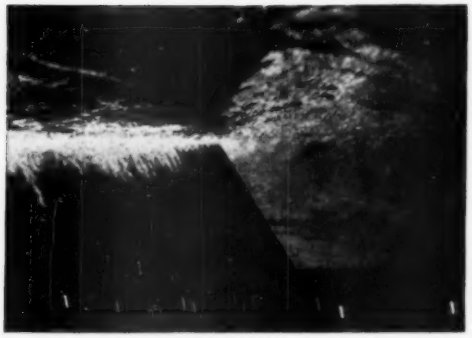

FIG. 7 STRUT SWEPT FORWARD 30 DEG, ZERO ANGLE OF ATTACK, SPEED 37 KNOTS

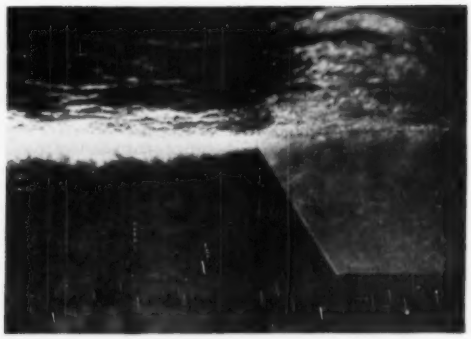

FIG. 8 STRUT SWEPT FORWARD 30 DEG, ZERO ANGLE OF ATTACK, SPEED 44 KNOTS

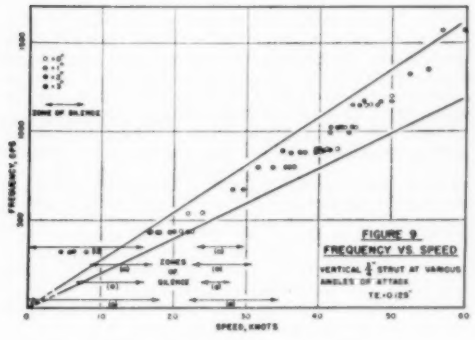

FIG. 9

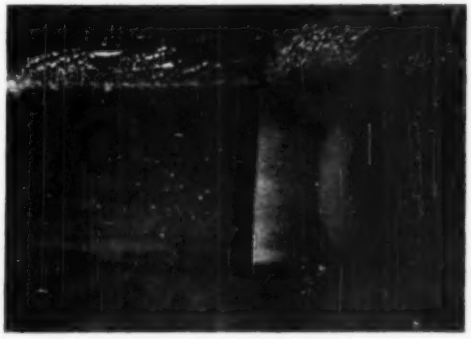

FIG. 10 VERTICAL STRUT FROM SUCTION SIDE, 2 DEG ANGLE OF ATTACK, SPEED 58 KNOTS

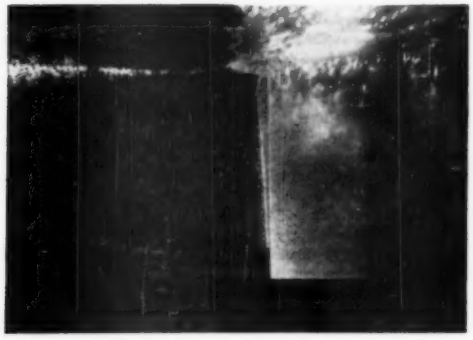

FIG. 11 EFFECT OF AERATION FROM SURFACE, VERTICAL STRUT WITHOUT AERATION PLATE, TRAILING-EDGE THICKNESS OF 0.125 IN., ZERO ANGLE OF ATTACK, SPEED 32 KNOTS

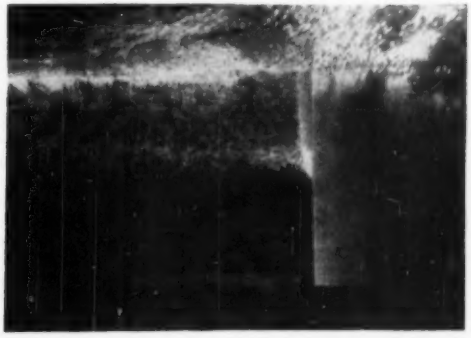

FIG. 12 VERTICAL STRUT WITHOUT AERATION PLATE, TRAILING-EDGE THICKNESS OF 0.125 IN., ZERO ANGLE OF ATTACK, SPEED 46 KNOTS

(Mode of vibration of lower unaerated portion indicated by distorted vortex street.)

TABLE 1 VALUES FOR TRAILING-EDGE THICKNESSES

b, in.		0.125	0.060	0.030	0.015	
$\frac{Nb}{U}$		0.160	0.147	0.118	0.0856	
$\frac{Nb'}{U} = \frac{N\left(b \text{ ft} + \frac{0.016}{12}\right)}{U}$		0.181	0.186	0.181	0.177	(Avg = 0.18)

The addition of 0.016 to b may be because the boundary layer of the plate provides a virtual plate thickness at the trailing edge which is greater than the actual trailing-edge thickness.

Table 2 shows a set of values of Nb/U and Nb'/U for different values of b obtained in another series of experiments where the trailing edge was thinned progressively. The values of Nb/U are taken as the averages over a range of speeds from 10 to 50 knots. The value of Nb'/U obtained is 0.19, which agrees closely with the previous value of 0.18 for the series presented in Table 1. Here, however, it was necessary to add 0.022 in. to the trailing-edge thickness, as a virtual boundary-layer effect, in order to make Nb'/U independent of b. Computation of the boundary layer of the strut considered as a flat plate edgewise to the flow at a speed of 15 knots, gives, for the thickness of the laminar sublayer at the trailing edge, 5×10^{-4} in. A value of 0.0295 in. is obtained for the displacement thickness. The momentum thickness is 0.0230 in. The flat-plate Reynolds number is 2.33×10^4. It is apparent that the contribution of the boundary layer must be doubled to allow for the two sides of the vane and that the experimentally determined virtual-thickness addition does not agree with any of the three thicknesses computed but is greater than the laminar sublayer and is approximately one half of the momentum and displacement thicknesses.

TABLE 2 VALUES OF Nb/U AND Nb'/U

b, in.		0.125	0.064	0.031	0.015	
$\frac{Nb}{U}$		0.166	0.137	0.117	0.076	
$\frac{Nb'}{U} = \frac{N\left(b \text{ ft} + \frac{0.022}{12}\right)}{U}$		0.195	0.184	0.200	0.187	Avg = 0.19

The value of a/b given by Goldstein[4] is 4.27 for a cylinder and 5.6 for a flat plate. For a strut at 15 knots when $b = 0.125$ in., a/b is 5.15. The agreement is seen to be reasonably good. Some significance can be ascribed to the virtual thickness when it is remembered that with a trailing-edge thickness of 0.007 in., the singing disappears. In other words, the trailing edge is submerged in the boundary layer and is, therefore essentially sharp. The agreement between 0.007 in. and 0.008 in., the virtual thickness, taken as half of the plate-thickness addition of 0.016 in. found previously, is better than the precision of determination of the limit of singing as a function of trailing-edge thickness.

Modes of Vibration. Inspection of the figures shows that the mode of vibration of the plate, and particularly the trailing edge, must increase in discrete steps as the speed increases. It is known from sand figures on flat plates excited by a bow or other means that the edges are divided into vibrating segments between which are nodal points and that the deflections of adjacent loops are of opposite sign. In Figs. 2, 3, and 4 can be seen the vortex streets coming from regions of the trailing edge which must be the loops. The frequency of singing is 720, 1070, and 1320 cycles per sec (cps) for these three tests. The number of vibrating segments can be seen to increase by 1 for each figure until, in Fig. 4, four separate loops can be seen with an additional loop indicated in the region of the aeration plate just under the surface of the water.

That adjacent streets of vortexes are of opposite sign when first shed is indicated in Fig. 4 where the adjacent streets can be seen faintly to link up about half a strut-chord length downstream but (by counting the number of cores to the trailing edge) the number of cores differs by 1 for adjacent streets. This produces a distortion in the linked vortexes, shown clearly in Figs. 5 and 12.

Strut Swept Forward. From the plot of the frequency of singing versus speed for the strut which was swept forward 30 deg, Fig. 6, it can be seen that the singing phenomenon is almost identical to that for the vertical strut. However, Nb'/U for the strut is 0.169, where b' is taken as $b + 0.019$ in., and 0.019 in. is the mean of the two determinations of the virtual-thickness addition. This value is lower than that for the vertical strut, but Nb'/U can be raised to 0.195 if U is taken as the component of velocity normal to the trailing edge. The then slightly better agreement with calculations made for the vertical strut indicates that frequency of the street is determined by the normal velocity component, within the precision of these determinations.

The photographs show the street inclined to the flow, but somewhat weaker than that for the vertical strut. This is because there was less tendency for the cores to cavitate, since the normal component of velocity also determines their strength, as well as their frequency.

Strength of Vortexes. An example will be worked out to illustrate the strength of a cavitating vortex. As shown in Fig. 4, the diameter of the cavitating core, measured just aft of the strut, is 0.044 in. At this diameter the whirl velocity is approximately known because the absolute pressure approximates the vapor pressure of the water at 60 deg, which is 1 ft of water. Since absolute pressure is 35 ft, the velocity of whirl at the core can be computed. $V = \sqrt{2g\,(H - ha)} = 46.8$ fps. Therefore the circulation Γ, of the vortex is $V \pi D = 46.8\,\pi \frac{0.044}{12} = 0.534$ ft^2 per sec. Since the momentary transverse force, or lift, associated with this circulation is $\rho\Gamma V$ per foot of span, the lift per foot of span for this vortex at 44 knots is

$$\frac{62.4}{32.2} \times 0.534 \times 44 \times 1.689 = 76.8 \text{ lb per ft.}$$

Since this force reverses sign at a frequency of 1320 cps, the vibration of the solid-steel strut is understandable.

Permissible Variation in Nb/U. Inspection of the plots in Figs. 1, 6, and 9 shows a range of speeds at which singing at a particular frequency will occur. The plots for the vanes indicate that the parameter Nb/U is not rigidly determined but can vary over a maximum permissible range of about 10 per cent. This indicates that for an actual singing propeller with the vortexes coming in separate streets from discrete patches on the trailing edges, the maximum permissible radial extent of a patch is probably 10 per cent of the radius. This is because, other things being equal, the variation of Nb/U over a patch on the trailing edge will be approximately the same as the radius variation percentagewise. Therefore the apparent contradiction between the production of discrete notes from a propeller in the absence of discrete values of Nb/U for the trailing edge is resolved. However, the principal velocity near the hub is the forward velocity, and the radial-velocity component is not controlling, therefore a wider region or patch of permissible range of Nb/U for a single-note production is available at this point.

Singing at Angle of Attack. The plot of frequency versus speed for different angles of attack α, is shown in Fig. 9. It can be seen that the note frequencies are the same at the same mean speeds for angles of attack of 0, 1, 2, and 3 deg. However, zones of silence between the notes appear at slight angles and widen, speedwise, as the angle increases. Fig. 10 shows that the vortex streets are less sensitive to cavitation and therefore much weaker. No vortex streets can be seen at 3 deg; at 2 deg the speed had to be raised to 47, 53, and 58 knots before the vortexes were visible. This

suppression of the vortexes by angle of attack is probably associated with the finite span of the strut. The low aspect ratio insures that a powerful vortex sheet oriented at right angles to the streets is left behind the strut. This makes the formation of the streets more difficult and distorts those that are formed. In Fig. 10 distorted streets can be seen at the lower trailing edge and at the surface.

In Fig. 10 leading-edge cavitation can be seen as well as successive strips at regular intervals following the cavitation. The spacing of these strips is equal to that between alternate vortexes of the vortex streets. The presence of these strips can be accounted for by the bubble-bouncing effects shown by Knapp,[5] but here modified by the strut singing, which causes leading-edge oscillations at the same frequency. This would account for the correspondence in spacing.

Correlation With a Singing Propeller. Data were obtained on one singing propeller from the Department of the Navy. These data are given in Table 3. An analysis of these data on the basis of the previously described theory follows.

TABLE 3 DATA FROM NAVY TESTS ON SINGING PROPELLER

Range of singing, rpm	Frequency cps
80 to 110	600
120 +	1000
Diameter..7.5 ft	Blade chord at 0.7R....28.44 in.
Pitch.....6.0 ft	Trailing-edge thickness .0.030 in.
Slip.....30 per cent	

It is not known at what radius from the axis of rotation the vortex street responsible for the singing is originating. For this example, it can be assumed to occur at the 0.7R point. This is the point used in many performance and design calculations for computing blade angles and corresponds to a mean radius in so far as average influence of the separate blade elements is concerned. The first note of 600 cps, from the Navy data, will now be considered. The mean rpm for the range of this note, 95 rpm, is used. The relative water velocity at the 0.7R point is then computed from the peripheral component and the advance speed derived from the pitch and the slip. This velocity U is 27 fps. It is now necessary to compute $b' = b + \delta$, where δ is the virtual thickness addition experimentally determined as in the foregoing. This will be taken as the same fraction of the computed displacement boundary-layer thickness as it was in the strut experiments.

The formula for the displacement thickness of a turbulent boundary layer is, for one side[4]

$$\delta_d = \frac{1}{8}\frac{0.37x}{\left(\frac{Ux}{\nu}\right)^{1/5}}$$

From the last paragraph in the section Vertical Strut, under Discussion of Results, the ratio of the mean virtual thickness addition

$$\delta_v = \left(\frac{0.016 + 0.022}{2}\right) = 0.019 \text{ in.}$$

for both sides to δ_d for the strut was

$$\frac{0.019}{0.0295} = 0.643$$

δ_d for this propeller is 0.0582 in. Therefore

$$\delta_v = 0.0582 \times \frac{0.019}{0.0295} = 0.0375 \text{ in.}$$

$$b' = \frac{0.030 + 0.0375}{12} = 0.00563 \text{ ft}$$

and

$$\frac{Nb'}{U} = \frac{600 \times 0.00563}{27} = 0.125$$

This is lower than the values of 0.18 and 0.19 for Nb'/U determined for the strut but may reflect the uncertainty in choosing the radius at which singing occurs.

Next, for the note at 1000 cps, given in the Navy data, the mean rpm is taken as slightly higher than 120 rpm, since this is the only figure given and is presumably the lower point of the speed range of this note. An rpm value of 130 rpm was taken in order not to extrapolate too far. The velocity U at the 0.7R point is then 37 fps, and

$$\delta_d = \frac{1}{8} \times \frac{0.37 \times \frac{28.44}{12}}{\left(\frac{37 \times \frac{28.44}{12}}{\nu}\right)^{1/5}} = 0.00455 \text{ ft}$$

The value of δ_v is determined from δ_d by applying the previously experimentally determined factor, 0.643. δ_v is then 0.00455 × 0.643 = 0.00293 ft or 0.0352 in., and b' is 0.030 + 0.0352 = 0.065 in. or 0.00541 ft. Therefore

$$\frac{Nb'}{U} = \frac{1000 \times 0.00541}{37} = 0.146$$

This value is also lower than the experimentally determined values of 0.18 and 0.19 and again reflects uncertainty in choosing the radius of the singing street. The angle between the trailing edges and the relative flow direction is assumed to be 90 deg at the street, but, if it is less, the normal component of relative velocity would take control, and this error would be in the direction of lowered apparent values of Nb'/U.

General Formula for Virtual-Thickness Addition. From the foregoing example the virtual-thickness addition to the measured trailing-edge thickness is given by

$$\delta_v = 0.643 \times \frac{1}{8} 0.37 \frac{x}{\left(\frac{Ux}{\nu}\right)^{1/5}} = 0.0297 \frac{x}{\left(\frac{Ux}{\nu}\right)^{1/5}}$$

or simply 0.643 times δ_d, the displacement turbulent-boundary-layer thickness. The corrected thickness b' is then b the actual thickness, plus δ_v, the virtual-thickness addition.

Summary and Conclusions

The experimental work performed in this study supports the following conclusions:

1 Singing of vanes, and incidentally of marine propellers, is caused by the action of von Kármán vortex streets which are generated at the trailing edge.

2 The critical length, which together with speed, determines the spacing of the street, and hence the frequency of singing is the thickness of the trailing edge of the vane.

3 The Strouhal number, Nb/U, can be made to apply to these streets and assume the customary range of values by increasing the length b by a fraction of the boundary-layer thickness.

4 Singing does not occur at speeds from 0 to 60 knots on vanes which have trailing edges thinner than 0.007 to 0.010 in. per ft of chord. This is suggested as a limit of trailing-edge thickness for marine propellers to suppress singing.

5 Singing will occur on a vane of the general type considered

[5] "Laboratory Investigations of the Mechanism of Cavitation," by R. T. Knapp and A. Hollander, Trans. ASME, vol. 70, 1948, pp. 419–435.

here whenever the plate can assume a mode of vibration such that the modified Strouhal number Nb'/U is approximately 0.18.

6 One of the principal types of vibration of the plate is with the trailing edge vibrating in scallops. Each scallop sheds a vortex street.

7 Vanes in which the trailing edge is not normal to the flow will sing and the corresponding vortex street is inclined to the flow. The component of velocity normal to the trailing edge controls in the Strouhal number for this case.

8 Thick vanes require a higher velocity for the inception of singing than thin ones, other things being equal.

9 The effect of angle of attack of the vane is to weaken the singing somewhat. This seems to be caused by the effect of finite span and the shedding of the lift vorticity which distorts and suppresses the vortex streets.

10 Leading edges and tips of vanes are not factors in the generation of the vortex streets and hence do not influence singing.

11 From consideration of the mechanism of the action, the singing note is radiated directly from the oscillating surfaces of the vane and not from the street or wake.

12 The vibration of the singing vane is generated by the oscillatory circulation produced about the vane as the oscillating vorticity is shed in the street. This results in oscillating transverse forces on the vane which drive the vibration.

13 In general, when the vane is not singing the vortex streets are not being generated.

Acknowledgment

The author wishes to thank the Office of Naval Research for sponsoring this study and permitting its publication. Thanks are also due to Mr. J. J. Marcinek for assisting in the experimental program and to Mr. Gordon Jarvis who was in charge of the photography.

Vibrations of Elastic Shells in a Fluid Medium and the Associated Radiation of Sound[1]

By MIGUEL C. JUNGER,[2] CAMBRIDGE, MASS.

This is a study of the vibrations of thin elastic shells freely suspended in a compressible fluid medium. The effect of the fluid reaction on the dynamic characteristics and, in particular, on the natural frequencies is investigated for cylindrical and spherical shells. The dynamic configuration of such shells undergoing forced vibration and the associated radiation of sound are determined. The problem is analyzed by means of the classical methods of the theory of mechanical vibrations; the Lagrange equations for the system are derived, the fluid reaction being introduced in the form of generalized forces. From the boundary condition that the normal shell deflection be equal to the normal fluid-particle displacement at the shell surface, and introducing the concept of acoustic impedance, it is shown that the fluid reaction is equivalent to an accession to the inertia of the shell and to a damping force. Numerical examples show that the effect of the fluid reaction on the dynamic characteristics of a shell may be of such magnitude as to render valueless calculations neglecting it.

Nomenclature

The following nomenclature is used in the paper:

- a = radius of shell
- c = velocity of sound in fluid medium
- E = Young's modulus
- h = half-thickness of shell
- j = $-\sqrt{-1}$
- k = wave number (ω/c)
- n = integer
- Q_n = generalized force
- r = radial distance in cylindrical and spherical systems
- t = time
- T = kinetic energy
- V = potential energy
- x = ka
- δ = radial displacement of shell surface
- ϵ_n = Neumann factor, equal to 1 for $n = 0$, and to 2 for $n \neq 0$
- ϵ_ϕ = normal strain in ϕ-direction in cylindrical and spherical systems
- ϵ_θ = normal strain in θ-direction in spherical system
- θ = spherical co-ordinate, Fig. 2
- ν = Poisson's ratio
- ρ = density of fluid medium
- ρ_s = density of shell material
- τ = tangential displacement of shell surface
- ϕ = cylindrical or spherical co-ordinate, Figs. 1 and 2
- χ_ϕ = change in curvature
- ω = frequency

Introduction

The dynamic characteristics of elastic structures vibrating in a fluid medium may differ considerably from their characteristics in vacuo. This is particularly true of structures having large areas of contact with the surrounding fluid, such as plates and shells. An analytical investigation of the latter is of practical interest, particularly in the domain of naval architecture. Such an analysis is presented here for the case of shells of cylindrical and spherical shape. The dynamic characteristics of the submerged shells are determined and compared with the corresponding characteristics in vacuo. Behavior of these shells under steady-state conditions is also studied.

The problem presents itself as follows: A thin elastic shell freely suspended in a compressible fluid medium is excited by a variable internal force. The resulting vibrations cause sound to be radiated from the shell. Connected with this sound radiation there is a reaction of the fluid on the shell; this fluid reaction, which is equivalent to a damping force and to an accession to the inertia of the shell, alters the dynamic characteristics of the system. It is assumed that the dynamic deflections and the thickness of the shell are small compared to its other dimensions and that it is composed of an isotropic material devoid of damping and obeying Hooke's law. The fluid medium satisfies the conditions for the validity of the simplified wave equation, viz., the absence of viscous forces.

Previous related studies in the field of mechanical vibrations were concerned with the free vibrations of thin, infinite, cylindrical and spherical shells in vacuo. Lord Rayleigh (1)[3] gives approximate solutions for purely flexural vibrations of cylindrical shells by assuming no extension of the middle surface. Rayleigh (2) also contributed an approximate treatment of extensional vibrations of cylindrical shells based on the assumption that the potential energy associated with bending of the shell is negligible when compared with the extensional energy. The chapter in reference (3)[4] dealing with shells is based largely on these two papers. Lamb (4), starting from the equations of static equilibrium of an element of cylindrical shell, derived an expression for the natural frequencies, taking into account the combined effect of both bending and extension of the middle surface. Lamb (5) also pro-

---

[1] This paper draws from a thesis submitted to the Faculty of Harvard University in partial fulfillment of the requirements for the degree of Doctor of Science. This research has been aided by funds made available under a contract with the ONR, and under a Gordon McKay Scholarship.

[2] Research Fellow in Acoustics, Department of Engineering Sciences and Applied Physics, Harvard University. Jun. ASME.

Presented at the National Conference of the Applied Mechanics Division, State College, Pa., June 19–21, 1952, of The American Society of Mechanical Engineers.

Discussion of this paper should be addressed to the Secretary, ASME, 29 West 39th Street, New York, N. Y., and will be accepted until January 10, 1953, for publication at a later date. Discussion received after the closing date will be returned.

Note: Statements and opinions advanced in papers are to be understood as individual expressions of their authors and not those of the Society. Manuscript received by ASME Applied Mechanics Division on November 19, 1951. Paper No. 52—APM-28.

[3] Numbers in parentheses refer to the Bibliography at the end of the paper.

[4] Vol. I, chapter Xa.

duced the first complete analysis of the vibrations of the spherical shell. A general survey of the subject is given by Love (6),[6] (7).

The present analysis of the cylindrical shell, which takes into account the combined effect of bending and extension, shows a slight discrepancy with Lamb's results (4). Lamb's two simultaneous equations of motion, which give consideration to the effect of shearing forces, display a peculiar assymmetry; i.e., the coupling terms are different in the two equations, while the corresponding homogeneous Lagrange equations in this analysis display the usual symmetry. The quantitative difference between the two solutions is of higher order and therefore of little significance. For limiting cases, both solutions give the value of natural frequencies obtained from Rayleigh's two approximate analyses (1), (2)—the first assuming purely flexural vibrations, the second purely extensional vibrations.

While the problem under consideration might be solved more elegantly by some other approach, the classical method of Lagrange equations is used because it can be extended conveniently to more complex, nonhomogeneous structures, such as shells provided with stiffeners.

The theory of sound radiation from cylindrical and spherical surfaces is used to deal with the acoustical aspects of the problem under consideration. This theory was introduced by Stokes (8) and developed by Rayleigh (3).[6] It was found convenient to borrow, from the terminology of acoustics, the concept of acoustic impedance to express the reaction of the fluid medium. The application of this concept to the vibrations of an elastic surface in a fluid medium has been confined generally to the case of plates and membranes (9),[7] (10). A procedure akin to the one here used was applied to the problem of scattering of a sound wave by elastic shells (11).

Dynamic Characteristics of Cylindrical Shells

Consider a cylindrical shell of infinite length as shown in Fig. 1. The exciting disturbance, which is independent of z and symmetrical with respect to the ($\phi = 0$) axis, exerts its action normally to the shell surface. The resulting dynamic configuration of the shell is two-dimensional (1), (2), (3),[8] and can be expressed in terms of two Fourier series

$$\left.\begin{aligned} \delta &= \sum_{n=0}^{\infty} a_n \cos n\phi \\ \tau &= \sum_{n=1}^{\infty} b_n \sin n\phi \end{aligned}\right\} \quad \ldots\ldots\ldots\ldots\ldots\ldots [1]$$

The generalized co-ordinates a_n and b_n must satisfy the Lagrange equations of the system. These equations form two sets; one, nonhomogeneous, in a_n; the other homogeneous, in b_n

$$\left.\begin{aligned} \frac{d}{dt}\frac{\partial T}{\partial \dot{a}_n} - \frac{\partial T}{\partial a_n} + \frac{\partial V}{\partial a_n} &= Q_n \\ \frac{d}{dt}\frac{\partial T}{\partial \dot{b}_n} - \frac{\partial T}{\partial b_n} + \frac{\partial V}{\partial b_n} &= 0 \end{aligned}\right\} \quad \ldots\ldots\ldots\ldots [2]$$

The quantities required for these equations will now be evaluated for a unit length of shell. The kinetic energy is the integral

$$T = a\lambda\rho_s \int_0^{2\pi} (\dot{\delta}^2 + \dot{\tau}^2) d\phi \ldots\ldots\ldots\ldots [3]$$

which can be expressed in terms of the generalized velocities $\dot{a}_n$ and $\dot{b}_n$ after substitution of the Fourier series [1].

The potential energy per unit area of thin shell (6)[9] is the sum of two terms, one representing the energy connected with extension in the middle surface, the other with change in curvature of the shell. Integrating this expression over the shell area, the potential energy takes the following form

$$V = \frac{Eha}{1-\nu^2} \int_0^{2\pi} \epsilon_\phi^2 d\phi + \frac{Eh^3 a}{3(1-\nu^2)} \int_0^{2\pi} \chi_\phi^2 d\phi \ldots [4]$$

The circumferential strain ϵ_ϕ and the change of curvature χ_ϕ may be expressed in terms of the displacements δ and τ (6),[10] and hence of the Fourier series [1]. Substituting the resulting series in the integral Equation [4], and integrating, an expression for the potential energy is obtained in terms of the generalized co-ordinates a_n and b_n.

The generalized force of order n on the cylindrical shell is evaluated by calculating the virtual work connected with an increment of the generalized co-ordinate a_n, and dividing this work by the increment. It may be verified that the generalized force associated with the sound pressure p in the fluid medium is

$$Q_n = -a \int_0^{2\pi} (p)_a \cos n\phi \, d\phi \ldots\ldots\ldots [5]$$

The fluid medium being nonviscous, tangential displacement of the shell surface does not give rise to any work by the fluid. It also may be assumed, for small deflections and changes in curvature, that the normal to the shell differs little from the radial direction. Under these conditions no generalized forces are associated with the b_n co-ordinates.

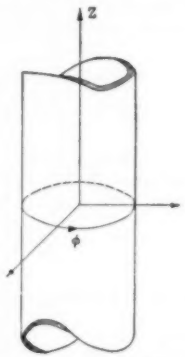

Fig. 1 Orientation of System of Cylindrical Co-Ordinates

The radiated sound pressure p is of the form of a solution of the cylindrical wave equation for an outgoing wave (9),[11] (12), i.e., of a series of products of trigonometric functions and of Hankel functions $H_n^{(2)}(kr)$ of the second kind. It is convenient to express these functions, and their derivatives, in terms of their magnitudes and phase angles in the complex plane

$$\left.\begin{aligned} H_n^{(2)}(y) &= J_n(y) - jN_n(y) = jC_n(y)e^{-j\beta_n(y)} \\ \frac{d}{dy}H_n^{(2)}(y) &= \frac{d}{dy}[J_n(y) - jN_n(y)] = -jC_n'(y)e^{-j\beta_n'(y)} \end{aligned}\right\} \ldots [6]$$

[6] Chapter XXIV.
[6] Vol. II, Chapters XVII and XVIII.
[7] Section V. 19–21.
[8] Vol. I, chapter Xa.
[9] See p. 530.
[10] See page 543.
[11] Section VII. 26.

The quantities C_n, C_n', δ_n, and δ_n' are tabulated in the "Scattering Tables" (12). Introducing these definitions, the radiated sound pressure now takes the form

$$p = j \sum_{n=0}^{\infty} c_n C_n(kr) e^{-j\delta_n(kr)} \cos n\phi \quad \ldots\ldots\ldots [7]$$

The undetermined coefficients c_n are related to the generalized co-ordinates a_n by the boundary condition that the radial displacement δ of the shell surface be equal to the radial component $(u)_a$ of the fluid-particle displacement at the boundary between fluid and shell. A relation between the radial component u of the fluid-particle displacement and the sound pressure p may be derived from Newton's second law (9)[12]

$$u = \frac{1}{\rho\omega^2} \frac{\partial p}{\partial r} \quad \ldots\ldots\ldots [8]$$

Calculating this quantity at $r = a$ by means of Equation [7], and equating the resulting series term by term to the Fourier series [1] for δ, the boundary conditions stated previously now take the form of a relation between the pressure coefficients c_n and the generalized co-ordinates a_n, or, assuming the latter to be proportional to $e^{j\omega t}$, the generalized velocities $\dot{a}_n = j\omega a_n$. Substituting these expressions for c_n, the sound pressure is finally written in terms of products of acoustic impedances and generalized velocities

$$p = \rho c \sum_{n=0}^{\infty} \zeta_n(kr) \dot{a}_n \cos n\phi \quad \ldots\ldots\ldots [9]$$

The acoustic impedance ratios $\zeta_n(kr)$ are defined by

$$\zeta_n(kr) = j \frac{C_n(kr)}{C_n'(x)} e^{-j[\delta_n(kr) - \delta_n'(x)]} \quad \ldots\ldots\ldots [10]$$

It is convenient to consider these complex quantities to be the sum of a real and of an imaginary term, respectively, the acoustic resistance and reactance ratios

$$\zeta_n(kr) = \theta_n(kr) + j\chi_n(kr) \quad \ldots\ldots\ldots [11]$$

$\chi_n(x)$ and $\theta_n(x)$ were plotted for values of n from 0 to 20, for the range from $x = 0$ to $x = 10$ (13).

Using Equations [9] to [11], the Integral [5] can now be evaluated and the generalized force Q_n written as the sum of a reactive and a resistive term

$$Q_n = -\frac{2\pi a \rho c}{\epsilon_n} \left[\frac{\chi_n(x)}{\omega} \ddot{a}_n + \theta_n(x) \dot{a}_n \right] \quad \ldots\ldots [12]$$

Substituting the proper derivatives of the energies, Equations [3] and [4], and the generalized forces, Equation [12], and transferring the forces to the left side of the equations, the Lagrange Equations [2] become

$$\left.\begin{aligned} &\frac{2\pi a}{\epsilon_n}\left[2h\rho_s + \frac{\rho}{k}\chi_n(x)\right]\ddot{a}_n + \left[\frac{2\pi a}{\epsilon_n}\rho c\theta_n(x)\right]\dot{a}_n \\ &+ \frac{4\pi E}{\epsilon_n(1-\mu^2)}\frac{h}{a}\left\{\left[1 + \frac{n^4}{3}\left(\frac{h}{a}\right)^2\right]a_n + n\left[1 + \frac{n^2}{3}\left(\frac{h}{a}\right)^2\right]b_n\right\} = 0 \\ &2\pi a h \rho_s \ddot{b}_n + \frac{2\pi E}{1-\mu^2}\left(\frac{h}{a}\right) n\left\{\left[1 + \frac{1}{3}\left(\frac{h}{a}\right)^2 n^2\right]a_n + n\left[1 + \frac{1}{3}\left(\frac{h}{a}\right)^2\right]b_n\right\} = 0 \end{aligned}\right\} \quad \ldots [13]$$

Each value of n larger than zero represents two coupled modes having loaded natural frequencies p_{n1} and p_{n2}, respectively. These frequencies are smaller than the corresponding frequencies of the shell vibrating in vacuo because of the damping effect and the accession to inertia. They are obtained from the characteristic equation of order n

$$\Delta(s_n^2) = 0 \quad \ldots\ldots\ldots [14]$$

where $\Delta(s_n^2)$ is the determinant of Equations [13] after substitution therein of solutions of the form $Ae^{s_n t}$. This fourth-degree equation admits roots of the form

$$\left.\begin{aligned} s_{n1} &= -n_{n1} \pm jp_{n1} \\ s_{n2} &= -n_{n2} \pm jp_{n2} \end{aligned}\right\} \quad \ldots\ldots\ldots [15]$$

where $n_{n1,2}$ and $p_{n1,2}$ are real numbers. The former is a measure of damping; the latter is the damped natural frequency of oscillation of the system.

Setting $n = 0$ in the Lagrange Equations [13], the second equation vanishes. The corresponding mode, which is a uniform radial pulsation of the shell, is therefore uncoupled.

The analysis presented in the foregoing takes into account coupling between extensional and flexural deformations. An approximate solution may be derived by neglecting extension entirely (3).[13] The condition that the middle surface undergo no extension then takes the place of the second set of Lagrange equations.

This condition is purely geometrical and therefore independent of frequency. The characteristic equations are thus quadratic, so that only one natural frequency is found for every value of n. This frequency corresponds to the smaller of the two roots of the characteristic Equation [14]. The accuracy of the approximate solution improves with decreasing values of p_n, i.e., of (h/a).

Forced Vibrations of Cylindrical Shells and Associated Radiation of Sound

It is now assumed that the shell is undergoing steady vibrations under the effect of a radial exciting force acting along the cylindrical generator located at $\phi = 0$. The force has a magnitude $fe^{j\omega t}$ per unit length. The corresponding generalized forces are all equal to $fe^{j\omega t}$. The introduction of the radial exciting force leaves the second of the Lagrange Equations [13] unchanged but renders the first equation (in a_n) nonhomogeneous, the term $fe^{j\omega t}$ appearing on its right side.

The particular solution of the resulting set of differential equations is expressed conveniently in terms of loaded mechanical impedances

$$Z_{nl} = Z_n + \rho c \zeta_n(x) \quad \ldots\ldots\ldots [16]$$

where the acoustic impedance ratios $\zeta_n(x)$ are defined by Equation [10], and where Z_n, the mechanical impedances of the shell vibrating in vacuo, are

[12] See p. 295.

[13] Vol. I, section 235.

$$Z_n = j\frac{2h}{\omega}\left\{\rho_s\omega^2 - \frac{E}{(1-\nu^2)a^2}\left[1+\frac{n^4}{3}\left(\frac{h}{a}\right)^2 + \frac{n^2\left[1+\frac{n^2}{3}\left(\frac{h}{a}\right)^2\right]^2}{\frac{\omega^2a^2\rho_s(1-\nu^2)}{E} - n^2\left[1+\frac{1}{3}\left(\frac{h}{a}\right)^2\right]}\right]\right\} \quad [17]$$

The particular solutions of the Lagrange equations may now be written in terms of Z_{ni}; substitution of these solutions in the series [1] yields expressions for the dynamic deflections

$$\left.\begin{aligned}\delta &= \frac{fe^{j\omega t}}{2j\pi a\omega}\sum_{n=0}^{\infty}\frac{\epsilon_n}{Z_{ni}}\cos n\phi \\ \tau &= \frac{fe^{j\omega t}}{j\pi a\omega}\sum_{n=1}^{\infty}\frac{n\left[1+\frac{n^2}{3}\left(\frac{h}{a}\right)^2\right]\sin n\phi}{Z_{ni}\left\{\frac{\omega^2a^2\rho_s(1-\nu^2)}{E} - n^2\left[1+\frac{1}{3}\left(\frac{h}{a}\right)^2\right]\right\}}\end{aligned}\right\} \quad [18]$$

Because the differential equations are linear, several solutions can be superimposed. Taking $f = 1$, the response to a unit harmonic force is obtained. Solution [18] can thus be used to calculate the response to an arbitrary distribution of normal harmonic forces, viz., bending moments. The same remark applies to the expression for the radiated wave pressure about to be given.

The sound pressure of the radiated wave is obtained by substituting in the series [9] the particular solution of the non-homogeneous Lagrange equations

$$p = \frac{\rho cfe^{j\omega t}}{2\pi a}\sum_{n=0}^{\infty}\frac{\epsilon_n\zeta_n(kr)}{Z_{ni}}\cos n\phi \quad [19]$$

The power of radiated sound is

$$P = \frac{\rho cf^2}{4\pi a}\sum_{n=0}^{\infty}\frac{\epsilon_n\theta_n(x)}{|Z_n| + \rho c\chi_n(x)|^2 + [\rho c\theta_n(x)]^2} \quad [20]$$

Dynamic Characteristics of Spherical Shells

Let us now turn to the case of the spherical shell in Fig. 2. The system of co-ordinates is rotated so that the exciting disturbance acts at the pole ($\theta = 0$), in a radial direction. The assumed solutions must be independent of ϕ and correspond to shell vibrations involving a radial displacement. According to Lamb's study of the free vibrations of spherical shells (5), these requirements are fulfilled by two coupled modes: A radial mode whose amplitude is of the form of a zonal surface harmonic $P_n(\cos\theta)$, i.e., of a Legendre polynomial of argument $\cos\theta$; and a tangential mode oriented in the θ-direction whose amplitude is of the form

$$\frac{d}{d\theta}P_n(\cos\theta) = -P_n^1(\cos\theta)$$

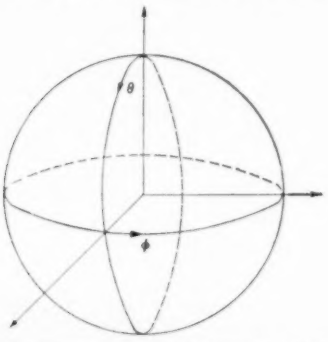

Fig. 2 Orientation of System of Spherical Co-Ordinates

The deflections may be written in the form of two series of such solutions

$$\left.\begin{aligned}\delta &= \sum_{n=0}^{\infty}a_nP_n(\cos\theta) \\ \tau &= -\sum_{n=1}^{\infty}b_nP_n^1(\cos\theta)\end{aligned}\right\} \quad [21]$$

The terms of the series form a complete orthogonal set (14)[14] and therefore may be used to represent an arbitrary configuration of the shell.

The analysis proceeds exactly as in the cylindrical case and hence will be carried through in somewhat less detail. The Lagrange equations are of the form of Equations [2]. The kinetic energy is again expressed in terms of $\dot{a}_n$ and $\dot{b}_n$. The procedure in obtaining the potential energy is, however, somewhat different from the cylindrical case; there the deformation tends to be mainly flexural, the extension of the middle surface becoming important only at high frequencies. This, however, is not true in the case of the complete spherical shell. A theorem derived by Jellett (15)[15] states: "The most general displacement which a closed, oval, inextensible surface admits, is that of a rigid body. Such a surface is therefore inextensible." In other words, a closed surface cannot be bent without stretching. The potential energy of a deformed spherical shell thus may be expressed without regard for changes in curvature

$$V = \frac{2\pi Eha^2}{1-\nu^2}\int_0^{\pi}[(\epsilon_\theta + \epsilon_\phi)^2 - 2(1-\nu)\epsilon_\theta\epsilon_\phi]\sin\theta d\theta \quad [22]$$

Relating the normal strains to the deflections (6),[16] the potential energy again may be expressed as a function of the generalized co-ordinates a_n and b_n.

The generalized forces are calculated as in the cylindrical case in terms of the radiated sound pressure. This function is of the form of a solution of the spherical wave equation for an outgoing wave, i.e., a series of products of zonal surface harmonics and of spherical Hankel functions $h_n^{(2)}(kr)$, (9),[17] (12). These functions and their derivatives may be expressed in terms of definitions in Equations [6], provided spherical Bessel and Neumann functions $j_n(kr)$ and $n_n(kr)$ are used in lieu of the corresponding cylindrical functions. Introducing these definitions and using, as in the cylindrical case, the boundary condition $\delta = (u)_a$ to correlate the undetermined pressure coefficients c_n and the generalized co-ordinates a_n, the pressure of radiated sound is again expressed in terms of acoustic impedance ratios and generalized velocities $\dot{a}_n$

$$p = \rho c\sum_{n=0}^{\infty}\zeta_n(kr)\dot{a}_nP_n(\cos\theta) \quad [23]$$

The impedance ratios $\zeta_n(kr)$ coincide formally with expression

[14] See p. 116.
[15] See p. 377.
[16] See p. 56.
[17] See Section VII. 27.

[10]. The corresponding reactance and resistance ratios $\chi_n(x)$ and $\theta_n(x)$ were plotted for a range of values of x and n (13). The generalized forces corresponding to Equation [23] are

$$Q_n = -\frac{4\pi a^2 \rho c}{2n+1}\left[\frac{\chi_n(x)}{\omega}\dot{a}_n + \theta_n(x)a_n\right] \quad \ldots\ldots [24]$$

The Lagrange Equations [2] can now be formed

$$\left.\begin{aligned}&\frac{4\pi a^2}{2n+1}\left[2h\rho_s + \frac{\rho}{k}\chi_n(x)\right]\ddot{a}_n + \left[\frac{4\pi a^2 \rho c}{2n+1}\theta_n(x)\right]\dot{a}_n \\ &\qquad + \frac{8\pi E h}{(1-\nu)(2n+1)}\left[2a_n - (n+1)nb_n\right] = 0 \\ &8\pi a^2 h\rho_s \frac{n(n+1)}{2n+1}\ddot{b}_n + \frac{4\pi E h}{1-\nu}\frac{2n(n+1)}{2n+1}\left[-a_n + \frac{n(n+1)-(1-\nu)}{1+\nu}b_n\right] = 0\end{aligned}\right\} \ldots [25]$$

As in the case of the cylindrical shell, the Lagrange Equations [25] show that the reaction of the fluid medium is equivalent to an accession to the inertia of the shell and to a damping force.

The characteristic equation is of the form of Equation [14] where $\Delta(s_n^2)$ is the determinant of Equations [25], after substitution of solutions proportional to $e^{s_n t}$. This determinant admits two roots of the form of Equation [15] for every value of $n > 0$. As in the cylindrical case, $n = 0$ corresponds to an uncoupled mode.

Forced Vibrations of Spherical Shells and the Associated Radiation of Sound

Now the case of forced vibrations will be considered. These vibrations are excited by a radial harmonic force $fe^{j\omega t}$ applied at the pole ($\theta = 0$). The corresponding Lagrange equations differ from Equations [25] only in that the term $fe^{j\omega t}$ appears on the right side of the equations in a_n. The particular solution to these equations will again be expressed in terms of loaded mechanical impedances of the form of Equation [16]; the mechanical impedance Z_n of a shell vibrating in vacuo at the mode n is given by

$$Z_n = j\frac{2h}{\omega}\left\{\rho_s\omega^2 - \frac{E}{(1-\nu)a^2}\left[2 - \frac{1+\nu}{1-\frac{1-\nu}{n(n+1)}\left[\frac{\omega^2\rho_s(1+\nu)a^2}{E}+1\right]}\right]\right\} \ldots [26]$$

Substituting the particular solution of the nonhomogeneous Lagrange equations in the series [21], expressions for the dynamic deflections are obtained

$$\left.\begin{aligned}\delta &= \frac{fe^{j\omega t}}{4j\pi a^2\omega}\sum_{n=0}^{\infty}\frac{2n+1}{Z_{nl}}P_n(\cos\theta) \\ \tau &= -\frac{(1+\nu)fe^{j\omega t}}{4j\pi a^2\omega}\sum_{n=1}^{\infty}\frac{(2n+1)P_n^1(\cos\theta)}{Z_{nl}\left[n(n+1) - \frac{\omega^2 a^2\rho_s(1-\nu^2)}{E} - (1-\nu)\right]}\end{aligned}\right\} \ldots [27]$$

As in the case of the cylindrical shell, the linearity of the differential equations permits superposition of the particular solutions.

Substituting the particular solutions for $\dot{a}_n$ in the series [23], the pressure of radiated sound is obtained

$$p = \frac{\rho c f e^{j\omega t}}{4\pi a^2}\sum_{n=0}^{\infty}\frac{(2n+1)\zeta_n(kr)}{Z_{nl}}P_n(\cos\theta) \quad \ldots\ldots [28]$$

The corresponding power of sound is

$$P = \frac{\rho c f^2}{8\pi a^2}\sum_{n=0}^{\infty}\frac{(2n+1)\theta_n(x)}{[|Z_n| + \rho c\chi_n(x)]^2 + [\rho c\theta_n(x)]^2} \quad \ldots\ldots [29]$$

Numerical Illustration

The solution for the cylindrical shell will be illustrated by a numerical example. The shell has a radius $a = 300$ cm and a thickness to radius ratio $(2h/a) = 1/10$. It is made of steel, having a Young's modulus E of 19×10^{11} g/cm sec^2, a Poisson's ratio ν of 0.27, and a density ρ_s of 7.7 g/cm^3. The fluid medium is water whose density ρ is 1.0 g/cm^3, and whose sound velocity c is 146,000 cm/sec.

The effect of the fluid reaction on the dynamic characteristics of the shell is studied first. The block diagram in Fig. 3 demonstrates the effect of the fluid reaction on the natural frequencies of the system.

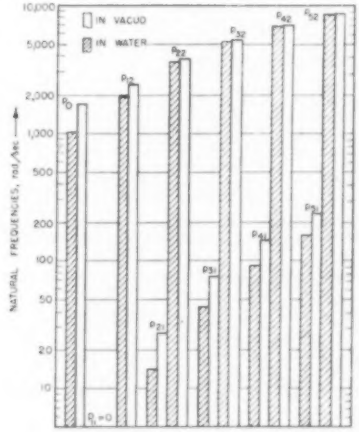

Fig. 3 Natural Frequencies p_{n1} and p_{n2} of a Cylindrical Shell in Vacuo and in Water

The damping ratios $\zeta_{n1,2} = n_{n1,2}\sqrt{p_{n1,2}^2 + n_{n1,2}^2}$ are a measure of relative damping of modes (n1, 2) of free vibration, and are associated with the resistive component of the fluid reaction. Damping ratios for certain values of n are given in the block diagram in Fig. 4.

The reactive component of the fluid reaction is equivalent to an accession to the inertia of the shell. Its relative importance is best illustrated by taking the ratio $\tau_{n1,2}$ of the increment of

kinetic energy owing to the fluid reaction and of the kinetic energy associated with the shell material, for a given mode of free vibration. These ratios are plotted in the block diagram in Fig. 5.

Turning now to forced vibrations, the radial deflection δ and the absolute value of the radiated sound pressure p are calculated for an exciting force of unit amplitude $f = 1$. The polar diagrams of these quantities are presented in Fig. 6 for a frequency corresponding to $x = 0.1$. Owing to a condition of mild resonance, the $n = 3$ mode is predominant.

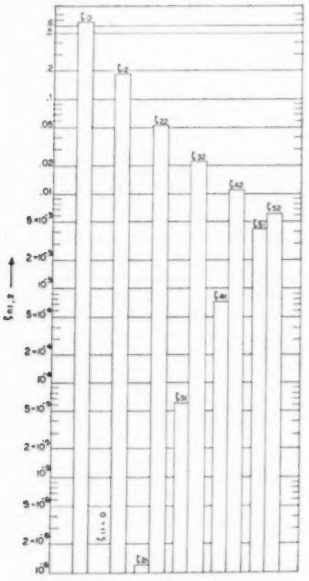

FIG. 4 DAMPING RATIOS $\zeta_{n1,2} = \pi_{n1,2}/\sqrt{p^2_{n1,2} + \pi^2_{n1,2}}$ OF A SUBMERGED CYLINDRICAL SHELL FOR CERTAIN MODES OF FREE VIBRATION

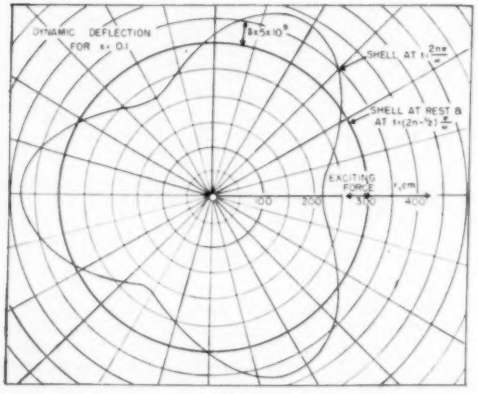

(a)

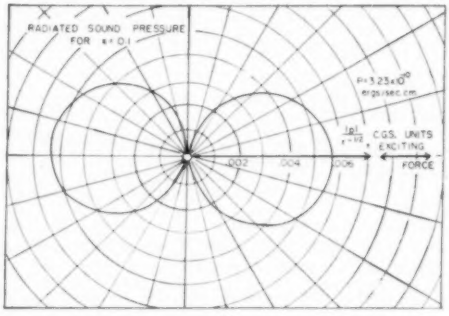

(b)

FIG. 6 POLAR DIAGRAMS OF AMPLITUDES OF DYNAMIC RADIAL DEFLECTION δ AND OF PRESSURE OF RADIATED SOUND p FOR A CYLINDRICAL SHELL EXCITED BY A HARMONIC FORCE OF AMPLITUDE $f = 1$, AND FREQUENCY $\omega = 48.7$ RADIANS PER SEC, $x = 0.1$

DISCUSSION

The effect of the fluid medium is primarily to cause a decrease of the natural frequencies; this decrease may be of the order of 50 per cent. At low frequencies, it is due mainly to the added inertia, and at high frequencies to the damping action. The acoustic reactance ratio $\chi_n(x)$ rises from zero to a maximum and again tends to zero as x increases from zero to infinity. The acoustic resistance ratio $\theta_n(x)$ rises from zero to a maximum, and then tends to a steady value of unity (13). The vanishing of the inertial effect at high frequencies may be interpreted as follows: Under these conditions, the shell surface oscillates with such rapidity that the disturbance does not spread far before the action is reversed; in other words, a low-frequency vibration tends to accelerate large quantities of fluid, while a high-frequency vibration compresses a small amount of fluid.

For predominantly extensional modes, i.e., p_{n2}-modes, and in

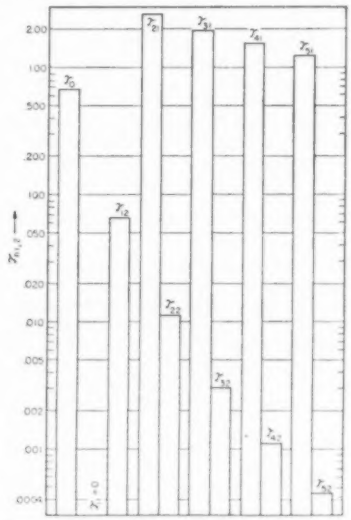

FIG. 5 RELATIVE INCREASE $\tau_{n1,2}$ OF KINETIC ENERGY OF A SUBMERGED CYLINDRICAL SHELL OWING TO FLUID REACTION FOR CERTAIN MODES OF FREE VIBRATION

particular, for the p_0-mode, the relative damping may be very large and approach a condition of critical damping, even though the fluid medium is nonviscous. For the low-frequency p_{s1}-modes, the relative damping provided by the resistive impedance is usually very small. Thus extreme resonance phenomena may be observed. A feature typical of such systems is that a small variation of the disturbing frequency may cause a considerable change in the amplitude of response of the system. In practice, of course, an actual structure provides its own damping, especially at resonance, when the inertia forces are large enough to overcome the static friction between metal surfaces; Coulomb damping is probably a more important factor in the dissipation of energy than the solid friction inherent in the metal or than the viscosity of the water. Unfortunately, information on this subject is very incomplete.

A few comments should be made about the natural frequencies of the system. The lower frequency (p_{s1})-mode corresponding to $n = 1$ represents a back-and-forth movement of the shell as a rigid body. Since no elastic forces are connected with such a condition, the corresponding natural frequency is zero. It also should be mentioned that the natural frequencies of a submerged shell may not be determined directly, but only through successive approximations. This difficulty arises from the fact that the reactive and resistive terms are themselves functions of x, i.e., of the frequency. Thus the characteristic equations are not, strictly speaking, equations with constant coefficients; however, the convergence of the calculation is usually rapid.

A development of the present investigation, which may lead to results of practical interest, is the study of more complicated shells, such asshel ls stiffened by periodically spaced rings.[18] Such an investigation is under way. The practical interest of these analyses also could be increased by not considering forces of a given amplitude acting directly on the shell, but assuming the transmission of disturbing forces through intermediary elastic members such as mounting brackets and vibration isolators. The parameters of these intermediary members then could be adjusted so as to obtain the desired dynamic characteristics for the system as a whole.

[18] Since the manuscript was submitted, the Lagrange equations have been derived for cylindrical shells provided with elastic stiffening rings, rigid septa, longitudinal stiffeners, and certain distributions of dead load. Numerical calculations are under way to determine the corresponding natural frequencies. Investigation of the sound field generated by a vibrating cylindrical shell with periodically spaced rigid septa (16) indicates: 1, that no sound energy will be radiated by certain modes of vibration, the fluid impedance being purely reactive; and 2, that the amplitudes of certain modes of vibration vanish at certain frequencies, the reactive impedance of the fluid medium being infinite; the action of this medium may then be likened to that of the familiar "dynamic vibration absorber" (17).

ACKNOWLEDGMENTS

The author wishes to extend his grateful appreciation to Professor F. E. Richart, Jr., Faculty of Arts and Sciences, Harvard University; to Dr. A. I. Bellin, Office of Naval Research, formerly Faculty of Arts and Sciences, Harvard University; and to Dr. J. J. Faran, Jr., Acoustics Research Laboratory, Harvard University, for their assistance in analyzing this problem; to Mr. C. E. Crede, Chief Engineer, The Barry Corporation, Watertown, Mass., for suggesting it and pointing out its practical interest; and to Mrs. E. Bockelman, for doing the numerical work.

BIBLIOGRAPHY

1 "On the Bending and Vibrations of Thin, Elastic Shells, Especially of Cylindrical Form," by Lord Rayleigh, Proceedings of the Royal Society of London, vol. 45, 1888, p. 105.

2 "Note on the Free Vibrations of an Infinitely Long Cylindrical Shell," by Lord Rayleigh, Proceedings of the Royal Society of London, vol. 45, 1888, p. 443.

3 "The Theory of Sound," by Lord Rayleigh, Dover Publications New York, N. Y., 1945.

4 "On the Deformation of an Elastic Shell," by H. Lamb, Proceedings of the London Mathematical Society, vol. 21, 1890, p. 119.

5 "On the Vibrations of a Spherical Shell," by H. Lamb, Proceedings of the London Mathematical Society, vol. 14, 1883, p. 50.

6 "A Treatise on the Mathematical Theory of Elasticity," by A. E. H. Love, Dover Publications, New York, N. Y., 1944.

7 "On the Small, Free Vibrations and Deformations of a Thin, Elastic Shell," by A. E. H. Love, Philosophical Transactions of the Royal Society, vol. 179, 1888, p. 520.

8 "On the Communication of Vibration From a Vibrating Body to a Surrounding Gas," by G. G. Stokes, Philosophical Transactions of the Royal Society, vol. 158, 1868, p. 447.

9 "Vibration and Sound," by P. M. Morse, McGraw-Hill Book Company, Inc., New York, N. Y., 1948.

10 "The Effect of Radiation on the Vibrations of a Circular Diaphragm," by M. Lax, *Journal of the Acoustical Society of America*, vol. 16, no. 1, 1944, p. 5.

11 "Sound Scattering by Thin Elastic Shells," by M. C. Junger, *Journal of the Acoustical Society of America*, vol. 24, July, 1952, p. 366.

12 "Scattering and Radiation From Circular Cylinders and Spheres," Mathematical Tables Project and M.I.T. Underwater Sound Laboratory, U. S. Navy Department, Office of Research and Inventions, Washington, D. C., 1946.

13 "Radiation Loading of Cylindrical and Spherical Surfaces," by M. C. Junger, *Journal of the Acoustical Society of America*, vol. 24, May, 1952, p. 288.

14 "Table of Functions," by E. Jahnke and F. Emde, McGraw-Hill Book Company, Inc., New York, N. Y., 1940.

15 "On the Properties of Inextensible Surfaces," by J. H. Jellett, Royal Irish Academy Transactions, vol. 22, part V, 1855, p. 343.

16 "The Physical Interpretation of the Expression for an Outgoing Wave in Cylindrical Coordinates," by M. C. Junger, *Journal of the Acoustical Society of America*, vol. 25, January, 1953.

17 "Vibration Problems in Engineering," by S. Timoshenko, second edition, D. Van Nostrand Co., New York, N. Y., 1947, pp. 240–252.

Large Deflection Theory for Orthotropic Rectangular Plates Subjected to Edge Compression[1]

By SYED YUSUFF,[2] BROOKLYN, N. Y.

A theory is presented of the large deflections of orthotropic (orthogonally anisotropic) rectangular plates when the plate is initially slightly curved and its boundaries are subjected to the conditions prevailing in edgewise compression tests. Results are given of computations carried out for four different combinations of load and lamination in Fiberglas panels. These theoretical results duplicate the substantial variations in the load-strain and load-deflection diagrams obtained earlier in experiments at the Polytechnic Institute of Brooklyn.

Introduction

An experimental investigation of the buckling loads and the postbuckling behavior of rectangular Fiberglas panels carried out at the Polytechnic Institute of Brooklyn (1)[3] disclosed substantial differences in the load-deflection and load-strain diagrams when the directions of lamination and loading were varied. As cross-laminated panels loaded in one of the grain directions can be assumed to behave approximately as isotropic panels, a theoretical investigation (2) was initiated in which the large deflections of initially slightly curved isotropic panels were analyzed.

This analysis, undertaken by Coan (2), was based on earlier work by Levy (3) as well as by Hu, Lundquist, and Batdorf (4) and took the boundary conditions along the unloaded edges more accurately into account than was done before. The results of the analysis compared well with the tests and led to suggestions regarding the evaluation of experimental data.

In the present paper this work is carried further through an analysis of plates that are orthogonally anisotropic. The results duplicate the load-deflection and load-strain diagrams of the experimental investigation, as can be seen from the diagrams given. In order to save space, only the most important equations are presented here and for many details omitted reference is made to similar parts of Coan's paper (2).

[1] This paper is based on a dissertation submitted to the Polytechnic Institute of Brooklyn in partial fulfillment of the requirements for the degree of Doctor of Aeronautical Engineering.

[2] Lecturer in Physics, University of Mysore, on leave of absence for advanced studies sponsored by the Government of Mysore, India. Now Stress Analyst, The Bristol Aeroplane Company, Ltd., Bristol, England.

[3] Numbers in parentheses refer to the Bibliography at the end of the paper.

Presented at the National Conference of the Applied Mechanics Division, State College, Pa., June 19-21, 1952, of The American Society of Mechanical Engineers.

Discussion of this paper should be addressed to the Secretary, ASME, 29 West 39th Street, New York, N. Y., and will be accepted until January 10, 1953, for publication at a later date. Discussion received after the closing date will be returned.

Note: Statements and opinions advanced in papers are to be understood as individual expressions of their authors and not those of the Society. Manuscript received by ASME Applied Mechanics Division on August 2, 1951. Paper No. 52—APM-38.

Orthotropic Plates With Edges Remaining Straight Under Loads

When von Kármán's derivation (5) is modified to take into account the anisotropic properties of the plate, and the plate is assumed to have initial deflections w_0, the following two equations are obtained (6)

$$D_1\frac{\partial^4(w-w_0)}{\partial x^4}+2D_3\frac{\partial^4(w-w_0)}{\partial x^2\partial y^2}+D_2\frac{\partial^4(w-w_0)}{dy^4}=h\left(\frac{p_z}{h}+\frac{\partial^2F}{\partial y^2}\frac{\partial^2w}{\partial x^2}+\frac{\partial^2F}{\partial x^2}\frac{\partial^2w}{dy^2}-2\frac{\partial^2F}{\partial x\partial y}\frac{\partial^2w}{\partial x\partial y}\right)\quad[1]$$

$$\frac{1}{E_y}\frac{\partial^4F}{\partial x^4}+\left(\frac{1}{G}-\frac{\nu_x}{E_x}-\frac{\nu_y}{E_y}\right)\frac{\partial^4F}{\partial x^2dy^2}+\frac{1}{E_x}\frac{\partial^4F}{\partial y^4}=\left(\frac{\partial^2w}{\partial x\partial y}\right)^2-\frac{\partial^2w}{\partial x^2}\frac{\partial^2w}{\partial y^2}-\left(\frac{\partial^2w_0}{\partial x\partial y}\right)^2+\frac{\partial^2w_0}{\partial x^2}\frac{\partial^2w_0}{\partial y^2}\quad[2]$$

where

$$\left.\begin{aligned}D_1&=(1/12)(E_xh^3)/(1-\nu_x\nu_y)\\D_2&=(1/12)(E_yh^3)/(1-\nu_x\nu_y)\\D_3&=(1/6)(3D_1\nu_y+3D_2\nu_x+h^2G)\end{aligned}\right\}\quad[3]$$

It is assumed that the edges of the plate are parallel to the principal directions of elasticity of the orthotropic plate which are designated by x and y. The initial deflection is w_0 and the total deflection w. Young's moduli and Poisson's ratios are represented by E_x, E_y, ν_x, and ν_y, and G is the shear modulus corresponding to the x- and y-directions. The thickness of the plate is h, and p_z is the transverse external load acting perpendicularly to the plate, that is, in the direction of the deflections w.

If the origin of the co-ordinates is the center of the plate and the edges correspond to $x=\pm a$ and $y=\pm b$, the initial deflection can be represented by the series

$$w_0=\sum_{m=1,3,\cdots}^{\infty}\sum_{n=1,3,\cdots}^{\infty}w_{0(mn)}\cos(m\pi x/2a)\cos(n\pi y/2b)\quad[4]$$

The stress function F is assumed in the form

$$F=-(1/2)p_xy^2-(1/2)p_yx^2+\sum_{p=0,2,\cdots}^{\infty}\sum_{q=0,2,\cdots}^{\infty}[b_{pq}-b_{0(pq)}]\cos(p\pi x/2a)\cos(q\pi y/2b)\quad[5]$$

and the total deflection w in the form

$$w=\sum_{m=1,3,\cdots}^{\infty}\sum_{n=1,3,\cdots}^{\infty}w_{mn}\cos(m\pi x/2a)\cos(n\pi y/2b)\quad[6]$$

Substitution from Equations [4], [5], and [6] into the compatibility equation, Equation [2], expression of all the trigono-

metric functions in terms of even cosines, and matching of the coefficients of like trigonometric terms lead to an expression for the coefficients b_{pq} in terms of the coefficients w_{mn}

$$b_{pq} = (1/4)\left\{(1/E_y)p^4(b/a)^3 + [(1/G) - (\nu_x/E_x) - (\nu_y/E_y)]p^2q^2 + (1/E_x)q^4(a/b)^3\right\}^{-1}\sum_{n=1}^{9} B_n \quad [7]$$

where

$$B_1 = \sum_{k=1}^{p-1}\sum_{t=1}^{q-1}[kt(p-k)(q-t) - k^2(q-t)^2]w_{kt}w_{(p-k)(q-t)} \quad [8]$$

if $q \neq 0$ and $p \neq 0$, and $B_1 = 0$ if $q = 0$ or $p = 0$. Values of B_n for $n \neq 1$ can be found in reference (2) following Equation [10]. Values of $b_{0(pq)}$ are obtained from Equation [7] if in the sums representing B_n one replaces w by w_0.

If the transverse load is

$$p_z = \sum_{r=1,3,\cdots}^{\infty}\sum_{s=1,3,\cdots}^{\infty} p_{rs}\cos(r\pi x/2a)\cos(s\pi y/2b) \quad [9]$$

substitution in the equilibrium equation, Equation [1], and manipulations yield the following expression for the coefficient p_{rs}

$$p_{rs} = (\pi^4/16)[D_1(r/a)^4 + 2D_3(rs/ab)^2 + D_2(s/b)^4] \times (w_{rs} - w_{0rs}) - hp_x(r\pi/2a)^2w_{rs} - hp_y(s\pi/2b)^2w_{rs} - h(\pi^2/8ab)^2\sum_{n=1}^{9}(A_n - A_{0n}) \quad [10]$$

where

$$A_1 = \sum_{k=1,3,\cdots}^{r}\sum_{t=1,3,\cdots}^{s}[(s-t)k - (r-k)t]^2b_{(r-k)(s-t)}w_{kt} \quad [11]$$

and for the values of A_n with $n \neq 1$ reference is made to Equation [18] of Coan's paper (2). Values of A_{0n} can be obtained from those of A_n by replacing b by b_0 in the expressions corresponding to Equation [11].

It can be easily shown that the equations given satisfy the boundary conditions of a plate upon the edges of which average stresses $\bar{p}_x$ and $\bar{p}_y$ are acting, provided all the edges are simply supported and are compelled to remain straight. Because of the requirement regarding displacements the edge stresses need not be distributed uniformly. With known initial deflections and a prescribed transverse load, Equation [10] represents an infinite number of simultaneous nonlinear equations in which the only unknowns are the displacement coefficients w_{mn}.

Orthotropic Plate With Unloaded Edges Free to Displace in Plane of Plate

In careful edgewise compression tests the test equipment insures that the four edges of the plate are simply supported. At the same time only the loaded edges are compelled to remain straight, while the unloaded ones are free to displace in the plane of the plate. Along the unloaded edges not only the average stress must vanish, but the stress at any point must be equal to zero. This condition can be realized in the calculations if a correction term is added to the stress function. Such a correction term was used in a different problem by Levy, et al. (7), and applied to the large deflection problem of the isotropic rectangular plate in edge compression by Coan (2). The final total stress function then becomes

$$F = -(1/2)\bar{p}_x y^2 + \sum_{p=0,2,\cdots}^{\infty}\sum_{q=0,2,\cdots}^{\infty}[e_{pq} - b_{0(pq)}] \times \cos(p\pi x/2a)\cos(q\pi y/2b) \quad [12]$$

when the total edgewise load along the edges $x = \pm a$ is $2bh\,\bar{p}_x$ and the edges $y = \pm b$ are free of stress. In Equation [12]

$$e_{pq} = b_{pq} + (-1)^{(q+2)/2}\frac{rp^2\sinh(p\pi b/2a)}{\pi a^2 b[(p/a)^2 + (q/b)^2]}C_p \quad [13]$$

with

$$\left.\begin{aligned} r &= 8 \text{ if } q \neq 0 \\ r &= 4 \text{ if } q = 0 \end{aligned}\right\} \quad [13a]$$

as was shown in connection with Equation [23] of reference (2).

In Equation [13] C_p is given by

$$\{[\cosh(p\pi b/2a) + (p\pi b/2a)]/\sinh(p\pi b/2a)\}\,C_p = \sum_{q=0,2,\cdots}^{\infty}(-1)^{q/2}[b_{pq} - b_{0(pq)}] \quad [14]$$

for $p = 2, 4 \ldots$

With the stress function of Equation [12] the expression given in Equation [10] is transformed into

$$p_{rs} = (\pi^4/16)[D_1(r/a)^4 + 2D_3(rs/ab)^2 + D_2(s/b)^4][w_{rs} - w_{0rs}] - h\bar{p}_x(r\pi/2a)^2w_{rs} - h(\pi^2/8ab)^2\sum_{n=1}^{9}(E_n - A_{0n}) \quad [15]$$

where E_n is determined in the same manner as A_n except that e_{pq} replaces b_{pq} in all the expressions corresponding to A_1 in Equation [11].

Solution for Square Plate

The main purpose of this analysis is the investigation of the behavior of orthotropic plates subjected to edgewise compression in the neighborhood of the buckling load. With plates which are reasonably plane before loading the Fourier component of the initial deflections corresponding to the first buckling load has a dominant influence upon the total deflections (4). It is permissible, therefore, to describe the initial deflections of the average plate by the single term

$$w_0 = w_{0(11)}\cos(\pi x/2a)\cos(\pi y/2b) \quad [16]$$

In the numerical work the plate was assumed to be square ($a = b$) and $w_{0(11)}$ was taken as $(h/10)$. This was a reasonable average value for the specimens which were noticeably warped because they were tested long after they were manufactured.

The final deflected shape at loads exceeding the buckling load by a factor not greater than 3 is represented accurately enough by the first three terms of the series given in Equation [6]

$$w = w_{11}\cos(\pi x/2a)\cos(\pi y/2b) + w_{13}\cos(\pi x/2a)\cos(3\pi y/2b) + w_{31}\cos(3\pi x/2a)\cos(\pi y/2b) \quad [17]$$

If all the other coefficients w_{mn} are assumed to vanish, Equation [8] yields the following expressions for the coefficients of the stress function of a square plate

$$\left.\begin{aligned} b_{02} &= -(E_x/32)(w_{11}^2 + 9w_{31}^2 + 2w_{11}w_{13}) \\ b_{04} &= -(E_x/64)w_{11}w_{13} \\ b_{06} &= -(E_x/288)w_{13}^2 \\ b_{20} &= -(E_y/32)(w_{11}^2 + 9w_{13}^2 + 2w_{11}w_{31}) \\ b_{40} &= -(E_y/64)w_{11}w_{31} \\ b_{60} &= -(E_y/288)w_{31}^2 \\ b_{22} &= -(E_1/4)(w_{11}w_{31} + w_{11}w_{13} + 4w_{13}w_{31}) \\ b_{24} &= -(E_2/16)(w_{11}w_{13} + 25w_{11}w_{31}) \\ b_{42} &= -(E_2/16)(w_{11}w_{31} + 25w_{11}w_{13}) \\ b_{44} &= -(E_1/16)w_{13}w_{31} \end{aligned}\right\} \quad [18]$$

where
$$\left.\begin{aligned} E_1 &= [(1/E_y) + R + (1/E_x)]^{-1} \\ E_2 &= [(1/E_y) + 4R + (16/E_x)]^{-1} \\ E_3 &= [(16/E_y) + 4R + (1/E_x)]^{-1} \end{aligned}\right\} \quad \ldots\ldots [18a]$$

and
$$R = (1/G) - (\nu_x/E_x) - (\nu_y/E_y) \quad \ldots\ldots [18b]$$

and all other b_{pq} values are zero.

As the initial deflections are represented by a single term, the only nonvanishing $b_{0(pq)}$ values are

$$\left.\begin{aligned} b_{0(02)} &= -(E_x/32)w_{0(11)}^2 = -(E_x/3200)h^2 \\ b_{0(20)} &= -(E_y/32)w_{0(11)}^2 = -(E_y/3200)h^2 \end{aligned}\right\} \quad \ldots [19]$$

With the values of the b_{pq} taken from Equations [18] expressions can be obtained for the A_{ik} in terms of the w_{mn} with the aid of Equation [11] and its associated equations. If in these calculations the b_{pq} are replaced by the ϵ_{pq} according to Equation [13], one obtains expressions for the E_{ik}, again in terms of the unknown w_{mn}. Finally, replacement of the w_{mn} by the $w_{0(mn)}$ in Equations [18] results in expressions for the A_{0ik}. Substitution of these expressions in Equation [15] leads to a set of nonlinear equations in the w_{mn}. In the problem to be solved here no transverse loads act upon the plate. Hence the left-hand side of Equation 15 is zero. With only three of the w_{mn}-coefficients assumed to be different from zero the following three equations are obtained for the square plate if the nondimensional coefficient

$$k_{mn} = w_{mn}/h \quad \ldots\ldots [20]$$

is introduced

$$\begin{aligned} &\{[(E_x/12)(1+\nu_y)/(1-\nu_x\nu_y)] + [(E_y/12)(1+\nu_x)/(1-\nu_x\nu_y)] \\ &+ (G/3) - (2a/\pi h)^2 p_z - 0.000238E_y - 0.000625E_x\}\, k_{11} \\ &- (0.0003719E_y + 0.000625E_x)k_{12} - 0.000625\,E_y k_{31} \\ &+ (0.0625E_x + 0.02378E_y)k_{11}^3 + (0.1875E_x + 0.03719E_y \\ &+ 0.30976E_1 - 0.0774E_2)k_{11}^2 k_{13} + (0.1100E_y + 0.30976E_1) \\ &\times k_{11}^2 k_{31} \\ &+(0.2500E_x + 0.2140E_y + 0.7028E_1 + 0.13688E_2)k_{11}k_{13}^2 \\ &+(2.942E_1 - 1.936E_3 + 0.07438E_y)k_{11}k_{13}k_{31} \\ &+(0.5625E_x + 0.2166E_y + 1.00E_1 + 0.1962E_3)k_{11}k_{31}^2 \\ &+ 0.3347E_y k_{13}^3 + (0.5626E_y + 2.811E_1 + 3.422E_2)k_{13}^2 k_{31} \\ &+ (0.5625E_x + 3.867E_1 + 4.904E_3)k_{13}k_{31}^2 = \{[(E_x/12) \\ &\times (1+\nu_y)/(1-\nu_x\nu_y)] + [(E_y/12)(1+\nu_x)/(1 \\ &\qquad - \nu_x\nu_y)] + (G/3)\}(w_{0(11)}/h) \quad \ldots [21] \end{aligned}$$

$$\begin{aligned} &-(0.000625E_x + 0.0003719E_y)k_{11} + \{[(E_x/12)(1+9\nu_y)/ \\ &(1-\nu_x\nu_y)] + [(3E_y/4)(\nu_x+9)/(1-\nu_x\nu_y)] + 3G \\ &- (2a/\pi h)^2 p_z - 0.00214E_y\}\, k_{13} - 0.001162E_y k_{31} \\ &+ (0.0625E_x + 0.0372E_y)k_{11}^3 + (0.25E_x + 0.2140E_y \\ &+0.7028E_1 + 0.13688E_2)k_{11}^2 k_{13} + (0.1906E_y + 0.7028E_1)k_{11}^2 k_{31} \\ &+ (0.33472E_y + 2.7878E_1 - 0.4280E_2)k_{11}k_{13}^2 + (0.3882E_y \\ &+ 8.6703E_1 + 5.2169E_2 + 0.1589E_3)k_{11}k_{13}k_{31} \\ &+ (0.5625E_x + 03518E_y + 3.0714E_1 + 1.08519E_3)k_{11}k_{31}^2 \\ &+ (0.06246E_x + 1.926E_y)k_{13}^3 \\ &+ (1.0461E_y + 11.151E_1 - 17.424E_2)k_{13}^2 k_{31} + (13.763E_1 \\ &+ 44.873E_2 + 27.530E_3)k_{13}k_{31}^2 = 0 \quad \ldots\ldots [22] \end{aligned}$$

$$\begin{aligned} &-0.000625E_y k_{11} - 0.001162E_y k_{13} + \{[(3E_x/4)(9+\nu_y)/(1 \\ &-\nu_x\nu_y)] + [(E_y/12)(1+9\nu_x)/(1-\nu_x\nu_y)] + 3G \\ &- 9(2a/\pi h)^2 p_z - 0.005635E_x\}\, k_{31} \\ &+ 0.0625E_y k_{11}^3 + (1.00E_1 + 0.1162E_y)k_{11}^2 k_{13} + (0.5625E_x \\ &+ 0.2165E_y + 1.00E_1 + 0.1962E_3)k_{11}^2 k_{31} + (0.5627E_y \\ &+ 3.074E_1 + 1.7949E_2)k_{11}k_{13}^2 \\ &+ (0.3518E_y + 1.125E_x + 6.9375E_1 + 5.9895E_3)k_{11}k_{13}k_{31} \\ &+ 1.046E_y k_{13}^3 + (44.873E_2 + 27.530E_3 + 13.763E_1)k_{13}^2 k_{31} \\ &+ (0.04937E_y + 5.0625E_x)k_{31}^3 = 0 \quad \ldots\ldots [23] \end{aligned}$$

These three equations suffice for the calculation of the deflections of an orthotropic square plate with slight initial deflections under the action of an edgewise compression.

Stresses and Strains

The median fiber normal stresses are

$$\sigma_x = \partial^2 F/\partial y^2,\ \sigma_y = \partial^2 F/\partial x^2 \quad \ldots\ldots [24]$$

and the corresponding strains are

$$\left.\begin{aligned} \epsilon_x &= (\sigma_x/E_x) - \nu_y(\sigma_y/E_y) \\ \epsilon_y &= -\nu_x(\sigma_x/E_x) + (\sigma_y/E_y) \end{aligned}\right\} \quad \ldots\ldots [25]$$

For the stresses at the center of the plate substitutions yield the following expressions

$$\begin{aligned} \sigma_x &= -p_z + (\pi h/2a)^2[(0.125E_x + 0.0139E_y)k_{11}^2 \\ &+(0.5E_x + 0.8888E_1 + 1.0279E_2)k_{11}k_{13} \\ &+ (0.01359E_y + 0.8888E_1 + 0.3071E_3)k_{11}k_{31} \\ &+ (0.125E_x + 0.1257E_y)k_{13}^2 + 1.125E_x k_{31}^2 \\ &+ (4.4975E_1 + 25.697E_2 + 8.0786E_3)k_{13}k_{31} \\ &\qquad - 0.000625E_x - 0.000139E_y] \quad \ldots\ldots [26] \end{aligned}$$

$$\begin{aligned} \sigma_y &= (\pi h/2a)^2[0.08634E_y k_{11}^2 + (1.3099E_1 - 0.07742E_2)k_{11}k_{13} \\ &+ (0.4049E_y + 1.3099E_1 + 1.07E_3)k_{11}k_{31} + 0.7767E_y k_{13}^2 \\ &+ 0.09846E_y k_{31}^2 + (6.17E_1 - 1.935E_2 + 27.1496E_3)k_{13}k_{31} \\ &\qquad - 0.000238E_y] \quad \ldots\ldots [27] \end{aligned}$$

The extreme fiber bending strain in the direction of the load is

$$\epsilon_x' = (\sigma_x'/E_x) - \nu_y(\sigma_y'/E_y) \quad \ldots\ldots [28]$$

with the extreme fiber bending stresses expressed as

$$\left.\begin{aligned} \sigma_x' &= -(1/2)[E_x h/(1-\nu_x\nu_y)]\,\{[\partial^2(w-w_0)/\partial x^2] \\ &\qquad + \nu_y[\partial^2(w-w_0)/\partial y^2]\} \\ \sigma_y' &= -(1/2)[E_y h/(1-\nu_x\nu_y)]\,\{[\partial^2(w-w_0)/dy^2] \\ &\qquad + \nu_x[\partial^2(w-w_0)/\partial x^2]\} \end{aligned}\right\} \quad \ldots [29]$$

Substitutions yield the following expression for the extreme fiber bending strain in the x-direction at the center of the plate

$$\epsilon_x = \pm\, 1/2(\pi h/2a)^2 \sum_{m=1,3,\cdots}^{\infty} \sum_{n=1,3,\cdots}^{\infty} m^2[k_{mn} - k_{0(mn)}] \quad \ldots [30]$$

The total extreme fiber strain at the center of the plate will be denoted by ϵ_1 on the concave side of the plate, and by ϵ_2 on its convex side. Hence

$$\epsilon_1 = \epsilon_x - \epsilon_x',\ \epsilon_2 = \epsilon_x + \epsilon_x' \quad \ldots\ldots [31]$$

The average of the extreme fiber strains is of course

$$\epsilon_A = (1/2)(\epsilon_1 + \epsilon_2) = \epsilon_x \quad \ldots\ldots [32]$$

The transverse deflection of the center of the plate is given by

$$\delta_c = h(k_{11} + k_{13} + k_{31} - 0.1) \quad \ldots\ldots [33]$$

when the initial deflection is $(h/10)$. Finally the total edgewise compressive load acting on the plate is

$$P = 2ah\, p_z \quad \ldots\ldots [34]$$

Numerical Work and Comparison With Experiment

The theory here presented was applied to the calculation of the postbuckling behavior of square panels tested earlier at the Polytechnic Institute of Brooklyn (1). The material of the panels was a low-pressure resin-bonded laminate of glass fibers commercially known as Fiberglas. Edgewise compression tests were carried out with four different combinations of lamination and load direction and the mechanical properties of the material were determined for the principal directions of elasticity. There was some scatter in the values obtained (8). The values selected

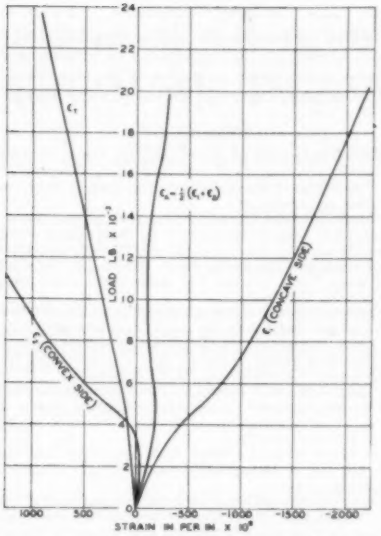

FIG. 1 THEORETICAL VALUES OF STRAIN IN CENTER OF PARALLEL-LAMINATED PANEL LOADED PARALLEL TO GRAIN

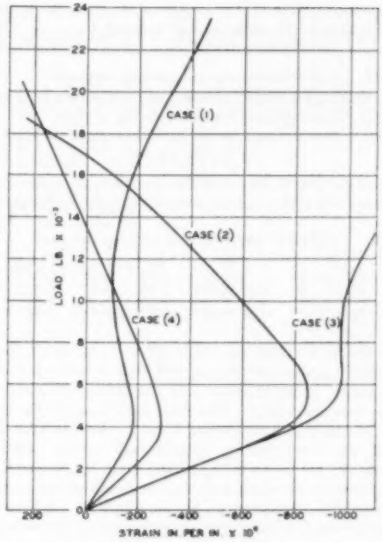

FIG. 2 THEORETICAL AVERAGE STRAIN PARALLEL TO LOAD IN CENTER OF PANEL

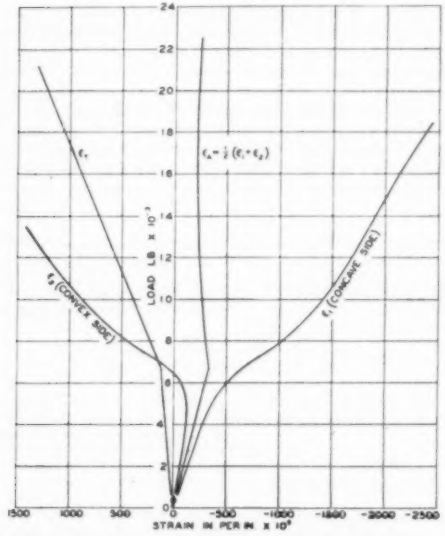

FIG. 3 EXPERIMENTAL VALUES OF STRAIN IN CENTER OF PARALLEL-LAMINATED PANEL LOADED PARALLEL TO GRAIN

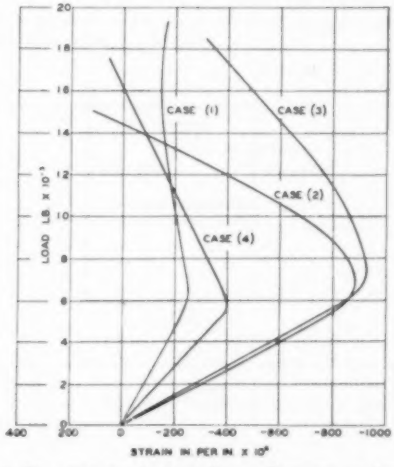

FIG. 4 EXPERIMENTAL AVERAGE STRAIN PARALLEL TO LOAD IN CENTER OF PANEL

for the computations were so chosen as to satisfy the conditions for the existence of a strain-energy function.

The four combinations investigated were as follows:

Case 1 Parallel laminate loaded parallel to grain.

Case 2 Parallel laminate loaded perpendicularly to grain.

Case 3 Cross laminate loaded at 45 deg to grain.

Case 4 Cross laminate loaded parallel to one of the grain directions.

The properties of the laminates are given in Table 1. The direction of the load is always designated as the x-direction.

TABLE 1 PROPERTIES OF LAMINATES

Case	E_x	E_y	ν_x	ν_y	G
1	3.75×10^6	1×10^6	0.30	0.08	0.5×10^6
2	1.00×10^6	3.75×10^6	0.08	0.30	0.5×10^6
3	1.00×10^6	1.00×10^6	0.55	0.55	0.323×10^6
4	2.20×10^6	2.20×10^6	0.14	0.14	0.965×10^6

The size of the plate was $20 \times 20 \times 1/4$ in. in all the cases calculated. Equations [21] to [23] were solved by a method of successive approximations and the deflections, strains, and stresses were calculated. The most interesting results are presented in graphical form in Figs. 1 and 2. For the sake of comparison the corresponding experimental curves, taken from reference (8), are shown in Figs. 3 and 4. It can be seen that the theory leads to the same variations in strain history as was observed in the experiments. In particular, it predicts tensile average strains in the direction of the applied compressive load in the center of the plate for Cases 2 and 4. Such tensile strains were measured in the tests, as is evident from Fig. 4.

ACKNOWLEDGMENTS

The author acknowledges his indebtedness to Dr. N. J. Hoff, his thesis adviser, for his suggestions and criticism during the preparation of this paper, as well as to Mr. Matthew G. Forte and Mr. Thomas J. Toomey for the tracing of the diagrams.

BIBLIOGRAPHY

1 "The Development of a Technique for Testing Stiff Panels in Edgewise Compression," by N. J. Hoff, Bruno A. Boley, and John M. Coan, Proceedings of the Society for Experimental Stress Analysis, vol. 5, 1948, pp. 14–24.

2 "Large-Deflection Theory for Plates With Small Initial Curvature Loaded in Edge Compression," by J. M. Coan, JOURNAL OF APPLIED MECHANICS, Trans. ASME, vol. 73, 1951, pp. 143–151.

3 "Bending of Rectangular Plates With Large Deflections," by Samuel Levy, NACA TN No. 846, May, 1942. (Also available as NACA TR No. 737, 1942.)

4 "Effect of Small Deviation From Flatness on Effective Width and Buckling of Plates in Compression," by Pai C. Hu, E. E. Lundquist, and S. B. Batdorf, NACA TN No. 1124, September, 1946.

5 "Theory of Elastic Stability," by S. Timoshenko, McGraw-Hill Book Company, Inc., New York, N. Y., 1936, p. 323.

6 "Large Deflection Theory for Orthotropic Plates With Small Initial Curvature," by Syed Yusuff, thesis for the Degree of Doctor of Aeronautical Engineering, Polytechnic Institute of Brooklyn, Brooklyn, N. Y., June, 1949.

7 "Analysis of Square Shear Web Above Buckling Load," by Samuel Levy, K. L. Fienup, and Ruth M. Woolley, NACA TN No. 962, February, 1945.

8 "Compression and Shear Tests on Fiberglas Panels," submitted by the Department of Aeronautical Engineering and Applied Mechanics of the Polytechnic Institute of Brooklyn to the Naval Air Experimental Station of the U. S. Navy, Philadelphia, Pa., September, 1947.

Bending of a Uniformly Loaded Rectangular Plate With Two Adjacent Edges Clamped and the Others Either Simply Supported or Free[1]

By M. K. HUANG[2] and H. D. CONWAY,[3] ITHACA, N. Y.

The distribution of deflection and bending moment in a uniformly loaded rectangular plate having two adjacent edges clamped and the others either simply supported or free, are obtained by a method of superposition. Numerical values are given for square plates and, in one case, the results are compared with those obtained by another method.

Introduction

THE problem of the bending of clamped rectangular plates has interested mathematicians and engineers for many years. In many cases it has been found impossible to find a function which will satisfy both the differential equation and the boundary conditions simultaneously. Various methods have been presented for obtaining approximate solutions. One important method, which was proposed by Timoshenko (1),[4] involves the determination of an infinite number of unknowns in an infinite number of equations obtained by the superposition of several known solutions. The method has been applied to other cases (2, 3, 4), but, in so far as the authors are aware, no attempt appears to have been made to analyze the problems discussed here, viz., the uniformly loaded rectangular plate with two edges clamped and the others either simply supported or free. These two problems will be treated separately in the following sections, as each requires a special method of superposition. The general assumptions relating to the small bending theory of plates are adopted.

Bending of a Uniformly Loaded Plate With Two Adjacent Edges Clamped and the Others Simply Supported

Analysis. The deflection w of the thin plate must satisfy the Lagrange differential equation

$$\frac{\partial^4 w}{\partial x^4} + 2\frac{\partial^4 w}{\partial x^2 \partial y^2} + \frac{\partial^4 w}{\partial y^4} = \frac{q}{D} \quad \ldots\ldots [1]$$

and the following boundary conditions

$$\left.\begin{array}{lll} \text{At } x = 0 & w = 0, & \dfrac{\partial w}{\partial x} = 0 \\ \text{At } x = a & w = 0, & \dfrac{\partial^2 w}{\partial x^2} = 0 \\ \text{At } y = 0 & w = 0, & \dfrac{\partial w}{\partial y} = 0 \\ \text{At } y = b & w = 0, & \dfrac{\partial^2 w}{\partial y^2} = 0 \end{array}\right\} \quad \ldots\ldots [2]$$

The usual notation is assumed. The plate has two clamped edges, $x = 0$ and $y = 0$, and two edges simply supported, $x = a$ and $y = b$, Fig. 1. As there is no known function which satisfies both the differential equation and the boundary conditions, the following approach was made:

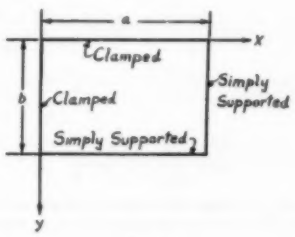

Fig. 1

Consider a uniformly loaded, simply supported, rectangular plate whose sides are twice the length of those of the actual plate to be investigated, Fig. 2(*a*). The deflection w_1 at any point obtained by the Levy method is

$$w_1 = \frac{64qa^4}{\pi^6 D} \sum_{m=1,3,5\ldots}^{\infty} \frac{(-1)^{\frac{m-1}{2}}}{m^6} \left(1 - \frac{\alpha_m \tanh \alpha_m + 2}{2\cosh \alpha_m} \cosh \frac{m\pi y}{2a} + \frac{1}{2\cosh \alpha_m} \frac{m\pi y}{2a} \sinh \frac{m\pi y}{2a}\right) \cos \frac{m\pi x}{2a} \quad \ldots [3a]$$

Along the X-axis

---

[1] Based on a thesis by M. K. Huang submitted to Cornell University in June, 1951, in partial fulfillment of the requirements for the degree of Doctor of Philosophy.

[2] Instructor of Mechanics, Cornell University.

[3] Professor of Mechanics, Cornell University. Jun. ASME.

[4] Numbers in parentheses refer to the Bibliography at the end of the paper.

Presented at the National Conference of the Applied Mechanics Division, State College, Pa., June 19–21, 1952, of The American Society of Mechanical Engineers.

Discussion of this paper should be addressed to the Secretary, ASME, 29 West 39th Street, New York, N. Y., and will be accepted until January 10, 1953, for publication at a later date. Discussion received after the closing date will be returned.

Note: Statements and opinions advanced in papers are to be understood as individual expressions of their authors and not those of the Society. Manuscript received by ASME Applied Mechanics Division, August 20, 1951. Paper No. 52—APM-14.

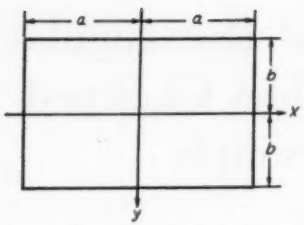

FIG. 2(a) SIMPLY SUPPORTED PLATE WITH UNIFORMLY DISTRIBUTED LOAD

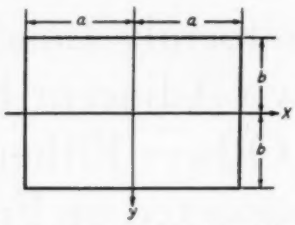

FIG. 2(b) SIMPLY SUPPORTED PLATE WITH A LOAD ALONG X-AXIS IN THE FORM OF A COSINE SERIES

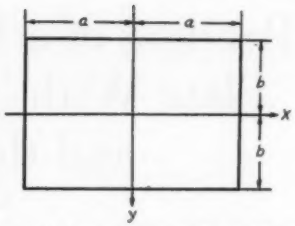

FIG. 2(c) SIMPLY SUPPORTED PLATE WITH A LOAD ALONG Y-AXIS IN THE FORM OF A COSINE SERIES

$$(w_1)_{y=0} = \frac{64qa^4}{\pi^5 D} \sum_{m=1,3,5\ldots}^{\infty} \frac{(-1)^{\frac{m-1}{2}}}{m^5} \left(1 - \frac{\alpha_m \tanh \alpha_m + 2}{2 \cosh \alpha_m}\right) \cos \frac{m\pi x}{2a} \quad \ldots\ldots [3b]$$

and along the Y-axis

$$(w_1)_{x=0} = \frac{64qb^4}{\pi^5 D} \sum_{m=1,3,5\ldots}^{\infty} \frac{(-1)^{\frac{m-1}{2}}}{m^5} \left(1 - \frac{\beta_m \tanh \beta_m + 2}{2 \cosh \beta_m}\right) \cos \frac{m\pi y}{2b} \quad \ldots\ldots [3c]$$

$$w_2 = \frac{2a^3}{D\pi^3} \sum_{m=1,3,5\ldots}^{\infty} (-1)^{\frac{m-1}{2}} \frac{A_m}{m^3} \left[\left(\tanh \alpha_m - \frac{\alpha_m}{\cosh^2 \alpha_m} \right) \cosh \frac{m\pi y}{2a} + \sinh \frac{m\pi y}{2a} - \frac{m\pi y}{2a} \cosh \frac{m\pi y}{2a} - \tanh \alpha_m \frac{m\pi y}{2a} \sinh \frac{m\pi y}{2a} \right] \cos \frac{m\pi x}{2a} \text{ for } -b \le y \le 0 \ldots [4b]$$

$$(w_2)_{y=0} = \frac{2a^3}{D\pi^3} \sum_{m=1,3,5\ldots}^{\infty} \frac{(-1)^{\frac{m-1}{2}} A_m}{m^3} \left(\tanh \alpha_m - \frac{\alpha_m}{\cosh^2 \alpha_m} \right) \cos \frac{m\pi x}{2a} \quad \ldots\ldots [4c]$$

Along the Y-axis

$$(w_2)_{x=0} = \frac{2a^3}{D\pi^3} \sum_{m=1,3,5\ldots}^{\infty} \frac{(-1)^{\frac{m-1}{2}} A_m}{m^3} \left[\left(\tanh \alpha_m - \frac{\alpha_m}{\cosh^2 \alpha_m} \right) \cosh \frac{m\pi y}{2a} - \sinh \frac{m\pi y}{2a} - \tanh \alpha_m \frac{m\pi y}{2a} \sinh \frac{m\pi y}{2a} + \frac{m\pi y}{2a} \cosh \frac{m\pi y}{2a} \right] \text{ for } 0 \le y \le b$$

$$(w_2)_{x=0} = \frac{2a^3}{D\pi^3} \sum_{m=1,3,5\ldots}^{\infty} \frac{(-1)^{\frac{m-1}{2}} A_m}{m^3} \left[\left(\tanh \alpha_m - \frac{\alpha_m}{\cosh^2 \alpha_m} \right) \cosh \frac{m\pi y}{2a} + \sinh \frac{m\pi y}{2a} - \tanh \alpha_m \frac{m\pi y}{2a} \sinh \frac{m\pi y}{2a} - \frac{m\pi y}{2a} \cosh \frac{m\pi y}{2a} \right] \text{ for } -b \le y \le 0 \quad \ldots [4d]$$

where

$$\alpha_m = \frac{m\pi b}{2a}, \quad \beta_m = \frac{m\pi a}{2b}$$

Next consider a similar plate, Fig. 2(b), simply supported along all edges but with a line load along the X-axis represented by the series

$$\sum_{m=1,3,5\ldots}^{\infty} (-1)^{\frac{m-1}{2}} A_m \cos \frac{m\pi x}{2a}$$

The expression for the deflection of this plate is[6]

$$w_2 = \frac{2a^3}{D\pi^3} \sum_{m=1,3,5\ldots}^{\infty} (-1)^{\frac{m-1}{2}} \frac{A_m}{m^3} \left[\left(\tanh \alpha_m - \frac{\alpha_m}{\cosh^2 \alpha_m} \right) \cosh \frac{m\pi y}{2a} - \sinh \frac{m\pi y}{2a} + \frac{m\pi y}{2a} \cosh \frac{m\pi y}{2a} - \tanh \alpha_m \frac{m\pi y}{2a} \sinh \frac{m\pi y}{2a} \right] \cos \frac{m\pi x}{2a} \quad \text{for } 0 \le y \le b \ldots [4a]$$

[6] Derivations of the expressions are given in the Appendix.

The expressions in parentheses in Equations [4d] vanish at the edges $y = \pm b$. They can be expanded into a Fourier series of the type

$$\sum_{i=1,3,5\ldots}^{\infty} C_i \cos \frac{i\pi y}{2b}$$

in which the coefficients C_i are calculated from the formula

$$C_i = \frac{1}{b} \left\{ \int_{-b}^{0} \left[\left(\tanh \alpha_m - \frac{\alpha_m}{\cosh^2 \alpha_m} \right) \cosh \frac{m\pi y}{2a} + \sinh \frac{m\pi y}{2a} - \tanh \alpha_m \frac{m\pi y}{2a} \sinh \frac{m\pi y}{2a} - \frac{m\pi y}{2a} \cosh \frac{m\pi y}{2a} \right] \cos \frac{i\pi y}{2b} \, dy \right.$$

$$+\int_0^b \left[\left(\tanh\alpha_m - \frac{\alpha_m}{\cosh^2\alpha_m}\right)\cosh\frac{m\pi y}{2a} - \sinh\frac{m\pi y}{2a} - \tanh\alpha_m\frac{m\pi y}{2a}\sinh\frac{m\pi y}{2a} + \frac{m\pi y}{2a}\cosh\frac{m\pi y}{2a}\right]\cos\frac{i\pi y}{2b}\,dy\Bigg\}$$

It follows that

$$C_i = \frac{8}{m\pi}\left(\frac{b}{a}\right)^3\frac{1}{\left(\frac{b^2}{a^2}+\frac{i^2}{m^2}\right)^2}$$

Substituting this in Equations [4d] gives

$$(w_2)_{x=0} = \frac{16b^3}{D\pi^4}\sum_{m=1,3,5\ldots}^{\infty}\frac{(-1)^{\frac{m-1}{2}}A_m}{m^4}\sum_{i=1,3,5\ldots}^{\infty}\frac{1}{\left(\frac{b^2}{a^2}+\frac{i^2}{m^2}\right)^2}\cos\frac{i\pi y}{2b} \quad \ldots\ldots [4e]$$

In a similar manner, if a simply supported plate is loaded by a line load represented by the series

$$\sum_{m=1,3,5\ldots}^{\infty}(-1)^{\frac{m-1}{2}}B_m\cos\frac{m\pi y}{2b}$$

along the Y-axis Fig. 2(c), the expressions for the deflections are

$$w_3 = \frac{2b^3}{D\pi^3}\sum_{m=1,3,5\ldots}^{\infty}\frac{(-1)^{\frac{m-1}{2}}B_m}{m^3}\left[\left(\tanh\beta_m - \frac{\beta_m}{\cosh^2\beta_m}\right)\cosh\frac{m\pi x}{2b} - \sinh\frac{m\pi x}{2b} + \frac{m\pi x}{2b}\cosh\frac{m\pi x}{2b} - \tanh\beta_m\frac{m\pi x}{2b}\sinh\frac{m\pi x}{2b}\right]\cos\frac{m\pi y}{2b} \text{ for } 0\le x\le a \ldots. [5a]$$

$$w_2 = \frac{2b^3}{D\pi^3}\sum_{m=1,3,5\ldots}^{\infty}\frac{(-1)^{\frac{m-1}{2}}B_m}{m^3}\left[\left(\tanh\beta_m - \frac{\beta_m}{\cosh^2\beta_m}\right)\cosh\frac{m\pi x}{2b} + \sinh\frac{m\pi x}{2b} - \frac{m\pi x}{2b}\cosh\frac{m\pi x}{2b} - \tanh\beta_m\frac{m\pi x}{2b}\sinh\frac{m\pi x}{2b}\right]\cos\frac{m\pi y}{2b} \text{ for } -a\le x\le 0 \ldots. [5b]$$

$$(w_3)_{x=0} = \frac{2b^3}{D\pi^3}\sum_{m=1,3,5\ldots}^{\infty}\frac{(-1)^{\frac{m-1}{2}}B_m}{m^3}\left(\tanh\beta_m - \frac{\beta_m}{\cosh^2\beta_m}\right)\cos\frac{m\pi y}{2b} \ldots\ldots [5c]$$

$$(w_3)_{y=0} = \frac{16a^3}{D\pi^4}\sum_{m=1,3,5\ldots}^{\infty}\frac{(-1)^{\frac{m-1}{2}}B_m}{m^4}\sum_{i=1,3,5\ldots}^{\infty}\frac{1}{\left(\frac{a^2}{b^2}+\frac{i^2}{m^2}\right)^2}\cos\frac{i\pi x}{2a} \ldots\ldots [5d]$$

The given problem is then solved by superposing the three cases in such a manner that the resultant deflections along the coordinate axes in Figs. 2(a), (b), and (c) are zero. The remaining boundary conditions are satisfied due to symmetry. In this manner, two infinite sets of equations containing two infinite sets of unknowns are obtained. For instance, when using Equations [3b], [4c] and [5d] and grouping the terms in $\cos(i\pi x)/(2a)$ to obtain zero resultant deflection along the X-axis, an infinite set of linear equations of the following type is obtained

$$\frac{32qa}{\pi^2}\frac{1}{i^4}\left(1-\frac{\alpha_i\tanh\alpha_i+2}{2\cosh\alpha_i}\right)+\frac{A_i}{i^2}\left(\tanh\alpha_i-\frac{\alpha_i}{\cosh^2\alpha_i}\right)+\frac{8i}{\pi}(-1)^{\frac{i-1}{2}}\sum_{m=1,3,5\ldots}^{\infty}(-1)^{\frac{m-1}{2}}\frac{B_m}{m^4}\times\frac{1}{\left(\frac{a^2}{b^2}+\frac{i^2}{m^2}\right)^2}=0 \ldots\ldots [6]$$

A similar set of equations is also obtained by equating to zero the resultant deflections along the Y-axis and using Equations [3c], [4e], and [5c].

Numerical Example. As an example, consider the case of a square plate. Since $a = b$, the two sets of equations are identical and $A_i = B_i$

$$\frac{A_i}{i^2}\left(\tanh\alpha_i-\frac{\alpha_i}{\cosh^2\alpha_i}\right)+(-1)^{\frac{i-1}{2}}\frac{8i}{\pi}\sum_{m=1,3,5\ldots}^{\infty}\frac{(-1)^{\frac{m-1}{2}}A_m}{(i^2+m^2)^2}=\frac{32qa}{\pi^2}\frac{1}{i^4}\left(\frac{\alpha_i\tanh\alpha_i+2}{2\cosh\alpha_i}-1\right) \ldots. [7]$$

By using first seven coefficients in the series, we obtain the following equations

$$1.30428\,A_1 - 0.0254648\,A_3 + 0.00376698\,A_5 - 0.00101859\,A_7 + 0.000378715\,A_9 - 0.000171088\,A_{11} + 0.0000881134\,A_{13} = 0.314385\,K$$

$$-0.0763944\,A_1 + 0.134501\,A_3 - 0.00660851\,A_5 + 0.00227094\,A_7 - 0.000943141\,A_9 + 0.000452038\,A_{11} - 0.000241113\,A_{13} = 0.0116014\,K$$

$$0.0188349\,A_1 - 0.0110142\,A_3 + 0.0450928\,A_5 - 0.00232513\,A_7 + 0.00113318\,A_9 - 0.000597316\,A_{11} + 0.000338304\,A_{13} = 0.00159388\,K$$

$$-0.00713014\,A_1 + 0.00529886\,A_3 - 0.00325518\,A_5 + 0.0222642\,A_7 - 0.00105475\,A_9 + 0.000616794\,A_{11} - 0.000375081\,A_{13} = 0.000416402\,K$$

$$0.00340843\,A_1 - 0.00282942\,A_3 + 0.00203972\,A_5 - 0.00135611\,A_7 + 0.0132190\,A_9 - 0.000561668\,A_{11} + 0.000366693\,A_{13} = 0.000152414\,K$$

$$-0.00188197\,A_1 + 0.00165747\,A_3 - 0.00131410\,A_5 + 0.000969249\,A_7 - 0.000686484\,A_9 + 0.00874276\,A_{11} - 0.000333071\,A_{13} = 0.000068301\,K$$

$$0.00114547\,A_1 - 0.00104482\,A_3 + 0.000879579\,A_5 - 0.000696579\,A_7 + 0.000529667\,A_9 - 0.000393629\,A_{11} + 0.00620693\,A_{13} = 0.0000350128\,K$$

Solving these equations yields the following values for the coefficients

$$A_1 = 0.245485\,K$$
$$A_3 = 0.224458\,K$$
$$A_5 = -0.010128\,K$$
$$A_7 = 0.042281\,K$$

$$A_9 = 0.002564\,K$$
$$A_{11} = 0.012279\,K$$
$$A_{13} = 0.004861\,K$$

where

$$K = -32qa/\pi^2$$

Values of the deflection at several points along the diagonal of symmetry (this includes the maximum deflection) have been calculated by superposition. The results are shown in Fig. 3, and it is observed that the maximum deflection of $0.002203\ qa^4/D$ occurs at $x = y = 0.566a$. The accuracy of the solution naturally depends upon the degree to which the deflection of the clamped edges approaches zero by this method of approximation. An inspection of the calculated results of deflection at several points along the clamped edge, Table 1, shows that they are exceedingly small in comparison with the deflections w_1. By assuming the deflection at the clamped edge exactly equal to zero, the bending moments along the clamped edge are calculated from the formula

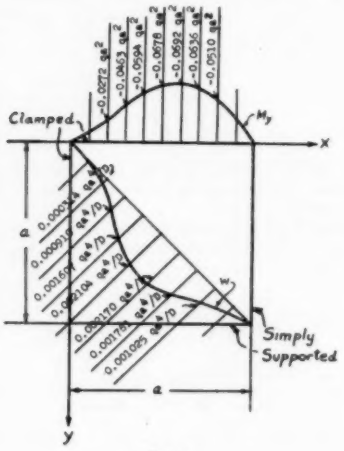

FIG. 3

$$(M_y)_{y=0} = -D\left(\frac{\partial^2 w_1}{\partial y^2} + \frac{\partial^2 w_2}{\partial y^2} + \frac{\partial^2 w_3}{\partial y^2}\right)_{y=0}$$

The moments along the clamped edge are also shown in Fig. 3 and the maximum bending moment is found to be $-0.0695\ qa^2$ at $x = 0.57a$.

TABLE 1 DEFLECTION ALONG CLAMPED EDGES BY SUPERPOSITION FOR UNIFORMLY LOADED PLATE WITH TWO ADJACENT EDGES CLAMPED AND OTHERS SIMPLY SUPPORTED

Location x	Location y	Deflections for plates shown in Fig. 2(a) w_1	Fig. 2(b) w_2	Fig. 2(c) w_3	Resultant deflection
0	0	0.310792	−0.155394	−0.155394	0.000004
0.2a	0	0.269749	−0.151078	−0.145664	0.000007
0.4a	0	0.255243	−0.135275	−0.119966	0.000002
0.6a	0	0.188409	−0.104120	−0.084276	0.000013
0.8a	0	0.100647	−0.057377	−0.043267	0.000003

NOTE: Each value should be multiplied by $64\ qa^4/D\pi^4$ to obtain the deflection.

This problem also has been discussed by Stiles (5) using a method due to Weinstein (6, 7). Table 2 gives the comparative values of deflection along the diagonal of symmetry by the two methods, while Table 3 gives the comparative values of the clamping moments.

TABLE 2 COMPARATIVE VALUES OF DEFLECTION ALONG DIAGONAL OF SYMMETRY FOR UNIFORMLY LOADED PLATE WITH TWO ADJACENT EDGES CLAMPED AND OTHERS SIMPLY SUPPORTED

Location x	Location y	Deflection × (D/qa^4) Present method	Stiles' method
0.2a	0.2a	0.000314	0.0003
0.4a	0.4a	0.001607	0.0016
0.6a	0.6a	0.002170	0.0022
0.8a	0.8a	0.001025	0.0010

TABLE 3 COMPARATIVE VALUES OF CLAMPING MOMENT FOR UNIFORMLY LOADED SQUARE PLATE WITH TWO ADJACENT EDGES CLAMPED AND OTHERS SIMPLY SUPPORTED

Location x	Location y	Clamping moments × $(1/qa^2)$ Present method	Stiles' method
0.2a	0	−0.0272	−0.0257
0.4a	0	−0.0594	−0.0608
0.6a	0	−0.0692	−0.0684
0.8a	0	−0.0510	−0.0515

BENDING OF A UNIFORMLY LOADED PLATE WITH TWO ADJACENT EDGES CLAMPED AND THE OTHERS FREE

Analysis. The deflection w of this plate must satisfy the Lagrange equation and the following boundary conditions

At $x = 0$

$$M_x = -D\left(\frac{\partial^2 w}{\partial x^2} + \nu\frac{\partial^2 w}{\partial y^2}\right) = 0 \text{ and } \frac{\partial^3 w}{\partial x^3} + (2-\nu)\frac{\partial^3 w}{\partial x \partial y^2} = 0 \quad [8a]$$

At $y = 0$

$$M_y = -D\left(\frac{\partial^2 w}{\partial y^2} + \nu\frac{\partial^2 w}{\partial x^2}\right) = 0 \text{ and } \frac{\partial^3 w}{\partial y^3} + (2-\nu)\frac{\partial^3 w}{\partial y \partial x^2} = 0 \quad [8b]$$

At $x = a$

$$w = 0 \text{ and } \frac{\partial w}{\partial x} = 0 \quad [8c]$$

At $y = b$

$$w = 0 \text{ and } \frac{\partial w}{\partial y} = 0 \quad [8d]$$

The plate has two clamped edges at $x = a$ and $y = b$, and two free edges at $x = 0$ and $y = 0$, Fig. 4. The solution of this problem

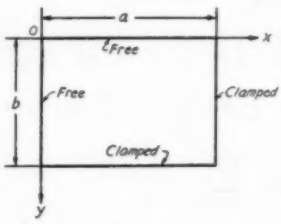

FIG. 4

is obtained by superimposing the five cases shown in Fig. 5. Fig. 5(*a*) shows a simply supported plate carrying a uniformly distributed load of intensity q, while Figs. 5(*b*) and 5(*c*), are simply supported plates bent by arbitrary edge moments

$$(M_x)_{x=\pm a} = \sum_{m=1,3,5\ldots}^{\infty} (-1)^{\frac{m-1}{2}} G_m \cos\frac{m\pi y}{2b} \quad [9]$$

or

$$(M_y)_{y=\pm b} = \sum_{m=1,3,5\ldots}^{\infty} (-1)^{\frac{m-1}{2}} H_m \cos\frac{m\pi x}{2a} \quad \ldots\ldots [10]$$

respectively. The expressions for the deflection, slope, and bending moment for the foregoing three cases can be obtained. In addition, the expressions

$$\left[\frac{\partial^3 w}{\partial x^3} + (2-\nu)\frac{\partial^3 w}{\partial x \partial y^2}\right]_{x=0} \text{ and } \left[\frac{\partial^3 w}{\partial y^3} + (2-\nu)\frac{\partial^3 w}{\partial x^2 \partial y}\right]_{y=0}$$

are zero for all three cases because of symmetry. Fig. 5(*d*) has no lateral load but is bent by moments at the edge $x = 0$ having the form

$$(M_x)_{x=0} = \sum_{m=1,3,5\ldots}^{\infty} (-1)^{\frac{m-1}{2}} E_m \cos\frac{m\pi y}{2b} \quad \ldots\ldots [11]$$

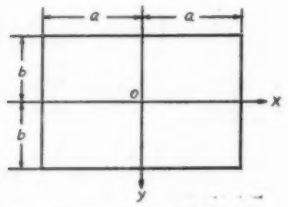

Fig. 5(*a*) Simply Supported Plate With Uniformly Distributed Load

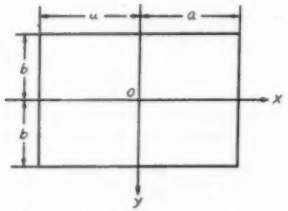

Fig. 5(*b*) Simply Supported Plate Bent by

$$(M_x)_{x=\pm a} = \sum_{m=1,3,5\ldots}^{\infty} (-1)^{\frac{m-1}{2}} G_m \cos\frac{m\pi y}{2b}$$

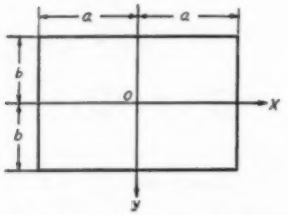

Fig. 5(*c*) Simply Supported Plate Bent by

$$(M_y)_{y=\pm b} = \sum_{m=1,3,5}^{\infty} (-1)^{\frac{m-1}{2}} H_m \cos\frac{m\pi x}{2a}$$

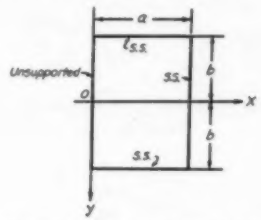

Fig. 5(*d*) Plate With Three Edges Simply Supported and the Other Edge Bent by

$$(M_x)_{x=0} = \sum_{m=1,3,5\ldots}^{\infty} (-1)^{\frac{m-1}{2}} E_m \cos\frac{m\pi y}{2b}$$

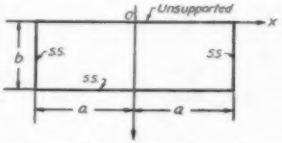

Fig. 5(*e*) Plate With Three Edges Simply Supported and the Other Edge Bent by

$$(M_y)_{y=0} = \sum_{m=1,3,5\ldots}^{\infty} (-1)^{\frac{m-1}{2}} F_m \cos\frac{m\pi x}{2a}$$

Similarly, Fig. 5(*e*) is a plate bent by moments at $y = 0$ having the form

$$(M_y)_{y=0} = \sum_{m=1,3,5\ldots}^{\infty} (-1)^{\frac{m-1}{2}} F_m \cos\frac{m\pi x}{2a} \quad \ldots\ldots [12]$$

Also, due to symmetry

$$\left[\frac{\partial^3 w}{\partial y^3} + (2-\nu)\frac{\partial^3 w}{\partial x^2 \partial y}\right]_{y=0}$$

in Fig. 5(*d*), and

$$\left[\frac{\partial^3 w}{\partial x^3} + (2-\nu)\frac{\partial^3 w}{\partial x \partial y^2}\right]_{x=0}$$

in Fig. 5(*e*), are both zero. These five cases are combined in such a manner that the boundary conditions in Equations [8] are satisfied. This gives four sets of simultaneous equations involving four sets of unknowns E_m, F_m, G_m, and H_m.

Equations for Figs. 5(a), (b), (c):

For Fig. 5(*a*)

$$w_1 = \frac{64qa^4}{D\pi^5} \sum_{m=1,3,5\ldots}^{\infty} (-1)^{\frac{m-1}{2}} \frac{\cos\frac{m\pi x}{2a}}{m^5} \left(1 - \frac{\alpha_m \tanh\alpha_m + 2}{2\cosh\alpha_m}\cosh\frac{m\pi y}{2a} + \frac{1}{2\cosh\alpha_m}\frac{m\pi y}{2a}\sinh\frac{m\pi y}{2a}\right) \quad \ldots\ldots [13a]$$

$$\left(\frac{\partial w_1}{\partial y}\right)_{y=b} = \frac{16qa^3}{D\pi^4} \sum_{m=1,3,5\ldots}^{\infty} (-1)^{\frac{m-1}{2}} \frac{\cos\frac{m\pi x}{2a}}{m^4} \left(\frac{\alpha_m}{\cosh^3\alpha_m} - \tanh\alpha_m\right) \quad \ldots\ldots [13b]$$

$$(M_y)_{y=0} = \frac{16qa^2}{\pi^3} \sum_{m=1,3,5...}^{\infty} (-1)^{\frac{m-1}{2}} \frac{\cos \frac{m\pi x}{2a}}{m^3}$$

$$\left[\frac{\alpha_m \tanh \alpha_m + \nu(2 \cosh \alpha_m - \alpha_m \tanh \alpha_m - 2)}{2 \cosh \alpha_m}\right] \quad [13c]$$

where

$$\alpha_m = \frac{m\pi b}{2a}$$

For Fig. 5(*b*)

$$w_2 = -\frac{2b^2}{D\pi^2} \sum_{m=1,3,5...}^{\infty} (-1)^{\frac{m-1}{2}} \frac{G_m}{m^2 \cosh \beta_m} \cos \frac{m\pi y}{2b}$$

$$\left(\frac{m\pi x}{2b} \sinh \frac{m\pi x}{2b} - \beta_m \tanh \beta_m \cosh \frac{m\pi x}{2b}\right) \quad [14a]$$

$$\left(\frac{\partial w_2}{\partial x}\right)_{x=a} = -\frac{b}{\pi D} \sum_{m=1,3,5...}^{\infty} (-1)^{\frac{m-1}{2}} \frac{G_m}{m} \cos \frac{m\pi y}{2b}$$

$$\left(\tanh \beta_m + \frac{\beta_m}{\cosh^2 \beta_m}\right) \quad [14b]$$

$$\left(\frac{\partial w_2}{\partial y}\right)_{y=b} = -\frac{8a^2}{D\pi^2 b} \sum_{m=1,3,5...}^{\infty} \frac{G_m}{m^3} \sum_{i=1,3,5...}^{\infty} \frac{(-1)^{\frac{i-1}{2}} i}{\left(\frac{a^2}{b^2} + \frac{i^2}{m^2}\right)^2} \cos \frac{i\pi x}{2a} \quad [14c]$$

$$(M_x)_{x=0} = \frac{1}{2} \sum_{m=1,3,5...}^{\infty} (-1)^{\frac{m-1}{2}} G_m \cos \frac{m\pi y}{2b}$$

$$\left[\frac{2 - (1-\nu)\beta_m \tanh \beta_m}{\cosh \beta_m}\right] \quad [14d]$$

$$(M_y)_{y=0} = \frac{1}{2} \sum_{m=1,3,5...}^{\infty} (-1)^{\frac{m-1}{2}} \frac{G_m}{\cosh \beta_m} \left\{[(1-\nu)\beta_m \tanh \beta_m + 2\nu] \cosh \frac{m\pi x}{2b} - (1-\nu) \frac{m\pi x}{2b} \sinh \frac{m\pi x}{2b}\right\}$$

$$= \frac{4}{\pi} \sum_{m=1,3,5...}^{\infty} (-1)^{\frac{m-1}{2}} \frac{G_m}{m^2} \sum_{i=1,3,5}^{\infty} \frac{(-1)^{\frac{i-1}{2}} i \left(\frac{a^2}{b^2} + \nu \frac{i^2}{m^2}\right)}{\left(\frac{a^2}{b^2} + \frac{i^2}{m^2}\right)^2} \cos \frac{i\pi x}{2a} \quad [14e][6]$$

where

$$\beta_m = \frac{m\pi a}{2b}$$

[6] When we expand $\{---\}$ into a Fourier cosine series, we tacitly assume that the function of period $4a$ represented by $\{---\}$ has finite jumps of $4\nu \cosh \beta_m$ at the points $x = \pm a$. It is seen that by the superposition process we remove all bending moments M_y along the X-axis except at the points $x = \pm a$, because at these points $(M_y)_{y=0}$ is not represented by the Fourier series. A similar state of affairs exists at the points $y = \pm b$ in Equation [15*d*].

For Fig. 5(*c*)

$$w_3 = -\frac{2a^2}{D\pi^2} \sum_{m=1,3,5...}^{\infty} H_m \frac{(-1)^{\frac{m-1}{2}}}{m^2 \cosh \alpha_m} \cos \frac{m\pi x}{2a}$$

$$\left(\frac{m\pi y}{2a} \sinh \frac{m\pi y}{2a} - \alpha_m \tanh \alpha_m \cosh \frac{m\pi y}{2a}\right) \quad [15a]$$

$$\left(\frac{\partial w_3}{\partial x}\right)_{x=a} = -\frac{8b^2}{D\pi^2 a} \sum_{m=1,3,5...}^{\infty} \frac{H_m}{m^3} \sum_{i=1,3,5...}^{\infty} \frac{(-1)^{\frac{i-1}{2}} i}{\left(\frac{b^2}{a^2} + \frac{i^2}{m^2}\right)^2} \cos \frac{i\pi y}{2b} \quad [15b]$$

$$\left(\frac{\partial w_3}{\partial y}\right)_{y=b} = -\frac{a}{D\pi} \sum_{m=1,3,5...}^{\infty} (-1)^{\frac{m-1}{2}} \frac{H_m}{m} \cos \frac{m\pi x}{2a}$$

$$\left(\tanh \alpha_m + \frac{\alpha_m}{\cosh^2 \alpha_m}\right) \quad [15c]$$

$$(M_x)_{x=0} = \frac{4}{\pi} \sum_{m=1,3,5...}^{\infty} (-1)^{\frac{m-1}{2}} \frac{H_m}{m^2} \sum_{i=1,3,5...}^{\infty} \frac{(-1)^{\frac{i-1}{2}} i \left(\frac{b^2}{a^2} + \nu \frac{i^2}{m^2}\right)}{\left(\frac{b^2}{a^2} + \frac{i^2}{m^2}\right)^2} \cos \frac{i\pi y}{2b} \quad [15d]$$

$$(M_y)_{y=0} = \frac{1}{2} \sum_{m=1,3,5...}^{\infty} (-1)^{\frac{m-1}{2}} H_m \cos \frac{m\pi x}{2a}$$

$$\left[\frac{2 - (1-\nu)\alpha_m \tanh \alpha_m}{\cosh \alpha_m}\right] \quad [15e]$$

Derivation of Equations for Figs. 5(d) and 5(e). Denote the deflections by w_4. Then w_4 must satisfy the differential equation

$$\frac{\partial^4 w_4}{\partial x^4} + 2 \frac{\partial^4 w_4}{\partial x^2 \partial y^2} + \frac{\partial^4 w_4}{\partial y^4} = 0 \quad [16]$$

and the boundary conditions

At $x = 0$

$$M_x = -D\left(\frac{\partial^2 w_4}{\partial x^2} + \nu \frac{\partial^2 w_4}{\partial y^2}\right) = \sum_{m=1,3,5...}^{\infty} (-1)^{\frac{m-1}{2}} E_m \cos \frac{m\pi y}{2b} \quad [17a]$$

$$\frac{\partial^3 w_4}{\partial x^3} + (2-\nu) \frac{\partial^3 w_4}{\partial x \partial y^2} = 0 \quad [17b]$$

At $x = a$

$$w_4 = 0 \quad \text{and} \quad \frac{\partial^2 w_4}{\partial x^2} = 0 \quad [17c]$$

At $y = b$

$$w_4 = 0 \quad \text{and} \quad \frac{\partial^2 w_4}{\partial y^2} = 0 \quad [17d]$$

Take the solution of Equation [16] in the form of the series

$$w_4 = \sum_{m=1,3,5\ldots}^{\infty} X_m \cos \frac{m\pi y}{2b} \quad \ldots\ldots\ldots\ldots [18]$$

in which X_m is a function of x alone. Then the function X_m is found to be

$$X_m = A_m \sinh \frac{m\pi x}{2b} + B_m \cosh \frac{m\pi x}{2b} + C_m \frac{m\pi x}{2b} \sinh \frac{m\pi x}{2b} + D_m \frac{m\pi x}{2b} \cosh \frac{m\pi x}{2b}$$

From the boundary conditions in Equations [17] the constants are

$$A_m = \frac{(-1)^{\frac{m-1}{2}} (1+\nu) \frac{E_m}{D} \frac{b^2}{m^2\pi^2}}{(1-\nu)(3+\nu)\tanh \beta_m + (1-\nu)^2 \beta_m \operatorname{sech}^2 \beta_m}$$

$$B_m = -\frac{(-1)^{\frac{m-1}{2}} \frac{E_m}{D} \frac{b^2}{m^2\pi^2} [(1+\nu)\tanh \beta_m + (1-\nu)\beta_m \operatorname{sech}^2 \beta_m]}{(1-\nu)(3+\nu)\tanh \beta_m + (1-\nu)^2 \beta_m \operatorname{sech}^2 \beta_m}$$

$$C_m = -\frac{(-1)^{\frac{m-1}{2}} (1-\nu) \frac{E_m}{D} \frac{b^2}{m^2\pi^2} \tanh \beta_m}{(1-\nu)(3+\nu)\tanh \beta_m + (1-\nu)^2 \beta_m \operatorname{sech}^2 \beta_m}$$

$$D_m = \frac{(-1)^{\frac{m-1}{2}} (1-\nu) \frac{E_m}{D} \frac{b^2}{m^2\pi^2}}{(1-\nu)(3+\nu)\tanh \beta_m + (1-\nu)^2 \beta_m \operatorname{sech}^2 \beta_m}$$

where $\beta_m = \dfrac{m\pi a}{2b}$

and $w_4 = \dfrac{b^2}{D\pi^2} \displaystyle\sum_{m=1,3,5\ldots}^{\infty} (-1)^{\frac{m-1}{2}} \frac{E_m}{m^2}$

$$\frac{\cos \frac{m\pi y}{2b}}{(1-\nu)(3+\nu)\tanh \beta_m + (1-\nu)^2 \beta_m \operatorname{sech}^2 \beta_m} \left\{ (1+\nu)\sinh \frac{m\pi x}{2b} - [(1+\nu)\tanh \beta_m + (1-\nu)\beta_m \operatorname{sech}^2 \beta_m] \cosh \frac{m\pi x}{2b} - (1-\nu)\tanh \beta_m \frac{m\pi x}{2b} \sinh \frac{m\pi x}{2b} + (1-\nu)\frac{m\pi x}{2b} \cosh \frac{m\pi x}{2b} \right\}$$

$$(M_y)_{y=0} = (1-\nu)^2 \sum_{m=1,3,5\ldots}^{\infty} \frac{(-1)^{\frac{m-1}{2}} E_m}{(1-\nu)(3+\nu)\tanh \beta_m + (1-\nu)^2 \beta_m \operatorname{sech}^2 \beta_m} \left\{ \sinh \frac{m\pi x}{2b} - (\tanh \beta_m + \beta_m \operatorname{sech}^2 \beta_m) \cosh \frac{m\pi x}{2b} - \tanh \beta_m \frac{m\pi x}{2b} \sinh \frac{m\pi x}{2b} + \frac{m\pi x}{2b} \cosh \frac{m\pi x}{2b} \right\}$$

The expression in parentheses in the last equation can be expanded into a cosine series of the form

$$\sum_{i=1,3,5\ldots}^{\infty} A_i \cos \frac{i\pi x}{2a}$$

from which it follows that

$$A_i = -\frac{8}{\pi} \frac{a}{b} \frac{i^2}{m^3 \left(\frac{a^2}{b^2} + \frac{i^2}{m^2} \right)^2}$$

and

$$(M_y)_{y=0} = -\frac{8(1-\nu)^2}{\pi} \frac{a}{b} \sum_{m=1,3,5\ldots}^{\infty} \frac{(-1)^{\frac{m-1}{2}} E_m}{m^3[(1-\nu)(3+\nu)\tanh \beta_m + (1-\nu)^2 \beta_m \operatorname{sech}^2 \beta_m]} \sum_{i=1,3,5\ldots}^{\infty} \frac{i^2 \cos \frac{i\pi x}{2a}}{\left(\frac{a^2}{b^2} + \frac{i^2}{m^2} \right)^2} \quad \ldots\ldots [19]$$

Similarly, the following equations are obtained

$$\left(\frac{\partial w_4}{\partial x} \right)_{x=a} = \frac{2b}{D\pi} \sum_{m=1,3,5\ldots}^{\infty} \frac{(-1)^{\frac{m-1}{2}} E_m [2 \operatorname{sech} \beta_m - (1-\nu)\beta_m \sinh \beta_m \operatorname{sech}^2 \beta_m]}{m[(1-\nu)(3+\nu)\tanh \beta_m + (1-\nu)^2 \beta_m \operatorname{sech}^2 \beta_m]} \cos \frac{m\pi y}{2b} \quad \ldots\ldots [20]$$

$$\left(\frac{\partial w_4}{\partial y} \right)_{y=b} = \frac{16}{\pi^2} \frac{a}{D} \sum_{m=1,3,5\ldots}^{\infty} \frac{E_m}{m^2[(1-\nu)(3+\nu)\tanh \beta_m + (1-\nu)^2 \beta_m \operatorname{sech}^2 \beta_m]} \sum_{i=1,3,5\ldots}^{\infty} \frac{\frac{i^2}{m^2} + \nu \frac{a^2}{b^2}}{\left(\frac{a^2}{b^2} + \frac{i^2}{m^2} \right)^2} \cos \frac{i\pi x}{2a} \quad \ldots\ldots [21]$$

The equations for Fig. 5(*e*) may then be written as follows

$$(M_x)_{x=0} = -\frac{8(1-\nu)^2}{\pi} \frac{b}{a} \sum_{m=1,3,5\ldots}^{\infty} \frac{(-1)^{\frac{m-1}{2}} F_m}{m^3[(1-\nu)(3+\nu)\tanh \alpha_m + (1-\nu)^2 \alpha_m \operatorname{sech}^2 \alpha_m]} \sum_{i=1,3,5\ldots}^{\infty} \frac{i^2 \cos \frac{i\pi y}{2b}}{\left(\frac{b^2}{a^2} + \frac{i^2}{m^2} \right)^2} \quad \ldots\ldots [22]$$

$$\left(\frac{\partial w_2}{\partial y}\right)_{y=b} = \frac{2a}{\pi D}\sum_{m=1,3,5\ldots}^{\infty} \frac{(-1)^{\frac{m-1}{2}} F_m[2\ \mathrm{sech}\ \alpha_m - (1-\nu)\alpha_m \sinh \alpha_m\ \mathrm{sech}^2 \alpha_m]}{m[(1-\nu)(3+\nu)\tanh \alpha_m + (1-\nu)^2\alpha_m\ \mathrm{sech}^2 \alpha_m]} \cos\frac{m\pi x}{2a} \quad \ldots\ldots [23]$$

$$\left(\frac{\partial w_2}{\partial x}\right)_{x=a} = \frac{16}{\pi^2}\frac{b}{D}\sum_{m=1,3,5\ldots}^{\infty} \frac{F_m}{m^2[(1-\nu)(3+\nu)\tanh \alpha_m + (1-\nu)^2\alpha_m\ \mathrm{sech}^2 \alpha_m]} \sum_{i=1,3,5\ldots}^{\infty} \frac{\frac{i^2}{m^2} + \nu\frac{b^2}{a^2}}{\left(\frac{b^2}{a^2} + \frac{i^2}{m^2}\right)^2} \cos\frac{i\pi y}{2b} \quad \ldots\ldots [24]$$

Solution of Problem. Since one boundary condition requires M_y to be zero at $y = 0$, we combine Equations [12], [13c], [14e], [15e], and [19], and write the sum equal to zero. In this way we obtain the following set of equations

$$\frac{F_i}{i} - \frac{8(1-\nu)^2}{\pi}(-1)^{\frac{i-1}{2}} i\frac{a}{b}\sum_{m=1,3,5\ldots}^{\infty} \frac{(-1)^{\frac{m-1}{2}} E_m}{[(1-\nu)(3+\nu)\tanh \beta_m + (1-\nu)^2\beta_m\ \mathrm{sech}^2 \beta_m]m^2\left(\frac{a^2}{b^2} + \frac{i^2}{m^2}\right)^2} + \frac{H_i}{i}\frac{2-(1-\nu)\alpha_i \tanh \alpha_i}{2\cosh \alpha_i} + \frac{4}{\pi}\sum_{m=1,3,5\ldots}^{\infty} (-1)^{\frac{m-1}{2}} G_m \frac{\left(\frac{a^2}{b^2} + \nu\frac{i^2}{m^2}\right)}{m^2\left(\frac{a^2}{b^2} + \frac{i^2}{m^2}\right)^2} = -\frac{16qa^2}{\pi^3}\frac{1}{i^4}\frac{\alpha_i \tanh \alpha_i + \nu(2\cosh \alpha_i - \alpha_i \tanh \alpha_i - 2)}{2\cosh \alpha_i} \quad \ldots\ldots [25]$$

Also, from the condition that the slope $\partial w/\partial y$ must be zero at $y = b$, the following set of equations is obtained

$$\frac{F_i}{i}\frac{2[2-(1-\nu)\alpha_i \tanh \alpha_i]}{\cosh \alpha_i[(1-\nu)(3+\nu)\tanh \alpha_i + (1-\nu)^2\alpha_i \mathrm{sech}^2 \alpha_i]} + (-1)^{\frac{i-1}{2}}\frac{16}{\pi}\sum_{m=1,3,5\ldots}^{\infty} \frac{E_m\left(\frac{i^2}{m^2} + \nu\frac{a^2}{b^2}\right)}{[(1-\nu)(3+\nu)\tanh \beta_m + (1-\nu)^2\beta_m\ \mathrm{sech}^2 \beta_m]m^2\left(\frac{a^2}{b^2} + \frac{i^2}{m^2}\right)^2} - \frac{H_i}{i}\left(\tanh \alpha_i + \frac{\alpha_i}{\cosh^2 \alpha_i}\right) - \frac{8i}{\pi}\frac{a}{b}\sum_{m=1,3,5\ldots}^{\infty} \frac{G_m}{m^3}\frac{1}{\left(\frac{a^2}{b^2} + \frac{i^2}{m^2}\right)^2}$$

$$= -\frac{16qa^2}{\pi^3}\frac{1}{i^4}\left(\frac{\alpha_i}{\cosh^2 \alpha_i} - \tanh \alpha_i\right) \quad \ldots\ldots [26]$$

In a similar manner, two other equations can be obtained from the other two boundary conditions, i.e., $M_x = 0$ at $x = 0$ and at $x = a$. Thus we have four sets of equations providing relations for determining the unknowns E_m, F_m, G_m, and H_m. After these constants have been determined numerically, the deflection and the bending moment at any point can be obtained by superposition.

Numerical Example. Consider the case of a square plate in which $a = b$, $E_i = F_i$, and $G_i = H_i$, and the four sets of equations are reduced to two sets. In the following, Poisson's ratio is assumed to be zero in order to reduce the arithmetical work. In this case, Equations [25] and [26] become

$$\frac{E_i}{i} - (-1)^{\frac{i-1}{2}}\frac{8i}{\pi}\sum_{m=1,3,5\ldots}^{\infty} \frac{(-1)^{\frac{m-1}{2}} E_m}{(3\tanh \alpha_m + \alpha_m\ \mathrm{sech}^2 \alpha_m)m^3\left(1 + \frac{i^2}{m^2}\right)^2} + \frac{G_i}{i}\frac{2-\alpha_i \tanh \alpha_i}{2\cosh \alpha_i} + \frac{4}{\pi}\sum_{m=1,3,5\ldots}^{\infty} \frac{(-1)^{\frac{m-1}{2}} G_m}{m^2\left(1 + \frac{i^2}{m^2}\right)^2} = -\frac{16qa^2}{\pi^3}\frac{1}{i^4}\frac{\alpha_i \tanh \alpha_i}{2\cosh \alpha_i} \quad \ldots\ldots [27]$$

$$\frac{E_i}{i}\frac{2(2-\alpha_i \tanh \alpha_i)}{\cosh \alpha_i(3\tanh \alpha_i + \alpha_i \mathrm{sech}^2 \alpha_i)} + (-1)^{\frac{i-1}{2}}\frac{16i^2}{\pi} \sum_{m=1,3,5\ldots}^{\infty} \frac{E_m}{(3\tanh \alpha_m + \alpha_m\ \mathrm{sech}^2 \alpha_m)(m^2 + i^2)^2} - \frac{G_i}{i}\left(\tanh \alpha_i + \frac{\alpha_i}{\cosh^2 \alpha_i}\right) - \frac{8i}{\pi}\sum_{m=1,3,5\ldots}^{\infty} \frac{G_m}{m^3\left(1 + \frac{i^2}{m^2}\right)^2} = \frac{16qa^2}{\pi^5 i^4}\left(\tanh \alpha_i - \frac{\alpha_i}{\cosh^2 \alpha_i}\right) \quad \ldots\ldots [28]$$

By taking the first four coefficients in each series, the following equations are obtained

$$0.78786\ E_1 + 0.025456\ E_3 - 0.006278\ E_5 + 0.002377\ E_7 + 0.42977\ G_1 - 0.11459\ G_3 + 0.04709\ G_5 - 0.02496\ G_7 = -0.28708\ K$$

$$0.57284\ E_1 + 0.016971\ E_3 + 0.002511\ E_5 + 0.000679\ E_7 - 1.8033\ G_1 - 0.07639\ G_3 - 0.01884\ G_5 - 0.00713\ G_7 = 0.66768\ K$$

$$0.025457\ E_1 + 0.30976\ E_3 + 0.011014\ E_5 - 0.005299\ E_7 + 0.012732\ G_1 - 0.043487\ G_3 + 0.027536\ G_5 - 0.018546\ G_7 = -0.0005225\ K$$

$$0.15274\ E_1 + 0.052552\ E_3 + 0.013217\ E_5 + 0.004542\ E_7 + 0.076394\ G_1 + 0.40452\ G_3 + 0.033043\ G_5 + 0.015897\ G_7 = -0.012325\ K$$

$$0.006276\,E_1 - 0.011010\,E_3 - 0.19151\,E_5 - 0.005425\,E_7 - 0.001884\,G_1 + 0.009913\,G_3 - 0.012278\,G_5 + 0.011393\,G_7 = 0.00000488\,K$$

$$0.062763\,E_1 + 0.036701\,E_3 + 0.016730\,E_5 + 0.005425\,E_7 - 0.018835\,G_1 - 0.033043\,G_3 - 0.22547\,G_5 - 0.016276\,G_7 = 0.001600\,K$$

$$0.002376\,E_1 - 0.005297\,E_3 + 0.005425\,E_5 + 0.13853\,E_7 + 0.0005093\,G_1 - 0.003406\,G_3 + 0.005813\,G_5 - 0.006518\,G_7 = -8 \times 10^{-6}\,K$$

$$0.033263\,E_1 + 0.024719\,E_3 + 0.015191\,E_5 + 0.008690\,E_7 + 0.007130\,G_1 + 0.015897\,G_3 + 0.016276\,G_5 + 0.15585\,G_7 = -0.0004165\,K$$

where

$$K = 16qa^2/\pi^2$$

Solving these equations yields the following values for the coefficients

$$\begin{aligned} E_1 &= -0.1254\,K, & G_1 &= -0.4134\,K \\ E_3 &= 0.0412\,K, & G_3 &= 0.0895\,K \\ E_5 &= 0.0046\,K, & G_5 &= -0.0152\,K \\ E_7 &= 0.0092\,K, & G_7 &= 0.0280\,K \end{aligned}$$

The maximum deflection occurs at the origin, Fig. 4, and is found to be

$$(w)_{max} = 0.03619\,qa^4/D$$

If six coefficients are taken for each series, the following values are obtained

$$\begin{aligned} E_1 &= -0.1251\,K, & G_1 &= -0.4133\,K \\ E_3 &= 0.0419\,K, & G_3 &= 0.0893\,K \\ E_5 &= 0.0055\,K, & G_5 &= -0.0147\,K \\ E_7 &= 0.0102\,K, & G_7 &= 0.0276\,K \\ E_9 &= 0.0015\,K, & G_9 &= -0.0115\,K \\ E_{11} &= 0.0045\,K, & G_{11} &= 0.0137\,K \end{aligned}$$

By using these values, the maximum deflection is found to be the same as in the foregoing.

In calculating the moments, a difficulty arises. At the junctions of the clamped and free edges, the moments actually become singular and, near these junctions, the moments are large. The present analysis makes use of a finite number of functions which are regular in the corners and hence cannot show this growth rate of the moments. It follows that moment calculations near the corners are not dependable. However, the deflection as given is probably quite accurate.

BIBLIOGRAPHY

1 "Bending of Rectangular Plates With Clamped Edges," by S. Timoshenko, Proceedings of the Fifth International Congress for Applied Mechanics, Cambridge, Mass., 1938, p. 40.

2 "The Clamped Rectangular Plate With a Concentrated Load," by Dana Young, JOURNAL OF APPLIED MECHANICS, Trans. ASME, vol. 61, 1939, p. A-114.

3 "Bending Moments in the Walls of Rectangular Tanks," by Dana Young, Proceedings of the ASCE, vol. 67, 1941, p. 1683.

4 "The Bending of the Clamped Sectorial Plate," by G. F. Carrier, JOURNAL OF APPLIED MECHANICS, Trans. ASME, vol. 66, 1944, p. A-134.

5 "Bending of Clamped Plates," by W. B. Stiles, JOURNAL OF APPLIED MECHANICS, Trans. ASME, vol. 69, 1947, p. A-55.

6 "Étude des spectres des équations aux dérivées partielles de la théorie des plaques élastiques," by A. Weinstein, Memorial des Science Mathematique, vol. 88, 1937, p. 1.

7 "On the Bending of a Clamped Plate," by A. Weinstein and D. H. Rock, *Quarterly of Applied Mathematics*, vol. 2, 1944, p. 262

Appendix

Derivation of Equation [4a]. Consider the case in which a concentrated load P acts at a point A on the X-axis, Fig. 6. The

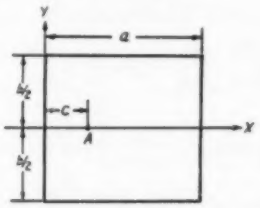

FIG. 6

deflection of the portion of the plate above the X-axis is given by the following equation[7]

$$w' = \sum_{m=1}^{\infty} \left(A_m' \cosh \frac{m\pi y}{a} + B_m' \sinh \frac{m\pi y}{a} + C_m' \frac{m\pi y}{a} \sinh \frac{m\pi y}{a} + D_m' \frac{m\pi y}{a} \cosh \frac{m\pi y}{a} \right) \sin \frac{m\pi x}{a}$$

for $y > 0$ ..... [29]

in which

$$A_m' = \frac{a_m \sinh 2\gamma_m}{\cosh \alpha_m} \left(\sinh \alpha_m - \gamma_m \coth 2\gamma_m \sinh \alpha_m - \frac{\alpha_m}{2 \cosh \alpha_m} \right)$$

$$B_m' = \frac{a_m \sinh 2\gamma_m}{\sinh \alpha_m} (-\sinh \alpha_m + \gamma_m \coth 2\gamma_m \sinh \alpha_m)$$

$$C_m' = -\frac{a_m}{2 \cosh \alpha_m} \sinh 2\gamma_m \sinh \alpha_m$$

$$D_m' = \frac{a_m}{2} \sinh 2\gamma_m$$

and

$$a_m = \frac{2Pa^3}{b_1 D\pi^4} \frac{\sin \frac{m\pi c}{a}}{m^4}, \quad \alpha_m = \frac{m\pi b}{2a}, \quad \gamma_m = \frac{m\pi b_1}{4a}$$

where b_1 is the infinitesimal width of the strip on which the load P acts. Let b_1 approach zero as a limit, and Equation [29] becomes

$$w' = \frac{Pa^3}{2D\pi^3} \sum_{m=1}^{\infty} \frac{\sin \frac{m\pi c}{a}}{m^3} \left[\left(\tanh \alpha_m - \frac{\alpha_m}{\cosh^2 \alpha_m} \right) \cosh \frac{m\pi y}{a} - \sinh \frac{m\pi y}{a} + \frac{m\pi y}{a} \cosh \frac{m\pi y}{a} - \tanh \alpha_m \frac{m\pi y}{a} \sinh \frac{m\pi y}{a} \right] \sin \frac{m\pi x}{a}$$ for $0 \leq y \leq b/2$ .. [30]

[7] See "Theory of Plates and Shells," by S. Timoshenko, McGraw-Hill Book Company Inc., New York, N. Y., 1940, pp. 147–157.

If the load along the X-axis is represented by the series

$$\sum_{n=1,3,5\ldots}^{\infty} A_n \sin \frac{n\pi x}{a} \quad \ldots\ldots\ldots\ldots\ldots [31]$$

the deflection w' can be obtained by integration of Equation [30]

$$w' = \frac{a^3}{2D\pi^3} \int_{c=0}^{a} \sum_{n=1,3,5\ldots}^{\infty} A_n \sin \frac{n\pi c}{a}\, dc \sum_{m=1}^{\infty} \frac{\sin \frac{m\pi c}{a}}{m^3} \left[\left(\tanh \alpha_m - \frac{\alpha_m}{\cosh^2 \alpha_m} \right) \cosh \frac{m\pi y}{a} - \sinh \frac{m\pi y}{a} - \tanh \alpha_m \frac{m\pi y}{a} \sinh \frac{m\pi y}{a} + \frac{m\pi y}{a} \cosh \frac{m\pi y}{a} \right] \sin \frac{m\pi x}{a}$$

$$= \frac{a^3}{4D\pi^3} \sum_{m=1,3,5\ldots}^{\infty} \frac{A_m}{m^3} \left[\left(\tanh \alpha_m - \frac{\alpha_m}{\cosh^2 \alpha_m} \right) \cosh \frac{m\pi y}{a} - \sinh \frac{m\pi y}{a} - \tanh \alpha_m \frac{m\pi y}{a} \sinh \frac{m\pi y}{a} + \frac{m\pi y}{a} \cosh \frac{m\pi y}{a} \right] \sin \frac{m\pi x}{a} \text{ for } 0 \le y \le b/2 \ldots [32]$$

Shifting the origin to the center of the plate, the load, Equation [31] becomes

$$\sum_{n=1,3,5\ldots}^{\infty} (-1)^{\frac{n-1}{2}} A_n \cos \frac{n\pi x}{a}$$

and the deflection, Equation [32], becomes

$$w' = \frac{a^3}{4D\pi^3} \sum_{m=1,3,5\ldots}^{\infty} (-1)^{\frac{m-1}{2}} \frac{A_m}{m^3} \left[\left(\tanh \alpha_m - \frac{\alpha_m}{\cosh^2 \alpha_m} \right) \cosh \frac{m\pi y}{a} - \sinh \frac{m\pi y}{a} - \tanh \alpha_m \frac{m\pi y}{a} \sinh \frac{m\pi y}{a} + \frac{m\pi y}{a} \cosh \frac{m\pi y}{a} \right] \cos \frac{m\pi x}{a} \text{ for } 0 \le y \le b/2$$

Changing the dimensions a to $2a$ and b to $2b$, we obtain

$$w' = \frac{2a^3}{D\pi^3} \sum_{m=1,3,5\ldots}^{\infty} (-1)^{\frac{m-1}{2}} \frac{A_m}{m^3} \left[\left(\tanh \alpha_m - \frac{\alpha_m}{\cosh^2 \alpha_m} \right) \cosh \frac{m\pi y}{2a} - \sinh \frac{m\pi y}{2a} - \tanh \alpha_m \frac{m\pi y}{2a} \sinh \frac{m\pi y}{2a} + \frac{m\pi y}{2a} \cosh \frac{m\pi y}{2a} \right] \cos \frac{m\pi x}{2a} \text{ for } 0 \le y \le b$$

which is Equation [4a]. Equation [4b] can be derived in a similar manner.

A Nonlinear Problem in the Bending Vibration of a Rotating Beam

By HSU LO,[1] WEST LAFAYETTE, IND.

The problem of bending vibration of a rotating beam is a nonlinear one when the vibration takes place in a plane not perpendicular to the plane of rotation. The nonlinear term arises from the Coriolis acceleration. From the nonlinear equation established, it is found that the existence of periodic solutions depends on the initial conditions, and the most important parameter which affects the periodic solutions is the nondimensional amplitude A. The percentage error in the frequency of vibration due to neglect of the Coriolis acceleration is a function of the parameter A only. For most of the present-day applications the error is negligible.

Introduction

In a recent paper,[2] Lo and Renbarger presented results of an investigation of the problem of bending vibration of a rotating beam, vibrating in a plane making an arbitrary angle $(\pi/2 - \beta)$ with the plane of rotation. It was found that except $\beta = 0$ (vibration perpendicular to the plane of rotation), the problem is nonlinear because of the Coriolis acceleration. By neglecting the nonlinear term, however, the authors of that paper established an interesting theory which states that the vibration modes are independent of the angle β and the vibration frequencies ω are related to the corresponding frequencies $\omega_\perp$ at $\beta = 0$ in the following simple manner

$$\omega^2 = \omega_\perp{}^2 - \Omega^2 \sin^2 \beta \quad \ldots\ldots\ldots\ldots\ldots\ldots [1]$$

where Ω is the speed of rotation. Since the bending vibration of rotating beams at $\beta = 0$ has been investigated by many authors, the results of their investigation can be used together with the foregoing theory to give the modes and frequencies for vibrations in any other planes β.

The questions remaining are (*a*) what are the errors induced by dropping the nonlinear term, and (*b*) what are the parameters that affect the error? It is the purpose of the present paper to seek an answer to those questions by studying the nonlinear equation itself. In order to simplify the problem, however, the beam is replaced by its semirigid representation; that is, the beam is assumed to be rigid in bending everywhere except at the root where a spiral spring is used to connect the beam to the rotating shaft. Guides are provided so that the bending vibration takes place in one plane only.

Equation of Motion

Shown in Fig. 1 are the elastic axis O-E of the beam at its neutral position and O-E' at an arbitrary deflected position. The line O-E' lies in the plane of vibration O-D which makes an angle β with the axis of rotation, O-z. The x-axis is chosen to coincide with the elastic axis O-E, and the y-axis is perpendicular to both O-x and O-z to form a left-hand system. Both the x and y-axes rotate with the beam.

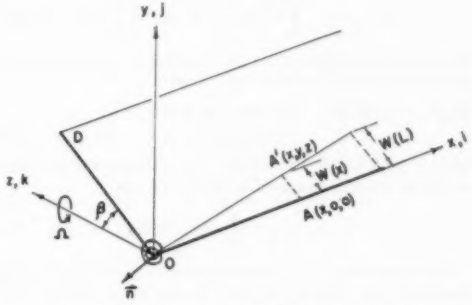

Fig. 1 Co-Ordinate System of Rotating Beam

With the same assumption used by Lo and Renbarger,[2] that the displacement in the z-direction is neglected for small oscillations, an element of the beam originally located at the point $A(x, O, O)$ is displaced to the position $A'(x, y, z)$ where $y = W(x) \sin \beta$ and $z = W(x) \cos \beta$. The symbol $W(x)$ is used to denote the displacement in the plane O-D of the beam at station x.

Let i, j, and k be the unit vectors along the x, y, and z-directions. The radius vector $\vec{R}$ to the deflected position $A'(x, y, z)$ is then

$$\vec{R} = ix + jW(x) \sin \beta + kW(x) \cos \beta \quad \ldots\ldots\ldots [2]$$

Differentiating twice with respect to the time t gives the acceleration

$$\frac{\partial^2 \vec{R}}{\partial t^2} = i[-2\Omega \dot{W}(x) \sin \beta - \Omega^2 x] + j[-\Omega^2 W(x) \sin \beta + \ddot{W}(x) \sin \beta] + k[\ddot{W}(x) \cos \beta] \quad \ldots\ldots\ldots [3]$$

where the dot refers to differentiation with respect to t. The first term on the right-hand side of Equation [3] is the Coriolis acceleration. The inertia force of the element $m(x)dx$ at the position $A'(x, y, z)$ is

$$d\vec{F} = -m(x)dx \frac{\partial^2 \vec{R}}{\partial t^2} \quad \ldots\ldots\ldots\ldots\ldots [4]$$

The bending moment at the root due to the inertia force $d\vec{F}$ is

---

[1] Associate Professor of Aeronautical Engineering, Purdue University.

[2] "Bending Vibrations of a Rotating Beam," by Hsu Lo and J. L. Renbarger, presented at the First United States National Congress of Applied Mechanics, Chicago, Ill., June, 1951; to be published in the Proceedings of that Congress.

Presented at the National Conference of the Applied Mechanics Division, State College, Pa., June 19–21, 1952, of The American Society of Mechanical Engineers.

Discussion of this paper should be addressed to the Secretary, ASME, 29 West 39th Street, New York, N. Y., and will be accepted until January 10, 1953, for publication at a later date. Discussion received after the closing date will be returned.

Note: Statements and opinions advanced in papers are to be understood as individual expressions of their authors and not those of the Society. Manuscript received by ASME Applied Mechanics Division, January 14, 1952. Paper No. 52—APM-35.

$$d\vec{M} = \vec{R} \times d\vec{F} = -s\ddot{s}(x)dx \left(\vec{R} \times \frac{\partial^2 \vec{R}}{\partial t^2}\right) \ldots\ldots [5]$$

and the total bending moment at the root due to the inertia forces of the whole beam is

$$\vec{M} = -\int_0^{\text{tip}} m(x) \left(\vec{R} \times \frac{\partial^2 \vec{R}}{\partial t^2}\right) dx \ldots\ldots [6]$$

Since we are only interested in the bending moment in the plane of vibration O-D, we take the dot product of the total bending moment with the unit vector

$$\vec{n} = -j \cos \beta + k \sin \beta \ldots\ldots [7]$$

which is normal to the plane O-D, as shown in Fig. 1. The result is the bending moment in the plane O-D at the root of the beam, or

$$M_{OD} = -\int_0^{\text{tip}} m(x) \left(\vec{n} \cdot \vec{R} \times \frac{\partial^2 \vec{R}}{\partial t^2}\right) dx \ldots\ldots [8]$$

Substituting Equations [2] to [7] into Equation [8] and making use of the relation $W(x) = (x/L)\, W(L)$ gives

$$M_{OD} = -m_e L \ddot{W}(L) - 2\Omega m_e \sin \beta\, W(L)\dot{W}(L) - m_e L \Omega^2 \cos^2 \beta\, W(L) \ldots\ldots [9]$$

where L is the length of the beam, $W(L)$ is the bending deflection at the tip, and m_e is an equivalent mass defined as

$$m_e = \frac{1}{L^2} \int_0^L m(x)\, x^2\, dx \ldots\ldots [10]$$

The equilibrium of the inertia moment M_{OD} and the spring moment $M_S = -SW(L)/L$, where S is the spring constant of the spiral spring, gives the following equation of motion

$$m_e \ddot{W}(L)\, L + 2\Omega\, m_e \sin \beta\, W(L)\dot{W}(L) + (m_e L\, \Omega^2 \cos^2 \beta + S/L)\, W(L) = 0$$

Substitution of the relation

$$\omega^2 = \Omega^2 \cos^2 \beta + S/m_e L^2 \ldots\ldots [11]$$

and dropping the symbol L in the parentheses of the term $W(L)$ gives

$$\ddot{W} + \left(2 \frac{\Omega}{L} \sin \beta\, W\right) \dot{W} + \omega^2 W = 0 \ldots\ldots [12]$$

This is the equation governing the motion of the vibrating beam.

Before the solution of Equation [12] is discussed, the following points are worth mentioning. (*a*) The nonlinear term, i.e., the middle term, of Equation [12] is due to the Coriolis acceleration. Had the Coriolis acceleration $-2\Omega\dot{W}(x) \sin \beta$ in Equation [3] been neglected, the resulting equation of motion would have been

$$\ddot{W} + \omega^2 W = 0 \ldots\ldots [13]$$

which is a harmonic vibration with the natural frequency ω. (*b*) When $\beta = 0$, i.e., when the plane of vibration is perpendicular to the plane of rotation, the Coriolis acceleration drops out automatically and the natural frequency becomes

$$\omega_\perp^2 = \Omega^2 + S/m_e L^2$$

(*c*) Substitution of this expression into Equation [11] gives

$$\omega^2 = \omega_\perp^2 - \Omega^2 \sin^2 \beta$$

which checks with Equation [1]. (*d*) Finally, the expression $S/m_e L^2$ in Equation [11] is the square of the natural frequency ω_0 of the beam when $\Omega = 0$. Therefore Equation [11] can be written as

$$\omega^2 = \omega_0^2 + \Omega^2 \cos^2 \beta$$

which agrees in general form with Southwell's equation.

A System by Analogy

Equation [12] is in effect the same equation of motion for a simple spring-mass system with a nonlinear viscous damping. The coefficient of the damping term is $(2\Omega/L \sin \beta\, W)$. This coefficient is an antisymmetric function of the displacement W. To the best of the author's knowledge, a nonlinear system with antisymmetric damping has not been discussed before. A general study of the existence and uniqueness of periodic motions of such a system is therefore desirable for general damping and spring functions. Because of space limitations the general discussion of this problem will not be included here. It is enough to mention at present that for positive W the damping is positive and the vibration is dissipative; for negative W the damping is negative and the vibration is self-excited. Because of the antisymmetric characteristics it can be expected that the energy dissipated in the first half cycle of vibration will be compensated by the energy gained in the second half cycle of vibration. Periodic solutions, therefore, can be anticipated.

Solution in Phase Plane

With the introduction of the following nondimensional parameters

$$\overline{W} = \frac{\alpha}{\omega} W \ldots\ldots [14]$$

$$\bar{t} = \omega t$$

where

$$\alpha = 2 \frac{\Omega}{L} \sin \beta \ldots\ldots [15]$$

Equation [12] can be written in the following nondimensional form

$$\overline{W}'' + \overline{W}\, \overline{W}' + \overline{W} = 0 \ldots\ldots [16]$$

where the prime system is used to denote the differentiation with respect to the nondimensional time $\bar{t}$.

Let $\bar{U} = \overline{W}'$ be the nondimensional velocity. Equation [16] can be written as

$$\bar{U}' = -\overline{W}\, \bar{U} - \overline{W}$$

The corresponding equation in the phase plane is

$$\frac{d\bar{U}}{d\overline{W}} = \frac{\bar{U}'}{\overline{W}'} = -\frac{1 + \bar{U}}{\bar{U}} \overline{W} \ldots\ldots [17]$$

The solution of this equation is

$$\frac{1}{2} \overline{W}^2 + \bar{U} - \log (1 + \bar{U}) = C_1, \text{ for } \bar{U} > -1 \ldots [18]$$

$$\frac{1}{2} \overline{W}^2 + \bar{U} - \log [-(1 + \bar{U})] = C_2, \text{ for } \bar{U} < -1 \ldots [19]$$

where C_1 and C_2 are the constants of integration.

Equations [18] and [19] represent two different types of solutions; the former is a family of concentric closed curves in the phase plane with the origin as the center while the latter is a family of open curves, as shown in Fig. 2. The line $\bar{U} = -1$ divides

the phase plane into two regions corresponding to the two different solutions. This line is called the "separatrix." For any given combination of the initial displacement and velocity lying above the separatrix, the resulting motion is periodic. For any given combination of the initial displacement and velocity lying below the separatrix, the motion of the system follows the arrow (the direction of increasing time) on the corresponding open curve with increasing amplitude and velocity until the system meets its destruction.

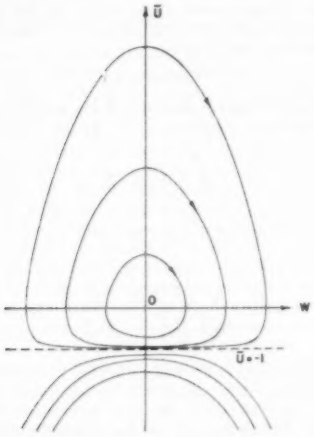

FIG. 2 PERIODIC AND NONPERIODIC SOLUTIONS

From the definition

$$\bar{U} = \bar{W}' = \frac{\alpha}{\omega^2}\dot{W}$$

it follows that the critical value $\bar{U} = -1$ becomes

$$\dot{W} = -\frac{\omega^2}{\alpha} \quad \ldots\ldots\ldots\ldots\ldots\ldots [20]$$

The negative sign means that the velocity is opposite to the direction of rotation. For any case where the velocity in that direction is greater than the critical value ω^2/α, the motion will follow the open curves.

PERIODIC SOLUTIONS

The constant of integration C_1 in the periodic solution as given by Equation [18] can be determined by the following condition, at

$$W = \text{amplitude } A, \quad \dot{W} = 0$$

In nondimensional notation, this condition becomes, at

$$\bar{W} = \frac{\alpha}{\omega} A = \bar{A}, \quad \bar{U} = 0$$

where $\bar{A}$ is the nondimensional amplitude. Substituting this condition into Equation [18] gives

$$\frac{1}{2}\bar{W}^2 + \bar{U} - \log(1+\bar{U}) = \frac{1}{2}\bar{A}^2, \quad \bar{U} > -1 \ldots [21]$$

For a given value of $\bar{A}$, the periodic solution is therefore uniquely determined.

It is interesting to note here that when the Coriolis acceleration is disregarded, Equation [16] becomes

$$\bar{W}'' + \bar{W} = 0$$

the solution of which in the phase plane is the circle

$$\bar{W}^2 + \bar{U}^2 = \bar{A}^2 \quad \ldots\ldots\ldots\ldots\ldots\ldots [22]$$

which represents a harmonic vibration. In Fig. 3 the nonlinear solution and the harmonic solution are plotted together for the

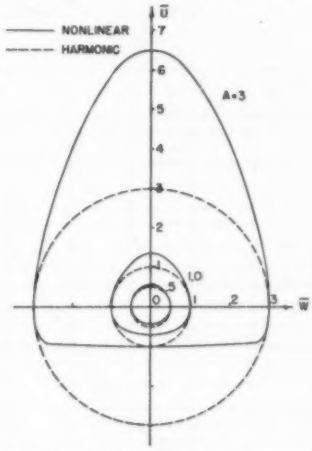

FIG. 3 COMPARISON OF NONLINEAR AND HARMONIC SOLUTIONS

three cases $\bar{A} = 0.5$, $\bar{A} = 1$, and $\bar{A} = 3$. As the value of $\bar{A}$ increases, the shape of the nonlinear solution departs more away from a circle. Solutions for many other values of $\bar{A}$ have been carried out by Marshall.[3]

From the nonlinear solution in the phase plane, the displacement $\bar{W}$ as a function of time $\bar{t}$ can be obtained by carrying out the following line integration

$$\bar{t} = \int_0^{\bar{W}} \frac{d\bar{W}}{\bar{W}'} = \int_0^{\bar{W}} \frac{d\bar{W}}{\bar{U}} \quad \ldots\ldots\ldots\ldots [23]$$

The line integration is to be performed in the clockwise direction, which is the direction of increasing time. For the case $\bar{A} = 3$, the $\bar{W} - \bar{t}$ curve is shown in Fig. 4.

In carrying out the line integration by numerical method, special attention should be paid to the region close to the points $\bar{U} = 0$, at which the integrand becomes infinite. A discussion of the proper method can be found in Appendix B of the paper by Marshall.[3]

From the $\bar{W} - \bar{t}$ curve and the corresponding curve in the $\bar{U}$, $\bar{W}$-plane, the velocity $\bar{U}$ can be obtained as a function of $\bar{t}$. Substitution of $\bar{W}$ and $\bar{U}(= \bar{W}')$ into Equation [16] gives the acceleration $\bar{W}''$ as a function of $\bar{t}$. The velocity and the acceleration curves are also plotted in Fig. 4 for the case $\bar{A} = 3$.

When the line integral in Equation [23] is carried around the

[3] "The Effect of Coriolis Acceleration on the Bending Vibration of a Rotating Beam," by H. M. Marshall; thesis submitted to School of Aeronautics, Purdue University, in partial fulfillment of the requirement for the degree of Master of Science in Aeronautical Engineering, January, 1952.

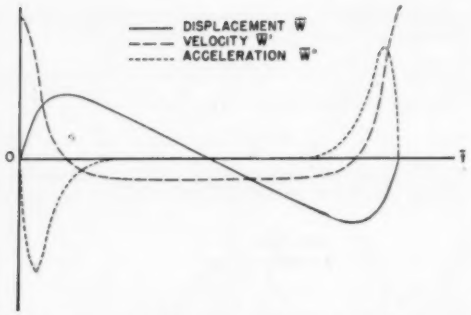

FIG. 4 DISPLACEMENT, VELOCITY, AND ACCELERATION CURVES FOR NONLINEAR SOLUTION, $\bar{A} = 3$

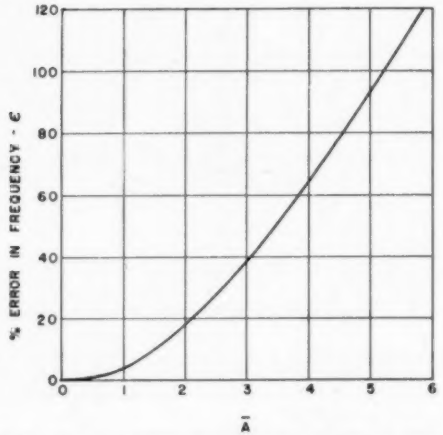

FIG. 5 PERCENTAGE ERROR IN FREQUENCY AS A FUNCTION OF PARAMETER $\bar{A}$

closed curve in the phase plane, the result is the nondimensional period $\bar{T}_c$ of the nonlinear vibration

$$\bar{T}_c = \oint \frac{d\bar{W}}{\bar{U}} \quad \ldots\ldots [24]$$

The subscript c is used to denote that the Coriolis acceleration has been taken into account. From the definition of the nondimensional time

$$\bar{T}_c = \omega T_c = 2\pi \frac{f}{f_c} \quad \ldots\ldots [25]$$

where T_c and f_c are the period and frequency of the nonlinear vibration, and f is the frequency of the harmonic vibration when the Coriolis acceleration is neglected. The percentage error in the vibration frequency resulting from the drop of the Coriolis acceleration is therefore

$$\epsilon \text{ per cent} = \frac{f}{f_c} - 1 = \frac{1}{2\pi} \oint \frac{d\bar{W}}{\bar{U}} - 1 \quad \ldots\ldots [26]$$

For $\bar{A} = 3$, the percentage error is 39.3 per cent.

Following the same procedure one can determine the percentage error for any other values of $\bar{A}$. In Fig. 5 the error curve is given with the percentage error ϵ per cent plotted against the nondimensional amplitude $\bar{A}$.

CONCLUSION

1 The most important parameter in the nonlinear solution is the nondimensional amplitude $\bar{A} = (\alpha/\omega)A$. From the definitions

$$\alpha = 2\frac{\Omega}{L}\sin\beta$$

and

$$\omega^2 = \omega_0^2 + \Omega^2\cos^2\beta$$

one obtains

$$\bar{A} = \frac{2\sin\beta}{\sqrt{\left(\frac{\omega_0}{\Omega}\right)^2 + \cos^2\beta}}\frac{A}{L} \quad \ldots\ldots [27]$$

The percentage error in frequency when the Coriolis acceleration is neglected is therefore a function of the following three physical quantities: (*a*) The ratio of the stationary frequency ω_0 of the beam to the rotating speed Ω; (*b*) the orientation of the plane of vibration defined by the angle β; and (*c*) the amplitude of vibration A in terms of the length of the beam L.

2 In the practical applications at the present time, the value of $\bar{A}$ seldom exceeds 0.4, for which case the percentage error is approximately 0.7 per cent. The dropping of the Coriolis acceleration in the paper by Lo and Renbarger is therefore justified.

3 In the case of nonlinear damping and asymmetric spring force, the periodic solution in the form of a limiting cycle may or may not exist. A general discussion has been given by Lo in an unpublished paper while the study of several special cases can be found in the paper by Marshall.[3]

It should be pointed out that the present investigation is based on the assumption of no displacement in x direction. The actual displacement in the axial direction is governed by the equilibrium condition of the stretching forces due to both rotation and vibration. The determination of the actual stretching of the beam requires the solution of two simultaneous nonlinear equations. If the stretching is completely ignored, the Coriolis acceleration disappears and the problem is reduced to a nonlinear one of a different type. The use of the assumption of no displacement in the x direction is, in the author's opinion, a conservative estimation of the error due to neglect of Coriolis acceleration for the stretched beam.

Plastic-Rigid Analysis of Long Beams Under Transverse Impact Loading[1]

By M. F. CONROY,[2] PROVIDENCE, R. I.

The object of this paper is to set forth the results of an investigation of the behavior of long beams under transverse, constant-velocity impact loading, when a plastic-rigid type of analysis is adopted. It was expected that such an analysis would be satisfactory for problems involving large strains, and easier to evaluate than the corresponding elastic-plastic solution. Consideration is first given to the case of ideal plasticity. Elastic strains are neglected and the material of the beam is assumed to flow plastically at a constant yield limit. In this case expressions for the bending moment, shear force, curvature and deflection distributions along the beam are obtained analytically for any given impact velocity. The manner in which the solution for a beam having an elastic-ideally plastic bending moment-curvature relationship converges to the plastic-rigid solution, as EI increases, is discussed. Consideration is next given to the case of work-hardening where the material is assumed to obey a plastic-rigid bending moment-curvature relationship consisting of a straight line with nonzero slope. Unfortunately, difficulty arises in finding a solution analytically in this case. However, by considering the solution for a beam having the corresponding elastic-plastic bending moment-curvature relationship and a large EI-value, some speculation as to the probable form of the solution may be made.

Nomenclature

The following nomenclature is used in the paper:

- x = distance along beam
- y = deflection
- K = $\partial^2 y/\partial x^2$, curvature of deflection curve
- m = mass per unit length of beam.
- E = Young's modulus
- I = moment of inertia of cross section
- M = bending moment
- Q = shearing force
- t = time
- M_0 = limiting value of M for elastic bending

Introduction

A theoretical analysis of the plastic deformation of long beams subjected to transverse impact load has been developed by H. F. Bohnenblust.[3] In this analysis the bending moment is assumed to depend on the curvature of the deflection curve according to a nonlinear relation $M(K)$, that is obtained from the stress-strain curve of the material. As in the case for the usual elastic analysis, the theory neglects both the shear displacements of the cross sections and the rotary kinetic energy of the motion of the beam. The beam is assumed to extend infinitely in both directions and to be initially at rest. At $t = 0$ the beam is struck at $x = 0$ with such a force that the point $x = 0$ moves at a constant velocity V_1. Bohnenblust, guided by Boussinesq's theory of the elastic deformation of a beam subjected to a transverse impact, shows that in the plastic case, as in the elastic case, y/t is a function of x^2/t, where y is the beam deflection at time t at a distance x from the point of impact.

The theory of Bohnenblust is the basis for the work described in this paper. However, the purpose of the paper is to consider the plastic deformation of long beams when a plastic-rigid analysis is adopted rather than the elastic-plastic type of analysis; that is, we will assume here that elastic strains are negligible compared to plastic strains and so the elastic material can be considered to be rigid. Other work in the field of plasticity has shown that problems in which elastic strains can be neglected are, in general, much easier to handle than the corresponding elastic-plastic problems. It was hoped that by making this assumption more general, boundary-value problems for beams would be amenable to analysis.

Plastic-Rigid Analysis

As before, the beam is assumed to extend infinitely in both directions and to be initially at rest. At $t = 0$ the beam is struck at $x = 0$ with such a force that it moves with a constant velocity V_1. The equation of motion for the beam is

$$\frac{\partial Q}{\partial x} + m\frac{\partial^2 y}{\partial t^2} = 0 \qquad [1]$$

We will assume that y is of the form $y = tf(\eta)$, where $\eta = x^2/4t$. However, while η as used here is analogous to the η-variable introduced in Bohnenblust's elastic-plastic analysis, it is not the same variable. The same η cannot be used here because we want to consider the limit of the solution when E approaches infinity, so that we cannot use E to form a nondimensional variable. Thus we have

$$y = tf(\eta);\ \eta = \frac{x^2}{4t} \qquad [2]$$

By differentiation and using the notation defined

$$K = \frac{\partial^2 y}{\partial x^2} = \frac{1}{2}(f' + 2\eta f'') \qquad [3]$$

$$\frac{\partial^2 y}{\partial t^2} = \frac{\eta^2 f''}{t} \qquad [4]$$

$$Q = \frac{\partial M}{\partial x} = \frac{\sqrt{\eta}}{\sqrt{t}}\frac{dM}{d\eta} \qquad [5]$$

---

[1] The results presented in this paper were obtained in the course of research sponsored by the Office of Naval Research under Contract N7onr-35801 (Task Order 1) with Brown University.

[2] Research Assistant, Graduate Division of Applied Mathematics, Brown University.

Presented at the National Conference of the Applied Mechanics Division, State College, Pa., June 19–21, 1952, of The American Society of Mechanical Engineers.

Discussion of this paper should be addressed to the Secretary, ASME, 29 West 39th Street, New York, N. Y., and will be accepted until January 10, 1953, for publication at a later date. Discussion received after the closing date will be returned.

Note: Statements and opinions advanced in papers are to be understood as individual expressions of their authors and not those of the Society. Manuscript received by ASME Applied Mechanics Division, November 19, 1951. Paper No. 52—APM-36.

[3] "The Behavior of Long Beams Under Impact Loading," by P. E. Duwez, D. S. Clark, and H. F. Bohnenblust, Journal of Applied Mechanics, Trans. ASME, vol. 72, 1950, pp. 27–34.

and

$$\frac{\partial Q}{\partial x} = \frac{\sqrt{\eta}}{t}\frac{\partial}{\partial \eta}\left(\sqrt{\eta}\,\frac{dM}{d\eta}\right) \quad [6]$$

Before substituting these expressions into Equation [1], let us, following Bohnenblust, introduce a new variable, $S(\eta)$

$$S = 2\sqrt{t}\,Q = 2\sqrt{\eta}\,\frac{dM}{d\eta} \quad [7]$$

Now

$$\frac{\partial Q}{\partial x} = \sqrt{\eta}\,\frac{S'(\eta)}{2}\,\frac{1}{t} \quad [8]$$

Substituting Equations [4] and [8] into Equation [1] we obtain as the equation of motion for the beam

$$S' + 2m\eta^{3/2}f'' = 0 \quad [9]$$

and by Equation [3] this is equivalent to

$$S' + m\sqrt{\eta}(2K - f') = 0 \quad [10]$$

By differentiation of Equation [10] and from Equation [3] it follows that

$$S'' + 2m\sqrt{\eta}\,\frac{dK}{d\eta} = 0 \quad [11]$$

Finally, since $dK/d\eta = dK/dM(dM/d\eta)$ and $S = 2\sqrt{\eta}\,dM/d\eta$, we see that

$$S'' + mS\frac{dK}{dM} = 0 \quad [12]$$

Solutions of this equation with appropriate boundary conditions give shear-force distributions for constant-velocity impacts.

S having been determined, Q, K, M, y, and V_1 may be obtained by means of integration. From Equation [7]

$$Q = \frac{S}{2\sqrt{t}}$$

from Equation [11]

$$K(\eta) = -\frac{1}{2m}\int_{\infty}^{\eta}\frac{S''}{\sqrt{\eta}}\,d\eta$$

and from Equation [7]

$$M(\eta) = M(\infty) + \frac{1}{2}\int_{\infty}^{\eta}\frac{S}{\sqrt{\eta}}\,d\eta \quad [13]$$

It will be shown later that in the plastic-rigid analysis $M(\infty) = M_0$, and K, y, and y' are equal to zero at $x = \infty$.

Because of the assumed form of y

$$\left.\frac{\partial y}{\partial \eta}\right|_{t=\text{const}} = tf'(\eta) \quad [14]$$

From Equation [9] we can obtain $f''(\eta)$ so that

$$f'(\eta) = -\int_{\eta}^{\infty} f''(\eta)d\eta = \frac{1}{2m}\int_{\eta}^{\infty}\frac{S'}{\eta^{3/2}}\,d\eta$$

If this expression is substituted into Equation [14] it can be shown that

$$y = -\frac{t}{2m}\int_{\eta}^{\infty}\frac{S'(\eta)}{\sqrt{\eta}}\,d\eta + \frac{t}{2m}\eta\int_{\eta}^{\infty}\frac{S'(\eta)}{\eta^{3/2}}\,d\eta \quad [15]$$

and

$$V_1 = \frac{y(0)}{t} = -\frac{1}{2m}\int_{0}^{\infty}\frac{S'(\eta)}{\sqrt{\eta}}\,d\eta \quad [16]$$

Since M, Q, K, y, and V_1 may be obtained from S, the main problem consists of finding S from our fundamental equation

$$S'' + mS\frac{dK}{dM} = 0 \quad [17]$$

in such a way as to satisfy the boundary conditions of the problem.

Let us assume that the material of the beam obeys the plastic-rigid bending moment-curvature relationship of Fig. 1. Then

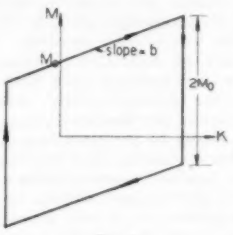

FIG. 1

dK/dM is either 0 or $1/b$, where b is the slope of the second straight line. From Equation [17] it is clear that S is composed of sections of a number of curves of the form

$$\left.\begin{array}{lll} \text{I} & S = A\cos\dfrac{1}{c}\eta & 0 \le \eta \le \eta_0 \\ \text{II} & S = -B(\eta - \eta_1) & \eta_0 \le \eta \le \eta_1 \\ \text{III} & S = -C\sin\dfrac{1}{c}(\eta - \eta_1) & \eta_1 \le \eta \le \eta_2 \\ \text{IV} & S = D(\eta - \eta_3) & \eta_2 \le \eta \end{array}\right\} \quad [18]$$

where $1/c = \sqrt{m/b}$, the occurrence of four regions being a special case. The unknowns, η_0, η_1, η_2, η_3, A, B, C, and D are determined by the following conditions: (1) Continuity of S at η_0; (2) continuity of S at η_2; (3) continuity of S' at η_0; (4) continuity of S' at η_1; (5) continuity of S' at η_2; (6) $M = M_0$ for $\eta \ge \eta_2$; plus the two integral conditions (7)

$$\frac{1}{2}\int_{\eta_0}^{\eta_1}\frac{S}{\sqrt{\eta}}\,d\eta = 2M_0$$

and (8)

$$-\frac{1}{2m}\int_{0}^{\infty}\frac{S'}{\sqrt{\eta}}\,d\eta = V_1$$

S must be continuous, for the shear-force distribution is continuous along the beam since no external forces are applied other than at the center. The bending-moment distribution is also continuous along the beam since no external moments are applied. In the case of a work-hardening material the curvature must be continuous, as a discontinuity in curvature would imply a discontinuity in bending moment. However, in the case of an ideally plastic material having a moment-curvature relationship of the form of Fig. 2 or Fig. 3, the curvature may be discontinuous. S' must be continuous when the curvature is continuous according to Equation [10]. Therefore, S' can be discontinuous if the material

FIG. 2

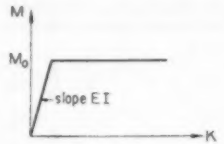

FIG. 3

of the beam is ideally plastic, but must be continuous for a work-hardening material.

Condition (7) imposes the condition that the change in bending moment during unloading is $2M_0$, Fig. 1. Condition (8) is merely Equation [16].

The last region must be the straight line $S = 0$ because any other straight line would lead to $M(\infty) = \infty$. Thus it is seen that in plastic-rigid analysis $S = 0$ and $M = M_0$ for $\eta \geq \eta_2$; this is true independently of the boundary conditions at ∞.

Also to be noted is that $\eta_0 \leq c\pi/2$ and $\eta_2 - \eta_1 \leq c\pi$. This follows from the fact that $S = 0$ corresponds to a maximum or minimum value of M. From the moment-curvature relationship it is clear that an elastic region occurs between a maximum and a minimum bending-moment value and so the inequalities mentioned must apply.

CASE OF IDEAL PLASTICITY

The bending moment-curvature relationship is as shown in Fig. 2. Since in this case $b = 0$ and $c = \sqrt{b/m} = 0$, regions I and III of Equations [18] shrink to the points $\eta = 0$ and $\eta = \eta_1$, respectively, as a consequence of the inequalities just cited; that is, in the case of an ideally plastic material, plastic hinges for min-stead of finite plastic regions. Since $\eta = x^2/4t$, plastic hinges appear at $x = 0$ and at $x = x_1$. As was mentioned before, the curvature of the beam may be discontinuous at these hinges and thus a discontinuity in S' is allowable at these points.

Equation [18] assumes the form, Fig. 4

$$\left.\begin{aligned} S &= -B(\eta - \eta_1) \quad 0 \leq \eta \leq \eta_1 \\ S &= 0 \qquad\qquad\quad \eta_1 \leq \eta \end{aligned}\right\} \qquad \ldots\ldots [19]$$

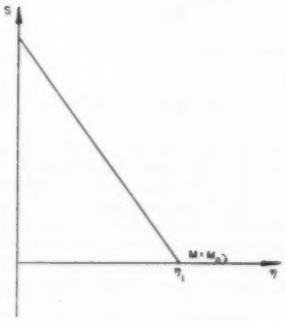

FIG. 4

Given the limiting bending moment of the material, M_0, and the impact velocity, V_1, the unknowns B and η_1 may be determined from conditions (7) and (8). Carrying out these integrations, we find that

$$\eta_1 = \frac{3M_0}{mV_1^2} \qquad \ldots\ldots [20]$$

and

$$B = \frac{3M_0}{\eta_1^{3/2}} \qquad \ldots\ldots [21]$$

Since B and η_1 are constants, we see from Equation [2] that

$$x_1 \sim \sqrt{t}$$

and from Equations [7] and [19]

$$Q(0) = \frac{S(0)}{2\sqrt{t}} = \frac{B\eta_1}{2\sqrt{t}} \sim \frac{1}{\sqrt{t}}$$

That is, the shear force at the center of the beam is proportional to $1/\sqrt{t}$, while the position of the hinge at $x = x_1$ is proportional to $\sqrt{t}$.

According to Equation [15] the deflection of the beam is given by

$$\left.\begin{aligned} y &= \frac{tB}{2m}\left[2\sqrt{\eta_1} - 2\sqrt{\eta} + 2\eta\left(\frac{1}{\sqrt{\eta_1}} - \frac{1}{\sqrt{\eta}}\right)\right] \quad 0 \leq \eta \leq \eta_1 \\ y &= 0, \qquad\qquad\qquad\qquad\qquad\qquad \eta \geq \eta_1 \end{aligned}\right\} \qquad [22]$$

y versus x may be computed from Equation [22] with the aid of Equation [2]. The beam shape is shown in a plot of y versus x taking $t = 1$ and $\eta_1 = 1$, Fig. 5. Note y is considered positive

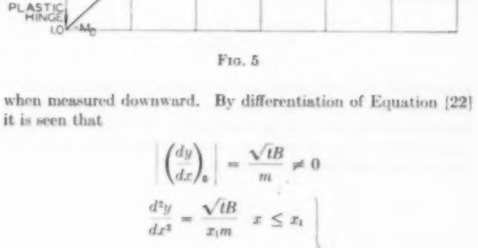

FIG. 5

when measured downward. By differentiation of Equation [22] it is seen that

$$\left.\begin{aligned} \left|\left(\frac{dy}{dx}\right)_0\right| &= \frac{\sqrt{tB}}{m} \neq 0 \\ \frac{d^2y}{dx^2} &= \frac{\sqrt{tB}}{x_1 m} \qquad x \leq x_1 \\ \frac{d^2y}{dx^2} &= 0 \qquad\qquad x \geq x_1 \end{aligned}\right\}$$

and hence the curvature of the beam is discontinuous at the plastic hinge at $x = x_1$.

The bending-moment distribution along the beam may be computed from Equation [13]. Since in the case of ideal plasticity $M = M_0$ for $\eta \geq \eta_1$, the lower limit may be replaced by $\eta = \eta_1$. Substituting for B from Equation [21] and integrating, we obtain

$$M(\eta) = M_0 - \frac{3M_0}{2\eta_1^{3/2}}\left(\frac{2}{3}\eta^{3/2} - 2\eta_1\sqrt{\eta} + \frac{4}{3}\eta_1^{3/2}\right) \qquad \eta \leq \eta_1$$

$$M(\eta) = M_0 \qquad \eta \geq \eta$$

But $\eta = x^2/4t$, so we can compute the bending-moment distribution along the beam. $M(x)$ versus x is shown in Fig. 6 for $t = 1$.

Hence it is clear that for the case of ideal plasticity, given the limiting bending moment M_0 and the impact velocity V_1, Equations [19], [20], [21], and [22] constitute the complete solution of the problem.

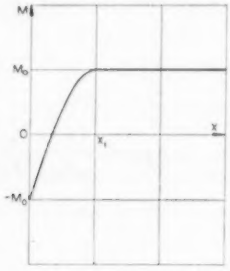

FIG. 6

Moreover, since for $x \geq x_1$ $y = 0$ and $M = M_0$, this solution is also the solution for a finite beam with fixed ends until such time as the hinge at $x = x_1$ reaches the end of the beam.

CONVERGENCE OF ELASTIC-PLASTIC SOLUTION TO PLASTIC-RIGID SOLUTION

Now that we have determined the complete solution for a beam of ideally plastic material under a plastic-rigid analysis, it is interesting to see in just what manner Bohnenblust's elastic-plastic solution converges to the plastic-rigid solution with increasing values of EI. A consideration of this convergence process also brings out the fact that in the case of ideal plasticity the number of plastic hinges along the beam is less than or at most equal to 3.

We will consider a beam which is subjected to a transverse impact loading at $x = 0$ such that the center of the beam moves with the constant velocity

$$V_1 = 0.006 \frac{M_0}{m}$$

where 0.006 in ft-sec units has dimensions of time/(distance)^2. This value for V_1 is chosen because it leads to large strains for normal practical values of the parameters. The beam is assumed to have the bending moment-curvature relation of Fig. 3. As before, we must determine a solution of

$$S'' + mS\frac{dK}{dM} = 0$$

satisfying the boundary conditions of the problem. Since dK/dM is equal either to $1/EI$ or ∞ and plastic regions shrink to hinges in the case of ideal plasticity, as shown by Bohnenblust, S is of the form

I Plastic hinge at $\eta = 0$

II $S = -A \sin \sqrt{\frac{m}{EI}}\,(\eta - \eta_1)$ $\quad 0 \leq \eta \leq \eta_1$

III Plastic hinge at $\eta = \eta_1$

IV $S = -B \sin \sqrt{\frac{m}{EI}}\,(\eta - \eta_1)$ $\quad \eta_1 \leq \eta$

A, B, and η_1 are determined from the velocity condition plus two bending moment conditions, i.e.

$$-\frac{1}{2m}\int_0^\infty \frac{S'(\eta)}{\sqrt{\eta}}\,d\eta = 0.006\,\frac{M_0}{m}$$

$$\frac{1}{2}\int_0^{\eta_1} \frac{S(\eta)}{\sqrt{\eta}}\,d\eta = 2M_0$$

$$-\frac{1}{2}\int_{\eta_1}^\infty \frac{S(\eta)}{\sqrt{\eta}}\,d\eta = +M_0$$

Bohnenblust has shown that the maximum impact velocity for which the beam remains entirely elastic is

$$V_e = \frac{M_0}{\sqrt{EI}\,\sqrt{m}}$$

Therefore, since the beam remains elastic throughout for $\sqrt{EI} \leq 167\,\sqrt{m}$, S is composed of only one region and no plastic hinges appear for such EI-values. The solution then for $\sqrt{EI} \leq 167\,\sqrt{m}$ is

$$S = A \cos \sqrt{\frac{m}{EI}}\,\eta \quad 0 \leq \eta$$

where A may be determined from the velocity condition. For $167\,\sqrt{m} \leq \sqrt{EI} \leq 347.83\,\sqrt{m}$, S is of the form

I Plastic hinge at $\eta = 0$

II $S = -B \sin \sqrt{\frac{m}{EI}}\,(\eta - \eta_1) \quad 0 \leq \eta$

This follows from Bohnenblust's conclusion that for an ideally plastic material one plastic hinge appears at the center of the beam for

$$V_e \leq V_1 \leq 2.087\,V_e$$

For $347.83\,\sqrt{m} \leq \sqrt{EI}$, S is of the form

I Plastic hinge at $\eta = 0$

II $S = -A \sin \sqrt{\frac{m}{EI}}\,(\eta - \eta_1) \quad 0 \leq \eta \leq \eta_1$

III Plastic hinge at $\eta = \eta_1$

IV $S = -B \sin \sqrt{\frac{m}{EI}}\,(\eta - \eta_1) \quad \eta \geq \eta_1$

Values of $\sqrt{EI}$ ranging from $167\,\sqrt{m}$ to $10^6\,\sqrt{m}$ (in ft-lb-sec units which are used throughout the numerical analysis) have been taken and the foregoing elastic-plastic solution considered. Several $S(\eta)$ solutions have been graphed in Fig. 7 to show the manner of convergence of the elastic-plastic solution, with increasing EI, to the plastic-rigid solution shown in the graph by the heavy black line. This plastic-rigid solution is obtained from Equations [20] and [21] very simply. Equation [19] becomes

$$\left.\begin{aligned} S &= -0.00027\,M_0(\eta - 500) \quad 0 \leq \eta \leq 500 \\ S &= 0 \qquad\qquad\qquad\qquad \eta \geq 500 \end{aligned}\right\}$$

A survey of the results obtained for the range of $\sqrt{EI}$ values considered is given in Table 1. Included in this table for each $\sqrt{EI} \geq 347.83\,\sqrt{m}$ is the value of the bending moment at the point of minimum bending moment following the hinge at $\eta = \eta_1$. If $M_{\min} \leq -M_0$ at this point another hinge would appear. How-

TABLE 1 RESULTS OBTAINED FOR RANGE OF $\sqrt{EI}$ VALUES

$\sqrt{\frac{EI}{m}}$	V_1	No. of hinges	A	B	η_1	$S(0)$	M at next min
167[a]	$0.006\frac{M_0}{m}$	1	$0.123\,M_0$			$0.123\,M_0$	
250	$0.006\frac{M_0}{m}$	1		$0.129\,M_0$	343	$0.126\,M_0$	
325	$0.006\frac{M_0}{m}$	1		$0.1369\,M_0$	409.6	$0.130M_0$	
347.83[b]	$0.006\frac{M_0}{m}$	2		$0.1400M_0$	428.61	$0.1320M_0$	$-0.606M_0$
370	$0.00600\frac{M_0}{m}$	2	$0.1423M_0$	$0.1352M_0$	439	$0.1319M_0$	$-0.606M_0$
400	$0.00599\frac{M_0}{m}$	2	$0.1457M_0$	$0.1279M_0$	450	$0.1315M_0$	$-0.600M_0$
450	$0.00599\frac{M_0}{m}$	2	$0.1524M_0$	$0.1175M_0$	465	$0.1309M_0$	$-0.5904M_0$
500	$0.00601\frac{M_0}{m}$	2	$0.1608M_0$	$0.1088M_0$	475	$0.1308M_0$	$-0.5816M_0$
600	$0.00602\frac{M_0}{m}$	2	$0.1792M_0$	$0.0954M_0$	490	$0.1306M_0$	$-0.5669M_0$
800	$0.00600\frac{M_0}{m}$	2	$0.2203M_0$	$0.0777M_0$	507	$0.1304M_0$	
10^3	$0.00600\frac{M_0}{m}$	2	$0.2661M_0$	$0.0664M_0$	513	$0.1306M_0$	$-0.5277M_0$
10^4	$0.00600\frac{M_0}{m}$	2	$2.6367M_0$	$0.01662M_0$	506	$0.1334M_0$	
10^5	$0.005997\frac{M_0}{m}$	2	$26.7524M_0$	$0.005070M_0$	501	$0.1340M_0$	
10^6	$0.006001\frac{M_0}{m}$	2	$268.35M_0$	$0.001597M_0$	500	$0.1342M_0$	
∞	$0.006\frac{M_0}{m}$	2		$0.00027M_0$	500	$0.1342M_0$	

[a] Hinge 1 first appears at center of beam.
[b] Hinge 2 first appears at η_1.

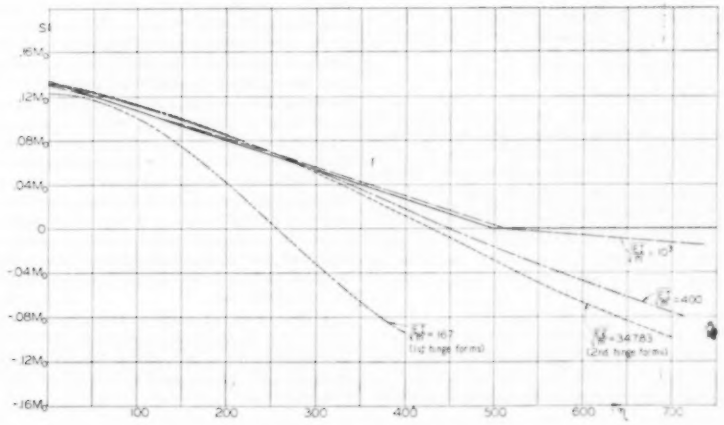

FIG. 7

ever, it is to be observed from the table that M_{min} at this point increases (from $-0.606\ M_0$) with increasing EI and hence never becomes $\leq -M_0$; that is, $M(\eta_1) - M_{min} < 2M_0$. But the theory demands that the change in bending moment between any two successive points of maximum and minimum bending moment decrease in absolute value as we proceed along the beam. Therefore it is clear that there will be at most three plastic hinges along the whole beam.

From column $S(0)$ in the table and from the fact that $Q(0) = S(0)/2\sqrt{t}$ we see that the shear force at the center of the beam increases with EI until such time as a hinge appears at η_1. After the formation of this hinge the shear force at the center of the beam decreases with increasing EI for some time and then increases to the value obtained by the plastic-rigid analysis.

From the η_1-column of the table and from Fig. 7 it is seen that η_1 increases with increasing EI to $\eta_1 = 513$ and then decreases

with increasing EI to $\eta_1 = 500$, the η_1-value determined by the plastic-rigid analysis.

Case of a Work-Hardening Material

The bending moment-curvature relationship is as shown in Fig. 1, and S is composed of curves of the form given by Equations [18]. Both $S(\eta)$ and $S'(\eta)$ must be everywhere continuous because the shear-force distribution and the bending moment are continuous along the beam. Also to be satisfied are boundary conditions of the type

$$\frac{1}{2}\int_{\eta_a}^{\eta_1}\frac{S}{\sqrt{\eta}}\,d\eta = 2M_0;\quad -\frac{1}{2m}\int_0^{\infty}\frac{S'}{\sqrt{\eta}}\,d\eta = V_1$$

and, since the material is plastic-rigid, $M = M_e$ for $\eta \geq \eta_b$. This last requirement, that M be constant for $\eta \geq \eta_b$, demands that $S = 0$ for $\eta \geq \eta_b$. However, it appears impossible to obtain a solution, $S(\eta)$, of the form of Equation [18] for which (1) $S(\eta)$ and $S'(\eta)$ are everywhere continuous, (2) $S = 0$ forms the last region, and (3) $S(\eta)$ has a finite number of regions. For this reason there is difficulty in obtaining a plastic-rigid solution analytically for the case of a work-hardening material.

A likely possibility, then, is that $S(\eta)$ is composed of an infinite number of regions in the case of a work-hardening plastic-rigid material. Bohnenblust encountered an elastic-plastic, Fig. 8,

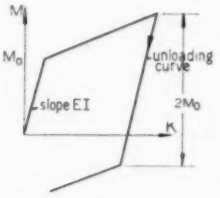

Fig. 8

solution consisting of more than four regions in the case of a copper beam for which $\sqrt{EI/m} = 216.5$ ft³/sec, and $\sqrt{b/m} = 30.31$ ft²/sec, and $V_1 = 100$ fps. The following question then arises: Does the number of regions increase indefinitely as $EI \to \infty$?

Let us consider a case where again $\sqrt{b/m} = 30.31$ ft²/sec, but now $\sqrt{EI/m} = 10^8$ ft³/sec. We seek a solution of our fundamental equation

$$S'' + mS\frac{dK}{dM} = 0$$

such that S and S' are everywhere continuous and the usual bending moment and velocity boundary conditions are satisfied. Let us assume, moreover, that V_1 is such that $\eta_b = \pi/4\sqrt{b/m}$.

If we assume that $S(\eta)$ is composed of six regions, it is found that all of the boundary conditions may be satisfied by the solution:

I $S = 2.1402\,M_e \cos \eta/30.31$
$0 \leq \eta \leq 23.8054$ (ft²/sec)

II $S = -49.9681\,M_e \sin 10^{-2}(\eta - 54.0961)$
$23.8054 \leq \eta \leq 54.0961$

III $S = -1.545\,M_e \sin \dfrac{\eta - 54.0961}{30.31}$
$54.0961 \leq \eta \leq 114.47$

IV $S = 20.471\,M_e \sin 10^{-2}(\eta - 182.04)$
$114.47 \leq \eta \leq 182.04$

V $S = 0.62047\,M_e \sin \dfrac{\eta - 182.04}{30.31}$
$182.04 \leq \eta \leq 230.046$

VI $S = -0.67474\,M_e \sin 10^{-2}(\eta - 1396.84)$
$230.046 \leq \eta$

But $M(1396.84) = 7.7893\,M_e$ and therefore another plastic region must appear at η_b. Hence there are more than six regions in this case. The calculations have not been carried out any further, but again it is indicated that the number of regions increases as EI increases and in particular that the number of regions may become infinite in the case of the plastic-rigid analysis for a work-hardening material, thus implying the difficulty mentioned previously.

Conclusion

It was hoped that by neglecting elastic strains and adopting a plastic-rigid type of analysis for beams under transverse-impact loading, rather than Bohnenblust's elastic-plastic analysis, it would be possible to evaluate solutions more easily and to make more general boundary-value problems amenable to treatment. In the case of problems involving large strains, it was expected that such a plastic-rigid solution would be satisfactory, and it has been demonstrated by other work in the field of plasticity that a plastic-rigid analysis of a problem is, in general, much easier to handle than an elastic-plastic analysis.

In the case of an ideally plastic material which flows plastically at a constant yield limit, this investigation showed that a plastic-rigid solution can be obtained very easily. The shear force, curvature, bending-moment, and deflection distributions can be obtained analytically for any given impact velocity. It was also shown that there will be at most three plastic hinges along the beam and that the solution obtained for an infinite beam is also the solution for a finite beam until such time as the hinges reach the end of the beam.

In the case of the work-hardening material, the investigation showed that a plastic-rigid analysis produced no simple solution. The analysis, while not carried through completely, seems to imply that an infinite number of localized plastic regions form along the beam.

Free Vibrations of Constrained Beams[1]

By WINSTON F. Z. LEE[2] and EDWARD SAIBEL,[3] PITTSBURGH, PA.

A general expression is developed from which the frequency equation for the vibration of a constrained beam with any combination of intermediate elastic or rigid supports, concentrated masses, and sprung masses can be found readily. The method also is extended to the case where the constraint is a continuous elastic foundation or uniformly distributed load of any length. This method requires only the knowledge of the natural frequencies and natural modes of the beam supported at the ends in the same manner as the constrained beam but not subjected to any of the constraints between the ends. The frequency equation is obtained easily and can be solved to any desired degree of approximation for any number of modes of vibration in a quick and simple manner. Numerical examples are given for a beam with one concentrated mass, for a beam with one sprung mass, and a continuous beam with one sprung mass.

Nomenclature

The following nomenclature is used in the paper:

- x = horizontal co-ordinate
- y = transverse deflection of beam
- Y = maximum transverse deflection of beam
- m = mass of beam per unit length
- h_i = distance from left end of beam to ith constraint
- M_i = magnitude of the ith concentrated mass
- K_i = spring constant of ith elastic support or the ith spring
- a_r = coefficient in series expansion of function
- $\phi_r(x)$ = eigenfunction of simple beam
- λ_r = eigenvalue of simple beam corresponding to $\phi_r(x)$
- p_r = natural circular frequency of rth mode of vibration of simple beam
- Λ = natural circular frequency of constrained beam
- L = length of beam
- V_1 = strain energy of bending of beam
- V_2 = potential energy of inertia force of mass of beam per unit length
- V_3 = strain energy stored in elastic supports.
- W = potential energy of vibrating system
- R_i = maximum support reaction of the ith intermediate rigid support
- k = modulus of elastic foundation, i.e., load per unit length of beam necessary to produce a compression in foundation equal to unity
- q = intensity of uniformly distributed load

Introduction

The classical method for finding the natural frequencies of a vibrating system becomes intractable when the beam is constrained by elastic supports, rigid supports, concentrated masses, or sprung masses, separately or combined. It is the object of this paper to develop a simple and readily applied method whereby the natural frequencies may be evaluated to any desired degree of approximation. This method also is extended to find the natural frequencies of a beam on a continuous elastic foundation or under uniformly distributed loads of any length. The method used is an extension of the method developed earlier for the solution of the natural frequencies of continuous beams.[4]

Essentially the method consists of developing the deflected shape of the beam with constraints in terms of the eigenfunctions of the same beam without the inner constraints. These eigenfunctions are presumed known and in most applications, this is the case.

Theory

The differential equation for the free vibrations of a beam is

$$\frac{\partial^2}{\partial x^2}\left[EI(x)\frac{\partial^2 y}{\partial x^2}\right] = -m(x)\frac{\partial^2 y}{\partial t^2} \quad \ldots\ldots [1]$$

where EI is the flexural rigidity, m, the mass per unit length, and y, the deflection. The deflection may be expressed in the form

$$y = Y(x)\sin(pt + e)$$

where p is the natural circular frequency and e is the phase angle. The differential equation which $Y(x)$ must satisfy is

$$\frac{d^2}{dx^2}\left[EI(x)\frac{d^2Y}{dx^2}\right] = m(x)p^2Y(x) \quad \ldots\ldots [2]$$

Associated with Equation [2] and the usual boundary conditions at the ends for simple or built-in supports or free ends, there is a complete set of eigenfunctions $\phi_r(x)$ and eigenvalues $\lambda_r = p_r^2$. These eigenfunctions satisfy Equation [2] and they are orthonormal, satisfying the following relations

$$\left.\begin{aligned}\int_0^L m\phi_r(x)\phi_s(x)dx &= 0 \text{ if } r \neq s\\ \int_0^L m\phi_r^2(x)dx &= 1\end{aligned}\right\} \quad \ldots\ldots [3]$$

Consider a beam of length L with given end conditions (simply supported, built-in, or free) with n intermediate elastic supports having spring constants $K_1, K_2, \ldots, K_n$, respectively, and located at distances $h_1, h_2 \ldots, h_n$ from the left end as shown in Fig. 1. If this composite beam is vibrating without external exciting loads with natural frequency Λ, the deflection may be expressed as

$$y = Y(x)\sin(\Lambda t + e) \quad \ldots\ldots [4]$$

Since the shape of the deflection curve $y(x, t)$ is continuous, and the set of eigenfunctions $\phi_r(x)$ of the simple beam is complete and satisfies the same end conditions, we may express

[1] The research underlying this paper was partially supported by funds from a U. S. Army Air Force contract with Carnegie Institute of Technology, and was done in part by Winston F. Z. Lee in partial fulfillment of the requirements for the degree of Doctor of Science at Carnegie Institute of Technology.

[2] Teaching Assistant, Mechanical Engineering Department, Carnegie Institute of Technology.

[3] Professor of Mechanics, Department of Mathematics, Carnegie Institute of Technology. Mem. ASME.

Presented at the National Conference of the Applied Mechanics Division, State College, Pa., June 19–21, 1952, of The American Society of Mechanical Engineers.

Discussion of this paper should be addressed to the Secretary, ASME, 29 West 39th Street, New York, N. Y., and will be accepted until January 10, 1953, for publication at a later date. Discussion received after the closing date will be returned.

Note: Statements and opinions advanced in papers are to be understood as individual expressions of their authors and not those of the Society. Manuscript received by ASME Applied Mechanics Division, January 4, 1952. Paper No. 52—APM-31.

[4] "Vibration Frequencies of Continuous Beams," by Edward Saibel, *Journal of the Aeronautical Sciences*, vol. 11, 1944, pp. 88–90

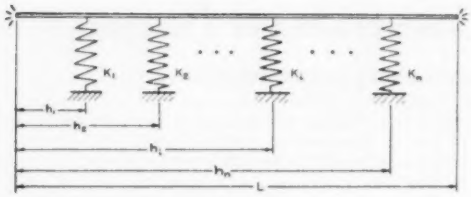

FIG. 1

$$Y(x) = \sum_{r=1}^{\infty} a_r \phi_r(x) \quad \ldots [5]$$

Consider the maximum deflection $Y(x)$ of the composite beam as being produced by the distributed inertia forces $[-\Lambda^2 m Y(x)]$ per unit length of the beam. The total potential energy W of the vibrating system consists of three parts, the strain energy V_1 of the beam, the potential energy V_2 of the distributed inertia forces, and the strain energies V_3 stored in the intermediate elastic supports.

For small deflections of a beam, the strain energy due to bending in its maximum deflection is given by

$$V_1 = \frac{1}{2} \int_0^L EI(x) \left(\frac{d^2Y}{dx^2} \right)^2 dx$$

Integrating by parts leads to

$$V_1 = \frac{E}{2} \left\{ \left[I(x) \frac{d^2Y}{dx^2} \frac{dY}{dx} \right]_0^L - \int_0^L \frac{dY}{dx} \frac{d}{dx} \left[I(x) \frac{d^2Y}{dx^2} \right] dx \right\}$$

The first term of this equation vanishes for any combination of standard end conditions, thus V_1 reduces to

$$-\frac{E}{2} \int_0^L \frac{dY}{dx} \frac{d}{dx} \left[I(x) \frac{d^2Y}{dx^2} \right] dx$$

Integrating by parts, we have

$$V_1 = -\frac{E}{2} \left\{ \left[\frac{d}{dx} \left(I(x) \frac{d^2Y}{dx^2} \right) Y \right]_0^L - \int_0^L Y \frac{d^2}{dx^2} \left[I(x) \frac{d^2Y}{dx^2} \right] dx \right\}$$

Again the boundary conditions at the ends of the beam make the first term zero. Therefore V_1 becomes by means of Equation [2]

$$\frac{E}{2} \int_0^L Y \frac{d^2}{dx^2} \left[I(x) \frac{d^2Y}{dx^2} \right] dx = \frac{E}{2} \int_0^L p^2 m(x) Y^2(x) dx$$

Substituting Equation [5] into this equation and using Equations [3] V_1 takes the form

$$V_1 = \frac{1}{2} \sum_{r=1}^{\infty} a_r^2 p_r^2 \quad \ldots [6]$$

where p_r is the natural circular frequency of the simple beam corresponding to its eigenfunction $\phi_r(x)$.

The potential energy of the distributed inertia forces $[-\Lambda^2 m Y(x)]$ is

$$V_2 = \frac{1}{2} \int_0^L [-\Lambda^2 m Y(x)] Y(x) dx$$

Substituting Equation [5] into this equation and using Equations [3] we get

$$V_2 = -\frac{1}{2} \Lambda^2 \sum_{r=1}^{\infty} a_r^2 \quad \ldots [7]$$

Corresponding to the maximum deflection of the beam, the spring force F_i of the ith elastic support is

$$F_i = K_i Y(h_i) \quad \ldots [8]$$

and the strain energy stored in it is

$$\frac{1}{2} K_i Y(h_i) Y(h_i) \quad \ldots [9]$$

Summing over all of the elastic intermediate supports, the total strain energy stored in them is

$$V_3 = \frac{1}{2} \sum_{i=1}^{n} K_i [Y(h_i)]^2 \quad \ldots [10]$$

The total potential energy of the vibrating system is

$$W = V_1 + V_2 + V_3$$

$$= \frac{1}{2} \sum_{r=1}^{\infty} p_r^2 a_r^2 - \frac{1}{2} \Lambda^2 \sum_{r=1}^{\infty} a_r^2 + \frac{1}{2} \sum_{i=1}^{n} K_i \left[\sum_{r=1}^{\infty} a_r \phi_r(h_i) \sum_{s=1}^{\infty} a_s \phi_s(h_i) \right] \quad \ldots [11]$$

This potential energy must be a minimum. Considering the coefficients a_r as independent variables, the necessary conditions for the total potential energy W of the vibrating system to be a minimum are

$$\frac{\partial W}{\partial a_r} = (p_r^2 - \Lambda^2) a_r + \sum_{i=1}^{n} Y(h_i) K_i \phi_r(h_i) = 0 \quad \ldots [12]$$

which lead to

$$a_r = -\frac{1}{p_r^2 - \Lambda^2} \left[\sum_{i=1}^{n} K_i Y(h_i) \phi_r(h_i) \right] \quad \ldots [13]$$

Multiplying this equation by $\phi_r(h_j)$ and summing on r, we have

$$\sum_{i=1}^{n} K_i \sum_{r=1}^{\infty} \frac{\phi_r(h_i) \phi_r(h_j)}{p_r^2 - \Lambda^2} Y(h_i) = -Y(h_j) \quad \ldots [14]$$

where $j = 1, 2, \ldots, i, \ldots n$.

Equations [14] represent a system of n homogeneous linear equations in the n unknowns $Y(h_i)$ which are the maximum deflections at the corresponding elastic supports. The number of homogeneous equations is equal to the number of intermediate constraints. The necessary conditions for a nontrivial solution is the vanishing of the determinant of the system. This yields the frequency equation in determinantal form

$$|A_{ij} + \delta_{ij}| = 0 \quad \ldots [15]$$

where

$$A_{ij} \equiv K_j \sum_{r=1}^{\infty} \frac{\phi_r(h_i) \phi_r(h_j)}{p_r^2 - \Lambda^2}$$

δ_{ij} is the Kronecker delta
$i, j = 1, 2, \ldots n$

A special case arises when $\phi_r(h_1), \phi_r(h_2), \ldots, \phi_r(h_n)$ all vanish. Equation [12] then becomes

$$\frac{\partial W}{\partial a_r} = a_r(p_r^2 - \Lambda^2) = 0$$

or

$$\Lambda = p_r \ldots\ldots\ldots\ldots\ldots\ldots\ldots\ldots [16]$$

In this case we have two frequency Equations [15] and [16], giving together the complete roots of natural frequencies of the vibrating system. Equation [15] or Equations [15] and [16] together constitute the frequency equation or equations for the composite beam with n elastic intermediate supports. This can be modified readily to include intermediate loadings of other kinds such as rigid supports, concentrated masses, sprung masses, continuous elastic foundations or uniformly distributed loads of any length, and so on. For simplicity, they will be dealt with separately as follows:

(*a*) *Rigid Supports.* Let the ith intermediate support be rigid instead of elastic. This condition may be obtained by letting the spring constant K_i approach infinity as the maximum deflection $Y(h_i)$ at the rigid support approaches zero, the product $K_iY(h_i)$ remaining a finite quantity and being the support reaction at the rigid support when the beam is at its maximum deflection. Let

$$R_i = K_iY(h_i)$$

then Equation [14] becomes

$$\sum_{s=1}^{n}{}' K_s \sum_{r=1}^{\infty} \frac{\phi_r(h_s)\phi_r(h_j)}{p_r^2 - \Lambda^2} Y(h_s) + R_i \sum_{r=1}^{\infty} \frac{\phi_r(h_i)\phi_r(h_j)}{p_r^2 - \Lambda^2} = Y(h_j)[\delta_{ij} - 1] \ldots [17]$$

where $j = 1, 2, \ldots n$, and $\sum_{s=1}^{n}{}'$ means summation with $s = i$ omitted, and δ_{ij} is the Kronecker delta.

The corresponding frequency equation is given by

$$|A_{st} + \delta_{st}'| = 0 \ldots\ldots\ldots\ldots\ldots\ldots [18]$$

where

$$A_{st} \equiv K_t \sum_{r=1}^{\infty} \frac{\phi_r(h_s)\phi_r(h_t)}{p_r^2 - \Lambda^2}$$

and

$$s, t = 1, 2, \ldots i, \ldots n$$

Also, K_t is replaced by unity and δ_{st}' is the Kronecker delta with the particular value, $\delta_{ii}' = 0$, where h_i is the location of the rigid support.

Equation [18] also can be obtained from Equation [15] by factoring out K_i from the ith column of the determinant in Equation [15] and taking the limit as K_i approaches infinity. Comparing Equations [18] and [15], it is evident that if the ith intermediate support is rigid instead of elastic, we need only to replace the corresponding column in the determinant of Equation [15] by

$$\sum_{r=1}^{\infty} \frac{\phi_r(h_s)\phi_r(h_i)}{p_r^2 - \Lambda^2}$$

where $s = 1, 2, \ldots i, \ldots n$, respectively. It is also clear that this is valid for any number of rigid intermediate supports.

(*b*) *Concentrated Masses.* Assume now that at the point $x = h_i$, there is attached to the beam a concentrated mass M_i instead of an elastic support. For the maximum deflection we have the inertia force

$$F_i = [-M_i\Lambda^2]Y(h_i) \ldots\ldots\ldots\ldots\ldots [19]$$

of the concentrated mass. Accordingly, the potential energy of this inertia force is $\frac{1}{2}[-M_i\Lambda^2]Y(h_i)Y(h_i)$ compared to the strain energy $\frac{1}{2}K_iY(h_i)Y(h_i)$ for an elastic support. The equations derived for a beam with elastic intermediate supports also will be valid here except that the spring constant K_i is replaced by $[-M_i\Lambda^2]$. The frequency equation for a beam with a concentrated mass M_i at h_i and $(n - 1)$ elastic intermediate supports is given by Equation [15] with the substitution of $[-M_i\Lambda^2]$ for K_i. It is evident that this is true for any number of concentrated masses.

(*c*) *Sprung Masses.* Consider that at $x = h_i$ we have a concentrated mass M_i supported by a spring of spring constant K_i instead of an elastic support K_i as shown in Fig. 2.

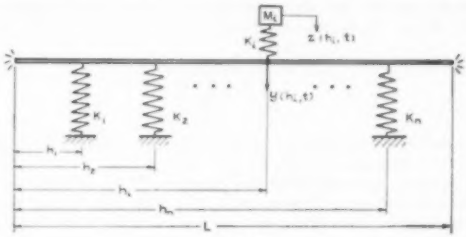

FIG. 2

The deflection of the beam at h_i is $y(h_i, t) = Y(h_i) \sin \Lambda t$. Let the corresponding displacement of the concentrated mass Mt be $z(h_i, t)$. Applying Newton's second law of motion to the mass, we have

$$K_i(y - z) = M_i \frac{d^2z}{dt^2}$$

or

$$\frac{d^2z}{dt^2} + \frac{K_i}{M_i} z = \frac{K_i}{M_i} Y(h_i) \sin \Lambda t$$

The steady-state solution is thus

$$z = \left[\frac{Y(h_i)}{1 - \dfrac{M_i\Lambda^2}{K_i}}\right] \sin \Lambda t$$

The spring force acting on the beam directed upward is

$$K_i(y - z) = \left[\frac{1}{\dfrac{1}{K_i} - \dfrac{1}{M_i\Lambda^2}}\right] Y(h_i) \sin \Lambda t \ldots\ldots [20]$$

Its maximum value corresponding to the maximum deflection of the beam is

$$F_i = \left[\frac{1}{\dfrac{1}{K_i} - \dfrac{1}{M_i\Lambda^2}}\right] Y(h_i) \ldots\ldots\ldots\ldots [21]$$

and the strain energy stored in the sprung mass is

$$\frac{1}{2}\left[\frac{1}{\dfrac{1}{K_i}-\dfrac{1}{M_i\Lambda^2}}\right]Y(h_i)Y(h_i)\ldots\ldots\ldots\ldots[22]$$

Referring to Equation [20]

$$\left[\frac{1}{\dfrac{1}{K_i}-\dfrac{1}{M_i\Lambda^2}}\right]$$

may be considered as the equivalent spring constant of the sprung mass. All the equations for elastic supports are valid for sprung mass if the equivalent spring constant

$$\left[\frac{1}{\dfrac{1}{K_i}-\dfrac{1}{M_i\Lambda^2}}\right]$$

of the sprung mass is substituted for the spring constant K_i of the elastic support. The frequency equation of the vibrating system as shown in Fig. 2, is the same as Equation [15] except for the substitution of the equivalent spring constant

$$\left[\frac{1}{\dfrac{1}{K_i}-\dfrac{1}{M_i\Lambda^2}}\right]$$

of the ith constraint for the elastic constant K_i in the ith column of the determinant.

Consider the case where the beam carries the concentrated mass M_i and spring K_i as shown in Fig. 3. The deflections of the concentrated mass, spring, and the beam at h_i are all the same.

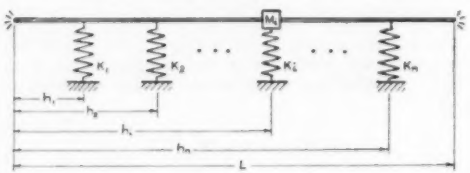

FIG. 3

It can be shown readily that the maximum force acting on the beam by the mass-spring system is

$$(K_i - M_i\Lambda^2)Y(h_i)\ldots\ldots\ldots\ldots\ldots\ldots[23]$$

and the corresponding energy stored in the system is

$$\frac{1}{2}\,[K_i - M_i\Lambda^2]Y(h_i)Y(h_i)$$

Referring to Equation [23] we may consider this mass-spring system as an equivalent elastic support of spring constant $(K_i - M_i\Lambda^2)$. Accordingly, the frequency equation of the vibrating system shown in Fig. 3 is given by Equation [15] with the substitution of equivalent spring constant $(K_i - M_i\Lambda^2)$ for the elastic constant K_i in the ith column of the determinant.

(d) *Continuous Elastic Foundations or Uniformly Distributed Loads of any Length.* Let the intermediate constraint be in the form of a continuous elastic foundation extending from $x = L_1$ to $x = L_2$ with modulus of the foundation k, this being the load per unit length of the beam necessary to produce a compression in the foundation equal to unity, as shown in Fig. 4. Assume that the mass of the foundation can be neglected. For the maximum

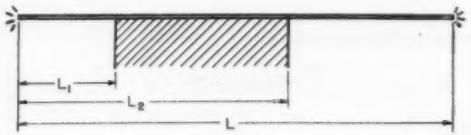

FIG. 4

deflection of the beam, the spring force at a distance x of the elastic foundation of length dx is

$$kY(x)dx$$

and the corresponding strain energy stored in it is

$$\frac{1}{2}\,kY(x)^2dx$$

The strain energy of the entire elastic foundation extending from L_1 to L_2 is thus

$$\frac{1}{2}\,k\int_{L_1}^{L_2}Y(x)Y(x)dx = \frac{1}{2}\,k\int_{L_1}^{L_2}\sum_{r=1}^{\infty}a_r\phi_r(x)\sum_{s=1}^{\infty}a_s\phi_s(x)dx\ldots[24]$$

The potential energy of the vibrating system as shown in Fig. 4 becomes

$$W = \frac{1}{2}\sum_{r=1}^{\infty}p_r^2a_r^2 - \frac{1}{2}\,\Lambda^2\sum_{r=1}^{\infty}a_r^2 + \frac{k}{2}\int_{L_1}^{L_2}\sum_{r=1}^{\infty}a_r\phi_r(x)\sum_{s=1}^{\infty}a_s\phi_s(x)dx$$

The necessary conditions for W to be a minimum require

$$k\sum_{s=1}^{\infty}a_s\int_{L_1}^{L_2}\frac{\phi_s(x)\phi_r(x)}{p_r^2-\Lambda^2}\,dx = -a_r\ldots\ldots[25]$$

and the condition for nontriviality of the solution leads to

$$|kB_{st} + \delta_{st}| = 0\ldots\ldots\ldots\ldots\ldots[26]$$

where

$$B_{st} = \int_{L_1}^{L_2}\frac{\phi_s(x)\phi_t(x)}{p_t^2-\Lambda^2}\,dx$$

and δ_{st} is the Kronecker delta.

This is the frequency equation of a beam on a continuous elastic foundation extended from L_1 to L_2. It can be shown that the infinite series expansion of the deflection of the beam

$$Y(x) = \sum_{r=1}^{\infty}a_r\phi_r(x)$$

converges so rapidly that only the first few nonzero terms will be enough for engineering applications. If the first two nonzero terms are taken, the frequency Equation [26] is reduced to a quadratic equation in Λ^2 from which a close approximation to the fundamental frequency and usually a good approximation to the next higher frequency can be obtained readily. The approximations to the lower frequencies are generally so good that as more

terms are taken these roots may be divided out and at each stage it is only necessary to solve a quadratic equation.

When the continuous elastic foundation extends over the entire length of the beam, i.e., from 0 to L, Equation [24] which is the strain energy stored in the entire elastic foundation becomes

$$\frac{1}{2}k\int_0^L \sum_{r=1}^{\infty} a_r\phi_r(x) \sum_{s=1}^{\infty} a_s\phi_s(x)\,dx = \frac{1}{2}\frac{k}{m}\sum_{r=1}^{\infty} a_r^2$$

and the total potential energy of the vibrating system is

$$W = \frac{1}{2}\sum_{r=1}^{\infty} p_r^2 a_r^2 - \frac{1}{2}\Lambda^2\sum_{r=1}^{\infty} a_r^2 + \frac{1}{2}\frac{k}{m}\sum_{r=1}^{\infty} a_r^2$$

The necessary conditions for W to be a minimum require

$$\frac{\partial W}{\partial a_r} = 0 = a_r\left[(p_r^2 - \Lambda^2) + \frac{k}{m}\right] = 0$$

This equation gives directly the natural circular frequencies of a beam on continuous elastic support as

$$\Lambda_r = \sqrt{p_r^2 + \frac{k}{m}} \qquad [27]$$

which checks with that given by Timoshenko.[5]

If the intermediate constraint is a uniformly distributed load of intensity q instead of continuous elastic foundation of modulus k, all the equations for the latter are valid for the former except that k is replaced by $[-q\Lambda^2]$ as worked out previously for the cases of concentrated masses and elastic supports. When the uniformly distributed load of intensity q extends over the entire range of the beam, Equation [27] becomes

$$\left.\begin{aligned} \Lambda &= \sqrt{p_r^2 - \frac{q\Lambda^2}{m}} \\ \text{or} \qquad \Lambda_r &= p_r\sqrt{\frac{m}{m+q}} \end{aligned}\right\} \qquad [28]$$

These are exactly the natural frequencies of the simple beam of mass $(m + q)$ per unit length of the beam.

Numerical Examples

Example 1. Consider a uniform beam of length L simply supported at both ends, carrying a mass M at its mid-point as shown in Fig. 5. In the classical approach,[6,7] the solution of eight simultaneous equations is required. For the symmetrical case, that is, a load at the center, this reduces to four equations. In the present method, the position of the concentrated mass does not affect appreciably the amount of labor involved. However, the case of mass at the center was selected for comparison because the exact solution by the classic approach is accessible.[6]

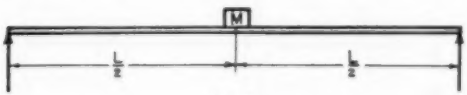

Fig. 5

The eigenfunctions for the simple beam with both ends simply supported are

$$\phi_r(x) = \sqrt{\frac{2}{Lm}}\sin\frac{r\pi x}{L}$$

and the corresponding eigenvalues are

$$\lambda_r = p_r^2 = r^4\frac{\pi^4 EI}{L^4 m}$$

The values of the eigenfunctions at the center of the simple beam where the concentrated mass is located are

$$\phi_r\left(\frac{L}{2}\right) = \sqrt{\frac{2}{Lm}}\sin\frac{r\pi}{2} = 0 \quad \text{for } r = 2, 4, 6, \ldots$$

Therefore the frequency equations of the system are given by Equation [16] and Equation [15] with the substitution of $(-M\Lambda^2)$ for K as follows

$$\frac{\Lambda}{p_1} = (r)^2 \text{ where } r = 2, 4, 6, \ldots \qquad [29]$$

and

$$\sum_{r=1}^{\infty}\frac{\left(\sin\frac{r\pi}{2}\right)^2}{r^4 - \frac{\Lambda^2}{p_1^2}} = \frac{1}{2}\frac{\left(\frac{mL}{M}\right)}{\frac{\Lambda^2}{p_1^2}} \qquad [30]$$

The first frequency Equation [29] gives directly the exact natural frequencies of all antisymmetrical modes of vibration while the second frequency Equation [30] yields the solutions of those of the symmetrical modes. Note that the second frequency Equation [30] converges as $1/r^4$. It reduces to a quadratic equation in Λ^2 if the first two nonzero terms are taken; and a cubic equation, if the first three nonzero terms are used. The former gives approximations to the natural frequencies of the first two symmetrical modes while the latter to the first three. They have been worked out for the case where the ratio of the concentrated mass M to the total mass of the beam mL is unity. The exact natural frequencies of antisymmetrical modes are given by Equation [29] and are independent of the mass ratio.

The results calculated from Equations [29] and [30] are listed in Table 1 together with their solutions by the classical method, see, for example, von Kármán and Biot.[6]

TABLE 1 RESULTS OF CALCULATIONS OF EQUATIONS [29] AND [30]

Modes of free vibrations	Present method: Equation [30] Two terms	Present method: Equation [30] Three terms	Present method: Equation [29]	von Kármán and Biot
$\frac{\Lambda_1}{p_1}$	0.5758	0.5756		0.5754
$\frac{\Lambda_2}{p_1}$			4	4
$\frac{\Lambda_3}{p_1}$	6.99	6.91		6.88
$\frac{\Lambda_4}{p_1}$			16	16
$\frac{\Lambda_5}{p_1}$		21.37		20.97

The numerical computations are simple and straightforward and the approximations are good even when only two terms of Equation [30] are used.

[5] "Vibration Problems in Engineering," by S. Timoshenko, D. Van Nostrand Company, Inc., New York, N. Y., 1937.

[6] "Mathematical Methods in Engineering," by T. von Kármán and M. A. Biot, McGraw-Hill Book Company, Inc., New York, N. Y., 1940.

[7] "Dynamik der Stabwerke," by K. Hohenemser and W. Prager, Julius Springer, Berlin, Germany, 1933.

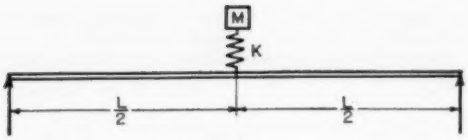

FIG. 6

Example 2. A uniform simply supported beam carries a spring-borne mass M at its mid-point, the spring constant being K in Fig. 6. The position of the mass does not affect the work involved using the present method but it complicates the solution greatly in the case of the classical approach. The eigenfunctions at the center of the simple beam where the sprung mass is located are

$$\phi_r\left(\frac{L}{2}\right) = \sqrt{\frac{2}{Lm}} \sin\frac{r\pi}{2} = 0 \quad \text{for } r = 2, 4, 6, \ldots$$

Therefore the frequency equations of the system are given by Equation [15] with the substitution of

$$\left[\frac{1}{\frac{1}{K} - \frac{1}{M\Lambda^2}}\right]$$

for K and Equation [16] as follows

$$\sum_{r=1}^{\infty} \frac{\left(\sin\frac{r\pi}{2}\right)^2}{\left(r^4 - \frac{\Lambda^2}{p_1^2}\right)} = \frac{1}{2}\left[\frac{\frac{mL}{M}}{\frac{\Lambda^2}{p_1^2}} - \frac{mL}{\frac{K}{p_1^2}}\right] \quad \ldots\ldots\ldots [31]$$

$$\frac{\Lambda}{p_1} = (r)^2 \quad \text{where } r = 2, 4, 6, \ldots\ldots\ldots [32]$$

The first frequency equation of the vibrating system gives the solutions of natural frequencies of symmetrical modes of vibration. If the first two nonzero terms are taken into account, it reduces to a cubic equation in Λ^2, from which the natural frequencies of the first three symmetrical modes can be obtained readily. These numerical values are worked out for the case where both the ratio of the concentrated mass M to the beam mass mL and the ratio of the spring constant K of the spring and the spring constant ($=48EI/L^3$) of the simple beam when centrally loaded are unity. The second frequency Equation [32] gives directly the exact natural frequencies of all antisymmetrical modes. These are independent of both mass ratio and spring ratio. The numerical results calculated from Equations [31] and [32] are listed in Table 2 together with the corresponding solutions as given by K. Hohenemser and W. Prager[7] using the classical approach.

TABLE 2 NUMERICAL RESULTS FROM CALCULATING EQUATIONS [31] AND [32]

Modes of free vibrations	Present method calculated from Equation [31] (two terms) and Equation [32]	Hohenemser and Prager
$\frac{\Lambda_1}{p_1}$	0.4655	0.4653
$\frac{\Lambda_2}{p_1}$	1.4995	1.4935
$\frac{\Lambda_3}{p_1}$	4	4
$\frac{\Lambda_4}{p_1}$	9.055	8.92

Example 3. Consider a continuous beam of length L carrying a spring-borne mass M at the mid-point of the entire beam, the spring constant of the spring being K. The continuous beam is simply supported at both ends and has an intermediate rigid support dividing the beam into two spans of span ratio $L_1 : L_2 = 6:4.5$ as shown in Fig. 7. The frequency equation of this vibrating system is given by Equation [18] with the substitution of

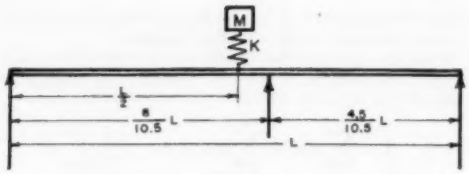

FIG. 7

$$\left[\frac{1}{\frac{1}{K} - \frac{1}{M\Lambda^2}}\right]$$

for K, and has the following form

$$\left\{\frac{\left[\sum_{r=1}^{\infty} \frac{\sin\frac{r\pi}{2}\sin\left(\frac{6}{10.5}r\pi\right)}{r^4 - \frac{\Lambda^2}{p_1^2}}\right]^2}{\left[\sum_{r=1}^{\infty} \frac{\left(\sin\frac{6}{10.5}r\pi\right)^2}{r^4 - \frac{\Lambda^2}{p_1^2}}\right]} - \left[\sum_{r=1}^{\infty} \frac{\left(\sin\frac{r\pi}{2}\right)^2}{r^4 - \frac{\Lambda^2}{p_1^2}}\right]\right\} = \frac{1}{2}\left[\frac{\pi^4}{48}\left(\frac{K_b}{K}\right) - \frac{\left(\frac{mL}{M}\right)}{\left(\frac{\Lambda^2}{p_1^2}\right)}\right] \quad \ldots [33]$$

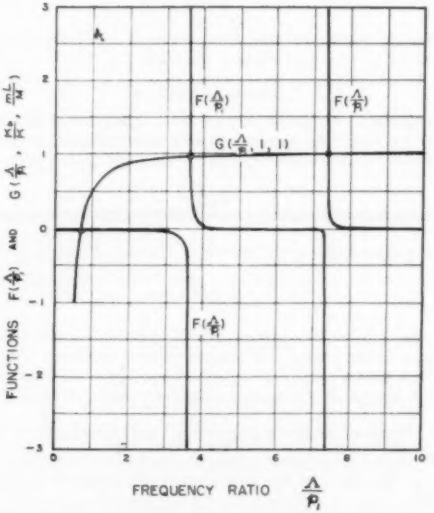

FIG. 8

where $K_b = 48EI/L^3$ is the spring constant of the simple beam when centrally loaded.

It is noted that the left side of the foregoing equation is a function of Λ alone while the right side is a function of Λ, the spring ratio K_b/K, and the mass ratio mL/M. Let

$$F\left(\frac{\Lambda}{p_1}\right) = \left\{ \frac{\left[\sum_{r=1}^{\infty} \frac{\sin\frac{r\pi}{2}\sin\frac{6}{10.5}r\pi}{r^4 - \frac{\Lambda^2}{p_1^2}}\right]^2}{\left[\sum_{r=1}^{\infty} \frac{\left(\sin\frac{6}{10.6}r\pi\right)^2}{r^4 - \frac{\Lambda^2}{p_1^2}}\right]} - \left[\sum_{r=1}^{\infty} \frac{\left(\sin\frac{r\pi}{2}\right)^2}{r^4 - \frac{\Lambda^2}{p_1^2}}\right] \right\}$$

and

$$G\left(\frac{\Lambda}{p_1}, \frac{K_b}{K}, \frac{mL}{M}\right) = \frac{1}{2}\left[\frac{\pi^4}{48}\left(\frac{K_b}{K}\right) - \frac{\left(\frac{mL}{M}\right)}{\left(\frac{\Lambda^2}{p_1^2}\right)}\right]$$

For given spring ratio and mass ratio, the function G becomes a function of Λ alone. The frequency Equation [33] may be solved graphically by plotting $F(\Lambda/p_1)$ and $G(\Lambda/p_1)$ and the intersections of these two curves give the natural frequencies Λ of the composite system. Fig. 8 shows the curves for one particular numerical example where both K_b/K and mL/M are taken as unity. The first three natural frequencies of this composite system as found in Fig. 8 are listed in Table 3.

TABLE 3 NATURAL FREQUENCIES OF COMPOSITE SYSTEMS

System	$\frac{\Lambda_1}{p_1}$	$\frac{\Lambda_2}{p_1}$	$\frac{\Lambda_3}{p_1}$	Source
Fig. 6 With $\frac{mL}{M} = 1$; $\frac{K_b}{K} = 1$	0.4655	1.4995	4	Example 2
Fig. 7 With $\frac{mL}{M} = 1$; $\frac{K_b}{K} = 1$	0.70	3.65	7.37	Fig. 8
Fig. 7 without the sprung-mass	2.17	4.25	8.25	Timoshenko, reference 5

The other two composite systems are listed together in Table 3 to show the effect of sprung-mass and intermediate support on the natural frequencies of the vibrating system.

Deflection and Stresses in Beams Subjected to Bending and Creep

By YOH-HAN PAO[1] and JOSEPH MARIN,[2] STATE COLLEGE, PA.

This paper presents theories for the determination of deflections and stresses in beams subjected to bending and creep. The theories are based on a creep-stress-time relation in simple tension which gives an accurate fit of most test data. The theory takes into account the variation in stress distribution in bending with time. For this purpose a time-hardening theory is used to express the stress variation or stress relaxation of each fiber in bending. A comparison between actual creep deflections for Plexiglas specimens subjected to pure bending and values predicted by the proposed theory shows good agreement between experimental and theoretical results. The creep behavior for other materials in tension indicates that this method could be used for predicting bending creep deflections for these materials. The application of the theory to the determination of deflections in various kinds of beams is also explained.

Theory for Stress and Deflections in Beams Subjected to Bending and Creep

VARIOUS theories have been developed for the determination of stresses and deflection in beams subjected to bending (1, 2, 3).[3] The theory presented in this paper has the advantages of greater accuracy for the initial stage of creep, combined with a reduction in the amount of effort required for specific solutions.

The theory developed is based on the assumption that the material is homogeneous and isotropic. It is also assumed that the creep-stress-time relations in tension and compression are identical and are defined by

$$\epsilon = \frac{\sigma}{E} + K\sigma^{\alpha}(1 - e^{-qt}) + B\sigma^{n}t \quad \ldots\ldots [1]$$

where

ϵ = creep strain plus elastic unit strain
σ = unit stress
t = time
e = natural base for logarithms
$E, K, \alpha, q, n,$ and B = experimental constants

In Equation [1] the first term on the right side represents the initial strain while the second and third represent the time-dependent creep strain. After the initial stage of creep, e^{-qt} becomes negligible and all the creep strain is then expressed by the third term $B\sigma^{n}t$ in Equation (1). The creep strain then varies linearly with time giving a constant creep rate. The agreement of test data and the empirical relation Equation [1] is shown in Fig 1 which represents test data for Plexiglas. The agreement in the initial stages could be improved if the expression $K\sigma^{\alpha}(1 - e^{-qt} - e^{-2qt})$ is used instead of $K\sigma^{\alpha}(1 - e^{-qt})$, but the ensuing mathematical difficulties do not make this refinement worth while.

In the following theoretical determination of stresses and deflections in bending and creep based on Equation [1], a member of rectangular cross section will be considered. Theory can be developed, however, for other types of cross section. Fig. 2 shows a straight member of rectangular cross section subjected to a pure bending moment M. To determine the stress σ for any fiber at a distance y from the neutral axis the conditions of equilibrium for the stress will be written, namely

$$b\int \sigma dy = 0 \quad \ldots\ldots [2]$$

$$b\int \sigma y dy = M \quad \ldots\ldots [3]$$

The strain ϵ at $t = 0$ for any fiber will be determined from Equation [1] by placing $t = 0$ or

$$\epsilon = \frac{\sigma}{E} \quad \ldots\ldots [4]$$

The stress distribution is then elastic and the stress on the outer fiber is

$$\sigma_{10} = (3)\frac{M}{2bh^2} \quad \ldots\ldots [5]$$

For bending accompanied by creep it has been shown (4, 5) that plane sections before bending remain plane after bending, or the strains are proportional to the distance from the neutral axis. Then, if ϵ and ϵ_1 are strains at distances y and h from the neutral axis, respectively

$$\frac{\epsilon}{\epsilon_1} = \frac{y}{h} \quad \ldots\ldots [6]$$

By l'Hospital's rule, using Equation [6]

$$\frac{\left(\frac{d\epsilon}{dt}\right)}{\left(\frac{d\epsilon_1}{dt}\right)} = \frac{y}{h} \quad \text{or} \quad \frac{C}{C_1} = \frac{y}{h} \quad \ldots\ldots [7]$$

That is, the ratio of the creep rates is proportional to the distance from the neutral axis. Using Equation [1] the creep rate for conditions of constant stress is by differentiation

$$C = qK\sigma^{\alpha}e^{-qt} + B\sigma^{n} \quad \ldots\ldots [8]$$

For varying stress conditions, Equation [8] for constant stress cannot be used unless certain assumptions are made. Two available simplifying assumptions are based on either the strain-

---

[1] Research Associate, Engineering Experiment Station, The Pennsylvania State College.

[2] Professor of Engineering Mechanics and Research Professor of Engineering Materials, The Pennsylvania State College. Mem. ASME.

[3] Numbers in parentheses refer to the Bibliography at the end of the paper.

Presented at the National Conference of the Applied Mechanics Division, State College, Pa., June 19–21, 1952, of The American Society of Mechanical Engineers.

Discussion of this paper should be addressed to the Secretary, ASME, 29 West 39th Street, New York, N. Y., and will be accepted until January 10, 1953, for publication at a later date. Discussion received after the closing date will be returned.

Note: Statements and opinions advanced in papers are to be understood as individual expressions of their authors and not those of the Society. Manuscript received by ASME Applied Mechanics Division, November 16, 1951. Paper No. 52—APM-34.

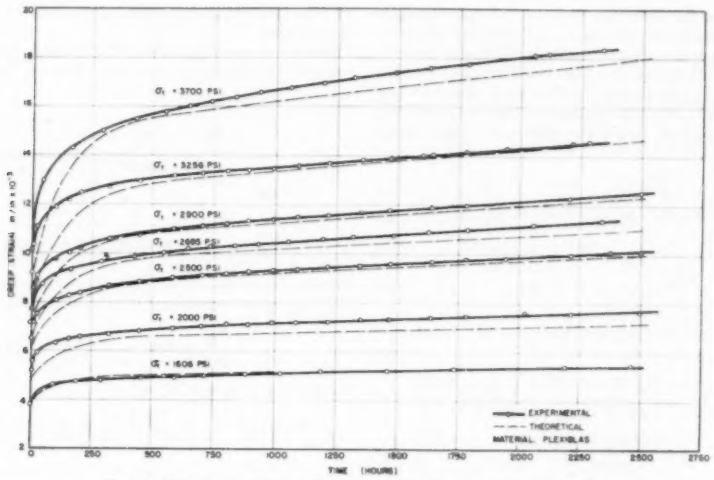

FIG. 1 REPRESENTATION OF TENSION-CREEP DATA BY EXPRESSION [1]

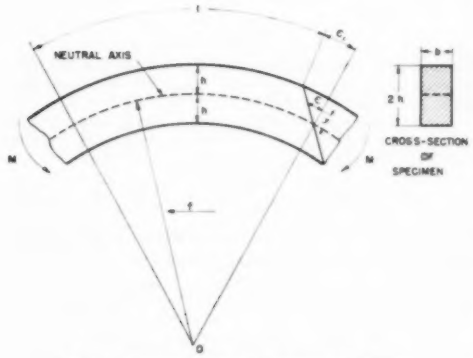

FIG. 2 ELEMENT OF BEAM SUBJECTED TO BENDING

hardening or the time-hardening laws (6). The strain-hardening law leads to complications in the development of the theory and for this particular application does not yield results greatly different from those obtained with the time-hardening law. Then, using the time-hardening assumption, the creep rate for conditions of varying stress is identical to that given by Equation [8]. Using Equation [8] to determine the creep rates C and C_1 for the inner and outer fibers, then by Equation [7]

$$\frac{C}{C_1} = \frac{qK\sigma^n e^{-\nu t} + B\sigma^n}{qK\sigma_1^n e^{-\nu t} + B\sigma_1^n} = \frac{y}{h} \quad \ldots\ldots\ldots\ldots [8a]$$

The first terms in the numerator and denominator of the left-hand side of Equation [8] represent the part of the creep rate contributed by the transient or initial creep component. For large values of $t = T$, $e^{-\nu t}$ approaches zero and then Equation [8] can be written

$$\frac{C}{C_1} = \frac{B\sigma_T^n}{B\sigma_{1T}^n} = \frac{y}{h} \quad \text{or} \quad \left(\frac{\sigma_T}{\sigma_{1T}}\right)^n = \frac{y}{h} \quad \ldots\ldots\ldots [9]$$

Then substituting the value of σ_T from Equation [9] for σ in Equation [3], and integrating the resulting equation

$$\sigma_{1T} = \frac{M}{2bh^2}\left(\frac{2n+1}{n}\right) \quad \ldots\ldots\ldots\ldots [10]$$

An examination of the stress values given by Equations [5] and [10] shows that the stress varies from a value

$$\sigma_{10} = \frac{M}{2bh^2} \quad (3)$$

to

$$\sigma_{1T} = \frac{M}{2bh^2}\left(\frac{2n+1}{n}\right)$$

for times varying from $t = 0$ to $t = T$, where T is large. A comparison of the creep rates in Equations [8] and [9], shows that the term which influences the change in stress from σ_{10} to σ_{1T} is $e^{-\nu t}$. It will then be assumed that the stress σ_1 at a time t between $t = 0$ and $t = T$, can be approximately defined by[4]

$$\sigma_1 = \left(\frac{M}{2bh^2}\right)\left[\frac{2n+1}{n} + \left(3 - \frac{2n+1}{n}\right)e^{-\nu t}\right] \quad \ldots [11]$$

For $t = 0$, $\sigma_1 = \sigma_{10}$ as given by Equation [5] and for $t = T$, where T is large, $\sigma_1 = \sigma_{1T}$ as given by Equation [10]. The value of σ_1 can be more conveniently written as

$$\sigma_1 = \frac{M}{2bh^2} k_n (1 + k_d e^{-\nu t}) \quad \ldots\ldots\ldots\ldots [12]$$

where

$$k_n = \frac{2n+1}{n} \quad \text{and} \quad k_d = \frac{3 - \dfrac{2n+1}{n}}{\left(\dfrac{2n+1}{n}\right)} \quad \ldots\ldots [13]$$

[4] The justification for the use of Equation [11] is given in the Appendix.

Equation [12] gives the maximum stress on the outer fiber as a function of the moment M and time t. To determine the creep deflections in beams subjected to bending, the strains must be considered. Since the stress on a fiber varies with time and the creep rate is a function of the stress, to determine the creep strain on a fiber at a time t, it will be necessary to integrate the influence of the varying stress; that is, the strain ϵ_1 at a time t for the outer fiber is

$$\epsilon_1 = \frac{\sigma}{E} + \int_0^t C_1\, dt = \frac{\sigma}{E} + \int_0^t \frac{d\epsilon_1}{dt}\, dt \ldots\ldots [14]$$

From Equation [1]

$$\frac{d\epsilon_1}{dt} = qK\sigma_1^{\alpha} e^{-qt} + B\sigma^n \ldots\ldots [15]$$

Placing the value of $(d\epsilon_1)/(dt)$ from Equation [15] in Equation [14] and integrating, the strain ϵ_1 at a time t is

$$\epsilon_1 = \frac{\sigma}{E} + K\left(\frac{Mk_n}{2bh^2}\right)^{\alpha}\left[\frac{(1+k_d)^{\alpha+1}}{k_d(\alpha+1)} - \frac{(1+k_d e^{-qt})^{\alpha+1}}{k_d(\alpha+1)}\right] + B\left(\frac{Mk_n}{2bh^2}\right)^{n}\left[t + \frac{nk_d}{q}(1-e^{-qt})\right] \ldots [16]$$

Equation [16] gives the strain ϵ_1 on the outer fiber in a member subjected to bending and creep. To obtain the deflection, note that by similar triangles, from Fig. 2

$$\frac{\epsilon_1}{1} = \frac{h}{f} \ldots\ldots [17]$$

where f = the radius of curvature.

For small deflections, if w is the deflection, the radius of curvature can be shown to be related to the deflection by the equation

$$\frac{1}{f} = \frac{\dfrac{d^2w}{dx^2}}{\left[1+\left(\dfrac{dw}{dx}\right)^2\right]^{3/2}} = \frac{d^2w}{dx^2} \ldots\ldots [18]$$

Then from Equations [17] and [18]

$$\frac{d^2w}{dx^2} = \frac{\epsilon_1}{h} \ldots\ldots [19]$$

For a given time t, Equation [16] can be written as

$$\epsilon_1 = K_1 M + K_2 M^{\alpha} + K_3 M^n \ldots\ldots [20]$$

where

$$\left.\begin{aligned} K_1 &= \frac{1}{E}\left(\frac{3}{2bh^2}\right) \\ K_2 &= K\left(\frac{k_n}{2bh^2}\right)^{\alpha}\left[\frac{(1+k_d)^{\alpha+1}}{k_d(\alpha+1)} - \frac{(1+k_d e^{-qt})^{\alpha+1}}{k_d(\alpha+1)}\right] \\ K_3 &= B\left(\frac{k_n}{2bh^2}\right)^{n}\left[t + \frac{nk_d}{q}(1-e^{-qt})\right] \end{aligned}\right\} \ldots [21]$$

From Equations [19] and [20] the differential equation for the deflection w becomes

$$h\frac{d^2w}{dx^2} = K_1 M + K_2 M^{\alpha} + K_3 M^n \ldots\ldots [22]$$

Equation [22] can now be used to determine the deflection in specific cases if the moment M can be expressed as a function of x. The application of Equation [22] is illustrated by the following examples.

Example 1—Cantilever Beam With an End Load. Fig. 3 shows a cantilever beam with an end load Q and of length L. To determine the maximum end deflection w at a time t, the value of $M = Qx$ will be substituted in Equation [22]. Then

FIG. 3 CANTILEVER BEAM WITH AN END LOAD

$$h\frac{d^2w}{dx^2} = K_1 Qx + K_2 Q^{\alpha} x^{\alpha} + K_3 Q^n x^n \ldots\ldots [23]$$

Integrating Equation [23] twice

$$h\frac{dw}{dx} = K_1 Q\frac{x^2}{2} + K_2 Q^{\alpha}\frac{x^{\alpha+1}}{\alpha+1} + K_3 Q^n \frac{x^{n+1}}{n+1} + c_1 \ldots [24]$$

$$hw = K_1 Q\frac{x^3}{6} + K_2\frac{Q^{\alpha}x^{\alpha+2}}{(\alpha+1)(\alpha+2)} + K_3\frac{Q^n x^{n+2}}{(n+1)(n+2)} + c_1 x + c_2 \ldots [25]$$

The boundary conditions for finding c_1 and c_2 are that the slope and deflection w at $x = L$ are zero. Then from Equations [24] and [25]

$$c_1 = -\left[\frac{K_1 QL^2}{2} + \frac{K_2 Q^{\alpha} L^{\alpha+1}}{\alpha+1} + \frac{K_3 Q^n L^{n+1}}{n+1}\right] \ldots [26]$$

$$c_2 = \left[K_1\frac{QL^3}{3} + \frac{K_2 Q^{\alpha} L^{\alpha+2}}{\alpha+2} + \frac{K_3 Q^n L^{n+2}}{n+2}\right] \ldots [27]$$

Substituting the values of c_1 and c_2 from Equations [26] and [27] in [25], the deflection w at a time t is expressed by

$$hw = K_1 Q\frac{x^3}{6} + \frac{K_2 Q^{\alpha} x^{\alpha+2}}{(\alpha+1)(\alpha+2)} + \frac{K_3 Q^n x^{n+2}}{(n+1)(n+2)} - \left[K_1\frac{QL^2}{2} + K_2\frac{Q^{\alpha}L^{\alpha+1}}{\alpha+1} + \frac{K_3 Q^n L^{n+1}}{n+1}\right]x + \left[K_1\frac{QL^3}{3} + \frac{K_2 Q^{\alpha}L^{\alpha+2}}{\alpha+2} + \frac{K_3 Q^n L^{n+2}}{n+2}\right] \ldots [28]$$

The maximum creep deflection at a time t is determined from Equation [22] since by inspection of the deflection diagram in Fig. 3 the maximum deflection occurs at $x = 0$. Then, by Equation [28]

$$hw_{\max} = K_1\frac{QL^3}{3} + K_2\frac{Q^{\alpha}L^{\alpha+2}}{\alpha+2} + K_3\frac{Q^n L^{n+2}}{n+2} \ldots [29]$$

where K_1, K_2, and K_3 are defined in Equations [21].

Example 2—Bar of Rectangular Cross Section Subjected to Pure Bending Moments at Ends. Fig. 4 represents a bar of length L subjected to pure bending by the couples m acting at the ends of the bar. To determine the maximum deflection $w_{\max}$ at the center of the bar, Equation [22] can be used. Since $M = M_0 = \text{const}$, Equation [22] can be written

$$h\frac{d^2w}{dx^2} = K_1 M_0 + K_2 M_0^{\alpha} + K_3 M_0^n \ldots\ldots [30]$$

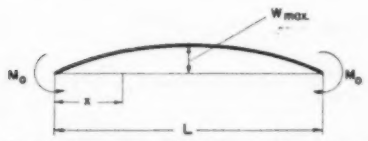

FIG. 4 BAR OF RECTANGULAR CROSS SECTION SUBJECTED TO PURE BENDING MOMENTS AT ENDS

Integrating Equation [30] twice

$$h\frac{dw}{dx} = K_1M_0x + K_2M_0^{\alpha}x + K_3M_0^{n}x + c_1 \dots [31]$$

$$hw = K_1\frac{M_0x^2}{2} + K_2\frac{M_0^{\alpha}x^2}{2} + K_3\frac{M^{n}x_2}{2} + c_1x + c_2 \dots [32]$$

Since $(dw)/(dx) = 0$ for $x = L/2$ and $w = 0$ for $x = 0$, by Equations [31] and [32]

$$c_1 = -\left(K_1M_0\frac{L}{2} + K_2M_0^{\alpha}\frac{L}{2} + K_3M_0^{n}\frac{L}{2}\right) \quad \text{and} \quad c_2 = 0$$

Then

$$hw = \left(\frac{K_1M_0}{2} + \frac{K_2M_0^{\alpha}}{2} + \frac{K_3M_0^{n}}{2}\right)x^2 - \left(\frac{K_1M_0}{2} + \frac{K_2M_0^{\alpha}}{2} + \frac{K_3M_0^{n}}{2}\right)Lx \dots [33]$$

The maximum deflection is obtained by Equation [33] by placing $x = L/2$ or

$$hw_{max} = -(K_1M_0 + K_2M_0^{\alpha} + K_3M_0^{n})\frac{L^2}{8} \dots [34]$$

Equation [34] can now be used to determine the maximum deflection, since K_1, K_2, K_3, α, n, L, h, and M_0 are known in any particular case.

Example 3—Statically Indeterminate Beam. Fig. 5 shows a statically indeterminate beam of length L, fixed at one end and simply supported at the other, and subjected to a concentrated load P at a distance c from the left end. To determine the reaction at the left end and the equations for the creep deflections, it is necessary to write differential equations for deflections covering x values from 0 to c, from c to a, and from a to L. These equations and their integration for the creep deflection become:

For $0 \leq x \leq c$

$$h\frac{d^2w_1}{dx^2} = K_1M_1 + K_2M_1^{\alpha} + K_3M_1^{n} \dots [35]$$

Since $M_1 = Rx$, Equation [35] can be written

$$h\frac{d^2w_1}{dx^2} = K_1Rx + K_2(Rx)^{\alpha} + K_3(Rx)^{n} \dots [35a]$$

Integrating Equation [35a] twice to determine the deflection w_1

$$h\frac{dw_1}{dx} = K_1\frac{Rx^2}{2} + K_2\frac{R^{\alpha}x^{\alpha+1}}{(\alpha+1)} + K_3\frac{R^{n}x^{n+1}}{(n+1)} + c_1 \dots [36]$$

and

$$hw_1 = K_1\frac{Rx^3}{6} + \frac{K_2R^{\alpha}x^{\alpha+2}}{(\alpha+1)(\alpha+2)} + \frac{K_3R^{n}x^{n+2}}{(n+1)(n+2)} + c_1x + c_2 \dots [37]$$

For $c \leq x \leq a$

$$h\frac{d^2w_2}{dx^2} = K_1M_2 + K_2M_2^{\alpha} + K_3M_2^{n} \dots [38]$$

Since $M_2 = Rx - P(x - c)$, Equation [38] can be written

$$h\frac{d^2w_2}{dx^2} = K_1[(R-P)x + Pc] + K_2[(R-P)x + Pc]^{\alpha} + K_3[(R-P)x + Pc]^{n} \dots [38a]$$

Integrating Equation [38a] twice to determine the deflection w_2

$$h\frac{dw_2}{dx} = K_1\frac{[(R-P)x + Pc]^2}{2(R-P)} + K_2\frac{[(R-P)x + Pc]^{\alpha+1}}{(R-P)(\alpha+1)} + K_3\frac{[(R-P)x + Pc]^{n+1}}{(R-P)(n+1)} + c_2 \dots [39]$$

and

$$hw_2 = \frac{K_1[(R-P)x + Pc]^3}{6(R-P)^2} + \frac{K_2[(R-P)x + Pc]^{\alpha+2}}{(R-P)^2(\alpha+1)(\alpha+2)} + \frac{K_3[(R-P)x + Pc]^{n+2}}{(R-P)^2(n+1)(n+2)} + c_2x + c_4 \dots [40]$$

For $a \leq x \leq L$:
For a value of $x = a$ in Fig. 5 there is a point of contraflexure.

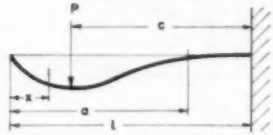

FIG. 5 A STATICALLY INDETERMINATE BEAM

The distance a is obtained from the condition that at the point of contraflexure the moment is zero or

$$Ra = P(a - c) \quad \text{and} \quad a = \frac{Pc}{P - R} \dots [41]$$

Now Equations [38], [39], and [40] for x-values from $x = a$ to $x = L$ do not apply, since for these values of x the stress and strain on the bottom fiber change sign and the strain has a value of

$$\epsilon = \frac{\sigma}{E} - K(-\sigma)^{\alpha}(1 - e^{-\gamma t}) - B(-\sigma)^{n}$$

This gives a differential equation for deflection for $a \leq x < L$ as follows

$$h\frac{d^2w_3}{dx^2} = K_1M_3 - K_2(-M_3)^{\alpha} - K_3(-M_3)^{n} \dots [42]$$

Since $M_3 = Rx - P(x - c)$, Equation [42] can be written

$$h\frac{d^2w_3}{dx^2} = K_1[(R-P)x + Pc] - K_2[-(R-P)x - Pc]^{\alpha} - K_3[-(R-P)x - Pc]^{n} \dots [42a]$$

Integrating Equation [42a] twice to determine the deflection w_3

$$h\frac{dw_3}{dx} = K_1\frac{[(R-P)x + Pc]^2}{2(R-P)} + K_2\frac{[-(R-P)x - Pc]^{\alpha+1}}{(R-P)(\alpha+1)} + K_3\frac{[-(R-P)x - Pc]^{n+1}}{(R-P)(n+1)} + c_3 \dots [43]$$

and

$$hw_2 = \frac{K_1[(R-P)x + Pc]^3}{6(R-P)} - \frac{K_2[-(R-P)x - Pc]^{\alpha+2}}{(R-P)^2(\alpha+1)(\alpha+2)} - \frac{K_3[-(R-P)x - Pc]^{n+2}}{(R-P)^2(n+1)(n+2)} + c_7x + c_8 \quad . . [44]$$

The constants of integration c_1 to c_8 and reaction R can be determined using the foregoing equations and the following boundary conditions

$$\left.\begin{aligned}(w_1)_{x=0} = 0,\ (w_1)_{x=c} = (w_2)_{x=c},\ \left(\frac{dw_1}{dx}\right)_{x=c} \\ = \left(\frac{dw_2}{dx}\right)_{x=c},\ (w_2)_{x=a} = (w_3)_{x=a},\ \left(\frac{dw_2}{dx}\right)_{x=a} \\ = \left(\frac{dw_3}{dx}\right)_{x=a},\ (w_3)_{x=L} = 0,\ \left(\frac{dw_3}{dx}\right)_{x=L} = 0\end{aligned}\right\} \quad . . [45]$$

With the constants of integration and reaction R evaluated, Equations [37], [40], and [44] can then be used to determine the creep deflections.

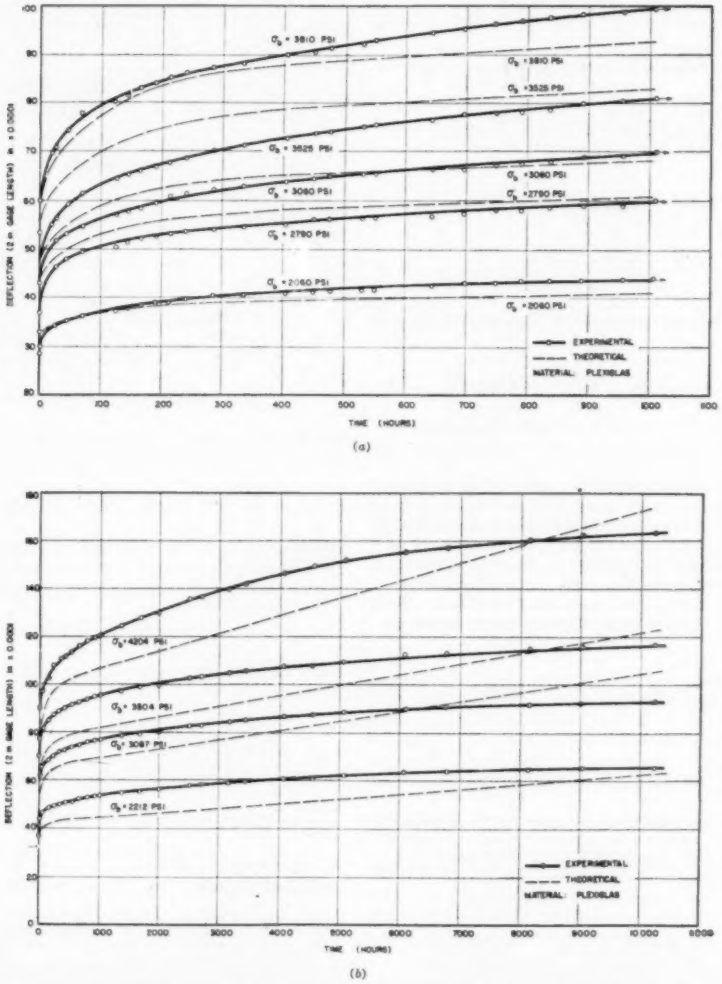

FIG. 6 COMPARISON BETWEEN EXPERIMENTAL AND THEORETICAL BENDING-CREEP DEFLECTIONS

TABLE 1 CONSTANT STRESS-CREEP CONSTANTS FOR PLEXIGLAS

$E = 4.10 \times 10^5$	$q = 8.00 \times 10^{-3}$
$K = 9.74 \times 10^{-9}$	$B = 7.69 \times 10^{-16}$
$\alpha = 1.89$	$n = 2.02$

TABLE 2 COMPARISON BETWEEN THEORETICAL AND EXPERIMENTAL BENDING-CREEP DEFLECTIONS FOR PLEXIGLAS

Specimen no.	Initial max fiber stress (elastic), psi	Bending-creep deflections for 2 in. gage length, in. $\times 10^{-4}$								
		At 50 hr			At 500 hr			At 1000 hr		
		Exp	Theor	Diff. per cent	Exp	Theor	Diff. per cent	Exp	Theor	Diff. per cent
Group A:										
1	3810	74.8	72.3	−2	91.8	88.8	−2	99.3	92.8	−7
2	3525	59.4	65.1	+10	74.5	79.5	+7	80.7	83.0	+3
4	3060	53.8	55.6	+3	65.0	65.7	+1	69.7	67.7	−3
5	2790	48.3	50.5	+5	56.3	58.6	+4	59.6	60.7	+2
7	2060	35.2	35.6	+1	41.9	39.7	−5	43.7	40.7	−7
Group B:		At 500 hr			At 5000 hr			At 10,000 hr		
		Exp	Theor	Diff. per cent	Exp	Theor	Diff. per cent	Exp	Theor	Diff. per cent
2	2212	51.1	42.6	−17	62.2	52.0	−16	65.2	62.0	−5
4	3087	73.8	66.8	−9	88.4	84.4	−4	93.2	104.5	+12
5	3504	91.2	79.0	−13	109.1	100.0	−8	115.0	122.0	+5
8	4204	113.1	101.2	−11	151.1	135.8	−10	163.8	172.8	+5

In some problems it is not possible to integrate directly, as in the foregoing examples. In such cases it is possible to express the right-hand side of the differential equation in the form of a series which then can be integrated.

Comparison of Theoretical and Experimental Creep Deflection

Values of creep deflections were measured for Plexiglas subjected to pure bending and for a series of specimens with different values of the bending moments. Two series of tests were conducted as indicated in Fig. 6. In one series, labeled group (*a*), the tests covered a period of 1000 hr, while in a second group (*b*), of longer duration, the tests lasted for 10,000 hr. The test procedure and other details of testing are given in reference (3). The theoretical creep deflection-time relations based on Equation [34] for pure bending, are also given in Fig. 6. The creep constants used for evaluating the theoretical creep-deflection relations are given in Table 1. A comparison of the theoretical and experimental creep deflections, as given in Fig. 6 and Table 2, shows good agreement between theory and test results when it is considered that the material variations were found to yield differences of 20 per cent in creep strains. Furthermore, the creep constants in Equation [1] for tension and compression were assumed the same and of value equal to the average of the tension and compression constants.

Conclusions

1 A theory for determining the creep deflections in bending is presented in this paper which gives a good approximation for short, intermediate, and long periods of time. Available theories are good only for long periods of time.

2 The theory developed provides for relaxation of fiber stresses with time and for elastic recovery.

3 The theory for creep deflections in bending can be applied to specific problems in bending with no greater difficulty than is present in the current available theories.

4 Tests on Plexiglas in bending accompanied by creep show good agreement with values given by the proposed theory.

Acknowledgments

The authors appreciate the financial assistance and sponsorship by Research Corporation in making possible this investigation.

Bibliography

1 "Mechanical Properties of Materials and Design," by Joseph Marin, McGraw-Hill Book Company, Inc., New York, N. Y., 1942.

2 "Bending of Beams With Creep," by E. P. Popov, *Journal of Applied Physics*, vol. 20, 1949, pp. 251–256.

3 "Creep Properties of Lucite and Plexiglas for Tension, Compression, Bending, and Torsion," by J. Marin, Y. H. Pao, and G. E. Cuff, Trans. ASME, vol. 73, 1951, pp. 705–719.

4 "An Experimental and Analytical Investigation of Creep in Bending," by G. H. MacCullough, Trans. ASME, vol. 55, 1933, pp. 55–60.

5 "Unpublished Data on the Bending of Polymethylmethacrylate Beams," by J. Marin and Y. H. Pao.

6 "Correlation of Creep and Relaxation Properties of Copper," by C. C. Davenport, Journal of Applied Mechanics, Trans. ASME, vol. 60, 1938, p. A-55.

Appendix

Justification for Use of Equation [11]

By Equation [8*a*] of the text

$$\frac{C}{C_1} = \frac{qK\sigma^\alpha e^{-\psi t} + B\sigma^n}{qK\sigma_1^\alpha e^{-\psi t} + B\sigma_1^n} = \frac{y}{h} \quad \ldots\ldots [46]$$

Also, by Equation [3] the condition of equilibrium at the cross section of the beam may be written as

$$2b\int^h \sigma y\, dy = M \quad \ldots\ldots [47]$$

From Equation [46]

$$y = \frac{h(qK\sigma^\alpha e^{-\psi t} + B\sigma^n)}{(qK\sigma_1^\alpha e^{-\psi t} + B\sigma_1^n)} \quad \ldots\ldots [48]$$

and after differentiation

$$dy = \frac{h\,(qK\alpha\sigma^{\alpha-1}e^{-\psi t} + nB\sigma^{n-1})d\sigma}{(qK\sigma_1^\alpha e^{-\psi t} + B\sigma_1^n)} \quad \ldots\ldots [49]$$

Substitution of Equations [48] and [49] into Equation [47] gives

$$\frac{2bh^2}{(qK\sigma_1^\alpha e^{-\psi t} + B\sigma_1^n)^2}\int_0^{\sigma_1} (qK\alpha\sigma^\alpha e^{-\psi t} + nB\sigma^n)$$

$$(qK\sigma^\alpha e^{-\psi t} + B\sigma^n)\, d\sigma = M \quad \ldots\ldots [50]$$

Integration of Equation [50] results in the following expression

$$\frac{\alpha}{2\alpha+1} q^2K^2\sigma_1^{2\alpha+1} e^{-\psi t} + \frac{n+\alpha}{n+\alpha+1} qKB\sigma_1^{\alpha+n+1}e^{-\psi t} + \frac{n}{2n+1} B^2\sigma_1^{2n+1}$$

$$\frac{}{q^2K^2\sigma_1^{2\alpha}e^{-\psi t} + 2qKB\sigma_1^{\alpha+n}e^{-\psi t} + B^2\sigma_1^{2n}} = \frac{M}{2bh^2} \quad [51]$$

Equation [51] may be solved to give time t as an explicit function of the stress σ_1

$$t = f(\sigma_1) \quad [52]$$

This was done but the resulting expression was much too complicated to be of further practical use in the analytical development of the theory.

A graphical plot of stress against time was then made using the relation represented by Equation [51]. It was found that a simpler expression, namely

$$\sigma_1 = \frac{2n+1}{n}\frac{M}{2bh^2} + \left[3\frac{M}{2bh^2} - \frac{2n+1}{n}\frac{M}{2bh^2}\right]e^{-qt} \quad [53]$$

could represent the relation given by Equation [51] quite well, except for the initial portion of the curve. However, Equation [51] is incorrect for small values of time. For example, at $t = 0$ the value of σ_1 obtained from Equation [51] would be approximately

$$\sigma_1 = \frac{2\alpha+1}{\alpha}\frac{M}{2bh^2} \quad [54]$$

If $\alpha \neq 1$, σ_1 would be not equal to $(3M)/(2bh^2)$ which is the initial stress value given by the initial elastic distribution.

The reason for this discrepancy is that in Equation [8a] the creep rates of the fibers are considered to be proportional to the distances of the fibers from the neutral axis. Actually, the total strain rates are proportional to the distances from the neutral axis and in writing Equation [8a] the terms representing the rate of change of the elastic strains have been neglected.

Determination of Theoretical Plastic Stress-Strain Relations for Variable Combined Stress Ratios

By L. W. HU[1] and JOSEPH MARIN,[2] STATE COLLEGE, PA.

To distinguish between the various theories of plastic flow defining plastic stress-strain relations under combined stresses, it is necessary to conduct combined stress tests in which the ratio of the stress components does not remain constant during the test. To compare these results with the flow theory of the second stress-invariant type, graphical methods have been used to determine the combined plastic stress-strain relations based upon the simple tension plastic stress-strain relations. This paper presents an analytical procedure for the determination of these theoretical stress-strain relations. For certain stress conditions the graphical methods have the disadvantage of yielding inaccurate results—an objection not present in the proposed method. Furthermore, the proposed analytical method is less time-consuming than the graphical methods.

Introduction

In recent years various theories of plasticity have been proposed to define plastic stress-strain relations for combined stresses and for metals and alloys with strain-hardening (1, 2).[3] In order to differentiate between these theories and to determine which one agrees best with the actual plastic stress-strain relations, it is necessary to consider combined stress-strain relations for loading conditions where the ratio of the stress components varies during loading. For evaluating the theoretical plastic stress-strain relations for these variable stress-ratio conditions by the flow-type theory (2), using the plastic stress-strain curve for simple tension, graphical methods have been used as proposed by Cunningham, Thomsen, and Dorn (3), and Shepherd (4). Except for small plastic strains these graphical methods are subject to considerable inaccuracies. Furthermore, the application of these graphical methods to determine plastic stress-strain relations involves a considerable amount of time. For these reasons the following analytical method was developed. The method is particularly suited to the range of large plastic strains. The proposed analytical method will first be described, followed by an application to show how the theory can be used.

Method of Analysis

For an element subjected to normal stress components σ_x, σ_y, and σ_z, and shear stress components τ_{xy}, τ_{yz}, and τ_{zx} in the plastic range, the strain components will be made up of elastic and plastic strains. The plastic-strain components will be designated by e_x, e_y, e_z, γ_{xy}, γ_{yz}, and γ_{zx}. Then, the flow theory based on the octahedral shear-stress criterion of plastic flow (1, 2) defines the changes of strain components in terms of the stress components by the following equations

$$\left.\begin{aligned} \delta e_x &= h(\bar{\sigma})\,\delta\bar{\sigma}\,(\sigma_x - \sigma_0) \\ \delta e_y &= h(\bar{\sigma})\,\delta\bar{\sigma}\,(\sigma_y - \sigma_0) \\ \delta e_z &= h(\bar{\sigma})\delta\bar{\sigma}\,(\sigma_z - \sigma_0) \\ \delta\gamma_{xy} &= 2h(\bar{\sigma})\,\delta\bar{\sigma}\,\tau_{xy} \\ \delta\gamma_{yz} &= 2h(\bar{\sigma})\,\delta\bar{\sigma}\,\tau_{yz} \\ \delta\gamma_{zx} &= 2h(\bar{\sigma})\,\delta\bar{\sigma}\,\tau_{zx} \end{aligned}\right\} \quad \ldots\ldots\ldots\ldots [1]$$

where

δe_x, δe_y, δe_z = incremental changes in normal plastic-strain components

$\delta\gamma_{xy}$, $\delta\gamma_{yz}$, $\delta\gamma_{zx}$ = incremental changes in shear-strain components

σ_0 = mean normal stress = $\frac{1}{3}(\sigma_x + \sigma_y + \sigma_z)$

$\bar{\sigma}$ = effective stress whose value is

$$\bar{\sigma} = \frac{1}{\sqrt{2}}\sqrt{(\sigma_x - \sigma_y)^2 + (\sigma_y - \sigma_z)^2 + (\sigma_z - \sigma_x)^2 + 6(\tau_{xy}^2 + \tau_{yz}^2 + \tau_{zx}^2)} \quad \ldots\ldots\ldots\ldots [2]$$

and $h(\bar{\sigma})$ = a function of the effective stress to be defined later. The effective strain corresponding to the effective stress $\bar{\sigma}$ is shown to be (1, 2)

$$\delta\bar{\epsilon} = \frac{\sqrt{2}}{3}\sqrt{(\delta\epsilon_x - \delta\epsilon_y)^2 + (\delta\epsilon_y - \delta\epsilon_z)^2 + (\delta\epsilon_z - \delta\epsilon_x)^2 + \frac{3}{2}[(\delta\gamma_{xy})^2 + (\delta\gamma_{yz})^2 + (\delta\gamma_{zx})^2]} \quad \ldots\ldots\ldots [3]$$

The case considered also must obey the conventional type of loading in which loading occurs for $\delta\bar{\sigma} > 0$ and unloading occurs for $\delta\bar{\sigma} < 0$.

If the state of stress considered can be defined in terms of principal stresses σ_1, σ_2, and σ_3 in place of the stress components σ_x, σ_y, σ_z, τ_{xy}, τ_{yz} and τ_{zx}, then Equations [1] can be written

$$\left.\begin{aligned} \delta e_1 &= H(\bar{\sigma})\delta\bar{\sigma}\left[\sigma_1 - \frac{1}{2}(\sigma_2 + \sigma_3)\right] \\ \delta e_2 &= H(\bar{\sigma})\delta\bar{\sigma}\left[\sigma_2 - \frac{1}{2}(\sigma_3 + \sigma_1)\right] \\ \delta e_3 &= H(\bar{\sigma})\delta\bar{\sigma}\left[\sigma_3 - \frac{1}{2}(\sigma_1 + \sigma_2)\right] \end{aligned}\right\} \quad \ldots\ldots [4]$$

where $H(\bar{\sigma})$ = a function of the effective stress $\bar{\sigma}$, and δe_1, δe_2, δe_3 = increments of principal strains. When the stresses are

---

[1] Research Associate in the Engineering Experiment Station, The Pennsylvania State College.

[2] Professor of Engineering Mechanics and Research Professor of Engineering Materials, The Pennsylvania State College. Mem. ASME.

[3] Numbers in parentheses refer to the Bibliography at the end of the paper.

Presented at the National Conference of the Applied Mechanics Division, State College, Pa., June 19–21, 1952, of The American Society of Mechanical Engineers.

Discussion of this paper should be addressed to the Secretary, ASME, 29 West 39th Street, New York, N. Y., and will be accepted until January 10, 1953, for publication at a later date. Discussion received after the closing date will be returned.

Note: Statements and opinions advanced in papers are to be understood as individual expressions of their authors, and not those of the Society. Manuscript received by ASME Applied Mechanics Division, November 15, 1951. Paper No. 52—APM-29.

defined in terms of the principal stresses in place of the stress components, the effective stress and strain become, respectively

$$\bar{\sigma} = \sqrt{\sigma_1^2 + \sigma_2^2 + \sigma_3^2 - \sigma_1\sigma_2 - \sigma_2\sigma_3 - \sigma_3\sigma_1} \quad \ldots [5]$$

$$\delta\bar{\epsilon} = \sqrt{\frac{2}{3}[(\delta\epsilon_1)^2 + (\delta\epsilon_2)^2 + (\delta\epsilon_3)^2]} \quad \ldots [6]$$

In obtaining Equation [6], the condition of constancy of volume was used or $\delta\epsilon_1 + \delta\epsilon_2 + \delta\epsilon_3 = 0$.

For simple tension $\sigma_2 = \sigma_3 = 0$ and $\sigma_1 = \sigma$ (the stress in simple tension), and $\delta\epsilon_2 = \delta\epsilon_3 = -\delta\epsilon_1/2$ for constancy of volume. Then by Equation [5] $\bar{\sigma} = \sigma_1$, and by Equation [6] $\delta\bar{\epsilon} = \delta\epsilon_1$, the axial plastic strain in simple tension. For simple tension, the first of Equations [4] becomes

$$\delta\epsilon = H(\bar{\sigma})\,\delta\bar{\sigma}\,\sigma = H(\sigma)\delta\sigma\,\sigma$$

or

$$H(\bar{\sigma}) = \frac{1}{\sigma}\frac{\delta\epsilon}{\delta\sigma} = \frac{1}{\bar{\sigma}}\frac{\delta\bar{\epsilon}}{\delta\bar{\sigma}} \quad \ldots [7]$$

Placing the value of $H(\bar{\sigma})$ from Equation [7] in Equations [4], the strain increments become

$$\left.\begin{aligned}
\delta\epsilon_1 &= \frac{1}{\bar{\sigma}}\frac{\delta\bar{\epsilon}}{\delta\bar{\sigma}}\left[\sigma_1 - \frac{1}{2}(\sigma_2 + \sigma_3)\right]\delta\bar{\sigma} \\
\delta\epsilon_2 &= \frac{1}{\bar{\sigma}}\frac{\delta\bar{\epsilon}}{\delta\bar{\sigma}}\left[\sigma_2 - \frac{1}{2}(\sigma_3 + \sigma_1)\right]\delta\bar{\sigma} \\
\delta\epsilon_3 &= \frac{1}{\bar{\sigma}}\frac{\delta\bar{\epsilon}}{\delta\bar{\sigma}}\left[\sigma_3 - \frac{1}{2}(\sigma_1 + \sigma_2)\right]\delta\bar{\sigma}
\end{aligned}\right\} \quad \ldots [8]$$

For strain-hardening materials it has been found that the true stress-strain relation in simple tension can be defined by

$$e = k\sigma^n \quad \ldots [9]$$

where k and n are experimental constants. Since for simple tension $e = \int d\bar{\epsilon}$ and $\sigma = \bar{\sigma}$, Equation [9] can be written

$$\bar{\epsilon} = k\bar{\sigma}^n \quad \ldots [9a]$$

Differentiating Equation [9a] with respect to $\bar{\sigma}$

$$\frac{d\bar{\epsilon}}{d\bar{\sigma}} = kn\bar{\sigma}^{n-1} \quad \ldots [10]$$

Since $d\bar{\epsilon}/d\bar{\sigma} = \delta\bar{\epsilon}/\delta\bar{\sigma}$, the value of $\delta\bar{\epsilon}/\delta\bar{\sigma}$ in Equations [8] can be replaced by $kn\bar{\sigma}^{n-1}$ or

$$\left.\begin{aligned}
\delta\epsilon_1 &= kn\bar{\sigma}^{n-1}\left[\sigma_1 - \frac{1}{2}(\sigma_2 + \sigma_3)\right]\delta\bar{\sigma} \\
\delta\epsilon_2 &= kn\bar{\sigma}^{n-1}\left[\sigma_2 - \frac{1}{2}(\sigma_1 + \sigma_3)\right]\delta\bar{\sigma} \\
\delta\epsilon_3 &= kn\bar{\sigma}^{n-1}\left[\sigma_3 - \frac{1}{2}(\sigma_1 + \sigma_2)\right]\delta\bar{\sigma}
\end{aligned}\right\} \quad \ldots [11]$$

For biaxial stresses, $\sigma_3 = 0$ and the strain increments become

$$\left.\begin{aligned}
\delta\epsilon_1 &= kn\bar{\sigma}^{n-1}\left[\sigma_1 - \frac{\sigma_2}{2}\right]\delta\bar{\sigma} \\
\delta\epsilon_2 &= kn\bar{\sigma}^{n-1}\left[\sigma_2 - \frac{\sigma_1}{2}\right]\delta\bar{\sigma} \\
\delta\epsilon_3 &= -\delta\epsilon_1 - \delta\epsilon_2
\end{aligned}\right\} \quad \ldots [12]$$

The effective stress by Equation [5] becomes

$$\bar{\sigma} = \sqrt{\sigma_1^2 - \sigma_1\sigma_2 + \sigma_2^2} = \sigma_1\sqrt{1 - \alpha + \alpha^2} \quad \ldots [13]$$

where α = the variable stress ratio σ_2/σ_1. Using the value of $\bar{\sigma}$ from Equation [13] in [12] and noting $\alpha = \sigma_2/\sigma_1$, the strain increments can be written as

$$\left.\begin{aligned}
\delta\epsilon_1 &= \left[kn\sigma_1^{n-1}(1 - \alpha + \alpha^2)^{\frac{n-2}{2}}\left(1 - \frac{\alpha}{2}\right)\right]\delta\left[\sigma_1\sqrt{1 - \alpha + \alpha^2}\right] \\
\delta\epsilon_2 &= \left[kn\sigma_1^{n-1}(1 - \alpha + \alpha^2)^{\frac{n-2}{2}}\left(\alpha - \frac{1}{2}\right)\right]\delta\left[\sigma_1\sqrt{1 - \alpha + \alpha^2}\right] \\
\delta\epsilon_3 &= -\delta\epsilon_1 - \delta\epsilon_2
\end{aligned}\right\} \quad \ldots [14]$$

Equations [14] may be integrated provided either σ_1 is a constant or α is a constant. If α is selected as a constant—representing the condition where the principal stress ratio remains constant—the integration of Equations [14] gives

$$\left.\begin{aligned}
e_1 &= k\sigma_1^n(1 - \alpha + \alpha^2)^{\frac{n}{2}}\left(1 - \frac{\alpha}{2}\right) \\
e_2 &= k\sigma_1^n(1 - \alpha + \alpha^2)^{\frac{n}{2}}\left(\alpha - \frac{1}{2}\right)
\end{aligned}\right\} \quad \ldots [15]$$

These equations are identical with those obtained using the deformation theory based on the octahedral shear-stress criterion and confirm the statement that for constant stress ratios the deformation and flow theories coincide.

The case of variable stress ratio, where a stress σ_1 is first applied, followed by a stress σ_2, has been studied experimentally by several investigators for the purpose of differentiating between the deformation and flow-type theories of plasticity. For this case of stress application σ_1 is a constant and $\alpha = \sigma_2/\sigma_1$ is a variable. To analyze this case, Equations [14] first can be replaced in differential form, or

$$\left.\begin{aligned}
de_1 &= kn\sigma_1^n(1 - \alpha + \alpha^2)^{\frac{n-2}{2}}\left(1 - \frac{\alpha}{2}\right)d\sqrt{1 - \alpha + \alpha^2} \\
de_2 &= kn\sigma_1^n(1 - \alpha + \alpha^2)^{\frac{n-2}{2}}\left(\alpha - \frac{1}{2}\right)d\sqrt{1 - \alpha + \alpha^2}
\end{aligned}\right\} \quad \ldots [16]$$

Integrating Equations [16] between limits α_1 and α_2 where $\alpha_2 > \alpha_1 \geqslant 1.0$, Equations [16] become

$$\left.\begin{aligned}
e_1 &= kn\sigma_1^n\int_{\alpha_1}^{\alpha_2}\left(1 - \frac{\alpha}{2}\right)(1 - \alpha + \alpha^2)^{\frac{n-2}{2}}d(1 - \alpha + \alpha^2)^{\frac{1}{2}} \\
e_2 &= kn\sigma_1^n\int_{\alpha_1}^{\alpha_2}\left(\alpha - \frac{1}{2}\right)(1 - \alpha + \alpha^2)^{\frac{n-2}{2}}d(1 - \alpha + \alpha^2)^{\frac{1}{2}}
\end{aligned}\right\} \quad \ldots [17]$$

Evaluating the integrals in Equations [17] using integration by parts gives

$$\left.\begin{aligned} e_1 &= \frac{kn\sigma_1^n}{n-1}\left[\left(1-\frac{\alpha}{2}\right)(1-\alpha+\alpha^2)^{\frac{n-1}{2}} + \frac{1}{2}\int(1-\alpha+\alpha^2)^{\frac{n-1}{2}}\,d\alpha\right]_{\alpha_1}^{\alpha_2} \\ e_2 &= \frac{kn\sigma_1^n}{n-1}\left[\left(\alpha-\frac{1}{2}\right)(1-\alpha+\alpha^2)^{\frac{n-1}{2}} - \int(1-\alpha+\alpha^2)^{\frac{n-1}{2}}\,d\alpha\right]_{\alpha_1}^{\alpha_2} \end{aligned}\right\} \quad [18]$$

If the stress σ_2 is kept constant in place of σ_1, equations for e_1 and e_2 can be obtained similar to Equations [18]. In this case

$$\left.\begin{aligned} e_1 &= \frac{kn\sigma_2^n}{n-1}\left[\left(\beta-\frac{1}{2}\right)(1-\beta+\beta^2)^{\frac{n-1}{2}} - \int(1-\beta+\beta^2)^{\frac{n-1}{2}}\,d\beta\right]_{\beta_1}^{\beta_2} \\ e_2 &= \frac{kn\sigma_2^n}{n-1}\left[\left(1-\frac{\beta}{2}\right)(1-\beta+\beta^2)^{\frac{n-1}{2}} + \frac{1}{2}\int(1-\beta+\beta^2)^{\frac{n-1}{2}}\,d\beta\right]_{\beta_1}^{\beta_2} \end{aligned}\right\} \quad [19]$$

where $\beta = \sigma_1/\sigma_2$ = ratio of stresses, and $\beta_2 > \beta_1 \geqslant 1.0$.

To evaluate the integrals in Equations [18] it first may be expressed as

$$\left.\begin{aligned} \int_{\alpha_1}^{\alpha_2}(1-\alpha+\alpha^2)^{\frac{n-1}{2}}\,d\alpha &= \int_{\alpha_1}^{\alpha_1'}(1-\alpha+\alpha^2)^{\frac{n-1}{2}}\,d\alpha + \int_{\alpha_1'}^{\alpha_1''}(1-\alpha+\alpha^2)^{\frac{n-1}{2}}\,d\alpha + \cdots \\ &\quad + \int_{\alpha_2-\Delta\alpha}^{\alpha_2}(1-\alpha+\alpha^2)^{\frac{n-1}{2}}\,d\alpha \end{aligned}\right\} \quad [20]$$

In order to evaluate the integrals in Equation [20] they may be expressed in the form of a Taylor series, that is

$$G(\alpha_1') - G(\alpha_1) = \int_{\alpha_1}^{\alpha_1'}(1-\alpha+\alpha^2)^{\frac{n-1}{2}}\,d\alpha$$

or

$$\left.\begin{aligned} G(\alpha_1') - G(\alpha_1) &= (\alpha_1'-\alpha_1)\left(\frac{dG}{d\alpha}\right)_{\alpha_1} + \frac{(\alpha_1'-\alpha_1)^2}{2!}\left(\frac{d^2G}{d\alpha^2}\right)_{\alpha_1} \\ &\quad + \frac{(\alpha_1'-\alpha_1)^3}{3!}\left(\frac{d^3G}{d\alpha^3}\right)_{\alpha_1} + \cdots \end{aligned}\right\} \quad [21]$$

where

$$\left.\begin{aligned} G &= \int(1-\alpha+\alpha^2)^{\frac{n-1}{2}}\,d\alpha \\ \frac{dG}{d\alpha} &= (1-\alpha+\alpha^2)^{\frac{n-1}{2}} \\ \frac{d^2G}{d\alpha^2} &= \frac{n-1}{2}(2\alpha-1)(1-\alpha+\alpha^2)^{\frac{n-3}{2}} \\ \frac{d^3G}{d\alpha^3} &= \frac{n-1}{2}(1-\alpha+\alpha^2)^{\frac{n-3}{2}}\left[\frac{n-3}{2}\frac{(2\alpha-1)^2}{(1-\alpha+\alpha^2)}+2\right] \end{aligned}\right\} \quad [22]$$

The accuracy of the evaluation as given by the expansion in Equation [21] will depend upon the interval $(\alpha_1' - \alpha_1)$ used and upon the number of terms selected in the series. In general, the first two or three terms in the series of Equation [21] are sufficient, if the interval $\Delta\alpha = (\alpha_1' - \alpha_1)$ is about 0.1. With each integral such as given in Equation [21] evaluated, the integral between α_1 and α_2 can be found as defined in Equation [20]. Finally, by Equations [18] the strains e_1 and e_2 can be determined.

For stress combinations where the σ_2 stress is kept constant and σ_1 is varied, Equations [19] in place of [18] are used, and a procedure similar to that outlined can be followed.

With the strains, initial dimensions, and loads known, the stresses can be determined and hence the theoretical stress-strain relations are defined completely.

Application of Method

The foregoing method of finding the theoretical stress-strain relations was applied to variable stress-ratio tests of thin-walled tubular specimens subjected to axial tension and internal pressure, producing biaxial stresses σ_1 and σ_2. The material considered was an aluminum alloy 14S-T4. The true stress-strain relation for this material in simple tension plotted in terms of log stress versus log strain is shown in Fig. 1. With this stress-strain

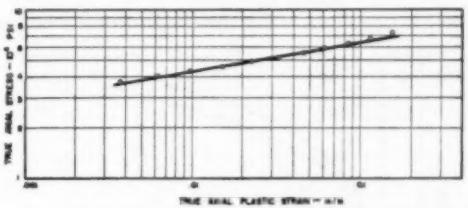

Fig. 1 True Stress-Plastic Strain Relation for Simple Tension Test $\sigma_2/\sigma_1 = 0$

curve as a basis, the theoretical strains for a tube subjected to combined stresses can be determined for a specified stress σ_1 followed by application of a stress σ_2. The procedure to be used based on the analysis consists of the following steps:

1 The best straight line representing the true stress-strain values for simple tension is obtained with test data in Fig. 1, using the method of least squares. The equation of this line is $\bar{s} = k\bar{\delta}^n$, where k and n are experimental constants. For the material Alcoa 14S-T4 considered, values of $k = 5.98 \times 10^{-38}$ and $n = 5.65$ were determined.

2 Selecting three terms of the Taylor series, values of $(dG)/(d\alpha)$, $(d^2G)/(d\alpha^2)$, and $(d^3G)/(d\alpha^3)$ were found using Equations [22] for values of $\alpha_1 = 1.0$ to $\alpha_1' = 1.1$, $\alpha_1' = 1.1$ to $\alpha_1'' = 1.2$, and so on, and for a value of $n = 5.65$.

3 Using values obtained under step 2, integrals as defined by Equation [21] were determined for each $\Delta\alpha$-interval.

4 By Equation [20] and using values from step 3, the values of $\int^{\alpha_2}(1-\alpha+\alpha^2)^{\frac{n-1}{2}}\,d\alpha$ were evaluated from the summation of integrals defined by Equation [20] for various values of α.

5 The remaining terms in Equations [18] were determined to various values of α.

6 For the initial stress value σ_1 used, the value of

$$\frac{kn\sigma_1^n}{(n-1)}$$

appearing in Equations [18] was determined.

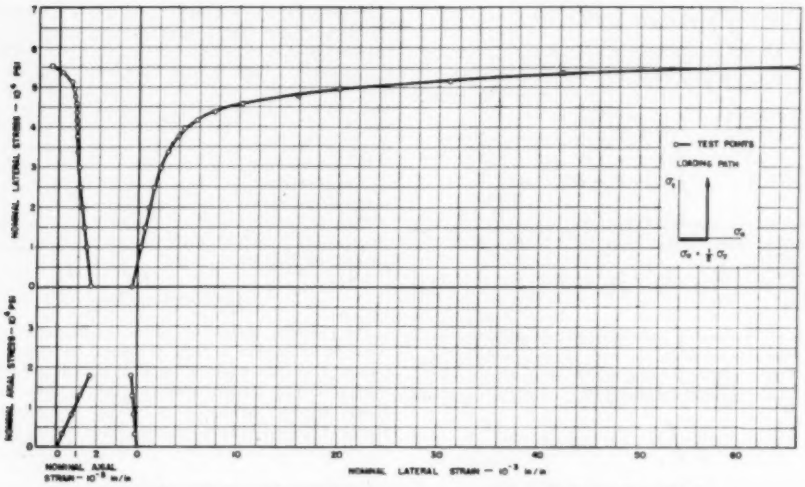
TEST POINTS
LOADING PATH
NOMINAL LATERAL STRESS - 10^3 PSI
NOMINAL AXIAL STRESS - 10^3 PSI
NOMINAL AXIAL STRAIN - 10^{-3} in/in
NOMINAL LATERAL STRAIN - 10^{-3} in/in

FIG. 2 NOMINAL STRESS-STRAIN RELATIONS FOR VARIABLE STRESS-RATIO TEST, B-108

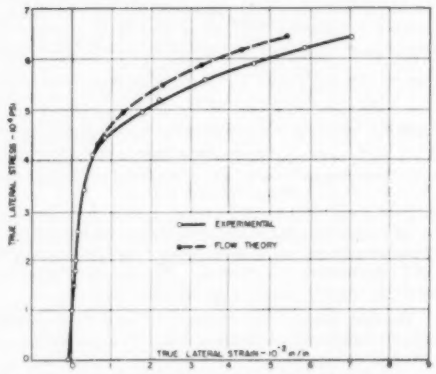

FIG. 3 COMPARISON OF TRUE STRESS-STRAIN RELATION FOR VARIABLE STRESS-RATIO TEST, B-108

7 With values of the various terms determined by steps 4, 5, and 6, Equations [18] were used to find the true strains e_1 and e_2 for selected values of α.

8 With the true stress values σ_1 and σ_2 calculated as described in reference (5), the theoretical stress-strain relations could then be plotted as shown in Fig. 3.

COMPARISON OF THEORETICAL AND EXPERIMENTAL STRESS-STRAIN RELATIONS

To compare the theoretical stress-strain relations obtained with actual values, variable stress-ratio tests on thin-walled tubes subjected to internal pressures and axial loading were made as described in reference (6) using various initial values of the stress σ_1. Fig. 2 shows the nominal stress-strain relation for a test in which an axial stress σ_1 was first applied of such magnitude as to be equal to one half of the yield stress. By means of internal pressure, with a provision to remove the axial-pressure component, a lateral or tangential stress σ_2 was then applied. Based on the nominal stress-strain relations in Fig. 2 and using equations given in reference (5), true stress-strain values were computed. The values of these experimental true stresses and strains are plotted in Fig. 3 for comparison with the theoretical stress-strain relation. Approximate agreement between the values predicted by the flow theory and the test results is indicated in Fig. 3.

ACKNOWLEDGMENTS

The analysis given in this paper was prepared as part of a project on "Plastic Flow of Metals," sponsored by the Office of Army Ordnance.

BIBLIOGRAPHY

1 "Theory of Plastic Flow of Solids," by A. Nadai, McGraw-Hill Book Company, Inc., New York, N. Y., 1950.

2 "Stress-Strain Relations in the Plastic Range—A Survey of Theory and Experiment," by D. C. Drucker, Brown University, Providence, R. I., 1950.

3 "Plastic Flow of a Magnesium Alloy Under Biaxial Stresses," by D. M. Cunningham, E. G. Thomsen, and J. E. Dorn, Proceedings of the ASTM, vol. 47, 1947, pp. 546–553.

4 "Plastic Stress-Strain Relations," by W. M. Shepherd, Proceedings of The Institution of Mechanical Engineers, vol. 159, 1948 pp. 95–99.

5 "Biaxial Plastic Stress-Strain Relations for 24S-T Aluminum Alloy," by J. Marin, et al., NACA Technical Note 1536, May, 1948.

6 "Plastic Biaxial Stress-Strain Relations for Alcoa 24S-T Subjected to Variable Stress Ratios," by J. Marin and B. J. Kotalik, JOURNAL OF APPLIED MECHANICS, Trans. ASME, vol. 72, 1950, p. 372.

A Simple Method of Determining Plastic Stresses and Strains in Rotating Disks With Nonuniform Metal Properties

By M. H. LEE WU,[1] CLEVELAND, OHIO

This paper presents a simple method of solving plastic deformation of a rotating disk having nonuniform metal properties. A stress-strain surface, which is formed by stress-strain curves obtained from the tensile specimens cut at different radii of the disk in the tangential direction, is introduced. The distributions of plastic stresses and strains can be obtained by a simple multiplication with the use of a short table given in the paper and a stress-strain curve along the radius of the disk determined from the stress-strain surface. The rotating-speed parameter is simplified to a simple algebraic function of maximum octahedral shear strain of the disk, and a parameter determined directly from the stress-strain curve along the radius of the disk. A chart calculated from such relations is given. The relation between rotating speed and maximum strain determined from the chart are compared with the experimental data of disk test; results agree well.

Introduction

THE metal properties of any machine member are quite nonuniform owing to the process of manufacturing, such as cold-working, heat-treating, and so forth. Nonuniformity also may be caused by external effects, such as temperature gradients. Therefore it is practical to consider problems of plastic deformation for members having nonuniform metal properties. The present paper considers the problem of a rotating disk, Fig. 1, having nonuniform metal properties in the radial direction.

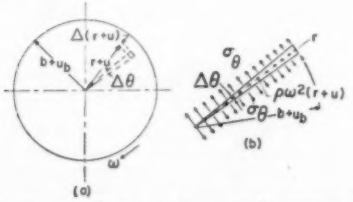

FIG. 1 ROTATING DISK AND A SECTOR IN DEFORMED STATE

For a rotating disk having uniform metal properties or other plane plastic stress problems with axial symmetry, the equations of the problem are reduced to two first-order nonlinear differential equations (1).[2] Solutions can be obtained by numerical integration for a given $\tau(\gamma)$-curve of the material, where τ and γ are octahedral shear stress and strain, respectively. When the metal properties are considered as uniform, only one $\tau(\gamma)$-curve is needed to represent the relations between τ and γ of the material for the whole member. For a disk having uniform metal properties, τ and γ are functions of radius r, but the relation between τ and γ of the material is known and independent of radius r. For disks having nonuniform metal properties, a single $\tau(\gamma)$-curve representing the relations between τ and γ at different radii as previously used can be applied no longer.

Furthermore, the relation between τ and γ along the radius of the disk is unknown because τ is not only a function of γ but also a function of radius r. This can be illustrated as follows: If the $\tau(\gamma)$-curves at different radii of the disk are plotted in a three-dimensional space (γ, τ and r/b, where b is the outer radius of the disk), as shown in Fig. 2. These $\tau(\gamma)$-curves form a surface which is referred to as the "stress-strain surface." The

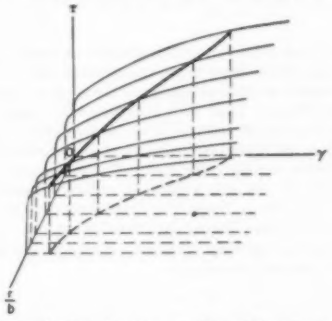

FIG. 2 STRESS-STRAIN SURFACE IN THREE-DIMENSIONAL SPACE (γ, τ, AND r/b)

relation of τ and γ along the radius of the disk at any load (or at any value of γ_0, where γ_0 is the maximum value of γ in the disk) must be a curve lying on the stress-strain surface. At the same time, the relation between γ and r/b should satisfy the two first-order differential equations obtained in (1).

The τ and γ relation along the radius of the disk can be obtained from the stress-strain surface when the relation between γ and r/b is known, but the relations between γ and r/b can be determined from the differential equations only when the relation between τ and γ along the radius of the disk is known. Thus iteration seems unavoidable for such cases without any approximation. However, the general plastic behavior obtained recently for a rotating disk (2), namely, that the ratio of principal stresses

[1] Formerly Aeronautical Research Scientist, Stress and Vibration Section, Lewis Laboratory, NACA. Mem. ASME.

Presented at the National Conference of the Applied Mechanics Division, State College, Pa., June 19–21, 1952, of THE AMERICAN SOCIETY OF MECHANICAL ENGINEERS.

Discussion of this paper should be addressed to the Secretary, ASME, 29 West 39th Street, New York, N. Y., and will be accepted until January 10, 1953, for publication at a later date. Discussion received after the closing date will be returned.

NOTE: Statements and opinions advanced in papers are to be understood as individual expressions of their authors and not those of the Society. Manuscript received by ASME Applied Mechanics Division, February 1, 1952. Paper No. 52—APM-25.

[2] Numbers in parentheses refer to the Bibliography at the end of the paper.

and the distributions of the proportionate strains are essentially independent of the stress-strain relations of the material, suggests a simple and accurate method of solving a plastically deformed rotating disk having nonuniform metal properties.

Before going into the detail of the method, a brief summary of the general plastic behavior of a rotating disk and also the final equations and results obtained in (2), which will be used in the present paper, are first given in the next section.

General Plastic Behavior of Rotating Disk Having Uniform Metal Properties

The two first-order nonlinear differential equations obtained in (1) for a rotating disk having uniform metal properties involve two dependent variables α and γ, one independent variable r/k, and a variable τ, which is an experimentally determined function of γ of the material from the simple tensile test, k is an arbitrary constant determined from the boundary condition, α is a parameter indicating the ratio of principal stresses and of principal strains. The relations between α and principal stresses and strains are given by the following equations

$$\left.\begin{aligned}\sigma_r &= \sqrt{\frac{3}{2}}\,\tau(\sqrt{3}\sin\alpha - \cos\alpha)\\ \sigma_\theta &= \sqrt{\frac{3}{2}}\,\tau(\sqrt{3}\sin\alpha + \cos\alpha)\end{aligned}\right\} \quad \ldots\ldots\ldots [1]$$

$$\left.\begin{aligned}\epsilon_r &= \frac{\gamma}{2\sqrt{2}}(\sin\alpha - \sqrt{3}\cos\alpha)\\ \epsilon_\theta &= \frac{\gamma}{2\sqrt{2}}(\sin\alpha + \sqrt{3}\cos\alpha)\end{aligned}\right\} \quad \ldots\ldots\ldots [2]$$

Equations [1] and [2] satisfy the relations of plastic stress and strain of the deformation theory for plane stress, because the yielding surfaces of plane plastic stress based on the deformation theory are ellipses. Thus these equations can be used only for the plane plastic stress problems to which the deformation theory is applicable. In Equations [1], τ, which is a function of γ, varies with radius and also with load. Similar relations as Equations [1] and [2] but with a constant value of τ (ideally plastic material) were used by Nadai for a thin plate with a circular hole (3), and by Nadai and Donnell for a rotating disk (4).

In (2) the two nonlinear differential equations obtained in (1) are partly linearized, resulting in

$$\frac{d\alpha}{d\left(\frac{r}{k}\right)} = \left(\frac{2H}{L}\right)\frac{1 + \sqrt{3}\,\frac{J}{L}\,n - \frac{K_1}{2H}\left[1 - 2\left(1 - \frac{\gamma}{\gamma_0}\right)n\right]^{-1}\left(\frac{r}{k}\right)^2}{\left[1 + \left(\frac{J}{L}\right)^2 n\right]\left(\frac{r}{k}\right)}$$

$$\frac{d\left(\frac{\gamma}{\gamma_0}\right)}{d\left(\frac{r}{k}\right)} = \left(-\frac{8H^2}{L^2}\right)\frac{\left\{1 - \frac{JK_1}{8H^2}\left[1 - 2\left(1 - \frac{\gamma}{\gamma_0}\right)n\right]^{-1}\left(\frac{r}{k}\right)^2\right\}\left(\frac{\gamma}{\gamma_0}\right)}{\left[1 + \left(\frac{J}{L}\right)^2 n\right]\left(\frac{r}{k}\right)} \quad [3]$$

where

$$H = \cos\alpha$$
$$J = \sqrt{3}\sin\alpha - \cos\alpha$$
$$L = \sqrt{3}\cos\alpha + \sin\alpha$$
$$K_1 = \sqrt{\frac{2}{3}}\,\frac{\rho(\omega k)^2}{\tau_0}$$ (where τ_0 is maximum value of τ in disk)

and

$$n = m - C_1\gamma_0 = m - 0.5\,\gamma_0 \quad \ldots\ldots\ldots [4]$$

In Equation [4] m is equal to the slope of a straight line approximating the $\tau(\gamma)$-curve on the logarithmic plot within the range of γ encountered along the radius of the disk, γ_b to γ_0, with γ_0/γ_b approximately equal to 5.5 (γ_b is the value of γ at outer radius b). Thus m is a function of γ_0 and can be determined directly from the $\tau(\gamma)$-curve of the material for a given value of γ_0. Once the value of γ_0 is chosen, the value of n can be obtained from Equation [4].

The variations of α and γ/γ_0 with r/b for $n = 0.05$, 0, 0.1, 0.2, and 0.3 are calculated from Equations [3]. These variations are shown in Figs. 3 (*a*) and (*b*). The value of n for most materials and for different values of γ_0 is determined from the $\tau(\gamma)$-curve given in references (5), (6), and (7) and varies from —0.05 to 0.3. Thus Figs. 3 (*a*) and (*b*) cover the variations of α and γ/γ_0 with r/b for most materials for the rotating disk having uniform metal properties. Numerical results obtained from these varia-

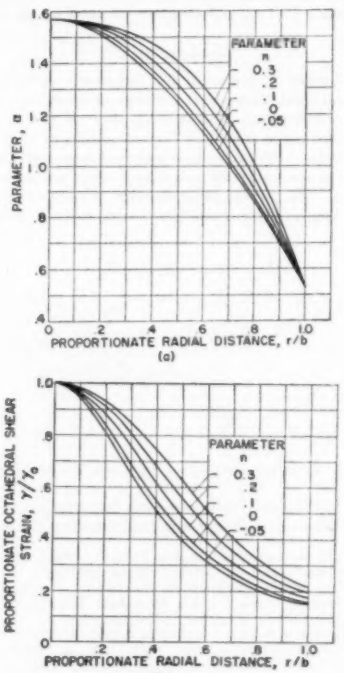

Fig. 3 Variations of Parameter α and Proportionate Octahedral Shear Strain γ/γ_0 With Proportionate Radial Distance r/b Obtained by Partly Linearized Solution for Different Values of n

tions of α and γ/γ_0 with r/b compared closely with those obtained from (1) (for simplicity, the results obtained in reference 1 are referred to as the exact solution). In addition, comparison of distributions of stresses and strains obtained from the exact solution with those obtained for the ideally plastic material (the constant τ-value of which is chosen equal to the value of τ of the exact solution at the center of the disk) show clearly that the distributions of proportionate strains (γ/γ_0, $\epsilon_\theta/[\epsilon_\theta]_0$ and $\epsilon_r/[\epsilon_r]_0$) are essentially independent of the $\tau(\gamma)$-curve of the material but that the distributions of the stresses depend on the material (2). It also is shown that the variation of α during loading is very small for most materials.

Basic Principle of Method

(*a*) *Approximate Relations of α and γ/γ_0 With r/b.* The general plastic behavior obtained for the rotating disk having uniform metal properties can be applied to the disk having nonuniform metal properties, if the value of n, determined from the $\tau(\gamma)$-curve along the radius of the disk, varies in about the same range of n as given in Fig. 3. Since the curves shown in Figs. 3 (*a*) and (*b*), give the relations of α and γ/γ_0 with r/b for the $\tau(\gamma)$-curve of most materials, the average value of these curves may be used as an approximate relation of α and γ/γ_0 with r/b for most materials, or the curves for $n = 0$ may be used as approximate relations for the materials having low n-values, and the curves for $n = .2$ used for the high n-values. In the paper detailed data for $n = 0$ will be given, because one special case of $n = 0$ is the case of ideally plastic material with infinitesimal strain, which often is considered in the stress analysis for plastic deformation. (For ideally plastic material and using infinitesimal strain concept, γ_0 is infinitesimal and $m = 0$; n obtained from Equation [4] is then equal to zero.) For $n = 0$, Equations [3] reduce to the following simple form

$$\left.\begin{aligned} \frac{d\alpha}{d\left(\frac{r}{b}\right)} &= \left(\frac{2H}{L}\right)\frac{1-\frac{K_1}{2H}\left(\frac{r}{b}\right)^2}{\left(\frac{r}{b}\right)} \\ \frac{d\left(\frac{\gamma}{\gamma_0}\right)}{d\left(\frac{r}{b}\right)} &= \left(-\frac{8H^2}{L^2}\right)\frac{\left[1-\frac{JK_1}{8H^2}\left(\frac{r}{b}\right)^2\right]\left(\frac{\gamma}{\gamma_0}\right)}{\left(\frac{r}{b}\right)} \end{aligned}\right\} \quad \ldots[5]$$

The relations of α, γ/γ_0, and r/b for $n = 0$ are calculated from Equations [5] and given in Table 1. These relations are used to represent the approximate relations of α, γ/γ_0, and r/b for most materials, because they are not sensitive with the material as shown in (2). If more accurate results are required, the data given in the paper for $n = 0$ can be used as the approximate solution for materials having low n-values only, and similar data for $n = .2$ or $n = .3$ can be obtained easily and used as the approximate solution for materials having high n-value. The accuracy of the method will be discussed quantitatively later.

(*b*) *Determination of $\tau(\gamma)$-Curve Along Radius of Disk.* The relation between τ and γ along the radius of the disk is needed for the evaluation of the distributions of stresses and the rotating speed, which are dependent on the stress-strain relation of the material. As mentioned in the introduction, the relation between τ and γ along the radius of the disk for any load (or for any value of γ_0) must be a curve lying on the stress-strain surface, Fig. 2. This curve is the intersection of the stress-strain surface and a surface, which is perpendicular to the (r/b) γ plane and on which the relation between r/b and γ/γ_0 is the same as those given in Table 1.

The stress-strain surface is introduced only for the purpose of explanation. In the process of obtaining the $\tau(\gamma)$-curve along the radius, this stress-strain surface is not needed. Only the projection of the curves on the $\gamma\tau$ plane is used. The procedure of determining the $\tau(\gamma)$-curve along the radius of the disk for a given γ_0 is very simple and is given as follows:

TABLE 1

	$n = 0$					
α	r/b	γ/γ_0	ϵ_θ/γ	ϵ_r/γ	σ_θ/τ	σ_r/τ
1.5708	0.0000	1.0000	0.3536	0.3536	2.1213	2.1213
1.5675	0.0510	0.9850	0.3556	0.3515	2.1253	2.1172
1.5615	0.0900	0.9675	0.3592	0.3478	2.1326	2.1098
1.5480	0.1325	0.9250	0.3674	0.3395	2.1487	2.0929
1.5300	0.1780	0.8710	0.3782	0.3283	2.1695	2.0696
1.5045	0.2250	0.8030	0.3933	0.3122	2.1978	2.0355
1.4820	0.2600	0.7500	0.4065	0.2979	2.2216	2.0044
1.4490	0.3050	0.6820	0.4253	0.2765	2.2544	1.9568
1.4105	0.3510	0.6150	0.4468	0.2513	2.2896	1.8986
1.3670	0.4000	0.5490	0.4702	0.2223	2.3253	1.8295
1.3180	0.4505	0.4875	0.4955	0.1892	2.3602	1.7476
1.2635	0.5025	0.4295	0.5222	0.1518	2.3924	1.6515
1.2045	0.5540	0.3790	0.5494	0.1108	2.4192	1.5419
1.1400	0.6060	0.3345	0.5770	0.0655	2.4389	1.4160
1.0705	0.6600	0.2950	0.6040	0.0165	2.4488	1.2738
0.9965	0.7150	0.2610	0.6295	−0.0358	2.4463	1.1157
0.9175	0.7700	0.2330	0.6530	−0.0915	2.4289	0.9401
0.8330	0.8240	0.2075	0.6735	−0.1503	2.3935	0.7458
0.7430	0.8780	0.1870	0.6902	−0.2118	2.3370	0.5331
0.6465	0.9330	0.1690	0.7018	−0.2758	2.2555	0.3003
0.5236	1.0000	0.1520	0.7071	−0.3536	2.1213	0.0000

Obtain the tensile $\tau(\gamma)$-curves from several specimens cut from the disk at different radii in the tangential direction as shown in Fig. 4 (the tangential direction is suggested because the rotating speed function $\rho(\omega b)^2$ is determined by the distribution of tangential stress and tangential strain as will be shown later,

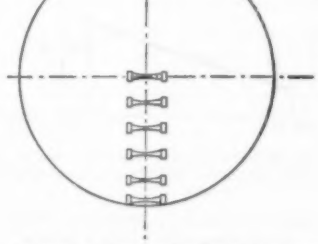

Fig. 4 Location of Tensile Specimens Cut From Disk

where ρ is the mass per unit volume and ω is the angular speed of the disk). Plot the $\tau(\gamma)$-curves at different radii as shown by the light solid curves in Fig. 5. Calculate the value of γ at the different radii for a given value of γ_0 using the values of γ/γ_0 and r/b given in Table 1. Locate these values of γ on the corresponding $\tau(\gamma)$-curves in Fig. 5. The curve obtained by joining these points gives the $\tau(\gamma)$-curve along the radius of the disk for a given γ_0 (shown in Fig. 5 by the heavy curve). The $\tau(\gamma)$-curve along the radius of the disk is also plotted on a logarithmic scale as indicated by the heavy solid curve in Fig. 6.

Determination of Principal Strains and Stresses

From Equations [1] and [2] it can be seen that ϵ_θ/γ, ϵ_r/γ, σ_θ/τ, and σ_θ/τ are functions of α only. These values are calculated and are also given in Table 1. From the relation of γ and r/b for a given γ_0 obtained in the previous section and the relations of ϵ_θ/γ and ϵ_r/γ with r/b given in Table 1, the distributions of the principal strains of the rotating disk for a given γ_0 is obtained by a simple multiplication.

From the relation between τ and γ along the radius of the

disk for a given γ_0, Fig. 5, and the relation between γ and r/b obtained in the previous section, the relation between τ and r/b for a given γ_0 can be obtained. In a manner similar to the principal strains, the principal stresses can be obtained from the relation between τ and r/b and from the values of σ_θ/τ and σ_r/τ given in Table 1 by a simple multiplication.

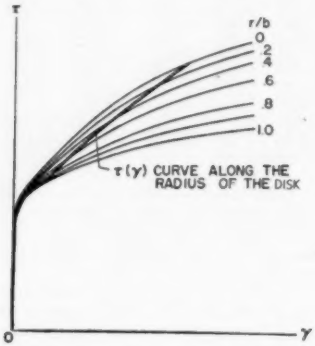

FIG. 5 RELATION BETWEEN OCTAHEDRAL SHEAR STRESS τ AND OCTAHEDRAL SHEAR STRAIN γ AT DIFFERENT RADII AND RELATION BETWEEN OCTAHEDRAL SHEAR STRESS AND STRAIN ALONG RADIUS OF DISK

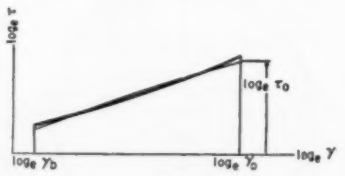

FIG. 6 RELATIONS BETWEEN OCTAHEDRAL SHEAR STRESS AND STRAIN ALONG RADIUS OF DISK ON LOGARITHMIC SCALE

DETERMINATION OF ROTATING SPEED FOR GIVEN MAXIMUM OCTAHEDRAL SHEAR STRAIN OF DISK

The rotating speed parameter $\rho(\omega b)^2$ for a given γ_0 of the disk can be determined from the distributions of tangential stress and of tangential strain of a circular sector of the disk as shown in Fig. 1(b). The component of force in the r-direction acting on the sector due to σ_θ is equal to

$$-\int_0^b 2\sigma_\theta h \sin\frac{\Delta\theta}{2}\frac{d(r+u)}{dr}\,dr$$

The centrifugal force on the same sector is equal to

$$\int_0^b \rho h_{\text{init}}\, r(\Delta\theta)\,\omega^2\,(r+u)\,dr$$

where h_{init} and h are the initial and instantaneous thickness of the disk. From the condition of equilibrium of the sector in the r-direction, the following is obtained

$$\rho(\omega b)^2 = \frac{\displaystyle\int_0^1 \sigma_\theta e^{-\epsilon_\theta}\,d\left(\frac{r}{b}\right)}{\displaystyle\int_0^1 \left(\frac{r}{b}\right)^2 e^{\epsilon_\theta}\,d\left(\frac{r}{b}\right)} \quad \ldots\ldots\ldots\ldots [6]$$

Equation [6] shows that the rotating-speed function $\rho(\omega b)^2$ is determined by the tangential stress and strain only.

Expanding e^{ϵ_θ} into a series, the denominator of Equation [6] becomes

$$\int_0^1 e^{\epsilon_\theta}\left(\frac{r}{b}\right)^2 d\left(\frac{r}{b}\right) = \int_0^1 \left[1+\left(\frac{\epsilon_\theta}{\gamma}\right)\left(\frac{\gamma}{\gamma_0}\right)\gamma_0 + \frac{1}{2!}\left(\frac{\epsilon_\theta}{\gamma}\right)^2\left(\frac{\gamma}{\gamma_0}\right)^2\gamma_0^2 + \ldots\right]\left(\frac{r}{b}\right)^2 d\left(\frac{r}{b}\right)$$

where γ_0 is a constant and can be taken out of the integral sign. Thus

$$\int_0^1 e^{\epsilon_\theta}\left(\frac{r}{b}\right)^2 d\left(\frac{r}{b}\right) = \frac{1}{3} + \gamma_0\int_0^1\left(\frac{\epsilon_\theta}{\gamma}\right)\left(\frac{\gamma}{\gamma_0}\right)\left(\frac{r}{b}\right)^3 d\left(\frac{r}{b}\right) + \gamma_0^2\int_0^1 \frac{1}{2}\left(\frac{\epsilon_\theta}{\gamma}\right)^2\left(\frac{\gamma}{\gamma_0}\right)^2\left(\frac{r}{b}\right)^3 d\left(\frac{r}{b}\right) + \ldots = \frac{1}{3} + G_1\gamma_0 + G_2\gamma_0^2 + \ldots\ldots [7a]$$

in which the integrands of $G_1, G_2 \ldots$ are functions of α and γ/γ_0 only.

The numerator of Equation [6] is a function of σ_θ, ϵ_θ, and r/b. The tangential strain ϵ_θ can be treated in a manner similar to that used for the denominator. The tangential stress σ_θ can be written as $(\sigma_\theta/\tau)\tau$, where σ_θ/τ is a function of α, and τ can be written as an approximate function of γ

$$\sigma_\theta = \left(\frac{\sigma_\theta}{\tau}\right)\tau = \left(\frac{\sigma_\theta}{\tau}\right)K\gamma^m$$

where m is the slope of a straight line approximating the $\tau(\gamma)$-curve along the radius of the disk on the logarithmic plot, Fig. 6, and K is a constant. The integrand of the numerator becomes

$$\sigma_\theta e^{-\epsilon_\theta} = K\gamma_0^m\left(\frac{\sigma_\theta}{\tau}\right)\left(\frac{\gamma}{\gamma_0}\right)^m e^{-\epsilon_\theta} = \tau_0\left(\frac{\sigma_\theta}{\tau}\right)e^{-\left(m\log_e\frac{\gamma_0}{\gamma}+\epsilon_\theta\right)}$$

Expanding the exponential function of e into a series

$$e^{-\left(m\log_e\frac{\gamma_0}{\gamma}+\epsilon_\theta\right)} = 1-\left(m\log_e\frac{\gamma_0}{\gamma}+\epsilon_\theta\right) + \frac{1}{2!}\left(m\log_e\frac{\gamma_0}{\gamma}+\epsilon_\theta\right)^2 - \frac{1}{3!}\left(m\log_e\frac{\gamma_0}{\gamma}+\epsilon_\theta\right)^3+\ldots$$

$$= 1 - m\log_e\frac{\gamma_0}{\gamma} + \frac{m^2}{2!}\left(\log_e\frac{\gamma_0}{\gamma}\right)^2 - \frac{m^3}{3!}\left(\log_e\frac{\gamma_0}{\gamma}\right)^3+\ldots - \frac{\epsilon_\theta}{\gamma}\frac{\gamma}{\gamma_0}\gamma_0 + m\gamma_0\left(\frac{\epsilon_\theta}{\gamma}\right)\left(\frac{\gamma}{\gamma_0}\right)\log_e\frac{\gamma_0}{\gamma} - \frac{m^2}{2!}\gamma_0\left(\frac{\epsilon_\theta}{\gamma}\right)\left(\frac{\gamma}{\gamma_0}\right)\left(\log_e\frac{\gamma_0}{\gamma}\right)^2+\ldots+\frac{\gamma_0^2}{2!}\left(\frac{\epsilon_\theta}{\gamma}\right)^2\left(\frac{\gamma}{\gamma_0}\right)^2 - \frac{m\gamma_0^2}{2!}\left(\frac{\epsilon_\theta}{\gamma}\right)^2\left(\frac{\gamma}{\gamma_0}\right)^2\left(\log_e\frac{\gamma_0}{\gamma}\right)+\ldots-\frac{\gamma_0^3}{3!}\left(\frac{\epsilon_\theta}{\gamma}\right)^3\left(\frac{\gamma}{\gamma_0}\right)^3+\ldots$$

The value of m and γ_0 remain constant along the radius, and, therefore, can be taken out of the integral sign. Denoting the individual integral in the numerator of Equation [6] by I_0, I_1, $I_2, \ldots$ the following is obtained

$$\int_0^1 \sigma_{8c}^{-n_0}\, d\left(\frac{r}{b}\right) = \tau_0(I_0 - I_1\gamma_0 + I_2\gamma_0^2 - I_3\gamma_0^3 + \ldots$$

$$-I_4\gamma_0 + I_5\gamma_0\gamma_0 + \ldots) \quad [7b]$$

in which the integrands of $I_0, I_1, \ldots$ are also functions of α and γ/γ_0 only.

Substituting Equations [7a] and [7b] into Equation [6] and neglecting the small terms, yields the following equation

$$\frac{\rho(\omega b)^2}{\tau_0} = \frac{I_0 - I_1 m + I_2 m^2 - I_3 m^3 - I_4\gamma_0 + I_5 m\gamma_0}{\frac{1}{3} + G_1\gamma_0 + G_2\gamma_0^2} \quad [8]$$

The values of $I_0, I_1, \ldots G_1$ and G_2 (for $n = 0$) are calculated by using the relation of α, γ/γ_0, and r/b given in Table 1. These values are as follows:

I_0	2.3031	I_4	0.5239
I_1	2.0281	I_5	0.3514
I_2	1.3131	G_1	0.0537
I_3	0.6362	G_2	0.0047

Equation [8] shows that $\rho(\omega b)^2/\tau_0$ is a function of m and γ_0, where γ_0 is the maximum value of γ in the disk. Once the value of γ_0 is given, m can be obtained from the $\tau(\gamma)$-curve along the radius of the disk, Fig. 6; τ_0 is the value of τ corresponding to γ_0 on the straight line approximating the $\tau(\gamma)$-curve. Equation [8] thus gives an approximate value of $\rho(\omega b)^2$ for a given γ_0 with the use of a parameter m determined directly from the tensile stress-strain curves at different radii of the disk. Curves of $\rho(\omega b)^2/\tau_0$ against γ_0 for different constant values of the parameter m are calculated and plotted in Fig. 7. The value of $\rho(\omega b)^2/\tau_0$ then can be read directly from the chart for any given value of γ_0 and m.

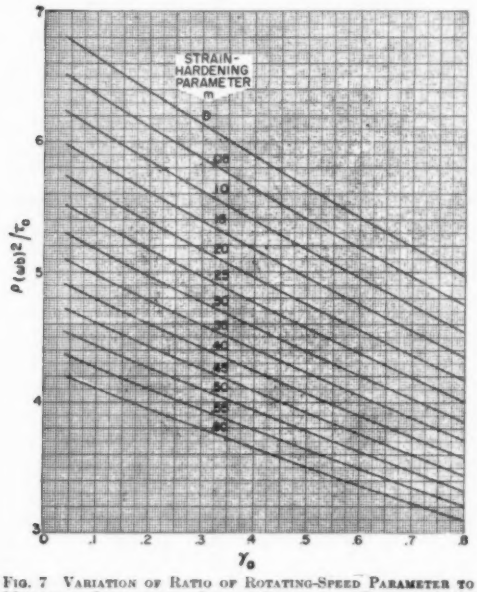

FIG. 7 VARIATION OF RATIO OF ROTATING-SPEED PARAMETER TO MAXIMUM OCTAHEDRAL SHEAR STRESS OF DISK $\rho(\omega b)^2/\tau_0$ WITH MAXIMUM OCTAHEDRAL SHEAR STRAIN AT CENTER OF DISK γ_0 FOR DIFFERENT VALUES OF PARAMETER m

DETERMINATION OF VARIATION OF RATIO OF PRINCIPAL STRESSES DURING LOADING

It was shown in (2) that the variation of a parameter n, Equation [4], of a material can be used to determine the variation of the ratio of the principal stresses of the rotating disk having uniform metal properties during loading, and consequently the variation of n can be used as a criterion of the applicability of deformation theory to the problem of rotating disk for the given material.

Furthermore, it was shown, see Fig. 3(*a*) and references (5), (6), and (7), that the variation of the ratio of principal stresses for a rotating disk of uniform metal properties is small for most materials and for different values of γ_0. However, for a disk having nonuniform metal properties, the variations of n during loading depend not only on the $\tau(\gamma)$-curve of the material at different radii of the disk but also on the variations of the $\tau(\gamma)$-curves with respect to the radius. Thus it is necessary to check the variation of n of the $\tau(\gamma)$-curve along the radius of the disk during loading for each case in order to see whether or not the deformation theory is applicable. The procedure is as follows:

Obtain several $\tau(\gamma)$-curves along the radius of the disk for different values of γ_0 by using the procedure described in the previous section. Plot these curves on a logarithmic scale, Fig. 6. Determine the values of n of the $\tau(\gamma)$-curves along the radius of the disk for different γ_0. Calculate n from Equation [4]. From the values of n for several γ_0 and the curves given in Fig. 3(*a*), the variation of α, or the variation of ratio of principal stresses is obtained.

NONUNIFORMITY DUE TO TEMPERATURE GRADIENT

Consider now rotating disks which have nonuniformity of metal properties resulting from an external effect such as temperature gradient of the surrounding gas. It should be emphasized that for such a case (nonuniformity in metal property due to temperature gradient), the method can be applied only in the range of temperature for which the viscous creep of the material is negligible and the transient creep is small, because the theory on which the method is based does not include time effect. The procedure of the method is the same as the one described previously except that the $\tau(\gamma)$-curve of the specimen cut from the disk at a certain radius should be obtained at the same temperature as that in the disk at the same radius during operation. Also the strain rate of the tensile test should be kept as close as possible to the strain rate of the disk at the given radius under consideration.

It is assumed that the plastic laws which have been proved valid at room temperature are also valid at the temperature range considered, such as (*a*) the incompressibility of metal, and (*b*) the unique relation between the octahedral shear stress and strain at the given temperature if the ratios and directions of principal stresses remain constant during loading.

The variations of the ratio of principal stresses during loading, that is, during acceleration, for a disk operating under a certain steady state of temperature gradient along the radius of the disk can be obtained by the procedure given in the preceding section. However, if the temperature at the center of the disk is low and it increases with r (any function, not necessarily linear) such as in a turbine or compressor disk, the stress-strain surface is qualitatively similar to the one shown in Fig. 2 because the stress-strain curve of a material at a higher temperature is flatter than that at a lower temperature. The value of m therefore increases with γ_0. Thus from Equation [4] the variation of n during loading (accelerating) is expected to be small.

Comparison of Experiment and Calculation

It is interesting to compare the experimentally determined relation between $\rho(\omega b)^2$ and γ_0 with those obtained from the chart. In order to make such a comparison, it would be necessary to measure γ_0 at the center of the disk during operation and also to obtain the tensile stress-strain curves from the specimens shown in Fig. 4. Such data are not available in the literature. If it is assumed that fracture in the rotating disk takes place when the maximum octahedral shear strain in the disk reaches the same value as the fracture octahedral shear strain in a simple tension, then the data given in (9) together with the additional data regarding the metal properties of the disk supplied by the Lewis laboratory of NACA, are sufficient to allow comparison between the calculation and the experiment. Also it is assumed that the metal properties of the disk in (9) are uniform. The tangential and radial stresses as well as the tangential and radial strains in the solid disk near the shaft are assumed to be equal. This assumption is shown to be justified by the strain measurements given in Figs. 17 and 18 of reference (8).

The calculated bursting speed is determined directly from the chart by using the value of m of the $\tau(\gamma)$-curve of the disk material for $\gamma_0 = \gamma_{fr}$, where γ_{fr} is the octahedral shear strain of the tensile specimen at fracture. The $\tau(\gamma)$-curves given in Fig. 8

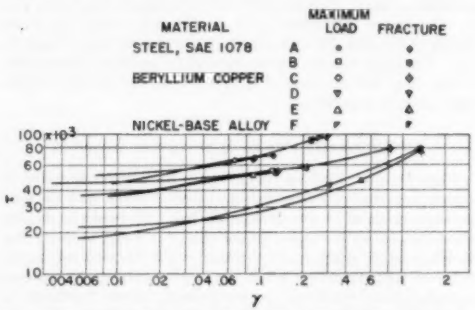

Fig. 8 Relation Between Octahedral Shear Stress τ and Octahedral Shear Strain γ of Tensile Specimens Cut From Disks for Six Materials

(SAE 1078 steel of two different heat-treatments, beryllium-copper alloy of three different heat-treatments and one nickel-base alloy.)

are calculated from the unpublished tensile-test data for reference (9). The tensile specimens were cut in the radial direction of the disks which show no imperfections upon x-ray and surface inspection. The specimen was 3.00 in. long with a 1.00-in. gage length. Six materials (SAE 1078 steel of two different heat-treatments, beryllium-copper alloy of three different heat-treatments, and one nickel-base alloy) are considered. For simplicity, these materials are herein designated as materials A, B, C, D, E, and F.

The calculated values of $\rho(\omega b)^2$ at disk failure (based on the previously mentioned assumptions) are plotted against the experimentally determined $\rho(\omega b)^2$ at bursting speed in Fig. 9. It can be seen that these points are very close to the 45-deg straight line. More reliable comparisons can be obtained, however, if (*a*) the $\tau(\gamma)$-curves of few tensile specimens taken at different radii of the disk in the tangential direction, Fig. 4, are used; (*b*) the tensile strain is obtained by measuring the diameter of the tensile specimen during loading rather than the elongation between a finite gage length; and (*c*) the $\tau(\gamma)$-curves obtained from the tensile test are corrected for the triaxiality and nonuniform stress distribution introduced by necking.

For material C the load-elongation curve shows that there is a large necking effect in tensile test. Therefore values of $\rho(\omega b)^2$ for several values of γ_0 between $\gamma_0 = 0.1342$ (the value of γ at the maximum load of the tensile test) and γ_{fr} are calculated. The calculated value of $\rho(\omega b)^2$ increases to a maximum (337×10^3 psi) at $\gamma_0 = 0.3$ to 0.4 then decreases to 324×10^3 at $\gamma_0 = \gamma_{fr} = 0.8224$. This indicates a case of instability of the rotating disk.

Accuracy of Method

In order to examine the accuracy of the method, especially the percentage error of $\rho(\omega b)^2$ (for a given γ_0) determined from the chart, the relations between $\rho(\omega b)^2$ and γ_0 are obtained from the chart for Inconel X and 16-25-6. These relations of $\rho(\omega b)^2$ and γ_0 are compared in Fig. 10 with those obtained from the exact solution (1). Fig. 10 shows that the difference of $\rho(\omega b)^2$ between the two solutions is small. The percentage deviation of $\rho(\omega b)^2$ of the approximate solution from the exact solution is much less than the percentage deviation of α, σ_θ, and ϵ_θ, as shown by the approximate figures of the two examples given in Table 2.

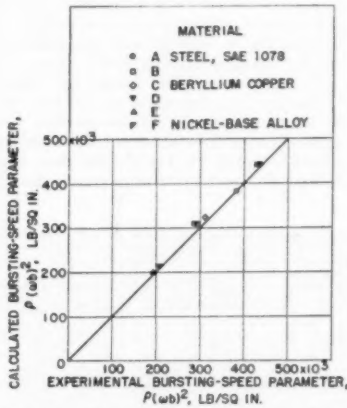

Fig. 9 Relation Between Calculated and Experimental Bursting Speed Parameter for Six Materials

(SAE 1078 steel of two different heat-treatments, beryllium-copper alloy of three different heat-treatments and one nickel-base alloy.)

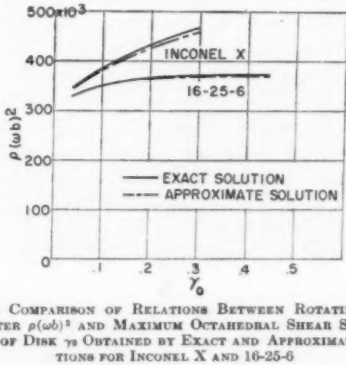

Fig. 10 Comparison of Relations Between Rotating-Speed Parameter $\rho(\omega b)^2$ and Maximum Octahedral Shear Strain at Center of Disk γ_0 Obtained by Exact and Approximate Solutions for Inconel X and 16-25-6

TABLE 2 PERCENTAGE DEVIATION OF $\rho(\omega b)^2$

Material	γ_0	Maximum percentage deviation (along radius of disk) of			Percentage deviation of
		n	σ_θ	ϵ_θ	$\rho(\omega b)^2$
Inconel X.....	0.1152	9.0	4.1	20	2.07
	0.3000	9.5	6.5	16	1.70

This can be explained by the following: (*a*) The maximum percentage deviations of α, σ_θ, and ϵ_θ occurred at the low strain region. In the high strain region, which is the region of importance, the percentage deviations of these quantities are small. (*b*) In Equation [6] $\rho(\omega b)^2$ increases with increasing value of σ_θ but decreases with increasing value of ϵ_θ; values of σ_θ and ϵ_θ obtained by the approximate solution differ from those of the exact solution in the same direction; hence part of the error cancels.

The accuracy of the method and the accuracy of the use of the chart depend only on the deviation of the value n for the $\tau(\gamma)$-curve from the value of $n = 0$. For a disk having uniform metal properties, n is determined from the $\tau(\gamma)$-curve of the material. For a disk having nonuniform metal properties, n is determined from the relation between τ and γ along the radius of the disk obtained from the stress-strain surface. The two numerical examples are chosen because they have relatively high n-values (0.195 and 0.150) among all the examples, and therefore give the maximum error. The numerical results of the two examples show that the error introduced in $\rho(\omega b)^2$ by the use of the chart ($n = 0$) is small, because even for the n-values equal to 0.195 and 0.150 the percentage deviations of $\rho(\omega b)^2$ introduced are only equal to 2.07 and 1.70, respectively.

BIBLIOGRAPHY

1 "Analysis of Plane-Plastic-Stress Problems With Axial Symmetry in Strain-Hardening Range," by M. H. Lee Wu, NACA Rep. 1021, 1951. (Formerly NACA TN 2217, 1950.)

2 "General Plastic Behavior and Approximate Solutions of Rotating Disk in Strain-Hardening Range," by M. H. Lee Wu, NACA TN 2367, May, 1951.

3 "Plasticity," by A. Nadai, McGraw-Hill Book Company, Inc., New York, N. Y., 1931.

4 "Stress Distribution in Rotating Disks of Ductile Material After the Yield Point Has Been Reached," by A. Nadai and L. H. Donnell, Trans. ASME, vol. 51, Paper APM—51-16, 1929, pp. 173–181.

5 "The Tension Test," by C. W. MacGregor, Proceedings of the ASTM, vol. 40, 1940, pp. 508–534.

6 "Precision Determination of Stress-Strain Curves in the Plastic Range," by John R. Low, Jr., and Frank Garofalo, Proceedings of the SESA, vol. 4, 1947, p. 16.

7 "Tensile Deformation," by John H. Hollomon, Trans. AIME, Iron and Steel Division, vol. 162, 1945, pp. 268–289.

8 "Developments in High-Speed Rotating Disk Research at MIT," by C. W. MacGregor and W. D. Tierney, *Welding Journal Supplement*, vol. 27, June, 1948, pp. 303S–309S.

9 "Effect of Strength and Ductility on Burst Characteristics of Rotating Disks," by Arthur G. Holms and Joseph E. Jenkins, NACA TN 1667, 1948.

Combined Tension-Torsion Tests for Aluminum Alloy 2S-O[1]

By ARIS PHILLIPS,[2] STANFORD UNIVERSITY, CALIF.

In this paper ten combined tension-torsion tests with thin-walled circular tubes of aluminum alloy 2S-O are described. All specimens were loaded with variable stress ratios. It has been found that the theory of plastic flow represents the experimental results with much greater accuracy than does the theory of plastic deformations.

Introduction

ONE of the most important problems in experimental plasticity is to find out which one of the theories of plasticity proposed up to now represents best the behavior of a given material in the plastic range. In this paper we shall describe some experiments which deal with this problem. In these experiments thin-walled circular tubes of aluminum alloy 2S-O have been submitted to combined tension and torsion in the plastic region. By means of these tests we shall compare the simplest forms of the two fundamental theories of plasticity, that is, of the theory of plastic deformations and of the theory of plastic flow.

Let us introduce the following notations

$\sigma_r, \sigma_\theta, \sigma_z, \tau_{r\theta}, \tau_{rz}, \tau_{\theta z}$ are the six stress components.

$$\sigma_m = \frac{\sigma_r + \sigma_\theta + \sigma_z}{3}$$

$$\tau_{oct} = \frac{1}{3}\sqrt{(\sigma_r - \sigma_\theta)^2 + (\sigma_\theta - \sigma_z)^2 + (\sigma_z - \sigma_r)^2 + 6(\tau_{r\theta}^2 + \tau_{\theta z}^2 + \tau_{zr}^2)}$$

is the octahedral shear stress.

$\epsilon_r', \epsilon_\theta', \epsilon_z', \gamma_{r\theta}', \gamma_{\theta z}', \gamma_{zr}'$ are the elastic strain components.

$\epsilon_r'', \epsilon_\theta'', \epsilon_z'', \gamma_{r\theta}'', \gamma_{\theta z}'', \gamma_{zr}''$ are the plastic strain components.

$\epsilon_r = \epsilon_r' + \epsilon_r'', \epsilon_z = \epsilon_z' + \epsilon_z'', \epsilon_\theta = \epsilon_\theta' + \epsilon_\theta''$

$\gamma_{r\theta} = \gamma_{r\theta}' + \gamma_{r\theta}'', \gamma_{\theta z} = \gamma_{\theta z}' + \gamma_{\theta z}'', \gamma_{zr} = \gamma_{zr}' + \gamma_{zr}''$

are the total strain components.

$$\epsilon_m = (\epsilon_r + \epsilon_\theta + \epsilon_z)/3$$

In plasticity we have with great accuracy

$$\epsilon_r'' + \epsilon_\theta'' + \epsilon_z'' = 0$$

Hence

$$\epsilon_m = \frac{\epsilon_r' + \epsilon_\theta' + \epsilon_z'}{3} = \sigma_m \frac{1 - 2\nu}{E}$$

The tests described in this paper are such that throughout each test the octahedral shear stress τ_{oct} increased monotonically starting from the zero value. For this case the stress-strain relations of the theory of plastic deformations are

$$\frac{\epsilon_r - \epsilon_m}{\sigma_r - \sigma_m} = \frac{\epsilon_\theta - \epsilon_m}{\sigma_\theta - \sigma_m} = \frac{\epsilon_z - \epsilon_m}{\sigma_z - \sigma_m} = \frac{\frac{1}{2}\gamma_{r\theta}}{\tau_{r\theta}} = \frac{\frac{1}{2}\gamma_{rz}}{\tau_{rz}} = \frac{\frac{1}{2}\gamma_{\theta z}}{\tau_{\theta z}} = f(\tau_{oct}) \quad [1]$$

where $f(\tau_{oct})$ is a function of τ_{oct} which depends on the material only. For this same case the stress-strain relations of the theory of plastic flow are

$$\frac{d\epsilon_r''}{(\sigma_r - \sigma_m)d\tau_{oct}} = \frac{d\epsilon_\theta''}{(\sigma_\theta - \sigma_m)d\tau_{oct}} = \frac{d\epsilon_z''}{(\sigma_z - \sigma_m)d\tau_{oct}} = \frac{\frac{1}{2}d\gamma_{r\theta}''}{\tau_{r\theta}d\tau_{oct}} = \frac{\frac{1}{2}d\gamma_{\theta z}''}{\tau_{\theta z}d\tau_{oct}} = \frac{\frac{1}{2}d\gamma_{zr}''}{\tau_{zr}d\tau_{oct}} = F(\tau_{oct}) \quad [2]$$

where $d\tau_{oct}, d\epsilon_r'', \ldots, d\gamma_{zr}''$ represent corresponding increments of $\tau_{oct}, \epsilon_r'', \ldots, \gamma_{zr}''$, respectively, during the loading process, and $F(\tau_{oct})$ represents a function of the τ_{oct} which depends only on the material.

In the case of combined tension and torsion of thin-walled tubes, we have

$$\sigma_r = \sigma_\theta = 0, \gamma_{r\theta} = \gamma_{rz} = 0, \gamma_{r\theta}'' = \gamma_{rz}'' = 0$$

$$\sigma_m = \sigma_z/3, \epsilon_m = \epsilon_m' = \sigma_z \frac{1 - 2\nu}{3E}$$

$$\tau_{oct} = \frac{\sqrt{2}}{3}\sqrt{\sigma_z^2 + 3\tau_{\theta z}^2}$$

Equations [1] become

$$\frac{\epsilon_r - \sigma_z \frac{1 - 2\nu}{3E}}{-\frac{\sigma_z}{3}} = \frac{\epsilon_\theta - \sigma_z \frac{1 - 2\nu}{3E}}{-\frac{\sigma_z}{3}} = \frac{\epsilon_z - \sigma_z \frac{1 - 2\nu}{3E}}{\frac{2\sigma_z}{3}} = \frac{\frac{1}{2}\gamma_{\theta z}}{\tau_{\theta z}} = f\left(\frac{\sqrt{2}}{3}\sqrt{\sigma_z^2 + 3\tau_{\theta z}^2}\right) \quad [3]$$

while Equations [2] become

$$\frac{d\epsilon_r''}{-\frac{\sigma_z}{3}d\tau_{oct}} = \frac{d\epsilon_\theta''}{-\frac{\sigma_z}{3}d\tau_{oct}} = \frac{d\epsilon_z''}{\frac{2}{3}\sigma_z d\tau_{oct}} = \frac{\frac{1}{2}d\gamma_{\theta z}''}{\tau_{\theta z}d\tau_{oct}} = F\left(\frac{\sqrt{2}}{3}\sqrt{\sigma_z^2 + 3\tau_{\theta z}^2}\right) \quad [4]$$

---

[1] The results presented in this paper were obtained in the course of research conducted under a contract sponsored by the Office of Naval Research.

[2] Assistant Professor, Division of Engineering Mechanics, Stanford University. Mem. ASME.

Presented at the West Coast Conference of the Applied Mechanics Division, Los Angeles, Calif., June 26–28, 1952, of The American Society of Mechanical Engineers.

Discussion of this paper should be addressed to the Secretary, ASME, 29 West 39th Street, New York, N. Y., and will be accepted until January 10, 1953, for publication at a later date. Discussion received after the closing date will be returned.

Note: Statements and opinions advanced in papers are to be understood as individual expressions of their authors and not those of the Society. Manuscript received by ASME Applied Mechanics Division, February 4, 1952.

where

$$d\tau_{oct} = \frac{\sqrt{2}}{3}\, d\left(\sqrt{\sigma_z^2 + 3\tau_{\theta z}^2}\right)$$

Our problem is to find which one of the systems, Equations [3] and [4], represents the experimental results with greater accuracy.

Test Procedure and Results

The test procedure consisted in applying stepwise definite increments of axial load and torque and measuring the corresponding increments in the gage length and the angle of twist. Then we calculated the quantities σ_z, $\tau_{\theta z}$, ϵ_z, $\gamma_{\theta z}$, $d\epsilon_z{}^p$, $d\gamma_{\theta z}{}^p$ for each loading step. By introducing these values into Equations [3] and [4] we could decide about the accuracy of these equations.

In Fig. 1 we see the results for test No. 3. The lower half of the figure represents the loading history. The specimen has been loaded stepwise in the axial direction up to $\sigma = 9330$ psi. The next loading step consisted of applying the shear stress $\tau = 950$ psi while keeping the axial stress constant. Then, the next step consisted of increasing the axial stress to $\sigma = 9350$ psi and simultaneously increasing the shear stress to $\tau = 1350$ psi. This step was followed by six other loading steps.

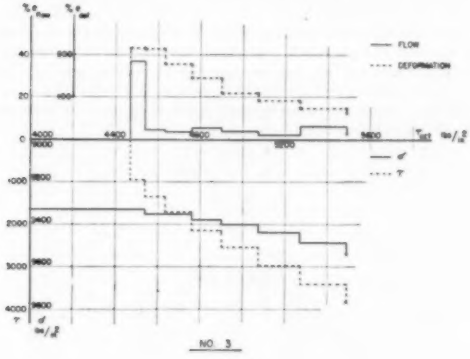

Fig. 1

In the upper half of Fig. 1 we see our results concerning the validity of equation

$$(\epsilon_z - \sigma_z(1-2\nu)/3E)/2\sigma_z/3 = \frac{1}{2}\,\gamma_{\theta z}/\tau_{\theta z} \quad \ldots\ldots [5]$$

of the theory of plastic deformations, and of equation

$$d\epsilon_z{}^p \Big/ \frac{2}{3}\,\sigma_i d\tau_{oct} = \frac{1}{2}\, d\gamma_{\theta z}{}^p/\tau_{\theta z} d\tau_{oct} \quad \ldots\ldots [6]$$

of the theory of plastic flow. Let us introduce the notations

$$A = \frac{2}{3}\,\sigma_z/\tau_{\theta z}, \quad B = \epsilon_z - \sigma_z(1-2\nu)/3E \Big/ \frac{1}{2}\,\gamma_{\theta z}$$

$$C = d\epsilon_z{}^p \Big/ \frac{1}{2}\, d\gamma_{\theta z}{}' \quad \ldots\ldots [7]$$

If Equation [5] were correct then we would have $A = B$. The experiments, however, show that $A \neq B$. The error of the theory of plastic deformations can be presented by

$$\left.\begin{aligned} e_{def} &= 100(A - B)/B, \; A \geq B \\ e_{def} &= 100(B - A)/A, \; A \leq B \end{aligned}\right\} \quad \ldots\ldots [8]$$

If Equation [6] were correct then we would have $A = C$. This, however, is not the case as the experiments show. Therefore the error of the theory of plastic flow can be presented by

$$\left.\begin{aligned} e_{flow} &= 100(A - C)/C, \; A \geq C \\ e_{flow} &= 100(C - A/A, \; A \leq C \end{aligned}\right\} \quad \ldots\ldots [9]$$

In Fig. 1 the full line represents e_{flow} while the dotted line represents e_{def}. We see that in so far as Equations [5] and [6] are concerned the theory of flow is much more accurate than the theory of plastic deformations.

In Figs. 2, 3, and 4 we give the results for tests Nos. 5, 8, and 10, respectively. The results for six additional tests can be found in a

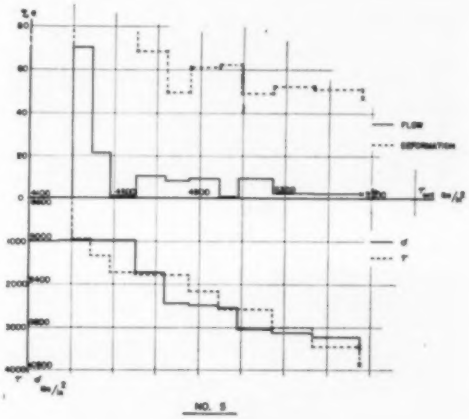

Fig. 2

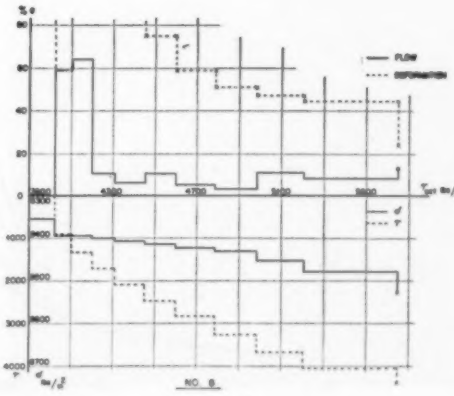

Fig. 3

technical report[3] by the author. In nine of these tests it has been found that the theory of plastic flow is superior to the theory of plastic deformations, while in one of the tests performed (test No. 10) the theory of plastic deformations gives slightly better results than does the theory of plastic flow.

It is also important to note that, in general, ϵ_{flow} becomes small only after the direction of loading remains substantially constant for a few loading steps. An abrupt and substantial change in the direction of loading produces a great increase in the value of ϵ_{flow}.

Equations [5] and [6] are only parts of the systems of Equations [3] and [4]. Another part of these same systems is the existence of the two functions $f(\tau_{oct})$ and $F(\tau_{oct})$. However, a prerequisite of the existence of these two functions is the validity of Equations [5] and [6].

From Figs. 1 to 4 it can be concluded that in the majority of cases ϵ_{def} is so large that Equation [5] cannot be considered as correct. Therefore function $f(\tau_{oct})$ cannot exist. On the other hand, ϵ_{flow} is in most cases smaller than 20 per cent. Therefore it would be worth while to investigate the existence of function $F(\tau_{oct})$. In Fig. 5 we give the values of the ratios

$$d\epsilon_s^p \Big/ \frac{2}{3}\,\sigma_s d\tau_{oct} \qquad [10]$$

and

$$\frac{1}{2}\,d\gamma_{\theta_s}^p / \tau_\theta d\tau_{oct} \qquad [11]$$

as functions of τ_{oct}. These ratios are denoted by ϕ in Fig. 5. Only tests Nos. 3, 5, 8, 9, and 10 have been considered, and these only for such values of τ_{oct} for which Ratio [10] does not differ from Ratio [11] by more than 20 per cent. From this figure we see that a function $F(\tau_{oct})$, which depends on the material only does not exist, because the lines representing the Ratios [10] and [11] for the different experiments do not lie near each other. It is clear that the history of loading has a great influence upon the value of the Ratios [10] and [11].

[3] "Combined Stress Experiments in Plasticity," by Aris Phillips, Technical Report No. 11, Contract N6onr-251-Task Order 11, prepared for the Office of Naval Research, Division of Engineering Mechanics, Stanford University, January 15, 1952.

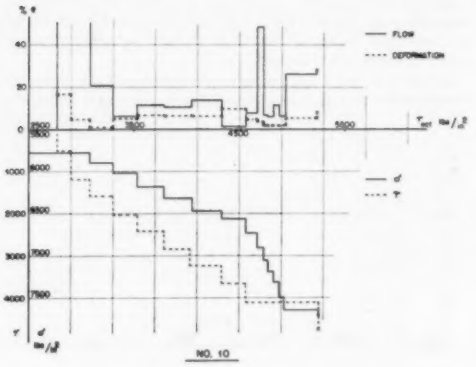

FIG. 4

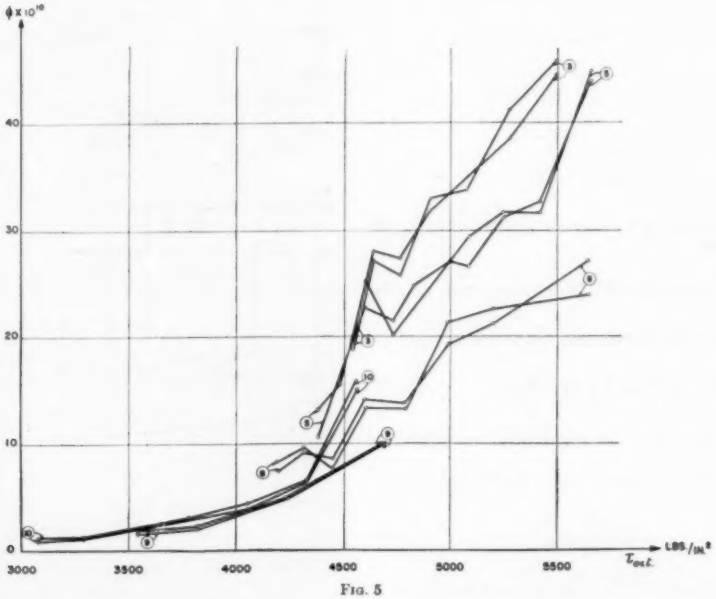

FIG. 5

Experimental Technique

The material used was annealed pure aluminum 28-O. It was supplied in the annealed condition in tubular extruded form with an internal diameter of 0.75 in. and a wall thickness of $^1/_4$ in. The specimens had an over-all length of 11 in., with an intermediate length of $6^3/_4$ in. of reduced wall thickness equal to 0.030 ± 0.001 in. The ratio of wall thickness to internal diameter of the specimen is 1:26.

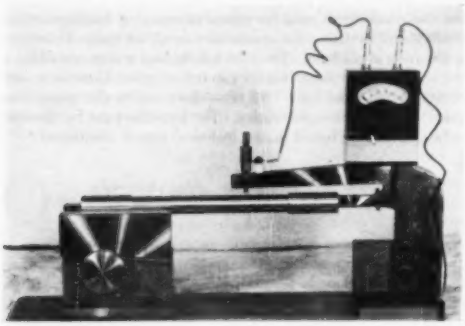

Fig. 6 Instrument for Measuring Tube Thickness

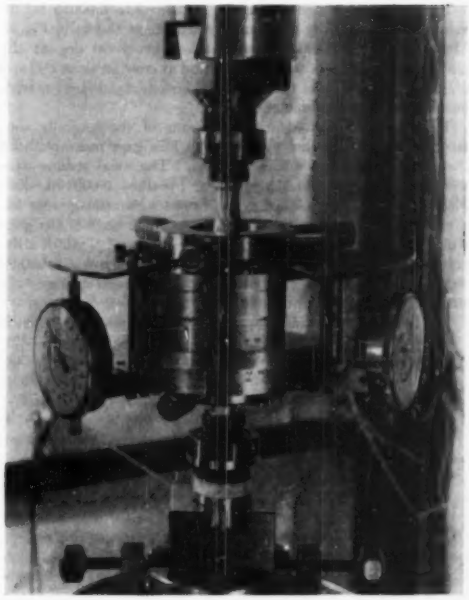

Fig. 7 Strain Gage

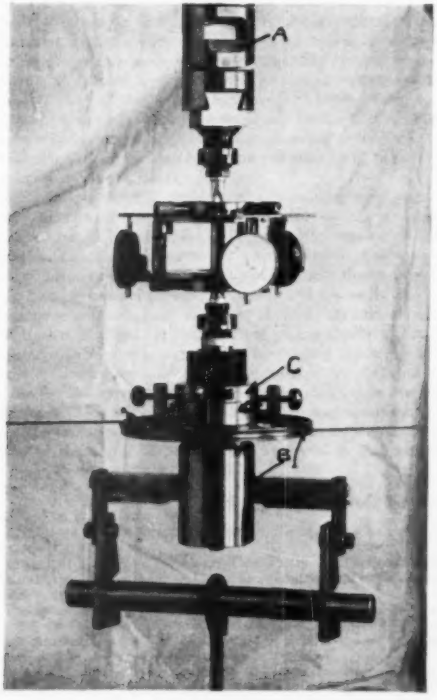

Fig. 8 Testing Machine

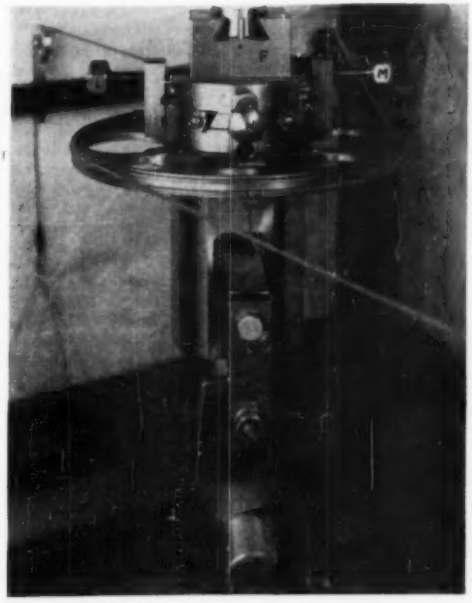

Fig. 9 Device for Measuring Axiality of Loading

The thickness of the tubes was measured to 0.00025 in. by means of the specially constructed instrument shown in Fig. 6. Measurements of thickness were taken every 90 deg at the middle cross section of the specimen and at cross sections $1^1/_4$ and $2^1/_2$ in. on either side of the middle. The external diameters were measured with a micrometer caliper.

The strains were measured by means of the specially constructed strain gage shown in Fig. 7. This gage measures both the axial strains and angles of twist. The axial strains were measured for a $4^1/_8$-in. gage length by three 0.0001-in. dials placed 120 deg apart. The angles of twist were measured for the same gage length by means of the twistmeter part of the gage which includes a vernier, allowing an accuracy of $^1/_{10}$th of a degree for the $4^1/_8$-in. gage length. The strain gage was attached to the specimen by three radial rods with preloaded springs. In this way slipping was prevented.

The load was applied by means of the testing machine shown in Fig. 8. This machine was designed for subjecting tubular specimens to combined axial tension and torsion. To insure axiality of the loading we use the two spherical seats A and B and the device denoted by C and shown in a greater scale in Fig. 9. This device consists of four screws and the blocks E, D, and F shown in Fig. 9. The block F slides with respect to the block E if pushed by any one of the screws L and M. The block E slides with respect to the block D if pushed by the screw N or by the opposite screw which is not shown in the figure.

The specimen was loaded first in tension up to a level well below the elastic limit, and by means of repeated loading and unloading and by using the special device C, we insured the axial application of the load. Then the tensile load was increased up to the level where torsional load began to be applied alone or in combination with axial load. All tests described in this paper were made with variable-stress ratios. The formulas used for the computations can be found in the technical report mentioned.[3]

A Matrix Method for Flexibility Analysis of Piping Systems

By J. E. BROCK,[1] ST. LOUIS, MO.

By use of matrix algebra a concise and strongly motivated method is developed for analyzing flexibility of piping systems. The method is particularly suited for systems which are complicated by multiple branches, additional constraints, inconvenient orientations, and so on, as well as for examination and modification for particular purposes of more widely known methods.

Introduction

ONE who undertakes to add to the already extensive literature on piping flexibility analysis is under obligation to give some cogent reasons for so doing. In the first place, increasing temperatures in modern power and process piping have made the problems of the piping designer more compelling and have resulted in the necessity of performing flexibility analyses for an increasing percentage of piping installations. Then too, the designer should be able to use any of a number of different methods depending on the nature of the problem at hand; for certain simple, uniplanar configurations of frequent occurrence, he should be able to make rapid use of appropriate available chart or graph solutions; for complicated three-dimensional configurations involving branches, intermediate partial constraints, and/or other complicating factors, he should be able to employ a method such as the one presented here. Finally, since all methods of analysis (which are known to the author) require too much labor to obtain results that are known to be within acceptable limits of engineering accuracy, a new point of view and philosophy of analysis may be of value in the evolution of the entire subject.

The basic structural problem of determining reactive forces and moments in hot piping systems involves only elementary structural theory. However, in all save the simplest of actual cases, it is necessary to carry out a large volume of arithmetical operations in order to arrive at a solution, and the bookkeeping (i.e., keeping track of the computations), and the motivation (i.e., deciding what to do next and how to do it) do involve serious practical difficulties. A "method" of piping flexibility analysis is, accordingly, simply a procedure for leading the analyst from one step to the next and of keeping track of his computations. A number of such methods have been described in the literature. Reference (1)[2] gives a bibliography of the most significant publications through 1945, and introduced by its publication, a series of papers on the subject has appeared in the periodical *Heating, Piping, and Air Conditioning.*

Since all methods of flexibility analysis involve assumptions and approximations of one kind or another, it is not strictly correct to speak of "exact" methods; however, this useful expression is sure to connote to the reader a method which, like the so-called graphoanalytical method described in the Piping Handbook (2) or the so-called analytical method (3), yields exact results subject only to the customary assumptions of elementary structural theory. Our further remarks will be concerned only with the exact methods, or methods which, like "square-corner" simplifications, imply the exact analysis of a simplified substitute configuration.

Examination of these methods reveals that while the sources of the motivation and the systems of bookkeeping vary widely from method to method, nevertheless ultimately, the same arithmetic operations are called for. This should not be surprising since indeed it is the same problem being attached by the different methods, the numerical input data is the same, and the final results are the same. The present analysis will disclose a strong motivation and a convenient bookkeeping system within the calculations themselves, as well as sufficient flexibility to attack the most complicated problems. Even in simple cases, though, the philosophy of the present method leads to an alternate, and thus a firmer, understanding of the basic behavior of the structure under consideration. The present method is of particular value in connection with the study or modification for particular purposes of one of the better-known methods.

The author does not recommend the present method for routine analysis in simple cases, but rather, one of the better-known methods. In this connection, the author's company expects to publish in the near future an extension of the so called tabular integration method (4), which will permit the user at his option, either to make a square-corner approximation or to take bends into account as such, without sacrificing the rigidly direct motivation and compact bookkeeping for which the method is known.

In more complicated cases, however, the method described herein may prove to be distinctly advantageous. Complications may arise from the following:

(*a*) Multiple anchor configurations.

(*b*) Partial constraints at intermediate points.

(*c*) Tangents (i.e., straight lengths) and bends oriented at inconvenient angles with respect to the configuration.

(*d*) Presence of bends whose axes are space curves or plane curves other than circular arcs.

(*e*) Desire to account for flexibility of equipment at ends of piping or of valves, specialties, or equipment at intermediate points.

The author has used the present method in several cases involving one or more of the complicating factors just cited. Especially, as the degree of redundancy increases, it is necessary to have a compact way of handling the systems of equations involved and a brief notation for conjuring with the notions involved.

Concerning the history of the method, while the author's analysis is his independent effort, priority for applying matrix ideas to piping flexibility analyses seems to belong to Com-

---

[1] Director of Research, Midwest Piping and Supply Company, Inc. Mem. ASME.

[2] Numbers in parentheses refer to the Bibliography at the end of the paper.

Presented at the West Coast Conference of the Applied Mechanics Division, Los Angeles, Calif., June 26–28, 1952, of The American Society of Mechanical Engineers.

Discussion of this paper should be addressed to the Secretary, ASME, 29 West 39th Street, New York, N. Y., and will be accepted until January 10, 1953, for publication at a later date. Discussion received after the closing date will be returned.

Note: Statements and opinions advanced in papers are to be understood as individual expressions of their authors and not those of the Society. Manuscript received by ASME Applied Mechanics Division, January 3, 1952.

mander P. T. Hoath whose interesting paper (5) exhibits in an almost incidental way, certain matrices which differ only in notation from some of those which follow in this paper. From correspondence with Commander Hoath, the date of his developments may be placed between 1944 and 1947. He regards the matrix formulation as fairly obvious, an opinion that the author does not share because of his stake in the matter and for two valid reasons as well: (*a*) The author's analysis seems to have been carried further than the earlier analysis of Commander Hoath, leading to analyses presented here and in the paper (6) which can hardly be said to be obvious. (*b*) While matrix analysis has been applied to structural problems in several recent studies, e.g., (7) and (8), the point of view and notation differ from those of the present paper, which accordingly does not seem to be obvious.

One final remark is in order concerning the notation used in this paper. To describe a complicated structure a fairly complicated notation is required. Use of superscripts has been avoided except in the very last portion which deals with multiply branched systems. Use of exotic alphabets has been avoided although a few Greek letters are used. In many cases, superscripts or subscripts could be suppressed without confusion; the author has, however, included all such symbols to avoid all possible misunderstandings. The attention of the reader is invited to the advantage of having brief symbols (whether or not complicated by the presence of subscripts) for naming and describing fairly complicated physical concepts (i.e., the force and displacement "vectors" and the flexibility tensors) which otherwise could be dealt with mentally only in a hazy fashion or a piece at a time. Since each symbol is defined as it is introduced and since the notation is such an intrinsic part of the theory, we do not here present a separate table or listing of notations. However, the reader should note that several letters serve a double duty. For example, EI denotes flexural rigidity while E and I separately are two quantities employed in constructing the flexibility matrix for bends and "inclined" tangents. The letters C, D, and F, without subscripts are similar quantities, while with subscripts they are elements of the matrices denoted by the same bold-face letters. Such usage will not prove to be a source of confusion.

Basic Theory

In this analysis we will use only elementary matrix algebra. Matrices will be denoted by bold-face letters, their elements by the same light-face letters with appropriate subscripts. When a matrix is exhibited *in extensio*, its elements will be enclosed in (square) brackets. Matrix addition and subtraction will be denoted by plus and minus signs, matrix multiplication by writing the matrices in juxtaposition, and the operation of transposition by writing a tilde ($\sim$) over the original matrix. The symbols $\mathbf{I}$ and $\mathbf{O}$ will denote the unit and the null matrices, respectively; their order will always be apparent from the context. For convenience we will sometimes use partitioned matrices, i.e., matrices the elements of which are also matrices; the use of such matrices will be indicated only by the fact that the matrix elements appear in bold face. Subject to a few obvious restrictions, partitioned matrices may be treated as if their elements were ordinary matrix elements, i.e., numbers. To conserve space we will use braces to indicate a column matrix and the letters "diag" followed by braces to indicate a diagonal matrix; thus:

$$\{a, b, \ldots, c\} = \begin{bmatrix} a \\ b \\ \cdot \\ \cdot \\ \cdot \\ c \end{bmatrix}, \quad \text{diag}\,\{a, b, \ldots, c\} = \begin{bmatrix} a & o & \ldots & o \\ o & b & \ldots & o \\ \cdot & \cdot & \cdot & \cdot \\ \cdot & \cdot & \cdot & \cdot \\ \cdot & \cdot & \cdot & \cdot \\ o & o & \ldots & c \end{bmatrix}$$

The reader who wishes to refresh himself concerning elementary matrix algebra will find his needs covered in the first chapter or so of any of a number of books on matrices. The books of Frazer, Duncan, and Collar (9), and of Zurmühl (10) are especially recommended as having been written particularly for engineers. Some of the necessary information is summarized in the following:

(*a*) If $\mathbf{A} = [A_{ij}]$ is an $m \times n$-matrix and $\mathbf{B} = [B_{ij}]$ is an $r \times s$-matrix, then the product symbol $\mathbf{AB}$ has meaning only if $n = r$. In this case $\mathbf{C} = \mathbf{AB} = [C_{ij}]$ is an $m \times s$-matrix with

$$C_{ij} = \sum_{k=1}^{n} A_{ik} B_{kj}$$

(*b*) In general, $\mathbf{AB} \neq \mathbf{BA}$ even when both sides have meaning.

(*c*) If $\mathbf{C} = \mathbf{AB}$, then $\tilde{\mathbf{C}} = \tilde{\mathbf{B}}\tilde{\mathbf{A}}$

(*d*) For any $\mathbf{A}$, $\mathbf{AI} = \mathbf{IA} = \mathbf{A}$ and $\mathbf{AO} = \mathbf{OA} = \mathbf{O}$

In what follows, we will use more than one set of right-handed rectangular co-ordinate axes (which hereafter we will call a "system"). We will generally employ one main x, y, z-system in any particular setup, as well as auxiliary local systems. We will not attempt to set up a notation which will automatically specify the origin and orientation it is used to denote, but will instead distinguish sufficiently in the text to avoid confusion.

Let $\mathbf{F} = \{F_1, F_2, F_3, F_4, F_5, F_6\}$ be a column matrix describing the forces and moments applied to a structure at a point; the elements (or components) F_1, F_2, F_3 are forces acting in the positive x, y, z-directions, respectively; the components F_4, F_5, F_6 are moments acting (in the positive sense of the right-hand rule) about the x, y, z-axes, respectively. Similarly, let $\mathbf{D} = \{D_1, D_2, D_3, D_4, D_5, D_6\}$ be a matrix describing the deflections which may be experienced by an infinitesimal element of a structure; the components D_1, D_2, D_3 are linear displacements in the x, y, z-directions, respectively; the components D_4, D_5, D_6 are rotations (positive according to the right-hand rule) about the x, y, z-axes, respectively. It is implicit here, and later, that the present analysis is valid only for small deflections.

Now let P and Q be two specified points in a definite structure (by "definite" we imply that we have specified completely just what elements or substructures comprise the structure in question and have also specified completely the constraints applied to the structure). Suppose also we have a system S_P: x, y, z at P and a system S_Q: ξ, η, ζ at Q. We are interested in the 6×6 square matrix $\mathbf{C}(P, Q)$ such that $\mathbf{C}(P, Q)\mathbf{F}(Q) = \mathbf{D}(P)$, i.e., a matrix relating the forces (forces and moments) applied at Q and specified in S_Q to the deflections they produce at P and specified in S_P. It is easily seen that the general element $C_{ij}(P, Q)$ of this matrix is an influence coefficient of the following nature:

$C_{ij}(P, Q) = i$-deflection (measured in S_P) of point P due to application of a unit j-force (measured in S_Q) to point Q $(i, j = 1, \ldots, 6)$

Thus, for example, C_{52} is the (positive) rotation about the y-axis experienced at P due to application of a unit force at Q in the (positive) ξ-direction.

The reciprocal theorems of Maxwell and Rayleigh assert that $\mathbf{C}(Q, P) = \mathbf{C}(P, Q)$. If points P and Q and their respective systems S_P and S_Q coincide, the corresponding matrix $\mathbf{C} = \mathbf{C}(P, P)$ of "self" influence coefficients is symmetrical, i.e., $C_{ij} = C_{ji}$.

It is convenient to define the following matrices:

$$\mathbf{k}_{UV} = \begin{bmatrix} \cos(x_U, x_V) & \cos(x_U, y_V) & \cos(x_U, z_V) \\ \cos(y_U, x_V) & \cos(y_U, y_V) & \cos(y_U, z_V) \\ \cos(z_U, x_V) & \cos(z_U, y_V) & \cos(z_U, z_V) \end{bmatrix}$$

i.e., the matrix of direction cosines between the two systems S_U: x_U, y_U, z_U and S_V: x_V, y_V, z_V

$$\mathbf{L}_{UV} = \begin{bmatrix} \mathbf{K}_{UV} & \mathbf{O} \\ \mathbf{O} & \mathbf{K}_{UV} \end{bmatrix}$$

$$\mathbf{b}_{U,W} = \begin{bmatrix} 0 & z & -y \\ -z & 0 & x \\ y & -x & 0 \end{bmatrix}$$

where the elements are co-ordinates of point U in system S_W,

$$\mathbf{b}_{UV,W} = \mathbf{b}_{U,W} - \mathbf{b}_{V,W}$$

(note that the subscripts following the commas are the same)

$$\mathbf{B}_{UV,W} = \begin{bmatrix} \mathbf{I} & \mathbf{O} \\ \mathbf{b}_{UV,W} & \mathbf{I} \end{bmatrix}$$

In later applications we may omit some of these subscripts if they can easily be supplied from the context; for the present we must use them faithfully.

In the structure shown in Fig. 1, suppose that the levers PQ and RS are attached to the main structure only at the points Q and

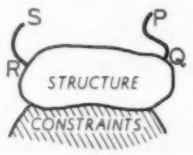

FIG. 1

R, respectively, where they are rigidly connected. For the following arguments we will use a notation (UV) to imply that the forces or deflections written preceding this notation are "observed at" the point U and "measured in" the system S_V. Suppose that we know the matrix $\mathbf{C}_{R3,Q2}$ which relates forces $\mathbf{F}(Q2)$ to deflections $\mathbf{D}(R3)$ according to the formula $\mathbf{C}_{R3,Q2}\mathbf{F}(Q_2) = \mathbf{D}(R3)$, and wish to determine the matrix $\mathbf{C}_{S4,P1}$ which relates forces $\mathbf{F}(P1)$ to deflections D $(S4)$ according to the formula $\mathbf{C}_{S4,P1}\mathbf{F}(P1) = \mathbf{D}(S4)$. We obtain the desired matrix by a series of fundamental transformations. The proofs, which are omitted to conserve space, can be supplied by application of elementary statics and elementary geometry; one possible line of argument is indicated in a previous paper of the author (6). These transformations are given in the following four equations; the notation has been selected for application to the problem at hand; it could of course be altered to apply to other situations and we will indeed repeatedly refer to the type of transformation given by these equations

$$\mathbf{F}(Q1) = \mathbf{B}_{QP,1}\mathbf{F}(P1) \quad [1]$$

$$\mathbf{F}(Q2) = \mathbf{L}_{21}\mathbf{F}(Q1) \quad [2]$$

$$\mathbf{D}(R4) = \bar{\mathbf{L}}_{44}\mathbf{D}(R3) \quad [3]$$

$$\mathbf{D}(S4) = \bar{\mathbf{B}}_{RS,4}\mathbf{D}(R4) \text{ (if } RS \text{ does not deform)} \quad [4]$$

Applying these as well as the condition

$$\mathbf{D}(R3) = \mathbf{C}_{R3,Q2}\mathbf{F}(Q2) \quad [5]$$

gives

$$\mathbf{D}(S4) = \bar{\mathbf{B}}_{RS,4}\bar{\mathbf{L}}_{44}\mathbf{C}_{R3,Q2}\mathbf{L}_{21}\mathbf{B}_{QP,1}\mathbf{F}(P1)$$

An alternate derivation gives

$$\mathbf{D}(S4) = \bar{\mathbf{L}}_{44}\bar{\mathbf{B}}_{RS,4}\mathbf{C}_{R3,Q2}\mathbf{B}_{QP,3}\mathbf{L}_{21}\mathbf{F}(P1)$$

Thus the desired transformation is

$$\mathbf{C}_{S4,P1} = \bar{\mathbf{B}}_{RS,4}\mathbf{C}_{R3,Q2}\mathbf{R}_{Q2,P1} \quad [6]$$

where

$$\mathbf{R}_{Q2,P1} = \mathbf{L}_{21}\mathbf{B}_{QP,1} = \mathbf{B}_{QP,3}\mathbf{L}_{21} \quad [7]$$

In the following we will use the symbol $\approx$ to mean "coincides with." If $P \approx S$ and $Q \approx R$, we still must be careful to distinguish between levers PQ and RS, for although the transformation of Equation [1] admits of the possible deformation in lever PQ, that of Equation [4] requires that lever RS experience only a rigid-body motion. In such a case, however, we can get by with only one lever if we specify that it be rigid.

Two special cases are of great interest. Suppose $P \approx Q \approx R \approx S$, $S_1 \approx S_4$, and $S_2 \approx S_3$. Then

$$\mathbf{C}_i = \bar{\mathbf{L}}_{2i}\mathbf{C}_i\mathbf{L}_{2i} \quad [8]$$

where $\mathbf{C}_i$ is the matrix of self influence coefficients at P with respect to S_i $(i = 1, 2)$. Such a transformation will be called an L-transformation for influence coefficients, or briefly, an L-transformation. The transformations of Equations [2] and [3] may be called L-transformations for forces and displacements, respectively.

Next, suppose $P \approx S$, $Q \approx R$, and $S_1 \approx S_2 \approx S_3 \approx S_4$; then

$$\mathbf{C}_P = \bar{\mathbf{B}}_{QP}\mathbf{C}_Q\mathbf{B}_{QP} \quad [9]$$

and we must specify that lever PQ be rigid. Here $\mathbf{C}_U$ is the matrix of self influence coefficients (with respect to the common system S_1) at the point U $(U = P, Q)$. The third subscript on the matrix $\mathbf{B}$ is superfluous. Such a transformation will be called a B-transformation for influence coefficients, or briefly, a B-transformation. The transformations of Equations [1] and [4] may be called B-transformations for forces and displacements, respectively.

In the application of this analysis to practical problems, most of the necessary transformations will be B-transformations. Because of the large number of zeroes in the matrices involved, the matrix multiplications involve many vanishing products, and it has been found convenient to construct Table 1 as a brief representation of the transformation given in Equation [9]. To avoid complications in subscripts, in Table 1 we have written $\mathbf{C}_Q = [C_{ij}]$, $\mathbf{C}_P = [\bar{C}_{ij}]$.

For the various piping elements and substructures which comprise a piping configuration, we will make use of the self influence coefficients $\mathbf{C}$ at a conveniently located base point BP, with respect to a conveniently oriented system S for the element PQ when one end of PQ is rigidly fixed and the other end is connected to BP by a rigid lever. Evidently, by failing to specify which end of PQ is fixed, we permit consideration of either situation shown in Figs. 2 (a and b). However, we may show that one and the same matrix $\mathbf{C}$ represents both situations. To see this, conceive of PQ as free in space as in Fig. 2 (c), with a rigid lever 1 fixed to it at P and extending to BP, and a rigid lever 2 fixed to it at Q and also extending to BP where it is not jointed to lever 1. Let S_1 be a system moving with lever 1, S_2 one moving with lever 2, and let S and S_3 both coincide originally with the original system S. Apply forces $\mathbf{F}$ to lever 1 at BP and forces $-\mathbf{F}$ to lever 2 at BP. The proof is essentially completed by noting that the deflections $\mathbf{D}$ experienced by the BP-end of lever 1 as measured in S_3 are the negatives of the displacements $-\mathbf{D}$ experienced by the BP-end of lever 2 as measured in S_1, Fig. 2(d).

TABLE 1 FORMULAS FOR THE B-TRANSFORMATION

$$C_P = \tilde{B}_{QP} C_Q B_{QP}$$

Elements of the matrix C_P are written with an overline ($\bar{}$), those of the matrix C_Q are written without the overline. The symbols x, y, z mean $(x_Q - x_P)$, $(y_Q - y_P)$, $(z_Q - z_P)$ respectively. The matrix C_Q is presumed to be symmetrical. Alternate formulas are given for $\bar{C}_{12}$, $\bar{C}_{13}$, and $\bar{C}_{23}$; in a particular application one will usually be found more convenient than the other. Determine results in the order indicated by the number at the point of the braces

$$1\begin{cases} \bar{C}_{44} = C_{44} \\ \bar{C}_{55} = C_{55} \\ \bar{C}_{66} = C_{66} \\ \bar{C}_{45} = C_{45} \\ \bar{C}_{46} = C_{46} \\ \bar{C}_{56} = C_{56} \end{cases} \qquad 2\begin{cases} \bar{C}_{14} = C_{14} - zC_{45} + yC_{46} \\ \bar{C}_{15} = C_{15} - zC_{55} + yC_{56} \\ \bar{C}_{16} = C_{16} - zC_{56} + yC_{66} \\ \bar{C}_{24} = C_{24} - xC_{46} + zC_{44} \\ \bar{C}_{25} = C_{25} - xC_{56} + zC_{45} \\ \bar{C}_{26} = C_{26} - xC_{66} + zC_{46} \\ \bar{C}_{34} = C_{34} - yC_{44} + zC_{45} \\ \bar{C}_{35} = C_{35} - yC_{45} + zC_{55} \\ \bar{C}_{36} = C_{36} - yC_{46} + zC_{56} \end{cases}$$

$$3\begin{cases} \bar{C}_{11} = C_{11} - z(\bar{C}_{15}+C_{15}) + y(\bar{C}_{16}+C_{16}) \\ \bar{C}_{22} = C_{22} - x(\bar{C}_{26}+C_{26}) + z(\bar{C}_{24}+C_{24}) \\ \bar{C}_{33} = C_{33} - y(\bar{C}_{34}+C_{34}) + x(\bar{C}_{35}+C_{35}) \end{cases}$$

$$4\begin{cases} \bar{C}_{12} = C_{12} - x\bar{C}_{16} + y\bar{C}_{26} + z(\bar{C}_{14}-C_{25}) = C_{12} - xC_{16} + y\bar{C}_{26} + z(C_{14}-\bar{C}_{25}) \\ \bar{C}_{13} = C_{13} - z\bar{C}_{35} + x\bar{C}_{15} + y(\bar{C}_{36}-C_{14}) = C_{13} - zC_{35} + x\bar{C}_{15} + y(C_{36}-\bar{C}_{14}) \\ \bar{C}_{23} = C_{23} - y\bar{C}_{24} + z\bar{C}_{34} + x(\bar{C}_{25}-C_{36}) = C_{23} - yC_{24} + z\bar{C}_{34} + x(C_{25}-\bar{C}_{36}) \end{cases}$$

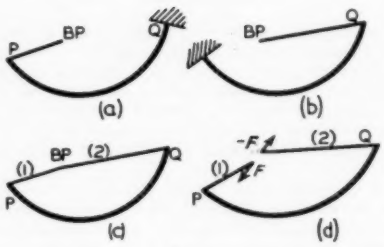

FIG. 2

TANGENTS AND CIRCULAR BENDS

The two principal fundamental elements into which a piping system may be divided are lengths of straight pipe (which will be referred to as "tangents") and plane circular arcs (which will be referred to as "bends"). In this section we present convenient data pertaining to such elements; the results are based on conventional methods of analysis and, as is customary for long, slender structures, neglect axial and cross-shearing deformations in comparison to flexural and torsional deformations.

It should be made clear that these data are not a part of the theory presented in this paper. In so far as the present theory is concerned, the source of the influence-coefficient data is immaterial. Such data could be obtained by alternate and more refined analyses, or by experiment. If it were desired to take into account the flexibility of valves, strainers, and other fittings, specialties, or items of equipment, an experimental determination of the appropriate influence coefficients would seem to be the most direct and accurate way of obtaining the desired information.

Analytic determination of the influence coefficients for spirals, helixes, and other curved elements can most easily be obtained by the method presented in reference (6). The latter method is basically the same as and essentially an outgrowth of the theory presented in this paper.

For tangents, it is convenient to choose the base point *BP* at the middle. Then, under the assumptions mentioned previously, and for orientations parallel to one of the co-ordinate axes, the matrix **C** of self influence coefficients at *BP* has only five nonvanishing elements, and these occur in the principal diagonal. Their values are indicated in Table 2 in which L denotes the length of the tangent, I denotes the second moment of (metallic) cross-sectional area of the pipe with respect to a diametral axis, E denotes the Young's modulus of elasticity at the temperature in question, and 0.3 has been used for Poisson's ratio. (For tangents which are not oriented parallel to a co-ordinate axis, an appropriate L-transformation is required. Further attention will be given this question later in the present section.)

If the tangent is oriented parallel to a co-ordinate axis, the

TABLE 2 NONVANISHING INFLUENCE COEFFICIENTS FOR TANGENTS ORIENTED PARALLEL TO A CO-ORDINATE AXIS

Matrix Element	Orientation: Parallel to: x	y	z
C_{11}	0	$L^3/12EI$	$L^3/12EI$
C_{22}	$L^3/12EI$	0	$L^3/12EI$
C_{33}	$L^3/12EI$	$L^3/12EI$	0
C_{44}	$1.3L/EI$	L/EI	L/EI
C_{55}	L/EI	$1.3L/EI$	L/EI
C_{66}	L/EI	L/EI	$1.3L/EI$

TABLE 3 FORMULAS FOR B-TRANSFORMATIONS FOR TANGENTS ORIENTED PARALLEL TO A CO-ORDINATE AXIS
(See notes accompanying Table 1.)

$$\begin{cases} \bar{c}_{44} = c_{44} \\ \bar{c}_{55} = c_{55} \\ \bar{c}_{66} = c_{66} \end{cases} \quad 3\begin{cases} \bar{c}_{15} = -z\, c_{55} \\ \bar{c}_{16} = y\, c_{66} \\ \bar{c}_{24} = z\, c_{44} \end{cases} \quad 4\begin{cases} \bar{c}_{12} = -x\, \bar{c}_{16} = y\, \bar{c}_{26} \\ \bar{c}_{13} = -z\, \bar{c}_{35} = x\, \bar{c}_{15} \\ \bar{c}_{23} = -y\, \bar{c}_{24} = z\, \bar{c}_{34} \end{cases}$$

$$2\begin{cases} \bar{c}_{45} = \bar{c}_{14} = 0 \\ \bar{c}_{46} = \bar{c}_{36} = 0 \\ \bar{c}_{56} = \bar{c}_{25} = 0 \end{cases} \quad 3\begin{cases} \bar{c}_{26} = -x\, c_{66} \\ \bar{c}_{34} = -y\, c_{44} \\ \bar{c}_{35} = x\, c_{55} \end{cases} \quad 5\begin{cases} \bar{c}_{11} = c_{11} + y\, \bar{c}_{16} - z\, \bar{c}_{15} \\ \bar{c}_{22} = c_{22} + z\, \bar{c}_{24} - x\, \bar{c}_{26} \\ \bar{c}_{33} = c_{33} + x\, \bar{c}_{35} - y\, \bar{c}_{34} \end{cases}$$

TABLE 4 FORMULAS FOR k AND β

R = bend radius
t = wall thickness
r = mean radius of cross section = 0.5(O.D.-t)
$h = tR/r^2$
$m = 12h^2$
$k = (m+10)/(m+1)$
$\beta = (m+10)^{5/6}/9(m+1)$ for $h<1.472$
$\beta = (m-2)/(m+1)$ for $h>1.472$

large number of zeros in the matrix of influence coefficients further simplifies the B-transformation, and the formulas of Table 1 reduce to those of Table 3.

In the case of pipe bends, we encounter four complicating factors. These concern (*a*) the choice of BP, (*b*) the flattening of cross section during bending, (*c*) the presence of inconvenient terms in the matrix, and (*d*) the multiplicity of orientations which may be encountered. In the case of tangents oriented parallel to one of the co-ordinate axes, the base point BP was chosen so as to eliminate all nondiagonal terms of the matrix. We cannot do this for bends. It is, however, possible, in many ways, to eliminate *some* of the nondiagonal terms. On the other hand, choices such as are indicated by the dots in Fig. 3, possess some advantages from the point of view of convenience and geometrical simplicity. For present purposes, we will select the point denoted by the letters BP in Fig. 3. However, it may profit the reader to investigate the convenience which may be brought to his particular application by other choices.

Because of the ability of noncompact cross sections, such as that of a pipe, to warp during bending, the use of elementary flexural theory may be attended by large errors. While, as pointed out in the second paragraph of this section, the present matrix analysis is capable of accommodating highly refined elastic analyses of pipe bends, we will here present only results based on the well-known Kármán-Hovgaard analysis which incorporates a factor k for increased bending flexibility in the plane of the bend and a stress intensification factor β, formulas for which are given in Table 4. The bibliography given in reference (1) cites the classical papers on this subject. More recent work has been done by Pardue, Symonds, and Vigness; reference (11) and its bibliography.

Using only elementary torsion and flexure theory except for the inclusion of the factor k, one may readily obtain the results displayed in Table 5 for the case (hereafter called Case 1) illustrated in Fig. 3. The formulas of Table 5 have been evaluated for the cases $\theta = 45°$, 90°, and 180°; these results are exhibited in Table 6. The letters $A, B, \ldots, L$ which appear in Tables 5 and 6 will be explained later.

We remark that the element C_{66}, while generally small in comparison to the other elements, does not vanish except for particular choices of θ_1 and θ_2. The presence of this term is a source of difficulty in the solution of the final flexibility equations; more will be said of this matter later.

Let us now consider orientations other than that shown in Fig. 3 and denoted as Case 1. In the general case, an L-transformation is evidently required, but if the plane of the bend is parallel to one of the co-ordinate planes, by suitably choosing angles θ_1 and θ_2 we can arrange so that the L-transformation

TABLE 5 INFLUENCE COEFFICIENTS FOR BENDS
(Elements C_{ij} refer to Case 1.)

A $C_{11} = kR^3[0.5(\theta_2 - \theta_1) + 0.25(\sin 2\theta_2 - \sin 2\theta_1)]/EI$
B $C_{12} = -0.25kR^3(\cos 2\theta_2 - \cos 2\theta_1)/EI$
C $C_{16} = -kR^2(\sin \theta_2 - \sin \theta_1)/EI$
D $C_{22} = kR^3[0.5(\theta_2 - \theta_1) - 0.25(\sin 2\theta_2 - \sin 2\theta_1)]/EI$
E $C_{26} = kR^2(\cos \theta_2 - \cos \theta_1)/EI$
F $C_{33} = 1.5R^3(\theta_2 - \theta_1)/EI$
G $C_{34} = 1.5R^2(\sin \theta_2 - \sin \theta_1)/EI$
H $C_{35} = -1.5R^2(\cos \theta_2 - \cos \theta_1)/EI$
I $C_{44} = R[1.15(\theta_2 - \theta_1) + 0.075(\sin 2\theta_2 - \sin 2\theta_1)]/EI$
J $C_{45} = -0.075R(\cos 2\theta_2 - \cos 2\theta_1)/EI$
K $C_{55} = R[1.15(\theta_2 - \theta_1) - 0.075(\sin 2\theta_2 - \sin 2\theta_1)]/EI$
L $C_{66} = k(\theta_2 - \theta_1)/EI$

$C_{21} = C_{12}$; $C_{61} = C_{16}$; $C_{62} = C_{26}$; $C_{43} = C_{34}$; $C_{53} = C_{35}$; $C_{54} = C_{45}$. All other C_{ij} are zero.

TABLE 6 SPECIAL CASES OF INFLUENCE COEFFICIENTS FOR BENDS
(Elements C_{ij} refer to Case 1.)

		$\theta_1=0°$ $\theta_2=45°$	$\theta_1=45°$ $\theta_2=90°$	$\theta_1=0°$ $\theta_2=90°$	$\theta_1=0°$ $\theta_2=180°$	Common Factor
A	C_{11}	0.64270	0.14270	0.78540	1.57080	kR^3/EI
B	C_{12}	0.25000	0.25000	0.50000	0.00000	kR^3/EI
C	C_{16}	−0.70711	−0.29289	−1.00000	0.00000	kR^2/EI
D	C_{22}	0.14270	0.64270	0.78540	1.57080	kR^3/EI
E	C_{26}	−0.29289	−0.70711	−1.00000	−2.00000	kR^2/EI
F	C_{33}	1.02102	1.02102	2.04204	4.08407	kR^3/EI
G	C_{34}	0.91924	0.38076	1.30000	0.00000	R^2/EI
H	C_{35}	0.38076	0.91924	1.30000	2.60000	R^2/EI
I	C_{44}	0.97821	0.82821	1.80642	3.61283	R/EI
J	C_{45}	0.07500	0.07500	0.15000	0.00000	R/EI
K	C_{55}	0.82821	0.97821	1.80642	3.61283	R/EI
L	C_{66}	0.78540	0.78540	1.57080	3.14159	$k\pi/EI$

$C_{21} = C_{12}$; $C_{61} = C_{16}$; $C_{62} = C_{26}$; $C_{43} = C_{34}$; $C_{53} = C_{35}$; $C_{54} = C_{45}$.

amounts merely to an interchange of matrix elements along with certain changes in algebraic sign; the transformation can then be exhibited usefully in the form of a tabulation.

In order to employ this simplification, we introduce an "orientation" symbol to describe the orientation of the bend. The orientation symbol consists of two of the three letters x, y, z in cyclic order, each preceded by a plus or a minus sign. The two letters denote the co-ordinate plane which is parallel to the plane of the bend. The method of determining the algebraic sign is most easily illustrated by means of an example. In Fig. 3 the

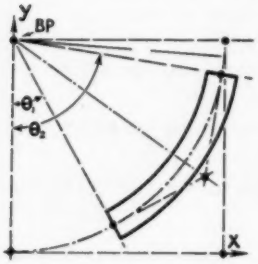

FIG. 3

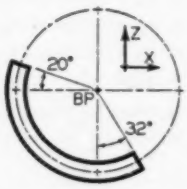

FIG. 4

bend "starts out" in the $+x$-direction (at angle θ_1) and bends toward the $+y$-direction (finishing at angle θ_2); the symbol is $(+x, +y)$. In the case shown in Fig. 4 we can think of the bend "starting out" in the $-z$-direction with $\theta_1 = -20°$ and bending toward the $+x$-direction with $\theta_2 = 122°$; the symbol would be $(-z, +x)$ with $\theta_1 = -20°$, $\theta_2 = 122°$. Likewise, we can arrive at $(-x, -z)$, $\theta_1 = 70°$, $\theta_2 = 212°$; $(-x, +z)$, $\theta_1 = -32°$, $\theta_2 = 110°$, $(-z, -x)$, $\theta_1 = 58°$, $\theta_2 = 200°$; (z, x), $\theta_1 = -122°$, $\theta_2 = 20°$, etc.; several of these symbols would have to be rejected since their letters are not in cyclic order xyz; any one of the remainder is a satisfactory symbol to describe the orientation of the bend shown in Fig. 4.

There are twelve basic cases to consider; with each orientation symbol we associate a case number for convenience. Further to illustrate the selection of the symbol, we show in Fig. 5 the twelve possible orientations of a 90-deg bend both tangents of which are parallel to co-ordinate axes. Shown also are the appropriate orientation symbols (in each case for $\theta_1 = 0$, $\theta_2 = 90°$) and the corresponding case numbers.

Table 7 is a tabulation of the interchanges which take place among the 21 independent elements for each of the twelve cases. Table 8 gives the interchange of the twelve nonvanishing elements $A, B, \ldots, L$ listed in Tables 5 and 6.

These same transformations are also useful in the case of a tangent inclined to all three of the co-ordinate axes but lying in a plane parallel to one of the co-ordinate planes. For Case 1, illustrated in Fig. 6(a), the influence coefficients are given in Table 9 for the general case and for the three special cases $\theta = 30°$, $45°$, and $60°$. It should be noted that the angle θ is measured from the direction of the first signed letter in the orientation symbol, around toward the second, and that each orientation may be described by either of two orientation symbols, and thus can be considered as falling under either of two distinct cases. Thus for the situation of Fig. 6 (b), we may consider the symbols $(y, -z)$ with $\theta = \alpha$; $(-z, y)$ with $\theta = \beta$, $(-y, z)$ with $\theta = \alpha$, and $(z, -y)$ with $\theta = \beta$. The first corresponds to Case 6, the third to Case 7, and the other two are not permissible since the letters are not in cyclic order. Note that the base point BP is at the center of the element.

For purposes of illustration we will now indicate the L-transformation for the case illustrated in Fig. 7 for which the preceding tabular arrangement is not adequate. The tangent is 13 ft long and its projections along the x, y, and z-axes are, respectively, 3, 12, and -4 ft. For the reference S_1 system we choose the ξ-axis along the tangent as illustrated so that $\cos(x, \xi) = 3/13$, $\cos(y, \xi) = 12/13$, and $\cos(z, \xi) = -4/13$. There is freedom in choosing the η- and ζ-axes subject to the condition that S_1: ξ, η, ζ forms a right-handed triad just as S_2: x, y, z does. In

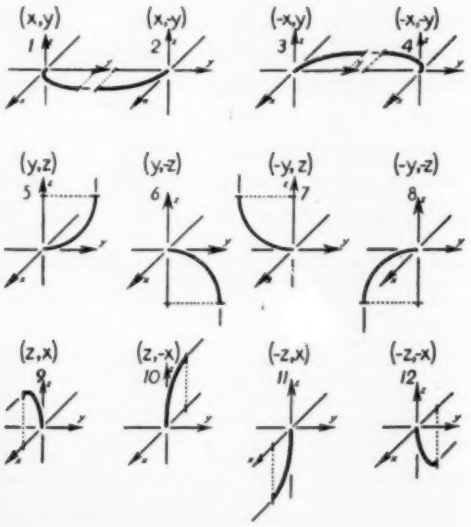

FIG. 5

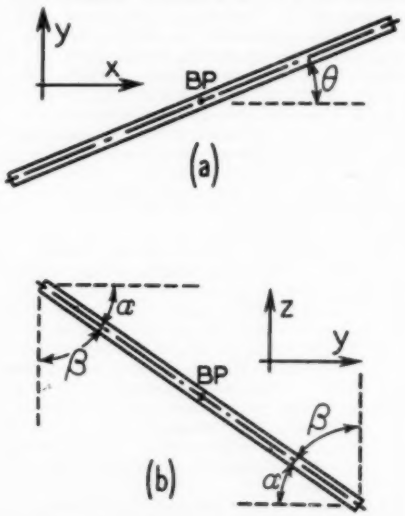

FIG. 6

TABLE 7 INTERCHANGE OF MATRIX ELEMENTS FOR TWELVE BASIC ORIENTATIONS[a]

Case	Symbol	C_{11}	C_{12}	C_{13}	C_{14}	C_{15}	C_{16}	C_{22}	C_{23}	C_{24}	C_{25}	C_{26}	C_{33}	C_{34}	C_{35}	C_{36}	C_{44}	C_{45}	C_{46}	C_{55}	C_{56}	C_{66}
1	(+x,+y)	C_{11}	C_{12}	C_{13}	C_{14}	C_{15}	C_{16}	C_{22}	C_{23}	C_{24}	C_{25}	C_{26}	C_{33}	C_{34}	C_{35}	C_{36}	C_{44}	C_{45}	C_{46}	C_{55}	C_{56}	C_{66}
2	(+x,-y)	C_{11}	$-C_{12}$	$-C_{13}$	C_{14}	$-C_{15}$	$-C_{16}$	C_{22}	C_{23}	$-C_{24}$	C_{25}	C_{26}	C_{33}	$-C_{34}$	C_{35}	C_{36}	C_{44}	$-C_{45}$	$-C_{46}$	C_{55}	C_{56}	C_{66}
3	(-x,+y)	C_{11}	$-C_{12}$	C_{13}	C_{14}	$-C_{15}$	C_{16}	C_{22}	$-C_{23}$	$-C_{24}$	C_{25}	$-C_{26}$	C_{33}	C_{34}	$-C_{35}$	C_{36}	C_{44}	$-C_{45}$	C_{46}	C_{55}	$-C_{56}$	C_{66}
4	(-x,-y)	C_{11}	C_{12}	$-C_{13}$	C_{14}	C_{15}	$-C_{16}$	C_{22}	$-C_{23}$	C_{24}	C_{25}	$-C_{26}$	C_{33}	$-C_{34}$	$-C_{35}$	C_{36}	C_{44}	C_{45}	$-C_{46}$	C_{55}	$-C_{56}$	C_{66}
5	(+y,+z)	C_{33}	C_{13}	C_{23}	C_{36}	C_{34}	C_{35}	C_{11}	C_{12}	C_{16}	C_{14}	C_{15}	C_{22}	C_{26}	C_{24}	C_{25}	C_{66}	C_{46}	C_{56}	C_{44}	C_{45}	C_{55}
6	(+y,-z)	C_{33}	$-C_{13}$	C_{23}	C_{36}	$-C_{34}$	C_{35}	C_{11}	$-C_{12}$	$-C_{16}$	C_{14}	$-C_{15}$	C_{22}	C_{26}	$-C_{24}$	C_{25}	C_{66}	$-C_{46}$	C_{56}	C_{44}	$-C_{45}$	C_{55}
7	(-y,+z)	C_{33}	C_{13}	$-C_{23}$	C_{36}	C_{34}	$-C_{35}$	C_{11}	$-C_{12}$	C_{16}	C_{14}	$-C_{15}$	C_{22}	$-C_{26}$	$-C_{24}$	C_{25}	C_{66}	C_{46}	$-C_{56}$	C_{44}	$-C_{45}$	C_{55}
8	(-y,-z)	C_{33}	$-C_{13}$	$-C_{23}$	C_{36}	$-C_{34}$	$-C_{35}$	C_{11}	C_{12}	$-C_{16}$	C_{14}	C_{15}	C_{22}	$-C_{26}$	C_{24}	C_{25}	C_{66}	$-C_{46}$	$-C_{56}$	C_{44}	C_{45}	C_{55}
9	(+z,+x)	C_{22}	C_{23}	C_{12}	C_{25}	C_{26}	C_{24}	C_{33}	C_{13}	C_{35}	C_{36}	C_{34}	C_{11}	C_{15}	C_{16}	C_{14}	C_{55}	C_{56}	C_{45}	C_{66}	C_{46}	C_{44}
10	(+z,-x)	C_{22}	C_{23}	$-C_{12}$	C_{25}	C_{26}	$-C_{24}$	C_{33}	$-C_{13}$	C_{35}	C_{36}	$-C_{34}$	C_{11}	$-C_{15}$	$-C_{16}$	C_{14}	C_{55}	C_{56}	$-C_{45}$	C_{66}	$-C_{46}$	C_{44}
11	(-z,+x)	C_{22}	$-C_{23}$	$-C_{12}$	C_{25}	$-C_{26}$	$-C_{24}$	C_{33}	C_{13}	$-C_{35}$	C_{36}	C_{34}	C_{11}	$-C_{15}$	C_{16}	C_{14}	C_{55}	$-C_{56}$	$-C_{45}$	C_{66}	C_{46}	C_{44}
12	(-z,-x)	C_{22}	$-C_{23}$	C_{12}	C_{25}	$-C_{26}$	C_{24}	C_{33}	$-C_{13}$	$-C_{35}$	C_{36}	$-C_{34}$	C_{11}	C_{15}	$-C_{16}$	C_{14}	C_{55}	$-C_{56}$	C_{45}	C_{66}	$-C_{46}$	C_{44}

[a] Opposite desired case number and under symbol for desired element find symbol of corresponding element in basic Case 1 preceded by appropriate algebraic sign. Thus C_{34} for Case 10 is negative of C_{13} for Case 1.

TABLE 8 INTERCHANGE OF MATRIX ELEMENTS FOR TWELVE BASIC ORIENTATIONS OF BENDS AND INCLINED TANGENTS[a]
(Refer to Tables 5, 6, 7, and 9.)

Case	Symbol	C_{11}	C_{12}	C_{13}	C_{15}	C_{16}	C_{22}	C_{23}	C_{24}	C_{26}	C_{33}	C_{34}	C_{35}	C_{44}	C_{45}	C_{46}	C_{55}	C_{56}	C_{66}
1	(+x,+y)	A	B	.	.	C	D	.	.	E	F	G	H	I	J	.	K	.	L
2	(+x,-y)	A	-B	.	.	-C	D	.	.	E	F	-G	H	I	-J	.	K	.	L
3	(-x,+y)	A	-B	.	.	C	D	.	.	-E	F	G	-H	I	-J	.	K	.	L
4	(-x,-y)	A	B	.	.	-C	D	.	.	-E	F	-G	-H	I	J	.	K	.	L
5	(+y,+z)	F	.	.	G	H	A	B	C	.	D	E	.	L	.	.	I	J	K
6	(+y,-z)	F	.	.	-G	H	A	-B	-C	.	D	E	.	L	.	.	I	-J	K
7	(-y,+z)	F	.	.	G	-H	A	-B	C	.	D	-E	.	L	.	.	I	-J	K
8	(-y,-z)	F	.	.	-G	-H	A	B	-C	.	D	-E	.	L	.	.	I	J	K
9	(+z,+x)	D	.	B	E	.	F	.	H	G	A	.	C	K	.	J	L	.	I
10	(+z,-x)	D	.	-B	E	.	F	.	H	-G	A	.	-C	K	.	-J	L	.	I
11	(-z,+x)	D	.	-B	-E	.	F	.	-H	G	A	.	C	K	.	-J	L	.	I
12	(-z,-x)	D	.	B	-E	.	F	.	-H	-G	A	.	-C	K	.	J	L	.	I

[a] Opposite desired case number and under symbol for desired element find letter together with algebraic sign giving desired entry. Thus C_{34} in Case 8 is negative of C-value given in Tables 5, 6, or 9. Elements C_{14}, C_{25}, C_{36} are zero.

TABLE 9 INFLUENCE COEFFICIENTS FOR TANGENTS
(Elements C_{ij} refer to Case 1.)

		Formula	$\theta = 30°$	$\theta = 45°$	$\theta = 60°$	Factor
A	C_{11}	$= (\sin^2\theta)/12$	0.02083	0.04167	0.06250	L^3/EI
B	C_{12}	$= -(\sin\theta\cos\theta)/12$	-0.03608	-0.04167	-0.03608	L^3/EI
D	C_{22}	$= (\cos^2\theta)/12$	0.06250	0.04167	0.02083	L^3/EI
F	C_{33}	$= 1/12$	0.08333	0.08333	0.08333	L^3/EI
I	C_{44}	$= 1 + .3\cos^2\theta$	1.22500	1.15000	1.07500	L/EI
J	C_{45}	$= .3\sin\theta\cos\theta$	0.12990	0.15000	0.12990	L/EI
K	C_{55}	$= 1 + .3\sin^2\theta$	1.07500	1.15000	1.22500	L/EI
L	C_{66}	$= 1$	1.00000	1.00000	1.00000	L/EI

$C_{21} = C_{12}$; $C_{54} = C_{45}$; all other elements C_{ij} are zero.

In particular, note that quantities C, E, G, and H are zero.

order to be definite here, we specify that the η-axis shall lie in the y, z-plane; the final results are independent of this specification. Then, by standard procedures, we arrive at the right-handed orthogonal matrix

$$\mathbf{K}_{12} = \begin{bmatrix} 3/13 & 12/13 & -4/13 \\ 0 & 1/\sqrt{10} & 3/\sqrt{10} \\ 40/\sqrt{1690} & -9/\sqrt{1690} & 3/\sqrt{1690} \end{bmatrix}$$

Also, with respect to the S_1 system, the nonvanishing influence coefficients are obtained from Table 2 as follows: $C_{22} = C_{33} = 316368/EI$, $C_{44} = 202.8/EI$, $C_{55} = C_{66} = 156/EI$, where we use inches as our unit and note that 13 ft equals 156 in. Writing

$$\mathbf{C}_1 = \begin{bmatrix} \mathbf{A}_1 & \mathbf{O} \\ \mathbf{O} & \mathbf{B}_1 \end{bmatrix}, \quad \mathbf{L}_{12} = \begin{bmatrix} \mathbf{K}_{12} & \mathbf{O} \\ \mathbf{O} & \mathbf{K}_{12} \end{bmatrix}$$

we easily see that

$$\mathbf{C}_2 = \tilde{\mathbf{L}}_{12}\mathbf{C}_1\mathbf{L}_{12} = \begin{bmatrix} \tilde{\mathbf{K}}_{12}\mathbf{A}_1\mathbf{K}_{12} & \mathbf{O} \\ \mathbf{O} & \tilde{\mathbf{K}}_{12}\mathbf{B}_1\mathbf{K}_{12} \end{bmatrix} = \begin{bmatrix} \mathbf{A}_2 & \mathbf{O} \\ \mathbf{O} & \mathbf{B}_2 \end{bmatrix}$$

Actually carrying out the computations yields

$$\mathbf{C}_2 = \begin{bmatrix} 299520 & -67392 & 22464 & 0 & 0 & 0 \\ -67392 & 46800 & 89856 & 0 & 0 & 0 \\ 22464 & 89856 & 286416 & 0 & 0 & 0 \\ 0 & 0 & 0 & 158.492 & 9.969 & -3.323 \\ 0 & 0 & 0 & 9.969 & 195.877 & -13.292 \\ 0 & 0 & 0 & -3.323 & -13.292 & 160.431 \end{bmatrix} \div EI$$

This is the matrix of influence coefficients for the tangent shown in Fig. 7, with respect to the S_2-system. A greater number of digits has been given in the foregoing than is customarily called for; this gives the reader a chance to check the calculation.

Applications

(*a*) *The Two-Anchor Problem Without Constraints.* In Fig. 8 the pipe AB is presumed to be made up of elements for which we know the influence coefficients at the corresponding base points with respect to a convenient x, y, z-system which will be used throughout this section of the present analysis. Let $\mathbf{C}_i$ be the influence coefficient matrix for the ith element $P_{i-1}P_i$, the corresponding base point being p_i. Then, using Equation [9], the contribution of the flexibility of this ith element alone to the flexibility matrix at B is given by $\tilde{\mathbf{B}}_{p_iB}\mathbf{C}_i\mathbf{B}_{p_iB}$.[3] Thus, for the entire line AB, the flexibility matrix at B is given by

$$\mathbf{\Delta} = \sum_i \tilde{\mathbf{B}}_{p_iB}\mathbf{C}_i\mathbf{B}_{p_iB} \quad \ldots\ldots\ldots\ldots\ldots\ldots [10]$$

the summation extending over all the elements comprising the line AB.

Let U be a point of the building structure or mechanical equipment to which piping is connected and let the column matrix $\mathbf{M}_U = [M_{U1}, \ldots, M_{U6}]$ represent the components of displacement which would be suffered by point U if the piping were absent or did not impose any forces on the structure or equipment at U, i.e., $\mathbf{M}_U$ is the matrix of free expansions at point U. Let V and W be any two points, let H be the unit expansion (co-

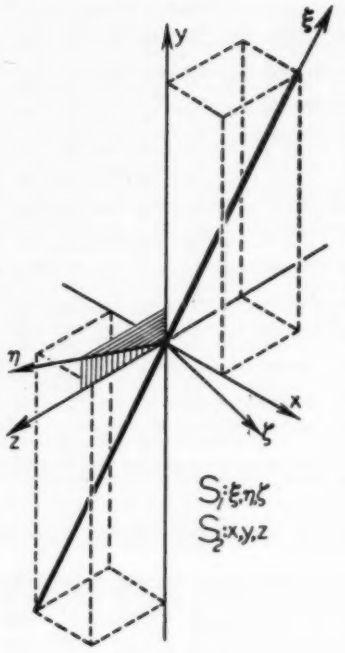

FIG. 7

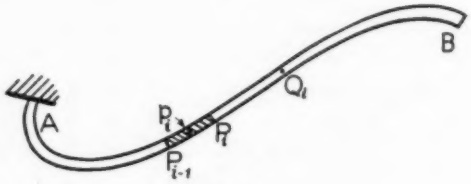

FIG. 8

[3] Here and later, when subscripts themselves possess subscripts, typographical limitations require that they be printed on the same horizontal level. Accordingly, some care is called for to avoid misinterpretations. Later, when superscripts are introduced and subscripts are encountered which possess superscripts, similar care is required.

efficient of linear expansion per degree times temperature change in degrees) of the piping material, and let the column matrix $\mathbf{N}_{VW} = H\{(x_V - x_W), (y_V - y_W), (z_V - z_W), 0, 0, 0\}$ represent the motion of point V relative to point W due to thermal expansion. (If more than one value of H applies, the definition of $\mathbf{N}_{VW}$ is modified in an obvious way.)

We will also use the following notion and notation: If a pipe is connected at point U to structure or equipment, we will use the letter U to refer to the point on the pipe and the overlined letter $\overline{U}$ to refer to the point on the structure. If the connection is maintained, the motion of U must correspond to that of $\overline{U}$ to an extent which depends upon the nature and rigidity of the connection.

For the first application of the theory, consider the problem of a two-anchor configuration AB with perfect fixity at A and B and with no intermediate constraints. (Our preparation so far has contemplated perfect fixity at A.) Relative to point A, the motion of B is $\mathbf{M}_B - \mathbf{M}_A$, while, relative to point A, the motion of B is $\mathbf{N}_{BA}$ due to thermal expansion and $\mathbf{\Delta F}$ owing to the reactive forces applied *to the pipe* at B. Since there is fixity at B, we have $\mathbf{\Delta F} + \mathbf{N}_{BA} = \mathbf{M}_B - \mathbf{M}_A$. By defining

$$\mathbf{D} = -\mathbf{N}_{BA} + \mathbf{M}_B - \mathbf{M}_A \quad [11]$$

we are led to the fundamental matrix equation

$$\mathbf{\Delta F} = \mathbf{D} \quad [12]$$

which, in effect, amounts to six equations in the six unknown components of $\mathbf{F}$. These equations are

$$\begin{aligned} \Delta_{11}F_1 + \Delta_{12}F_2 + \ldots + \Delta_{16}F_6 &= D_1 \\ \Delta_{21}F_1 + \Delta_{22}F_2 + \ldots + \Delta_{26}F_6 &= D_2 \\ \ldots\ldots\ldots\ldots\ldots\ldots\ldots\ldots\ldots\ldots \\ \Delta_{61}F_1 + \Delta_{62}F_2 + \ldots + \Delta_{66}F_6 &= D_6 \end{aligned}$$

In the general case, the method of P. D. Crout (12) is the best method of handling six equations in six unknowns. However, under certain circumstances (which incidentally are always met in the case of a system composed only of tangents oriented parallel to the x, y, z-axes), the coefficients Δ_{14}, Δ_{24}, Δ_{34}, Δ_{45}, Δ_{46}, Δ_{56} all vanish. Since usually $D_4 = D_5 = D_6 = 0$, it is advantageous to solve the last three equations for F_4, F_5, and F_6 in terms of F_1, F_2, F_3, and upon substituting into the first three, to solve the resulting system of three equations in three unknowns. It is this simplification which was alluded to in the preceding section in discussing the complications introduced by bends. There we saw that in Case 1 the coefficient C_{46} did not vanish. For other orientations, coefficients C_{45} or C_{56} would fail to vanish. Such terms, contributing to the matrix $\mathbf{\Delta}$, would prevent taking advantage of the procedure just described. This procedure of reducing the "number of degrees of freedom from six to three" is not uncommon among the well-known methods of flexibility analysis.

If the equipment to which the piping connects at A is itself flexible with matrix $\mathbf{C}_A$, this flexibility may be taken into account by adding to $\mathbf{\Delta}$ as given by Equation [10], the term $\bar{\mathbf{B}}_{AB}\mathbf{C}_A\mathbf{B}_{AB}$. If the equipment at B is flexible with matrix $\mathbf{C}_B$, we can take this into account by adding the term $\mathbf{C}_B$ to $\mathbf{\Delta}$ as given by Equation [10]. The correction for flexibility at A is obvious; that for flexibility at B involves the following reasoning: The forces $-\mathbf{F}$ applied by AB to $\overline{B}$ cause additional deflections $-\mathbf{C}_B\mathbf{F}$ of $\overline{B}$. Then $\mathbf{\Delta F} = \mathbf{D} - \mathbf{C}_B\mathbf{F}$ or $(\mathbf{\Delta} + \mathbf{C}_B)\mathbf{F} = \mathbf{D}$. Henceforth we presume that the symbol $\mathbf{\Delta}$ includes not only the terms given in Equation [10], but also the correction terms $\bar{\mathbf{B}}_{AB}\mathbf{C}_A\mathbf{B}_{AB}$ and $\mathbf{C}_B$ if they apply. (One should note that $\mathbf{C}_B$ is computed with respect to the same x, y, z-system at B that we started with; there seems to be a temptation to reverse the senses of these axes in computing $\mathbf{C}_B$.)

(*b*) *The Two-Anchor Problem With Constraints.* Let us now suppose that there are n-constraints $J_1, \ldots, J_n$ at points $Q_1, \ldots, Q_n$ (not necessarily distinct) along AB. The nature of these J-constraints is such that the constraint J_i offers no resistance to any motion except in the (generalized) J_i-direction to which it offers a resistance with spring "compliance" k_i (a constant). More precisely, let the J_i-axis have direction cosines $u_i = \cos(x, J_i)$, $v_i = \cos(y, J_i)$, and $w_i = \cos(z, J_i)$. Let $\mathbf{u}_i = \{w_i, v_i, w_i\}$, and let the 6×1 column matrix $\mathbf{v}_i$ be defined by $\{\mathbf{u}_i, \mathbf{O}\}$ if "motion in the J_i-direction" means translation along the (positive) J_i-axis, and by $\{\mathbf{O}, \mathbf{u}_i\}$ if motion in the J_i-direction means rotation (in the positive sense) about the J_i-axis. Then the J_i-constraint is such that if a generalized displacement $\mathbf{D} = \{D_1, \ldots, D_6\}$ is imposed upon the constraint so that the J_i displacement is $\mathbf{v}_i\mathbf{D}$, the constraint will exert a resistance (in the negative J_i-direction) of magnitude $\mathbf{v}_i\mathbf{D}/k_i$.

The J_i-constraint results in the application by the constraint upon the pipe of a reactive force G_i in the J_i-direction, and an equal and opposite force applied by the pipe to the constraint. We are concerned with determining the six components $F_1, \ldots, F_6$ applied at B and the n-reactive forces $G_1, \ldots, G_n$ applied at $Q_1, \ldots, Q_n$, respectively, which cause displacements at B and $Q_1, \ldots, Q_n$ consistent with the thermal expansion of the pipe and the prescribed motion of these points. Let

$$\left.\begin{aligned} e_{ij} &= i\text{-defl at } B \text{ due to a unit } J_j\text{-force at } Q_j \\ &= J_j\text{-defl at } Q_j \text{ due to a unit } i\text{-force at } B \end{aligned}\right\} \quad \begin{aligned} (i &= 1, \ldots, 6) \\ (j &= 1, \ldots, n) \end{aligned}$$

$g_{ij} = J_i$-defl at Q_i due to a unit J_j-force at Q_j
$(i, j = 1, \ldots, n)$

The structure referred to is the line AB presumed rigidly fixed at A and otherwise free.* The reciprocal theorems give the alternate definitions of e_{ij} and also assert that $g_{ij} = g_{ji}$.

Introduce the notations

$$\begin{aligned} \mathbf{G} &= \{G_1, \ldots, G_n\} \\ \mathbf{F}^* &= \{\mathbf{F}, \mathbf{G}\} \\ \mathbf{h} &= [g_{ij}] + \text{diag}\,\{k_1, \ldots, k_n\}\ (i, j = 1, \ldots, n) \\ \mathbf{e} &= [e_{ij}]\ (i = 1, \ldots, 6;\ j = 1, \ldots, n) \\ d_i &= \mathbf{v}_i(-\mathbf{N}_{Q_iA} + \mathbf{M}_{Q_i} - \mathbf{M}_A) \\ \mathbf{d} &= \{d_1, \ldots, d_n\} \\ \mathbf{D}^* &= \{\mathbf{D}, \mathbf{d}\} \text{ (see Equation [11])} \\ \mathbf{\Delta}^* &= \begin{bmatrix} \mathbf{\Delta} & \mathbf{e} \\ \bar{\mathbf{e}} & \mathbf{h} \end{bmatrix} \end{aligned}$$

By equating all six components of motion of B and $\overline{B}$, we are led to the matrix equation

$$\mathbf{\Delta F} + \mathbf{eG} = \mathbf{D} \quad [13]$$

By equating the J_i-motions of Q_i and $\overline{Q}_i$, we are led to the scalar equation

$$\sum_{j=1}^{6} e_{ji}F_j + \sum_{j=1}^{n} g_{ij}G_j + \mathbf{v}_i\bar{\mathbf{N}}_{Q_iA} = \mathbf{v}_i(\mathbf{M}_{Q_i} - \mathbf{M}_A) - G_ik_i$$

and the n-equations of this type may be combined into the single matrix equation

$$\bar{\mathbf{e}}\mathbf{F} + \mathbf{hG} = \mathbf{d} \quad [14]$$

Finally, Equations [13] and [14] may be combined into the single matrix equation

$$\mathbf{\Delta}^*\mathbf{F}^* = \mathbf{D}^* \quad [15]$$

which amounts to $6 + n$ equations in as many unknowns. Again, the method of P. D. Crout (12) is recommended.

It remains only to describe the calculation of the $6n$-quantities e_{ij} and the n^2-quantities g_{ij}. Let $\mathbf{\Delta}_{Q_i}$ denote the contribution to $\mathbf{\Delta}$ of only those elements of AB which lie between A and Q_i; this should include the term $\bar{\mathbf{B}}_{AB}\mathbf{C}_A\mathbf{B}_{AB}$ if the equipment at A is flexible. Then $\mathring{\mathbf{\Delta}}_{Q_i} = \bar{\mathbf{B}}_{BQ_i}\mathbf{\Delta}_{Q_i}\mathbf{B}_{BQ_i}$ represents the matrix at point Q_i of the portion Q_iA. Now the matrix $\mathbf{v}_i$ may be considered to represent the components with respect to an x, y, z-system at Q_i of a unit J_i-force at Q_i. Then the column matrix $\mathring{\mathbf{\Delta}}_{Q_i}\mathbf{v}_i$ gives the deflections at Q_i due to a unit J_i-force applied to the piping at Q_i. Since we may easily show that $\bar{\mathbf{B}}_{Q_iB}\bar{\mathbf{B}}_{BQ_i} = \mathbf{I}$, we find the corresponding deflections at B to be

$$\left.\begin{aligned}\mathbf{e}_i &= \{e_{1i}, \ldots, e_{6i}\} = \bar{\mathbf{B}}_{Q_iB}\mathring{\mathbf{\Delta}}_{Q_i}\mathbf{v}_i = \bar{\mathbf{B}}_{Q_iB}\bar{\mathbf{B}}_{BQ_i}\mathbf{\Delta}_{Q_i}\mathbf{B}_{BQ_i}\mathbf{v}_i \\ &= \mathbf{\Delta}_{Q_i}\mathbf{B}_{BQ_i}\mathbf{v}_i = \mathbf{\Delta}_{Q_i}\mathbf{r}_i\end{aligned}\right\} \ldots [16]$$

where

$$\mathbf{r}_i = \mathbf{B}_{BQ_i}\mathbf{v}_i \ldots [17]$$

is an easily computed column matrix. Thus

$$e_{ij} = (\mathbf{\Delta}_{Q_j}\mathbf{r}_j)_i \ldots [18]$$

that is, the ith component of the column matrix $\mathbf{\Delta}_{Q_j}\mathbf{r}_j$.

In computing the numbers g_{ij} we must distinguish two cases (a) Q_j lies on the segment AQ_i, and (b) Q_i lies on the segment AQ_j, Fig. 9. We wish to determine the J_i-deflection at Q_i due to a unit J_j-force at Q_j. In either case the column matrix $\mathbf{v}_j$ represents the components in an x, y, z-system at Q_j of the unit J_j-force at Q_j. In case (a), the deflections at Q_j are $\mathring{\mathbf{\Delta}}_{Q_j}\mathbf{v}_j$. Since the portion Q_jQ_i is unstrained, these transform according to Equation [3] to give $\bar{\mathbf{B}}_{Q_jQ_i}\mathring{\mathbf{\Delta}}_{Q_j}\mathbf{v}_j$ as the actual corresponding deflections at Q_i. We may write this as

$$\bar{\mathbf{B}}_{Q_jQ_i}\bar{\mathbf{B}}_{BQ_j}\mathbf{\Delta}_{Q_j}\mathbf{B}_{BQ_j}\mathbf{v}_j = \overbrace{(\mathbf{B}_{BQ_j}\mathbf{B}_{Q_jQ_i})}\,\mathbf{\Delta}_{Q_j}\mathbf{B}_{BQ_j}\mathbf{v}_j = \bar{\mathbf{B}}_{BQ_i}\mathbf{\Delta}_{Q_j}\mathbf{B}_{BQ_j}\mathbf{v}_j$$

since it may easily be shown that the matrix $\mathbf{B}_{UV}$ is transitive, i.e., that $\mathbf{B}_{UV}\mathbf{B}_{VW} = \mathbf{B}_{UW}$. Now consider case ($b$); the unit J_j-

FIG. 9

force at Q_j becomes $\mathbf{v}_j$ in an x, y, z-system at Q_i. The (elastic) lever Q_jQ_i transmits this force according to Equation [2] so that the forces at Q_i are $\mathbf{B}_{Q_iQ_j}\mathbf{v}_j$ and the corresponding deflections at Q_i are $\mathring{\mathbf{\Delta}}_{Q_i}\mathbf{B}_{Q_iQ_j}\mathbf{v}_j = \bar{\mathbf{B}}_{BQ_i}\mathbf{\Delta}_{Q_i}\mathbf{B}_{BQ_j}\mathbf{B}_{Q_iQ_j}\mathbf{v}_j = \bar{\mathbf{B}}_{BQ_i}\mathbf{\Delta}_{Q_i}\mathbf{B}_{BQ_j}\mathbf{v}_j$. This formula differs from that holding for case (a) only in the subscript on the matrix $\mathbf{\Delta}$. If we define

$$\mathbf{\Delta}_{Q_{ij}} = \mathbf{\Delta}_{Q_{ji}} = \left\{\begin{array}{l}\mathbf{\Delta}_{Q_i} \text{ if } Q_i \text{ lies on are } AQ_j \\ \mathbf{\Delta}_{Q_j} \text{ if } Q_j \text{ lies on are } AQ_i\end{array}\right\} \ldots [19]$$

both formulas become $\bar{\mathbf{B}}_{BQ_i}\mathbf{\Delta}_{Q_{ij}}\mathbf{B}_{BQ_j}\mathbf{v}_j$. Finally, the J_i-component of this deflection is $\mathbf{v}_i'\bar{\mathbf{B}}_{BQ_i}\mathbf{\Delta}_{Q_{ij}}\mathbf{B}_{BQ_j}\mathbf{v}_j$, and employing the notation of Equation [17] we have

$$g_{ij} = \mathbf{r}_i'\mathbf{\Delta}_{Q_{ij}}\mathbf{r}_j \ldots [20]$$

which obviously is symmetrical.

(*c*) *The Multiple-Anchor Problem With Constraints.* We confine our attention to the case illustrated in Fig. 10 where all the branches meet at a common point B. There are $m + 1$ branches originating from points $A_0, A_1, \ldots, A_m$. The ith branch, A_iB,

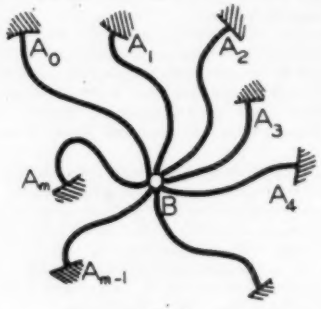

FIG. 10

contains n_i J-constraints as discussed in the preceding subsection. The number of unknown forces is $6(m + 1) + \sum_{i=0}^{m} n_i$. To find them we have $6m + \sum_{i=0}^{m} n_i$ equations of elasticity plus six equations of statics. It is advantageous in practice to forego the mathematical parallelism that could be maintained in the analysis of the various branches, and by regarding one branch, say, A_0B as "basic," to incorporate the six conditions of statics and reduce by six the number of unknowns in the system. This attitude was implicit in the two preceding subsections.

We will let subscripts play the rôle they have played previously and use superscripts to distinguish among the several branches. Let x, y, z be a convenient orientation of axes which will be used throughout this development.

Let $\mathbf{D}_U = -\mathbf{N}_{UA_0} + \mathbf{M}_U - \mathbf{M}_{A_0}$ using notations introduced previously. For simplicity, write $\mathbf{D}^i = \mathbf{D}_{A_i}$. Note the special role of point A_0. Let $d_i{}^j = \mathbf{v}_i'\mathbf{D}_{Q_i}{}^j - G_i{}^jk_i{}^j$. In the following definitions the structure involved is the entire configuration of Fig. 10 freed at all points $A_i (i = 1, \ldots, m)$ and $Q_i{}^j (i = 1, \ldots, n_j; j = 0, 1, \ldots, m)$ but maintaining the connection at A_0. Then let

$\Delta_{ij}{}^{kl} = i$-defl at A_k due to a unit j-force at A_l $(i, j = 1, \ldots, 6; k, l = 1, \ldots, m)$

$e_{ij}{}^{kl} = i$-defl at A_k due to a unit $J_j{}^l$-force at $Q_j{}^l$ $= J_i{}^l$-defl at $Q_i{}^l$ due to a unit i-force at A_k $(i = 1, \ldots, 6; j = 1, \ldots, n_l; k = 1, \ldots, m; l = 0, 1, \ldots, m)$

$g_{ij}{}^{kh} = g_{ji}{}^{hk} = J_i{}^k$-defl at $Q_i{}^k$ due a unit $J_j{}^h$-force at $Q_j{}^h$ $(i = 1, \ldots, n_k; j = 1, \ldots, n_h; k, l = 0, 1, \ldots, m)$

Also, define

$F_i{}^j =$ induced reactive i-force on piping at A_j $(i = 1, \ldots, 6; j = 1, \ldots, m)$

$G_i{}^j =$ induced reactive $J_i{}^j$-force at $Q_i{}^j$ $(i = 1, \ldots, n_j; j = 0, 1, \ldots, m)$

Then for the i-deflection at A_k, we have

$$\sum_{l=1}^{m}\sum_{j=1}^{6}\Delta_{ij}{}^{kl}F_j{}^l + \sum_{l=0}^{m}\sum_{j=1}^{nl}e_{ij}{}^{kl}G_j{}^l = (\mathbf{D}^k)_i$$
$$(i = 1, \ldots 6;\ k = 1, \ldots, m) \ldots [21]$$

the last symbol denoting the ith component of $\mathbf{D}^k$. Similarly, for the $J_s{}^k$ deflection at $Q_s{}^k$ we have

$$\sum_{l=1}^{m}\sum_{j=1}^{nl} e_{ij}{}^{kl}F_j{}^l + \sum_{l=0}^{m}\sum_{j=1}^{nl} g_{ij}{}^{kl}\,G_j{}^l = d_i{}^k$$
$$(k = 0, 1, \ldots, m;\ i = 1, \ldots, n_k) \quad [22]$$

Introducing the notations

$\mathbf{G}^l = \{G_1{}^l, G_2{}^l, \ldots, G_{nl}{}^l\}$ (n_l rows, one column)
$\mathbf{F}^l = \{F_1{}^l, F_2{}^l, \ldots, F_6{}^l\}$ (6 rows, one column)
$\mathbf{\Delta}^{kl} = [\Delta_{ij}{}^{kl}]$ (6 rows, 6 columns)
$\mathbf{e}^{kl} = [e_{ij}{}^{kl}]$ (6 rows, n_l columns)
$\mathbf{g}^{kl} = [g_{ij}{}^{kl}]$ (n_k rows, n_l columns)
$\mathbf{d}^k = \{d_1{}^k, d_2{}^k, \ldots, d_{nk}{}^k\}$ (n_k rows, one column)

we can rewrite Equations [21] and [22] as

$$\sum_{l=1}^{m}\mathbf{\Delta}^{kl}\mathbf{F}^l + \sum_{l=0}^{m}\mathbf{e}^{kl}\mathbf{G}^l = \mathbf{D}^k \quad [23]$$

$$\sum_{l=1}^{m}\mathbf{e}^{kl}\mathbf{F}^l + \sum_{l=0}^{m}\mathbf{g}^{kl}\mathbf{G}^l = \mathbf{d}^k \quad [24]$$

Next, introduce the partitioned matrices

$\bar{\mathbf{D}} = \{\mathbf{D}^1, \mathbf{D}^2, \ldots, \mathbf{D}^m\}$ (m rows, one column)
$\bar{\mathbf{d}} = \{\mathbf{d}^0, \mathbf{d}^1, \ldots, \mathbf{d}^m\}$ ($m + 1$ rows, one column)
$\bar{\mathbf{F}} = \{\mathbf{F}^1, \mathbf{F}^2, \ldots, \mathbf{F}^m\}$ (m rows, one column)
$\bar{\mathbf{G}} = \{\mathbf{G}^0, \mathbf{G}^1, \ldots, \mathbf{G}^m\}$ ($m + 1$ rows, one column)

$$\bar{\mathbf{\Delta}} = \begin{bmatrix} \mathbf{\Delta}^{11} & \mathbf{\Delta}^{12} & \ldots & \mathbf{\Delta}^{1m} \\ \mathbf{\Delta}^{21} & \mathbf{\Delta}^{22} & \ldots & \mathbf{\Delta}^{2m} \\ \cdot & \cdot & \ldots & \cdot \\ \cdot & \cdot & \ldots & \cdot \\ \cdot & \cdot & \ldots & \cdot \\ \mathbf{\Delta}^{m1} & \mathbf{\Delta}^{m2} & \ldots & \mathbf{\Delta}^{mm} \end{bmatrix} \quad (m \text{ rows, } m \text{ columns})$$

$$\bar{\mathbf{e}} = \begin{bmatrix} \mathbf{e}^{10} & \mathbf{e}^{11} & \ldots & \mathbf{e}^{1m} \\ \mathbf{e}^{20} & \mathbf{e}^{21} & \ldots & \mathbf{e}^{2m} \\ \cdot & \cdot & \ldots & \cdot \\ \cdot & \cdot & \ldots & \cdot \\ \cdot & \cdot & \ldots & \cdot \\ \mathbf{e}^{m0} & \mathbf{e}^{m1} & \ldots & \mathbf{e}^{mm} \end{bmatrix} \quad (m \text{ rows, } m + 1 \text{ columns})$$

$$\bar{\mathbf{g}} = \begin{bmatrix} \mathbf{g}^{00} & \mathbf{g}^{01} & \ldots & \mathbf{g}^{0m} \\ \mathbf{g}^{10} & \mathbf{g}^{11} & \ldots & \mathbf{g}^{1m} \\ \cdot & \cdot & \ldots & \cdot \\ \cdot & \cdot & \ldots & \cdot \\ \cdot & \cdot & \ldots & \cdot \\ \mathbf{g}^{m0} & \mathbf{g}^{m1} & \ldots & \mathbf{g}^{mm} \end{bmatrix} \quad (m + 1 \text{ rows, } m + 1 \text{ columns})$$

Then, we can write Equations [23] and [24] in the form

$$\begin{bmatrix} \bar{\mathbf{\Delta}} & \bar{\mathbf{e}} \\ (\bar{\mathbf{e}}) & \bar{\mathbf{g}} \end{bmatrix}\begin{bmatrix} \bar{\mathbf{F}} \\ \bar{\mathbf{G}} \end{bmatrix} = \begin{bmatrix} \bar{\mathbf{D}} \\ \bar{\mathbf{d}} \end{bmatrix} \quad [25]$$

Next let

$\mathbf{k}^l = \text{diag } \{k_1{}^l, \ldots, k_{nl}{}^l\}$
$\bar{\mathbf{k}} = \text{diag } \{\mathbf{k}^0, \mathbf{k}^1, \ldots, \mathbf{k}^m\}$
$\bar{\mathbf{d}}^* = \bar{\mathbf{d}} + \bar{\mathbf{k}}\bar{\mathbf{G}}$
$\bar{\mathbf{h}} = \bar{\mathbf{g}} + \bar{\mathbf{k}}$

and we can write Equation [25] in the form

$$\begin{bmatrix} \bar{\mathbf{\Delta}} & \bar{\mathbf{e}} \\ (\bar{\mathbf{e}}) & \bar{\mathbf{h}} \end{bmatrix}\begin{bmatrix} \bar{\mathbf{F}} \\ \bar{\mathbf{G}} \end{bmatrix} = \begin{bmatrix} \bar{\mathbf{D}} \\ \bar{\mathbf{d}}^* \end{bmatrix} \quad [26]$$

where $\bar{\mathbf{d}}^*$ does not depend upon the unknowns $G_i{}^l$ as did $\mathbf{d}$. Finally, letting

$$\bar{\mathbf{\Delta}}^* = \begin{bmatrix} \bar{\mathbf{\Delta}} & \bar{\mathbf{e}} \\ (\bar{\mathbf{e}}) & \bar{\mathbf{h}} \end{bmatrix},\ \bar{\mathbf{F}}^* = \begin{bmatrix} \bar{\mathbf{F}} \\ \bar{\mathbf{G}} \end{bmatrix},\ \bar{\mathbf{D}}^* = \begin{bmatrix} \bar{\mathbf{D}} \\ \bar{\mathbf{d}}^* \end{bmatrix}$$

we arrive at the final equation

$$\bar{\mathbf{\Delta}}^*\bar{\mathbf{F}}^* = \bar{\mathbf{D}}^* \quad [27]$$

We must still show how to calculate the numbers $\Delta_{ij}{}^{kl}$, $e_{ij}{}^{kl}$, and $g_{ij}{}^{kl}$. Denote by $\mathbf{\Delta}_s (i = 0, 1, \ldots, m)$ the matrix of influence coefficients at B of the branch A_sB presumed restrained at A_s and otherwise free. By the concluding observations of the section, "Basic Theory," we note that $\bar{\mathbf{B}}_{BAi}\mathbf{\Delta}_s\mathbf{B}_{BAi}$ then denotes the matrix at A_i of the branch A_sB presumed fixed at B and otherwise free. This matrix $\mathbf{\Delta}_s$ is calculated just as was the matrix $\mathbf{\Delta}$ in the two-anchor problem without constraints. Then, forces $\mathbf{F}^l$ at A_l cause forces $\mathbf{B}_{BAl}\mathbf{F}^l$ to be applied by the (flexible) lever A_lB to the line BA_0, and due to the distortion of BA_0, point B experiences deflections $\mathbf{\Delta}_0\mathbf{B}_{BAl}\mathbf{F}^l$. Thus, due only to the distortion of BA_0, point A_k experiences deflections $\bar{\mathbf{B}}_{BAk}\mathbf{\Delta}_0\mathbf{B}_{BAl}\mathbf{F}^l$. If $A_k \neq A_l$, portion A_kB is undistorted and these are the total deflections of A_k. If, however, $A_k = A_l$, the distortion in the branch A_lB causes A_l to suffer additional displacements $\bar{\mathbf{B}}_{BAl}\mathbf{\Delta}_l\mathbf{B}_{BAl}\mathbf{F}^l$. Thus

$$\mathbf{\Delta}^{kl} = \bar{\mathbf{B}}_{BAk}\mathbf{\Delta}_0\mathbf{B}_{BAl}\ (k \neq l) \quad [28]$$

$$\mathbf{\Delta}^{ll} = \bar{\mathbf{B}}_{BAl}(\mathbf{\Delta}_0 + \mathbf{\Delta}_l)\mathbf{B}_{BAl} \quad [29]$$

The components $\Delta_{ij}{}^{kl}$ are the elements of these matrices.

By similar arguments which are omitted here for brevity, we can obtain the numbers $e_{ij}{}^{kl}$ and $g_{ij}{}^{kl}$. It is useful to introduce the following notations: Let $\mathbf{\Delta}_{Q_i}{}^k$ denote the contribution of the portion Q_iA_k of the branch BA_k to the matrix $\mathbf{\Delta}_k$ (introduced previously) at B. Let $\mathbf{\Delta}_{Q_ij}{}^k$ denote the contribution of the "shorter" and $\mathbf{\Delta}^*{}_{Q_ij}{}^k$ the contribution of the "longer" of the two portions Q_iA_k and Q_jA_k of the branch BA_k (for both points Q falling on the same branch) to the matrix $\mathbf{\Delta}_k$. Then we can show that

$$e_{ij}{}^{kl} = (\bar{\mathbf{B}}_{BAk}\mathbf{\Delta}_{Q_j}{}^0\mathbf{r}_j{}^0)_i \quad [30a]$$
$$(i = 1, \ldots, 6;\ k = 1, \ldots, m;\ j = 1, \ldots, n_0)$$

$$e_{ij}{}^{kl} = (\bar{\mathbf{B}}_{BAk}\mathbf{\Delta}_{Ql}\mathbf{r}_j{}^l)_i \quad [30b]$$
$$(i = 1, \ldots, 6;\ k, l = 1, \ldots, m;\ k \neq l;\ j = 1, \ldots, n_l)$$

$$e_{ij}{}^{kk} = (\bar{\mathbf{B}}_{BAk}(\mathbf{\Delta}_0 + \mathbf{\Delta}_k - \mathbf{\Delta}_{Q_j}{}^k)\mathbf{r}_j{}^k)_i \quad [30c]$$
$$(i = 1, \ldots, 6;\ k = 1, \ldots, m;\ j = 1, \ldots, n_k)$$

$$g_{ij}{}^{00} = \mathbf{f}_i{}^0\mathbf{\Delta}_{Q_ij}{}^0\mathbf{r}_j{}^0 \quad [31a]$$
$$(i, j = 1, \ldots, n_0)$$

$$g_{ij}{}^{k0} = \mathbf{f}_i{}^k\mathbf{\Delta}_{Q_j}{}^0\mathbf{r}_j{}^0 \quad [31b]$$
$$(i = 1, \ldots, n_k;\ j = 1, \ldots, n_0;\ k = 1, \ldots, m)$$

$$g_{ij}{}^{kl} = \mathbf{f}_i{}^k\mathbf{\Delta}_{Ql}\mathbf{r}_j{}^l \quad [31c]$$
$$(i = 1, \ldots, n_k;\ j = 1, \ldots, n_l;\ k, l = 1, \ldots m;\ k \neq l)$$

$$g_{ij}{}^{kk} = \mathbf{f}_i{}^k(\mathbf{\Delta}_0 + \mathbf{\Delta}_k - \mathbf{\Delta}^*{}_{Q_ij}{}^k)\mathbf{r}_j{}^k \quad [31d]$$
$$(i, j = 1, \ldots, n_k;\ k = 1, \ldots m)$$

The derivations which are similar to those evaluating $\Delta_{ij}{}^{kl}$ are omitted for the sake of brevity. Here $\mathbf{r}_j{}^k$ is an obvious extension of the notation introduced in Equation [17].

Example

To indicate the sort of procedure which may be followed in

TABLE 10 EXAMPLE, SHEET 1

HOVGAARD BEND SHEET 1 OF 4

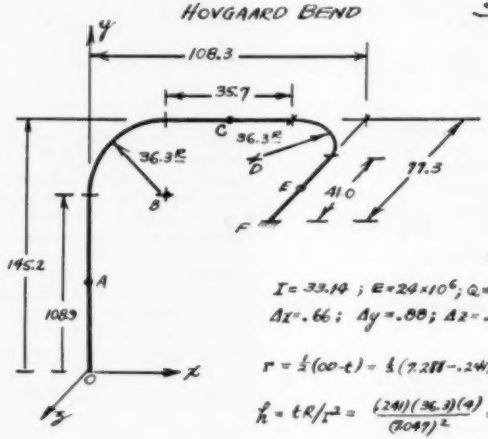

$I = 33.14$; $E = 24 \times 10^6$; $Q = 100$

$\Delta x = .66$; $\Delta y = .88$; $\Delta z = .47$

$r = \frac{1}{2}(OD - t) = \frac{1}{2}(7.288 - .241) = 7.047/2$

$k_h = tR/I^2 = \frac{(241)(36.3)(9)}{(7047)^2} = .7046527$

$m = 12k^2 = 5.958425$

$k = (m+N)/(mN) = 2.293396$

$R = .363$ $R^2 = .131769$ $R^3 = .047832$

$kR = .832503$ $kR^2 = .302198$ $kR^3 = .109698$

$A = .086157$
$B = .054849$
$C = -.302198$
$D = .086157$
$E = -.302198$
$F = .097675$
$G = .171300$
$H = .171300$
$I = .655730$
$J = .054450$
$K = .655730$
$L = 1.307696$

TABLE 10 EXAMPLE, SHEET 2

HOVGAARD BEND

SHEET 2 OF 4

ITEM NR 1
☑ TANGENT - LENGTH 1.089
☐ ELL - RADIUS ___, ARC ___
ORIENTATION Y, CASE ___
COORDS OF B REL. TO O
X = 0 ; Y = .5445 ; Z = 0

.107622					
	0				
		.107622			
			1.089		
.430483				1.4157	
0	0				1.089
0	0	.430483			
0	0	-.592960	1.089		
0	0	0	0	1.4157	
.592960	0	0	0	0	1.089

ITEM NR 2
☐ TANGENT - LENGTH ___
☑ ELL - RADIUS .362, ARC 30°
ORIENTATION -X -Y, CASE 4
COORDS OF B REL. TO O
X = .362 ; Y = 1.082 ; Z = 0

.086157	.054849				.302198
	.086157				.302198
		.097675	-.171300	-.171800	
			.655730	.054450	
2.295168				.655730	
-.242697	.039075				1.307696
0	0	1.167403			
0	0	-.365625	.655730		
0	0	.007434	.054450	.655730	
1.726279	-.172496	0	0	0	1.307696

ITEM NR 3
☑ TANGENT - LENGTH .357
☐ ELL - RADIUS ___, ARC ___
ORIENTATION X, CASE ___
COORDS OF C REL. TO O
X = .5415 ; Y = 1.452 ; Z = 0

0					
	.003792				
		.003792			
			.4641		
.752665				.357	
-.280694	.108473				.357
0	0	1.086936			
0	0	-.673873	.4641		
0	0	.193316	0	.357	
.518364	-.193316	0	0	0	.357

TABLE 10 EXAMPLE, SHEET 3

HOVGAARD BEND — SHEET 3 OF 4.

ITEM Nº 4
☐ TANGENT - LENGTH ____
☑ ELL-RADIUS .262, ARC 90
ORIENTATION -Z:X, CASE 12
COORDS OF 2 REL. TO 0
x = .720 ; y = 1.452 ; z = .363

.086157		.054849		.302198	
	.097675		-.171300		-.171300
		.086157		.302198	
			.655730		.054450
1.421553				1.307696	
-.905554	.617856				.655730
-.293842	-.039965	2.581710			
.079061	.027526	-.952120	.655730		
-.172496	0	1.243739	0	1.307696	
.952120	-.623660	-.079061	.054450	0	.655730

ITEM Nº 5
☑ TANGENT - LENGTH .410
☐ ELL-RADIUS ____, ARC ____
ORIENTATION X, CASE ____
COORDS OF E REL. TO 0
x = 1.083 ; y = 1.452 ; z = .568

.005743					
	.005743				
		0			
			.41		
1.261745				.41	
-.838151	.763169				.533
-.252209	-.338142	1.345289			
0	.232880	-.535320	.41		
-.232880	0	.444030	0	.41	
.773916	-.579239	0	0	0	.533

ITEM Nº ENTIRE CONFIGURATION
☐ TANGENT - LENGTH ____
☐ ELL-RADIUS ____, ARC ____
ORIENTATION ____, CASE ____
COORDS OF ____ REL. TO ____
x = ____ ; y = ____ ; z = ____

6.161620					
-2.267096	1.528573				
-.546051	-.378110	6.611827			
.079061	.260406	-3.679898	3.274560		
-.405376	0	1.888519	.054450	4.146126	
4.563639	-1.566711	-.079061	.054450	0	3.942426

TABLE 10 EXAMPLE, SHEET 4

HOYGARD BEND SHEET 4 OF 4

1 A-MATRIX

	1	2	3	4	5	6	Δ	Σ	5 CHECK OF RESULTS Δ	ERROR
1	6.161620	-2.267096	-.546051	.079061	-.405376	4.563639	.660000	8.245797	.660001	.000001
2	-2.267096	1.528573	-.378110	.260406	0	-1.566711	.880000	-1.542938	.879996	-.000004
3	-.546051	-.378110	6.688427	-3.679898	1.888519	-.079061	.470000	4.287226	.469990	-.000010
4	.079061	.260406	-3.679898	3.214560	.054450	.054450	0	.043029	.000003	.000003
5	-.405376	0	1.888519	.054450	4.146126	0	0	5.683719	-.000004	-.000004
6	4.563639	-1.566711	-.079061	.054450	0	3.942426	0	6.914743	.000001	.000001

2 B-MATRIX

	1	2	3	4	5	6	Δ₁	Σ₁	Δ′	Σ′
1	6.161620	-.367938	-.088621	.012831	-.065790	.740656	.107115	1.338251 ✓	.660000	8.245797
2	-2.267096	.694422	-.833820	.416885	-.214787	.161897	1.616941	2.147116 ✓	1.122840	1.491005
3	-.546051	-.579023	6.080634	-.564333	.284218	.068926	.240885	1.029697 ✓	1.464736	6.261209
4	.079061	.289496	-3.411504	1.216347	.901985	.152544	.287772	2.342302 ✓	.350031	2.849053
5	-.405376	-.149153	1.728227	1.097127	2.606635	.014544	-.171652	.842888 ✓	-.447433	2.197101
6	4.563639	.112425	.419115	.185546	.037910	.486395	-1.682717	-.682698 ✓	-.818465	-.332061

3

E = 24 · 10^6 psi

I = 33.14 in^4

EI = 795.36 · 10^6 lbs·in^2

Q = 10 in

Q^2 = 1 · 10^6 in^3

$f_1 = EI/Q^3$ = 795.36 lbs/in

$F_0 = Qf_1$ = 795.36 lbs

4

	FINAL MATRIX (START AT BOTTOM)	FACTOR	FINAL RESULT	UNITS
REACTIONS AT "0" F_1	2.223488	795.36	1768.47	POUNDS
F_2	2.226541	"	1770.90	
F_3	.780873	"	621.08	
F_4	.677214	795.36.	53863	INCH-POUNDS
F_5	-.147179	"	-11706	
F_6	-1.682717	"	-133837	

applying this method to practical cases, we here consider the simple, two-anchor problem involved in the well-known "Hovgaard" bend described in Fig. 2 of reference (1). The calculations are shown in Table 10 which is a reproduction of the four $8^1/_2$-in. × 11-in. sheet actually used for the calculation. Sheet 1 of Table 10 shows the configuration and some preliminary calculations. Sheets 2 and 3 show the calculations pertaining to the five individual elements into which the configuration is divided. For each element the upper-right triangular array represents the elasticity matrix at the appropriate base point and the lower-left array represents the elasticity matrix transferred to the origin, point 0. The summation is indicated at the bottom of Sheet 3. Sheet 4 contains the solution of the simultaneous equations by means of Crout's method. Once the reactive forces and moments are known, the solutions for force and moment at any point of the configuration and for stresses can be accomplished by customary procedures.

Only a few remarks need be made concerning the computations. The flexural rigidity EI is taken as unity in the body of the computation and a length unit of $Q = 100$ in. is used in the dimensions of the configuration so as to permit dealing with figures of the order of unity. This unit was not used for thermal expansions which were left in inches. At the end of the computation correction factors $EI/Q^2 = 795.36$ for forces and $EI/Q^3 = 79{,}536$ for moments are applied. The calculations shown in Table 10 represent far greater accuracy than is justified in practice; this was done to permit the reader to compare every step of the calculation if he wishes. On Sheet 4 the columns headed Δ_i' and Σ_i' are the values shown in columns Δ_i and Σ_i, respectively, before division by the diagonal element.

ACKNOWLEDGMENT

The author wishes to acknowledge his appreciation to Mr. C. E. Buettner of the Union Electric Company of Missouri, for having introduced him to the study of piping.

BIBLIOGRAPHY

1 "Methods of Making Piping Flexibility Analyses," by S. Crocker and A. McCutchan, *Heating, Piping and Air Conditioning*, vol. 18, June, 1946, pp. 69–73.

2 "Piping Handbook," by S. Crocker, McGraw-Hill Book Company, Inc., New York, N. Y., fourth edition, 1945, pp. 779–816; (A. W. McCutchan is coauthor of this section.)

3 "Expansion Stresses and Reactions in Piping Systems," Anon., (short title: "Design of Piping Systems"), M. W. Kellogg Company, (pub.), Jersey City, N. J., 1941. (Now out of print.)

4 "Methods of Making Piping Flexibility Analyses, Tabular Integration Method," by W. G. Hooper, *Heating, Piping and Air Conditioning*, vol. 18, November, 1946, pp. 70–75.

5 "Steam Pipework Design in Ships," by P. T. Hoath, Trans. Institution of Marine Engineers, vol. 59, 1947, pp. 189–214; discussion, pp. 214–220.

6 "Matrix Analysis of Flexible Filaments," by J. E. Brock, Proceedings of the First U. S. National Congress for Applied Mechanics, Chicago, Ill., 1951, to be published in January, 1953, by THE AMERICAN SOCIETY OF MECHANICAL ENGINEERS.

7 "Le calcul systématique des charactéristiques elastiques des systèmes hyperstatiques," by H. Falkenheiner, La Recherche Aéronautique, No. 17, September–October, 1950, pp. 17–31.

8 "Estructuras espaciales," by M. G. Ortega, Revista de Ciencia Aplicada, Num. 13, Ano IV, Fasc. 2, March–April, 1950, pp. 97–116; Num. 14, Ano IV, Fasc. 3, May–June, 1950, pp. 209–226.

9 "Elementary Matrices," by R. A. Frazer, W. J. Duncan, and A. R. Collar, Cambridge University Press, and The Macmillan Company, New York, N. Y., 1947.

10 "Matrizen," by R. Zurmühl, Springer Verlag, Berlin, Germany, 1950.

11 "Properties of Thin-Walled Curved Tubes of Short-Bend Radius," by T. E. Pardue and I. Vigness, Trans. ASME, vol. 73, 1951, pp. 71–87.

12 "A Short Method of Evaluating Determinants and Solving Systems of Linear Equations With Real or Complex Coefficients," by P. D. Crout, Trans. AIEE, vol. 60, 1941, pp. 1235–1240. See also Marchant Method No. 182, available on request to Marchant Calculating Machine Company, Oakland, Calif.

Calibration of Pressure Gages for Work in Ballistics

By S. RAYNOR,[1] CHICAGO, ILL.

For ballistics work where pressures of several thousand psi are encountered, it is essential that the gages used to measure transient pressures be checked against a "standard gage" of known behavior. Such a standard gage and the method of calibrating it are described in the paper.

THE measurement of transient pressure is of importance in many research programs. Numerous gages are available for this purpose, but a common shortcoming of these instruments is the difficulty of predicting their response to a transient. The reason for this is that such gages are rather complicated mechanical systems, having many coupled modes of vibration, and a damping that is difficult to evaluate. Therefore it is necessary to provide a calibration device in order to measure the error in the reproduction of a transient. Two approaches are possible: the first approach is to provide a pressure transient of known shape; the second is to calibrate the pressure gage against a standard gage of known behavior. The routine use of the standard gage might be inconvenient owing to its bulk.

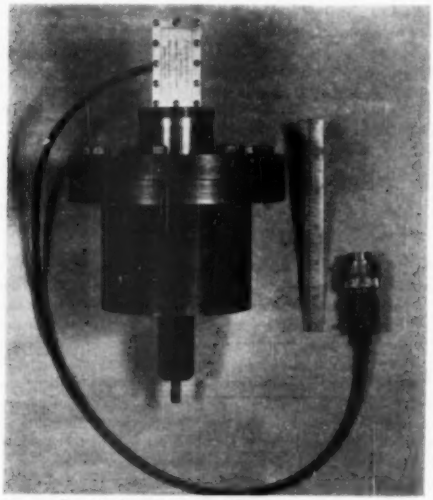

FIG. 1 ACCELEROMETER PRESSURE ADAPTER

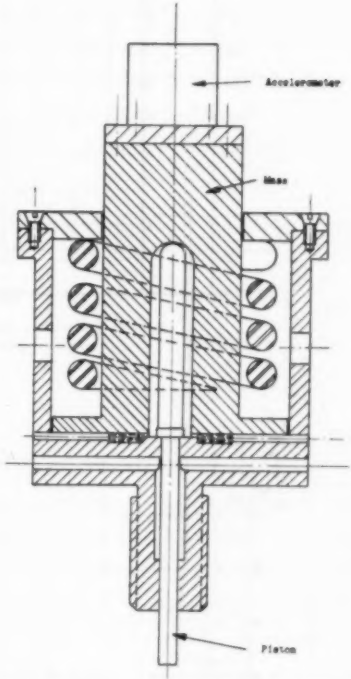

FIG. 2 CROSS SECTION OF ACCELEROMETER PRESSURE ADAPTER

The first approach can be applied successfully by the use of a shock wave in a shock tube. The pressure is approximately a step function of time, with a pressure rise time of the order of 10^{-9} sec. Unfortunately, the application of the shock tube is limited at the present time to pressures up to several hundred psi.

THE STANDARD GAGE

For ballistic work, where pressures of at least several thousand psi are encountered, the second approach is advisable and offers good possibilities if a standard gage can be built successfully. Such a gage, consisting of a $^1/_8$-in-diam piston connected to a large mass which carries a calibrated accelerometer, as shown in Figs. 1 and 2, has been built. It has the following characteristics: range, 10,000 psi; time of rise, of the order of 1 millisec; piston diameter, $^1/_4$ in.; moving weight, 4.57 lb. The accelerometer used has a range from 0 to 200 g, a resonant frequency of 1600 cycles, and its damping is 0.4 of the critical damping, according to the manufacturer's calibration. While the mass is propelled by the gas forces alone, accelerations are recorded. Then a buffer spring

[1] Armour Research Foundation.

Presented at the West Coast Meeting of the Applied Mechanics Division, Los Angeles, Calif., June 26–28, 1952, of THE AMERICAN SOCIETY OF MECHANICAL ENGINEERS.

Discussion of this paper should be addressed to the Secretary, ASME, 29 West 39th Street, New York, N. Y., and will be accepted until January 10, 1953, for publication at a later date. Discussion received after the closing date will be returned.

NOTE: Statements and opinions advanced in papers are to be understood as individual expressions of their authors and not those of the Society. Manuscript received by ASME Applied Mechanics Division, West Coast Group, January 9, 1952.

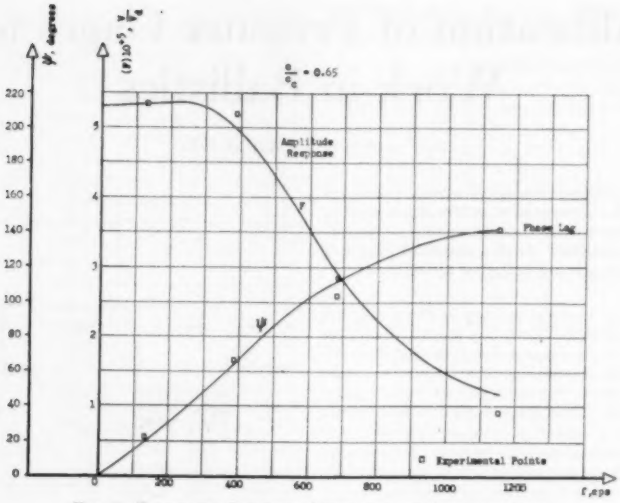

FIG. 3 FREQUENCY RESPONSE CURVE FOR AN ACCELEROMETER
(Resonant frequency 526 cps)

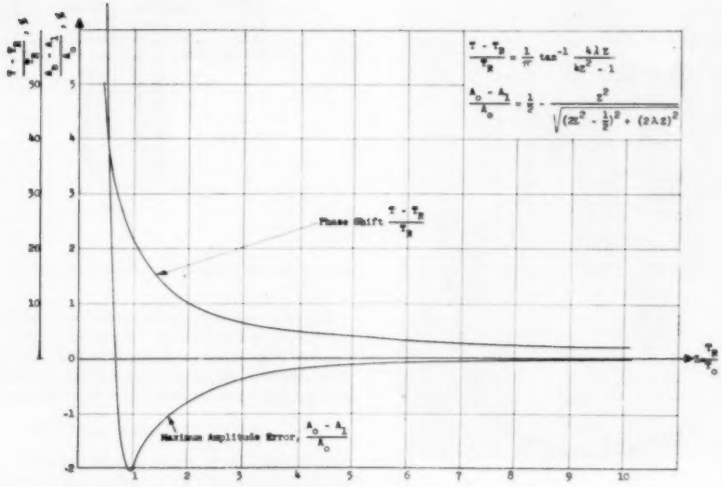

FIG. 4 ERROR CURVES FOR ACCELEROMETER ($\lambda = 0.6$) FOR THE INPUT $\frac{A_0}{2}\omega^2(1 - \cos \omega t)$

A_0 = Amplitude input in accelerometer
A_i = Recorded acceleration
T = Recorded time or rise
T_R = Time of input rise = π/ω
T_0 = Natural period
Z = T_R/T_0

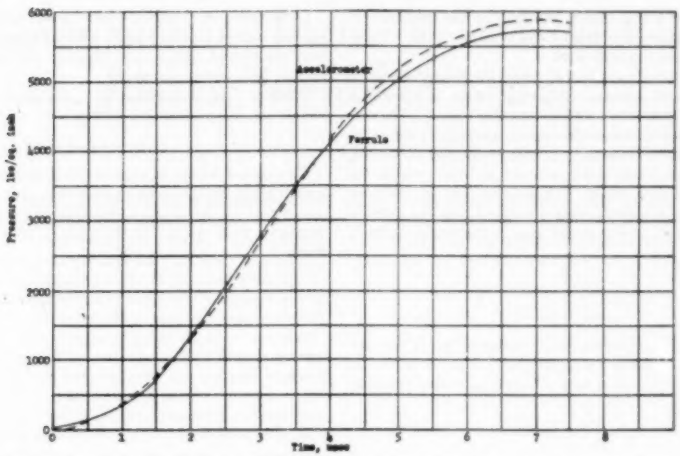

FIG. 5 PRESSURE VERSUS TIME AS MEASURED BY FERRULE-TYPE GAGE AND ACCELEROMETER

brings the mass to rest. Up to the time when the spring action begins, the pressure equals the acceleration multiplied by the ratio of the mass to the piston area. This relation holds only if the friction force is negligible, and it can be made so by proper choice of piston diameter. The friction force is estimated to be of the order of 2 to 5 lb, whereas the driving force on the $^1/_4$-in. piston diameter due to a peak pressure of 10,000 psi is 491 lb. Thus the error introduced by friction is considered negligible.

The problem of pressure measurement is thus reduced to the measurement of acceleration. By proper choice of the moving mass and the plunger area a commercially available accelerometer can be selected satisfying the requirements of range and frequency response.

CALIBRATING THE STANDARD GAGE

The calibration of the standard gage is accomplished by calibration of the accelerometer. If the accelerometer is not already calibrated satisfactorily by the manufacturer, a precise calibration can be carried out in the laboratory by vibrating the accelerometer through the required frequency range and measuring the amplitude output and the phase shift. Fig. 3 shows these measured data compared with the theoretical values obtained by considering the accelerometer as a simple degree of freedom seismic instrument having a viscous damping of 0.65 of the critical damping, where V is the voltage output, V_d is the voltage input to the bridge of a strain-gage-type accelerometer, and F is the calibration factor in units of V/V_d. This comparison demonstrates that the accelerometer can be idealized by the mathematical model. This does not imply that the reading of the accelerometer represents exactly the acceleration to which the instrument was subjected, but that by proper choice of the range, natural frequency and damping of the accelerometer, the errors can be made small and evaluated.

In Fig. 4 the relative errors in amplitude and time of rise computed for the input consisting of $\frac{A_0}{2}\omega^2 (1 - \cos \omega t)$ pulse are plotted for an accelerometer with natural period T_0 and damping of 0.6 of the critical damping ($\lambda = 0.6$). When the input time of rise, T_R, is 2 milliseconds, and the natural period of

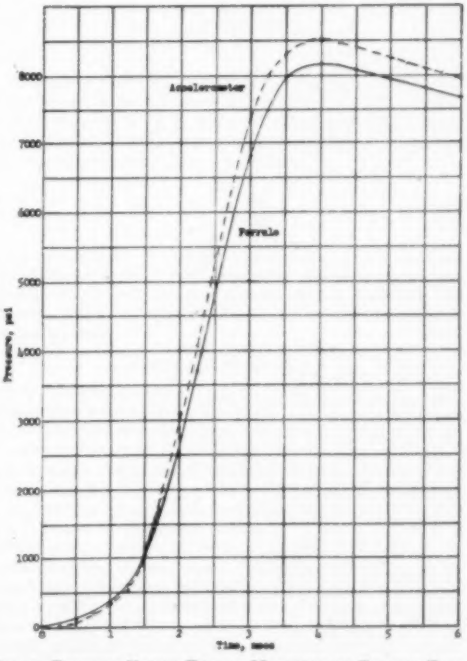

FIG. 6 PRESSURE VERSUS TIME AS MEASURED BY FERRULE-TYPE GAGE AND ACCELEROMETER

the accelerometer is 1 millisecond, the error in the amplitude is 0.8 per cent and the error in time of rise is 10 per cent. These values are acceptable in ballistic work.

Figs. 5 and 6 show a comparison between the records obtained with the Ferrule-type resistance strain gage used as a pressure gage and the records obtained with the standard gage. The corrections to be applied to the accelerometer readings, based on an accelerometer's natural frequency of 1600 cycles, are as follows: The error in the amplitude is 0.1 per cent and the error in the time of rise is 3 per cent, Fig. 6. These errors are not excessive for many applications and the diagram shows that the Ferrule-type strain gage used as a pressure gage is acceptable without major corrections.

In the process of pressure-gage design and calibration a comparison with a standard gage, whose behavior is predictable, is very useful and permits investigation of changes of parameters such as stiffness and damping.

Work is now in progress for a standard gage with range of 50,000 psi, using a 600 g accelerometer.

Acknowledgment

The author wishes to express his appreciation to Armour Research Foundation for sponsoring this work, and to Mr. Channon Price, of the Applied Mechanics Department of Armour Research Foundation, for the experimental work which he performed.

On Longitudinal Plane Waves of Elastic-Plastic Strain in Solids

By D. S. WOOD,[1] PASADENA, CALIF.

A theoretical description is given for the propagation of longitudinal plane waves of large lateral extent in solids, for waves of plastic as well as elastic strain. The importance of the hydrostatic compressibility in determining the nature of the waves is brought out. The results are illustrated by a computation of the velocities of propagation of such waves in 24S-T aluminum alloy, and by a computation of the propagation of a pressure pulse of short duration through a flat plate. The later results illustrate the attenuation and change in shape of the pressure pulse during its propagation. The effects of the pressure dependence of the compressibility, the temperature changes accompanying compression, and the time and rate dependence of the mechanical properties, upon the propagation of such waves are discussed qualitatively.

Introduction

A RECENT paper by Rinehart (1)[2] on the scabbing of metals under explosive attack has suggested the desirability of determining the nature and properties of certain types of longitudinal strain waves of high intensity in solids. This paper treats the simple case in which the waves are plane and extend over lateral distances which are large compared to the distance traveled by the waves.

The case of longitudinal strain waves in long thin bars has been treated by von Kármán (2) and others (3, 4, 5), and has been investigated experimentally (6). Pack, Evans, and James (7), in considering waves of large lateral extent, have pointed out that shock waves may be produced in metals under suddenly applied high pressures (as by explosives) due to the decrease in compressibility with increasing pressure. They demonstrated experimentally that a shock wave of 280,000 atm amplitude propagates at a rate greater than the speed of sound in lead, but at a rate less than the speed of sound in steel. However, they did not discuss the complete problem of the combined propagation of elastic and plastic waves.

The method of treatment employed by von Kármán (2) may be applied to the present case with suitable modifications to account for the lateral boundary conditions which apply for waves of large lateral extent.

Equation of Motion

The motion associated with a longitudinal plane wave of infinite lateral extent must be strictly unidirectional. Hence the displacement of the material u must always be in the direction of wave travel, denoted by the Lagrangian co-ordinate x. Thus the equation of motion may be written in the familiar form

$$\frac{\partial^2 u}{\partial t^2} = \frac{1}{\rho}\frac{\partial \sigma_x}{\partial \epsilon_x}\frac{\partial^2 u}{\partial x^2} \quad \ldots\ldots [1]$$

where σ_x is the component of stress in the x-direction, ϵ_x the component of strain in the x-direction, ρ the initial density of the material, and t the time. It may be noted that

$$\epsilon_x = \frac{\partial u}{\partial x}$$

is an engineering type of strain defined by the change in length per unit initial length of an element of material, and furthermore, Equation [1] is valid for large strains. Equation [1] is formally identical with that used by von Kármán (2) in his description of the plastic strain waves in long thin bars. As he has shown, the solution may be expressed in terms of strain waves whose velocity of propagation is given by

$$c = \left(\frac{1}{\rho}\frac{\partial \sigma_x}{\partial \epsilon_x}\right)^{1/2} \quad \ldots\ldots [2]$$

The wave velocity c is a function of strain ϵ_x in the general case of plastic as well as elastic deformations. If Δt is the time interval required for the increment of strain $d\epsilon_x$ at ϵ_x to traverse the interval of distance Δx, in the unstrained state, between two particles of the material, then c is defined by

$$c(\epsilon_x) = \frac{\Delta x}{\Delta t} \quad \ldots\ldots [3]$$

In the case of waves in long thin bars Equation [1] represents an approximation in which the kinetic energy and shear stresses associated with lateral motion of the material are neglected. In the present case that approximation is not made since no lateral motion is possible.

Stress-Strain Relation

The stress-strain relation σ_x versus ϵ_x must be known in order to determine the wave velocities by Equation [2]. This relation would be quite difficult to determine directly by experiment, and no such measurements are available at present. Hence it is necessary to derive it from indirect experimental data by means of a suitable theory of plasticity. Fortunately, a good approximation for the present problem may be obtained by the use of a very simple form of the theory of plasticity.

The desired σ_x versus ϵ_x relation will be derived from the stress-strain relation in simple tension and compression which is assumed to be given from experiment. To do this the stress and strain σ_y and ϵ_y in a direction normal to x must be considered. From the symmetry of the problem it is clear that σ_y and ϵ_y are the same for all directions in the plane normal to the x-direction. The strains may be separated into their elastic and plastic components, thus

---

[1] Assistant Professor of Mechanical Engineering, California Institute of Technology. Jun. ASME.

[2] Numbers in parentheses refer to the Bibliography at the end of the paper.

Presented at the West Coast Conference of the Applied Mechanics Division, Los Angeles, Calif., June 26–28, 1952, of The American Society of Mechanical Engineers.

Discussion of this paper should be addressed to the Secretary, ASME, 29 West 39th Street, New York, N. Y., and will be accepted until January 10, 1953, for publication at a later date. Discussion received after the closing date will be returned.

Note: Statements and opinions advanced in papers are to be understood as individual expressions of their authors and not those of the Society. Manuscript received by ASME Applied Mechanics Division, March 17, 1952.

$$\left.\begin{aligned}\epsilon_x &= \epsilon_x^e + \epsilon_x^p \\ \epsilon_y &= \epsilon_y^e + \epsilon_y^p\end{aligned}\right\} \quad \ldots\ldots [4]$$

where the superscripts e and p denote elastic and plastic-strain components, respectively.

Three principal assumptions will be made regarding the stress-strain behavior of the material: (a) The elastic components of strain are given by Hooke's law, which may be written

$$\left.\begin{aligned}\epsilon_x^e &= \frac{1}{E}\,[\sigma_x - 2\nu\sigma_y] \\ \epsilon_y^e &= \frac{1}{E}\,[(1-\nu)\sigma_y - \nu\sigma_x]\end{aligned}\right\} \quad \ldots\ldots [5]$$

where E and ν are Young's modulus and Poisson's ratio, respectively. (b) Plastic strains produce no change in density of the material. This is expressed by

$$\epsilon_x^p + 2\epsilon_y^p = 0 \quad \ldots\ldots [6]$$

(c) The plastic stress-strain law will be assumed to be independent of strain rate and of the form

$$\sigma_x - \sigma_y = \sigma(\epsilon_x^p) \quad \ldots\ldots [7]$$

in which the function $\sigma(\epsilon_x^p)$ is defined by

$$\sigma = \sigma(\epsilon^p) \quad \ldots\ldots [8]$$

where σ and ϵ^p are the stress and plastic component of strain, respectively, in a simple tension and compression test.

The later assumption corresponds to the Mises-Henky yield conditions and also to the maximum shear-stress yield criterion, the two giving equivalent results in the present case. In the terminology used by Drucker (8) the stress-strain law of Equation [7] involves the assumption of isotropic work-hardening. It can be shown that the so-called deformation and incremental theories of plasticity lead to the same result under the foregoing assumptions.

Since the conditions of the present problem permit no motion of the material in any direction normal to x, we have

$$\epsilon_y = 0$$

Then from Equations [4] and [6]

$$\epsilon_y^e = -\epsilon_y^p = \frac{1}{2}\,\epsilon_x^p$$

and using Equation [5] it can readily be shown that

$$\sigma_y = \frac{1}{2}\,\frac{E}{(1-\nu)}\,\epsilon_x^p + \frac{\nu}{(1-\nu)}\,\sigma_x \quad \ldots\ldots [9]$$

Substituting Equation [9] into Equation [7] and rearranging yields

$$\sigma_x = \frac{(1-\nu)}{(1-2\nu)}\,\sigma(\epsilon_x^p) + \frac{1}{2}\,\frac{E}{(1-2\nu)}\,\epsilon_x^p \quad \ldots\ldots [10]$$

Also, substituting Equations [9] and [10] into Equations [5] gives

$$\epsilon_x^e = \frac{1}{2}\,\epsilon_x^p + \frac{(1+\nu)}{E}\,\sigma(\epsilon_x^p) \quad \ldots\ldots [11]$$

Finally, the stress-strain relation in the purely elastic range is well known to be

$$\sigma_x = E\,\frac{(1-\nu)}{(1+\nu)(1-2\nu)}\,\epsilon_x \quad \ldots\ldots [12]$$

Equations [10], [11], and [12], together with the first of Equations [4] provide a means for computing the desired σ_x versus ϵ_x relation from the given data represented by Equation [8].

Plane Compression Waves in 24S-T Aluminum Alloy

A specific example of the calculations just discussed has been made for 24S-T aluminum alloy. The given data are represented by the portion of the stress-strain curve for simple compression shown in Fig. 1, which is indicated by the line 0′–e′–2′. Young's modulus E, and Poisson's ratio ν, are taken to be

$$E = 10.6 \times 10^6 \text{ psi}$$

and

$$\nu = 0.33$$

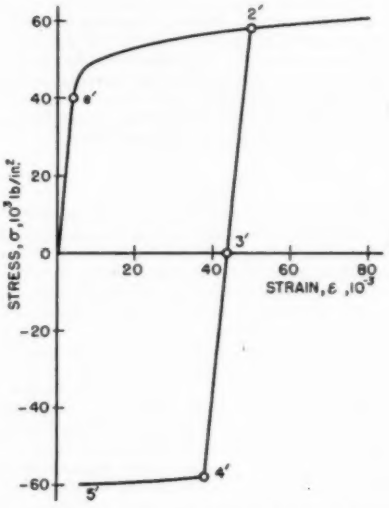

Fig. 1 Stress-Strain Relation σ Versus ϵ, for 24S-T Aluminum Alloy in Simple Compression and Tension

respectively. These values are only constants for moderate values of the hydrostatic component of the stress system. At very high values of the hydrostatic stress these vary with stress, since the hydrostatic compressibility decreases with increasing pressure. For the present, E and ν will be considered to be constant. The effect of varying compressibility will be discussed later.

The σ_x versus ϵ_x relation determined by the foregoing method is shown in Fig. 2 by the portion of the curve 0–e–2, where point e indicates the limit of elastic behavior. The points 0′, e′, 2′ in Fig. 1 bear a one to one correspondence with the points 0, e, 2 in Fig. 2. From Fig. 2 it is seen that the σ_x versus ϵ_x relation may be approximated quite closely by the two straight lines 0–1 and 1–2, where the approximate limit of elastic behavior indicated by point 1 is the intersection of these two lines.

The velocity of propagation of waves of various amplitudes may now be determined from Fig. 2 by the use of Equation [2]. For strain increments in the range 0 to 1 in Fig. 2, the velocity of propagation is the normal velocity of sound in the material, given by

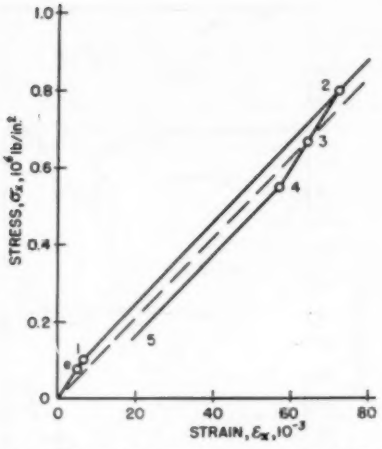

FIG. 2 STRESS-STRAIN RELATION σ_x VERSUS ϵ_x, FOR 24S-T ALUMINUM ALLOY IN CASE OF COMPLETE LATERAL CONSTRAINT

$$c_0 = \left[\frac{E}{\rho}\frac{(1-\nu)}{(1+\nu)(1-2\nu)}\right]^{1/2}$$

or numerically

$$c_0 = 2.46 \times 10^5 \text{ ips}$$

using a value of 0.100 lb per cu in. for the specific weight. For strain increments in the range 1 to 2, the velocity of propagation according to Equation [2] is found to be

$$c_1 = 2.01 \times 10^5 \text{ ips}$$

or about 18 per cent slower than the elastic wave. This numerical result is in marked contrast with the velocity of propagation of plastic strain in long thin bars. In the latter case the velocity of propagation of a plastic strain of a few per cent is typically of the order of one tenth of the elastic-wave velocity.

The physical interpretation of these results for the present case may be seen readily. If the material exhibits no resistance to shearing distortion, then it would behave like a liquid of low compressibility. The stress-strain relation would be

$$\sigma_{xh} = K\epsilon_{xh} = \sigma_{yh} \quad \ldots\ldots\ldots\ldots\ldots\ldots [13]$$

where the subscript h denotes hydrostatic behavior, and

$$K = \frac{E}{3(1-2\nu)}$$

is the reciprocal of the hydrostatic compressibility. In such a material all strains would propagate with the velocity

$$c_h = \sqrt{\frac{K}{\rho}} \quad \ldots\ldots\ldots\ldots\ldots\ldots [14]$$

The relation given by Equation [13] for 24S-T aluminum alloy is shown in Fig. 2 by the dashed line, and the corresponding velocity of strain propagation is

$$c_h = 2.00 \times 10^5 \text{ ips}$$

which is essentially the same as the velocity c_1, given previously. Thus the behavior of the material may be thought of as being composed of a stress associated with hydrostatic compression plus a stress associated with its resistance to shear deformation. In fact, it can be shown that the stress-strain relation represented by Equations [9], [10], and [11] also may be expressed in the form

$$\sigma_x = K\epsilon_x + 2/3\,\sigma\,(\epsilon_x{}^p) \quad \ldots\ldots\ldots\ldots [15]$$

The first term represents the hydrostatic stress component, and the second the contribution of the shear strength of the material.

UNLOADING WAVES

Thus far the treatment has considered only those cases in which the stress σ_x increases monotonically. In many problems involving the propagation of these types of waves it is necessary to know the nature of the σ_x versus ϵ_x relation when the stress σ_x, is decreased after it has previously reached a value such as that at point 2 in Fig. 2. As the stress is reduced, the strain will at first decrease elastically and the following relations hold

$$\sigma_{x_1} - \sigma_x = E\,\frac{(1-\nu)}{(1+\nu)(1-2\nu)}\,(\epsilon_{x_1} - \epsilon_x) \quad \ldots\ldots [16]$$

and

$$\sigma_{y2} - \sigma_y = \frac{\nu}{(1-\nu)}\,(\sigma_{x2} - \sigma_x) \quad \ldots\ldots\ldots [17]$$

where

$$\sigma_x < \sigma_{x2}$$

At some stress $\sigma_{x3} < \sigma_{x2}$ the stress system will become hydrostatic, i.e., $\sigma_{y3} = \sigma_{x3}$. Putting this condition into Equation [17] and using the yield condition $\sigma_{x2} - \sigma_{y2} = \sigma_2$

$$\sigma_{x2} - \sigma_{x3} = \frac{(1-\nu)}{(1-2\nu)}\,\sigma_2 \quad \ldots\ldots\ldots\ldots [18]$$

is obtained. Now using Equation [16] and replacing ϵ_{x2} by its value as given by Equation [15] and σ_{x2} by its value as obtained from Equation [18], and rearranging, it can be shown that

$$\sigma_{x3} = \frac{E}{3(1-2\nu)}\,\epsilon_{x3} = K\epsilon_{x3} \quad \ldots\ldots\ldots\ldots [19]$$

Thus the hydrostatic stress σ_{x3} is related to the total strain ϵ_{x3} in the same manner as if the material had been brought to that stress along a purely hydrostatic path rather than the path 0-1-2-3 in Fig. 2.

The point 3′ in Fig. 1 at which $\sigma_3 = 0$ corresponds to the point 3 in Fig. 2. Now if the stress σ_x is reduced still further along the elastic line 3–4 in Fig. 2, the corresponding point in Fig. 1 goes to negative stresses along 3′–4′. At some point 4′, yielding takes place in a reverse direction and the σ_x versus ϵ_x relation in Fig. 2 becomes plastic again along the line 4–5. This line is very nearly parallel to the hydrostatic line as was the line 1–2 during the initial loading. In Fig. 1 it has been assumed that reversed yielding begins when $\sigma_4 = -\sigma_2$, i.e., the material does not exhibit a Baushinger effect. However, this assumption is made only for convenience and is not essential to the argument.

Thus it has been shown that unloading in the σ_x versus ϵ_x plane can produce reversed plastic deformation before the stress σ_2 has been removed completely. Therefore unloading is associated with waves of plastic as well as elastic deformation. This result is the second characteristic of the present case which differs markedly from the case of waves in long thin rods. In the latter case unloading waves are completely elastic.

Specific Wave-Propagation Problems

The preceding discussion provides the basis for the construction of solutions for the propagation of laterally extended longitudinal waves under various boundary and initial conditions. Such solutions may be constructed graphically by means of the method of characteristics. This method has been illustrated by von Kármán and Duwez (2), and von Kármán, Bohnenblust, and Hyers (5) in the case of waves in long thin rods.

A solution has been constructed for the propagation of waves of the type considered in the present paper for the following particular set of boundary and initial conditions. A pressure pulse of short duration is applied to one surface of a flat plate of finite thickness. The pulse consists of an instantaneous rise to a peak pressure followed by a decay over a finite but short period of time. The pressure-decay curve is represented by a series of finite steps in order to simplify the calculations somewhat, but such an idealization is not essential to the method of computation. It is essential to assume that the pressure is applied uniformly over an area of the plate whose lateral dimensions are large compared to the thickness of the plate. This insures that the motion of the plate in the central portion of the area to which pressure is applied can be described completely in terms of waves of the type considered in the present paper.

The form of the applied pressure pulse is shown in Fig. 3 in

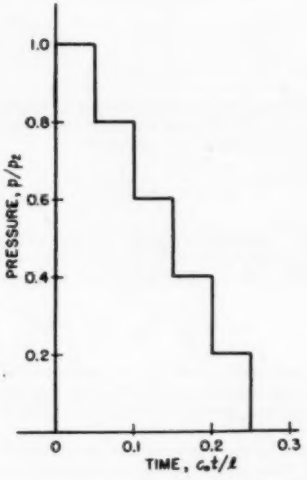

Fig. 3 Pressure Pulse, p/p_2 Versus c_0t/l, Applied at Surface, $x = 0$ of a Flat Plate

dimensionless form p/p_2 versus c_0t/l, where p is the pressure at any time, t, p_2 the peak pressure, l the thickness of the plate, and c_0 the velocity of propagation of elastic waves in the material. The peak pressure p_2 is taken to be 10 times the maximum stress σ_{s1}, for purely elastic behavior. The decay of the pressure pulse is taken to occur in five equal steps and to be completed in one quarter of the time required for an elastic wave to traverse the thickness of the plate. This pulse is applied to the surface $x = 0$. The σ_x versus ϵ_x relation of the plate material is taken to be of the type illustrated in Fig. 2. The velocity of propagation of the waves associated with plastic strain is 82 per cent of the velocity of elastic waves.

Some of the results of this sample calculation are shown in Fig.

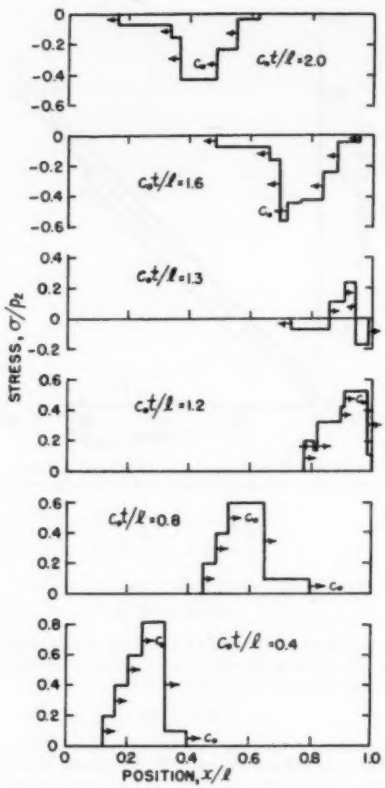

Fig. 4 Stress Distribution, σ_x/p_2 Versus x/l, in a Plate at Various Times c_0t/l, After Beginning of Applied Pressure Pulse

4. This shows the distribution of stress σ_x/p_2 versus x/l, in the plate at various times c_0t/l, after the beginning of the applied pressure pulse. The figure illustrates the attenuation and change in form of the pressure pulse as it progresses through the plate and reflects at the free surface $x/l = 1$. The attenuation of the pulse is brought about by the partially elastic nature of the unloading wave which enables the unloading wave to overtake the plastic portion of the initial loading wave progressively. The elastic portions of the wave fronts are indicated in Fig. 4 by a notation of the elastic-wave velocity c_0. The negative (tensile) stresses associated with the reflected pressure pulse are responsible for the phenomenon of scabbing (1). The triaxiality of this state of tension stress and the extremely rapid rate of application of the stress which occurs in such pressure pulses are both conditions which contribute to the brittle nature of scabbing failures even in normally ductile materials.

Effect of Variable Compressibility

The preceding discussion has assumed that the hydrostatic compressibility K^{-1}, is independent of pressure. Since this is not true at very high pressures, some modifications of the treatment are required. Bridgman (9) has determined the hydrostatic compression of pure aluminum up to 30,000 kg per sq cm (427,000

psi). It may be reasonably assumed that 24S-T aluminum alloy exhibits the same behavior in this respect. Hence Bridgman's data have been used to compute the stress-strain relation, σ_x versus ϵ_x, for 24S-T aluminum alloy taking the effect of variable compressibility into account. This may be accomplished conveniently by the use of Equation [15]. The results are shown in Fig. 5. The dashed line represents Bridgman's data, and the solid line the corresponding σ_x versus ϵ_x relation.

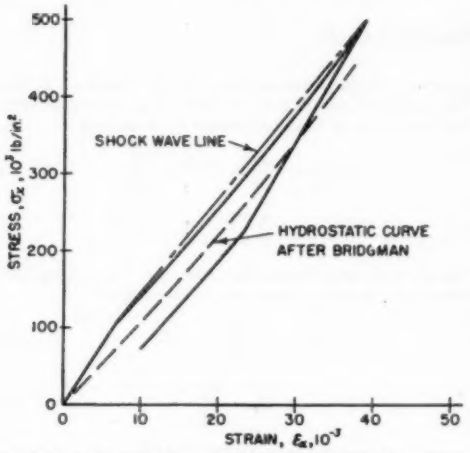

FIG. 5 STRESS-STRAIN RELATION, σ_x VERSUS ϵ_x, FOR 24S-T ALUMINUM ALLOY, TAKING INTO ACCOUNT VARIATION IN COMPRESSIBILITY WITH PRESSURE

This illustrates the fact that the stress-strain relation is concave upward in the region of plastic strains. This behavior leads to the formation of shock waves similar to those which occur in gases, as has been pointed out by Pack, Evans, and James (7), and White and Griffis (10). Such shock waves correspond to a jump across the concave upward portion of the stress-strain relation as shown by the dash-dot line in Fig. 5. The velocity of propagation of the shock wave may be obtained from Equation [2] by replacing the quantity $\partial\sigma_x/\partial\epsilon_x$ by the slope of the shock-wave line in the stress-strain relation. The velocity of propagation of the shock wave associated with the line shown in Fig. 5 is found to be

$$c_s = 2.17 \times 10^5 \text{ ips}$$

The shock-wave velocity clearly increases with increasing peak stress. Eventually, at very high stresses, the shock velocity will become equal to and exceed the velocity of elastic waves. In the latter case the shock will correspond to a straight line from the origin to the peak pressure point on the stress-strain relation, and all strains in such a wave front propagate with the same velocity. Pack, Evans, and James (7) have shown that this behavior occurs in lead subjected to the pressure of explosives (280,000 atm), but not in steel.

Unloading waves also will be modified somewhat under conditions of variable hydrostatic compressibility. The elastic portion of such unloading waves will propagate at a rate greater than the normal velocity of sound. The plastic portion of an unloading wave will exhibit a continuous variation of wave velocity dependent upon strain, with strain increments at lower values of the total strain propagating at lower velocities than those at higher values of total strain. These effects are due to the increased slopes of the unloading portion of the stress-strain relation which reflect the decreased value of the compressibility at high pressures. This is illustrated by the unloading line shown in Fig. 5.

EFFECT OF TEMPERATURE VARIATIONS

The stress-strain relation, and hence the various wave velocities, is affected by the changes in temperature produced by rapid and large pressure variations. An increase in temperature accompanying rapid compression to a high pressure increases the slope of the stress-strain relation due to the thermal expansion. Hence the wave velocities are increased. Furthermore, the amount of upward curvature of the stress-strain relation is increased, and hence the tendency toward shock-wave formation is enhanced. The magnitude of these effects is difficult to estimate due to the lack of suitable data.

TIME AND RATE EFFECTS

Since the stress-strain characteristics of materials are, in general, dependent upon the duration and rates of loading, their wave-propagation properties will differ somewhat from those predicted from their static stress-strain relations. For many metals these effects are not very pronounced. Furthermore, they are confined primarily to the resistance of the metals to plastic shear strains. Since the waves considered in this paper are largely associated with nondistortional strains the dependence of the inherent mechanical properties upon time and rate effects probably does not have a marked influence upon the nature and behavior of these waves. However, the very short times and extremely high rates of deformation associated with these waves may lead to detectable effects in their behavior. In particular, the initial yield stress and entire flow curve may be raised somewhat. This will be reflected in a somewhat increased amplitude of the elastic-wave components, but should have very little effect upon the wave velocities.

The determination of the magnitudes of these various effects must depend upon experimental studies of the waves themselves. Such studies also could provide measurements of the compressibilities of solids at considerably higher pressures than heretofore.

BIBLIOGRAPHY

1 "Some Quantitative Data Bearing on the Scabbing of Metals Under Explosive Attack," by J. S. Rinehart, *Journal of Applied Physics*, vol. 22, 1951, pp. 555–560.

2 "The Propagation of Plastic Deformation in Solids," by Theodore von Kármán and Pol Duwez, *Journal of Applied Physics*, vol. 21, 1950, pp. 987–994.

3 "The Plastic Wave in a Wire Extended by an Impact Load," by G. I. Taylor, British Official Report RC329, 1942.

4 "The Permanent Strain in a Uniform Bar Due to Longitudinal Impact," by M. P. White and Le Van Griffis, JOURNAL OF APPLIED MECHANICS, Trans. ASME, vol. 69, 1947, p. A-337.

5 "The Propagation of Plastic Waves in Tension Specimens of Finite Length, Theory and Methods of Integration," by Theodore von Kármán, H. F. Bohnenblust, and D. H. Hyers, NDRC Report No. A-103 (OSRD No. 946), 1942.

6 "An Experimental Study of the Propagation of Plastic Deformation Under Conditions of Longitudinal Impact," by P. E. Duwez and D. S. Clark, Proceedings of the American Society for Testing Materials, vol. 47, 1947, pp. 502–522.

7 "The Propagation of Shock Waves in Steel and Lead," by D. C. Pack, W. M. Evans, and H. J. James, Proceedings of the Physical Society, London, England, vol. 60, part 1, 1948, pp. 1–8.

8 "Relations of Experiments to Mathematical Theories of Plasticity," by D. C. Drucker, JOURNAL OF APPLIED MECHANICS, Trans. ASME, vol. 71, 1949, pp. 349–357.

9 "Linear Compressions to 30,000 Kg/Cm^2, Including Relatively Incompressible Substances," by P. W. Bridgman, Proceedings of the American Academy of Arts and Sciences, vol. 77, 1949, pp. 187–234.

10 "The Propagation of Plasticity in Uniaxial Compression," by M. P. White and Le Van Griffis, JOURNAL OF APPLIED MECHANICS, Trans. ASME, vol. 70, 1948, pp. 256–260.

Stress Singularities Resulting From Various Boundary Conditions in Angular Corners of Plates in Extension

By M. L. WILLIAMS,[1] PASADENA, CALIF.

As an analog to the bending case published in an earlier paper, the stress singularities in plates subjected to extension in their plane are discussed. Three sets of boundary conditions on the radial edges are investigated: free-free, clamped-clamped, and clamped-free. Providing the vertex angle is less than 180 degrees, it is found that unbounded stresses occur at the vertex only in the case of the mixed boundary condition with the strength of the singularity being somewhat stronger than for the similar bending case. For vertex angles between 180 and 360 degrees, all the cases considered may have stress singularities.

In amplification of some work of Southwell, it is shown that there are certain analogies between the characteristic equations governing the stresses in extension and bending, respectively, if ν, Poisson's ratio, is replaced by $-\nu$. Finally, the free-free extensional plate behaves locally at the origin exactly the same as a clamped-clamped plate in bending, independent of Poisson's ratio.

In conclusion, it is noted that the free-free case analysis may be applied to stress concentrations in V-shaped notches.

Introduction

IN an earlier paper[2] the stress singularities at the vertex of a sector plate in bending were discussed, where it was shown that unbounded stresses may occur for certain vertex angles if the radial edges of the sector were (1) simply supported-simply supported, (2) clamped-free, (3) simply supported-free, or (4) clamped-simply supported. The analogous problem for a thin plate in a state of plane stress or strain is now considered for three cases, (*a*) clamped-clamped, (*b*) free-free, and (*c*) clamped-free, and it will be shown that of these three cases, only the last, namely, the clamped-free boundary condition, may have unbounded stresses at the corner for certain vertex angles.

Method of Solution

Following the extensional development for generalized plane stress in thin plates as given by Coker and Filon[3] the polar displacements in the radial and circumferential directions, U_r and U_θ, respectively, may be written in terms of the biharmonic stress function χ and the harmonic function ψ_1 in the form

$$2\mu U_r = -\frac{\partial \chi}{\partial r} + (1-\sigma) r \frac{\partial \psi_1}{\partial \theta} \quad [1]$$

$$2\mu U_\theta = -\frac{1}{r}\frac{\partial \chi}{\partial \theta} + (1-\sigma) r^2 \frac{\partial \psi_1}{\partial r} \quad [2]$$

where μ is the shear modulus and $\sigma \equiv \nu/(1+\nu)$, ν being Poisson's ratio. Also, the stresses may be expressed as

$$\sigma_r = \frac{1}{r^2}\frac{\partial^2 \chi}{\partial \theta^2} + \frac{1}{r}\frac{\partial \chi}{\partial r} \quad [3]$$

$$\sigma_\theta = \frac{\partial^2 \chi}{\partial r^2} \quad [4]$$

$$\tau_{r\theta} = -\frac{1}{r}\frac{\partial^2 \chi}{\partial r \partial \theta} + \frac{1}{r^2}\frac{\partial \chi}{\partial \theta} \quad [5]$$

χ is related to ψ_1 by

$$\nabla^2 \chi = \frac{\partial}{\partial r}\left(r \frac{\partial \psi_1}{\partial \theta}\right) \quad [6]$$

The boundary conditions will be considered on two radial edges of a sector including a variable vertex angle α; the boundary conditions along the circumferential edge will be unspecified inasmuch as the stresses near the vertex will be locally determined solely by the boundary conditions along the radial edge providing the circumferential boundary is greater than several plate thicknesses from the vertex.

Let us assume solutions for χ and ψ_1 in the form

$$\chi = r^{\lambda+1}[b_1 \sin(\lambda+1)\theta + b_2 \cos(\lambda+1)\theta + b_3 \sin(\lambda-1)\theta + b_4 \cos(\lambda-1)\theta] \equiv r^{\lambda+1} F(\theta;\ \lambda) \quad [7]$$

$$\left.\begin{aligned} \psi_1 &= r^m(a_1 \cos m\theta + a_2 \sin m\theta) \\ &\equiv r^m G(\theta;\ m) \end{aligned}\right\} \quad [8]$$

On account of Equation [6], it must follow that $\lambda = m + 1$ in order that the powers of r be compatible and further

$$a_1 = -\frac{4}{\lambda-1} b_3;\quad a_2 = \frac{4}{\lambda-1} b_4 \quad [9]$$

by equating coefficients of like trigonometric terms.

Substitution of Equations [7] and [8] into [1], through Equation [5] utilizing Equation [9] gives

$$2\mu U_r = r^\lambda[-(\lambda+1)F(\theta) + (1-\sigma)G'(\theta)] \quad [10]$$

---

[1] Assistant Professor, Guggenheim Aeronautical Laboratory, California Institute of Technology.

[2] "Surface Singularities Resulting From Various Boundary Conditions in Angular Corners of Plates Under Bending," by M. L. Williams, U. S. National Congress of Applied Mechanics, Illinois Institute of Technology, Chicago, Ill., June, 1951.

[3] "A Treatise on Photoelasticity," by E. G. Coker and L. G. N. Filon, Cambridge University Press, 1931, p. 163.

Presented at the West Coast Conference of the Applied Mechanics Division, Los Angeles, Calif., June 26–28, 1952, of The American Society of Mechanical Engineers.

Discussion of this paper should be addressed to the Secretary, ASME, 29 West 39th Street, New York, N. Y., and will be accepted until January 10, 1953, for publication at a later date. Discussion received after the closing date will be returned.

Note: Statements and opinions advanced in papers are to be understood as individual expressions of their authors and not those of the Society. Manuscript received by ASME Applied Mechanics Division, February 28, 1952.

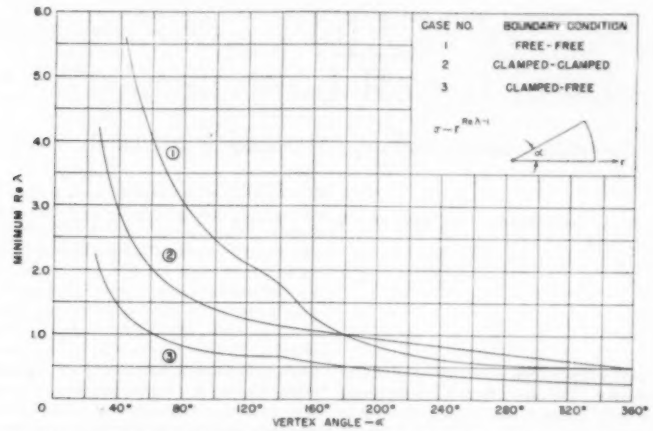

FIG. 1 VARIATION OF MINIMUM REAL PART OF EIGEN VALUE WITH VERTEX ANGLE

$$2\mu U_\theta = r^\lambda[-F'(\theta) + (1-\sigma)(\lambda-1)G(\theta)] \quad [11]$$

$$\sigma_r = r^{\lambda-1}[F''(\theta) + (\lambda+1)F(\theta)] \quad [12]$$

$$\sigma_\theta = r^{\lambda-1}[\lambda(\lambda+1)F(\theta)] \quad [13]$$

$$\tau_{r\theta} = r^{\lambda-1}[-\lambda F'(\theta)] \quad [14]$$

Having therefore a representation of the stresses and displacements for the sector plate in extension, the effects of different homogeneous boundary conditions may be investigated.

FREE-FREE EDGES

If both radial edges are prescribed to be free, $\sigma_\theta(0) = \tau_{r\theta}(0) = 0$, $\sigma_\theta(\alpha) = \tau_{r\theta}(\alpha) = 0$ which by Equations [13] and [14] require $F(0) = F'(0) = F(\alpha) = F'(\alpha) = 0$ where the primes indicate differentiation with respect to θ. While $F(\theta)$ contains four undetermined constants $b_i (i = 1, 2, 3, 4)$, and four boundary conditions are prescribed, the constants cannot be determined uniquely because the four equations are homogeneous. For there to be a solution, the determinant must vanish. In the case of the plate with free-free edges, this eigen equation is

$$\sin z = C_1 z \quad [15]$$

where $z = \lambda\alpha$ and $C_1 = \pm(\sin\alpha)/\alpha$. Equation [15] determines the value or values of the eigen value λ as a function of α.

Inasmuch as the continuity of displacements requires $\lambda > 0$, any value of Equation [15] satisfying this restriction will give an admissible solution for the extensional problem. Furthermore, as may be seen from Equations [12] to [14], a value of λ such that $0 < \lambda < 1$ will give unbounded stresses near the vertex of the sector. The purpose of this paper is to investigate the occurrence of any values of λ (or its real part if λ is complex) which lie in this region. Stated alternatively, it is desired to find the minimum root of Equation [15] with the restriction that $\lambda > 0$.

The results, showing min Re λ as a function of α for Poisson's ratio $\nu = 0.3$, ($\sigma = {}^3/_{13}$) are presented in Fig. 1.

CLAMPED-CLAMPED EDGES

Fixed edges at $\theta = 0$ and $\theta = \alpha$ require that $U_r(0) = U_\theta(0) = 0$, $U_r(\alpha) = U_\theta(\alpha) = 0$. Upon using Equations [10] and [11] and again formulating the four simultaneous homogeneous equations, the eigen equation in this case again becomes

$$\sin z = C_2 z \quad [16]$$

where $z = \lambda\alpha$ and

$$C_2 = \pm\frac{\sin\alpha}{(3-4\sigma)\alpha}$$

The min Re$\lambda(\alpha)$ for this case are also shown in Fig. 1 for $\nu = 0.3$.

CLAMPED-FREE

The mixed boundary condition of a clamped-free plate in extension requires $\sigma_\theta(0) = \tau_{r\theta}(0) = U_r(\alpha) = U_\theta(\alpha) = 0$. Using Equations [10], [11], [13], and [14] the eigen equation is found to be of somewhat different form, namely

$$\sin^2 z = \left[\frac{4(1-\sigma)^2}{3-4\sigma}\right] - \left[\frac{\sin^2\alpha}{(3-4\sigma)\alpha^2}\right] z^2 \quad [17]$$

The minimum values of the eigen parameter for this case are also shown in Fig. 1 as a function of vertex angle for $\nu = 0.3$.

COMPARISON OF RESULTS

A study of Fig. 1 reveals that of the three cases considered, only the plate with mixed boundary conditions, namely, clamped-free, may have a singularity if the vertex angle lies between 63 and 180 degrees.

As discussed elsewhere,[5] this does not mean that a singularity must occur, because other higher eigenvalues from Equation [17], at 90 deg, for example, will not introduce singular behavior at the origin. On the other hand, an arbitrary loading along the circumferential boundary formed by a linear combination of the eigen functions in the manner suggested by the author[4] will contain the eigen function giving rise to the singularity and hence locally in the vicinity of the origin introduce unbounded stresses.

For vertex angles between 180 and 360 degrees, all the cases considered may have stress singularities.

[5] "Theoretical and Experimental Effect of Sweep Upon the Stress and Deflection Distribution in Aircraft Wings of High Solidity. Part 6—The Plate Problem for a Cantilever Sector of Uniform Thickness," by M. L. Williams, AFTR 5761, November, 1950.

TABLE 1 EIGEN EQUATIONS FOR BENDING AND EXTENSION

Case no.	Boundary condition	Eigen equation	Loading	Constants
1	Free-free	$\sin z = C_1 z$	Bending	$C_1 = \pm \frac{1-\nu}{3+\nu} \frac{\sin \alpha}{\alpha}$
			Extension	$C_1 = \pm \frac{\sin \alpha}{\alpha}$
2	Clamped-clamped	$\sin z = C_2 z$	Bending	$C_2 = \pm \frac{\sin \alpha}{\alpha}$
			Extension	$C_2 = \pm \frac{1+\nu}{3-\nu} \frac{\sin \alpha}{\alpha}$
3	Clamped-free	$\sin^2 z = K_1^2 - K_2^2 z^2$	Bending	$K_1 = \pm \left[\frac{4}{(3+\nu)(1-\nu)}\right]^{1/2}$
				$K_2 = \pm \left[\frac{1-\nu}{3+\nu}\right]^{1/2} \frac{\sin \alpha}{\alpha}$
			Extension	$K_1 = \pm \left[\frac{4}{(3-\nu)(1+\nu)}\right]^{1/2}$
				$K_2 = \pm \left[\frac{1+\nu}{3-\nu}\right]^{1/2} \frac{\sin \alpha}{\alpha}$

Another conclusion can be drawn from a comparison of the extensional and bending results. For easy reference a table giving the eigen equations for both extension and bending is herein as Table 1. It is seen that the eigen equations for the free-free extensional case are exactly the same as for the clamped-clamped bending case which means that locally a clamped bent plate behaves as a free extensional plate.

For the cases of generalized plane stress the eigen equations for the free-free bending and clamped-clamped extension cases, and for the clamped-free bending and extension cases are the same if ν is replaced by $-\nu$. Southwell noted this association of Poisson's ratio between the bending and extension cases[5] and, furthermore, derived the correspondence of the boundary conditions. The point to be observed here is that the characteristic equation for the eigen values of the stress and deformation behavior are also analogous in the two cases.

In conclusion it is suggested that the analysis for the free-free case be applied to determine the type of stress variation at the base of V-shaped notches in plates or rods.

[5] "On the Analogues Relating Flexure and Extension of Flat Plates," by R. V. Southwell, *Quarterly Journal of Mechanics and Applied Mathematics*, vol. 3, part 3, September, 1950, pp. 257–270.

The Stresses in a Flat Curved Bar Due to Concentrated Radial Loads[1]

By C. W. NELSON,[2] C. J. ANCKER, JR.,[3] AND NING-GAU WU,[4] BERKELEY, CALIF.

This paper presents a Fourier integral solution for the plane-stress problem of a curved bar bounded by two concentric circles and loaded by any combination of radial loads on the circular boundaries. It is an extension of an earlier investigation (1)[5] which dealt with only the particular case of a curved bar in equilibrium under the action of two equal and opposite radial forces, one on each boundary. Numerical results are given for one of two basic cases from which the stresses for any combination of concentrated radial loads may be obtained by superposition. An example is included to show how superposition may be used to obtain the stresses for a loading condition which may occur frequently in practical machine-design problems. It is believed that the procedures developed in this paper will be useful in the solution of other elasticity problems by the Fourier integral method.

Introduction

IN an earlier paper by one of the authors, a Fourier integral solution was presented for a portion of a circular ring loaded as shown in Fig. 1(*a*). In the present paper the Fourier integral method is applied to the problem illustrated in Fig. 1(*b*). By superposition of the solutions for the two types of loading shown in Figs. 1 (*a*) and (*b*), the solution for any combination of concentrated radial loads acting on a portion of a circular ring can be obtained. For example, by subtracting one half of the stresses for Fig. 1(*b*) from one half of the stresses for Fig. 1(*a*), the stresses for Fig. 2(*a*) are obtained. Similarly, by adding one half of the stresses for Fig. 1(*b*) to one half of the stresses for Fig. 1(*a*), the stresses for Fig. 2(*b*) are obtained. In the solutions for Fig. 1(*b*) and Fig. 2 (*a* and *b*) the location of the wall at the built-in end of the curved beam is not specified. The wall is a fictitious one in the sense that the solution does not hold in the immediate vicinity of the wall and the wall is shown only in order to indicate which end of the beam is supported. In Figs. 1 and 2 and throughout this paper, the thicknesses of the bodies perpendicular to the plane of the paper are always assumed to be unity so that any load P should be thought of as force per unit thickness.

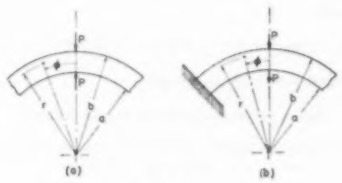

FIG. 1

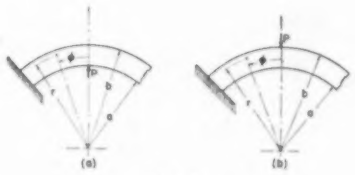

FIG. 2

In the solution of the curved-bar problems illustrated in Figs. 1 and 2, the authors have been assisted greatly by results obtained by other investigators (2, 3, 4, 5, 6, 7) in the solution of straight-beam problems.

Review of General Theory

In this paper, as in the earlier paper (1) where the problem of Fig. 1(*a*) was presented, the solutions of the plane-stress problems considered will be derived in terms of Airy's stress function which will be denoted by ψ. This stress function must satisfy the biharmonic equation

$$\nabla^2\nabla^2\psi = 0 \qquad [1]$$

where ∇^2 stands for the Laplace operator which, in polar co-ordinates (r, ϕ) is

$$\nabla^2 = \frac{\partial^2}{\partial r^2} + \frac{1}{r}\frac{\partial}{\partial r} + \frac{1}{r^2}\frac{\partial^2}{\partial \phi^2}$$

The stresses are to be determined from the stress function by the equations

$$\sigma_r = \frac{1}{r}\frac{\partial \psi}{\partial r} + \frac{1}{r^2}\frac{\partial^2 \psi}{\partial \phi^2} \qquad [2]$$

$$\sigma_\phi = \frac{\partial^2 \psi}{\partial r^2} \qquad [3]$$

$$\tau_{r\phi} = -\frac{\partial}{\partial r}\left(\frac{1}{r}\frac{\partial \psi}{\partial \phi}\right) \qquad [4]$$

Stresses determined by the foregoing procedure will satisfy equi-

[1] Some of the material presented in this paper was taken from a thesis submitted by C. J. Ancker, Jr., at the University of California in partial fulfillment of the requirements for the degree of Mechanical Engineer, 1950, and some from a thesis submitted by Ning-Gau Wu at the University of California in partial fulfillment of the requirements for the degree of Doctor of Philosophy, 1952.

[2] Associate Professor of Engineering Design, University of California. Mem. ASME.

[3] Assistant Professor of Engineering Design, University of California., Jun. ASME.

[4] Graduate student and Harry H. Hilp Research Fellow in Engineering, 1951–1952, University of California.

[5] Numbers in parentheses refer to the Bibliography at the end of the paper.

Presented at the West Coast Conference of the Applied Mechanics Division, Los Angeles, Calif., June 26–28, 1952, of THE AMERICAN SOCIETY OF MECHANICAL ENGINEERS.

Discussion of this paper should be addressed to the Secretary, ASME, 29 West 39th Street, New York, N. Y., and will be accepted until January 10, 1953, for publication at a later date. Discussion received after the closing date will be returned.

NOTE: Statements and opinions advanced in papers are to be understood as individual expressions of their authors and not those of the Society. Manuscript received by ASME Applied Mechanics Division, March 15, 1952.

librium and compatibility requirements. In any particular problem, a proper combination of solutions of Equation [1] must be formed so that boundary conditions will be satisfied.

The problem illustrated in Fig. 1(*b*) is not symmetrical with respect to ϕ because one end of the bar is built in while the other end is not supported. The stress function for Fig. 1(*b*) will be obtained by combining a well-known solution which is antisymmetrical with respect to ϕ with a symmetrical solution obtained in integral form by taking the limit of the sum of many terms of the form (8*a*)

$$\psi_n = (a_n r^n + b_n r^{n+2} + a'_n r^{-n} + b_n' r^{-n+2}) \cos n\phi \ldots [5]$$

where n is not necessarily an integer.

Basic Problem of Symmetrical Bending

Fig. 3(*a*) shows a portion of a circular ring with curved boundaries $r = a$ and $r = b$ and radial boundaries which, for convenience, are taken at $\phi = \pi$ and at $\phi = -\pi$ radians. Radial boundaries at $\phi = 3\pi$ and $\phi = -3\pi$, for example, would be equally convenient and such a choice of radial boundaries should be regarded as being physically possible since the problem considered is one of plane stress and the thickness of the ring may be very small so that the ends may slip past each other. The ring is loaded by normal forces uniformly distributed from $\phi = -\beta$ to $\phi = \beta$ on both boundaries $r = a$ and $r = b$. These normal forces are compressive on the outer boundary and tensile on the inner boundary. Furthermore, in order to make the downward force resultant on the inner boundary equal to that on the outer boundary, it will be specified that, for $-\beta < \phi < \beta$

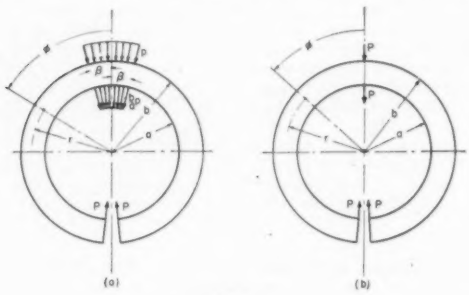

Fig. 3

$$(\sigma_r)_{r=a} = -\frac{b}{a}(\sigma_r)_{r=b} = \frac{b}{a}p \ldots [6]$$

After the stress function for Fig. 3(*a*) has been derived, the stress function for Fig. 3(*b*) will be obtained by letting β approach zero in the solution for Fig. 3(*a*), at the same time specifying that the downward resultant force on each curved boundary shall remain finite and of magnitude P. Thereafter, a known solution, presented in the following, will be superposed on the solution for Fig. 3(*b*), so as to obtain the solution for Fig. 1(*b*).

Derivation of a Stress Function for the Symmetrical Bending Problem

The boundary-stress conditions for Fig. 3(*a*) are

$$(\sigma_r)_{r=a} = -\frac{b}{a}(\sigma_r)_{r=b} \ldots [7]$$

$$(\sigma_r)_{r=b} = F(\phi) \ldots [8]$$

$$(\tau_{r\phi})_{r=a} = 0 \ldots [9]$$

$$(\tau_{r\phi})_{r=b} = 0 \ldots [10]$$

where $F(\phi)$ is an even function of ϕ such that

$$\begin{aligned} F(\phi) &= (\sigma_r)_{r=b} = 0 && \text{for } -\infty < \phi < -\beta \\ F(\phi) &= -p && \text{for } -\beta < \phi < \beta \\ F(\phi) &= 0 && \text{for } \beta < \phi < \infty \end{aligned}$$

In reference (1) the formula

$$F(\phi) = \frac{2}{\pi}\int_0^\infty d\lambda \int_0^\infty F(\lambda) \cos n\phi \cos n\lambda \, d\lambda \ldots [11]$$

which expresses $F(\phi)$ as a Fourier cosine integral, valid for $-\infty < \phi < \infty$ in the case of an even function of ϕ, was applied to the same function $F(\phi)$ which occurs here. The result of performing the inner integration in Equation [11] was found to be

$$F(\phi) = -\frac{2}{\pi}\int_0^\infty \left(\cos n\phi \, dn \, \frac{p}{n} \sin n\beta\right) \ldots [12]$$

It is not desirable to perform the remaining integration. For the limiting case when β becomes very small but the total load on each boundary remains finite and equal to P, Equation [12] reduces to

$$\lim_{\beta \to 0} F(\phi) = -\frac{2}{\pi}\int_0^\infty \left(\cos n\phi \, dn \, \frac{P}{2b}\right) \ldots [13]$$

Equation [13] is applicable for Fig. 3(*b*).

It is proposed to form a sum of many stress functions ψ_n such as given by Equation [5]. Boundary Conditions [7], [9], and [10] can be satisfied separately by each ψ_n. When this is done, three of the four constants a_n, b_n, a_n', b_n' in Equation [5] will be expressed in terms of the remaining one. The result is

$$\psi_n = \frac{a_n' \cos n\phi}{(n-1)ab(b^{n-1} + a^{n-1})} \left\{ \begin{aligned} &\frac{n(b^2 - r^2)}{b}\left(\frac{r^n}{a^n} + \frac{a^n}{r^n}\right) \\ &- \frac{n(r^2 - a^2)}{a}\left(\frac{b^n}{r^n} + \frac{r^n}{b^n}\right) \\ &+ \frac{(b^2 + r^2)}{b}\left(\frac{r^n}{a^n} - \frac{a^n}{r^n}\right) \\ &- \frac{(r^2 + a^2)}{a}\left(\frac{b^n}{r^n} - \frac{r^n}{b^n}\right) \end{aligned} \right\} \ldots [14]$$

Considerable algebra which is required in order to arrive at Equation [14] has been omitted. The steps omitted are essentially the same steps that are described in reference (1) in the process of arriving at a similar result for slightly different boundary conditions. The stress function

$$\sum_{n=0, \Delta n, 2\Delta n, \ldots}^{\infty} \psi_n \, \Delta n$$

obtained by forming an infinite series of stress functions of the type given by Equation [14], each multiplied by Δn, will still satisfy boundary Conditions [7], [9], [10]. The same is true of the stress function

$$\psi = \int_0^\infty \psi_n \, dn \ldots [15]$$

which is the limit of the foregoing infinite series of stress functions as Δn approaches zero.

Boundary Condition [8] remains to be satisfied. Application of Equation [2] to the stress function of Equation [15] gives

$$\sigma_r = \int_0^\infty \left(\frac{1}{r} \frac{\partial \psi_n}{\partial r} + \frac{1}{r^2} \frac{\partial^2 \psi_n}{\partial \phi^2} \right) dn \quad \ldots\ldots [16]$$

Substitution of $r = b$ in Equation [16] and application of Equation [8] lead to the result

$$F(\phi) = \int_0^\infty \left(\frac{1}{r} \frac{\partial \psi_n}{\partial r} + \frac{1}{r^2} \frac{\partial^2 \psi_n}{\partial \phi^2} \right)_{r=b} dn \quad \ldots\ldots [17]$$

Subtraction of Equation [13] from Equation [17] gives an equation of the form

$$\int_0^\infty f(n) \cos n\phi \, dn = 0 \quad \ldots\ldots [18]$$

and, if this equation is to hold for all values of ϕ, it is necessary that $f(n)$ shall be zero, from which

$$a_n' = \frac{P}{2\pi} \frac{ab(b^{n-1} + a^{n-1})}{(n+1)\left[\left(\frac{b^n}{a^n} - \frac{a^n}{b^n}\right) - n\left(\frac{b}{a} - \frac{a}{b}\right)\right]} \quad \ldots\ldots [19]$$

Therefore the stress function for Fig. 3(*b*) is

$$\psi = \frac{P}{2\pi} \int_0^\infty \frac{j(r, n) \cos n\phi \, dn}{(n^2 - 1)\left[\left(\frac{b^n}{a^n} - \frac{a^n}{b^n}\right) - n\left(\frac{b}{a} - \frac{a}{b}\right)\right]} \quad \ldots\ldots [20]$$

where $j(r, n)$ is the quantity in the braces of Equation [14].

It is advantageous to introduce the new symbols

$$z = n \ln \frac{1}{\alpha} \quad \ldots\ldots [21]$$

where $\alpha = \dfrac{a}{b}$

and

$$\left.\begin{aligned} \Phi = \frac{\phi}{\ln \frac{1}{\alpha}}, \; A = \frac{\ln \frac{r}{a}}{\ln \frac{1}{\alpha}}, \; B = \frac{\ln \frac{b}{r}}{\ln \frac{1}{\alpha}} \\ X = \frac{\sinh \ln \frac{1}{\alpha}}{\ln \frac{1}{\alpha}} = \frac{1 - \alpha^2}{2\alpha \ln \frac{1}{\alpha}} \end{aligned}\right\} \quad \ldots\ldots [22]$$

In terms of these symbols, Equation [20] becomes

$$\psi_s = \frac{P}{2\pi} \int_0^\infty \left\{ \frac{\left[\begin{aligned} &\frac{(b^2 - r^2)}{b \ln \frac{1}{\alpha}} z \cosh Az \\ &- \frac{(r^2 - a^2)}{a \ln \frac{1}{\alpha}} z \cosh Bz \\ &+ \frac{(b^2 + r^2)}{b} \sinh Az \\ &- \frac{(r^2 + a^2)}{a} \sinh Bz \end{aligned} \right]}{\left[\left(\frac{z}{\ln \frac{1}{\alpha}}\right)^2 - 1\right][\sinh z - Xz]} \right\} \frac{\cos \Phi z \, dz}{\ln \frac{1}{\alpha}} \quad \ldots\ldots [23]$$

where the subscript s has been attached to ψ to indicate that this is the stress function for the symmetrical problem of Fig. 3(*b*).

Stress Function for Unsymmetrical Bending

The stress function for the unsymmetrical bending problem of Fig. 1(*b*) will be denoted by ψ_U and it may be expressed as

$$\psi_U = \psi_S + \psi_K \quad \ldots\ldots [24]$$

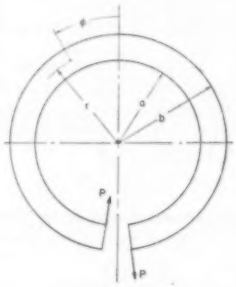

Fig. 4

(The loads in this figure are actually equal, opposite, and collinear. The width of the gap is very small but is exaggerated in the drawing.)

where ψ_K is the known stress function for the case shown in Fig. 4. The expression for ψ_K is (8*b*)

$$\psi_K = \frac{-P\left[\frac{a^2b^2}{r} + 2(a^2 + b^2)r \ln r - r^3\right]}{2\left[a^2 - b^2 + (a^2 + b^2)\ln \frac{b}{a}\right]} \sin \phi \quad \ldots [25]$$

The stress function ψ_U given by Equation [24] is valid for Fig. 1(*b*), except in the immediate vicinity of the wall. Another limitation on this solution for Fig. 1(*b*) is that the derivation is based on the assumption that the curved bar extends indefinitely to the right of the loads P in the figure. However, the stresses obtained from ψ_U will be sufficiently accurate for practical purposes if the curved beam extends as much as one beam depth to the right of the loads P. This will become apparent from calculations which will be given.

Curved Bar Loaded Only on Inner Circular Boundary

If the stress function (1) for Fig. 1(*a*) is denoted by ψ_P, then the stress function for Fig. 2(*a*) is

$$\psi_I = \frac{1}{2}\psi_P - \frac{1}{2}\psi_U \quad \ldots\ldots [26]$$

or

$$\psi_I = \frac{P\left[\frac{a^2b^2}{r} + 2(a^2 + b^2)r \ln r - r^3\right]}{4\left[a^2 - b^2 + (a^2 + b^2)\ln \frac{b}{a}\right]} \sin \phi$$

$$+\frac{P}{2\pi}\int_0^\infty \left\{ \begin{array}{l} \sinh z \left[\begin{array}{l} \dfrac{(r^2-a^2)}{a\ln\dfrac{1}{\alpha}}\, z\cosh Bz \\ +\dfrac{(a^2+r^2)}{a}\sinh Bz \end{array} \right] \\ -\mathrm{X}z \left[\begin{array}{l} \dfrac{(b^2-r^2)}{b\ln\dfrac{1}{\alpha}}\, z\cosh Az \\ +\dfrac{(b^2+r^2)}{b}\sinh Az \end{array} \right] \end{array} \right\} \frac{\cos \Phi z\, dz}{\ln\dfrac{1}{\alpha}}$$
$$\div\left[\left(\frac{z}{\ln\dfrac{1}{\alpha}}\right)^2-1\right][\sinh^2 z-\mathrm{X}^2z^2] \qquad \ldots\ldots[27]$$

The corresponding stresses, derived by application of Equations [2], [3], [4], are

$$\sigma_r+\sigma_\phi=\frac{P\left[-2r+\dfrac{a^2+b^2}{r}\right]\sin\phi}{\left[a^2-b^2+(a^2+b^2)\ln\dfrac{b}{a}\right]}$$
$$+\frac{2P}{\pi\ln\dfrac{1}{\alpha}}\left[\begin{array}{l}\dfrac{\mathrm{X}}{b}\displaystyle\int_0^\infty \frac{z\sinh Az\cos\Phi z\,dz}{\sinh^2 z-\mathrm{X}^2z^2} \\ -\dfrac{1}{a}\displaystyle\int_0^\infty \frac{\sinh z\sinh Bz\cos\Phi z\,dz}{\sinh^2 z-\mathrm{X}^2z^2}\end{array}\right] \qquad \ldots[28]$$

$$\sigma_r-\sigma_\phi=\frac{P\left[r-\dfrac{a^2b^2}{r^3}\right]\sin\phi}{\left[a^2-b^2+(a^2+b^2)\ln\dfrac{b}{a}\right]}$$
$$+\frac{P}{\pi\left(\ln\dfrac{1}{\alpha}\right)^2}\left[\begin{array}{l}\dfrac{\mathrm{X}\left(\dfrac{b^2}{r^2}-1\right)}{b}\displaystyle\int_0^\infty \frac{z^2\cosh Az\cos\Phi z\,dz}{\sinh^2 z-\mathrm{X}^2z^2} \\ -\dfrac{\left(1-\dfrac{a^2}{r^2}\right)}{a}\displaystyle\int_0^\infty \frac{z\sinh z\cosh Bz\cos\Phi z\,dz}{\sinh^2 z-\mathrm{X}^2z^2}\end{array}\right] \qquad \ldots\ldots[29]$$

$$\tau_{r\phi}=\frac{P\left[r-\dfrac{a^2+b^2}{r}+\dfrac{a^2b^2}{r^3}\right]\cos\phi}{2\left[a^2-b^2+(a^2+b^2)\ln\dfrac{b}{a}\right]}$$
$$-\frac{P}{2\pi\left(\ln\dfrac{1}{\alpha}\right)^2}\left[\begin{array}{l}\dfrac{\mathrm{X}\left(\dfrac{b^2}{r^2}-1\right)}{b}\displaystyle\int_0^\infty \frac{z^2\sinh Az\sin\Phi z\,dz}{\sinh^2 z-\mathrm{X}^2z^2} \\ +\dfrac{\left(1-\dfrac{a^2}{r^2}\right)}{a}\displaystyle\int_0^\infty \frac{z\sinh z\sinh Bz\sin\Phi z\,dz}{\sinh^2 z-\mathrm{X}^2z^2}\end{array}\right] \qquad \ldots\ldots[30]$$

Before considering these stresses further, it will be well to derive the stresses for Fig. 2(*b*) since there are several similarities between the expressions for the stresses for Fig. 2(*a*) and those for Fig. 2(*b*).

Curved Bar Loaded Only on Outer Circular Boundary

The stress function for Fig. 2(*b*) is

$$\psi_0=\frac{1}{2}\psi_P+\frac{1}{2}\psi_U \qquad \ldots\ldots[31]$$

or

$$\psi_0=\frac{-P\left[\dfrac{a^2b^2}{r}+2(a^2+b^2)r\ln r-r^3\right]}{4\left[a^2-b^2+(a^2+b^2)\ln\dfrac{b}{a}\right]}\sin\phi$$
$$+\frac{P}{2\pi}\int_0^\infty \left\{ \begin{array}{l} \sinh z \left[\begin{array}{l} \dfrac{(b^2-r^2)}{b\ln\dfrac{1}{\alpha}}\, z\cosh Az \\ +\dfrac{(b^2+r^2)}{b}\sinh Az \end{array} \right] \\ -\mathrm{X}z \left[\begin{array}{l} \dfrac{(r^2-a^2)}{a\ln\dfrac{1}{\alpha}}\, z\cosh Bz \\ +\dfrac{(a^2+r^2)}{a}\sinh Bz \end{array} \right] \end{array} \right\} \frac{\cos \Phi z\, dz}{\ln\dfrac{1}{\alpha}}$$
$$\div\left[\left(\frac{z}{\ln\dfrac{1}{\alpha}}\right)^2-1\right][\sinh^2 z-\mathrm{X}^2z^2] \qquad \ldots[32]$$

The corresponding stresses are

$$\sigma_r+\sigma_\phi=\frac{P\left[2r-\dfrac{a^2+b^2}{r}\right]\sin\phi}{\left[a^2-b^2+(a^2+b^2)\ln\dfrac{b}{a}\right]}$$
$$+\frac{2P}{\pi\ln\dfrac{1}{\alpha}}\left[\begin{array}{l}\dfrac{\mathrm{X}}{a}\displaystyle\int_0^\infty \frac{z\sinh Bz\cos\Phi z\,dz}{\sinh^2 z-\mathrm{X}^2z^2} \\ -\dfrac{1}{b}\displaystyle\int_0^\infty \frac{\sinh z\sinh Az\cos\Phi z\,dz}{\sinh^2 z-\mathrm{X}^2z^2}\end{array}\right] \qquad \ldots[33]$$

$$\sigma_r-\sigma_\phi=\frac{-P\left[r-\dfrac{a^2b^2}{r^3}\right]\sin\phi}{\left[a^2-b^2+(a^2+b^2)\ln\dfrac{b}{a}\right]}$$
$$+\frac{P}{\pi\left(\ln\dfrac{1}{\alpha}\right)^2}\left[\begin{array}{l}\dfrac{\mathrm{X}\left(1-\dfrac{a^2}{r^2}\right)}{a}\displaystyle\int_0^\infty \frac{z^2\cosh Bz\cos\Phi z\,dz}{\sinh^2 z-\mathrm{X}^2z^2} \\ -\dfrac{\left(\dfrac{b^2}{r^2}-1\right)}{b}\displaystyle\int_0^\infty \frac{z\sinh z\cosh Az\cos\Phi z\,dz}{\sinh^2 z-\mathrm{X}^2z^2}\end{array}\right] \qquad \ldots\ldots[34]$$

$$\tau_{r\phi}=\frac{-P\left[r-\dfrac{a^2+b^2}{r}+\dfrac{a^2b^2}{r^3}\right]\cos\phi}{2\left[a^2-b^2+(a^2+b^2)\ln\dfrac{b}{a}\right]}$$

$$+\frac{P}{2\pi\left(\ln\frac{1}{\alpha}\right)^2}\left[\begin{array}{l}\dfrac{X\left(1-\dfrac{a^2}{r^2}\right)}{a}\displaystyle\int_0^\infty \frac{z^2\sinh Bz\sin\Phi z\,dz}{\sinh^2 z-X^2z^2} \\ +\dfrac{\left(\dfrac{b^2}{r^2}-1\right)}{b}\displaystyle\int_0^\infty \frac{z\sinh z\sinh Az\sin\Phi z\,dz}{\sinh^2 z-X^2z^2}\end{array}\right] \quad \ldots\ldots\ldots [35]$$

From Saint Venant's principle, it is known that the stresses at one or two beam depths to the right of the load in Fig. 2(*b*) must be very small. Therefore, considering Equation [34] for instance, it may be surmised that for absolute values of Φ greater than about 2, that part of $\sigma_r - \sigma_\phi$ containing the integrals contributes about the same magnitude of stress as the first term containing the factor $\sin\phi$. Only if this is true, will it be possible for the value of $(\sigma_r - \sigma_\phi)$ to approach zero as Φ varies through negative values of increasing magnitude. The assumption that $(\sigma_r - \sigma_\phi)$ approaches zero at moderate distances to the right of the load in Fig. 2(*b*) also implies that the value of $(\sigma_r - \sigma_\phi)$ to the left of the load rapidly approaches the value

$$\frac{-2P\left[r-\dfrac{a^2b^2}{r^3}\right]\sin\phi}{\left[a^2-b^2+(a^2+b^2)\ln\dfrac{b}{a}\right]}$$

when Φ increases in the positive sense.

Aside from such generalizations as the one just made, not much can be learned about the stresses given by Equations [28] to [30], and [33] to [35] by mere inspection. It is necessary to be able to evaluate the integrals before any practical use can be made of these equations.

Evaluation of Integrals for Φ Less Than Unity

The numerator of the integrand in any of the integrals in Equations [28] to [30], and [33] to [35] can be expressed as a Maclaurin series in powers of z. Thus the integral can be replaced by a series of integrals of the type

$$\int_0^\infty \frac{z^n dz}{\sinh^2 z - X^2z^2}, \text{ where } n = 2, 4, 6, \ldots\ldots$$

each multiplied by a polynomial involving products of powers of Φ and either A or B. By the partial-fractions method it can be shown that

$$\int_0^\infty \frac{z^{k+1}\,dz}{\sinh^2 z - X^2z^2} = \frac{k!}{X}(H_k - I_k) \quad \ldots\ldots\ldots [36]$$

where

$$I_k = \frac{1}{2(k!)}\int_0^\infty \frac{z^k\,dz}{\sinh z + Xz} \quad \ldots\ldots\ldots [37]$$

and

$$H_k = \frac{1}{2(k!)}\int_0^\infty \frac{z^k\,dz}{\sinh z - Xz} \quad \ldots\ldots\ldots [38]$$

and the values of k which need to be considered are

$$k = 1, 3, 5, 7, \ldots\ldots\ldots$$

It should be pointed out that the integrals H_k are not ordinary integrals because the denominator of the integrand in Equation [38] passes through zero at a value of $z = z_1$ such that

$$z_1 = \ln\frac{1}{\alpha} \quad \ldots\ldots\ldots [39]$$

According to mathematical convention (9), H_k should not be written as an ordinary integral and, instead, the following notation should be used

$$2(k!)H_k = P\int_0^\infty \frac{z^k\,dz}{\sinh z - Xz} = \lim_{h\to 0}\left[\int_0^{z_1-h}\frac{z^k\,dz}{\sinh z - Xz} + \int_{z_1+h}^\infty \frac{z^k\,dz}{\sinh z - Xz}\right] \quad \ldots [40]$$

where the symbol P is used to indicate the special nature of the integral and is read as "the principal value of the integral." This symbol P will be omitted hereafter in this paper since the letter P has already been used to represent force per inch of length along an element of the cylindrical surface of a curved bar and it hardly seems necessary to repeatedly call attention to the special nature of the definite integrals H_k.

The integrals I_k were treated in reference (1). Table 1 of reference (1) gives values of the coefficients a_k, b_k, and so on, for the Taylor's series expansion

$$I_k(X) = a_k - b_k(X-1) + c_k(X-1)^2 - d_k(X-1)^3 + \ldots\ldots\ldots [41]$$

Table 1 of the present paper gives values of the coefficients α_k, β_k, γ_k, and so on, for the Taylor's series expansion

$$H_k(X) = \alpha_k + \beta_k(X-1) + \gamma_k(X-1)^2 + \delta_k(X-1)^3 + \ldots\ldots\ldots [42]$$

It should be noted that $(X - 1)$ is small compared to unity if $a/b > 0.5$.

TABLE 1 VALUES OF COEFFICIENTS IN TAYLOR SERIES FOR $H_k(X)$

k	α_k	β_k	γ_k	δ_k	ϵ_k	ζ_k	η_k
1	−1.179153868	0.679153868	−0.457134988	0.326565936	−0.240845284	0.181212229	−0.138263028
3	2.038710667	−1.675223637	1.243480123	−0.932437596	0.708242900	−0.543583773	0.420642023
5	1.156864366	0.425655803	−0.616366464	0.573397020	−0.486737494	0.400187474	−0.324610876
7	1.039251312	0.053556636	0.049414207	−0.101740014	0.114367412	−0.109389888	0.097685997
9	1.010870147	0.012345768	0.002366511	0.003558326	−0.009482599	0.012529344	−0.013375580
11	1.003084774	0.003265641	0.000228801	0.000082834	0.000173383	−0.000585575	0.000894736
13	1.000876180	0.000899749	0.000026810	0.000004159	0.000002264	0.000000083	−0.000024232
15	1.000247139	0.000250274	0.000003377	0.000000264	0.000000067	0.000000049	0.000000161
17	1.000069073	0.000069492	0.000000437	0.000000019	0.000000003	0.000000001	0.000000001
19	1.000019128	0.000019184	0.000000057	0.000000001	0.000000000	0.000000000	
21	1.000005252	0.000005260	0.000000007	0.000000000			
23	1.000001431	0.000001432	0.000000001				
25	1.000000388	0.000000388	0.000000000				
27	1.000000104	0.000000104					
29	1.000000028	0.000000028					
31	1.000000007	0.000000007					
33	1.000000002	0.000000002					
35	1.000000001	0.000000001					
37	1.000000000	0.000000000					

The details of the derivation of the values of α_k, β_k, and so on are given in reference (10).

The application of Table 1, together with Table 1 of reference (1), toward obtaining the stresses in a curved beam for values of Φ less than unity will be demonstrated in a later section.

The method presented in the foregoing is comparable to the procedure used by Howland (6, 7) in the treatment of straight-beam problems, while the method discussed in the next section is an extension of the method used by von Kármán (2) and Seewald (3) for straight-beam problems. The latter method was discussed in detail in 1904 by Dougall (11) in connection with similar integrals arising in flat-plate problems, but Dougall did not give any numerical results.

Evaluation of Integrals for Larger Values of Φ

A satisfactory method of integration for Φ greater than unity, and even for values of Φ somewhat less than unity, is the method of contour integration based on the residue theorem of complex variable theory (12). The method can be applied to any of the integrals which occur in Equations [28] to [30] and [33] to [35]. The application of the contour-integral method to the evaluation of the integrals

$$\int_0^\infty \frac{z \cos \Phi z \, dz}{\sinh z \pm Xz}$$

is presented in reference (13).

Numerical Examples

In order to show some numerical results of the procedures described in the foregoing, further consideration will be given to the circumferential stress σ_ϕ, for the curved bar loaded as in Fig. 2(*b*). For small values of Φ the circumferential stress on the outer boundary of Fig. 2 (*b*) can be calculated from the formula

$$(\sigma_\phi)_{r=b} = (\sigma_r)_{r=b} + \frac{P \sin \phi}{b\left[\dfrac{1+\alpha^2}{1-\alpha^2} \ln \dfrac{1}{\alpha} - 1\right]} + \frac{2PX}{\pi b \ln \dfrac{1}{\alpha}}$$

$$[(I_1 - H_1) - 3\Phi^2(I_3 - H_3) + 5\Phi^4(I_5 - H_5) - 7\,\Phi^6(I_7 - H_7) + \ldots .] \quad [43]$$

derived by applying Equations [37] and [38] to the following equation obtained by substituting $r = b$ into Equation [34]

$$(\sigma_\phi)_{r=b} = (\sigma_r)_{r=b} + \frac{P \sin \phi}{b\left[\dfrac{1+\alpha^2}{1-\alpha^2} \ln \dfrac{1}{\alpha} - 1\right]} + \frac{PX}{\pi b \ln \dfrac{1}{\alpha}} \left[\int_0^\infty \frac{z \cos \Phi z \, dz}{\sinh z + Xz} - \int_0^\infty \frac{z \cos \Phi z \, dz}{\sinh z - Xz}\right] \quad [44]$$

For values of Φ greater than 0.5, it is more convenient to apply the contour integral method to the latter equation.

The circumferential stress on the inner boundary of Fig. 2(*b*), obtained by substituting $r = a$ into Equation [34] is

$$(\sigma_\phi)_{r=a} = -\frac{P \sin \phi}{a\left[\dfrac{1+\alpha^2}{1-\alpha^2} \ln \dfrac{1}{\alpha} - 1\right]} + \frac{PX}{\pi a \ln \dfrac{1}{\alpha}} \left[\int_0^\infty \frac{z \cos \Phi z \, dz}{\sinh z + Xz} + \int_0^\infty \frac{z \cos \Phi z \, dz}{\sinh z - Xz}\right] \quad [45]$$

For values of Φ greater than about 0.5, the contour integral method again may be used to evaluate the integrals in Equation [45]. For smaller values of Φ, Equation [45] may be put in the form

$$(\sigma_\phi)_{r=a} = -\frac{P \sin \phi}{a\left[\dfrac{1+\alpha^2}{1-\alpha^2} \ln \dfrac{1}{\alpha} - 1\right]} + \frac{2PX}{\pi a \ln \dfrac{1}{\alpha}}$$

$$[(I_1 + H_1) - 3\Phi^2(I_3 + H_3) + 5\Phi^4(I_5 + H_5) - \ldots .] \quad [46]$$

For the problem in Fig. 2(*b*), Table 2 contains values of $(\sigma_\phi)_{r=b}$

TABLE 2. VALUES OF CIRCUMFERENTIAL STRESS AT OUTER BOUNDARY FOR LOADING SHOWN IN FIG. 2(*b*)

$\left[(\sigma_\phi)_{r=b} + \dfrac{P}{b-a}\right]$

Φ	For $\alpha = 1.0$	For $\alpha = 0.9$	For $\alpha = 0.8$	For $\alpha = 0.7$
−3.0	0.000 002	0.000 002	0.000 002	0.000 002
−2.8	−0.000 003	−0.000 003	−0.000 002	−0.000 001
−2.6	−0.000 02	−0.000 02	−0.000 02	−0.000 02
−2.4	−0.000 08	−0.000 07	−0.000 07	−0.000 06
−2.2	−0.000 21	−0.000 20	−0.000 19	−0.000 18
−2.0	−0.000 45	−0.000 43	−0.000 41	−0.000 39
−1.8	−0.000 75	−0.000 71	−0.000 68	−0.000 66
−1.6	−0.000 72	−0.000 69	−0.000 68	−0.000 69
−1.4	0.0010	0.0010	0.0009	0.0007
−1.2	0.0082	0.0078	0.0073	0.0067
−1.0	0.0294	0.0279	0.0262	0.0245
−0.8	0.0807	0.0766	0.0724	0.0680
−0.6	0.1892	0.1798	0.1701	0.1604
−0.4	0.3923	0.3727	0.3530	0.3334
−0.2	0.7313	0.6948	0.6584	0.6221
0	1.2400	1.1780	1.1161	1.0543
0.2	1.9313	1.8345	1.7371	1.6391
0.4	2.7923	2.6516	2.5084	2.3622
0.6	3.7893	3.5968	3.3978	3.1907
0.8	4.8807	4.6304	4.3659	4.0844
1.0	6.0294	5.7163	5.3771	5.0065
1.2	7.2082	6.8283	6.4048	5.9290
1.4	8.4010	7.9506	7.4323	6.8332
1.6	9.5993	9.0745	8.4499	7.7073
1.8	10.7993	10.1960	9.4522	8.5435
2.0	11.9996	11.3133	10.4360	9.3366
2.2	13.1998	12.4255	11.3989	10.0821
2.4	14.3999	13.5321	12.3390	10.7762
2.6	15.6000	14.6326	13.2545	11.4154
2.8	16.8000	15.7266	14.1435	11.9965
3.0	18.0000	16.8136	15.0044	12.5166
$\Phi > 3.0$	$6\,\Phi$ where $\Phi = \dfrac{x}{b-a}$	$54.0900 \sin \phi$ where $\phi = \Phi \ln \dfrac{1}{\alpha}$	$24.1796 \sin \phi$ where $\phi = \Phi \ln \dfrac{1}{\alpha}$	$14.2686 \sin \phi$ where $\phi = \Phi \ln \dfrac{1}{\alpha}$

for four values of α, i.e., for four ratios of inner radius to outer radius of the curved bar. The results given in Table 2 were calculated by means of Equation [43] or, for larger values of Φ, by means of the contour-integral method. Fig. 5 shows a graphical representation of the results presented in Table 2.

In a similar way, Table 3 and Fig. 6 show values of $(\sigma_\phi)_{r=a}$ for four values of α, again for the problem in Fig. 2(*b*).

In each of Figs. 5 and 6 and in Tables 2 and 3, one of the cases considered is the case of a straight beam for which $\alpha = 1$. These previously known results (3) for a straight beam are included for the sake of comparison with those for the curved bars having $\alpha = 0.9$, $\alpha = 0.8$, and $\alpha = 0.7$. The indications of the curves in Figs. 5 and 6 for negative values of Φ may be summarized by pointing out that at one beam depth to the right of the load in Fig. 2 (*b*), the value of σ_ϕ on either circular boundary has already decreased to about 3 per cent of $P/(b-a)$ for any value of α in the range $\alpha = 0.7$ to $\alpha = 1.0$.

According to the discussion following Equation [35] it is to be expected that, with increasing Φ, the values of σ_ϕ to the left of the load in Fig. 2 (*b*) will rapidly approach those given by the expression

$$(\sigma_\phi)_{\Phi>1} \approx \frac{P\left(3r - \dfrac{a^2+b^2}{r} - \dfrac{a^2b^2}{r^3}\right) \sin \phi}{\left[a^2 - b^2 + (a^2+b^2) \ln \dfrac{b}{a}\right]} \quad [47]$$

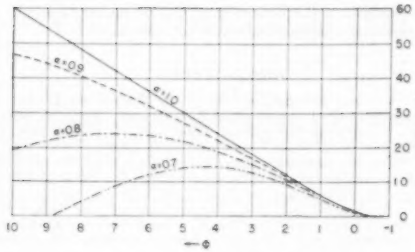

FIG. 5 CIRCUMFERENTIAL STRESS σ_ϕ AT OUTER BOUNDARY FOR LOADING SHOWN IN FIG. 2(b)

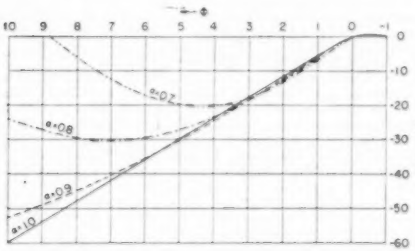

FIG. 6 CIRCUMFERENTIAL STRESS σ_ϕ AT INNER BOUNDARY FOR LOADING SHOWN IN FIG. 2(b)

It should be noted that the error which results from using Equation [47] to calculate σ_ϕ at $\Phi = K_1$ is numerically the same as the error which results from taking $\sigma_\phi = 0$ at $\Phi = -K_1$.

The curves in Figs. 5 and 6 have been carried to comparatively large values of Φ to help the reader in interpreting Φ in terms of an angle ϕ measured in degrees or radians. For example, the point at which the curve for $\alpha = 0.7$ crosses the horizontal axis (at $\Phi = 8.808$) in Fig. 5 corresponds to an angle $\phi = 180$ deg for $\alpha = 0.7$. Similarly, $\Phi = 14.079$ corresponds to an angle $\phi = 180$ deg for $\alpha = 0.8$, and $\Phi = 29.818$ corresponds to an angle $\phi = 180$ deg for $\alpha = 0.9$.

A PRACTICAL APPLICATION

Fig. 7 shows a portion of a circular ring subjected to a loading condition approaching one which may actually occur in certain machine parts. The solutions developed in this paper make it possible to find the stresses at any point in the curved bar of Fig. 7. If the loads are concentrated as shown in the figure, there will be infinite stresses at each of the three points where the concentrated radial loads are applied. However, if the loads are distributed over a small area, as always would be the case in practice, one may still use the formulas derived in this paper in order to calculate with good approximation the stress at point A in Fig. 7. Furthermore, there will be some cases, depending on the material, where failure of a machine part loaded as in Fig. 7, will be governed by the maximum tensile stress which occurs at point A. The value of this maximum tensile stress is

$$(\sigma_\phi)_A = \frac{P}{b-a}\frac{4X^2}{\pi(1+\alpha)}\left[\frac{1}{2}\int_0^\infty \frac{z\,dz}{\sinh z - Xz} + \frac{1}{2}\int_0^\infty \frac{z\,dz}{\sinh z + Xz} - \frac{1}{2\cos\omega}\left[\int_0^\infty \frac{z\cos\Omega z\,dz}{\sinh z - Xz} - \int_0^\infty \frac{z\cos\Omega z\,dz}{\sinh z + Xz}\right]\right] \quad [48]$$

TABLE 3 VALUES OF CIRCUMFERENTIAL STRESS AT INNER BOUNDARY FOR LOADING SHOWN IN FIG. 2(b)

$$\left[(\sigma_\phi)_{r=a} \div \frac{P}{b-a}\right]$$

Φ	For $\alpha = 1.0$	For $\alpha = 0.9$	For $\alpha = 0.8$	For $\alpha = 0.7$
−3.0	0.000 002	0.000 002	0.000 002	0.000 003
−2.8	−0.000 003	−0.000 003	−0.000 003	−0.000 002
−2.6	−0.000 02	−0.000 02	−0.000 02	−0.000 02
−2.4	−0.000 08	−0.000 08	−0.000 09	−0.000 09
−2.2	−0.000 21	−0.000 22	−0.000 23	−0.000 25
−2.0	−0.000 45	−0.000 47	−0.000 51	−0.000 55
−1.8	−0.000 74	−0.000 79	−0.000 85	−0.000 95
−1.6	−0.000 70	−0.000 75	−0.000 82	−0.000 96
−1.4	0.0011	0.0011	0.0011	0.0011
−1.2	0.0083	0.0087	0.0091	0.0096
−1.0	0.0283	0.0298	0.0316	0.0337
−0.8	0.0717	0.0757	0.0805	0.0864
−0.6	0.1419	0.14975	0.1595	0.1721
−0.4	0.2019	0.2132	0.2275	0.2460
−0.2	0.1297	0.1371	0.1467	0.1596
0	−0.2614	−0.2756	−0.2928	−0.3141
0.2	−1.0703	−1.1292	−1.2018	−1.2933
0.4	−2.1981	−2.3189	−2.4667	−2.6523
0.6	−3.4581	−3.6470	−3.8750	−4.1569
0.8	−4.7283	−4.9841	−5.2865	−5.6512
1.0	−5.9717	−6.2907	−6.6570	−7.0835
1.2	−7.1917	−7.5697	−7.9878	−8.4509
1.4	−8.3989	−8.8318	−9.2882	−9.7597
1.6	−9.6007	−10.0843	−10.5650	−11.0123
1.8	−10.8007	−11.3305	−11.8170	−12.2069
2.0	−12.0004	−12.5713	−13.0460	−13.3391
2.2	−13.2002	−13.8066	−14.2491	−14.4034
2.4	−14.4001	−15.0358	−15.4239	−15.3947
2.6	−15.6000	−16.2585	−16.5682	−16.3077
2.8	−16.8000	−17.4740	−17.6794	−17.1379
3.0	−18.0000	−18.6817	−18.7555	−17.8809
	$-6\,\Phi$	$-60.1000 \sin\phi$	$-30.2245 \sin\phi$	$-20.3837 \sin\phi$
$\Phi > 3.0$	where $\Phi = \frac{x}{b-a}$	where $\phi = \Phi \ln\frac{1}{\alpha}$	where $\phi = \Phi \ln\frac{1}{\alpha}$	where $\phi = \Phi \ln\frac{1}{\alpha}$

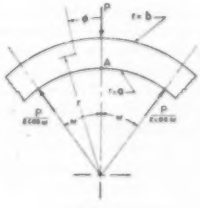

FIG. 7

where

$$\Omega = \frac{\omega}{\ln\frac{1}{\alpha}} \quad [49]$$

Equation [48] was obtained from Equations [29] and [34] by using the principle of superposition. Equation [48] may be written in the form

$$(\sigma_\phi)_A = K_A \frac{P}{b-a} \quad [50]$$

Values of K_A are given in Table 4 for values of Ω ranging from 0 to 3.0 in increments of 0.2 and for values of $\alpha = 0.7$, 0.8, 0.9, 1.0.

Additional results for the problem illustrated in Fig. 7 are

TABLE 4 VALUES OF K_A FOR EQUATION [50]

	Value of K_A in Equation [50]			
Ω	For $\alpha = 1.0$	For $\alpha = 0.9$	For $\alpha = 0.8$	For $\alpha = 0.7$
0	0.9786[a]	1.0332[a]	1.1023[a]	1.1920[a]
0.2	1.0699	1.1298	1.2058	1.3052
0.4	1.3309	1.4060	1.5027	1.6311
0.6	1.7279	1.8267	1.9573	2.1354
0.8	2.2193	2.3487	2.5259	2.7769
1.0	2.7680	2.9333	3.1701	3.5209
1.2	3.3469	3.5528	3.8628	4.3461
1.4	3.9394	4.1901	4.5889	5.2459
1.6	4.5379	4.8378	5.3434	6.2272
1.8	5.1379	5.4918	6.1251	7.3050
2.0	5.7382	6.1514	6.9376	8.5050
2.2	6.3384	6.8170	7.7854	9.8629
2.4	6.9385	7.4891	8.6745	11.4294
2.6	7.5386	8.1684	9.6119	13.2768
2.8	8.1386	8.8558	10.6059	15.5132
3.0	8.7386	9.5521	11.6659	18.3079

[a] At a point immediately adjoining A. The value of the stress exactly at A, for $\Omega = 0$, is minus infinity.

given in reference (14) which includes a partial photoelastic check of the calculated results.

Conclusions

The Fourier integral method can be applied to the plane-stress problem of a curved bar loaded by any combination of radial loads on the inner and outer circular boundaries. Numerical results for the stresses can be obtained by using procedures described in this paper and in an earlier paper (1) by one of the authors.

By superposition of the solutions presented in this paper, results for various practical problems, such as the one illustrated in Fig. 7, can be obtained. In particular, the procedure used in this paper can be applied to problems involving distributed radial loads on the circular boundaries of a curved bar.

All of the integrals encountered in the present paper can now be evaluated by procedures shown in this paper and in references (1, 10, 13). These procedures are based on those used by other investigators in treating straight-beam problems but considerable original work was required for the evaluation of the integrals occurring in this paper. In any case, since the mathematical difficulties of the Fourier integral method have been overcome for the problem of a curved bar, it may be concluded that the solution of other elasticity problems by the Fourier integral method may be attempted with more confidence than would have been warranted before the present investigation.

Acknowledgments

Several valuable suggestions made by Mr. Reuben Bond, Research Engineer at the University of California, were followed in the mathematical derivations required for this paper.

Bibliography

1 "A Fourier Integral Solution for the Plane-Stress Problem of a Circular Ring With Concentrated Radial Loads," by C. W. Nelson, Journal of Applied Mechanics, Trans. ASME, vol. 73, 1951, pp. 173–182.

2 "Über die Grundlagen der Balkentheorie," by Th. von Kármán, Abhandlungen aus dem Aerodynamischen Institut an der Technischen Hochschule Aachen, vol. 7, 1927, pp. 3–10.

3 "Die Spannungen und Formänderungen von Balken mit rechteckigem Querschnitt," by Friedrich Seewald, Abhandlungen aus dem Aerodynamischen Institut an der Technischen Hochschule Aachen, vol. 7, 1927, pp. 11–33.

4 "A Treatise on Photo-Elasticity," by E. G. Coker and L. N. G. Filon, Cambridge University Press, London, England, 1931, chapter 5, pp. 415–443.

5 "On an Approximate Solution for the Bending of a Beam of Rectangular Cross Section Under Any System of Load, With Special Reference to Points of Concentrated or Discontinuous Loading," by L. N. G. Filon, Philosophical Transactions of the Royal Society of London, England, series A, vol. 201, 1903, pp. 63–155.

6 "On the Stresses in the Neighborhood of a Circular Hole in a Strip Under Tension," by R. C. J. Howland, Philosophical Transactions of the Royal Society of London, England, series A, vol. 229, 1929–1930, pp. 49–86.

7 "Bi-Harmonic Analysis in a Perforated Strip," by R. C. J. Howland and A. C. Stevenson, Philosophical Transactions of the Royal Society of London, England, vol. 232, series A, 1933–1934, pp. 155–222.

8 "Theory of Elasticity," by S. Timoshenko and J. N. Goodier, McGraw-Hill Book Company, Inc., New York, N. Y., 1951, (*a*) chapter 4, pp. 116–117; (*b*) chapter 4, pp. 73–76.

9 "Methods of Mathematical Physics," by Harold Jeffreys and Bertha S. Jeffreys, Cambridge University Press, London, England, 1946, pp. 348–349.

10 "Evaluation of Definite Integrals Encountered in Elasticity Problems Involving Curved Flat Bars, I," by C. W. Nelson, Ning-Gau Wu, and C. J. Ancker, Jr., University of California Institute of Engineering Research Report, Series No. 53, Issue No. 1, March, 1952.

11 "An Analytical Theory of the Equilibrium of an Isotropic Elastic Plate," by John Dougall, Transactions of the Royal Society of Edinburgh, Scotland, vol. 41, 1903–1906, pp. 129–228.

12 "Introduction to Complex Variables and Applications," by Ruel V. Churchill, McGraw-Hill Book Company, Inc., New York, N. Y., 1948, pp. 116–134.

13 "Evaluation of Definite Integrals Encountered in Elasticity Problems Involving Curved Flat Bars, II," by C. W. Nelson and Ning-Gau Wu, University of California Institute of Engineering Research Report, Series No. 53, Issue No. 2, March, 1952.

14 "A Fourier Integral Solution for the Stresses in a Curved Bar Bent by Concentrated Radial Loads," by C. J. Ancker, Jr., thesis (unpublished), University of California, Berkeley, Calif., September, 1950.

Gravitational Stresses on Deep Tunnels

By YI-YUAN YU,[1] ST. LOUIS, MO.

Gravitational stresses around a horizontal tunnel opening are determined by means of Muschelišvili's complex variable method for solving two-dimensional elasticity problems. The tunnel is located at a large but finite depth underneath the horizontal ground surface. It has the shape of a general ovaloid, including the rounded-cornered square, the ellipse, and the circle as its special cases. The surrounding material is assumed to be elastic, isotropic, and homogeneous. Two problems are solved. In one problem an unlined tunnel is considered, which has a boundary free from external stresses. In the other the tunnel has a rigid lining, and a perfect bond is assumed to exist between the lining and the surrounding material so that the displacements at the boundary are zero.

Introduction

MUSCHELIŠVILI'S complex variable method of solving two-dimensional elasticity problems consists in determining for each state of stress two analytical functions from which stress and displacement components may readily be determined (1).[2] The method also can be extended for solving gravitational stress problems. This will be shown in the paper, and two problems relating to a horizontal tunnel of the shape of a general ovaloid at a large finite depth underneath the horizontal ground surface will be solved by means of the method thus extended.

Method

Stress Function. When gravity acts along the negative y-direction, it effects, on any body located in its field, a body force the components of which are

$$X_b = 0, \quad Y_b = -w$$

w being the specific weight of the material of the body. These components can be written as

$$X_b = -\frac{\partial V_1}{\partial x}, \quad Y_b = -\frac{\partial V_1}{\partial y}$$

in which the potential function for the body force

$$V_1(x,y) = wy$$

is obviously harmonic. If the stress function U is now defined by

$$\frac{\partial^2 U}{\partial x^2} = \tau_{xx} - V_1, \quad \frac{\partial^2 U}{\partial y^2} = \tau_{yy} - V_1, \quad -\frac{\partial^2 U}{\partial x \partial y} = \tau_{xy} \ldots [1]$$

in which τ_{xx}, τ_{yy}, and τ_{xy} are the normal and shearing stress components in rectangular co-ordinates, it easily can be shown that the compatibility equation reduces finally to the same biharmonic equation as in the case involving no body forces (2). Thus, as shown by Muschelišvili, the stress function U can be expressed in terms of two analytic functions $\varphi_1(z)$ and $\psi_1(z)$ of the complex variable $z = x + iy$ as follows

$$2U = \bar{z}\,\varphi_1(z) + z\,\bar{\varphi}_1(\bar{z}) + \psi_2(z) + \bar{\psi}_2(\bar{z}) \ldots\ldots [2]$$

in which the bars indicate the conjugates of the complex quantities and

$$\psi_2(z) = \int \psi_1(z)dz$$

Boundary Conditions. The boundary conditions

$$\tau_x = \tau_{xx}\frac{dy}{ds} - \tau_{xy}\frac{dx}{ds}$$

$$\tau_y = \tau_{xy}\frac{dy}{ds} - \tau_{yy}\frac{dx}{ds}$$

in which τ_x and τ_y are the surface force components and ds is an element of length along the boundary, will be seen to lead to some result different from what is obtained for the case having no body force. When stress components are substituted from Equations [1] into these conditions, we have

$$\left.\begin{aligned} \tau_x - V_1\frac{dy}{ds} &= \frac{d}{ds}\left(\frac{\partial U}{\partial y}\right) \\ \tau_y + V_1\frac{dx}{ds} &= -\frac{d}{ds}\left(\frac{\partial U}{\partial x}\right) \end{aligned}\right\} \ldots\ldots [3]$$

We multiply the second equation by i and add up the two equations. The result is further multiplied through by $i\,ds$ and integrated. Finally, making use of Equation [2], we obtain

$$\varphi_1(z) + z\,\bar{\varphi}_1'(\bar{z}) + \bar{\psi}_1(\bar{z}) = i\int(\tau_x + i\,\tau_y)\,ds - \int V_1(z)dz \ldots [4]$$

in which the function V_1 is now in its complex form

$$V_1 = wy = -\frac{1}{2}iw(z - \bar{z}) \ldots\ldots [5]$$

Comparing this with the boundary condition for the case of zero body forces we see that the body force may be considered as equivalent to a surface force. As was observed by Biot (3), the equivalent surface force is a normal hydrostatic pressure equal to V_1. It also may be seen by observing Equations [3] that its components are

$$-V_1\frac{dy}{ds} \quad \text{and} \quad V_1\frac{dx}{ds}$$

Stresses and Displacements. Stress and displacement components can be derived in terms of the analytic functions in a similar manner following Muschelišvili (4). Only the final results will be presented here. The stress components are given by

$$\left.\begin{aligned} \tau_{xx} + \tau_{yy} &= 2[\varphi_1'(z) + \bar{\varphi}_1'(\bar{z})] + 2V_1(z) \\ \tau_{yy} - \tau_{xx} + 2i\tau_{xy} &= 2\,[\bar{z}\,\varphi_1''(z) + \psi_1'(z)] \end{aligned}\right\} \ldots\ldots [6]$$

The x and y-components of the displacement u and v, are given by

$$2\mu(u + iv) = \kappa\varphi_1(z) - z\bar{\varphi}_1'(\bar{z}) - \bar{\psi}_1(\bar{z}) + 2(\kappa - 1)\gamma_1(z) \ldots [7]$$

---

[1] Assistant Professor, Department of Applied Mechanics, Washington University. Jun. ASME.

[2] Numbers in parentheses refer to the Bibliography at the end of the paper.

Presented at the West Coast Conference of the Applied Mechanics Division, Los Angeles, Calif., June 26–28, 1952, of The American Society of Mechanical Engineers.

Discussion of this paper should be addressed to the Secretary, ASME, 29 West 39th Street, New York, N. Y., and will be accepted until January 10, 1953, for publication at a later date. Discussion received after the closing date will be returned.

Note: Statements and opinions advanced in papers are to be understood as individual expressions of their authors and not those of the Society. Manuscript received by ASME Applied Mechanics Division, January 11, 1952.

in which

$$\kappa = \frac{\lambda + 3\mu}{\lambda + \mu}$$

and λ and μ are Lamé's constants. The function $\gamma_1(z)$ is constructed from $V_1(x, y) = wy$ and its conjugate harmonic function $W_1(x, y) = -wx$ according to

$$\gamma_1(z) = \frac{1}{4}\int (V_1 + iW_1)dz$$

which yields

$$\gamma_1(z) = -\frac{1}{8} iwz^2 \quad [8]$$

Conformal Mapping. Let the function

$$z = \omega(\zeta) \quad [9]$$

map the boundary C of a given region in the z-plane into the unit circle γ in the ζ-plane. As a result of this, curvilinear co-ordinates (ρ, θ) are introduced into the z-plane which are the maps of the polar co-ordinates in the ζ-plane as given by $\zeta = \rho e^{i\theta}$. The stress components $\tau_{\rho\rho}$, $\tau_{\theta\theta}$, and $\tau_{\rho\theta}$ with reference to the curvilinear co-ordinates thus obtained may be derived from Equations [6]; thus

$$\tau_{\rho\rho} + \tau_{\theta\theta} = 2[\Phi(\zeta) + \bar{\Phi}(\bar{\zeta})] + 2V(\zeta) \quad [10]$$

$$\tau_{\theta\theta} - \tau_{\rho\rho} + 2i\tau_{\rho\theta} = \frac{2\zeta^2}{\rho^2\bar{\omega}'(\bar{\zeta})}\,[\bar{\omega}(\bar{\zeta})\Phi'(\zeta) + \omega'(\zeta)\Psi(\zeta)] \quad [11]$$

where

$$\Phi(\zeta) = \frac{\varphi'(\zeta)}{\omega'(\zeta)}, \quad \Psi(\zeta) = \frac{\psi'(\zeta)}{\omega'(\zeta)}$$

$$\varphi(\zeta) = \varphi_1[\omega(\zeta)] = \varphi_1(z), \quad \psi(\zeta) = \psi_1[\omega(\zeta)] = \psi_1(z)$$

and

$$V(\zeta) = V_1[\omega(\zeta)] = V_1(z)$$

Similarly, Equation [7] is transformed into

$$2\mu(u + iv) = \kappa\varphi(\zeta) - \frac{\omega(\zeta)}{\bar{\omega}'(\bar{\zeta})}\,\bar{\varphi}'(\bar{\zeta}) - \bar{\psi}(\bar{\zeta}) + 2(\kappa - 1)\gamma(\zeta) \quad [12]$$

where

$$\gamma(\zeta) = \gamma_1[\omega(\zeta)] = \gamma_1(z)$$

Boundary Equations of Two Fundamental Problems. In the first fundamental boundary-value problem of elasticity, stresses are prescribed at the boundary C of the body. If we define

$$f_1 + if_2 = i\int(\tau_x + i\tau_y)ds - \int V_1 dz \quad [13]$$

then, according to Equation [4], the boundary equation is

$$\varphi_1(z) + z\,\bar{\varphi}_1'(\bar{z}) + \bar{\psi}_1(\bar{z}) = f_1 + if_2 \quad (\text{on } C)$$

Transforming by means of the mapping function [9], we have

$$\varphi(\sigma) + \frac{\omega(\sigma)}{\bar{\omega}'(\bar{\sigma})}\,\bar{\varphi}'(\bar{\sigma}) + \bar{\psi}(\bar{\sigma}) = f_1 + if_2 \,(\text{on } \gamma) \quad [14]$$

in which $f_1 + if_2$ has also been transformed and is now a function of $\sigma = e^{i\theta}$, namely, the value of ζ on the boundary γ.

In the second fundamental boundary-value problem the displacements are prescribed at the boundary. We define

$$2\mu(g_1 + ig_2) = 2\mu(u + iv) - 2(\kappa - 1)\gamma_1 \quad [15]$$

and obtain the boundary equation from Equation [7]

$$\kappa\varphi_1(z) - z\bar{\varphi}_1'(\bar{z}) - \bar{\psi}_1(\bar{z}) = 2\mu(g_1 + ig_2) \,(\text{on } C)$$

Transforming by means of Equation [9], we have

$$\kappa\varphi(\sigma) - \frac{\omega(\sigma)}{\bar{\omega}'(\bar{\sigma})}\,\bar{\varphi}'(\bar{\sigma}) - \bar{\psi}(\bar{\sigma}) = 2\mu(g_1 + ig_2)\,(\text{on } \gamma) \quad [16]$$

in which $2\mu(g_1 + ig_2)$ is now also a function of σ.

Thus, except with different definitions for the functions $f_1 + if_2$ and $2\mu(g_1 + ig_2)$, the boundary Equations [14] and [16] assume the same forms as the ones for zero body forces.

Tunnel Problems

We shall be concerned with a horizontal tunnel of the shape of a general ovaloid located at a large but finite depth underneath the horizontal ground surface as shown in Fig. 1. The tunnel

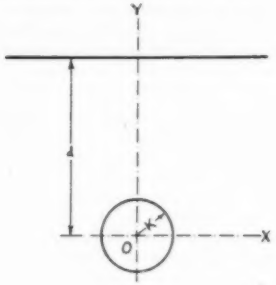

FIG. 1

may either be unlined, or it may have a rigid lining. In the former problem we consider the tunnel opening to be free from any surface loading. In the latter problem we assume a perfect bond between the tunnel lining and its surrounding material so that the displacement at the boundary may be considered to be zero. Stresses due to gravity in the neighborhood of the tunnel opening will be determined. Since these are plane-strain problems, the foregoing method may be used. The co-ordinate axes are chosen as shown in Fig. 1 with the origin at the center of the tunnel. The depth of the tunnel underneath the upper surface of the ground is denoted by d, which is measured from the center of the tunnel. The material surrounding the tunnel opening is assumed to be elastic, isotropic, and homogeneous, and has a specific weight w.

Mapping Function. The shape of the tunnel is obtained by means of the function

$$z = \omega(\zeta) = K\left(\zeta + \frac{m}{\zeta} + \frac{n}{\zeta^3}\right) \quad [17]$$

which maps the unit circle γ in the ζ-plane into a general ovaloid in the z-plane, as was first used by Greenspan (5) in a different form. When m is zero, a square with rounded corners may be obtained in the z-plane; when n is zero, an ellipse may be obtained; and when both m and n vanish, the unit circle is simply mapped into another circle of radius K.

At the boundary the function reduces to

$$z = \omega(\sigma) = K\left(\sigma + \frac{m}{\sigma} + \frac{n}{\sigma^3}\right) \quad [18]$$

and the functions $V_1(z)$ and $\gamma_1(z)$ in Equations [5] and [8] are transformed, respectively, into

$$V(\sigma) = -\frac{1}{2} iwK \left(\sigma + \frac{m}{\sigma} + \frac{n}{\sigma^2} - \frac{1}{\sigma} - m\sigma - n\sigma^2 \right) \quad [19]$$

and

$$\gamma(\sigma) = -\frac{1}{8} iwK^2 \left(\sigma + \frac{m}{\sigma} + \frac{n}{\sigma^2} \right)^2 \quad [20]$$

We have also the integral

$$-\int V_1(z)dz = -\int V(\sigma)\omega'(\sigma)d\sigma = \frac{1}{2} iwK^2 \left[-\frac{n}{4}\sigma^4 + \frac{1-m+mn}{2}\sigma^2 - (1-m^2-3n^2)\log\sigma + \frac{2n-m+m^2-3mn}{2\sigma^2} + \frac{4mn-3n}{4\sigma^4} + \frac{n^2}{2\sigma^6} \right] \quad [21]$$

which, according to Equation [13], represents that part of the function $f_1 + if_2$ which is contributed by the body force.

Forms of Analytic Functions. The functions $\varphi(\zeta)$ and $\psi(\zeta)$ which determine the state of stress of the present problems have the forms

$$\left.\begin{aligned} \varphi(\zeta) &= BK\zeta - \frac{X+iY}{2\pi(\kappa+1)} \log\zeta + \varphi^0(\zeta) \\ \psi(\zeta) &= (B' + iC')K\zeta + \frac{\kappa(X-iY)}{2\pi(\kappa+1)} \log\zeta + \psi^0(\zeta) \end{aligned}\right\} \quad [22]$$

which are the same as those for an infinite region exterior to some closed boundary and subjected to constant stresses at infinity (1). In each expression the first term will be determined by the condition at the upper ground surface, the second term will be determined by the unbalanced force at the tunnel opening, and the last term represents the analytic part of the function.

According to our former discussion the equivalent surface loading at the upper ground surface is a hydrostatic pressure equal to

$$V_1 = (wy)_{y=d} = wd$$

and its x and y-components are

$$-V_1 \frac{dy}{ds} = 0, \quad V_1 \frac{dx}{ds} = wd(-1) = -wd$$

The negative sign in the second expression is due to the fact that ds is positive when the boundary is described with the body kept to the left and therefore has a sign opposite to that of dx. The loading is thus seen to be a constant hydrostatic pressure over the entire upper boundary, and the principal stresses due to this loading are

$$\sigma_1 = \sigma_2 = -wd$$

By means of formulas given by Muschelišvili (1), we find

$$\left.\begin{aligned} B &= \frac{\sigma_1+\sigma_2}{4} = -\frac{1}{2}wd \\ B' &= -\frac{\sigma_1-\sigma_2}{2}\cos 2\alpha = 0 \\ C' &= \frac{\sigma_1-\sigma_2}{2}\sin 2\alpha = 0 \end{aligned}\right\} \quad [23]$$

where α is the angle between the x-axis and the direction of σ_1.

With surface load acting on the inner boundary of an infinite region, its resultant force (X, Y) is given by

$$X + iY = -i[f_1 + if_2]_A^A$$

where the bracket denotes the increase in the value of $f_1 + if_2$ when the boundary is described from any point A on the boundary back to A in the positive or clockwise sense (1). This expression may be applied to the tunnel opening when the depth d is large compared with its size. Since the body force has contributed to $f_1 + if_2$ an amount given by the expression in Equation [21], its equivalent surface load at the tunnel opening has a resultant given by

$$X + iY = -i\left[-\int V(\sigma)\omega'(\sigma)d\sigma \right]_A^A = iw\pi K^2(1 - m^2 - 3n^2) \quad [24]$$

where $\pi K^2(1-m^2-3n^2)$ can easily be shown to be the area of the ovaloid-shaped opening. Since the actual surface forces on the boundary are zero for the tunnel with no lining and are in equilibrium[2] for the tunnel with a rigid lining, the foregoing constitutes the only unbalanced force to be used in Equations [22].

When the depth d is large, functions $\varphi^0(\zeta)$ and $\psi^0(\zeta)$ may be considered to be analytic in the entire region exterior to the opening and therefore have the forms

$$\left.\begin{aligned} \varphi^0(\zeta) &= \frac{\alpha_1+i\beta_1}{\zeta} + \frac{\alpha_2+i\beta_2}{\zeta^2} + \cdots \\ \psi^0(\zeta) &= \alpha_0' + i\beta_0' + \frac{\alpha_1'+i\beta_1'}{\zeta} + \frac{\alpha_2'+i\beta_2'}{\zeta^2} + \cdots \end{aligned}\right\} \quad [25]$$

where α and β are real constants.

By virtue of Equations [23] and [24], the functions in Equations [22] become

$$\left.\begin{aligned} \varphi(\zeta) &= -\frac{1}{2}wdK\zeta - \frac{iwK^2(1-m^2-3n^2)}{2(\kappa+1)}\log\zeta + \varphi^0(\zeta) \\ \psi(\zeta) &= -\kappa\frac{iwK^2(1-m^2-3n^2)}{2(\kappa+1)}\log\zeta + \psi^0(\zeta) \end{aligned}\right\} \quad [26]$$

in which only $\varphi^0(\zeta)$ and $\psi^0(\zeta)$ remain to be determined.

Determination of $\varphi^0(\zeta)$ and $\psi^0(\zeta)$. The boundary equation for the unlined tunnel in the first problem has the form given in Equation [14]. Since surface forces τ_x and τ_y are zero, the function $f_1 + if_2$ defined in Equation [13] consists of only the integral as evaluated in Equation [21]. Function $\omega(\sigma)$ is given by Equation [18], and $\varphi(\sigma)$ and $\psi(\sigma)$ can be obtained from Equations [26]. Substituting these into Equation [14] yields

$$\begin{aligned} &-\frac{wdK}{2}\sigma - \frac{iwK^2(1-m^2-3n^2)}{2(\kappa+1)}\log\sigma + \varphi^0(\sigma) \\ &+ \frac{\sigma^4+m\sigma^2+n}{\sigma^2(1-m\sigma^2-3n\sigma^4)}\left[-\frac{wdK}{2} + \frac{iwK^2(1-m^2-3n^2)}{2(\kappa+1)}\sigma + \bar{\varphi}^0(\bar{\sigma}) \right] - \frac{\kappa iwK^2(1-m^2-3n^2)}{2(\kappa+1)}\log\sigma + \bar{\psi}^0(\bar{\sigma}) \\ &= \frac{iwK^2}{2}\left[-\frac{n}{4}\sigma^4 + \frac{1-m+mn}{2}\sigma^2 - (1-m^2-3n^2)\log\sigma + \frac{2n-m+m^2-3mn}{2\sigma^2} + \frac{4mn-3n}{4\sigma^4} + \frac{n^2}{2\sigma^6} \right] (\text{on } \gamma) \end{aligned} \quad [27]$$

Terms including $\log\sigma$ are observed to cancel each other. Multiplying the equation through by

$$\frac{1}{2\pi i}\frac{d\sigma}{\sigma-\zeta}$$

[2] The effect due to the weight of the lining will not be considered here but may be computed separately (6).

and integrating around γ, we obtain an integral equation, in which the integrals can be evaluated by means of several theorems developed by Muskhelishvili (1). The result gives

$$-\varphi^0(\zeta)+\frac{wdK}{2}\frac{n}{\zeta^2}+\frac{wdK}{2}\frac{m(1+n)}{\zeta}-\frac{iwK^2(1-m^2-3n^2)}{2(\kappa+1)}\frac{n}{\zeta^2}+(\alpha_1-i\beta_1)\frac{n}{\zeta}=\frac{iwK^2}{2}\left[\frac{m-2n-m^2+3mn}{2\zeta^2}+\frac{3n-4mn}{4\zeta^4}-\frac{n^2}{2\zeta^6}\right]$$

Constants α_1 and β_1 may be determined by comparing the coefficients of $1/\sigma$ on both sides of Equation [27]; thus

$$\alpha_1=\frac{wdK}{2}\frac{m(1+n)}{1-n},\qquad \beta_1=0$$

Therefore

$$\varphi^0(\zeta)=\frac{wdK}{2}\frac{m(1+n)}{1-n}\frac{1}{\zeta}-\frac{iwK^2}{2}\left(n\frac{1-m^2-3n^2}{\kappa+1}+\frac{m-2n-m^2+3mn}{2}\right)\frac{1}{\zeta^2}+\frac{wdK}{2}\frac{n}{\zeta^2}+\frac{iwK^2}{2}\frac{4mn-3n}{4}\frac{1}{\zeta^4}+\frac{iwK^2}{2}\frac{n^2}{2\zeta^6}\qquad[28]$$

Formulating the conjugate of Equation [27], multiplying the result through by

$$\frac{1}{2\pi i}\frac{d\sigma}{\sigma-\zeta}$$

and integrating around γ, we obtain an expression for $\psi^0(\zeta)$ which also includes some unknown constant terms. The sum of these constant terms can be shown to be zero by multiplying the conjugate of Equation [27] through by

$$\frac{1}{2\pi i}\frac{d\sigma}{\sigma}$$

and integrating around γ. We thus have

$$\psi^0(\zeta)=-\frac{wdK}{2}n\zeta^2-\frac{iwK^2(1-m^2-3n^2)}{2(\kappa+1)}n\zeta^2-\frac{wdK}{2}\frac{m(1+n)}{1-n}\zeta+\frac{wdK}{2}\frac{1}{\zeta}-\frac{iwK^2}{2}\frac{1-m+mn}{2\zeta^2}+\frac{iwK^2}{2}\frac{n}{4\zeta^2}-\frac{\zeta^2(1+m\zeta^2+n\zeta^4)}{\zeta^4-m\zeta^2-3n}\left[-\frac{wdK}{2}-\frac{iwK^2(1-m^2-3n^2)}{2(\kappa+1)}\frac{1}{\zeta}+\varphi^{0\prime}(\zeta)\right]$$

Determination of $\varphi^0(\zeta)$ and $\psi^0(\zeta)$ for the second problem, in which the tunnel has a rigid lining, is entirely similar. Since we have assumed zero displacements at the boundary, Equation [15] reduces to

$$2\mu(g_1+ig_2)=-2(\kappa-1)\gamma_1(z)=-2(\kappa-1)\gamma(\sigma)$$

where $\gamma(\sigma)$ is given by Equation [20]. Substituting this together with $\varphi(\sigma)$, $\psi(\sigma)$, and $\omega(\sigma)$ into the boundary Equation [16], we may proceed to solve for the unknown functions $\varphi^0(\zeta)$ and $\psi^0(\zeta)$, which turn out to be

$$\varphi^0(\zeta)=-\frac{wdK}{2}\frac{m(1+n)}{\kappa+n}\frac{1}{\zeta}+\frac{iwK^2}{2}\frac{n(1-m^2-3n^2)}{\kappa(\kappa+1)}\frac{1}{\zeta^2}-\frac{wdK}{2}\frac{n}{\kappa}\frac{1}{\zeta^2}+\frac{iwK^2(\kappa-1)}{4\kappa}\left(\frac{m^2+2n}{\zeta^2}+\frac{2mn}{\zeta^4}+\frac{n^2}{\zeta^6}\right)$$

$$\psi^0(\zeta)=-\frac{wdK}{2}n\zeta^2-\frac{iwK^2}{2}\frac{n(1-m^2-3n^2)}{\kappa+1}\zeta^2-\frac{wdK}{2}\frac{\kappa m(1+n)}{\kappa+n}\zeta-\frac{wdK}{2}\frac{\kappa}{\zeta}+\frac{iwK^2}{4}\frac{\kappa-1}{\zeta^2}-\frac{\zeta^2(1+m\zeta^2+n\zeta^4)}{\zeta^4-m\zeta^2-3n}\left[-\frac{wdK}{2}-\frac{iwK^2(1-m^2-3n^2)}{2(\kappa+1)}\frac{1}{\zeta}+\varphi^{0\prime}(\zeta)\right]\qquad[29]$$

Boundary Stresses at Tunnel Opening. Since the boundary of the unlined tunnel in the first problem is free from external forces, the only nonvanishing stress component there is the normal stress in a direction tangent to the boundary, namely, $\tau_{\theta\theta}$. This is given by Equation [10]

$$(\tau_{\theta\theta})_{\rho=1}=2[\Phi(\sigma)+\bar{\Phi}(\bar{\sigma})]+2V(\sigma)$$

where

$$\Phi(\sigma)=\frac{\varphi'(\sigma)}{\omega'(\sigma)}$$

Substituting into this expression the functions $\varphi(\sigma)$, $\varphi^0(\sigma)$, $\omega(\sigma)$, and $V(\sigma)$ according to Equations [26], [28], [18], and [19], we have

$$(\tau_{\theta\theta})_{\rho=1}=2wK[(1-m)\sin\theta-n\sin 3\theta]+\frac{2w}{1+m^2+9n^2+2(3mn-m)\cos 2\theta-6n\cos 4\theta}\left\{\left(\frac{4mn}{1-n}\right)d\cos 2\theta-\left(1-9n^2-m^2\frac{1+n}{1-n}\right)d-\left[m^2-5mn+15n^2-m^3+6m^2n-21mn^2+\frac{1}{\kappa+1}(1+m+2mn-6n^2)(1-m^2-3n^2)\right]K\sin\theta+\left[m-2n-m^2+4m^2n+9n^2-\frac{n}{\kappa+1}(1-m^2-3n^2)\right]K\sin 3\theta+(3n-4mn+3mn^2)K\sin 5\theta-(3n^2)K\sin 7\theta\right\}\qquad[30]$$

For a circle, the expression reduces to

$$(\tau_{\theta\theta})_{\rho=1}=2w\left(-d+\frac{K\kappa}{\kappa+1}\sin\theta\right)\qquad[31]$$

which is the same as was obtained by Mindlin (7) for a circular tunnel when the depth d is large.

None of the stress components at the boundary vanishes in the second problem in which the tunnel has a rigid lining, and they can be computed by means of both of Equations [10] and [11]. Functions $\varphi^0(\zeta)$ and $\psi^0(\zeta)$ as obtained in Equations [29] should now be used. The mathematical manipulation is rather tedious for the general case of an ovaloid. The results for the case of a circular tunnel only are given here as follows

$$(\tau_{\theta\theta} + \tau_{\rho\rho})_{\rho=1} = -2wd + \frac{2wK\kappa}{\kappa+1}\sin\theta$$

$$(\tau_{\theta\theta} - \tau_{\rho\rho} + 2i\tau_{\rho\theta})_{\rho=1} = -wd(1-\kappa) - i\frac{wK\kappa^2}{\kappa+1}(\cos\theta - i\sin\theta) - i\frac{wK\kappa}{\kappa+1}(\cos\theta + i\sin\theta)$$

from which

$$\left.\begin{aligned}(\tau_{\theta\theta})_{\rho=1} &= \frac{3-\kappa}{2}w\left(-d + \frac{K\kappa}{\kappa+1}\sin\theta\right)\\ (\tau_{\rho\rho})_{\rho=1} &= \frac{1+\kappa}{2}w\left(-d + \frac{K\kappa}{\kappa+1}\sin\theta\right)\\ (\tau_{\rho\theta})_{\rho=1} &= -\frac{wK\kappa}{2}\cos\theta\end{aligned}\right\} \quad \ldots\ldots[32]$$

It is noted that

$$\left(\frac{\tau_{\theta\theta}}{\tau_{\rho\rho}}\right)_{\rho=1} = \frac{3-\kappa}{1+\kappa} = \frac{\nu}{1-\nu}$$

ν being Poisson's ratio, which can be verified by applying Hooke's law to the boundary. It is also interesting to note the similarity between the two expressions of $(\tau_{\theta\theta})_{\rho=1}$ in Equations [31] and [32].

Numerical Examples

In the following numerical examples the depth d is taken to be $5K$. Poisson's ratio ν of the surrounding material is taken to be 0.15 (for instance, that of concrete), and thus we have $\kappa = 3 - 4\nu = 2.40$.

The examples show only cases of the first problem of an unlined tunnel having different shapes. The expression for the boundary stress $(\tau_{\theta\theta})_{\rho=1}$ in each case is obtained from Equation [30] by a substitution of the proper numerical values of the constants. Figs. 2 to 5 show the results for the boundary stress plotted normal to the boundary in units of wK.

Example 1 (Fig. 2)—Circle ($m = 0$, $n = 0$)

$$(\tau_{\theta\theta})_{\rho=1} = wK\,(1.413\sin\theta - 10)$$

Example 2 (Fig. 3)—Ellipse ($m = 0.2$, $n = 0$)

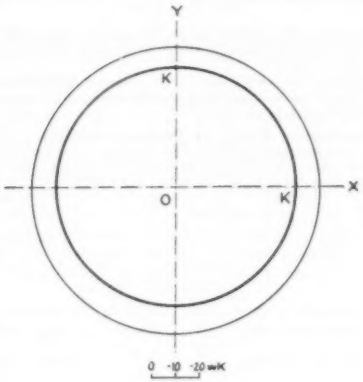

Fig. 2

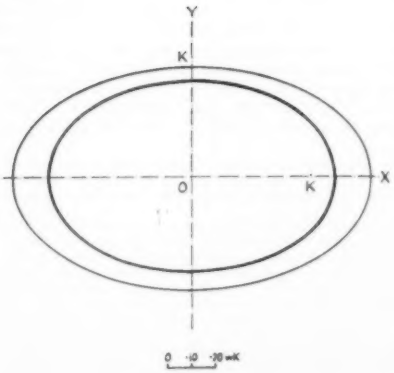

Fig. 3

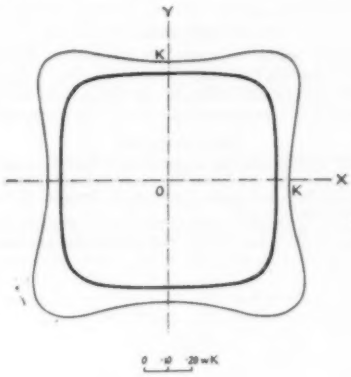

Fig. 4

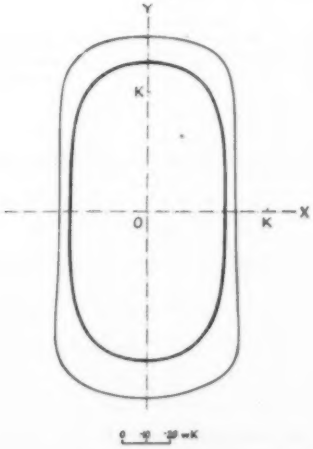

Fig. 5

$$(\tau_{\theta\theta})_{\rho=1} = wK\left(1.600\sin\theta - \frac{4.800 + 0.372\sin\theta - 0.160\sin 3\theta}{0.520 - 0.200\cos 2\theta}\right)$$

Example 3 (Fig. 4)—Rounded-cornered square ($m = 0$, $n = -0.1$)

$$(\tau_{\theta\theta})_{\rho=1} = wK\left(2\sin\theta + 0.200\sin 3\theta - \frac{4.550 + 0.418\sin\theta - 0.220\sin 3\theta + 0.300\sin 5\theta + 0.030\sin 7\theta}{0.545 + 0.300\cos 4\theta}\right)$$

Example 4 (Fig. 5)—Ovaloid ($m = -0.3$, $n = -0.05$)

$$(\tau_{\theta\theta})_{\rho=1} = wK\left(2.600\sin\theta + 0.100\sin 3\theta + \frac{0.572\cos 2\theta - 8.962 - 0.538\sin\theta - 0.602\sin 3\theta - 0.420\sin 5\theta - 0.015\sin 7\theta}{1.113 + 0.690\cos 2\theta + 0.300\cos 4\theta}\right)$$

It can be seen that as the depth d increases, the stress distribution around the upper and lower halves of the tunnel tends to become symmetrical.

ACKNOWLEDGMENT

The author wishes to express his gratitude to Prof. R. D. Mindlin of Columbia University, for informing him of the analogy between body force due to gravity and surface force, and to Prof. M. Hetényi of Northwestern University for his encouragement.

BIBLIOGRAPHY

1 "Praktische Lösung der fundamentalen Randwertaufgaben der Elastizitätstheorie in der Ebene für einige Berandungsformen," by N. Muschelišvili, *Zeitschrift für angewandte Mathematik und Mechanik*, vol. 13, 1933, pp. 264–282.

2 "Theory of Elasticity," by S. Timoshenko, McGraw-Hill Book Company, Inc., New York, N. Y., first edition 1934, pp. 25–26.

3 "Distributed Gravity and Temperature Loading in Two-Dimensional Elasticity Replaced by Boundary Pressure and Dislocations," by M. A. Biot, JOURNAL OF APPLIED MECHANICS, Trans. ASME, vol. 57, 1935, pp. A-41–45.

4 "Recherches sur les problèms aux limites relatifs à l'équation biharmonique et aux équations de l'elasticité à deux dimensions," by N. Muschelišvili, *Mathematische Annalen*, vol. 107, 1932, pp. 282–312.

5 "Effect of a Small Hole on the Stresses in a Uniformly Loaded Plate," by Martin Greenspan, *Quarterly Applied Mathematics*, vol. 2, 1944, pp. 60–71.

6 "Solution for the Exterior of a General Ovaloid Under Arbitrary Loading," by Yi-Yuan Yu, doctoral dissertation, Northwestern University, Evanston, Ill., 1951.

7 "Gravitational Stresses in Bipolar Coordinates," by R. D. Mindlin, Proceedings of the Fifth International Congress for Applied Mechanics, edited by J. P. Den Hartog and H. Peters, John Wiley & Sons, Inc., New York, N. Y., 1939, pp. 112–116.

On a General Method of Solving Second-Order Ordinary Differential Equations by Phase-Plane Displacements

By L. S. JACOBSEN,[1] STANFORD, CALIF.

The phase-plane-delta method of solving second-order differential equations has been illustrated by numerous examples involving graphical constructions. Test cases show good accuracy for practicable size of steps, but, in general, the degree of approximation can be inferred empirically only. The delta method is extremely simple to apply, even to complicated equations. A subprofessional assistant can be instructed quickly in how to use the method, and ordinarily will develop enough speed to become useful in a short time.

Introduction

THE object of this study is to present a simple, graphical method of solving second-order differential equations by phase-plane constructions. Three excellent textbooks on nonlinear problems have appeared recently in English by Minorsky (1),[2] Andronow and Chaikin (2), and Stoker (3). They deal to some extent with the graphical method of solution by isoclines, but they do not give a straightforward general method that will be presented here.

Originality for the method cannot be claimed by the author since the germs from which it has been grown may be found in the writings of Lamoën (4) and Fuchs (5). It appears, however, that the generalization and conscious formulation of the method as an efficient working tool have not been fully realized before.

The method will be referred to as the "phase-plane-delta" method or simply the δ-method. The phase plane will consist of the usual co-ordinates $\left(\frac{\dot{x}}{p},\ x\right)$. The geometry of the phase trajectories will be described by a series of circular arcs having their centers located on the x-axis only. This arbitrary restriction of locating the centers of the arcs on the displacement axis at δ gives the method its name.

Since there is no simple drafting gadget by means of which a continuous, independent variation in radius as well as in center location δ can be accomplished, we are forced to use an ordinary compass and consequently to make the graphical process a stepwise one. As the individual steps diminish in size and their number increases, the results obtained by the method theoretically will approach those of an exact solution, but the possibility for purely graphical errors of the "personal-equation" type will usually increase when the number of steps becomes large. Therefore a compromise must be made, leading to the philosophically unsatisfying, but practically tenable, situation that the degree of approximation can be known only empirically.

Development of Solution

Physically, the differential equation describing the force equilibrium may be given by various terms relating to inertia, dissipation, restoration, and driving. Let us assume that either inherently or by a suitable division it is possible to reduce the equation to a form where the coefficient for $\ddot{x}$ is constant. Then we have

$$m\ddot{x} + G(x, \dot{x}, t) = 0 \qquad [1]$$

The method of solution is based on the assumption that it will always be found possible to separate out from the G-term or to add to it a positive linear component in x which, if added, will be of a fictitious nature. An alternative development, not dependent on the existence or artificial creation of a positive linear component has been worked out by Prof. K. Klotter and may be found in the Appendix.

Placing $G(x, \dot{x}, t) = g(x, \dot{x}, t) + kx$ in Equation [1], dividing through by m, and letting $k/m = p^2$, we obtain

$$\ddot{x} + p^2(x + \delta) = 0 \qquad [2]$$

in which the displacement δ is

$$\delta = \frac{1}{k}\, g(x, \dot{x}, t) \qquad [3]$$

The geometrical significance of Equation [2] in a phase-plane representation will be made clear by introducing the phase-plane co-ordinates

$$x = x \quad \text{and} \quad \frac{\dot{x}}{p} = v$$

From the v-co-ordinate the following identities are seen to exist

$$\ddot{x} = p\,\frac{dv}{dt} = p\,\frac{dv}{dx}\,\dot{x} = p^2 v\,\frac{dv}{dx}$$

Equation [2] then becomes a first-order differential equation

$$v\,\frac{dv}{dx} + x + \delta = 0 \qquad [2a]$$

giving the geometrical relation

$$\frac{dx}{dv} = \frac{v}{x + \delta} \qquad [4]$$

In the present study the displacement axis x will be taken vertical so as to facilitate subsequent projection of the displace-

---

[1] Executive Head, Mechanical Engineering Department, School of Engineering, Stanford University. Mem. ASME.

[2] Numbers in parentheses refer to the Bibliography at the end of the paper.

Contributed by the Applied Mechanics Division and presented at the Annual Meeting, New York, N. Y., November 30–December 5, 1952, of The American Society of Mechanical Engineers.

Discussion of this paper should be addressed to the Secretary, ASME, 29 West 39th Street, New York, N. Y., and will be accepted until January 10, 1953, for publication at a later date. Discussion received after the closing date will be returned.

Note: Statements and opinions advanced in papers are to be understood as individual expressions of their authors and not those of the Society. Manuscript received by ASME Applied Mechanics Division, Sept. 11, 1951. Paper No. 52—A-1.

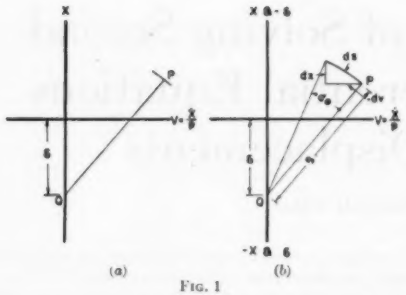

(a) (b)

FIG. 1

ment on a horizontal time axis. Fig. 1(*a*) shows that the slope of the line *Q-P* will be $(x + \delta)/v$; consequently the equation of the normal to the line *Q-P* will be identical with Equation [4]. Therefore the phase trajectory will pass through P_o and it will be normal to the direction *Q-P*. Moreover, since a step method requires that δ be held constant for the step, an integration of Equation [4] gives the equation of a circle with its center at *Q*.

The time element, of course, is implied by the phase trajectory. An explicit expression for time can be obtained from the relation $\dot{x} = pv$, namely

$$dt = \frac{dx}{pv} \quad \ldots\ldots [5]$$

This expression will be integrated by considering the differential geometry of the phase trajectory as shown in Fig. 1(*b*). Let $\rho = Q\text{-}P$, the average radius of curvature of the trajectory for the step, then

$$d\theta = \frac{ds}{\rho} = \frac{\sqrt{dx^2 + dv^2}}{\sqrt{v^2 + (x + \delta)^2}} = \sqrt{\frac{1 + \left(\frac{dv}{dx}\right)^2}{1 + \left(\frac{x + \delta}{v}\right)^2}}\,\frac{dx}{v} = \frac{dx}{v}$$

Introducing this expression into Equation [5], we get

$$dt = \frac{1}{p}\,d\theta \quad \ldots\ldots [5a]$$

This expression can be integrated for the duration of the step, and gives

$$t - t_o = \frac{1}{p}\,(\theta - \theta_o) \quad \ldots\ldots [5b]$$

It is therefore seen that positive time is proportional to the counterclockwise angular variation in the normal to the phase trajectory. If x had been taken horizontal and $v = \dot{x}/p$ vertical, positive time would correspond to clockwise angular variations in the normal to the phase trajectory.

It is interesting to note that the Liénard method is a special case of the more general "delta" method. In Liénard's analysis δ is a function of $\dot{x}$ only, and therefore not as general as given by Equation [3].

The graphical solution of Equation [2] therefore can be effected by the stepwise construction shown in Fig. 1(*b*) if the operative displacement δ, Equation [3], is known. The following examples will illustrate the method.

Autonomous Systems

Free Vibration of an Ideal Linear System With Positive Restoration. Fig. 2(*a*) shows the conventional method when $\delta = 0$ and obviously the preferred one for such a simple case. The restoring-force diagram is a straight line with positive slope k. The phase trajectory is a circle of radius R_o about the origin on which the phase point will move with the angular velocity of $\sqrt{k/m} = p$ radians per sec.

Fig. 2(*b*) illustrates the δ-method, utilizing one of the infinite number of arbitrary parameters capable of solving the problem. The parameter introduced is represented by a fictitious linear restoring force diagram of an "arbitrary" slope k_1. The differential equation then becomes

$$m\ddot{x} + kx + k_1x - k_1x = 0$$

$$\ddot{x} + p_1^2\,x + \frac{k}{m}\,x - p_1^2x = 0$$

$$\ddot{x} + p_1^2\,(x + \delta) = 0 \text{ with } \delta = \left(\frac{k}{k_1} - 1\right)x$$

The foregoing equation employs the arbitrary and physically fictitious, angular frequency of $p_1 = \sqrt{k_1/m}$ radians per sec.

Method of Construction: A graphical solution of a specific problem is begun by first assuming an arbitrary value for $|k/k_1|$, say, 3/2, and plotting $\delta = x/2$ against the x-axis of the phase plane. The construction of a phase curve is then commenced by assuming suitable specific starting conditions. Let the start occur at ① with $x = R_o$. The initial value of δ is then $R_o/2$ which means that the center of the initial circular arc must be located that distance below the $\dot{x}/p_1$ axis. Therefore the displacement R_o will decrease. Assuming that for a finite step it decreases from R_o to 0.8 R_o with an average value of 0.9 R_o, we use $\delta_1 = 0.45\ R_o$

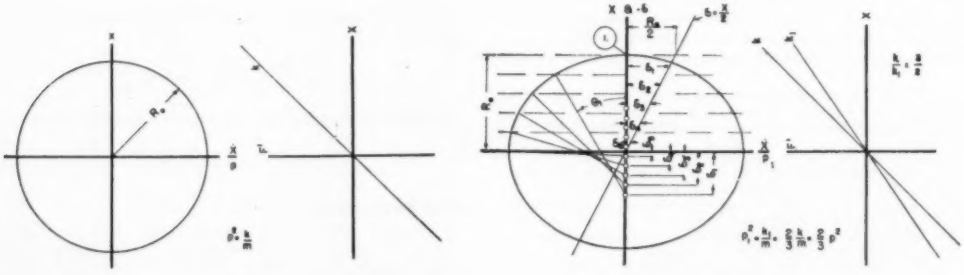

(a) (b)

FIG. 2

for the center location of the circular arc describing the phase trajectory from R_o to 0.8 R_o. It should be remembered that δ_1 must be laid off in the positive δ-direction, i.e., in the negative x-direction. The angle θ_1 divided by p_1 will then give the time it takes the system to move from $x = R_o$ to $x = 0.8\ R_o$. For the second step we assume that x changes from 0.8 R_o to 0.6 R_o with an average value of $\delta_2 = 0.35\ R_o$, and so on.

The closed phase trajectory, made up of 5 circular arcs for each quadrant, will describe the approximate motion of the system. Fig. 2(*a*) illustrates that for a simple system the δ-method is far more involved than the conventional representation, but it also shows that great flexibility in representation may be obtained by using fictitious restoring force diagrams with arbitrary slopes k_1.

Free Vibration of an Ideal Linear System With Negative Restoration. Fig. 3 gives the conventional $\left(\frac{\dot{x}}{p}, x\right)$ phase-plane representation for such a simple system. The restoring force diagram is a straight line with negative slope k. The complete phase trajectory consists of four equilateral hyperbolas with vertexes on the co-ordinate axes and with asymptotes along the 45-deg axes. The actual plotting of the hyperbolas can be accomplished either by calculating points or by purely graphical means. Notice that for any specific start the phase trajectory is located within one of the four quadrants separated by the asymptotes. The origin is in this case a "saddle" point.

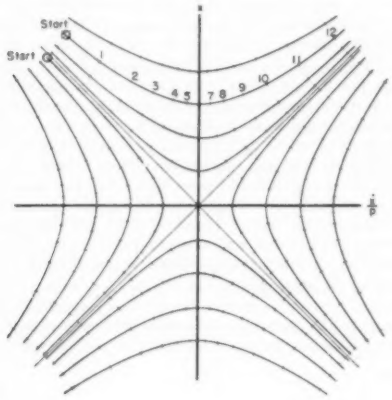

FIG. 3

Fig. 4 illustrates the δ-method of treating the negative restoration problem by introducing an arbitrary, fictitious, positive restoring force diagram of slope k_1. The differential equation is then

$$m\ddot{x} - kx + k_1 x - k_1 x = 0$$

$$\ddot{x} + p_1^2\left(x - \frac{k}{k_1}\,x - x\right) = 0$$

$$\delta = -\left(\frac{k}{k_1} + 1\right)x$$

Letting $|k/k_1| = 1$ in a specific case, we get $\delta = -2x$. Plotting the δ-values against the x-axis, and taking starting condition ① we notice that as x increases from R_o to 1.1 R_o the average δ-value will be $-2(1.05\ R_o)$. We therefore locate the center of the

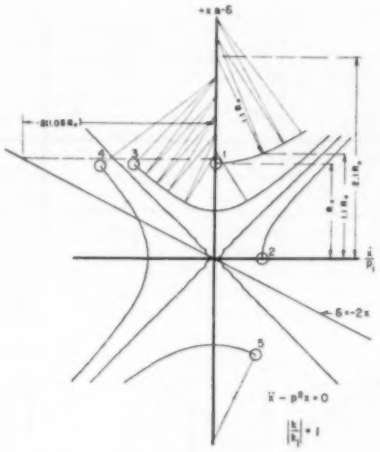

FIG. 4

circular arc at the distance 2.1 R_o along the positive x-axis and swing the arc of radius 2.1 R_o — R_o between the x-limits of R_o and 1.1 R_o. Similar reasoning enables us to draw another circular arc between the x-limits of 1.1 R_o and 1.2 R_o, and so on. A phase trajectory made up of circular arcs and approximating an equilateral hyperbola will be the result. The time marks can be located on the trajectory by measuring the angles subtended by the component circular arcs and dividing them by $p_1 = \sqrt{k_1/m}$. Five specific starts have been shown. The saddle point nature of the diagram and the implied instability of the system are clear.

Free Vibration of an Ideal Nonlinear System. Assume that $G(x, \dot{x}, t)$ is given by the straight line and the second-degree parabola

$$kx \pm a|x|x$$

If we use the plus sign the vibrating system "stiffens" indefinitely. If we use the minus sign the system "softens" toward zero restoration at $x_{cr} = \pm k/a$. It has negative restoration for values of x larger than x_{cr}.

Fig. 5(*a*) illustrates the nonlinear system with stiffening spring. The construction of the δ-curve from the restoring-force curve is clearly indicated by the distances labeled D. It is obvious that whatever be the start, a closed trajectory oblong on the $\dot{x}/p$ axis will result. The free vibrational period of the system will depend on the start; it will be different for each member of the family of trajectories and can be found for a specific member by adding the $\Delta\theta$-values for one quadrant of the curve and dividing their sum by $p/4$. This system is stable for any start.

Fig. 5(*b*) shows the nonlinear system with a "softening" spring. Again the transfer of the restoring-force curve into a delta curve is simple. It will be seen that a vortex point occurs at the origin and that any start of the system lying within the phase-plane area bounded by the closed part of the critical curves passing through $x = \pm\ k/a$ will have closed trajectories and therefore will be stable. These curves will be oblong on the x-axis. Any start falling outside the critical curve, the separatrix, will result in the system being unstable.

Free Vibration of an Ideal Pendulum With Large Amplitude. Since the restoring moment is sinusoidal $G(x, \dot{x}, t)$ will be $mgl \sin x$. We will take the initial slope mgl to be the arbitrary refer-

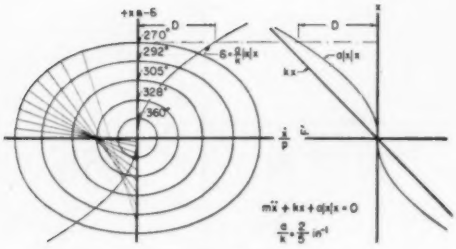

(a)

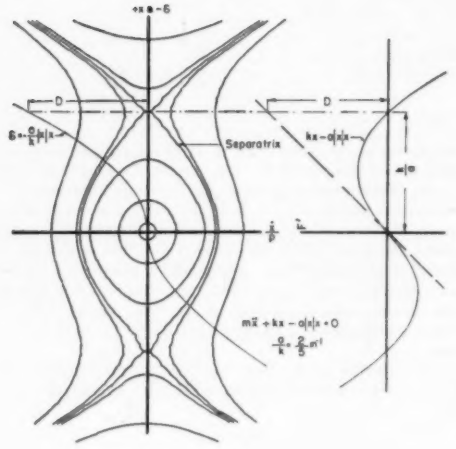

(b)

FIG. 5

ence slope by which we calculate the fictitious, in this case basic, frequency $p_1 = \sqrt{g/l}$. The delta curve is then related to the difference between the reference line of slope mgl and the sinusoidal curve $mgl \sin x$.

Fig. 6 shows the construction for a pendulum swinging between ± 3 radians $= \pm 172$ deg. Since the accuracy of the graphical method can be tested in this case, one quadrant of the phase trajectory has been constructed by the circular arcs related to 30 equal steps in x, i.e., $\Delta x = 0.1$ radians. The addition of the 30 unequal angles $\Delta\theta$ gives 219.4 deg. Consequently,

$$p = \frac{90}{219.4}\, p_1 \text{ or } 0.410\sqrt{\frac{g}{l}}$$

By tables of "elliptic integrals" of the first kind we find that the exact value of p should be $0.3875\sqrt{g/l}$. Our result is therefore 5.7 per cent too high, an appreciable error. To reduce this discrepancy somewhat, let us reconstruct the first two steps involving the angles of 55.5 deg and 22.7 deg. It is obvious that a relatively long time must be spent by the system in getting started and that inaccuracies will occur by taking angles as large as 55.5 deg and 22.7 deg.

A second, fivefold enlarged, diagram of the cross-sectioned region appears on the left of Fig. 6. It will be seen that the first new angle obtained by using five additional subdivisions adds up to 66.3 deg, and the second new angle becomes 23.3 deg. The sum of the angles due to a reconsideration of the first two steps will be 230.8 deg and give a corrected value of p equal to 0.390 $\sqrt{g/l}$. This is only 0.6 per cent higher than the exact value.

If the initial amplitude had been very nearly π radians, the graphical method would of course break down since the starting motion would have been extremely slow. It can be concluded that in the immediate neighborhood of a saddle point the accuracy obtainable by any step-by-step method is poor.

Free Vibration of an Ideal System With Multilinear Restoration. When the restoring-force diagram can be represented by straight lines within definite regions, the phase-plane methods employed by Lamoën (4), Bruce (8) and others consist in drawing the phase trajectory in a multiphase plane where the co-ordinates $(\dot{x}/p_i, x)$ are used for the ith linear region in which $p_i = \sqrt{k_i/m}$. The stepwise jumps in the $\dot{x}/p_i$ co-ordinate therefore require corresponding jumps in the geometry of the phase trajectory in order that velocity continuity may be preserved. For positive restoration,

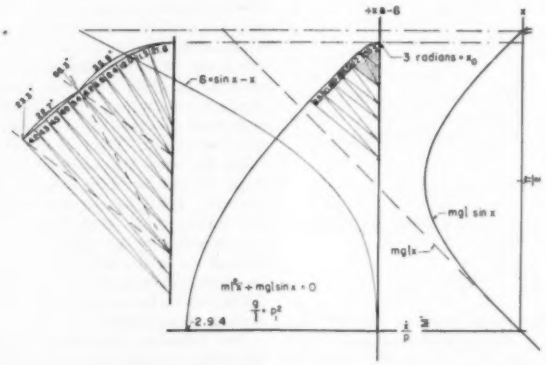

FIG. 6

the trajectories are then circular arcs with their centers located on the z-axis, the actual locations of the centers being determined from the restoring-force diagram. If the slopes of some of the straight lines in the restoring-force diagram are negative, the phase trajectories for those regions will be segments of hyperbolas, while regions with zero slopes of restoring forces will be parabolas.

The δ-method lends itself especially well to multilinear restoration problems by being capable of using the same graphical construction regardless of plus, minus, or zero slopes of the restoring-force diagram. As an example, a bilinear, stiffening elastic system is shown in Fig. 7. It is seen that a family of trajectories about the origin as a vortex point will describe the motion of the system. The smallest one of these is the circle representing the maximum harmonic motion that can occur wholly within the k_1 region of the restoring-force diagram. The "isotemporal" line for $t = \pi/2p_1$ is labeled 90 deg. The free vibrational periods of the system in the various trajectories are proportional to the cyclic angles shown for one revolution, namely, 360 deg, 272 deg, 232 deg, and 212 deg. It is obvious that the limiting period of the system for very large motion will be proportional to a cyclic angle of 180 deg since k_2/k_1 is taken equal to 4.

The bilinear system in Fig. 8 has a linear region Δ followed by an indefinitely large region of zero slope. This is therefore a soft system with an infinite period as a limit. The isotemporal line for $t = \pi/2p_1$ is again marked 90 deg, and the cyclic angles for one revolution are shown.

Referring to the largest trajectory in Fig. 8, it is seen that the segment a'-a is circular with its center at 0 while the seven circular segments from a to b, on account of F' being constant, constitute the δ-approximation of a parabola with vertex at b. Since the vertex bisects the subtangent d-c, it is possible to obtain point b by calculation alone. For time-reckoning purposes the equivalent circular arc of the parabolic segment a-b is given by the trigonometric tangent of the angle a-o-b. With the dimensions $\Delta = 0.6$ in., o-$a = 1.414$ in., angle a-o-b becomes 64.9 deg, and the calculated period of the largest trajectory becomes proportional to 590 deg instead of the graphically obtained 584 deg.

Free Vibration of a System With Viscous Damping and Linear Restoration. In this case the dissipative term will be given by $c\dot{x}$, and the restorative term by kx, consequently

$$\delta = \frac{1}{k}\, c\dot{x}$$

Letting

$$\frac{c}{c_{cr}} = \nu = \frac{c}{2\sqrt{km}}$$

we obtain, if $p = \sqrt{k/m}$

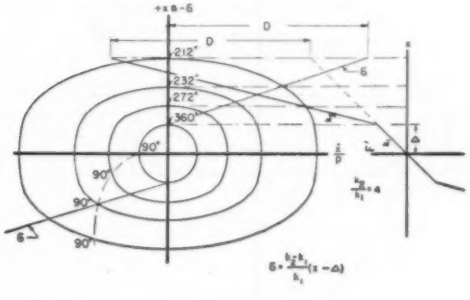

Fig. 7

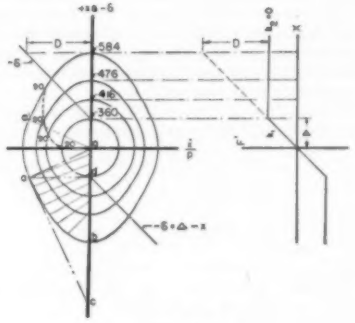

Fig. 8

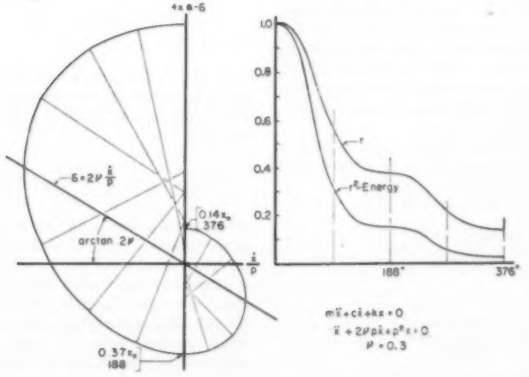

Fig. 9

$$\delta = 2\nu \frac{\dot{x}}{p}$$

The δ-curve is therefore a straight line of slope 2ν on the $\dot{x}/p$ axis. Remembering that the positive δ-direction coincides with the negative x-direction, we construct the diagram for $\nu = 0.3$ shown in Fig. 9(*a*).

A solution involving 7 unequal steps for the first swing and 5 unequal steps for the second is given. The calculated values of r at the x-axis intercepts are 1.00, 0.373, and 0.139, while those determined by the 12-step graphical solution are 1.00, 0.37, and 0.14, indicating a satisfactory agreement. The sum of the angles $\Delta\theta$ corresponding to the first half cycle or to the first seven steps is 188 deg; this corresponds to a natural frequency of

$$\frac{180}{188} p = 0.957 \sqrt{\frac{k}{m}} \text{ radians per sec}$$

which compares favorably with the calculated frequency of $0.955\sqrt{\frac{k}{m}}$.

A time plot of r, rather than a time projection of r, will illustrate the action of the dissipative term, in this case $c\dot{x}$ Fig. 9(*b*) shows time plots of r and of r^2. It is seen that the slopes of the curves are zero at $\theta = 0$, 188 deg, and 376 deg. They reach their negative maximums when the velocities are maximums.

While the phase-plane-delta method illustrates clearly the energy variation in the system as well as the dynamic velocities and displacements, the step-by-step nature of the graphical solution with its involved time marking cannot be advocated for a problem as simple as the one outlined.

Free Vibration of a Linear System With Damping Proportional to Square of Velocity. The motion of the system is governed by

$$m\ddot{x} + s|\dot{x}|\dot{x} + kx = 0$$

or by

$$\ddot{x} + p^2\left(x + \frac{s}{m}\frac{|\dot{x}|}{p}\frac{\dot{x}}{p}\right) = 0$$

This gives

$$\delta = +\frac{s}{m}\frac{|\dot{x}|}{p}\frac{\dot{x}}{p}$$

Fig. 10 shows the square velocity damping problem for the parameter $s/m = 1/2x_o$, and with the trajectory originally drawn to the scale of $x_o = 5$ in. The construction made use of 32 steps for the first convolution, 20 steps for the second, and 16 steps for the third. The circled points show excellent agreement with the Milne tables (9). The period corresponding to the first cyclic angle of 368 deg is $^1/_4$ per cent smaller than the one found by Milne's analysis.

Free Vibration of a Linear System With Negative as Well as With Positive Damping. As an example consider the system governed by the equation

$$m\ddot{x} - c\dot{x} + s|\dot{x}|\dot{x} + kx = 0$$

In the equivalent δ-form this becomes

$$\ddot{x} + p^2(x + \delta) = 0$$

with

$$\delta = 2\nu\frac{\dot{x}}{p} + \frac{s}{m}\frac{|\dot{x}|}{p}\frac{\dot{x}}{p}$$

The curve for the assumed parameters is plotted in Fig. 11, giving $\delta = 0$ at $\dot{x}/p = \pm 2.5$. An initial start with $\dot{x}_o/p = 0$ and $x_o = 4$ in. is seen to make the phase trajectory spiral inward about the origin for about one convolution; then it forms a closed curve. The cyclic angle of the closed curve is 372 deg, corresponding to a period of

$$T = \frac{372}{360}\frac{2\pi}{p} = 1.033 \times 2\pi\sqrt{\frac{m}{k}} \text{ sec}$$

If we choose a start with $\dot{x}/p = 0$, and $x = ^1/_2$ in., the resulting phase trajectory will spiral outward about the origin for about $2^1/_2$ convolutions and join the closed curve already traced by the system set into motion by the first start. Any start lying outside the closed curve therefore will have a phase trajectory spiraling inward, while starts lying inside the closed curve will have trajectories spiraling outward so that any arbitrary start eventually will land the system's phase trajectory on the closed one. For this reason the closed-phase curve is called a "limit cycle trajectory." The origin is an unstable focal point.

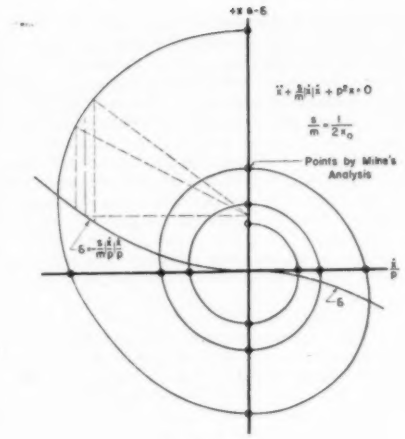

FIG. 10

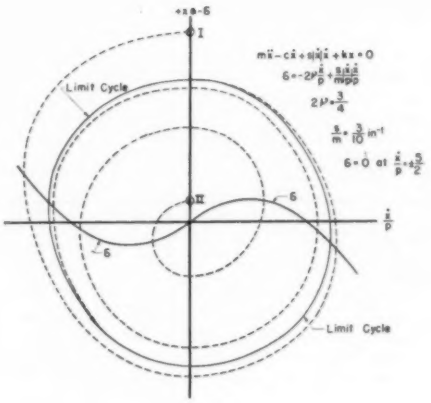

FIG. 11

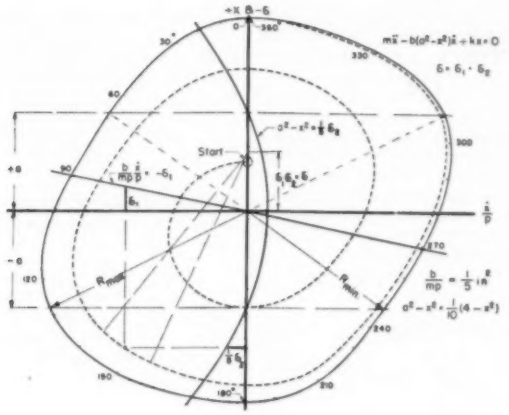

FIG. 12

Free Vibration of a Linear System in Which Damping Is a Function of Both Phase Co-Ordinates. Such a system may be represented by Van der Pol's equation

$$m\ddot{x} - b(a^2 - x^2)\dot{x} + kx = 0$$

$$\delta = -\frac{b}{mp}(a^2 - x^2)\frac{\dot{x}}{p} = \delta_1\delta_2$$

Taking the parameters $b/(mp) = 1/5$ in.$^{-2}$, and $a^2 - x^2 = (4 - x^2)/2$ in.^{2}, we plot $\delta_1 = -(1/5)(\dot{x}/p)$ along the $(\dot{x}/p)$ axis, and $\delta_2/5 = (4 - x^2)/10$ along the x-axis in Fig. 12. The construction then proceeds by reading off the average values of δ_1 and δ_2 for the estimated location of a phase-trajectory segment, multiplying the two to give δ, then locating δ on the x-axis as a center, and striking the circular, segmental arc.

It is seen that a start represented by a phase point near the origin, on account of the negative damping for small values of x, will make the point spiral out and finally move onto the limit-cycle trajectory. The construction center of the phase trajectory will be located at the origin when $\dot{x}/p = 0$, and also when $x = \pm a$; this places the minimum and maximum radii of the limit-cycle trajectory as shown. It should be noted that the cyclic angle of the limit cycle, constructed in 28 steps, is 360 deg, making the natural frequency equal to $\sqrt{k/m}$, but that the system spends approximately 101/180 or 56 per cent of its period in the second and fourth quadrants. A start outside the limit-cycle trajectory of course will make the phase point spiral inward to reach the stable closed trajectory.

Solutions by Means of Auxiliary Backgrounds. An alternative way of dealing with problems in which δ or a part of δ is a product of the phase co-ordinates was employed by Fuchs (5). Assume that the damping is proportional to $x(\dot{x}/p)$, so that

$$m\ddot{x} + a|x|\frac{\dot{x}}{p} + kx = 0$$

with

$$\delta = \frac{a}{mp}|x|\frac{\dot{x}}{p}$$

If the family of curves $x(\dot{x}/p) = c$ be plotted for equal increments in c, the resulting contour plot, consisting of equilateral hyperbolas, can be used as a "background" on which to construct the phase trajectory on transparent paper. Then the local contour value multiplied by $a/(mp)$ gives the operative displacement δ.

Two such backgrounds, Figs. 13 and 14, have been constructed for the families

$$u\,v = c,\ u\,v^2 = c$$

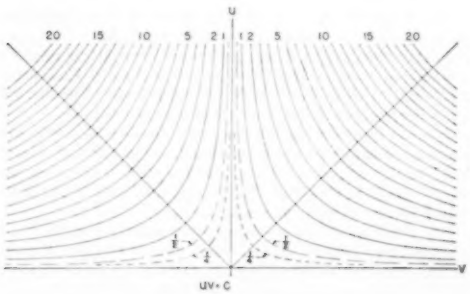

FIG. 13

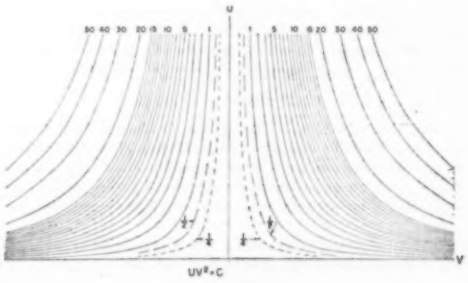

FIG. 14

By means of identifying either u or v with either x or $\dot{x}/p$ it is possible to use the two families as backgrounds for the following three combinations of phase co-ordinates

$$|x|\frac{\dot{x}}{p};\quad |x^2|\frac{\dot{x}}{p};\quad |x\frac{\dot{x}}{p}|\frac{\dot{x}}{p}$$

The phase trajectories of the system in which damping is proportional to $|x|\,\dot{x}/p$ have been drawn by means of the background given in Fig. 13, and are shown in Fig. 15. Any start, originating with $\dot{x}/p$ lying between $\mp mp/a$ in the second and in the fourth quadrants, will never have any subsequent value of $\dot{x}/p$ exceed the limit $\mp mp/a$. This limiting value will be reached asymptotically for all starts with large initial displacements.

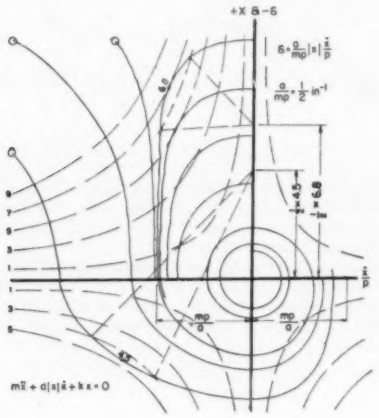

FIG. 15

Van der Pol's equation can be solved readily by using the background provided by Fig. 14. In this case we let

$$\delta = \delta_1 + \delta_2$$

with

$$\delta_1 = \frac{ba^2}{mp}\frac{\dot{x}}{p}$$

$$\delta_2 = \frac{b}{mp}|x^2|\frac{\dot{x}}{p}$$

This means that δ_1 is plotted as the straight line in Fig. 16 and that δ_2 is obtained from Fig. 14 by identifying x^2 with v^2. The background method furnishes an extremely rapid way of constructing the phase trajectory of Van der Pol's equation.

NONAUTONOMOUS SYSTEMS

When time enters explicitly into the differential equation it is sometimes desirable to make a plot of the part of δ due to the independent variable t. This is especially true if an arbitrary disturbance of external origin contributes to δ. Let us now consider two well-known differential equations of the nonautonomous type.

Solution of Bessel's Equation. The general differential equation of Bessel contains the independent variable t explicitly

$$\ddot{x} + \frac{1}{t}\dot{x} + \left(p^2 - \frac{n^2}{t^2}\right)x = 0$$

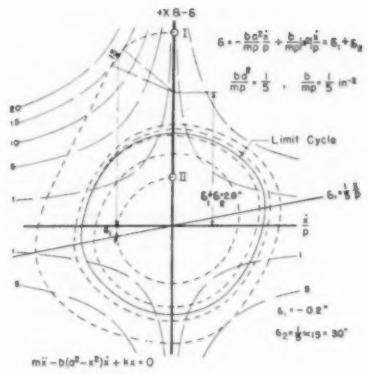

FIG. 16

it can be solved analytically for any value of n, but in our graphical study we will assume that n is zero and write

$$\ddot{x} + \frac{1}{t}\dot{x} + p^2x = 0$$

Changing this equation into the δ-form we get

$$\ddot{x} + p^2(x + \delta) = 0$$

with

$$\delta = \frac{1}{pt}\frac{\dot{x}}{p} = \frac{1}{\theta}\frac{\dot{x}}{p}$$

As a start we let $t = 0$; $\dot{x}/p = 0$, and $x = 1.00$. This means that the initial value of δ will be

$$\delta_o = \lim \frac{1}{\Delta\theta}\frac{\Delta\dot{x}}{p} \quad \text{as} \quad \left(\frac{\Delta\dot{x}}{\Delta\theta}\right) \to 0$$

From geometry it is seen that

$$\frac{\Delta\dot{x}}{p} = -(x_o - \delta_o)\sin\Delta\theta = -(x_o - \delta_o)\Delta\theta$$

Consequently the limit becomes

$$\delta_o = \lim\left[-\frac{1}{\Delta\theta}(x_o - \delta_o)\,\Delta\theta\right] = -(x_o - \delta_o) = -\frac{x_o}{2}$$

Fig. 17 not only shows the phase trajectory of Bessel's equation up to an angle of 12 radians, using increments of $\Delta\theta = 1/8$ radian, but it also shows angle or time projections of x and $\dot{x}/p$ in which the x-projection is equal to $J_0(pt)$, and the $\dot{x}/p$ projection is equal to $J_1(pt)$. Therefore we have obtained graphically the 0th and the first-order Bessel functions of the first kind.

It is obvious that another start with $\dot{x}/p \neq 0$ at $t = 0$ will cause graphical difficulties by making $\delta_o \to \infty$. To take care of this situation we may assume a particular start by using any one set of computed values of the 0th and first-order Bessel function of the second kind (Neumann functions).

Fig. 18 shows the phase trajectory of Bessel's equation for a start leading to the $N_0(pt)$ and $N_1(pt)$ functions by simple angle or time projections. It is obvious from the geometry of construction that the two trajectories in Figs. 17 and 18 will not be alike; however, they will begin to resemble each other with a phase lag of $\pi/2$ as the argument $\theta = pt$ increases. The circled points

on the time projections have been obtained from tables of J_0, J_1, N_0, and N_1.

The reason for including the solution of Bessel's equation in the examples is of pedagogical rather than of practical value.

Solution of Weber's Equation and Its Associate. In the general form we have

$$\ddot{x} + \left(n + \frac{1}{2} \mp \frac{1}{4} a^2 t^2\right) x = 0$$

Letting $n = 0$, $a^2 = 1$, and $p^2 = 1/2$ we get a specific equation

$$\ddot{x} + (p^2 \mp p^4 t^2)\, x = 0$$

Which in the δ-form will be

$$\ddot{x} + p^2 (x + \delta) = 0$$

with

$$\delta = \mp p^2 t^2 x = \mp \theta^2 x$$

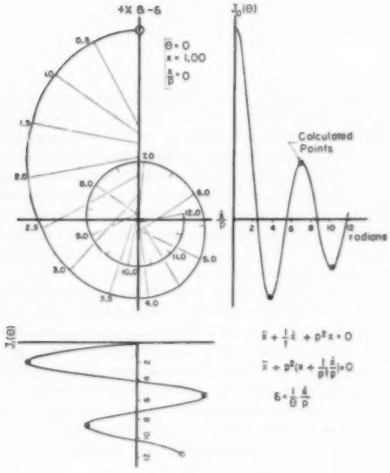

FIG. 17

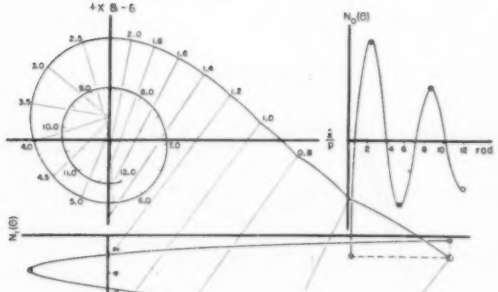

FIG. 18

The lower sign refers to the associate equation. Phase trajectories for both equations are shown in Fig. 19 for a pure displacement start and for angular steps of 10 deg. It is seen that Weber's equation gives an unstable solution while the associate equation represents an oscillatory, damped motion with a period that decreases with time. Thus the four first-half cycles are proportional to the angles 155 deg, 135 deg, 106 deg, and 93 deg, respectively.

Systems With Distinct Driving Term. If the driving term $F(t)$ is a distinct external force acting directly on the mass, we may write Equation [1] as

$$m\ddot{x} + G(x, \dot{x}, t) = F(t) \quad \ldots\ldots [6]$$

Rearrangement then gives

$$\ddot{x} + p^2 \left(x + \delta - \frac{1}{k} F(t)\right) = 0 \quad \ldots\ldots [6a]$$

from which

$$\delta_{ett} = \delta - \frac{1}{k} F(t) \quad \ldots\ldots [6b]$$

Moreover, if the external driving term $X(t)$ is a distinct ground displacement acting through the restoring element on the mass of the system, Equation [1] can be written

$$m\ddot{x} + k(x - X(t) + \delta) = 0 \quad \ldots\ldots [7]$$

Denoting the relative displacement $x - X(t)$ of the mass with respect to the ground by y, we have

$$\ddot{y} + p^2 \left(y + \delta + \frac{1}{p^2} \bar{X}(t)\right) = 0 \quad \ldots\ldots [7a]$$

from which

$$\delta_{att} = \delta + \frac{1}{p^2} \bar{X}(t) \quad \ldots\ldots [7b]$$

It is seen that the same type of expression for δ_{att} results for the two cases when the absolute displacements x are used in the force case and the relative displacements y are used in the ground-motion case.

Bilinear, Hysteretic System With Stepwise Driving. A bilinear, restorative force F is shown in the left-hand diagram of Fig. 20. When the displacement has extended into the second linear region, a reduction in displacement or a return will not

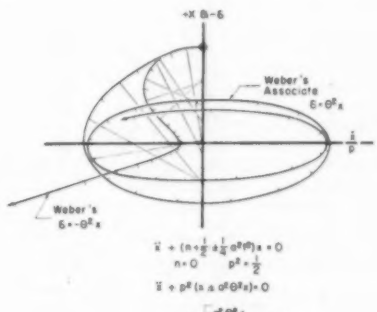

FIG. 19

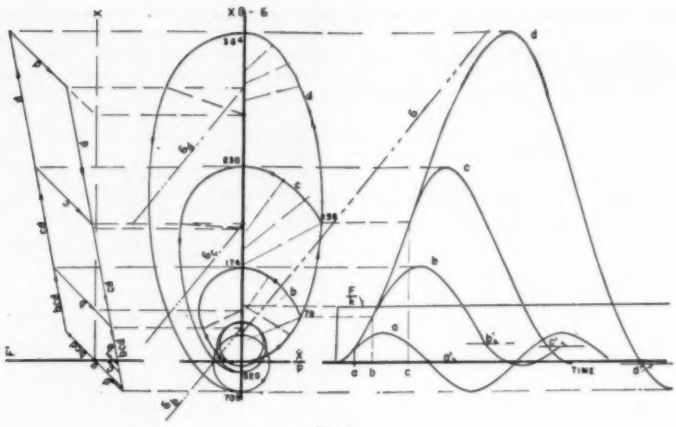

FIG. 20

make the restoring force follow the same curve back. Instead, a new bilinear, inverted diagram will govern the force, as indicated by the arrows, and hysteresis will be present. The bilinear hysteretic system is being driven by a stepwise force pulse F of four durations, indicated by a, b, c, and d in the time diagram on the right of Fig. 20.

For the shortest duration of pulse a, the system remains in the first linear region. The phase curve for this situation is not shown, but the time plot of the ensuing simple harmonic motion is labeled a. If the force acts for the durations b and c, the corresponding phase trajectories, their restoring-force traces, and their time projections have been indicated by b and c. They both finally oscillate about the indicated positive displacements or "permanent sets" b' and c'. If the force continues to act for an indefinitely long time the phase trajectory, force trace, and time projection marked d will result.

The construction of the trajectories is made according to Equation [6b], the δ-part being obtained from the plots marked δ, δ_b, δ_c, and δ_d, and the F/k part from its time plot. It should be noticed that the phase-plane-delta method gives a very compact solution and that the simplicity of the method is in no way dependent on the assumed bilinearity of the restoring-force diagram. If a more complicated restoring-force diagram had been desired, its shape would have affected the δ-plots, but it would not have caused additional difficulties. Experimentally obtained stress-strain curves therefore can be introduced easily into the method. Attention should be called to the fact that the initial reference slope k of the restoring force curve F' always should be drawn equal to unity in the diagrams.

Another bilinear restorative force F' diagram is shown on the left of Fig. 21. In this case the second region is characterized by a negative slope. The physical reason for this may be due to gravitational instability or to other causes. Seven durations of the rectangular force pulse are indicated by the numbers 1 to 7 in the time plot of the force displacement F/k of Fig. 21.

Phase trajectories, restoring-force traces, and time projections are shown for the eight durations. The first of these keeps the system within its first linear region, while durations 2, 3, 4, and 5

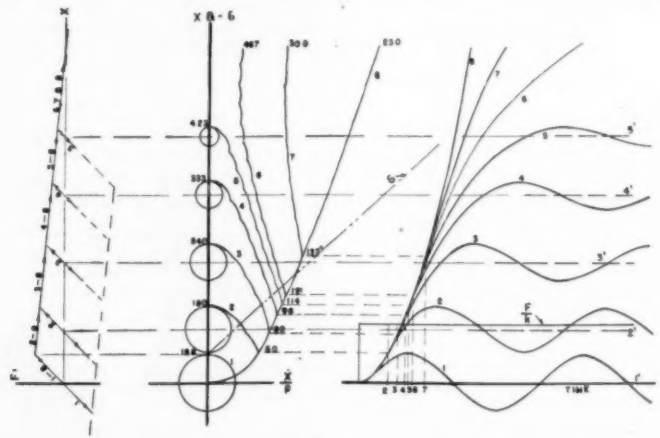

FIG. 21

produce the four permanent sets indicated. Durations 6 and 7 make the system unstable, and duration 8—indefinitely long—gives the system a continuous, positive acceleration. Notice that one δ-curve is sufficient for the construction of all eight diagrams.

It can be concluded that the phase-plane-delta method is extremely useful for problems in which stepwise variation of driving term can be postulated.

Conclusions and Summary

1 The phase-plane-delta method relegates all the terms of an ordinary second-order differential equation into the type form

$$\ddot{x} + p^2 (x + \delta) = 0$$

Consequently the variable displacement δ is often a complicated function.

2 Numerous examples show that the method is practical and that nonlinearity can be dealt with almost as readily as linearity.

3 Terms involving x, $\dot{x}$, and t can be analytically messy and still be simple graphically, as for instance a friction term proportional to the nth power of the velocity when n is any real number.

4 Any graphically defined term can be introduced without first subjecting it to auxiliary analysis. Thus the plastic stress-strain relations of materials with their effects on the restorative properties of a system can be taken into account without any complication if they are experimentally known.

5 Accuracy of the graphical method depends on a judicious choice of size of steps. Test cases involving elliptic integrals, Bessel and Neumann functions, show good accuracy for practicable size of steps. In a general case the degree of approximation can be inferred empirically only.

6 Solutions involving long durations, as for instance in the Mathieu types of equations, will suffer in accuracy by the many steps necessary. Consequently the method is not recommended for long-duration phenomena.

7 Time projection of the phase trajectory in either the displacement or in the velocity direction is especially simple since the trajectory is continuous. Slope discontinuities in the trajectory will cause slope discontinuities in the velocity plot only.

8 The delta method is extremely simple to apply, even to complicated equations. A subprofessional assistant can be instructed quickly in how to use the method, and ordinarily will develop enough speed to become useful in a short time. The drafting implements are a scale, a compass, and a protractor. Auxiliary implements in the form of an adjustable angle V, and various backgrounds can be constructed easily if found desirable.

BIBLIOGRAPHY

1 "Introduction to Non-Linear Mechanics," by N. Minorsky, Edwards Bros., Ann Arbor, Mich., 1947.

2 "Theory of Oscillations," by A. A. Andronow and C. E. Chaikin, Princeton University Press, Princeton, N. J., 1949.

3 "Non-Linear Vibrations," by J. J. Stoker, Interscience Publishers, Inc., New York, N. Y., 1950.

4 "Étude Graphique des Vibrations de Systemes a un Seul Degré de Liberté," by J. Lamoën, Révue Universelle des Mines, May, 1935.

5 "Spiral Diagrams to Solve Vibration Problems," by H. O. Fuchs, *Product Engineering*, vol. 7, 1936, pp. 294–296.

6 "Étude des oscillations entréténues," by A. Lienard, Révue Générale d'Electricité, 1928.

7 "Response of an Elastically Non-Linear System to Transient Disturbances," by R. L. Evaldson, R. S. Ayre, and L. S. Jacobsen, *Journal of The Franklin Institute*, vol. 248, 1949, pp. 473–494.

8 "A Graphical Method for Solving Vibration Problems of a Single Degree of Freedom," by V. Bruce, Bulletin Seismological Society of America, vol. 41, January, 1951.

9 "Damped Vibrations General Theory Together With Solutions of Important Specific Cases," by W. E. Milne, University of Oregon Publication, vol. 2, 1923.

Acknowledgment

The author wishes to acknowledge the sponsorship by the Office of Naval Research and the Armed Forces Special Weapons Project of a research contract at Stanford University under which he has had a chance to work.

Appendix

Let the differential equation governing the motion of the system in question be

$$\ddot{x} + H(x, \dot{x}, t) = 0 \quad \ldots\ldots [8]$$

without specifying any particular kind of function H. Then, after choosing an arbitrary constant κ (of dimension T^{-1}), Equation [8] may be written as

$$\ddot{x} + \kappa^2 h(x, \dot{x}, t) = 0 \quad \ldots\ldots [8a]$$

with h of the same dimension as $\ddot{x}$. Adopting the phase-plane co-ordinates x and $\dot{y} = \dot{x}/\kappa$, we may replace Equation [8a] by

$$\left.\begin{aligned} \dot{x} &= \kappa y \\ \dot{y} &= -\kappa h \end{aligned}\right\} \quad \ldots\ldots [9]$$

Dividing the second of these equations by the first one, we arrive at the differential equation of the trajectories in the phase plane

$$\frac{dy}{dx} = -\frac{h}{y} \quad \ldots\ldots [10]$$

Equation [10] is a differential equation of the first order. This indicates clearly that only the slopes of the trajectories are fully determined. The tangent of the trajectory at point P, Fig. 22,

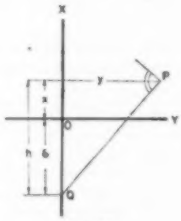

Fig. 22

will be perpendicular to the line QP. A graphical procedure, leading to an approximation of the trajectory by a sequence of straight-line segments, can be based on this geometric relationship.

It is apparent that if κ (as used here) coincides with the quantity p (as used in the paper) the co-ordinates y and v will coincide. The length h may be split into the two components x and δ so that $h = x + \delta$. Equations [10] and [4] are then completely equivalent, and so are Figs. 1(*a*) and 22.

In the paper the trajectories are not approximated by straight-line segments but by circular-arc segments, the centers of which are located on the x-axis (point Q) since δ was assumed constant in the integration of Equation [4]. In reality δ is not constant. This means that the true centers of curvature will be located somewhere on the straight line passing through points P and Q, but not necessarily at Q.

On the other hand, the increment of time is determined by the arc $d\theta$ measured at point Q, as indicated by Equation [5*a*] of the paper.

Torsion of Uniform Rods With Particular Reference to Rods of Triangular Cross Section

By HENRY NUTTALL,[1] BIRMINGHAM, ENGLAND

A solution of the Saint-Venant torsion problem is presented which is alternative to that usually adopted. When the cross section has the shape of an isosceles triangle the method also provides a close and useful Rayleigh-Ritz solution. The torsional rigidity has been evaluated for a range of section proportions, and simple expressions for an approximate evaluation of the maximum shearing stress are provided. Use is made of the hydrodynamic analogy to extend the application of these solutions to the problem of the flow of a viscous incompressible fluid in a tube of triangular section.

THE variational approach to the torsion problem, when the cross section of the rod is simply connected, is to determine a stress function $\varphi(x, y)$ which has a zero value along the boundary of the section, and for which the total potential energy of the deformed rod in the configuration of equilibrium is a minimum.

The total potential energy of a rod of length l, shearing modulus of elasticity G, twisted through an angle θ radians per unit length, is given by the expression

$$U = \frac{l}{2G} \int_R \int \left[\left(\frac{\partial \varphi}{\partial x} \right)^2 + \left(\frac{\partial \varphi}{\partial y} \right)^2 - 4G\theta\varphi \right] dx\, dy \ldots [1]$$

If $\varphi(x, y)$ is the stress function required, it must satisfy the Euler equation of the problem which for this case reduces to

$$\frac{\partial^2 \varphi}{\partial x^2} + \frac{\partial^2 \varphi}{\partial y^2} = \nabla^2 \varphi = -2G\theta \ldots\ldots\ldots\ldots [2]$$

The procedure usually followed in the treatment of the torsion problem is to determine a stress function $\varphi(x, y)$ which has zero value along the boundary of the cross section and which satisfies Equation [2]. The method to be discussed approaches the problem by determining a function $\varphi_r(x, y)$ which has zero value along the boundary and which satisfies the following equation

$$\nabla^2 \varphi_r(x, y) = -\lambda_r^2 \varphi_r(x, y) \ldots\ldots\ldots\ldots [3]$$

If λ_r^2 and λ_s^2 are the eigenvalues corresponding to the eigenfunctions φ_r and φ_s, an application of Green's theorem gives

$$\int_R \int [\varphi_r \nabla^2 \varphi_s - \varphi_s \nabla^2 \varphi_r]\, dx\, dy = (\lambda_r^2 - \lambda_s^2) \int_R \int \varphi_r \varphi_s dx dy$$

$$= \int_C \left[\varphi_r \frac{\partial \varphi_s}{\partial n} - \varphi_s \frac{\partial \varphi_r}{\partial n} \right] ds = 0$$

since $\varphi_r = \varphi_s = 0$ along the boundary. If $\lambda_r^2 \neq \lambda_s^2$ the orthogonal relationship $\int_R \int \varphi_r \varphi_s\, dx dy = 0$ is satisfied.

If the stress function $\varphi(x, y)$ be expanded in the form $\varphi = \Sigma_r A_r \varphi_r$ and this expanded form be substituted in the energy integral Equation [1], after some simplification and the use of Equation [3] this gives

$$U = \frac{l}{2G} \left[\sum_r A_r^2 \lambda_r^2 \int_R \int \varphi_r^2\, dx dy - 4G\theta \sum_r A_r \int_R \int \varphi_r\, dx dy \right]$$

The condition that U shall have a stationary value is that

$$\frac{\partial U}{\partial A_1} = 0, \frac{\partial U}{\partial A_2} = 0, \ldots \frac{\partial U}{\partial A_r} = 0, \ldots$$

This condition provides the equations for determining the values of the constants A_r; thus

$$A_r = 2G\theta \frac{k_r^2}{\lambda_r^2} \int_R \int \varphi_r\, dx dy$$

where

$$k_r^2 \int_R \int \varphi_r^2\, dx dy = 1$$

The stress function φ may now be written as

$$\varphi = 2G\theta \sum_r \left[\frac{k_r^2}{\lambda_r^2} \int_R \int \varphi_r\, dx dy \right] \varphi_r$$

and it may be shown that this function satisfies the Euler equation.

By this method, solutions of the torsion problem have been obtained when the cross section of the rod has the shape of a rectangle, an equilateral triangle, a right-angled isosceles triangle, a circular sector, and a curvilinear rectangle. In the former cases the eigenfunctions are trigonometrical functions but the two latter solutions are in terms of Bessel functions. In order to illustrate the method, the main steps of the two solutions for rods of triangular cross section are presented. A method also is outlined whereby the forms of these exact solutions may be used to obtain a close and useful Rayleigh-Ritz approximate solution when the cross section has the shape of any isosceles triangle.

In the calculations which follow, the base of an isosceles triangle is taken to be of length $2a$ and the height from the center of

---

[1] Lecturer in Mechanical Engineering, The University.

Presented at the National Conference of the Applied Mechanics Division, State College, Pa., June 19–21, 1952, of THE AMERICAN SOCIETY OF MECHANICAL ENGINEERS.

Discussion of this paper should be addressed to the Secretary, ASME, 29 West 39th Street, New York, N. Y., and will be accepted until January 10, 1953, for publication at a later date. Discussion received after the closing date will be returned.

NOTE: Statements and opinions advanced in papers are to be understood as individual expressions of their authors and not those of the Society. Manuscript received by ASME Applied Mechanics Division, October 2, 1951. Paper No. 52—APM-27.

the base to the vertex is taken as $3b$. The length of each of the equal sides is denoted by c.

For an equilateral triangle $a = b\sqrt{3}$

For a right-angled isosceles triangle $a = 3b$

FOR A CROSS SECTION IN THE FORM OF AN EQUILATERAL TRIANGLE

$$\varphi_r(x, y) = 2 \sin\frac{\pi nx}{3b}\frac{\cos \pi ny}{b\sqrt{3}} - \sin\frac{2\pi nx}{3b},\ \lambda_r^2 = \frac{4}{9}\frac{\pi^2 n^2}{b^2}$$

$$\int_R\int \varphi_r\, dxdy = \frac{27b^2}{\pi n\sqrt{3}},\ k_r^2\frac{9b^2\sqrt{3}}{2} = 1,\ A_r = \frac{9b^2G\theta}{\pi^2 n^2}$$

$$\varphi(x, y) = \frac{9b^2G\theta}{\pi^2}\sum_1^\infty \frac{1}{n^2}\,\varphi_r(x, y)$$

Twisting moment

$$M = 2\int_R\int \varphi\, dxdy = \frac{486G\theta b^4}{\pi^4\sqrt{3}}\sum_1^\infty \frac{1}{n^4} = \frac{5.4G\theta b^4}{\sqrt{3}}$$

The maximum shearing stress which occurs at the center of each side is given by

$$\tau = -\left(\frac{\partial\varphi}{\partial x}\right)_{\substack{x\,=\,3b\\ y\,=\,0}} = \frac{12G\theta b}{\pi^2}\sum_{1,3,5}^\infty \frac{1}{n^2} = \frac{3}{2}G\theta b$$

FOR A CROSS SECTION IN THE FORM OF A RIGHT-ANGLED ISOSCELES TRIANGLE

$$\varphi_r(x, y) = \cos\left[\frac{\pi}{6b}(m+n)x\right]\cos\left[\frac{\pi}{6b}(m-n)y\right]$$

$$-\cos\left[\frac{\pi}{6b}(m-n)x\right]\cos\left[\frac{\pi}{6b}(m+n)y\right]\begin{matrix}m\text{ odd}\\ n\text{ even}\end{matrix}$$

$$\lambda_r^2 = \frac{\pi^2}{18b^2}(m^2+n^2),\int_R\int \varphi_r\, dxdy = \frac{72b^2}{\pi^2}\frac{n}{m(m^2-n^2)}$$

$$k_r^2\frac{9b^2}{2} = 1$$

$$A_r = \frac{576b^2G\theta}{\pi^4}\frac{n}{m(m^4-n^4)},$$

$$\varphi(x, y) = \frac{576b^2G\theta}{\pi^4}\sum_{\substack{m\\ \text{Odd}}}\sum_{\substack{n\\ \text{Even}}}\frac{n\,\varphi_r(x, y)}{m(m^4-n^4)}$$

Twisting moment $M = 2\int_R\int \varphi\, dx\, dy$

$$= \frac{82{,}944b^4G\theta}{\pi^6}\sum_{\substack{m\\ \text{Odd}}}\sum_{\substack{n\\ \text{Even}}}\frac{n^2}{m^2(m^4-n^4)(m^2-n^2)}$$

It can be shown that the double summation term in the expression for the twisting moment is reducible to the form

$$\frac{\pi^6}{3072} - \frac{\pi}{16}\frac{31}{32}\sum_1^\infty \frac{1}{n^5} - \frac{\pi}{8}\sum_{1,3,5}^\infty \frac{1}{n^5(e^{n\pi}-1)}$$

The series in this latter expression converges rapidly and is readily summed, giving

$$M = 8.4532b^4G\theta \quad\text{or}\quad M = \frac{c^4G\theta}{38.328}$$

where c is the length of equal sides of the triangle. The maximum shearing stress which occurs at the center of the hypotenuse is given by

$$\tau = -\left(\frac{\partial\varphi}{\partial x}\right)_{\substack{x\,=\,3b\\ y\,=\,0}} = \frac{576bG\theta}{3\pi^3}\sum_{\substack{m\\ \text{Odd}}}\sum_{\substack{n\\ \text{Even}}}\frac{\cdots\sin\cdots/2\,(m+n)}{m(m^4-n^4)}$$

By means of the series[2]

$$\sum_{-\infty}^{\infty}\frac{(-)^n}{n^2+z^2} = \frac{\pi}{z\sinh \pi z}$$

the double summation term in the expression for the stress may be reduced to the form

$$\frac{\pi^3}{64} - \frac{\pi}{8}\left[\frac{1}{\sinh\frac{1}{2}\pi} - \frac{1}{3^2\sinh\frac{3}{2}\pi} + \frac{1}{5^2\sinh\frac{5}{2}\pi} - \cdots\cdots\right]$$

The series in this latter expression converges rapidly and is readily summed, giving

$$\tau = 1.9482G\theta b, \text{ or } \tau = 0.45919G\theta c$$

where c is the length of equal sides of the triangle.

RAYLEIGH-RITZ APPROXIMATE SOLUTIONS

It is possible to obtain two Rayleigh-Ritz solutions of the torsion problem when the cross section of the rod has the shape of any isosceles triangle. In each case the approximate stress function φ is written in the form $\varphi = \Sigma A_r\varphi_r$ where φ_r is given by one or other of the following expressions

$$\varphi_r(x, y) = \frac{2\sin\pi nx}{3b}\frac{\cos\pi ny}{a} - \sin\frac{2\pi nx}{3b} \quad\cdots\cdots[4]$$

$$\varphi_r(x, y) = \cos\left[\frac{\pi}{6b}(m+n)x\right]\cos\left[\frac{\pi}{2a}(m-n)y\right]$$

$$-\cos\left[\frac{\pi}{6b}(m-n)x\right]\cos\left[\frac{\pi}{2a}(m+n)y\right]\begin{matrix}m\text{ odd}\\ n\text{ even}\end{matrix}\quad\cdots[5]$$

Each of these functions has a zero value along the boundary of the cross section and they also have the merit that Equation [4] gives an exact solution when $a = b\sqrt{3}$ while Equation [5] gives an exact solution when $a = 3b$.

Each of the functions φ_r is of the form $f_{r1} - f_{r2}$, and it may be shown that the following relationships are satisfied

$$\nabla^2 f_{r1} = -\lambda_{r1}^2 f_{r1},\ \nabla^2 f_{r2} = -\lambda_{r2}^2 f_{r2}$$

$$\nabla^2\varphi_r = -\lambda_{r1}^2 f_{r1} + \lambda_{r2}^2 f_{r2}$$

$$\int_R\int f_{r1}f_{r2}\,dx\,dy = \int_R\int f_{s1}f_{s2}\,dx\,dy = \int_R\int f_{r1}f_{s1}\,dx\,dy$$

$$= \int_R\int f_{r1}f_{s2}\,dx\,dy = \int_R\int f_{r2}f_{s1}\,dx\,dy = \int_R\int f_{r2}f_{s2}\,dx\,dy = 0$$

These relationships lead to considerable simplification when $\varphi = \Sigma A_r\,\varphi_r$ is substituted for φ in the energy integral Equation [1].

The solution corresponding to Equation [4] gives

$$\text{Twisting moment } M = 3.6\frac{G\theta a^2b^2}{a^2+3b^2} \quad\cdots\cdots[6]$$

(exact when $a = b\sqrt{3}$)

[2] "A Course in Modern Analysis," by E. T. Whittaker and G. N. Watson, §7.4 example 5, Cambridge University Press, London, England, 1946.

Maximum shear stress

$$-\left(\frac{\partial\varphi}{\partial x}\right)_{\substack{x=3b\\y=0}} = \frac{3G\theta a^2 b}{a^2+3b^2} \quad \ldots\ldots [7]$$

(exact when $a = b\sqrt{3}$)

A closer approximation to the value of the maximum shear stress is obtained by regarding $\nabla^2\varphi + 2G\theta$ as the error arising at any point of the cross section when φ has any value other than the exact value. If the approximate stress function is taken in the form $\varphi = \sum_r A_r\varphi_r$ where φ_r has the value given by Equation [4]

$$\nabla^2\varphi + 2G\theta = \sum_r (A_r\nabla^2\varphi_r) + 2G\theta$$

If $\int_R\int\left[\left(\sum_r A_r\nabla^2\varphi_r\right) + 2G\theta\right]^2 dx\,dy$ is to be a minimum

$$\frac{\partial}{\partial A_1} = \frac{\partial}{\partial A_2} = \frac{\partial}{\partial A_r} = \ldots$$

$$\int_R\int\left[\left(\sum_r A_r\nabla^2\varphi_r\right) + 2G\theta\right]\nabla^2\varphi_r\,dx\,dy = 0$$

This gives

$$A_r = -2G\theta\,\frac{\int_R\int\nabla^2\varphi_r\,dx\,dy}{\int_R\int(\nabla^2\varphi_r)^2\,dx\,dy} = \frac{6G\theta a^2b^2(2a^2+6b^2)}{\pi^5 n^2(a^4+2a^2b^2+9b^4)}$$

Maximum stress $\tau = -\left(\frac{\partial\varphi}{\partial x}\right)_{\substack{x=3b\\y=0}}$

$$= \frac{G\theta a^2 b(2a^2+6b^2)}{a^4+2a^2b^2+9b^4} \quad \ldots\ldots [8]$$

(exact when $a/b = \sqrt{3}$)

The solution corresponding to Equation [5] gives

$$M = \frac{55{,}296G\theta a^4b^4}{\pi^6(a^2+9b^2)} \sum_{\substack{m\\\text{Odd}}}\sum_{\substack{n\\\text{Even}}} \frac{n^2}{m^2(m^4-n^4)(m^2-n^2) + \dfrac{32\,a^2-9b^2}{\pi^2\,a^2+9b^2}\,m^4n^2} \quad \ldots\ldots [9]$$

When $a = 3b$, the value of M given by Equation [9] is exact.

Accuracy of Rayleigh-Ritz Solutions

In the following discussion the term "error by defect" is used to denote that a value obtained by calculation is less than the exact value, while "error by excess" denotes that the calculated value exceeds the exact value.

The expressions for the twisting moment and shearing stress given by Equations [6] to [9], when evaluated for any given value of the ratio a/b have the form

$$\text{Twisting moment } M = AG\theta b^4$$

$$\text{Maximum shearing stress } \tau = BG\theta b$$

The constants A and B depend upon the ratio a/b of the cross section and also upon the expression used in the evaluation of M and τ. It is a fundamental property of the Rayleigh-Ritz solution of the torsion problem that the value of the twisting moment obtained is in error by defect of the exact value. Each of the two solutions which have been obtained is exact for one particular value of the ratio a/b and, therefore, each serves to check the accuracy of the other within the range $\sqrt{3} \le a/b \le 3$.

It is possible, using the two solutions to obtain values of A which are exact for $a/b = \sqrt{3}$ and and for $a/b = 3$ and which are in error by defect of the exact value by less than 4 per cent for the range $\sqrt{3} < a/b < 3$.

A set of values of A corresponding to the range $1 \le a/b \le 5.2$ is given in Table 1. For values of a/b less than $\sqrt{3}$, Equation [6] is used, while Equation [9] is more accurate for values of a/b greater than 3. For small values of the apex angle it is more accurate to use the exact solution for the torsion of a circular sector,[1] and a comparison suggests that the value of the twisting moment given by Equation [6] will be in error by defect to the order of about 4 per cent when the apex angle is 40 deg, the magnitude of the error increasing for smaller angles. An estimate of the error involved in the use of Equation [9] for large values of the apex angle is obtained by a relaxation calculation for the case where the apex angle is 120 deg.

TABLE 1 TWISTING MOMENT $M = AG\theta b^4$

$\frac{a}{b}$	A	$\frac{a}{b}$	A	$\frac{a}{b}$	A
1.0	0.900	2.0	4.11	3.2	9.43
1.1	1.14	2.1	4.50	3.4	10.41
1.2	1.40	2.2	4.89	3.6	11.40
1.3	1.69	2.3	5.28	3.8	12.40
1.4	1.99	2.4	5.68	4.0	13.39
1.5	2.31	2.5	6.08	4.2	14.39
1.6	2.65	2.6	6.54	4.4	15.38
1.7	3.00	2.7	7.01	4.6	16.37
$\sqrt{3}$	3.118	2.8	7.49	4.8	17.37
1.8	3.36	2.9	7.97	5.0	18.35
1.9	3.74	3.0	8.453	5.2	19.35

NOTE: The values of A are exact when $a/b = \sqrt{3}$ and when $a/b = 3$. For other values of a/b the maximum error is not greater than about 4 per cent.

The relaxation solution was obtained by using a lattice of triangular mesh, i.e., six strings meeting at a nodal point, the distance between nodal points being $b/10$. The relaxation solution gives a value of $M = 19.25b^4G\theta$ for the twisting moment as compared with the value $M = 19.35b^4G\theta$ obtained from Equation [9]. Since the value obtained from Equation [9] being a Rayleigh-Ritz solution is in error by defect of the exact value, it follows that Equation [9] gives a value of M which is slightly more accurate than that obtained by relaxation.

The relaxation solution also has been used to estimate the magnitude of maximum shearing stress occurring at the center of the side opposite to the vertex. This calculation was made on a lattice three times finer than that used to calculate the twisting moment, and the value of the maximum shearing stress is estimated as $2.30\,G\theta b$.

The two expressions for the shearing stress obtained in Equations [7] and [8] are compared in Table 2. It will be noted that both solutions are exact when $a/b = \sqrt{3}$, but Equation [7] overestimates the magnitude of the stress when $a/b > \sqrt{3}$ while Equation [8] gives a close approximation in error by excess when

TABLE 2 MAGNITUDE OF MAXIMUM SHEARING STRESS $\tau = BG\theta b$

$\frac{a}{b}$	τ from Equation [7]	τ from Equation [8]	τ exact
$\sqrt{3}$	$\frac{3}{2}\,G\theta b$	$\frac{3}{2}\,G\theta b$	$\frac{3}{2}\,G\theta b$
3	$\frac{9}{4}\,G\theta b$	$2G\theta b$	$1.948G\theta b$
$3\sqrt{3}$	$2.7G\theta b$	$2.05G\theta b$	Relaxation estimate $2.30G\theta b$

$$\tau = \frac{3G\theta a^2 b}{a^2+3b^2} \quad \ldots\ldots [7]$$

$$\tau = \frac{G\theta a^2 b(2a^2+6b^2)}{a^4+2a^2b^2+9b^4} \quad \ldots\ldots [8]$$

[1] "Theory of Elasticity," by S. Timoshenko, McGraw-Hill Book Company, Inc., New York, N. Y., 1934, pp. 250–253.

$a = 3b$ and in error by defect at higher values of a/b. Thus the two solutions taken together provide a useful approximation to the value of the maximum stress.

Flow of a Viscous Incompressible Fluid in a Uniform Tube

As stated by Boussinesq,[4] the equations of the torsion problem for a uniform rod are analogous to the equations which govern the flow of a viscous incompressible fluid through a uniform tube having the same shape of cross section as the rod. Because of this analogy it is possible to state the equation for the volume flow through a uniform tube of triangular cross section in the form

$$V = \frac{APb^4}{4L\mu}$$

In this equation P is the pressure drop over a length L of the tube, and μ is the coefficient of viscosity. The values of the constant A for different proportions a/b of the cross section are those given in Table 1.

Acknowledgments

From time to time during the course of the work the author has been grateful for the kindly help and advice of Prof. G. N. Watson, F.R.S. His thanks are also due to Prof. L. G. H. Huxley for a very helpful discussion of eigenvalue problems.

[4] "Étude nouvelle sur l'équilibre et le mouvement des corps solides élastiques dont certaines dimensions sont très-petites par rapport à d'autres," by J. Boussinesq, Journal de Math. (Mathématiques. Pure et Appliquées.) Series 2, vol. 16, 1871, pp. 125–274.

Design Data and Methods

It is important that the data contained in technical papers be made readily available to designing engineers. In order to satisfy these needs of industry, this section of the Journal includes a concise presentation of data and information drawn chiefly from papers previously published by the Applied Mechanics Division of The American Society of Mechanical Engineers.

A Chart for Oblique Shock Waves in Water

By REUBEN BOND[1] AND WERNER GOLDSMITH,[2] BERKELEY, CALIF.

Introduction

THE subject of shock-wave propagation in water, with particular emphasis on the effects of underwater explosions, has received increasing attention in recent years. The reflections of these waves at bounding surfaces, governed by the nonlinear equations of wave propagation and the properties of the medium, frequently lead to the formation of oblique shocks. An analysis of these shock waves is quite tedious, and the numerical evaluation is facilitated by the use of a design chart.

Calculations for normal shocks in both fresh and salt water based on empirical equations of state have been published,[3,4] but no information on oblique shocks for these media is available. Oblique-shock charts for air, on the other hand, are a familiar tool in the analysis of shock phenomena in this medium.[5] The diagram presented here for sea water is patterned according to the form found to be most useful for air shocks, but covers a considerably different range of variables in view of the wide differences in the physical properties of the two media.

Method of Calculation

The procedure employed in the present calculations consists of the superposition of a tangential velocity upon a normal shock. The values for this normal component have been obtained from the computations of Arons and Halverson[4] for sea water initially at 25 C and atmospheric pressure p_0. These data do not admit of simple analytical formulation and consequently are most conveniently expressed in graphical form in terms of the shock pressure rise $p - p_0$, as shown in Fig. 1. Since the acoustic velocity behind the shock front is not included in the data of reference 4 but is contained in reference 3 for an initial temperature of 20 C, these values are adjusted to conform to the same initial temperature as the remainder of the data.

Fig. 2 illustrates the velocity relations for a stationary shock front oblique to the direction of incident flow. In this diagram the normal and tangential velocity components are represented, respectively, by u and v, the resultant velocity by w, the flow angles by β, and the deflection angle by θ. Initial and final conditions are denoted by the subscripts 1 and 2. Mach numbers are indicated by the symbol $\mathbf{M}$.

The following geometrical relations are illustrated in Fig. 2

$$\theta = \beta_1 - \beta_2 \quad [1]$$

$$\tan \beta_1 = u_1/v_1 \quad [2]$$

$$\tan \beta_2 = u_2/v_2 = u_2/v_1 \quad [3]$$

since $v_1 = v_2$.

It follows by substitution that

$$\tan \theta = \frac{\tan \beta_1 - \tan \beta_2}{1 + \tan \beta_1 \tan \beta_2} = \frac{\frac{u_1}{v_1} - \frac{u_2}{v_1}}{1 + \frac{u_1 u_2}{v_1^2}} \quad [4]$$

$$v_1 = \frac{1}{2}\left[(u_1 - u_2)\cot\theta \pm \sqrt{(u_1 - u_2)^2 \cot^2\theta - 4u_1u_2}\right] \quad [5]$$

$$\mathbf{M}_1 = w_1/c_1 = \frac{\sqrt{u_1^2 + v_1^2}}{c_1} \quad [6]$$

$$\mathbf{M}_2 = w_2/c_2 = \frac{\sqrt{u_2^2 + v_2^2}}{c_2} = \frac{\sqrt{u_2^2 + v_1^2}}{c_2} \quad [7]$$

The maximum value of θ for a given value of pressure is obtained from Equation [5] when the radical in this expression vanishes. Then

$$\sin \theta_{max} = \frac{u_1 - u_2}{u_1 + u_2} \quad [8]$$

In the calculations, values of u_1, u_2, c_1, and c_2 were obtained from Fig. 1 for a series of shock pressures. The dependent variables β_1, $\mathbf{M}_1$, and $\mathbf{M}_2$ were computed from Equations [2], [5], [6], and [7] employing these values of velocity and a series of selected values of the angle θ.

The results of these computations are shown in Fig. 3. Lines of constant pressure and constant deflection angle are plotted on rectangular co-ordinates of initial Mach number and flow angle. Curves of constant final Mach number, also shown on the diagram, were not computed directly but were obtained by interpolation from an auxiliary figure.

Discussion

The oblique shock chart for water exhibits the same features as those found in the corresponding diagram for air.[5] The principal differences in the two cases are the larger pressures and

[1] Research Engineer, Institute of Engineering Research, University of California.

[2] Assistant Professor of Engineering Design, University of California. Jun. ASME.

[3] "The Pressure Wave Produced by an Underwater Explosion. III: Properties of Salt Water at a Shock Front," by J. G. Kirkwood and J. N. Richardson, OSRD 813, 1942.

[4] "Hugoniot Calculations for Sea Water at the Shock Front," by A. B. Arons and R. R. Halverson, OSRD 6577, 1946.

[5] "Aerodynamics of a Compressible Fluid," by H. W. Liepmann and A. E. Puckett, John Wiley & Sons, Inc., New York, N. Y., 1947.

Discussion of this paper should be addressed to the Secretary, ASME, 29 West 39th Street, New York, N. Y., and will be accepted until January 10, 1953, for publication at a later date. Discussion received after the closing date will be returned.

Note: Statements and opinions advanced in papers are to be understood as individual expressions of their authors and not those of the Society. Manuscript received by ASME Applied Mechanics Division, May 5, 1952.

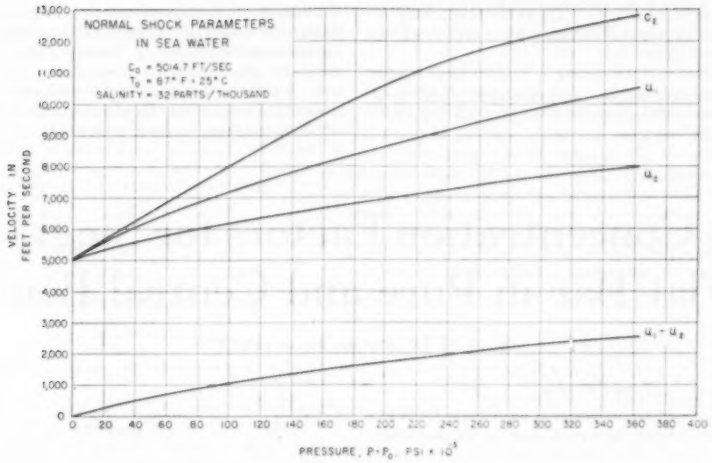

FIG. 1

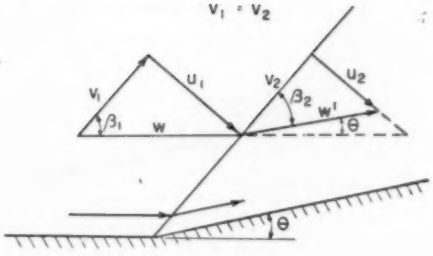

FIG. 2

smaller deflection angles which occur in water shock waves. The range of pressures covered by Fig. 3 corresponds to that expected to be of significance in the propagation phenomena associated with underwater explosions.

The diagram demonstrates that a stationary oblique shock does not exist for every arbitrarily prescribed initial condition. For a given initial Mach number, there is a maximum angle through which the flow may be deflected and, conversely, a minimum initial Mach number exists for a given deflection angle. When a stationary shock wave can exist, there are two possible solutions corresponding to different reductions in the flow velocity. The shock exhibiting the larger velocity change is designated as a strong shock, while the term weak shock is applied to the other. At the limiting conditions, these combine into a single solution with a supersonic emergent flow, but usually the strong shock exhibits a subsonic emergent flow. Furthermore, there exist a minimum pressure for a given deflection angle and a maximum deflection angle for a prescribed pressure. Both these extreme values lie on line *A-B* in Fig. 3 and always occur at a flow angle in excess of 45 deg.

The initial conditions are incompatible with the existence of a stationary oblique shock whenever they fall outside the limits just described. Under these circumstances, some other phenomenon must arise, such as a detached shock, a Mach reflection,

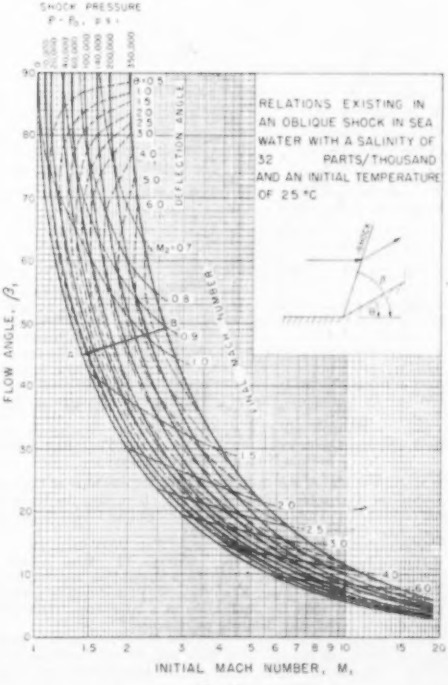
SHOCK PRESSURE
$P-P_0$, PSI
RELATIONS EXISTING IN AN OBLIQUE SHOCK IN SEA WATER WITH A SALINITY OF 32 PARTS/THOUSAND AND AN INITIAL TEMPERATURE OF 25 °C
DEFLECTION ANGLE
MACH LINE
FLOW ANGLE, β_1
INITIAL MACH NUMBER, M_1

FIG. 3

or some other type of irregularity. The entire phenomenon exhibits features and limitations analogous to those occurring in the more familiar case of air shocks.

It may be observed that the spacing of the final Mach number curves is somewhat nonuniform. This same nonuniformity appears in the normal shock data and must be attributed to the properties of the medium.

A variation of initial temperature is accompanied by a positive temperature coefficient of the acoustic velocity amounting to approximately 0.002/deg C. However, the relative values of shock and acoustic velocity are much less sensitive to this variation. Furthermore, in view of the small differences of the properties of the fluids, it may be presumed that the chart also can be employed for shock waves in fresh water.

Stress-Concentration Factors for Single Notch in Flat Bar in Pure and Central Bending[1]

By M. M. LEVEN[2] and M. M. FROCHT[3]

Pure Bending

THE factors of stress concentration for a single notch in a field of pure bending have been investigated photoelastically for flat bars. The maximum stress developed at the base of the notch is a function of the three parameters, r/d, D/d

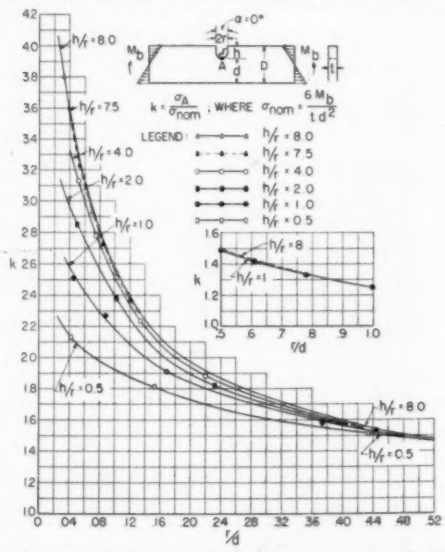

FIG. 1 STRESS-CONCENTRATION FACTOR k, FOR FLAT BAR WITH A SINGLE NOTCH IN PURE BENDING

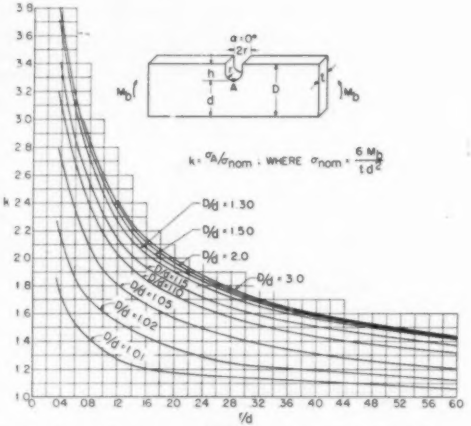

FIG. 2 STRESS-CONCENTRATION FACTOR k, FOR FLAT BAR WITH A SINGLE NOTCH IN PURE BENDING

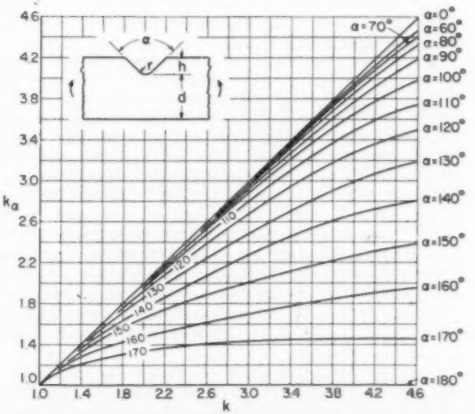

FIG. 3 VARIATION OF k_α WITH k FOR CONSTANT VALUES OF α

[1] Most of this work was done when both authors were at Carnegie Institute of Technology, Pittsburgh, Pa. Recently, the work has been rechecked and amplified at the Westinghouse Research Laboratories, East Pittsburgh, Pa.

[2] Westinghouse Research Laboratories, East Pittsburgh, Pa.

[3] Illinois Institute of Technology, Chicago, Ill. Mem. ASME.

Discussion of this paper should be addressed to the Secretary, ASME, 29 West 39th Street, New York, N. Y., and will be accepted until January 10, 1953, for publication at a later date. Discussion received after the closing date will be returned.

NOTE: Statements and opinions advanced in papers are to be understood as individual expressions of their authors and not those of the Society. Manuscript received by ASME Applied Mechanics Division, September 4, 1952.

(or h/r), and α, where r is the radius at the base of the notch, D is the over-all depth, d is the minimum depth of the beam, h is the depth of the notch, and α is the notch or flank angle, Fig. 1.

The curves in Fig. 1, giving the factors of stress concentration k are the basic experimental curves for the case in which the notch angle α is 0 deg. The range of r/d in these curves varies from 0.03 to 1.0 for notch-depth ratios of h/r = 0.5, 1, 2, 4, 7.5, and 8. The maximum stress which occurs at the base of the notch, point A, Fig. 1, was obtained photoelastically and divided by the nominal stress

$$\sigma_{nom} = \frac{Mc}{I} = \frac{6M_b}{bd^2}$$

to give the factor of stress concentration

$$k = \sigma_{max}/\sigma_{nom}$$

The variation of k with r/d for constant values of D/d is shown in Fig. 2.

Fig. 3 shows the effect of notch angle α, on the factor of stress concentration k_α. For given dimensions, r, h, d, and D, the factor of stress concentration k for α = 0 deg is obtained from Fig. 1 or Fig. 2. This value of k is then extended vertically until it intersects the desired curve for α, Fig. 3, and k_α is read on the ordinate.

Central Bending

For the case of a notched flat bar which is simply supported and centrally loaded, an additional parameter L/D, the ratio of the

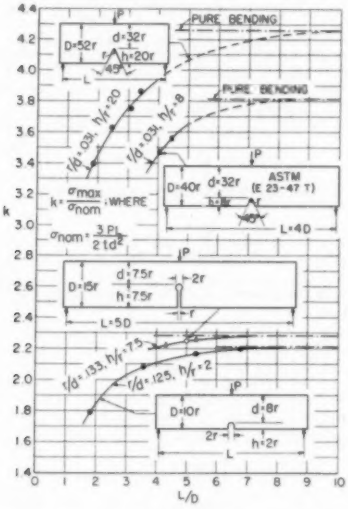

Fig. 4 Curves Showing Variation of Stress-Concentration Factor, k, With Ratio of Beam Span to Depth, L/D, for Various Impact Test Models

length of span to the depth of the beam, affects the factor of stress concentration.

Fig. 4 shows the effect of this parameter for four typical impact test models.

Brief Notes

On the recommendations of the Executive Committee of the ASME Applied Mechanics Division, it has been decided to initiate a section devoted to brief notes on technical matters in mechanics. These notes must not be longer than 750 words (about 2½ double-spaced typewritten pages, including figures) and will be subject to the usual review procedure prior to publication. After approval such notes will be published in the next issue of the Journal. The notes should be submitted to the Secretary of the ASME Applied Mechanics Division.

Graphical Analysis of Axially Symmetrical Plates With Variable Thickness

By P. F. Chenea[1] and P. M. Naghdi[2]

In recent times, considerable attention has been given to the bending of plates with variable thickness especially when the variation in thickness is linear.[3] Generally, however, it is difficult to obtain analytical solutions for plates of variable thickness when the thickness variation is other than linear. In such cases, the notion of splitting the plates into concentric rings has been used quite frequently. Since the problems of rotating disk and bending of axially symmetrical plate are mathematically analogous, Timoshenko[4] suggests, with reference to a paper by Grammel, the method for rotating disk of variable thickness when the plate is divided into concentric rings. The idea of concentric rings has been used by others and more recently, by Gittleman.[5]

Even though the plate is divided into concentric rings in the present method, the analysis is somewhat different from those of the previous authors. This method is applicable to circular plates with axial symmetry and of any variation in thickness within the scope of the classical theory of thin plates. The numerical calculations involved are relatively simple and rapid.

Let the radius of the plate, subjected to axially symmetrical loading but otherwise arbitrary, be divided into n finite divisions, each of incremental length[6] (Δr), from the inner portion at radius

[1] Professor of Engineering Mechanics, Purdue University, Lafayette, Ind.; formerly, Associate Professor of Engineering Mechanics, University of Michigan.

[2] Assistant Professor of Engineering Mechanics, University of Michigan, Ann Arbor, Mich. Jun. ASME.

[3] (*a*) "The Bending of Symmetrically Loaded Circular Plates of Variable Thickness," by H. D. Conway, Journal of Applied Mechanics, Trans. ASME, vol. 70, 1948, pp. 1–6, and the references cited; see also (*b*) "Axially Symmetrical Plates With Linearly Varying Thickness," by H. D. Conway, Journal of Applied Mechanics, Trans. ASME, vol. 73, 1951, pp. 140–142.

[4] "Theory of Plates and Shells," by S. Timoshenko, McGraw-Hill Book Company, Inc., New York, N. Y., 1941, p. 287.

[5] "Circular Plates of Non-Uniform Thickness," by W. Gittleman, *Aircraft Engineering*, vol. 22, 1950, p. 224.

[6] It is not necessary, although convenient, that these divisions be all equal.

Discussion of this paper should be addressed to the Secretary, ASME, 29 West 39th Street, New York, N. Y., and will be accepted until January 10, 1953, for publication at a later date. Discussion received after the closing date will be returned.

Note: Statements and opinions advanced in papers are to be understood as individual expressions of their authors and not those of the Society. Manuscript received by ASME Applied Mechanics Division, June 5, 1952.

r_i to outer radius r_o (for a plate without discontinuity at the center $r_i = 0$); let $(\Delta\varphi)/(\Delta r)$ and φ/r be the normal and tangential curvatures[7] and let M_r, M_t, and Q represent the conventional bending moments and transverse shear (per unit length); then the moment-curvature relations are

$$M_r = D\left(\frac{\Delta\varphi}{\Delta r} + \nu\,\frac{\varphi}{r}\right) \text{ and } M_t = D\left(\frac{\varphi}{r} + \nu\,\frac{\Delta\varphi}{\Delta r}\right)$$

D being the flexural rigidity of the plate

$$\frac{Eh^3}{12(1-\nu^2)}$$

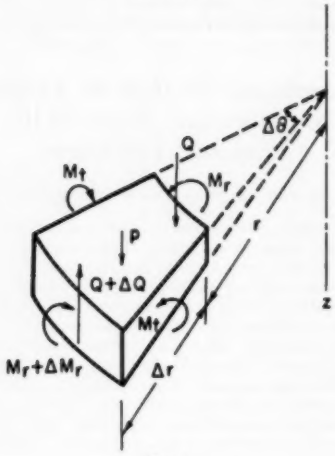

FIG. 1

The axial equilibrium of an element shown in Fig. 1 gives $\Delta(rQ) = pr\Delta r$ from which

$$rQ = \sum_{r_i}^{r} pr\Delta r + (rQ)_{r=r_i} \quad \ldots\ldots [1]$$

and the moment equilibrium yields

$$(M_r - M_t)\Delta r + r\,(\Delta M_r) + rQ\Delta r = 0 \quad \ldots\ldots [2]$$

From the moment-curvature relations, there is obtained

$$(1+\nu)(M_t - M_r)\Delta r + r(\Delta M_t - \nu\Delta M_r) = 0$$

which, together with Equation [2] yields

$$\Delta(M_r + M_t) = -(1+\nu)\,Q\Delta r$$

or

$$M_r + M_t = -(1+\nu)\sum_{r_i}^{r} Q\Delta r + (M_r + M_t)_{r=r_i} = \bar{M} + (M_r + M_t)_{r=r_i} \quad \ldots [3]$$

Substitution of the moment-curvature relations into Equation [3] yields

$$\Delta(r\varphi) = \frac{1}{D(1+\nu)}\,[\bar{M}r\Delta r + (M_r + M_t)_{r=r_i}\,r\Delta r]$$

or

$$r\varphi = \frac{1}{1+\nu}\left[\sum_{r_i}^{r}\frac{\bar{M}}{D}\,r\Delta r + (M_r + M_t)_{r=r_i}\sum_{r_i}^{r}\frac{r\Delta r}{D}\right] + (r\varphi)_{r=r_i} \quad \ldots [4]$$

To illustrate the use of the preceding equations to a particular problem, let us consider the case of a clamped circular plate without discontinuity at the center subjected to a uniformly distributed load. In this case, $r_i = 0$ and Equations [1], [3], and [4] reduce in order to

$$Q = \frac{p}{r}\sum_{0}^{r} r\Delta r \quad \ldots\ldots [1a]$$

$$M_r + M_t = -(1+\nu)\sum_{0}^{r} Qr\Delta r + 2M_c \quad \ldots\ldots [3a]$$

$$\varphi = \frac{1}{r(1+\nu)}\left[\sum_{0}^{r}\frac{\bar{M}}{D}\,r\Delta r + 2M_c\sum_{r_i}^{r} r\Delta r\right] \quad \ldots [4a]$$

where M_c is the bending moment at the center of the plate. It is easily seen that invariant $(M_r + M_t)$ at any material point of the plate is equal to the sum of twice the bending moment at the center and the variation of bending moment due to the action of the transverse shear. Since for a clamped edge $\varphi = 0$ at $r = r_o$, the last equation yields

$$M_c = -\sum_{0}^{r_0}\frac{\bar{M}}{D}\,r\Delta r \Big/ 2\sum_{0}^{r_0}\frac{r\Delta r}{D} \quad \ldots\ldots [5]$$

Again with the aid of the moment curvature relations and Equation [5], there is obtained

$$M_r = \frac{\bar{M} + 2M_c}{1+\nu} - (1-\nu)\,D\,\frac{\varphi}{r} \quad \ldots\ldots [6]$$

$$M_t = \bar{M} + 2M_c - M_r \quad \ldots\ldots [7]$$

The deflection of the plate can be obtained from

$$W = -\sum_{r_i}^{r}\varphi\Delta r + (W)_{r=r_i}$$

For numerical integration, the following step-by-step procedure may be used:

Calculate

1 $$Q = \frac{p}{r}\sum_{0}^{r} r\Delta r$$

2 $$\sum_{0}^{r} Q\Delta r$$

3 $$\bar{M} = -(1+\nu)\sum_{0}^{r} Q\Delta r$$

4 M_c from Equation [5]

5 M_r and M_t from Equations [6] and [7]

In this computation, any one of the well-known graphical integration procedures may be used.

It is clear that the foregoing procedure may be applied to any

[7] The notation used is that of Timoshenko, reference 4, pp. 55–58.

edge conditions, as well as to plates with discontinuity at the center for which in Equation [3] and succeeding expressions the quantity $2M_r$ should be replaced by $(M_r + M_t)_b = r_b$.

To indicate the accuracy of the procedure outlined, it will suffice to state that the example (*a*) in Conway's paper[5] was worked out and his results were checked within 1 per cent when the radius of the plate was divided into twelve equal parts.

A Simple Approximation for the Natural Frequencies of Partly Restrained Bars

By N. M. NEWMARK[1] and A. S. VELETSOS,[2] URBANA, ILL.

THIS paper gives a simple approximation for the natural frequencies of flexural vibration of a bar of constant mass per unit of length m, of constant flexural rigidity of cross section EI, and of span length L between supports which are nondeflecting but which offer a linear resistance to end rotations of the bar.

Consider the bar to be oscillating in one of its natural modes of free vibration. Let θ_L and θ_R be the angular rotations of the bar at the left and right ends, respectively, and M_L and M_R the restraining moments at the corresponding ends. The relation between these moments and the end rotations is expressed by the equations

$$M_L = K_L \theta_L \quad \text{and} \quad M_R = K_R \theta_R \ldots\ldots\ldots [1]$$

The stiffnesses of the restraints are related to the characteristics of the bar by dimensionless coefficients β as follows

$$\beta_L = K_L L/EI \quad \text{and} \quad \beta_R = K_R L/EI \ldots\ldots\ldots [2]$$

For a hinged end $\beta = 0$, and for a clamped end $\beta =$ infinity.

The frequencies f_n, expressed in cycles per second, of the elastically restrained bar can be stated as the product of a dimensionless coefficient C_n multiplied by the fundamental frequency f_0 of the same bar with hinged ends

$$f_n = C_n f_0 = C_n \frac{\pi}{2L^2} \sqrt{EI/m} \ldots\ldots\ldots [3]$$

From the results of numerical calculations based on the exact solution, the following simple approximation is developed for the coefficient C_n for the fundamental frequency ($n = 1$) and all the higher natural frequencies

$$C_n = \left[n + \frac{1}{2}\left(\frac{\beta_L}{5n + \beta_L}\right)\right]\left[n + \frac{1}{2}\left(\frac{\beta_R}{5n + \beta_R}\right)\right] \ldots [4]$$

This formula is applicable to bars having positive end restraints. The maximum error of Equation [4] is 4 per cent for the fundamental and a little over 1 per cent for the higher frequencies.

Errors greater than 2 per cent in the fundamental frequency occur only for bars having one end either hinged or practically unrestrained ($\beta < 0.9$) and the other end clamped or very nearly fixed ($\beta > 10$). The absolute maximum error is obtained for a hinged-clamped bar, for which the approximate fundamental frequency given by Equation [4] is $1.50 f_0$ and the true value is $1.56 f_0$.

When the end restraints are very small, i.e., for values of β approaching zero, the value of C_n is expressed more conveniently by the relation

$$C_n \cong n^2 + 0.1\,(\beta_L + \beta_R) \ldots\ldots\ldots [5]$$

Equation [5] is in error by less than 1.5 per cent when $\beta_L + \beta_R$ is less than 1.0, and the approximate value is always too large.

The approximate formulas are based on exact solutions derived from the ordinary theory of flexure of beams, which neglects the effects of shearing deformation and of rotatory inertia. Because the influence of these neglected factors may become significant in the higher modes, the present formulas should not be used without regard for the limitations imposed by the ordinary theory of flexure.

The approximate equations are similar to those given in a previous paper[3] relating to buckling loads for partly restrained bars.

Acknowledgment

The calculations and detailed study were made as a part of a program sponsored by the Office of Naval Research (Mechanics Branch) in the Structural Research Laboratory, Department of Civil Engineering, of the University of Illinois.

Complementary Energy Analysis of the Failing Load of a Clamped Beam

By N. J. HOFF,[1] BROOKLYN, N. Y.

THE purpose of this note is to report on an investigation of the fundamental assumptions of limit analysis (or limit design). A beam of length L is clamped at both ends, but one end is permitted to move axially to avoid axial loads. The cross section is an idealized I with the area concentrated in the two flanges and the weightless web perfectly rigid in shear. The stress-strain curve is a straight line with slope E from zero stress to the yield stress σ_y and from there on a straight line of slope E/C up to fracture. If the uniformly distributed load is increased gradually from zero to a value w sufficiently high to exceed the yield stress at the two ends of the beam and in the middle, the total complementary energy U' stored is

$$U'/M_y^2 = (1/EI)\left[\int_0^p (C-1)(m-1)^2 dx + \int_q^{L/2} (C-1)(m+1)^2 dx + \int_0^{L/2} m^2 dx\right] \ldots [1]$$

[5] "The Bending of Symmetrically Loaded Circular Plates of Variable Thickness," by H. D. Conway, JOURNAL OF APPLIED MECHANICS, Trans. ASME, vol. 70, 1948, pp. 1–6.

[1] Research Professor of Structural Engineering, University of Illinois. Mem. ASME.

[2] Department of Civil Engineering, University of Illinois.

Discussion of this paper should be addressed to the Secretary, ASME, 29 West 39th Street, New York, N. Y., and will be accepted until January 10, 1953, for publication at a later date. Discussion received after the closing date will be returned.

NOTE: Statements and opinions advanced in papers are to be understood as individual expressions of their authors and not those of the Society. Manuscript received by ASME Applied Mechanics Division, April 15, 1952.

[3] "A Simple Approximate Formula for Effective End-Fixity of Columns," by N. M. Newmark, *Journal of the Aeronautical Sciences*, vol. 16, 1949, p. 116.

[1] Head of Department of Aeronautical Engineering and Applied Mechanics, Polytechnic Institute of Brooklyn. Mem. ASME.

Discussion of this paper should be addressed to the Secretary, ASME, 29 West 39th Street, New York, N. Y., and will be accepted until January 10, 1953, for publication at a later date. Discussion received after the closing date will be returned.

NOTE: Statements and opinions advanced in papers are to be understood as individual expressions of their authors and not those of the Society. Manuscript received by ASME Applied Mechanics Division, June 20, 1952.

where m is the ratio of the bending moment M to the moment M_y at which σ_y is reached, I the moment of inertia $Ah^2/4$, x the axial co-ordinate measured from a fixed end, and the yielded regions extend from $x = 0$ to $x = p$ and from $x = q$ to $x = L/2$. The bending moment M can be calculated from

$$m = -6R[(x/L) - (x/L)^2] + n \quad \ldots\ldots [2]$$

where n is the ratio of the clamping moment N to the yield moment M_y, and R is the ratio of the load w to the value w_y of the load at the onset of yielding in the clamped sections. From the requirement that the complementary energy be a minimum with respect to the clamping moment it follows that

$$R\{6(q/L)^2 - 4(q/L)^3 - 6(p/L)^2 + 4(p/L)^3 - [C/(C-1)]\} + n\{2(p/L) - 2(q/L) + [C/(C-1)]\} - 2(p/L) - 2(q/L) + 1 = 0 \quad \ldots [3]$$

At $x = p$ the moment M is M_y and at $x = q$ it is $-M_y$. Hence

$$-6R[(p/L) - (p/L)^2] + n = 1 \quad \ldots\ldots [4]$$

$$-6R[(q/L) - (q/L)^2] + n = -1 \quad \ldots\ldots [5]$$

Computations were carried out for a wide-flanged I-beam 12 in. × 10 in., weighing 64 lb per ft for which $A = 18.83$ sq in. and $I = 528.3$ in.^{4} The idealization was accomplished by assuming $h = 10.6$ in. which is not a significant deviation from reality. The length was $L = 12$ ft. The modulus was $E = 29 \times 10^6$ psi, the yield stress $\sigma_y = 38{,}000$ psi, and $C = 290$, which corresponds to an ultimate stress of 70,000 psi at an elongation of 32.1 per cent.

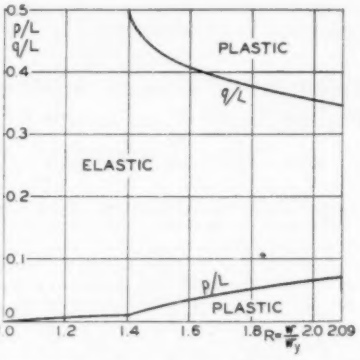

FIG. 1 SPREADING OF PLASTIC REGIONS WITH INCREASING LOAD

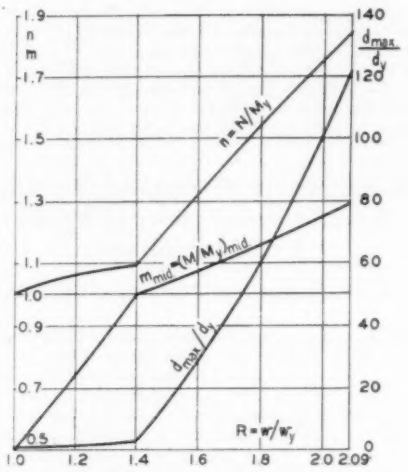

FIG. 2 VARIATION OF MOMENTS AND DEFLECTIONS WITH INCREASING LOAD

The numerical values plotted in Figs. 1 and 2 reveal that the yielded region increases from zero to only 1.12 per cent of L while the load is increased from w_y to 1.4 w_y. During the same time the clamping moment increases from M_y to 1.08 M_y and the mid-deflection, calculated from the principle of virtual displacements, reaches 0.42 in., which is not excessive although it is 2.62 times the value at the onset of yielding. At $R = 1.4$ the mid-section begins to yield and the deflections from there on grow catastrophically. At $R = 2.09$ the ultimate stress is reached in the end sections and the mid-deflection is 19.52 in. Hence the assumption of a yield hinge which permits rotation without an appreciable change in moment is justified below $R = 1.4$. At the load corresponding to this value the beam loses its practical usefulness simultaneously with the appearance of the third yield hinge. The statements contained in the last two sentences justify the fundamental assumptions of limit analysis.

Discussion

Stresses and Deformations of Toroidal Shells of Elliptical Cross Section[1]

WALTER WUEST.[2] The Bourdon tube, invented in 1845 by the German engineer Schinz, has gained a wide field of application for industrial-pressure measurements. For a long time the tubes were manufactured quite empirically. The originally elliptical form of the cross section was changed to a form consisting of two half circles and two straights. During the last war the latter form was investigated by thorough experiments in the Schäffer & Budenberg spring laboratory (Germany). The measured values were found in agreement with theoretical results of the writer, who simplified and improved M. Tueda's theory of Bourdon tubes. Some experimental results also were gained with Bourdon tubes of elliptical cross section.

It is now interesting to compare these experimental results with the theory presented in this paper. The theoretical results for the pressure sensitivity show about double the value of the measurements. Also, taking into account that it is difficult to retain the exact elliptical form during the manufacturing process, this disagreement seems to be very high. Further measurements are needed to clarify this situation. Such measurements would be very interesting, because the results of the authors' theory indicate an extraordinarily great influence of the form of the cross section.

The general theory of thin-walled Bourdon tubes is quite complicated. Apart from the elastic properties of the material the elastic behavior of such tubes depends for a given form of cross section mainly on the following two geometrical parameters:

1 The ratio α of the axes of the cross section.

2 The parameter $\Lambda = c^2/ah$ with c = great semiaxis of the cross section, a radius of curvature, h thickness of the wall.

There are two special cases for which the solution is rather simplified:

(a) Λ small (in practice $\Lambda < 1$), arbitrary α.

(b) $\alpha \to 0$, arbitrary Λ.

The first limiting case may be called "mean pressure tube," for this simplification is only justified for tubes of mean pressure range (lying in practice approximately between 700 and 7000 psi). The elementary theory of mean pressure tubes has often been treated. C. B. Biezeno and J. J. Koch[3] have discussed a numerical method for determining arbitrary cross sections. By an iterative process they extended the range of validity of the elementary theory up to approximately $\Lambda = 3$; but in practice values up to $\Lambda = 50$ happen.

Also, in the other limiting case $\alpha \to 0$ the theory is simplified greatly. A detailed analysis will be treated in a paper by the writer to be published in the *Ingenieure Archiv*.[4] If the cross section is supposed to be of double symmetry and given by

$$y = \pm bf(x)$$

with $f(x)$ an odd function in x, the analysis leads to the following differential equation for the normal deformation w^*

$$w^{iv}(\xi) + 4n^4 w = 4n^4[\alpha\omega f(\xi) - A] \quad \ldots\ldots\ldots\ldots [1]$$

with $w = w^*/c$, $\xi = x/c$, $\omega = \Delta a/a$

$$n^4 = 3(1 - \nu^2)c^4/a^2h^2$$

$$A = 3(1 - \nu^2)c^5 p/n^4 h^3 E$$

The boundary conditions are

$$w = w' = 0 \text{ for } \xi = \pm 1$$

and the general solution is given by

[1] By R. A. Clark, T. I. Gilroy, and E. Reissner, published in the March, 1952, issue of the JOURNAL OF APPLIED MECHANICS, Trans. ASME, vol. 74, pp. 37–48.

[2] Max Planck Institut für Strömungsforschung, Göttingen, Germany.

[3] "On the Elastic Behaviour of the So-Called Bourdon Pressure Tube," by C. B. Biezeno and J. J. Koch, Proceedings, Amsterdam, vol. 44, 1940, pp. 779–786, and 914–920.

[4] "The Influence of the Form of Cross Section on the Behaviour of Bourdon Tubes" (in German), by Wuest, *Ingenieure Archiv*, vol. 20, 1952, pp. 116–125.

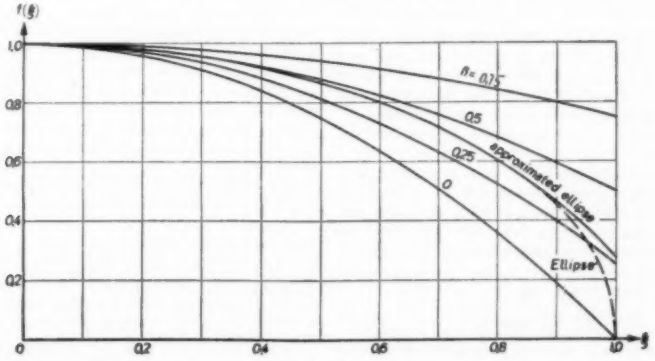

FIG. 1

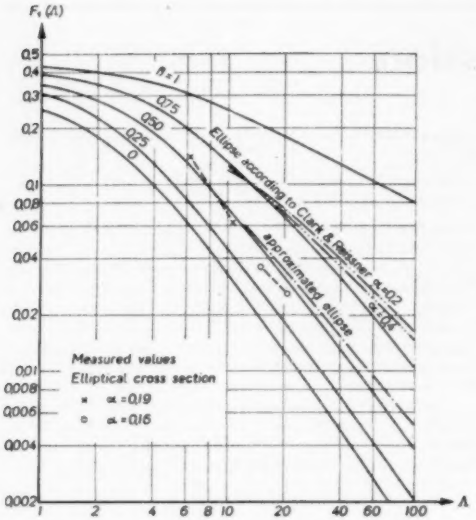

FIG. 2

$$w = A(1 + C_1 \cosh n\xi \cos n\xi + C_2 \sinh n\xi \sin n\xi) + n\alpha\omega \int_0^\xi \bar{w}(\xi - \xi')f(\xi')d\xi' \quad \ldots [2]$$

with $\bar{w}(\xi) = \cosh n\xi \sin n\xi - \sinh n\xi \cos n\xi$

Explicit solutions are possible for $f(\xi)$ given by a polynom, exponential, or trigonometric functions.
The pressure sensitivity is given by

$$\Delta a/a = \frac{1}{\alpha} \frac{\int_0^1 wf d\xi}{\int_0^1 xf^2 d\xi} \quad \ldots [3]$$

Fig. 1 of this discussion shows a family of cross sections given by $f(\xi) = 1 - \beta\xi^2$. $\beta = 0.5$ is a very rough approximation of an ellipse. A better approximation is given in the figure by a polynom of 6th degree (approximated ellipse). The evaluation of Equation [3] of this discussion leads to

$$\Delta a/a = F_1(1 - \nu^2)c^3 p/\alpha h^3 E \quad \ldots [4]$$

In general, F_1 is a function of Λ and in minor dependence also of α. Here only the value $\lim F_1(\alpha, \Lambda)$ for $\alpha \to 0$ is investigated and shown in Fig. 2 of this discussion, for the forms of cross section of Fig. 1. The values of the authors' theory, interpolated for $\alpha = 0.2$ and 0.4 and the measurements mentioned are represented by dotted lines. The measured values lie near the limit curve of the approximated ellipse.

Also, other forms of cross section have been investigated by this method. The approximated analysis concerns also the bending of curved tubes and the stresses. An interesting problem is also the protection of the Bourdon spring from damage by excessive pressures and the behavior of dynamical differential manometers. These problems, too, have been investigated by approximate analysis, i.e., for the limiting case $\alpha \to 0$.

AUTHORS' CLOSURE

Dr. Wuest's comments on the portion of our paper having to do with the sensitivity of Bourdon tubes are of considerable interest and the paper which he has just published[4] represents an important contribution to the subject.

Dr. Wuest's calculations (see Figs. 1 and 2) show that for sufficiently large values of Λ the sensitivity of the tube depends very greatly on the form of its cross section. Dr. Wuest also refers to previously unpublished experimental results concerning tubes with elliptical cross section. We feel that these experimental results are not incompatible with our calculations in view of the important effect which relatively small changes in shape are seen to have and in view of the discusser's statement[4] "Die bei den Messungen verwandten Röhrenfedern sind zunächst mit elliptischen Ziehdornen gezogen worden. Doch besteht immerhin die Möglichkeit, dass bei dem 'Rollvorgang,' bei dem das ursprünglich grade Rohr eine kreisförmige Krümmung erhält, die elliptische Form nicht streng erhalten blieb."

As we see it, Dr. Wuest's calculations are based on the assumptions that

$$\Lambda \text{ finite}, \alpha \to 0 \quad \ldots [1]$$

and there seems to be an upper limit, at least when $\beta \neq 0$, for the admissible values of Λ for which the boundary conditions $w'(\pm 1) = 0$ result in a true picture of what happens. This is in accordance with the fact that as Λ increases the shape of the cross section and what happens in the immediate vicinity of the ends of the major axis is of major importance.

Our own calculations for the elliptical cross section were for

$$\alpha \text{ finite} \quad \ldots [2]$$

and we did not offer results which were intended to be valid when $\alpha \to 0$. On the other hand, our results were for Λ finite where we used trigonometric series *and* for $\Lambda \to \infty$ where we used a method of asymptotic integration. We think it would be interesting to consider the problem further, in particular with reference to what happens when simultaneously

$$\alpha \to 0, \Lambda \to \infty \quad \ldots [3]$$

Gas Cooling of a Porous Heat Source[1]

EDWARD ADAMS RICHARDSON.[2] The writer, and his partner, hold patents on thermal insulation,[3] chemical apparatus,[4] and furnaces,[5] involving the use of permeable bodies with fluid flowing between two faces at different temperatures. In view of such inventions, it was obvious to the partners that such permeable bodies with heat liberation in the mass thereof could be cooled by methods such as those proposed.

We find the work done by the author of interest. However, it seems well to discuss certain aspects of this paper.

The significance, or necessity, for certain of the assumptions made deserves consideration. Though customarily made, the first assumption to the effect that the permeable body and permeating fluid are at the same temperature is not essential. If H is the rate of heat flow between solid and fluid in Btu per cu

[1] By Leon Green, Jr., published in the June, 1952, issue of the JOURNAL OF APPLIED MECHANICS, Trans. ASME, vol. 74, pp. 173–178.

[2] Partner of Edward (Nellie), and George Richardson of Bethlehem, Pa. Mem. ASME.

[3] U. S. Patent No. 2,215,532, Method and Apparatus Relating to Insulated Vessels and Structures of Great Variety, issued to E. A. Richardson, September 24, 1940.

[4] U. S. Patent No. 2,235,644, Process and Apparatus for Effecting Chemical Reactions Involving a Melt and a Gas-Like Body, issued to E. A. Richardson, March, 18, 1941.

[5] U. S. Patent No. 2,311,350, Method and Apparatus for Controlling Combustion, issued to E. A. Richardson, February 16, 1943.

in. per sec per 1 deg F, T the solid temperature, and t the fluid temperature at x, the differential equation required is

$$H(T - t) = Gc_p \left(\frac{dt}{dx}\right) \quad \ldots\ldots\ldots\ldots\ldots [1]$$

This equation is easily combined with Equation [1] of the paper and the resulting differential equation in t is solved easily. Or Equation [1] herewith may be used to estimate the order of error introduced by assuming $T = t$. The finer the degree of subdivision of the porous body and the smaller G, the better justified the first assumption. It cannot be assumed that, with the coarser bodies and higher rates of flow G, the first assumption will be justified.

The second assumption (regarding convection) may be considerably in error for low fluid flow rates G. When G is of the order of 0.10 lb-mol of air per sq ft per hr, convection may be so important that nearly all heating of the entering fluid takes place before the laminar film along the wall is reached. Obviously, if convection could carry heat to the surroundings, this effect would become important.

The third assumption is substantially true (all heat conduction in the wall takes place in the solid) when k_s is large and k_g and G are small. This is certainly not true for rock wool with G of the order of 0.10 lb-mol of air per sq ft per hr.

The fourth assumption (temperature independence of coefficients) is necessary to insure the exactness of the mathematical solutions. In fact, most of these assumptions have as their aim the simplification of the studies which follow.

The conditions set by Equations [3] and [4] of the paper are appropriate where Equation [2] (gas before entering the wall) applies. Those set by Equations [5] and [6] are quite special. It is implied that there can be no radiation from the surface at T_1 to the surroundings at T_0. This condition effectively assumes that the porous body comprises a series of parallel slabs slightly spaced from each other, with fluid entrance faces and fluid exit faces of adjacent slabs facing. Only under such conditions, where radiation escape is negligible, excepting adjacent to the edges of the slab, may these assumptions be justified. For any arrangement permitting radiation from the surface at T_1 to surroundings, at, say, T_0, the effective entering fluid temperature for points within the porous body is less than T_0 by an amount $Q_r/(Gc_p)$ where Q_r is the heat lost by radiation from the surface at T_1 to the surroundings. If radiation occurs from the surface at T_1, then T_2 in Equation [6] of the paper must be reduced by the quantity $Q_r/(Gc_p)$. Furthermore, Equation [6] assumes that there is no loss or gain of heat by radiation from the surface at T_2 to the surroundings.

We appreciate the importance of these simplified mathematical studies, but it is well to emphasize the nature of the omissions involved in the assumptions.

Above Equation [9] of the paper, it is stated that wall-temperature uniformity is desirable from the thermal-stress viewpoint. If a single solid slab is used as an element, this statement has validity. If the heating element is subdivided, or permitted to subdivide under heating stresses, perhaps with the pressure drop controlled by a second layer of high heat conductivity, presumably low or negligible heat generation, there is little limitation due to thermal stresses.

Most of the work done by the writer has been limited somewhat to the lower rates of fluid flow so that laminar-flow resistance or the use of the first term only of flow Equation [13] of the paper is adequate. Flows of the order of 2500 lb per sq ft per hr will involve full use of Equation [13].

It is noted that this study involves an extrapolation of viscosity data for helium. It is presumed facilities for test were not available. The properties of permeable bodies with heat flow and fluid permeation are such that apparatus may be set up quite readily for measuring such things as viscosity at high or low temperature and likewise thermal conductivities at all temperatures. Excepting for a purely mathematical study, such extrapolations as that used are scarcely warranted. Suffice that the partners measured, in 1941, rock-wool conductivity to 1000 F using relatively crude apparatus.

The conclusions reached in this paper are of interest. If the author were to refer to the specifications of our first patent[5] (first filed in 1933), he would find that there is nothing original in the heat-insulation suggestions offered and that even the so-called "sweat-cooling" of Duwez[6] was duly anticipated in our specifications. Our patents were duly called to the attention of the National Inventors' Council in 1943, and it was suggested that the methods could be applied to rockets, gas turbines, and the like. At that time the need for the cooling of atomic reactors was not known, or that might have been mentioned. We are pleased to note that the author does appreciate the possibilities of the method, which possibilities he has presented very well. He appears to appreciate fully that our methods lead directly to the substitution of low-temperature materials for high-temperature work through principles of engineering design based on the properties of these porous bodies with fluid flow from cold, through to, and through, the hot face. This is an extremely important conclusion in view of the great efforts being made to develop extreme high-temperature structural materials when, by and large, such materials are far from essential and require excessive amounts of materials of strategic importance.

It is regretted that space prevents the deserved favorable comments on the general character of the paper and the studies included.

P. J. Schneider.[7] The thermal and dynamic performance of a hypothetical porous graphite helium-heating wall is investigated wherein the steady, one-dimensional temperature distribution of gas and wall are computed from derived analytical solutions, and the familiar relations between system pressure, flow rate, and pumping-power/heat-removal rate uniquely exhibited.

The tractableness of the gas and wall temperature-profile solutions stems from a number of initial thermal and geometric simplifications. Assumption (1) in the paper concerning equal gas and wall temperature is fully justified by the analytical study of Weinbaum. Assumption (2) is controlled by geometry and mode of operation, and assumption (3) follows from specification of an equivalent porosity or wall bulk. Assumption (4) is permissible for most materials which are likely to find application as porous heat sources, although for large temperature differences the influence of nonuniform thermal conductivity and specific heat becomes more pronounced, in which case the analytical device of Kirchhoff might prove useful.

A factor which was not taken into account, in the derivation of the author's Equation [7] for the wall is that electrical heat sources ordinarily exhibit a substantial point-to-point variation in the generated Joulean heat at elevated temperatures. This nonuniformity stems from the temperature dependency of the electrical resistivity, and is approximately identified as a linear relation with the local wall temperature $T(x)$ as $q(T) = q_0(1 + \alpha_0 T)$, wherein α_0 (not to be confused with the viscous resistance coefficient α) is a temperature coefficient of electrical resistivity

[6] "Experimental Study of Cooling by Infiltration of a Fluid Through a Porous Material," by P. Duwez, Sixth International Congress of Applied Mechanics, Paris, France, 1946.

[7] Instructor and Research Assistant, Department of Mechanical Engineering, The State University of Iowa, Iowa City, Iowa. Jun. ASME.

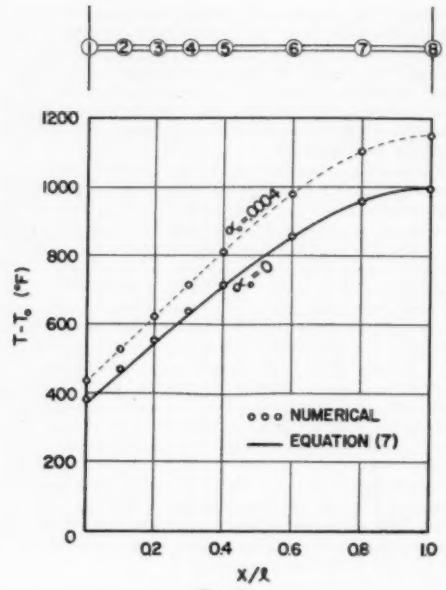

FIG. 1

at a base temperature $T = 0$. Exact analytical solutions analogous to Equations [7] and [8] of the paper, for $q = q(T)$ are found to be tractable but awkward to evaluate numerically. This in turn might suggest an alternate approach using the numerical-relaxation method of Emmons and Southwell.

Let a lin² section of the porous wall in Fig. 1 be subdivided geometrically into eight subregions as in Fig. 1 of this discussion, choosing a finer subdivision in the region of expected maximum temperature gradient. These subregions are then replaced with a network of fictitious heat-conducting rods of appropriate thermal conductance $K = k_s A/L$ Btu/sec-deg F, wherein $A = \text{lin}^2$ is the wall area normal to the assumed linear path of steady heat flow and L is this path length, and a similar network of fictitious pipes to transport the helium gas and its heat-content rate AGC_pT Btu/sec.

For the case of uniform heat development $q = q_0$, choose $q = 10$ Btu/sec-in³, $GC_p = 0.5 \times 10^{-2}$ Btu/sec-in²-deg F, and $k_s = 10^{-3}$ Btu/sec-in-deg F. Then the approximate heat residuals Q at nodal points in the network such as 1 and 2 are

$$Q_1 = K_{2-1}(T_2 - T_1) + GC_pT_0 - GC_pT_1 + qv_1$$

$$Q_2 = K_{1-2}(T_1 - T_2) + K_{3-2}(T_3 - T_2) + GC_pT_1 - GC_pT_2 + qv_2$$

Writing all such residuals for the eight nodal-point network of subregion volume v_i ãñd evaluating each numerically gives

$$\begin{aligned}
\bar{Q}_1' &= 2T_2 + 25 - 2.5T_1 \\
\bar{Q}_2' &= 2.5T_1 + 2T_3 + 50 - 4.5T_2 \\
\bar{Q}_3' &= 2.5T_2 + 2T_4 + 50 - 4.5T_3 \\
\bar{Q}_4' &= 2.5T_3 + 2T_5 + 50 - 4.5T_4 \\
\bar{Q}_5' &= 2.5T_4 + T_6 + 75 - 3.5T_5 \\
\bar{Q}_6' &= 1.5T_5 + T_7 + 100 - 2.5T_6 \\
\bar{Q}_7' &= 1.5T_6 + T_8 + 100 - 2.5T_7 \\
\bar{Q}_8' &= T_7 + 33.3 - T_8
\end{aligned}$$

Temperatures T_1 through T_8 ($T_0 = 0$) obtained through relaxation of this set of residual equations are plotted in Fig. 1 of this discussion, along with $T(x)$ given by Equation [7] of the paper. It appears that the two solutions are in substantial agreement.

For the extended case of nonuniform heat development one simply sets $q_i = q_0(1 + \alpha_0 T_i)$, or, in general, $q_i = q(T_i)$, with α_0 chosen appropriate to the wall in question. The effect of a variable heat source begins to exhibit itself with $\alpha_0 = 10^{-3}$/deg F. The residuals $\bar{Q}_i$ with $\alpha_0 = 4 \times 10^{-3}$ read

$$\begin{aligned}
\bar{Q}_1' &= 2T_2 + 25 - 2.49T_1 \\
\bar{Q}_2' &= 2.5T_1 + 2T_3 + 50 - 4.48T_2 \\
\bar{Q}_3' &= 2.5T_2 + 2T_4 + 50 - 4.48T_3 \\
\bar{Q}_4' &= 2.5T_3 + 2T_5 + 50 - 4.48T_4 \\
\bar{Q}_5' &= 2.5T_4 + T_6 + 75 - 3.47T_5 \\
\bar{Q}_6' &= 1.5T_5 + T_7 + 100 - 2.46T_6 \\
\bar{Q}_7' &= 1.5T_6 + T_8 + 100 - 2.46T_7 \\
\bar{Q}_8' &= 1.5T_7 + 50 - 1.48T_8
\end{aligned}$$

and their relaxation gives the solution plotted in Fig. 1 of this discussion, as $\alpha_0 = 0.0004$. No data seem to be available on the temperature coefficient of electrical resistivity for graphite in particular, and the author does not list k and C_p for helium gas used in his calculations. Also a typographical error appears in the incomplete units for k_s in Table 1.

H. S. TSIEN.[8] The author should be complimented for having demonstrated the effectiveness of cooling a porous heat source by gas. In view of its possible application to high-temperature devices, where the experimental setup will be complicated, it might be worth while to explore the theoretical approach more fully.

The following remarks are motivated by this idea:

Equation [13] of the paper shows that the first term of the pressure gradient is proportional to a power of temperature higher than 1. Therefore the method of average temperature used by the author will underestimate the pressure differential. A more accurate result might be obtained by taking the viscosity as a linear function of temperature between the surface temperatures T_1 and T_2. To extrapolate the viscosity to higher temperatures where no experimental data are available, theoretical relations from the kinetic theory as given by J. O. Hirschfelder[9] could be utilized.

The question of stability is intriguing. A theoretical solution based upon the concept of small perturbations could be made by starting from the following generalized equations for nonsteady flow through porous media

$$-\nabla p = \alpha\mu\mathbf{v} + \beta\rho v\mathbf{v}$$

$$\frac{\partial \rho}{\partial t} + \nabla\cdot(\rho\mathbf{v}) = 0$$

$$\frac{p}{\rho} = \frac{R}{M}T$$

$$\nabla\cdot(k_s\nabla T) + q = \frac{\partial}{\partial t}(\rho_s c T) + \rho\left[\frac{\partial c_p T}{\partial t} + \mathbf{v}\nabla c_p T\right]$$

where $\mathbf{v}$ the velocity vector of the gas, v its magnitude, ρ_s and c are the density and heat capacity of the solid, respectively. The

[8] Robert H. Goddard Professor, Daniel and Florence Guggenheim Jet Propulsion Center, California Institute of Technology, Pasadena, Calif. Mem. ASME.

[9] "Viscosities and Other Physical Properties of Gases and Gas Mixtures," by J. O. Hirschfelder, R. B. Bird, and Ellen L. Spotz, Trans. ASME, vol. 71, 1949, pp. 921–937.

theoretical analysis may be able to decide whether the high performance given in the author's paper is practically possible.

Author's Closure

The author is gratified by the response to his exploratory study of heat removal from a power-producing porous solid, and wishes to thank Messrs. Richardson, Schneider, and Tsien for their constructive comments. In view of the prefatory nature of the study, the idealizations involved therein are certainly justified. Should a more detailed analysis of the problem be warranted, however, the refinements suggested in the foregoing discussion will indeed deserve consideration.

Partially Plastic Thick-Walled Cylinder Theory[1]

P. G. Reynolds.[2] In analyzing test results in relation to theory, it must be borne in mind that consistent test data are exceptionally difficult to obtain. Most alloy-steel cylinders which can be used for experimental work have substantial residual stresses locked in the metal as a result of the heat-treatment used. These residual stresses, in some of our work, have been observed to change the pressure at which plasticity is initiated by as much as ± 50 per cent from the calculated value. This in turn affects the plastic behavior of the cylinder until it is overstrained all the way through the wall. Consideration must be given to factors such as this when evaluating theories in relation to practical results.

Author's Closure

The author thanks Mr. Reynolds for his remarks, with which he is in general agreement.

An Alternative Formulation of the Laws of Mechanics[1]

F. K. Bielitz.[2] A novel aspect of a mathematical symmetry that is often called duality is presented in these studies. Although the basic principle can be traced back to Clerk Maxwell, it is seldom mentioned in present literature on mechanics. In electrical circuit systems, however, such a duality is commonly employed.

The method advanced in the paper has great advantage and deserves to be recommended for application in engineering. The writer employed inverted equations for solving practical mechanical-vibration problems for more than 20 years. It has been his experience that the inversion method very often leads to a quicker solution and in all cases offers new insight into the nature of the problem. The inversion method establishes a new system analogous to the original by interchanging mass and compliance. The author's method provides a further short cut by writing inverted equations directly for the original system.

Two details seem worth mentioning as useful in applying the new method. The inertial reference system that is considered with the loop-type analysis has its counterpart in the usual (nodal) methods of analysis. Certain mechanical systems have two or more ground connections or other closed loops. In some members of such systems forces may be present even in the state of rest. This is a preload that does not have to be known, because it does not affect the motions of the nodal points; neither does the velocity of the inertial system affect the forces within the members.

Another detail which is brought to attention often may be encountered in the analysis of vehicle power plants. It is a certain kind of branched system involving levers in the diagram; the actual components are reduction gears or other mechanical transformers. A loop containing such an element needs special consideration in setting the equations of the type of Equations [11] in the author's presentation. More details can be found in a publication by the writer.[3] This earlier paper is not easily available; and, except for amplifying on the different kinds of branched systems, it is contained within the wider range of the present paper.

C. Truesdell.[4] Fifty years of vigorous controversy after the publication of the "Principia Mathematica" were required in order to demonstrate that the predictions of Newton's system were more or less in agreement with all mechanical phenomena known at the time. The universal popular acceptance of the Newtonian method was caused less by this ultimate scientific accord than by the literary activities of Voltaire and other interested laymen.

Although the established practical success of the Newtonian formulation is admitted and admired, students of the principles ever after have sought to establish the same or nearly the same results from a conceptually clearer and sounder foundation. Thus many "alternative formulations," not altogether equivalent, have been proposed. Every great geometer of the eighteenth century and several of the principal physicists of the nineteenth constructed his own mechanics. Some of these are described in the interesting but unreliable old book of Mach; a more trustworthy but still incomplete account is given in a new book by R. Dugas.[5] In some respects the old fundamental difficulties are removed in the general theory of relativity.

Slightly suggestive of the author's system is that of Lazare Carnot,[6] since it, too, emphasizes the transmissibility of force. The author, however, does not attempt to traverse the quicksands of the foundations of mechanics, for his use of the vague words "force," "transmitted force," and "measurable force" is that customary in the Newtonian method. Rather, he draws out of the conventional Newtonian scheme an admirably easy method of setting up directly equations for the interaction forces.

While the author's analogy to Kirchhoff's laws is interesting, it does not seem that his postulate 3 is used in his example. The following scheme seems to be an equivalent method of putting into practice the author's ideas:

1 Divide the system into loops, taking care to include an inertial reference as a member of the system.

2 Write down the algebraic identities $(\vec{a}_1 - \vec{a}_2) + (\vec{a}_2 - \vec{a}_3) + \ldots = 0$ for each loop, where $\vec{a}_i$ is the acceleration of the ith particle. This gives the derivative of the author's Equations [11].

3 Replace the foregoing differences by the data of the problem if possible, otherwise by the action of unknown forces ac-

---

[1] By M. C. Steele, published in the June, 1952, issue of the Journal of Applied Mechanics, Trans. ASME, vol. 74, pp. 133–140.

[2] Supervisor, Mechanical Research Section, E. I. du Pont de Nemours & Company, Wilmington, Del.

[1] By H. M. Trent, published in the June, 1952, issue of the Journal of Applied Mechanics, Trans. ASME, vol. 74, pp. 147–150.

[2] Project Engineer, Wright-Patterson Air Force Base, Components and Systems Laboratory, Dayton, Ohio.

[2] "Die Umkehrung der linearen mechanischen Schwingungsgebilde," by F. Bielitz, Dissertation, Dresden, Germany, 1934. Published also by *Zeitschrift des Vereines deutscher Ingenieure*, Verlag, Berlin, 1934, Forschungsheft No. 368.

[4] Professor of Mathematics, Graduate Institute for Applied Mathematics, Indiana University, Bloomington, Ind.

[5] "Histoire de la Mécanique," by R. Dugas, Dunod, Neuchâtel and Paris, France, 1950.

[6] "Essai sur les machines en général," by Lazare Carnot, 1783.

cording to Newton's second law, taking care to note that that law reads $\vec{f}_i = m_i(\vec{a}_i - \vec{a}_0)$, where naught refers to the inertial reference.

There result the derivatives of the author's Equations [13].

Since many engineering problems require determination of interaction forces, the author has done great service in showing how to write down equations for them alone, without having first to find the motion. His use of the inertial reference is important and must be understood fully. The fact that the equations for the forces are simpler than those for the positions makes the author's work particularly valuable.

Author's Closure

Bielitz in his comments has mentioned two concepts which are important in practice; so important that it is unfortunate they are relegated to a section on comments. These concepts are duality and perfect couplers.

It appears that Bielitz has employed duality in the following manner: Suppose we have a linear system in vibration and we wish to compute the forces acting in the system. We begin by constructing a dual system in which masses are replaced by compliances and vice versa. We now analyze this dual system in the conventional fashion; i.e., we compute its kinematics. The velocities so obtained will be equal to the corresponding forces in the original system. This can be done in many relatively simple situations. However, there are two pitfalls: Such a duality exists on a one-to-one basis in a physically realizable form only if the connection diagram of the original system can be mapped on a plane without crossovers. In general, this cannot be done. If the one-to-one correspondence requirement can be relaxed so that the conceptual addition of perfect unity-ratio couplers is permissible, then a dual can be found by methods summarized in a paper by Bloch.[7]

Another pitfall concerns the conceptual problem of connecting a mass between two moving junction points, which must be done, in general, if each spring is to be replaced by a mass when forming the dual. The paper shows that masses are to be considered as always connected to the inertial reference; hence they cannot be connected as implied in all situations. A mechanical high-pass filter is a case in hand. The situation can be handled, however, by the conceptual or actual introduction of perfect unity-ratio couplers. A forthcoming paper[8] by P. Le Corbeiller and Ying-Wa Yeung is recommended reading for those interested.

It is seen that the proposal by Bielitz on duality can be carried through in any case, provided perfect couplers are admitted into the situation. This tends to confirm the importance of Bielitz's remarks on couplers. However, couplers go much deeper than this, for they are not only exemplified by levers and gears but they are the equivalent of a broad class of workless constraints. Unfortunately, the literature does not contain, to the author's knowledge, a systematic procedure to treating these devices on a perfectly general basis. This deficiency gives promise of being corrected in the near future.

The remark by Dr. Truesdell on the author's postulate 3 deserves some comment. He describes a three-step process which is correct. However, his step 3 contains a joker. His replacement process, to give a solvable set of equations, must contain only an "independent" set of unknown forces. How does one get such an independent set? Either Newton's third law or postulate 3 of the paper is invoked. These two are equivalent in the sense that one implies the other and vice versa. Postulate 3 is more in keeping with the spirit of a mesh analysis with its emphasis on transmitted forces while Newton's third law is in the spirit of a nodal analysis with its emphasis on the motion of points.

[7] "On Methods for Construction of Networks Dual to Nonplanar Networks," by A. Bloch, Proceedings of the Physical Society, London, England, vol. 58, 1946, pp. 677–694.

[8] "Duality in Mechanics," by P. Le Corbeiller and Ying-Wa Yeung, to be published in the *Journal of the Acoustical Society*.

Bending of a Circular Beam Resting on an Elastic Foundation[1]

M. C. Ek.[2] Some of the results of this paper have been checked by a method developed by the writer. This method was developed to solve such problems as thin flanges with widely spaced bolts and rocket-motor dome thrust rings with concentrated thrust-mount loads; in these cases it is required that a twisting foundation coefficient K_0 be taken into account as well as the deflection foundation coefficient K.[3]

If the basic problem is considered to be a closed ring on an elastic foundation with a single concentrated load at $\phi = 0$, then the series

$$v = a_0 + \sum_{n=1}^{\infty} a_n \cos n\phi \qquad [1a]$$

$$R\beta = b_0 + \sum_{n=1}^{\infty} b_n \cos n\phi \qquad [1b]$$

satisfy the symmetry conditions about $\phi = 0, \pi$.

The expressions for bending and twisting moment are then

$$M_x = f\left[b_0 + \sum_{n=1}^{\infty} (b_n + n^2 a_n) \cos n\phi\right] \qquad [2a]$$

$$M_z = -h \sum_{n=1}^{\infty} n(a_n + b_n) \sin n\phi \qquad [2b]$$

where $f = \dfrac{EI_x}{R^2}, \qquad h = \dfrac{C}{R^2}$

The elastic energy V, due to the bending, twisting, and foundation effects, is then given by

$$\frac{2}{\pi} RV = f\left[2b_0^2 + \sum_{n=1}^{\infty} (b_n + n^2 a_n)^2\right] + h \sum_{n=1}^{\infty} n^2 (a_n + b_n)^2 + R^2 K\left[2a_0^2 + \sum_{n=1}^{\infty} a_n^2\right] + K_0\left[2b_0^2 + \sum_{n=1}^{\infty} b_n^2\right] \qquad [3]$$

Since

$$\frac{\partial V}{\partial a_n} = P, \quad \frac{\partial V}{\partial b_n} = 0, \quad \text{and } a_0 = \frac{P}{2\pi RK}, \; b_0 = 0$$

we have

$$\left.\begin{aligned} \frac{RP}{\pi} &= a_n(fn^4 + hn^2 + R^2K) + b_n n^2 (f + h) \\ 0 &= n^2 a_n (f + h) + b_n (f + hn^2 + K_0) \end{aligned}\right\} \qquad n = 1, 2, 3, \ldots \qquad [4a, b]$$

[1] By Enrico Volterra, published in the March, 1952, issue of the Journal of Applied Mechanics, Trans. ASME, vol. 74, pp. 1–4.

[2] Supervisor, Applied Mechanics Unit, North American Aviation, Inc., Downey, Calif. Jun. ASME.

[3] Unless otherwise specified, the nomenclature is the same as in the paper.

Then, if $f/h = \epsilon$, and $\lambda = \frac{R^2K}{h}$, it follows that

$$a_n = \frac{P}{RK\pi}\left[\frac{\lambda}{\epsilon n^4 + n^2 + \lambda - \frac{n^4(1+\epsilon)^2}{n^2 + K_0/h + \epsilon}}\right]$$

$$b_n = \frac{-n^2(1+\epsilon)a_n}{n^2 + K_0/h + \epsilon} \qquad \left.\begin{array}{l} \\ \\ n = 1, \\ 2, 3, \ldots \end{array}\right\} \quad \ldots\ldots [5a, b]$$

Superimposing four solutions of this type with the loads 90 deg apart, a check is obtained against the author's Table 2 for $K_0 = 0$, $\lambda = 100$, $\mu = 1 = 1/\epsilon$, $\phi = 45$ deg (same as $\phi = 0$ in the writer's notation):

	β/v	y/v	M_x/av	M_t/av
Volterra	—0.00851	0.01087	0.1088	0
Writer (12 terms)	—0.00846	0.01082	0.0862	0

For the case of a single concentrated twisting moment M_0, applied at $\phi = 0$, we obtain $a_0 = 0$, $b_0 = M_0/2\pi(f + K_0)$

$$a_n = \frac{-n^2(1+\epsilon)b_n}{\epsilon n^4 + n^2 + \lambda}$$

$$b_n = \frac{M_0}{\pi h}\,\frac{1}{(n^2 + K_0/h + \epsilon) - \frac{n^4(1+\epsilon)^2}{\epsilon n^4 + n^2 + \lambda}} \qquad \left.\begin{array}{l} \\ \\ n = 1, 2, 3, \ldots \end{array}\right\} \quad \ldots\ldots [6a, b]$$

Although this method is approximate in the sense that its accuracy depends on the number of terms used in the series, a good check of the values in the author's Table 2 was obtained. It has the advantage of taking into account, when necessary, the foundation twisting coefficient K_0.

It is felt that a real gap in the theory of rings has been filled by this paper.

Author's Closure

The author thanks Mr. Ek for his valuable contribution to the discussion of his paper. However, he wants to point out that on May 5, 1952, i.e., more than one and one-half months prior to receipt of Mr. Ek's comments, he sent to the Applied Mechanics Division of The American Society of Mechanical Engineers a paper under the title "Deflections of Circular Beams Resting on Elastic Foundations Obtained by Methods of Harmonic Analysis". This paper, which will be presented at the 1952 Annual Meeting of the Society, will be published in the JOURNAL OF APPLIED MECHANICS. In the new paper a solution is given in terms of trigonometric series for the problem in absence of symmetric restrictions. This solution offers a simple approximate method for evaluating deflections, angles of twist, bending and twisting moments for any case of external loading. In order to facilitate the necessary computations, numerical tables are presented giving the first twenty-four terms in the required series development for different beam characteristics.

Lateral Vibrations as Related to Structural Stability[1]

E. A. RICHARDSON.[2] Several years ago a set of whiskey racks designed under the direction of F. E. Fahy,[3] was tested by the writer's company. Having been consulted with respect to certain aspects of the design, the writer was present as an observer. These racks were five tiers high, loaded with whiskey barrels water-filled to whiskey-barrel weight. The lower three tiers were braced longitudinally, but the upper two tiers were left unbraced. It was hoped that the rigidly fastened rails, cross members, and struts would be adequately stiff without such longitudinal bracing.

Upon test with the full load in place, a small longitudinal disturbance gave rise to longitudinal oscillations of large amplitude which were so slow the period amounted to several seconds.

In his report, the writer noted that the extremely slow oscillations of large amplitude proved that the structure had very little reserve of strength for handling such oscillations; hence full longitudinal bracing should be provided. This observation rested entirely on the known behavior of columns as the critical load is approached. It is well known that such a critical load is characterized by the increase without limit of a slight imposed lateral deflection. It is also well known that the imposed deflection is limited at lower loads substantially according to the formula $1/(1 - P/P_0)$ given by the author. With a very small available recovery force, obviously the frequency of oscillation must be low. Conversely, finding the period long, failure is not far off.

The author is to be congratulated on his comprehensive study of the relations between oscillation frequencies of structures and the loads upon them. The writer is particularly able to appreciate these contributions in view of the fact he touched upon them relatively qualitatively without recognizing the possibilities for further work and wide generalizations in the field.

The emphasis upon the vibration method, because it makes due allowance for actual boundary conditions, is important. Though some allowance was made for joint rigidities in the case of the whiskey racks, it was of the routine type.

The use of constant cross sections for the truss members tested seems open to question. The joint rigidity of the more lightly loaded members could exert an undue effect upon the behavior of those more heavily loaded. This could result in unduly wide departure of the relation between square of the truss frequency and the load thereon. Furthermore, the solid sections of members used do not have the relatively high stiffness of built-up members of open type, based on a given loading. This would affect individual member frequencies and might influence the behavior of the truss as a whole. It seems well to consider these points.

In the case of plates, emphasis was placed on the need for the employment of the theory of large deflections for securing better agreement between theory and practice. Comparison of the studies of Massonnet,[4] as exhibited in Fig. 11 of the paper, with the results of tests shows the importance of such considerations. The practical application of such theory seems open to question.

It happens that the writer served as a member of the American Iron and Steel Institute committee which drew up the handbook of "Light Gage Steel Sections." In view of the nature of the stress and deflection formulas developed by the Committee on Specifications, he reviewed some seven years of tests, carried on by Dr. George Winter of Cornell University for the latter committee, which served as the basis for the formula. Failures were largely determined by exceeding the yield point determined for the material. In such failure, flat-plate compression elements stiffened on the longitudinal edges ranged in behavior from theoretical flat plates supported along the longitudinal edges to those clamped along these edges. (It will be recalled that the effective plate width is used in design.)

[1] By Harold Lurie, published in the June, 1952, issue of the JOURNAL OF APPLIED MECHANICS, Trans. ASME, vol. 74, pp. 195–204.

[2] Publications Department, Bethlehem Steel Company, Bethlehem, Pa. Mem. ASME.

[3] Engineer, Research Department, Bethlehem Steel Company.

[4] "Le Voilement des Plaques Planes Sollicitees dans leur Plan," by Ch. Massonnet, Final Report of the Third Congress of the International Association for Bridge and Structural Engineering, Liége, Belgium, September, 1948.

In two cases, plate curvature so increased on loading that the sections behaved substantially as solid sections up to the yield point. In all other cases the distribution according to actual flat-plate edge condition lay quite at random between the two limiting conditions. It would seem that there would be little to gain in such a case through study based on large deflection methods, at least in so far as practical design is concerned. In view of this observation based on beam behavior with thin, stiffened flanges and quite random types and amounts of initial curvature, it would seem necessary to correlate a relatively large number of tests of normally fabricated plates loaded and subject to vibration to ascertain adequately the range of behavior to be expected in practice.

Author's Closure

The author first wishes to express his thanks to Mr. Richardson for his interest in the paper.

In reply to the points raised in regard to the truss tests, the relationship between the frequency and the loading should be valid irrespective of the particular cross sections employed in the trusses. If the members fail purely by elastic instability, one should be able to use the vibration method in general, constant and solid cross sections not excepted.

The plate experiments were conducted to determine whether, for thin plates, the theoretically linear relationship between the square of the frequency and the applied load was obeyed in practice. The tests showed that it was not, and the results of the large deflection theory were introduced merely to explain the discrepancy. It was not proposed that such theory might be the basis for practical application.

Regarding Mr. Richardson's final comments, two reports dealing with the vibration method applied to normally fabricated plates have become available since the presentation of this paper. The first of these,[5] conducted on solid web bridge girders designed to buckle between stiffeners, confirmed the inapplicability of the method to nonlinear systems. The second[6] was conducted on stiffened plating for ships, and the panels were designed so that the plate-stiffener combination would buckle. In this case, the point of general instability was accurately predicted by the vibration method.

Heat-Exchanger Tube-Sheet Design 2—Fixed Tube-Sheets[1]

G. Horvay.[2] The author's original suggestion, in 1948,[3] that perforated-sheet deflections be calculated by solid-plate formulas, replacing in the various expressions the solid-sheet bending stiffness

$$D = ET^3/12\,(1-\nu^2) \qquad [1a]$$

by the effective stiffness

$$D_b = \eta_w D \qquad [1b]$$

of the perforated sheet, represented an important advance over earlier design procedures. In Equation [1b] η_w may be an experimental constant, as it was in the 1948 paper, or it may have a semiempirical-semitheoretical value, as it does in reference I, equation [40]. In the present paper the author further utilizes the idea of representing tube sheets by equivalent solid sheets, and solves several problems of practical importance.

The writer's comments will be concerned with determination of simpler, and at the same time more reliable expressions for D_b—both for the case of triangular pitch, and for square pitch—than were available heretofore. Since the author's use and the writer's use of the symbols h, H, etc., is conflicting, a third set of symbols, T, 2λ, $2R$, I_s, I, B, C, Γ, will be introduced to denote tube-sheet thickness, average ligament width, tube pitch, moment of inertia of solid sheet per unit length ($T^3/12$), moment of inertia of ligament ($2\lambda I_s$), bending stiffness of ligament (EI), torsional stiffness (GJ), stiffness ratio (C/B). These quantities were denoted by h, $P-d+2t$ (approximate), P, $h^3/12(1-\nu^2)$, —, —, —, in reference I, and by H, $2\bar{h}$, $2R$, I_s, I, B, C, K, in reference II.[4]

The bending rigidity of a perforated sheet of triangular layout has been determined—though not stated—in reference II. It can be written, on the basis of reference II Equations [2], [3], in the form

$$D_b = I_s E_b/(1-\nu_b^2) = I_s E\lambda/R(1+\nu_b) = B/2R(1+\nu_b) \qquad [2]$$

where

$$\left.\begin{aligned} \nu_b &= (1-\Gamma)/(1+3\Gamma) \\ E_b &= (1-\nu_b)E\lambda/R \\ G_b &= E/2(1+\nu_b) \end{aligned}\right\} \qquad [3]$$

are the effective Poisson ratio, Young's modulus, and shear modulus of the perforated sheet, respectively.[5] Since the value of the effective Poisson ratio ν_b varies, by reference II Equation [15], from—0.1 (for very flat ligaments, $T \ll \lambda$) to 1.0 (for very tall ligaments, $T \gg \lambda$; all the time it is assumed that the ligaments are slender, $\lambda \ll R$), its replacement by the actual ν ($\sim$0.3) value in the few innocuous places it still appears in the deflection formula (as for instance in the formula

$$\delta = (5+\nu_b)qa^4/64(1+\nu_b)D_b$$

for central deflection of a uniformly loaded simply supported circular plate) does not cause a significant error. This then fully bears out the author's observation that solid-plate deflection formulas can be used for perforated plates, only the substitution $D \to D_b$ must be made.

The situation for the case of square pitch is more delicate. While it is clear from Fig. 1 of this discussion,[6] that when moments and torques M_x, M_y, $M_{xy} = M_{xy}$ (per inch length) are applied to the edges of such a plate, moments and torques

$$\left.\begin{aligned} M_1 &= M_3 = 2RM_x, \quad T_1 = T_3 = 2RM_{xy} \\ M_2 &= M_4 = 2RM_y, \quad T_2 = T_4 = 2RM_{yx} \end{aligned}\right\} \qquad [4]$$

are developed in the ligaments which cause bending and twist angles

$$\varphi_k = 2M_k R/B, \quad \psi_k = 2T_k R/C \qquad [5]$$

and curvatures

[5] "Experimental Investigation of the Resistance to Buckling of the Web of Solid Web Girders," by Ch. Massonnet, Bulletin Centre Étud. Constr. Génie civ. Hyd. Fluviale 5, 67–240, 1951.

[6] "A Determination of the Critical Load of a Column or Stiffened Panel in Compression by the Vibration Method," by E. E. Johnson and B. F. Goldhammer, Report 800, The David W. Taylor Model Basin, Washington, D. C., February, 1952.

[1] By K. A. Gardner, published in the June, 1952, issue of the Journal of Applied Mechanics, Trans. ASME, vol. 74, pp. 159–166. This will be referred to hereinafter as reference I.

[2] Development Engineer, Knolls Atomic Power Laboratory. The Knolls Atomic Power Laboratory is operated by the General Electric Company for the Atomic Energy Commission.

[3] "Heat-Exchanger Tube-Sheet Design," by K. A. Gardner, Journal of Applied Mechanics, Trans. ASME, vol. 70, 1948, p. 377.

[4] Discussion of paper, "Bending of Honeycombs and of Perforated Plates," Journal of Applied Mechanics, Trans. ASME, vol. 74, 1952, pp. 406-407. To be referred to hereinafter as II.

[5] Needless to say, that increased rigidity of plate, which results from the stiffening effect of the tubes, can be taken care of by suitable increase of B and C.

[6] Labeling of M_y, M_2 on the right of Fig. 1 should be changed to M_x, M_4.

$$\left.\begin{aligned} \kappa_x &= \varphi_1/2R = 2RM_x/B, \quad \kappa_y = 2RM_y/B \\ \kappa_{xy} &= \psi_1/2R = 2RM_{xy}/C, \kappa_{yx} = 2RM_{yx}/C \end{aligned}\right\} \quad [6]$$

a comparison with the solid plate-moment curvature relations

$$\left.\begin{aligned} E_x I_x \kappa_x &= M_x - \nu_y M_y \\ E_y I_y \kappa_y &= M_y - \nu_x M_x \\ 2\,G_{xy} I_x \kappa_{xy} &= M_{xy} \end{aligned}\right\} \quad [7]$$

now leads to the equivalent elastic constants

$$\left.\begin{aligned} \nu_x = \nu_y = 0 = \nu_b,\ E_x = E_y = E\lambda/R = E_b \\ G_{xy} = (1/2)\,\Gamma E\lambda/R = G_b \end{aligned}\right\} \quad [8]$$

and to the equivalent bending rigidity

$$D_x = D_y = B/2R = D_b \quad [9]$$

which (except for $\Gamma = 1$) no longer adhere to the condition of isotropy[7]

$$G_b = E_b/2\,(1 + \nu_b)$$

Indeed, the plate-deflection equation now assumes the form

$$[\nabla^4 + 2(\Gamma - 1)\mathfrak{D}^4]w = q/D_x, \qquad \mathfrak{D}^4 = \partial^4/\partial x^2\partial y^2 \quad [10]$$

$$\nabla^4 = (\partial^2/\partial x^2 + \partial^2/\partial y^2)^2$$

and, when written in polar co-ordinates, it involves, for $\Gamma \neq 1$, the azimuth angle φ, explicitly. Because of the ensuing complications the equation does not lend itself readily to a Gardner type of elastic-foundation analysis. Nevertheless, a simple appraisal of the relative merits of tube sheets of triangular pitch and of square pitch can be obtained by comparing their central deflections when they are in the form of simply supported square plates. By Timoshenko,[8] the deflection, for uniform load q, side length a, is

$$w_t = \frac{32\,qa^4}{\pi^6 B/R}\,\frac{2 + 2\Gamma}{1 + 3\Gamma} \sum_{m,n=1,3,5\ldots}\sum \frac{\sin\,(1/2)\,m\pi \sin\,(1/2)\,n\pi}{mn(m^2 + n^2)^2} \quad [11]$$

when the pitch is triangular, and is[9]

$$w_s = \frac{32\,qa^4}{\pi^6 B/R} \sum_{m,n=1,3,5\ldots}\sum \frac{\sin\,(1/2)m\pi \sin\,(1/2)\,n\pi}{mn(m^2 + n^2)^2\,[1 + 2(\Gamma - 1)\,(mn)^2/(m^2 + n^2)^2]} \quad [12]$$

when the pitch is square. In Fig. 2 of this discussion we plot w_s/w_t versus the stiffness ratio Γ when the B/R ratio of the two sheets is the same. It is seen that for $\Gamma < 1$ the sheet of triangular pitch is stiffer, for $\Gamma > 1$ the sheet of square pitch is stiffer.

Author's Closure

The author is indebted to Dr. Horvay for his discussion contributing to the evaluation of the flexural efficiency η_w, in the tube-sheet design equations. Since his result differs from that derived from Malkin's paper (reference 3 of the paper), it may be helpful to include a comparison of the two.

[7] In the proof of isotropy of a perforated plate for which the constants ν_x, E_x of the x-direction repeat at some other angle α (Journal of Applied Mechanics, June, 1952, p. 229) H. Poritsky and the writer failed to point out that for the special case $\alpha = \pi/2$ only the relations $E_x = E_y$, $\nu_x = \nu_y$ are established (but these now constitute merely a restatement of the assumptions), and the third relation $G = E_x/2\,(1 + \nu_x)$ of the proof degenerates into $0 = 0$. Thus, in the case of $\alpha = \pi/2$ isotropy cannot be proved, and, as the present example indicates, where $D_x/4 = (1/2)\,(\Gamma + 1)\,D_x \neq D_x$ when $\Gamma \neq 1$, it need not exist.

[8] "Plates and Shells," by S. Timoshenko, McGraw-Hill Book Company, Inc., New York, N. Y., 1940, p. 118.

[9] Ibid., p. 192.

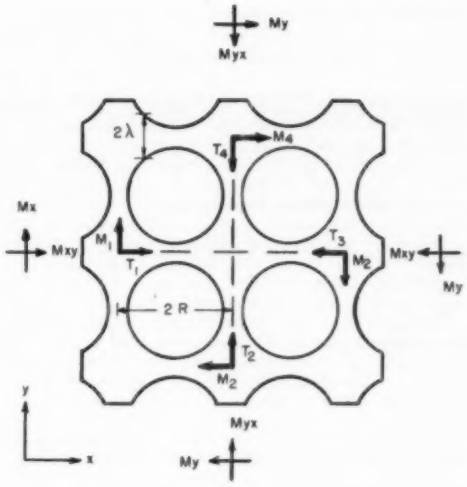

Fig. 1

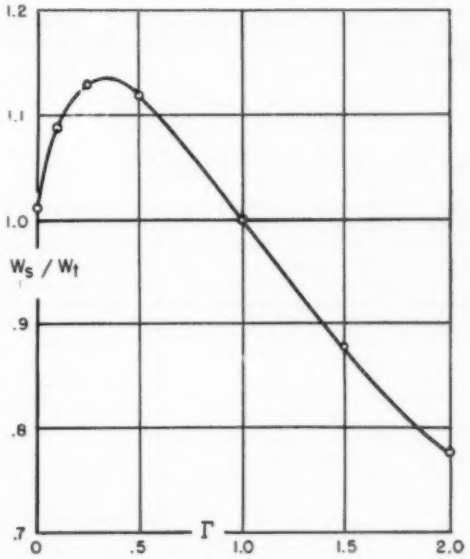

Fig. 2

According to Malkin a plate perforated uniformly by circular holes on a triangular layout may be treated as a solid plate whose effective modulus of elasticity and Poisson ratio are given by

$$E_b = E\left(\frac{1 + \Gamma}{3 + \Gamma}\right)\frac{8\sqrt{3}\,\lambda\,l}{(2R)^2}$$

$$\nu_b = \frac{1 - \Gamma}{3 + \Gamma}$$

The corresponding flexural efficiency may be computed as

$$\eta_w = (3 + \Gamma)(1 - \nu^2)\frac{\sqrt{3}\,\lambda\, l}{4R^2}$$

or, since he suggests defining the mean ligament width × length product $(2\lambda l)$ as $(R^2/\sqrt{3})\ [1 - (\pi\sqrt{3}d^2/24R^2)]$

$$\eta_w = \frac{(3 + \Gamma)(1 - \nu^2)}{8}\left(1 - \frac{\pi\sqrt{3}}{6}\frac{d^2}{P^2}\right) \text{(Malkin)}$$

For the same conditions, Horvay gives

$$E_b = E\frac{4\Gamma}{(1 + 3\Gamma)}\frac{\lambda}{R}$$

$$\nu_b = \frac{1 - \Gamma}{1 + 3\Gamma}$$

from which

$$\eta_w = \frac{(1 + 3\Gamma)}{2(1 + \Gamma)}(1 - \nu^2)\frac{\lambda}{R}$$

If Malkin's suggestion as to the evaluation of the mean ligament width $(2\lambda = 2R - 0.952d)$ is adopted, the result is

$$\eta_w = \frac{(1 + 3\Gamma)(1 - \nu^2)}{2(1 + \Gamma)}\left(1 - 0.952\,\frac{d}{P}\right) \text{(Horvay)}$$

In a discussion of Malkin's paper, the author indicated that the normal range of Γ lay between 0 and 0.12, so that the final comparisons become

$$\eta_w = 0.35\left(1 - 0.908\,\frac{d^2}{P^2}\right) \text{(Malkin)}$$

and

$$\eta_w = 0.50\left(1 - 0.952\,\frac{d}{P}\right) \text{(Horvay)}$$

where the error in the numerical constant due to variation in Γ is approximately ±2.5 per cent in the former and ±10 per cent in the latter. For the example given in this paper the numerical results are 0.171 and 0.143, respectively. The author does not feel competent at the moment to act as arbiter between the two methods; a more detailed discussion has been published.[4]

In conclusion it should be mentioned that the author has only recently received from England a preprint of a paper[10] by Dr. K. A. G. Miller in which he has derived, independently and simultaneously, equations for fixed tube-sheet design identical to those presented in the paper under discussion here. Miller has furthermore made strain measurements on a tube sheet of a floating-head-type exchanger which show very good agreement with what would be predicted from the author's original paper[3] in the case of radial strains; the tangential strains are not so close to theory so, as a result, the comparison between predicted and observed radial stresses is not so good as between predicted and observed radial strains. However, Miller in effect advocates the use of a flexural efficiency (and a ligament efficiency) given by

$$\eta_w = \eta_\sigma = 1 - \frac{\pi\sqrt{3}}{6}\frac{d^2}{P^2}$$

for plates uniformly perforated on a triangular pitch, and the favorable experimental results referred to are based on the use of η_w from this equation. For the example, in the paper under discussion here, this would give a numerical value of 0.489.

A Variational Principle for the Mesh-Type Analysis of a Mechanical System[1]

C. Truesdell.[2] In the first part of the paper the author gives a systematic method for carrying out Dr. Trent's scheme of writing down directly equations for the interaction forces in a mechanical system. It would be interesting to see how extraneous forces can be brought in by the method which the author just mentions.

The author's subsequent derivation of a new variational principle for obtaining equations for the forces in any system subject only to conservative mutual forces and linear internal damping is commendably clear and brief. Some worked-out examples would be valuable.

[10] "The Design of Tube Plates in Heat Exchangers," by K. A. G. Miller, to be published in the Transactions of The Institution of Mechanical Engineers.

[1] By R. A. Toupin, published in the June, 1952, issue of the Journal of Applied Mechanics, Trans. ASME, vol. 74, pp. 151–152.

[2] Professor of Mathematics, Graduate Institute for Applied Mathematics, Indiana University, Bloomington, Ind.

Book Reviews

Drag

AERODYNAMIC DRAG. By Sighard F. Hoerner. Published by the author, 148 Busteed, Midland Park, N. J., 1951. Cloth, 6 × 9 in., illus., index, bibliography, tables, v and 259 pp., $5.50.

REVIEWED BY PAUL A. LIBBY[1]

THIS book is a collection of data on aerodynamic drag presented within the framework of aerodynamic theory. The devotion of an entire book to such a specialized aspect of aeronautical engineering is rather unusual. It may be useful, however, as collateral reading in a graduate course in viscous flow theory and as a reference book for practicing engineers in the aeronautical, civil, mechanical, and marine fields.

The material is arranged in the following manner: Drag due to incompressible viscous effects is treated first. Thus skin-friction and pressure-drag data for blunt and streamlined bodies are presented. Induced drag is discussed next and is followed by a presentation of drag data for various aircraft components; vehicles such as cars, trains, and so on; and internal flow systems. Compressibility effects on low-speed drag characteristics, supersonic wave drag, and drag in free molecule flow are treated in this order.

Analytical Mechanics

ANALYTICAL MECHANICS FOR ENGINEERS. By Fred B. Seely and Newton E. Ensign. John Wiley & Sons, Inc., New York, N. Y., fourth edition, 1952. Cloth, 5½ × 8¼ in., xiv and 443 pp., 569 figs., $5.50.

REVIEWED BY NICHOLAS GROSSMAN[2]

WITH memories mellowed by time, the reviewer recalls the days when he was initiated into his first "engineering" course through an earlier edition of "Analytical Mechanics," which has served many fledgling engineers since its first publication in 1921. The present edition retains the salient features which have made this work a classic among the abundant texts in this field, namely: the emphasis of physical entities and comely everyday experiences; mathematics utilized as a tool, not as an end; reiteration of the free-body concept; a great wealth of well-balanced and profusely illustrated problems—which are neither too easy to cause undue overconfidence nor too involved or lengthy to discourage students; review questions at the end of the chapters; a conscientious effort to make each chapter self-contained and in toto, thus avoiding cross references, the latter being objectionable in elementary texts.

One cannot constructively review this textbook without effectively evaluating both the subject matter and its traditional method of presentation. The reviewer feels that a more compact and unified presentation of the chapters on the resultants of force systems and the equilibrium of force systems would enhance the clarity and purpose of the whole text. In the same tenor the equilibrium of coplanar and noncoplanar force systems could be advantageously integrated into an over-all treatment of statics. This would aid students in grasping basic and general ideas of spacial force systems instead of subdivisions and special cases.

The treatment of first moments and second moments is the weakest section of the text. Here the authors fall short of their avowed purpose of making this an engineeringly tangible presentation rather than an adjunct to mathematics. One fails to derive an organic unity between this appendix and the main body of the text. This poses an additional problem for the instructor and a psychological handicap for the students. The text on moments is not sufficiently complete and product of inertia should not have been omitted and Mohr's circles for inertias might be introduced at this level as a powerful tool in the general field of mechanics.

As for some minor points, the reviewer feels that relative motion and Coriolis's Law can be more advantageously assimilated in kinetics, than in kinematics, especially if it serves as preliminary to rotation in space and gyroscopes. The merit of including a short chapter each on vibration and balancing is a moot one. They seem too lengthy to be incorporated into an already overcrowded sophomore course, yet not self-sufficient to serve as a textbook in those fields. The reviewer feels that elements of mechanical vibrations should be integrated with the text in the appropriate sections.

The reviewer could not fail to observe with growing alarm that with the steadily increasing textbook prices there has been a concomitant reduction of marginal space, resulting in less legible, more eye-straining texts, a most serious handicap for students.

In this fourth edition of "Analytical Mechanics for Engineers" the authors have retained or successfully improved all those features of this text which have made it a clear, concise, and well-balanced introductory book in mechanics.

Engineering Mathematics

ADVANCED ENGINEERING MATHEMATICS. By C. R. Wylie, Jr. McGraw-Hill Book Company, Inc., New York, N. Y., 1951. Cloth, 6 × 9 in., xiii and 640 pp., illus., $7.50.

REVIEWED BY R. F. RINEHART[3]

THIS work provides a treatment of "those branches of mathematics with which the average analytical engineer must be reasonably familiar to carry on his own work effectively and keep abreast of current developments in his field." The author has made a good selection of material for this purpose, and the book should serve admirably as a text for a one-or-more semester course for upper-level undergraduates in science and engineering.

The book opens with three chapters on ordinary differential equations and one on applications to mechanical and electrical circuits. There follow chapters on Fourier series and integrals, and the Laplace transform with application to the development of the Heaviside methods. Chapter 7 deals with partial differential equations with emphasis on the wave equation. Chapter 8 is devoted to Bessel functions. Chapters 9 through 14 contain, from the standpoint of the engineer, an excellent and complete treatment of functions of a complex variable, culminating with applications to fluid mechanics. One chapter each is devoted to vector analysis and numerical analysis. An appendix contains selected refresher and supplementary material from algebra and calculus for the student's reference.

The presentation of the material maintains a high pedagogical standard. Proofs are written for maximum understandability by the reader. Motivations are usually given for any tack in a proof which might otherwise be obscure to the student. Refreshing phraseology, a departure from the customary language of mathematical proof, increases the intelligibility. The excellent exposi-

[1] Associate Professor of Aeronautical Engineering, Polytechnic Institute of Brooklyn, Brooklyn, N. Y.

[2] Mechanical Engineer, Sylvania Electric Products, Inc., Bayside, L. I., N. Y. Mem. ASME.

[3] Professor of Mathematics, Case Institute of Technology, Cleveland, Ohio.

tion has been achieved without any reduction in the level of rigor attained by the better books in this field.

Some 950 exercises of graded order of difficulty illustrate most of the text material. Some instructors will doubtless feel the need of supplementing some of the lists.

The typography is good and few printing errors were noted. The major shortcoming in the format is the practice of printing statements of theorems without any distinguishing features, either in type or in spacing, relative to the rest of the text matter. This seems an unnecessary inconvenience to inflict upon the reader.

Vibration

MECHANICS OF VIBRATION. By H. M. Hansen and Paul F. Chenea. John Wiley & Sons, Inc., New York, N. Y., 1952. Cloth, 6 × 9 in., tables, figs. problems, index, xiii and 417 pp., $8.

REVIEWED BY G. HORVAY[4]

"THERE appears to be a need for a treatment of vibrations designed primarily as a textbook." This statement of the authors in the preface, where they explain the reason for writing the book, took this reviewer quite by surprise. He was under the impression that there are a number of very commendable texts on the subject.

Since the authors aim so high, they invite close scrutiny. What are the ingredients of a good textbook? In this reviewer's opinion, at least, it must teach the student how to recognize a problem, it must teach him how to formulate a problem, it must teach him how to solve a problem, and it must teach him how to utilize the solution of the problem.

Acquisition of the knack of recognizing the variables of a problem, of recognizing the parameters of the problem, of recognizing and discarding the irrelevant features of the problem requires training and self-discipline. So does the formulation of the equations of equilibrium or of motion, and the determination of the correct boundary conditions. And so does the skill in drawing conclusions from solutions which do not fit the existing situation, or in generalizing the implications of partial results. Nevertheless, many textbooks spend all their energy on the easiest task, number 3, the teaching of the routines of the solution, and leave the more vital steps, 1, 2, and 4, largely unattended. The present book is no exception.

This is the problem, these are the pertinent differential equations and boundary conditions—is the way a topic is usually introduced in the first 120 pages (which deals with systems of one degree of freedom and of several degrees of freedom). Then comes a lengthy discourse on how to solve the problem (as if a person who knew how to set up his problem needed further indoctrination on how to solve linear differential equations with constant coefficients), and then an overlengthy explanation—not of the implications of the solution, but rather of its various mathematical and geometrical niceties.

Considering the presentation as a reference book, such an approach invites much less criticism. But then some other shortcomings of the presentation become apparent, such as limited coverage of the subject, lack of literature references, insufficient correlation with the work and terminology of other authors.

After a brief section on Lagrange's equations there follows the main feature of the book, discussion of the mobility method (80 pages). The method utilizes, as most readers will know, the analogy that exists between electric circuits and mechanical systems (charge corresponds to displacement, voltage to force), but only to define the notion of mechanical impedance as force per unit displacement, with proper phase relations. The analogy is then discarded (its further use would constitute an unnecessary drag), and mechanical systems are analyzed as such. The authors give a very thorough presentation of this laborsaving device, and illustrate the technique of setting up problems by numerous examples. They treat exhaustively complicated multimass systems, branched systems, lever systems, and platform problems. It should, however, be remembered that the impedance concept, as used, is limited to systems where all elements translate in one direction only, and where, correspondingly, rotation occurs only about an axis which is perpendicular to the translation axis.

The third part of the book (100 pages) consists of brief chapters on the solution of the frequency equation, on systems with distributed constants, on transient vibrations, and on nonlinear vibrations. In short accounts like these, where the author is hampered by space limitations, there arises the question of what to include, what to omit. Perhaps this reviewer will be pardoned for suggesting two items that could be readily replaced by things more important (such as more extensive discussion of systems with continuous parameters, or of nonlinear problems.) One is the lengthy explanation of Graeffe's method in solving for the complex roots of an equation. Quite apart from the fact that the method is usually explained also in other courses, and that its use depends on the availability of a first-class computer who makes no numerical mistakes, there really never arises—in the vibration problem of a slightly damped system—a need for such an unpleasant method of solution. A preferable procedure is to solve first the undamped frequency equation, writing it in the form $(\omega^2-p_1^2)(\omega^2-p_2^2)\ldots$, then approach the factored form of the damped equation $(\omega^2+\alpha_1\omega+\beta_1)(\omega^2+\alpha_2\omega+\beta_2)\ldots$ by means of Horner type synthetic divisions, using quadratic factors (the undamped factors are the first approximations), as explained in Milne's Numerical Analysis, page 54. The second suggestion is somewhat personal. When a mass M is attached to a spring of stiffness k, mass m, Rayleigh's rule gives $\omega^2 = k/(M + m/3)$ for the approximate squared natural frequency. When one attempts to extend this formula to multimass systems, there arises the need for first determining the nodes of the system (with respect to which the masses m must be counted). This is, with the one exception that is treated by the authors, quite a laborious job. There exists, however, another method of lumping the distributed constants of the spring; and this method requires no knowledge of the node locations. The method consists in lumping $^1/_2$ of the total shaft mass m into each end as concentrated mass, and replacing the shaft stiffness k by an effective stiffness $k + m\omega^2/6$.[5] For the one-mass system the squared frequency $\omega^2 = (k + m\omega^2/6)/(M + m/2)$ is readily seen to reduce to the Rayleigh formula; for more complicated systems the appearance of ω^2 in the spring terms causes no difficulty, since in a Holzer (or some other) scheme the calculation of a new set of spring constants for each assumed frequency causes but a small increase in labor.

There are three sections in the book which particularly impressed this reviewer. One is the valuable account of the mobility method; the second, the lively presentation of "systems with distributed physical constants"; the third, the remarkable collection, at the end of the book, of some 350 problems, with solutions included. These problems, by no means trivial, and frequently challenging, are a tribute to the authors' thorough familiarity with the field. They are likely to prove also of invaluable aid to the practicing engineer, as he will be enabled to relate many of his problems to the examples treated in the collection. It is hoped that future editions of the book will further enhance the value of this section, by providing more "hints for solution."

[4] Development Engineer, General Electric Co., Knolls Atomic Power Laboratory, Schenectady, N. Y.

[5] "Static and Dynamic Spring Constants," by G. Horvay and J. Ormondroyd, JOURNAL OF APPLIED MECHANICS, Trans. ASME, Vol. 65, 1943, p. A-214.

RESOLUTION CHART

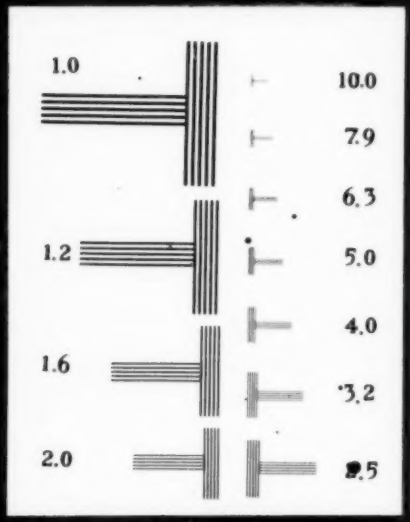

100 MILLIMETERS

INSTRUCTIONS Resolution is expressed in terms of the lines per millimeter recorded by a particular film under specified conditions. Numerals in chart indicate the number of lines per millimeter in adjacent "T-shaped" groupings.

In microfilming, it is necessary to determine the reduction ratio and multiply the number of lines in the chart by this value to find the number of lines recorded by the film. As an aid in determining the reduction ratio, the line above is 100 millimeters in length. Measuring this line in the film image and dividing the length into 100 gives the reduction ratio. Example: the line is 20 mm. long in the film image, and 100 / 20 = 5.

Examine "T-shaped" line groupings in the film with microscope, and note the number adjacent to finest lines recorded sharply and distinctly. Multiply this number by the reduction factor to obtain resolving power in lines per millimeter. Example: 7.9 group of lines is clearly recorded while lines in the 10.0 group are not distinctly separated. Reduction ratio is 5, and 7.9 x 5 = 39.5 lines per millimeter recorded satisfactorily. 10.0 x 5 = 50 lines per millimeter which are not recorded satisfactorily. Under the particular conditions, maximum resolution is between 39.5 and 50 lines per millimeter.

Resolution, as measured on the film, is a test of the entire photographic system, including lens, exposure, processing, and other factors. These rarely utilize maximum resolution of the film. Vibrations during exposure, lack of critical focus, and exposures yielding very dense negatives are to be avoided.

THIS PUBLICATION IS REPRODUCED BY AGREEMENT WITH THE COPYRIGHT OWNER. EXTENSIVE DUPLICATION OR RESALE WITHOUT PERMISSION IS PROHIBITED.